Transactions of the ASME

The Piston Gage as a Precise Pressure-Measuring Instrument . . . . . *D. P. Johnson and D. H. Newhall* 301

A High-Pressure Wire Gage Using Gold-Chrome Wire . . . . . *H. E. Darling and D. H. Newhall* 311

An Application of High Pressure in Geophysics: Experimental Rock Deformation . . . . . *John Handin* 315

Techniques and Equipment for Generation of Dynamic High Pressures . *E. J. Mickevicz* 325

A Sensitive Pressure Controller for High-Pressure Service . . . . . *P. L. Golden and A. F. Headrick* 329

High-Pressure Research in Chemical Engineering Department of Yale University . . . . . *B. F. Dodge* 331

Influence of Residual Stress on Behavior of Thick-Wall Closed-End Cylinders . . . . . *J. H. Faupel and A. H. Furbeck* 345

Rupture-Disk Design Evaluation and Bursting Tests . . . . . *G. R. Prescott* 355

Design and Application of Controlled-Volume Pumps for High Pressure in the Range of 10,000 to 30,000 Psi . . . . . *D. H. Jones* 361

Seals to Minimize Leakage at Higher Pressure . . . . . *B. A. Niemeier* 369

Static-Dynamic Load Machine for High Pressure . . . . . *E. T. Fleischbauer and E. G. Dorsey, Jr.* 381

Local Coefficients of Mass Transfer by Evaporation of Water Into an Air Jet . . . . . *Maurice Spielman and Max Jakob* 385

Design and Development of a Broad-Range, High-Efficiency Centrifugal Compressor for a Small Gas-Turbine-Compressor Unit . . . . . *Ivan E. Speer* 395

Some Investigations With Wet Compression . . . *J. T. Hamrick and W. L. Beede* 409

Transient and Steady-State Heat Transfer in Irradiated Citrus Fruit . *H. F. Poppendiek* 421

Operation of Sunbury Steam-Electric Station Using Pulverized-Anthracite Fuel . . . . . *T. B. Richards* 427

Cyclone Dust Collectors for Boilers . . . . . *A. J. ter Linden* 433

Mechanical Design in Oil-Shale Retorting Plants. . . . . *L. H. Brakel* 441

Engineering Features of the Union Oil-Shale Retort . . . *H. C. Reed and Clyde Berg* 453

Low-Temperature Insulation for Refinery Service. . . . . *W. L. Martin* 459

Full-Scale Fatigue Testing of Compressor Cylinders . . . . . *T. O. Kuivinen* 467

TRANSACTIONS OF THE AMERICAN SOCIETY OF MECHANICAL ENGINEERS

VOLUME 75 APRIL 1953 NUMBER 3

Transactions

of The American Society of Mechanical Engineers

Published on the tenth of every month, except March, June, September, and December

OFFICERS OF THE SOCIETY:

FREDERICK S. BLACKALL, JR., *President*

JOSEPH L. KOPF, *Treasurer* — C. E. DAVIES, *Secretary*
EDGAR J. KATES, *Ass't Treasurer*

COMMITTEE ON PUBLICATIONS:

GEORGE R. RICH, *Chairman*

PAUL T. NORTON, JR. — COLIN CARMICHAEL
OTTO DE LORENZI — W. E. REASER
MORRIS GERR, JOSEPH SCHMERLER } *Junior Advisory Members*
GEORGE A. STETSON, *Editor* — K. W. CLENDINNING, *Managing Editor*

REGIONAL ADVISORY BOARD OF THE PUBLICATIONS COMMITTEE:

KERR ATKINSON—I
JOHN DE S. COUTINHO—II
WILLIAM N. RICHARDS—III
FRANCIS C. SMITH—IV
HENDLEY BLACKMON—V
CHESTER R. EARLE—VI
RAYMOND G. ROSHONG—VII
VENTON L. DOUGHTIE—VIII

Published monthly by The American Society of Mechanical Engineers. Publication office at 20th and Northampton Streets, Easton, Pa. The editorial department is located at the headquarters of the Society, 29 West Thirty-Ninth Street, New York 18, N. Y. Cable address, "Dynamic," New York. Price $1.50 a copy, $12.00 a year for Transactions and the *Journal of Applied Mechanics;* to members and affiliates, $1.00 a copy, $6.00 a year. Changes of address must be received at Society headquarters four weeks before they are to be effective on the mailing list. Please send old as well as new address.... By-Law: The Society shall not be responsible for statements or opinions advanced in papers or ... printed in its publications (B13, Par. 4).... Entered as second-class matter March 2, 1928, at the Post Office at Easton, Pa., under the Act of August 24, 1912....

Copyrighted, 1953, by The American Society of Mechanical Engineers. Reprints from this publication may be made on condition that full credit be given the Transactions of the ASME and the author, and that date of publication be stated.

The Piston Gage as a Precise Pressure-Measuring Instrument

By D. P. JOHNSON[1] and D. H. NEWHALL[2]

The errors which must be considered for accurate measurements of pressure with piston gages are discussed. A new design of piston gage is described which permits the operator to control the clearance between piston and cylinder at any operating pressure. Instrumental errors are thus substantially reduced, particularly those resulting from elastic distortion. A check list of errors inherent to piston gages is presented. These errors are to be considered when instruments are used to accuracies better than $\frac{1}{2}$ of 1 per cent. The need for a check on the long-time variations of the piston gage is supplied by the fixed points, changes of state of some very pure materials which take place at definite pressures. Such are the melting pressure of solid mercury at 0 C, the melting pressure of water at 30 C, the transition between crystalline states of bismuth. As an indication of its possibilities the experimental model of the controlled-clearance piston gage was used to measure the melting point of mercury at 0 C. Results were in satisfactory agreement with Bridgman's value.

Introduction

INDUSTRIAL engineers sometimes ask how they may benefit by the concern of the National Bureau of Standards over a primary standard of pressure with an accuracy of 0.01 per cent or better. An industrial engineer may be concerned with processes which require the control of pressures within, say, ±1 per cent. To be sure of holding the pressures within the required range, he will have on his control panel, pressure gages with an accuracy of, say, 0.3 per cent. The manufacturer of the pressure gages will have in his production line a calibration bench. Here the gages will be checked against standards which should be better than the instruments calibrated by at least a factor of 3, preferably a factor of 10, that is, from 0.1 to 0.03 per cent. The manufacturer should have in his standards room instruments somewhat better than the bench standards, with an accuracy better than 0.03 per cent, preferably about 0.01 per cent.

There are many research laboratories in industry engaged in getting fundamental engineering data with an accuracy of 0.1 per cent or better. Phenomena which are sensitive to pressure may require instrumentation accurate to 0.03 or even 0.01 per cent.

The National Bureau of Standards should have primary standards which are somewhat more accurate than any instrument portable enough to be brought in for calibration. There are pressure-measuring instruments which are capable of an accuracy of 0.01 per cent at pressures up to a few thousand pounds per square inch. The primary standards against which these are calibrated should be definitely better, with an accuracy of 0.003 per cent. The possible accuracy drops off as the pressures increase, and considerable effort is required to develop primary standards adequate to the present requirements in the high-pressure field.

Pressure-Standards Apparatus

In a primary standard the measurement of any physical quantity is referred directly to the standards of mass, length, and time. The device should be so simple in principle that all of the errors inherent in the instrument either can be eliminated or evaluated. Two commonly used primary standards are the mercury column and the dead-weight piston gage. The choice of instrument is not limited by accuracy, but by convenience. Twenty pounds per square inch is approximately equal to the head of a convenient 40-in. column of mercury. To measure 30,000 psi would require a column of mercury about 1 mile high.

The first extensive use of the free-piston gage was by Amagat (1).[3] The basic form and two modifications are in current use. They are illustrated in Figs. 1, 2, and 3.

Simple Piston Gage. The most familiar form of piston gage is shown in Fig. 1. It is a fitted piston-and-cylinder arrangement with means to apply known weights on the piston. The piston is rotated or oscillated to reduce friction. When the pressure applied to the piston develops a force sufficient to support the dead weights, they will be lifted. The weights may be placed on top of the piston or be suspended below it by a yoke. The weights may rotate with the piston or the piston may be rotated or oscillated independently of the weights. It is necessary for some fluid to leak past the piston for lubrication. The leak should be kept small to provide sufficient floating time to establish equilibrium and to make the required observations. This is particularly important at high pressure.

Differential Piston. Professor Michels (2) of Holland has designed a sensitive piston gage for high pressure, Fig. 2. It is a series of two differential-area pistons both carrying dead weights. The first piston (A) is suitable to pressures of 3000 kg/cm² (43,000 psi).

When its output is piped to the upper side of the second piston (B), the force developed is additive to the dead-weight load. The second piston makes the unit suitable to 10,000 kg/cm² (142,000 psi). Leakage is controlled by an interference fit between piston and cylinder. At high pressure the piston becomes free to rotate. The use of similar pistons of various sizes permits measurements over a wide range.

Re-entrant Cylinder. Professor Bridgman (3), early in his work developed a free-piston gage with re-entrant cylinder, Fig. 3. The bottom tip portion of the piston (p) and outside surface of cylinder (C) are subjected to the measured pressure. The bore of the re-entrant cylinder (C) grows smaller as pressure increases, regardless of the wall ratio (W = OD/ID). Since the clearance between the piston and cylinder diminishes with increasing pressure, and the leakage is reasonably small, the upper limit of the range is determined by the initial clearance. The initial clear-

[1] National Bureau of Standards, Washington, D. C.

[2] Harwood Engineering, Inc., Walpole, Mass.; formerly with Foxboro Company, Foxboro, Mass.

Contributed by the Industrial Instruments and Regulators Division of The American Society of Mechanical Engineers and presented at the Seventh National Instrument Conference, Cleveland, Ohio, September 9–10, 1952.

Note: Statements and opinions advanced in papers are to be understood as individual expressions of their authors and not those of the Society. Manuscript received at ASME Headquarters June 30, 1952. Paper No. 52—IIRD-2.

[3] Numbers in parentheses refer to the Bibliography at the end of the paper.

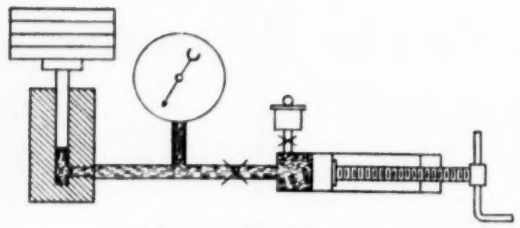

FIG. 1 SIMPLE PISTON GAGE

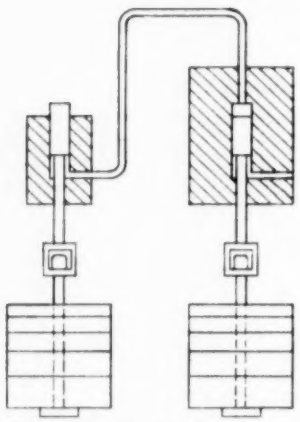

A, Low-pressure section B, High-pressure section

FIG. 2 DIFFERENTIAL-AREA PISTON GAGE

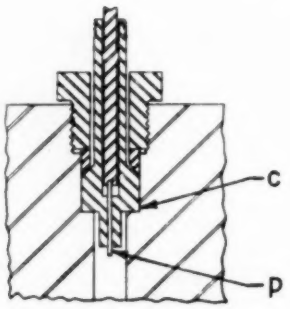

P, Piston
C, Cylinder

FIG. 3 PISTON GAGE WITH RE-ENTRANT CYLINDER

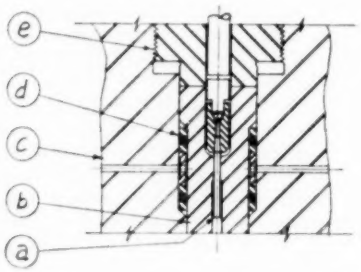

a, Piston
b, Cylinder
c, Jacketing cylinder
d, Packing rings
e, Closing nut

FIG. 4 CONTROLLED-CLEARANCE PISTON GAGE

ance was chosen so that the crevice closed completely at approximately 210,000 psi, and the instrument was used to approximately 190,000 psi to a precision of approximately 0.1 per cent. The fluid used was a mixture of glucose, glycerin, and water.

The literature abounds with descriptions of instruments which are variations of the basic concept of the simple piston gage. Mostly, they are clever arrangements to allow the operator to handle small weights. It is probably fair to say that uncertainties are built into the devices in proportion to the departure from the simply loaded piston.

CONTROLLED-CLEARANCE PISTON GAGE

The clearance between the cylinder and piston must be kept small if the piston gage is to be useful on the score of (*a*) knowledge of the effective area, (*b*) high sensitivity, (*c*) manageable leakage of the fluid past the piston. The large elastic distortions, particularly in the cylinder, have set severe limitations on the useful range.

The controlled-clearance piston gage, Fig. 4, permits a size adjustment of the cylinder bore to the desired clearance. The measuring piston (a) is contained in a jacketed cylinder (b). An independent pressure is used between the jacketed and jacketing cylinder (c) to deform the jacketed cylinder to the desired clearance. The pressure in the jacketing cylinder is sealed off by Bridgman unsupported area rings (d) whose initial seal is accomplished by a mechanical load from nut (e).

The relation between the pressure P_J required in the jacketing cylinder and the pressure P_M being measured is expressed approximately by

$$P_J = K + L P_M$$

in which K is the pressure required to close the crevice at zero internal pressure. The value of L depends on the position of the ring of minimum clearance. If the ring is near the top of the cylinder, L will be about 0.7; if away from either end, the preferred condition, L will be about 0.35. Depending on the initial clearance, the jacketing pressure can be either greater or less than the pressure being measured. The jacketed cylinder and piston are disposed in the design so that the seal between them will be accomplished sufficiently far from the ends of the piston to avoid local distortions which result from end effects. To avoid end effect further, the jacket cylinder is "bellmouthed" at both ends of its bore.

The free-falling time is controlled readily by minor adjustments of jacket pressure. If the close clearance is maintained, the effect of the distortion of the cylinder is eliminated. It will be shown later that this is a notable improvement since in other designs the elastic distortion of the cylinder is one order greater than the distortion of the piston. A still further improvement probably will result from the use of carboloy pistons. Otherwise the apparatus is more elaborate than unique. The elaborations take advantage of well-known design points with a view to maintaining accuracy and precision, and to securing ease in manipulation.

The dead-weight system, Fig. 5, is patterned after the 10,100-lb dead-weight system in the Engineering Mechanics Section at the National Bureau of Standards (4). The dead weights themselves (f) are made of austenitic stainless steel for long-time stability and freedom from oxidation, corrosion, and magnetism. The loading system has 1000 lb of dead weight, consisting of nine 100-lb platters held in a chain suspension attached to the yoke (g). The weights are lifted on and off the suspension by the power cylinder (h) on the base. Smaller 10 and 5-lb weights (i)

are provided for hand-loading on the yoke. The piston is rotated either clockwise or counterclockwise by means of a pulley (j) and motor arrangement to eliminate the corkscrew effect. It is patterned after that described by Meyers and Jessup (5). The yoke suspension rods (k) are insulated electrically from the upper cross rail (l). Thus, by electrical sensing, there is assurance that the weights supported by the piston are free of other parts.

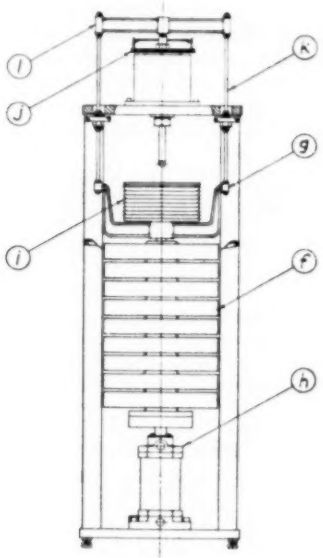

f, Large dead weights of 100 lb each
g, k, l, Yoke suspension
h, Power cylinder to load large dead weights
i, Small dead weights of 5 and 10 lb
j, Pulley for rotating piston

FIG. 5 LOADING MACHINE FOR CONTROLLED-CLEARANCE PISTON GAGE

The measuring piston and cylinder are so arranged that they may be removed readily and interchanged with similar components for other ranges. The cost of the piston assemblies is on the order of 3 per cent of the total cost of the instrument, while the piston itself represents only a fraction of 1 per cent of the total cost of the instrument. The change-over from one piston size to another is done readily with hand tools.

ERRORS OF A PISTON GAGE

Definitions. A pressure is a force per unit area. A force of 1 lb will be defined as that which will accelerate a mass of 1 lb at the normal acceleration of gravity, 980.665 cm/sec^2 or 32.174 ft/sec.^{2} The U. S. pound is defined as the 0.4535924277 part of the international kilogram. The U. S. standard inch is defined as 100/3937 international meters (6).

To obtain the pressures as so defined, the indications of a practical dead-weight piston gage are subject to a number of corrections. The more important of these, which will be of concern to those who hope to measure a pressure to a part in a thousand, will be discussed in some detail. Some of these errors can be evaluated and corrections applied, but in every case there will remain some residual uncertainty which may or may not be important.

Effective Area. The effective area of a piston gage is the mean of the area of the cylinder and that of the piston, provided the piston is concentric with the cylinder and falling at a rate at which the volume displaced by the piston is equal to the leak between it and the cylinder. This is true for any clearance and for fluid of any viscosity. If, because of other volume changes in the system, the piston is falling at any other rate, of the same order of magnitude, the effective area will be changed by an amount of the order of the square of the clearance distance.

Elastic Distortions. The following formulas may be found with the assistance of standard texts on elasticity (7):

The change Δd in the diameter d, in a solid piston subjected to end pressure P and surrounded by pressure P_c (P is the pressure being measured and P_c the pressure in the crevice) is given by

$$\frac{\Delta d}{d} = \frac{\nu P}{E} + \frac{P_c}{E}(\nu - 1) \quad [1]$$

where ν is Poisson's ratio and E is Young's modulus.

The change Δa in the bore radius a of a hollow cylinder of outside radius $b = wa$, where P_o is the pressure on the outside, P_a is the pressure on the inside, and P_z is the pressure on the end face, is

$$\frac{\Delta a}{a} = \frac{P_a}{E}\left[\frac{(1-\nu) + (1+\nu)W^2}{W^2 - 1}\right] - \frac{P_o}{E}\left(\frac{2W^2}{W^2 - 1}\right) + \frac{\nu P_z}{E} \quad [2]$$

In the piston gage the pressure varies along the length of the crevice between piston and cylinder. At the bottom it equals the pressure being measured; at the top it falls to zero. The fall of pressure probably will be concentrated in a small portion of the length. The effective pressure in the crevice, to be used in calculating the distortion, will depend on the location of the region of falling pressure. If this region is at the bottom of the piston, the effective pressure will be small. If it is at the top, so that the crevice is filled with liquid at high pressure, then the effective pressure may be nearly as high as that being measured.

Small variations in dimensions may have a great effect on the position of the pressure drop. (It is even possible that the position may be a function of pressure.) The variations may occur because of the design, because of irregularities in machining, or because of distortions in use. For example, when a piezoelectric gage is calibrated by a sudden release of pressure, the piston of a gage connected to the system will drop violently. If it is stopped at the blind end of a cylinder it may mushroom slightly, Fig. 6(*a*). If it is stopped by contact with the open end of the cylinder, the latter may develop a burr, Fig. 6(*b*). Therefore it can be said with certainty, only that the effective pressure in the crevice is less than the pressure measured. The distortions of the piston and cylinder may be calculated on the basis of an effective pressure in the crevice which is the mean between that at the two ends, provided that the fall of pressure takes place in a region remote from the ends of the piston, and of the bore of the cylinder. "Remote" can be taken as one diameter in the case of the piston, and three bore diameters for the cylinder.

Piston. Case 1: When the pressure in the crevice is one half the pressure being measured, we have the following change ΔA in the area A using Equation [1], a value of 0.28 for Poisson's ratio and 30×10^6 psi for Young's modulus

$$\frac{\Delta A}{A} = \frac{2\Delta d}{d} = -0.53\,\frac{P}{10^6} \quad [3]$$

At 200,000 psi this amounts to −0.11 per cent.

Case 2: If the fall of pressure is at the top of the piston and occurs over a length which is small compared to the diameter, $P_c = P$

$$\frac{\Delta A}{A} = \frac{2\Delta d}{d} = \frac{-2.9P}{10^6} \quad [4]$$

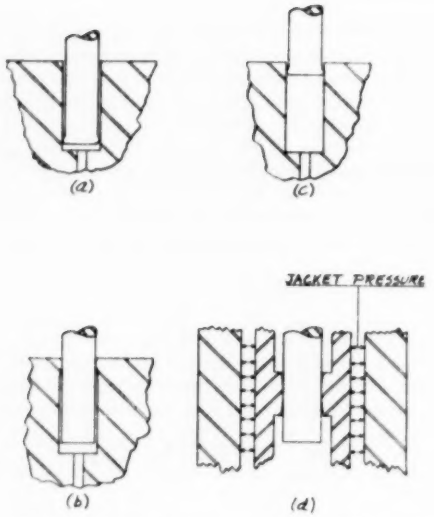

FIG. 6 PRESSURE DISTRIBUTION IN PISTON GAGES

(*a*, Piston and cylinder at low pressure; *b*, piston and cylinder at high pressure; *c*, piston at low pressure, cylinder at high pressure; *d*, top of piston at low pressure, bottom at high pressure. Cylinder controlled to fit piston.)

At 200,000 psi this amounts to —0.58 per cent.

Case 3: If the fall of the pressure is at the bottom of the piston $P_c = 0$

$$\frac{\Delta A}{A} = \frac{2\Delta d}{d} = \frac{+1.9P}{10^6} \quad [5]$$

At 200,000 psi this amounts to +0.38 per cent.

Piston Gage, Simple Cylinder, and Piston. Here the cylinder is subjected only to the pressure in the crevice. Equation [2] is applicable, with the terms

$$P_o = 0,\ P_s = 0,\ \text{and}\ P_a = P_c = \frac{P}{2}$$

For a wall ratio $W = 3$

$$\text{The change in area} = \frac{\Delta A}{A} = \frac{2\Delta a}{a} = \frac{5.1P}{10^6} \quad [6]$$

At 200,000 psi this amounts to +1.02 per cent.

The change in effective area of the gage will be the mean of the changes in the cylinder and piston (Case 1) or

$$\frac{\Delta A_{eff}}{A} = \frac{\Delta d}{d} + \frac{\Delta a}{a} = \frac{2.3P}{10^6} \quad [7]$$

At 200,000 psi this amounts to +0.46 per cent.

If the piston is expanded at the lower tip (Case 3), in a blind cylinder, Fig. 6(*a*), the distortion at 200,000 psi might vary from +0.19 per cent at the bottom of the stroke, to +0.70 per cent when the tip of the piston has risen several bore diameters away from the end of the cylinder, Fig. 6(*c*).

Piston Gage With Re-entrant Cylinder. The end face and outside of the re-entrant cylinder are subjected to the pressure measured so that $P_s = P_o = P$. If $P_a = P/2$ the distortion $\Delta A/A$ of the cylinder of wall ratio 3 is

$$\frac{\Delta A}{A} = \frac{2\Delta a}{a} = \frac{-4.02P}{10^6} \quad [8]$$

At 200,000 psi this amounts to —0.8 per cent.

The change in effective area of the piston gage (piston Case 1) is

$$\frac{\Delta A}{A} = \frac{\Delta d}{d} + \frac{\Delta a}{a} = \frac{-2.28P}{10^6} \quad [9]$$

At 200,000 psi this amounts to —0.46 per cent.

Controlled-Clearance Piston. In this instrument the dimensions of the cylinder change with those of the piston. The piston extends outside the section of close clearance with the cylinder by several diameters, so that the conditions for using the mean value of the pressure in the cylinder are satisfied, Fig. 6(*d*). Therefore the elastic distortion is that of the piston alone. For steel with $\nu = 0.28$ and $E = 30 \times 10^6$ psi, the change in area is

$$\frac{\Delta A}{A} = -\frac{0.53P}{10^6} \quad [10]$$

At 200,000 psi this amounts to —0.11 per cent.

For carboloy, with $\nu = 0.22$ and $E = 88 \times 10^6$ psi

$$\frac{\Delta A}{A} = -\frac{0.39P}{10^6} \quad [11]$$

At 200,000 psi this amounts to —0.08 per cent.

Measurement of Area. In the size range used in pressure gages, the piston diameters can be measured to 10 microinches or a little less. The corresponding uncertainties in the measured error are given in Table 1.

TABLE 1 EFFECT OF A 10-MICROINCH ERROR IN DIAMETER

Nominal area, sq in.	Approximate diameter, in.	Error in area, per cent
1/200	0.0798	0.025
1/100	0.1128	0.018
1/50	0.1596	0.012
1/20	0.2523	0.008
1/10	0.3568	0.006
1/5	0.5046	0.004
1/2	0.7979	0.0025

The gain in accuracy by increasing the size of the piston is somewhat more than that shown in the table since more precise methods of measurement are available for the largest size.

Measurement of Mass. The weights should be of the materials and quality required for the better commercial-scale weights. The material should be nonporous, corrosion and wear resistant, nonmagnetic. Weights usually are adjusted by the manufacturer to about 0.01 per cent. They can be calibrated to 0.001 per cent. In precise work, these corrections should be applied.

Gravity. The readings of Bourdon-tube pressure gages, manganin-wire gages, and such phenomena as elasticities, viscosities, phase changes, and chemical reactions, are functions of the absolute pressure. They are not sensibly affected by the local value of gravity. The pressure measured by a piston gage loaded with a particular set of dead weights is proportional to the local value of gravity. The convention here used is that the readings of elastic and dead-weight pressure gages should correspond when the dead weights are acted upon by gravity at the standard value of 980.665 cm/sec^2.

In the southern part of the United States, the value of gravity will be more than 0.1 per cent smaller than the standard value. In Canada and the northern part of the United States the local value will be higher.

If the latitude ϕ and the elevation h in feet above sea level are known, the gravity correction C_g will be given approximately by

$$C_g = -R\,(0.00261 \cos 2\,\phi + 0.000000095\,h + 0.00006)$$

where R is the reading of the piston gage.

This correction usually will compensate for gravitational

variation with an error of less than 0.005 per cent in any part of the United States.

For example: At Boulder, Colo., the reading on a piston gage, before gravity correction, was 101,200 psi. The latitude was 40°01′ (sin 80°02′ = +0.1730) the elevation 5350 ft

$$C'_g = -101{,}200\,(0.00261 \times 0.1730 + 0.000000095 \times 5350 + 0.00006)$$
$$= -101{,}200\,(0.00102) = -103$$

so that the corrected pressure = 101,200 −103 = 101,097 psi.

In this case had the value observed at this location by the U. S. Coast and Geodetic Survey been used, the corrected pressure would have been 101,091 psi. This difference of 6 psi is reasonable, since the errors in the formula are largest in mountainous country.

Air Buoyancy. The mass of the piston and loading weights is determined on the ordinary commercial basis, i.e., by weighing in air, on an equal-arm balance, against standard brass weights (density 8.4 grams per cc). In precise work, the mass of the load on the piston should be reduced by an amount equal to the mass of the air displaced by the weights.

The density of air at room temperature and sea-level pressure is about 0.0012 gram per cc; and the mass under these conditions will be reduced by 1 part in 7000.

Temperature. The effective area of a carbon-steel piston and cylinder may be expected to increase about 13 ppm per deg F temperature rise; for a stainless-steel piston and cylinder the increase in area will be about 18 ppm per deg F.

The temperature of the piston is somewhat higher than that of the surroundings because of the dissipation of energy in the fluid escaping between the piston and cylinder. The temperature rise in the piston is difficult to estimate because of the uncertainty in the thermal transfer between the piston and the exterior. Since the dissipated energy is proportional to the rate of leak, measurements can be made at various rates, and an extrapolation made to zero leak.

Aging. Over a period of years the dimensions of the piston and cylinder may change by as much as 1 part in 1000 because of aging effects. Wear also will change the dimensions, and is likely to result in irregular performance. Extreme precautions to keep grit out of the fluid are required. The dead weights may lose weight from wear, or may gain weight by oxidation or collection of dirt.

Height and Piston-Buoyancy Corrections. It usually happens that the gage being tested, or the point at which the pressure is to be measured, is not at the same level as the lower end of the piston. Therefore correction should be made for the pressure difference due to the head of oil between these points. The correction is negative when the gage is above the piston. When oil is used in the piston gage, the correction will be approximately 0.03 psi for each inch difference in level.

When the submerged part of the piston is of uniform cross section, the pressure measured is that at the level of the lower end of the piston. In some designs the piston is enlarged to provide a stop for its upward motion or to give increased strength. If these enlargements are submerged in liquid, the weight of the fluid displaced by the enlargement should be subtracted from the dead-weight load.

With some designs it is not possible to observe the liquid level, and therefore not possible to determine the submerged volume. In such a case it is necessary to determine the buoyancy correction by test. It will usually be less than a pound per square inch.

Pressure Drops in Lines. Whenever possible, the piston gage should be connected into a leak-tight system, with tubing of the largest bore consistent with strength and safety, in order to avoid pressure drops in the lines. If this is impossible, the layout of tubing should be such that the piston gage is connected to the test vessel with a line through which the least possible flow of fluid occurs.

Friction. If the piston and cylinder come into contact, or if any part of the dead weight touches the supporting frame, sliding friction will introduce uncertainties. A film of fluid between piston and cylinder is usually maintained by rotation or oscillation. With rotation there is the possibility of a corkscrew effect, an axial thrust produced by helical irregularities on the surface of the piston and cylinder. Observations should be repeated with the piston rotating in the opposite direction. If the hydraulic fluid is a good lubricant and has a suitable viscosity, a film can be maintained with either rotation or oscillation. A lubricating film can be maintained with a fluid of very low viscosity (even air) provided the piston is rotated above a critical speed. This speed depends on the fluid, the symmetry of loading, and the clearances, etc. It must be determined experimentally for each instrument.

Intercomparison Techniques

Since the percentage accuracy of the measurements of the diameter is better for a large piston than for a small one, the intercomparison of piston gages of differing ranges provides an opportunity of improving the accuracy of the latter. In addition, there is the opportunity of averaging out some of the effects of varying properties of the materials of the piston, and of picking up possible mistakes in measurements.

In an intercomparison by cross floating, two piston gages are connected together and to a common pressure generator, such as the intensifier, of suitable range and capacity. Either piston gage can be isolated by means of valves in the connecting tubing. A telescope with an eyepiece scale or the equivalent, is set up to observe the position of one of the pistons in its range of motion. At the selected pressure, the rate of fall of each piston is observed with the gage isolated. The two gages are connected together and one of the loads adjusted by adding small weights until both pistons fall at approximately the same rate as when isolated. An exact balance is usually not obtained, but by observing rates of fall at various loads, an interpolation can be made to the load for which the rates of fall would be the same with the gages connected as when they are isolated.

By having one of the pistons fall repeatedly over the same interval, while the other falls through various parts of its range it is possible to observe small variations in diameter. By this method a commercial piston gage with a simple cylinder was ascertained to have an effective area constant over its length to within 1 part in 50,000. Since the diameter of this piston was about 0.16 in., it must have been uniform to 1.6 microinch or better.

This particular observation happened to have been made at a pressure of about 1000 psi. When the same kind of comparison was attempted at 5000 psi, the rate of fall was so much greater that the comparison was quite unsatisfactory. The enormous change in sensitivity was caused by an increase in the bore of the cylinder estimated to be only about 8 microinches.

Calibration Against a Mercury Column

An alternative primary standard is the mercury column. Readings on it are also subject to a large number of corrections most of which are counterparts of those for the piston gage. The reader may refer to Glazebrook (8) or Meyers and Jessup (5) for a discussion of them. The latter authors set up a 150-psi mercury column, with an accuracy of 0.01 per cent, compared it with piston gages of 0.01 per cent accuracy, and had agreement within 0.01 per cent at pressures up to 1050 psi. They set up a

pressure on one piston gage, added the pressure measured by the mercury column, and compared the sum with the pressure on a second piston gage. The pressure measured by the mercury column was then added to that on the second gage and compared with a new pressure set up on the first. The process was continued until the glass tubing broke. Keyes (9) has carried a similar procedure up to pressures as high as 15,000 psi.

While this method is quite satisfactory at low pressures, the accuracy falls off rapidly at higher pressures. For example, suppose that a 150-psi mercury column is used to calibrate a pair of 30,000-psi piston gages, which have a sensitivity of 1 ppm of their range or 0.03 psi. Then each 150-psi step in this comparison can be done to 0.03 psi, or 1 part in 5000. But the area of a piston good enough to attain this sensitivity probably can be measured to better than 1 part in 10,000.

The small distortion of the cylinder or piston in the 150-psi step of pressure gives rise to just as large a correction, in relation to the 150 psi, as the larger distortion under 30,000 psi is with respect to the 30,000-psi range of the instrument.

A satisfactory comparison with a mercury column will give the user of the piston gage the valuable assurance that he has not overlooked some large systematic error in the latter. But a calibration of a piston gage against a mercury column cannot be regarded as inherently better than a standardization by direct measurement on piston and weights.

Fixed Points on the Pressure Scale

Primary pressure standards are not portable. In order to attain an over-all accuracy of 1 part in 10,000, attention must be paid to a great many factors. As a result, although the mercury column or piston gage is simple in principle, it will be surrounded by so many auxiliaries that its bulk will be large in the aggregate. To tear it up by the roots and send it to another laboratory for a calibration is a formidable task. Even if all this were done, there would be no assurance that essential parts would endure the hazards of shipment. There is a real need for a means of calibration that can be put in a suitcase, or even better, sent by first-class mail.

One solution to this problem is a set of experiments which can be repeated at any laboratory and will reproduce definite pressures. In some cases a suitable transfer instrument and a set of fixed-pressure points would replace the primary standard. The analogous situation exists in the field of temperature measurement. The platinum-resistance thermometer and four fixed-temperature points define the temperature scale over a range of 600 C to the satisfaction of most users.

The fixed-pressure points may be based on changes of state or polymorphic transformations which should satisfy the following conditions:

1 The substances involved should be obtainable in a pure state.

2 The transition should take place at a sharply defined pressure, with no range of indifference.

3 There should be a large volume change, or other effect, for ready identification.

4 The reaction should run rapidly.

5 The dependence of the pressure on temperature or other possible parameters should be slight.

6 It should be possible to contain the substances so as not to damage the pressure vessel.

Triple points are particularly suitable since they are unique in both temperature and pressure, provided all three phases are present. In a two-phase system a volume change is associated with a thermal change, and time is required to approach equilibrium. At a triple point, adjustments among all the components take care of thermal and volume changes simultaneously.

Bridgman's value of the freezing pressure of mercury at 0 C, 7640 kg/cm² (108,660 psi), has been used by a number of observers. Occasionally a higher temperature has been used when a higher pressure was required. The temperature coefficient of the melting pressure is about 3000 psi per deg C, so that accurate temperature measurements and precise control are required. These are much easier at 0 C, where an ice bath can be used.

In his work at the high pressures Bridgman has used the bismuth I–II transition at about 360,000 psi for the calibration of his manganin-wire pressure cells.

The four triple points between liquid water and various ices appear to be promising. These are L-I-III at about 30,000 psi; L-III-V near 50,000 psi; L-V-VI near 90,000 psi, L-VI-VII near 320,000 psi. Between these points the melting-point pressure at various temperatures can be used. The Geophysical Laboratory of the Carnegie Foundation (10) is reporting its pressure measurements on the basis of a value of 9630 bars (139,670 psi) for the freezing pressure of water at 30 C, with the expectation of adjustment if a better determination should change that value.

Professor Bridgman measured pressures at the phase changes of water and of mercury in 1912. Since then, in so far as is known, there has not been an independent determination. Rather, the value reported by him has been used without question. While the Bridgman values were sufficiently accurate for his pioneering work, a vast amount of data reported with greater accuracy than that claimed by Bridgman are still dependent on his value. This is not as serious as it might seem at first glance. Bridgman's value should stand until an independent determination has been made with the improved tools of the present day. Quantitative work reported prior to the publication of the new value will have to be corrected when correlated to subsequent work—should a correction for Bridgman's value be indicated.

Mercury-Point Determination

In order to test the possibilities of the controlled-clearance piston gage, and to get the "feel" of the experiment, a determination was made of the melting pressure of mercury at 0 C. Use was made of a transfer gage, at first a manganin-wire pressure cell, and for the final runs, a gold-chromium-wire pressure cell. The determination can be broken into three steps as follows:

(*a*) Measurement of melting pressure of mercury in terms of transfer instruments.

(*b*) Calibration of transfer instruments in terms of piston gage.

(*c*) Direct measurement of area of piston and mass of dead-weight load.

Mercury-Point Comparisons. The apparatus found to be convenient was arranged as shown schematically in Fig. 7. Two laboratory-type intensifiers were used. The intensifiers were driven and charged by hand-operated 10,000-psi pumps. White gasoline was the high-pressure fluid used. Kerosene had been found unsuitable in an earlier experiment. The upper side of the low-pressure piston of the intensifier A (normally vented to the air), was filled with a liquid and connected to a sight glass to indicate the piston displacement, and hence the changes in volume. With a $^1/_8$-in-bore sight glass, the displacement of the column was 360 times that of the piston.

The mercury bomb was a simple high-pressure vessel with a cavity 1 in. diam and approximately 5 in. long. Freshly distilled mercury was sealed in a polyethylene sack and placed in the bomb cavity.

A gold-chromium resistance element, subjected to the high pressure, was used as a transfer device. The gold-chromium resistance was part of a 120-ohm equal-arm bridge. The other arms were in a bath at room temperature, close to the pressure cell. The bridge was driven by alternating current at 1000 cps,

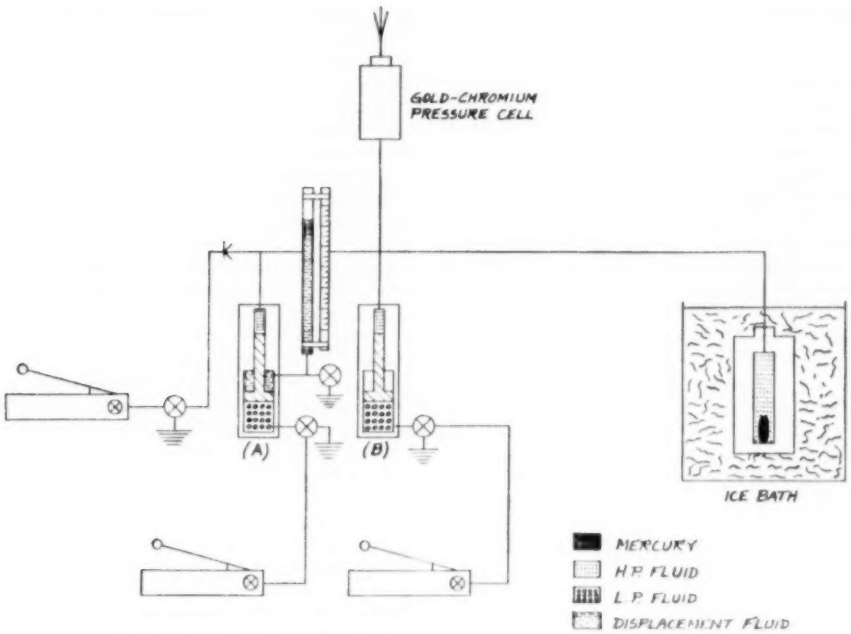

FIG. 7 APPARATUS FOR DETERMINATION OF MERCURY FREEZING PRESSURE

50 milliamp total current. One arm of the bridge was shunted by an adjustable resistance box. An a-c null indicator was used to detect balance. The sensitivity of the indicator was adequate to detect changes in the resistance of the gold-chromium wire of 1 part in 10^7. A duplicate bridge in a temperature-controlled bath was used to correct for drift in the null indicator. The drift during a run was not more than 1 part in 10^6.

The system was charged to about 10,000 psi by a hand pump. This pressure was held in the system by a check valve when the hand pump was removed. The piston of intensifier (B) was then advanced to the end of its stroke raising the pressure to about 90,000 psi. Another check valve held the pressure in the rest of the system after the pressure in intensifier (B) was released. During the rest of the experiment the pressure was raised by advancing the piston of intensifier (A). The movement of the piston of this intensifier was followed in the sight glasses.

If the volume is plotted against pressure, at constant temperature, there is obtained a nearly straight line *A-B*, Fig. 8, representing the compression of the liquid, a horizontal straight line *B-C*, representing the change in volume at constant pressure of the mixture of liquid and solid, and the nearly straight line *C-D* representing the compression of the solid. This is under isothermal conditions, which are never realized by the experimenter. When the specimen is compressed, it is heated, and is therefore at a pressure which is a little high. If only one phase is present, either liquid or solid, the approach to equilibrium is nearly completed after 5 min. With both phases present, the latent heat of the phase change is large, and a relatively long time is required for the system to come to equilibrium as this heat is transferred to the bath.

In these measurements the pressure is increased in steps of about 5000 psi, and the piston held stationary at each step for 5 min. As long as only liquid mercury is present, the pressure drops back slightly and stabilizes during each hold period, *A* to *B*, Fig. 8. When solid mercury makes its appearance, the pressure drops back farther in the 5-min period and the curve drops off,

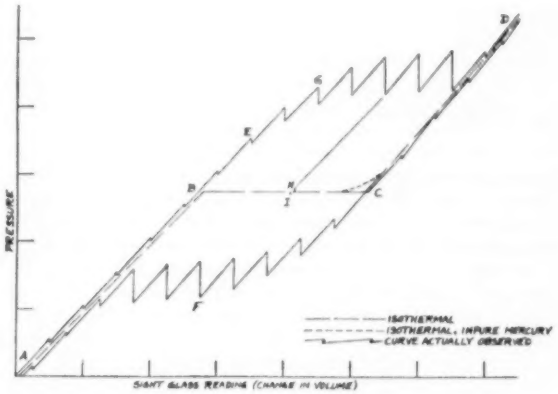

A-B—Liquid phase only
C-D—Solid phase only
B-C—Liquid and solid phases present at 0 C
A-B-E-G-D—Mercury compressed in steps; specimen heated by freezing
D-C-F-A—Mercury expanded in steps; specimen cooled by melting
H, I—Approaches to equilibrium with both phases present

FIG. 8 IDENTIFICATION OF FREEZING PRESSURE OF MERCURY BY VOLUME CHANGE

as at *E*. When the all-solid line *C-D* is reached, there is an abrupt transition to the quick equilibrium condition, and on further compression, the curve resembles *A-B*.

On expansion, a zig-zag line *D-C-F-A* would be described. If at the point *G*, the volume were held constant the pressure would settle out toward the equilibrium point. The time of several hours required for a close approach to equilibrium may exceed the experimenter's patience. A quicker way is to juggle pressures so as to start close to the expected asymptote, as at *H* or *I*. Then the equilibrium pressure can be approached from both sides,

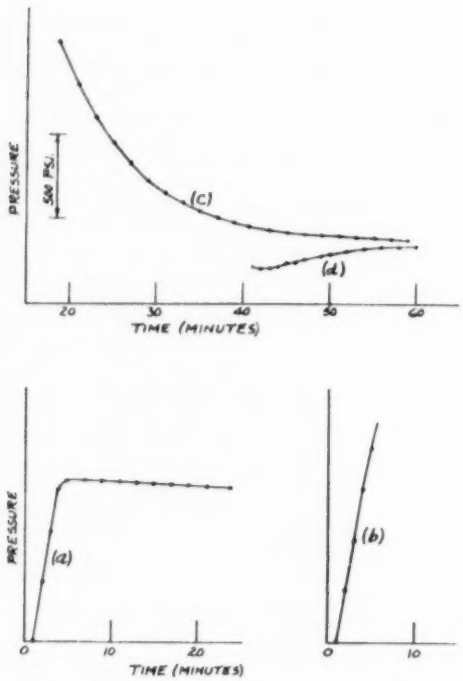

(*a*) Approach to equilibrium after expansion; one phase present
(*b*) Pressure change immediately after expansion; both phases present
(*c*) Approach to equilibrium after compression; both phases present
(*d*) Approach to equilibrium after expansion; both phases present

FIG. 9 DETERMINATION OF MERCURY FREEZING PRESSURE; PRESSURE-TIME RELATIONS

the decay being followed only long enough to predict the position of the asymptote. This should be repeated at several points along the line *B-C'*, including one point close to *C'*. If the mercury is impure, the corner at *C'* will not be sharp, as in the dotted line.

In addition to the plot of pressure (or what is more convenient, readings on the transfer gage) against volume, it is also desirable to plot pressure against time. In Fig. 9 are such curves. In (*a*) only liquid is present, and the decay is rapid. This is a leak check showing a loss of about 3 psi per min after disappearance of the initial transient following an expansion; (*b*) was taken near (F) with both phases present; (*c*) and (*d*) were taken at (H) and (I) and define the melting pressure as their common asymptote.

It is desirable that the system be absolutely tight. If the leak in, say, 30 min cannot be detected by the pressure-measuring means when only one phase is present, its effect may be neglected. If it is perceptible but small, its effect can be estimated and a correction applied.

From a curve such as (*a*), Fig. 9, with only one phase present, the leak in psi per minute may be estimated. The flow through the leak is supplied by the expansion of the fluids, mostly gasoline, and the contraction of the pressure vessel under this pressure change. The fall of pressure with both phases present, as (*c*) Fig. 9, can be divided into two parts, the pressure drop associated with the expansion of the fluid under the leak, and that associated with the change in volume due to the phase change. When the pressure is falling rapidly, as at the beginning of curve (*c*), the mercury is freezing, the sample is warmer than its surroundings and is giving up heat to the pressure vessel. When the pressure is falling very slowly, the fluids are expanding very slowly, and most of the leak is supplied by the expansion which results from melting of the sample. The sample then will be absorbing heat from the pressure vessel and will be a little cooler. At the point of (*c*) where the slope is the same as that of the leak curve, the sample is neither melting nor freezing and its temperature is the same as that of its surroundings. The difference between the pressure at this point and that at the asymptote is approximately the leak correction.

An alternative and equivalent estimate of the effect of leak is obtained by multiplying the rate of leak from curve (*a*) by the time constant of the decay of pressure in curve (*c*) or (*d*).

Calibration of Transfer Instrument. The arrangement of apparatus used in calibrating the gold-chromium pressure cell is shown in Fig. 10. A pressure was generated by intensifier (A), and admitted to the controlled-clearance piston gage (B). This pressure was indicated on the gold-chromium pressure cell (C) with the same bridge and null indicator used in the observations on the mercury point. The jacketing cylinder of the piston gage was subjected to pressures generated by intensifier (D) and measured by a manganin cell (E) which was part of a Wheatstone bridge of the strain-indicator type.

A dead-weight load was set up on the piston gage, the pressure raised until the piston was at the top of its travel. While the piston fell through its range ($^1/_8$-in.) observations were made on the pressure under the piston with the gold-chromium cell, on the jacketing pressure with the manganin cell, and on the time of fall. The jacketing pressure was adjusted until the rate of fall was about 30 sec. Readings were made at the top and the bottom of the travel. The dead-weight load on the piston was increased in 20-lb steps until the pressure used in the mercury-point measurements had been exceeded. The load corresponding to the mercury point was obtained by interpolation between calibration points on the basis of the resistance change in the gold-chromium cell.

Measurement of Piston and Dead Weights. The 20-lb weights

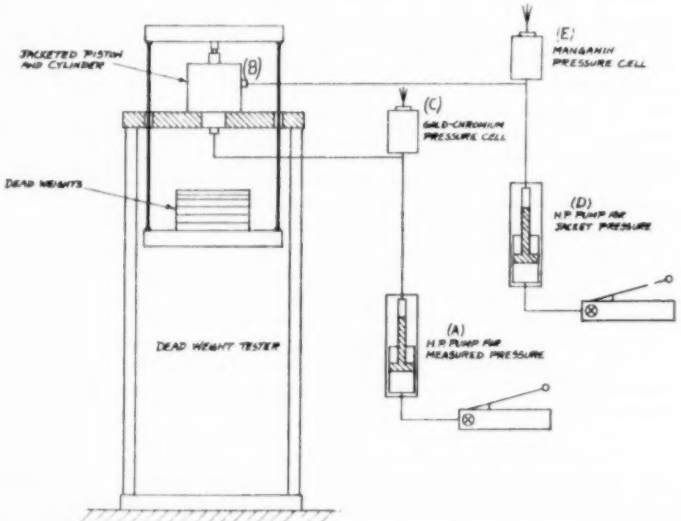

FIG. 10 CALIBRATION OF GOLD-CHROMIUM PRESSURE CELL

had been adjusted by the Massachusetts State Sealer of Weights and Measures to within 0.001 lb of their nominal mass. The yoke, weight hanger, piston, and so on, were weighed to an accuracy of about 0.001 lb.

The piston was measured by the Gage Section of the National Bureau of Standards with an accuracy of about ±0.00002 in.

Results. The results of the measurement and the estimates of the various errors are summarized in Table 2. The errors characteristic of piston gages, in general, have already been discussed at length.

TABLE 2 SUMMARY OF RESULTS

Weights: 268 73 lb
Area: 0 0024446 sq in.
Pressure uncorrected: 109,930 psi

	Correction, psi	Residual error, psi
Zero shifts, in mercury-point runs	...	∓ 65
Zero shifts, in piston-gage runs	...	±215
Correction for leakage	+ 20	± 10
Piston measurement, ±0.00002 in.	...	± 80
Piston taper, 0.00003 in.	...	±120
Residual clearance, 0.000010 to 0.000020 in.	— 30	± 10
Elastic distortion	+ 65	± 10
Temperature of piston	— 25	± 15
Weight measurement	...	± 10
Buoyant effect of air on weights	— 15	
Gravity at Foxboro	— 35	± 5
Temperature of ice bath, ±0.02 C	...	± 60
Conduction down tubing	—150	±150
Total correction	—170	
Corrected pressure	109760	±750

The mass load on the piston gage at the pressure for which the resistance change was the same as that observed in the mercury fixed-point runs was obtained by interpolation between observations in the piston-gage runs. The area was the average in the upper 1/4 in. of the piston, based on direct measurement. The uncorrected pressure is the mass load divided by the area.

There were differences in zero before and after the mercury-point and the piston-gage runs. The two zero readings were averaged, on the assumption of equal changes during increase and decrease.

The system was found to be losing pressure at a rate of about 2 psi per min when only liquid was present. This rate was multiplied by the 10-sec time constant of the approach to equilibrium conditions when both phases were present.

The residual clearance between piston and cylinder was estimated from the leakage rate, including the effect of the expansion of the fluid under the pressure change during the fall of the piston, and assuming that the drop in pressure occurred in 1/10 in. of length of the piston.

The elastic distortion of the steel piston was calculated from Equation [10].

The value of gravity was interpolated from Coast and Geodetic Survey data at points within 10 miles of Foxboro, Mass., where the experiment was conducted.

The temperature of an ice bath, using good commercial ice, usually can be expected to be 0.00 ± 0.02 C. Several measurements of samples during these tests fell within this range. The conduction of heat down the pipe to the mercury cell would raise the temperature of the latter by an amount estimated not to exceed 0.1 C.

A difference between pressures at the upper and lower limits of travel of the piston was observed. This was found to be caused by a taper in the piston which developed when the piston had been scored in previous tests. (This taper of 0.00012 in. in 1/2 in. of length was 10 to 100 times that which would be tolerated in a new piston.) The ratio of 0.7 between change of jacket pressure and change of measured pressure indicated that the line of contact between piston and cylinder was near the top. The area of the piston was computed on the diameter of 0.05579 ± 0.00002 in. measured 1/8 in. from the top. An additional uncertainty in area was taken as that corresponding to the taper in 1/8 in. of length.

Additional possible errors, not evaluated, include those resulting from possible changes in the resistance in the gold-chromium wire which were not reflected in the zero shift. This alloy is a new one for pressure measurement, and very little experience has been accumulated. In particular, little or nothing is known as to the proper pressure-seasoning treatment. (This particular element had been subjected to two applications of pressure to 140,000 psi.)

Difficulties Encountered. A number of mechanical difficulties resulted from the escape of mercury from its container in an early experiment. A small quantity got into other parts of the system, and amalgamated with brass packing rings, the heads of pistons, and the like. Numerous failures of these parts resulted. No autofrettaged cylinders failed. It was found that a polyethylene bag was tough and flexible enough to hold the mercury. Wherever possible, the inlets to pressure cells, intensifiers, and the like, should be at the bottom, and the inlet to the mercury bomb at the top, and the tubing arranged so that escaped mercury droplets will drain to the mercury bomb.

In the manganin and gold-chromium cells the packing used for the insulated electrical lead included a plastic which softened in contact with kerosene or gasoline, and was responsible for a progressively increasing electrical leakage. This was serious since one corner of the Wheatstone bridge is grounded, and a leakage through 100 megohms will produce a significant error. Other packing materials are being tried.

Conclusions

The measurements of the melting pressure of mercury were of value in trying out new equipment in the high-pressure field and in pointing out the direction of future improvements in technique and apparatus.

The controlled-clearance piston gage was used at pressures as high as 120,000 psi, with no indication that the limit of its range was being approached. (The pressures to which this instrument was used were limited by fittings rated at 100,000 psi.) Adequate floating times for the measurements were obtained. Indications were that clearances could be held to a few microinches, provided the surfaces of the piston and cylinder were that good. The small clearances make necessary precautions to eliminate abrasive particles in the working fluid. The use of carboloy pistons may be indicated from considerations of wear.

The gold-chromium pressure cell seemed promising. The time required to reach constant readings seemed somewhat shorter than for manganin. The very small temperature coefficient should be valuable. The elastic defects of hysteresis, drift, and after-effect, required further study since they were obscured by the electrical leakages in other parts of the bridge.

These measurements give a value 1 per cent higher than obtained by Bridgman for the melting pressure of mercury. This difference is not serious in view of the rather large experimental error of ±0.7 per cent due to identifiable sources.

The largest errors can be reduced substantially in future work. A better choice of the insulating material in the electrical leads should reduce the troubles with zero shift. An unworn piston would have variations in diameter less than a tenth as great as those in the one used. The temperature of the mercury sample can be measured directly.

Acknowledgments

This work was carried out with the support of the Foxboro Company, Harwood Engineering, Inc., and the National Bureau of Standards. The authors are indebted to numerous people in those organizations for assistance. They particularly wish to

thank Dr. Brombacher of the National Bureau of Standards, and Mr. Howe of the Foxboro Company for their encouragement; Mr. George Champagne for his technical assistance; Mr. Howard Fuller, who designed and operated the a-c null indicator used. The authors have profited from many suggestions made by Professor Bridgman.

BIBLIOGRAPHY

1 "Mémoires sur l'élasticité et la dilatabilité des fluides jusqu'aux très hautes pressions," by E. H. Amagat, *Annales de Chemie et de Physique*, vol. 29, 1893, pp. 68–136 and 505–574.

2 "Einfluss der Rotation auf die Empfindlichkeit einer absoluten Druckwage," by A. Michels, *Annalen der Physik*, vol. 72, 1923, pp. 285–320; vol. 73, 1924, p. 577.

3 "The Measurement of Hydrostatic Pressures Up to 20,000 Kilograms Per Square Centimeter," by P. W. Bridgman, Proceedings of the American Academy of Arts and Sciences, vol. 47, 1912, p. 321.

4 "Dead-Weight Machines of 111,000 and 10,100 Pound Capacities," by B. L. Wilson, D. R. Tate, and George Borkowski, NBS Circular C446, June, 1943.

5 "A Multiple Manometer and Piston Gages for Precision Measurements," by C. H. Meyers and R. H. Jessup, National Bureau of Standards, *Journal of Research*, vol. 6, 1931, p. 1061, RP324.

6 "Units of Weight and Measure, Definitions and Tables of Equivalents," National Bureau of Standards Miscellaneous Publication M121.

7 "Strength of Materials, Part II. Advanced Theory and Problems," by S. Timoshenko, The Macmillan Company, New York, N. Y., 1936.

8 Glazebrook-Dictionary of Applied Physics.

9 "Methods and Procedures Used in the M.I.T. Program of Investigation of the Pressures and Volumes of Water to 460 C," by F. G. Keyes, Proceedings of the American Academy of Arts and Sciences, vol. 68, 1933, p. 505.

10 "Equilibrium in Binary Systems Under Pressure I. An Experimental and Thermodynamic Investigation of the System, $NaCl-H_2O$, at 25°," by L. H. Adams, *Journal of the American Chemical Society*, vol. 53, October, 1931, p. 3769.

A High-Pressure Wire Gage Using Gold-Chrome Wire

By H. E. DARLING[1] and D. H. NEWHALL[2]

Precision experiments with manganin wire for the measurement of high pressures are made difficult by virtue of the temperature-resistance response of the manganin. The equilibrium time required for this material to steady out after rapid pressure changes makes manganin generally unsuited for uses in industrial-control applications. For this reason, a study was made of the pressure and temperature response characteristics of several new materials. An alloy of 2.1 per cent chromium in gold was found to have much less sensitivity to temperature, varying from +1 to —1 ppm per deg F over the range of 40 F to 200 F, while manganin varies from +5 to —40 ppm in this same interval. This alloy also has a strong pressure coefficient. Typical values are 0.67 to 0.72 × 10^{-7} ohm/ohm/psi for gold chrome as compared to 1.69 to 1.72 × 10^{-7} ohm/ohm/psi for the manganin tested. Although the pressure sensitivity is only 33 per cent that of manganin, the smaller temperature sensitivity of the gold chrome results in good discrimination between temperature and pressure changes. Gold chrome responds rapidly to pressure changes, quickly coming to equilibrium, and does not show the annoying drift so characteristic of manganin. It is generally pressure seasoned with a single application of pressure, as compared to several cycles usually required for manganin. Its long-term stability compares favorably with manganin.

Introduction

IN the laboratory investigation of high-pressure phenomena, the use of a coil of manganin wire whose resistance changes linearly with exposure to fluid pressure, has been adopted, universally as a pressure-sensing device, as a result of the pioneering work of Dr. Bridgman.[3]

Manganin is especially suitable for the measurements of pressure from 50,000 psi up to values that are limited only by the structure used. Its resistance changes in the order of 1.7 ohms per 100 ohms of wire per 100,000 psi, a value which makes accurate resistance measurements quite simple.

It is well known that manganin changes its resistance slightly with temperature, and this resistance change is small only over a fairly narrow temperature range. If the temperature of the fluid departs very much from room temperature, an appreciable change in coil resistance results, and this cannot be distinguished from a pressure change. When precision measurements are attempted on fluids whose pressure has undergone a rapid change, a fairly long period of time is usually required for the manganin coil to come to equilibrium. This is due in part, at least, to the temperature change produced in the liquid by the pressure change. Although the equilibrium time is a nuisance in laboratory measurements, it can be tolerated, but this is not the case where high-pressure sensing devices are required for control of continuous industrial processes.

A great deal of work has been done in Germany on the development of alloys of gold, silver, and copper, for the purpose of developing resistance wire that has better temperature-resistance properties than manganin.[4] Of these, alloys containing 2 to 4 per cent chromium in gold have shown the most promise. The remarkable temperature properties of these alloys have been investigated at length by the Bureau of Standards with the objective of using gold chrome as a primary standard of resistance.[5] Material similar to that supplied to the Bureau of Standards was obtained from Sigmund Cohn and tested at Foxboro. An excellent agreement between our samples and those reported by the Bureau has been a gratifying check on the accuracy of our measurement technique. Their probable sensitivity to pressure also was predicted by the Germans. Experiment has shown that gold chrome is suitable for measurement of high pressure to values of the same order as manganin.

Gold-chromium wire has properties which make it particularly suitable for a pressure-sensing element for industrial purposes. It responds rapidly to pressure changes, it has a high degree of discrimination between temperature and pressure effects, it has adequate pressure-resistance sensitivity, and material with a high degree of uniformity is available.

Temperature Versus Resistance Properties—Experimental Procedure

Manganin. Samples to be tested were either loosely wound on a ceramic bobbin of small size to facilitate handling, or were self-supporting coils as in the case of pressure-sensing units. The coils thus wound contained locked-in mechanical strains which of necessity had to be removed before the coils became stable. For manganin coils, this stabilizing process was accomplished by the use of the Bridgman cycle. This consisted of exposing the completed coils to temperatures of —100 F for a period of at least 2 hr, and then placing them in an oven at a temperature of +250 F for a period of at least 8 hr. This cycle was recommended by Dr. Bridgman to produce the greatest stability in manganin wire, and frequently it was found that several such cycles were necessary before complete stability was attained. Coils were wound non-inductively, since all measurements were made at 1000 cycles, in order to avoid contact-potential difficulties.

Measurements of the resistance of the coils were made by an automatic two-function recorder developed at Foxboro for this purpose. The recording chart was positioned according to the temperature of an oil bath in which the sample was placed, and the recording pen moved across the chart in response to resistance changes. The temperature sensitivity of this instrument had a

[1] The Foxboro Company, Foxboro, Mass.

[2] Harwood Engineering Company, Inc., Walpole, Mass.; formerly with The Foxboro Company. Jun. ASME.

[3] "The Physics of High Pressure," by P. W. Bridgman, The Macmillan Company, New York, N. Y., 1931.

Contributed by the Industrial Instruments and Regulators Division of The American Society of Mechanical Engineers and presented at The Seventh National Instrument Conference, Cleveland, Ohio, September 9–10, 1952.

Note: Statements and opinions advanced in papers are to be understood as individual expressions of their authors and not those of the Society. Manuscript received at ASME Headquarters, June 30, 1952. Paper No. 52—IIRD-1.

[4] "Werkstoffe für Widerstandsmanometer und Widerstandsthermometer," by Alfred Schulze, *Chemiker-Zeitung*, vol. 19, July, 1943, p. 228.

[5] "Gold Chromium Resistance Alloys," by J. L. Thomas, U. S. Bureau of Standards, *Journal of Research* (Research Paper No. 737), vol. 13, 1934, pp. 681–688.

reproducibility of ½ deg F, while the resistance measurement was accurately repeatable to 10 ppm change. Samples were placed in a well-stirred oil bath, and the temperature of the bath slowly raised through the temperature interval desired. When the temperature cycle was completed, a continuous record of resistance changes was obtained. From such records, the accompanying curves were plotted. Thus several spools of manganin were found which had exceptionally good temperature characteristics for the construction of pressure coils.

Gold Chromium. Samples were prepared by either winding the wire on ceramic bobbins or were formed into self-supporting coils, as in the case of the manganin samples. It was found that the gold-chrome wire was quite sensitive to mechanical handling or cold-working. These locked-in strains disappear with extensive baking at 300 F. Subjecting the wire to temperatures of —100 F was found to have little effect on its temperature properties, so the Bridgman cycle, as used in the preparation of manganin coils, was abandoned in favor of extensive baking at 300 F. Care must be taken not to expose the wire to temperatures greater than 350 F, as the material will be many times more sensitive to temperature change after such a treatment.

The gold-chrome wire amalgamates readily with solder, so care must be exercised when the soldering technique is used. Spot-welding is recommended.

Experimental Results. The temperature-resistance properties of a typical sample of gold chrome are shown in Fig. 1. This illustrates the effect upon the temperature properties by extensive baking at 300 F. A temperature coefficient of from —1 to +1 ppm per deg F can be obtained readily over a temperature range of 80 deg F. The sample shown contained 2.1 per cent chromium in gold and was in a dead-soft annealed condition. This appears to be the combination that has the least sensitivity to temperature.

A comparison of the temperature-resistance properties of gold-chrome, manganin, and Advance wire are shown in Fig. 2, all being plotted to the same scale. The advantages of the use of gold chrome over manganin are at once evident. Advance, which also has an excellent temperature property, unfortunately has a very small pressure coefficient.

The properties of alloys containing different percentages of chrome in gold are shown in Fig. 3, from which it is evident that almost any coefficient, positive, negative, or nearly zero, can be obtained by suitable choice of alloy composition and heat-treatment. Hard-drawn wires of all alloy proportions do not respond to baking procedures, but always have a large temperature coefficient. For this reason, half-hard or dead-soft wire is recommended for precision resistors and pressure coils. Half-hard wire will have a 2 to 4 per cent elongation, while soft wire will have 15 to 16 per cent elongation on a rupture test.

Pressure Measurements

Experimental Procedure. The material used in the construction of manganin coils was selected on the basis of uniformity of resistance, and minimum temperature-resistance properties. The manganin wire was of No. 38 gage, double-silk and double-silk plus nylon-braid insulation. Coils were wound noninductively, using a small piece of spaghetti as a starting form, and were interleaved for several layers. Then the coil was lashed securely with strong thread, forming a firm, self-supporting unit, which could be handled readily for mounting in pressure cells. Although the finished coil appears bulky, its cross section is mostly porous insulating material, allowing pressure fluids readily to penetrate the structure. Where a smaller physical size was required, the nylon braid was omitted, and the coils were wound as before with thin paper between layers to minimize the possibility of shorts. Coils were usually of 60 or 120-ohm resistance.

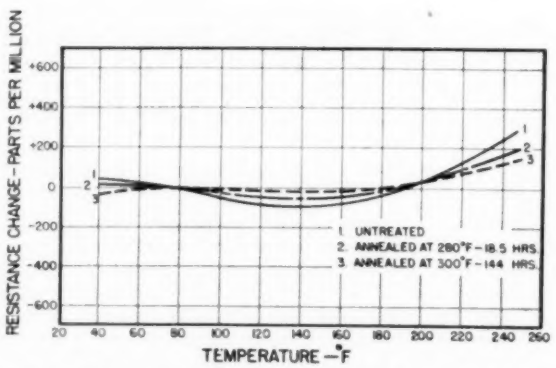

Fig. 1 Temperature Versus Resistance Change of 2.1 Per Cent Gold Chrome

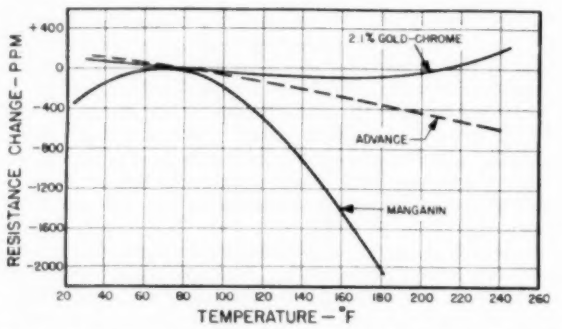

Fig. 2 Comparison of Temperature Versus Resistance Change for Gold Chrome, Advance, and Manganin

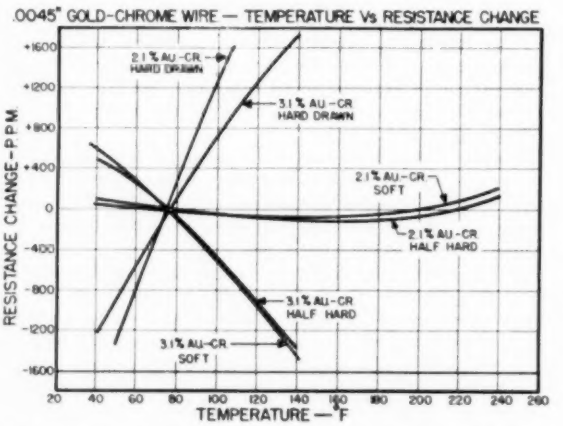

Fig. 3 Temperature Versus Resistance Change for 0.0045-In. Gold-Chrome Wire

Manganin coils were first stabilized by the use of the Bridgman cycle, and then exposed to several applications of pressure to a value greater than that for which they were to be used.

The gold-chrome wire was of No. 36 gage, and was specially covered with a quadruple layer of nylon. Coils also were wound noninductively, starting with a spaghetti core, and using a double layer of onionskin paper between layers to minimize the possibility of shorts and to make a firmer coil. Lacing of the coil with thread, as before, makes a firm structure.

The gold-chrome coils are stabilized by baking at 300 F for at least 36 hr. Pressure-seasoning was accomplished by a single application of pressure.

Finished manganin and gold-chrome coils are shown in Fig. 4.

Pressure Equipment. Initial pressure measurements were made with the co-operation of the high-pressure laboratory of the Watertown Arsenal, where pressures up to 150,000 psi were available. Measurements were referred to the manganin-coil standards as calibrated in Dr. Bridgman's laboratory.

Later measurements were made in the Foxboro high-pressure laboratory with equipment designed and built by D. H. Newhall. A typical pressure-cell assembly is shown in Fig. 5.

Our present high-pressure laboratory was designed and built by the Harwood Engineering Company. A view of the laboratory

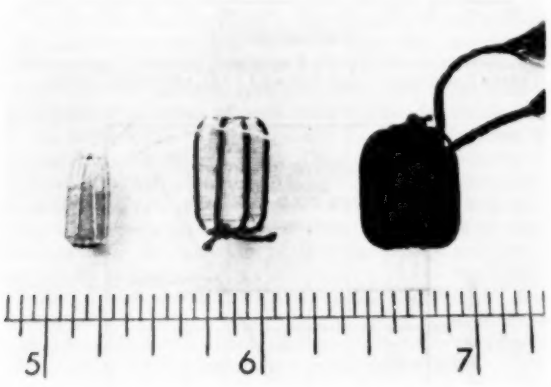

FIG. 4 FINISHED MANGANIN AND GOLD-CHROME COILS

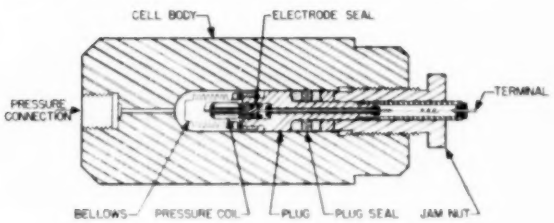

FIG. 5 ASSEMBLY OF 150,000-PSI PRESSURE CELL

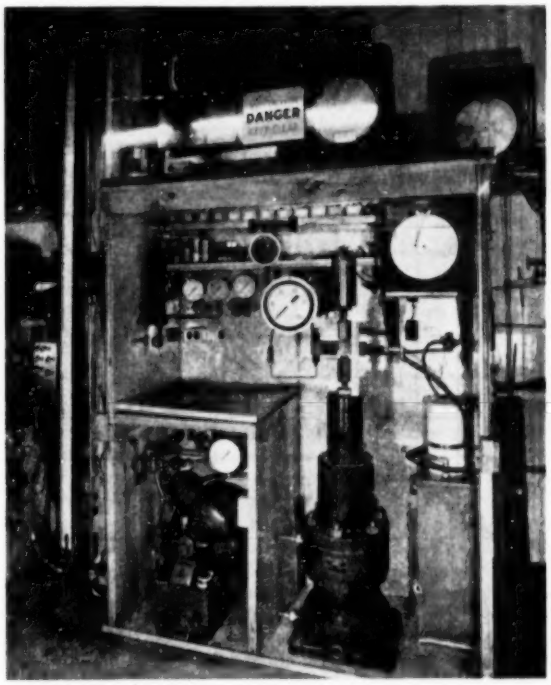

FIG. 6 VIEW IN HIGH-PRESSURE LABORATORY

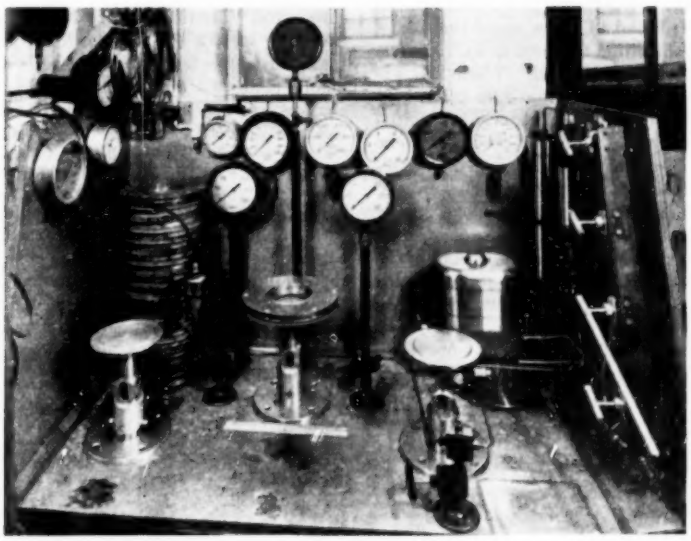

FIG. 7 DEAD-WEIGHT ASSEMBLY FOR MEASURING PRESSURES UP TO 30,000 PSI

is shown in Fig. 6. The low-pressure pump, intensifier, controls, and pressure cell are plainly visible in this view.

In addition to the high-pressure equipment, a dead-weight assembly was constructed for measurement of pressures up to 30,000 psi, Fig. 7. Pressure coils were calibrated with reference to this dead-weight assembly, and periodic checks were made with the Watertown standard and Dr. Bridgman's laboratory.

All measurements were made with specially adapted Foxboro instruments or with specially designed alternating-current bridges. Accuracies of measurement were in most cases better than 0.1 per cent.

Experimental Results. All measurements on gold chrome were compared to manganin standards. Fig. 8 shows the pressure-resistance characteristics of two typical gold-chrome samples. The two samples had received a different degree of annealing after the drawing process, and had been baked after being formed into a coil as described previously.

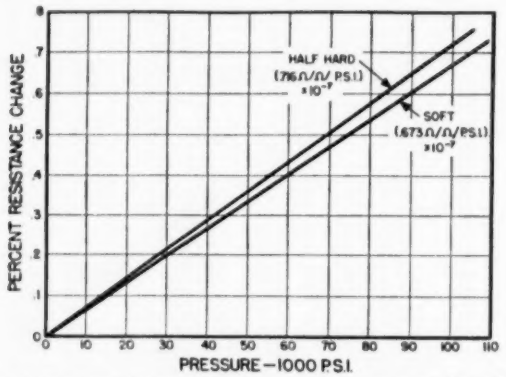

FIG. 8 PRESSURE VERSUS RESISTANCE CHANGE FOR 2.1 PER CENT GOLD CHROME

The pressure coefficients of 0.716 and 0.673 $\times 10^{-7}$ ohm/ohm/psi are typical of several samples tested. A remarkable degree of linearity of resistance change versus pressure was noted and, even more important, the complete absence of drift, so annoying with manganin. Linearity was good to less than 0.25 per cent.

The gold-chrome alloy was found to follow rapid changes of pressure, coming to equilibrium within a second or so. No hysteresis during pressure-cycling was observed. When first exposed to pressure, the gold-chrome coils showed an initial zero shift, but in all cases this was well under 1 per cent of the initial value. Furthermore, all measurable zero shift occurred in the first pressure cycle, as compared with manganin, which often required several cycles before repeatable results would be obtained.

Fig. 9 shows the temperature-resistance properties of a 2.1 per cent gold-chrome coil which had been pressurized to greater than 100,000 psi several times. It is interesting to note that one of the effects of exposure to pressure-cycling is to perform the same type of stabilization to temperature as accomplished by extended baking of the new coil.

For purposes of comparison, Fig. 10 shows the pressure sensitivity of a Foxboro manganin coil as compared to a typical gold-chrome coil. The manganin coils had pressure coefficients ranging from 1.69 to 1.72 $\times 10^{-7}$ ohm/ohm/psi. Therefore it appears that gold chrome has about 33 per cent of the sensitivity of good-quality manganin, but its ability to discriminate between pressure changes and temperature changes more than overweighed this loss in sensitivity.

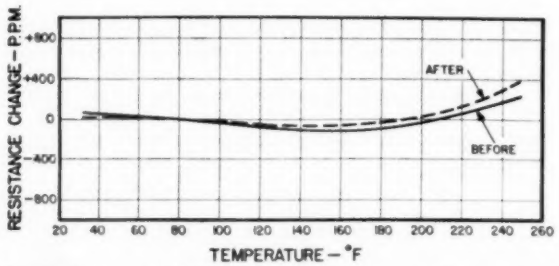

FIG. 9 EFFECT OF 100,000-PSI PRESSURE CYCLE ON TEMPERATURE VERSUS RESISTANCE CHANGE FOR 2.1 PER CENT GOLD CHROME

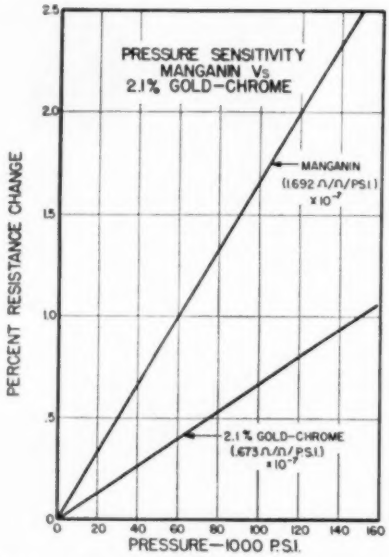

FIG. 10 PRESSURE SENSITIVITY OF MANGANIN VERSUS 2.1 PER CENT GOLD CHROME

CONCLUSION

Recent observations on gold chrome have confirmed these earlier findings on the linearity and stability of the pressure characteristics. Since 2.1 per cent gold chrome so nearly fulfills all of the requirements of a pressure-sensing device for industrial-control applications, it is recommended that this material be considered seriously as a standard for pressure measurements, replacing the existing manganin standard for application to industrial-control problems.

An Application of High Pressure in Geophysics: Experimental Rock Deformation

By JOHN HANDIN,[1] HOUSTON, TEXAS

For proved laboratory methods through which to study phenomena within the earth's crust the geophysicist often turns to the engineer and physicist who have largely developed the high-pressure art. The paper reports on the geophysical problem of rock deformation in which there is an application of high pressure and with which the reader may not be familiar. Of the four important environmental factors involved in natural rock deformation, namely, pressure, temperature, time, and the presence of solutions, only pressure and time have received much attention in the laboratory. Descriptions of current research by Griggs and his collaborators at the Institute of Geophysics, University of California, and by the Shell Research Laboratory show what is being done to determine the combined effects of these factors in an effort to simulate geological conditions more realistically.

Introduction

THE investigator of phenomena occurring deep within the earth's crust finds himself at once in the realm of high pressure. For proved laboratory methods the geophysicist often turns to the engineer and physicist who have largely developed the high-pressure art, and who indeed did much of the early work on rock deformation. Von Kármán, 1911, made the first triaxial tests on rocks in which the high confining pressure was truly hydrostatic, by compressing small jacketed marble and sandstone cylinders surrounded by a liquid under pressure. Böker, 1915, observed the deformation when the axial stress was made less than the hydrostatic stress. Ros and Eichinger, 1928, tested a number of nonmetallic materials, including marble. More recently at the Denver laboratories of the Bureau of Reclamation, 1946, triaxial tests have been made on rock samples to determine their engineering properties. We are all indebted to Professor Bridgman for the basic techniques used in handling high pressure, but we also are grateful for his contributions to earth physics in his studies of viscosity, compressibility, polymorphic transitions, and plasticity among others (Bridgman, 1949, 1951).

However, it is perhaps appropriate to report on some of the work of geophysicists in which there is an application of high pressure and with which the reader may not be familiar because for the most part what has been published at all appears in geological journals. Engineers may be most interested in the techniques employed, but may well find the results of interest too. Some of the experiments to be described have been performed under conditions not duplicated for any materials other than rocks, so that the results enhance our understanding of the inelastic behavior under multiaxial stress of solids in general.

[1] Exploration and Production Research Laboratory, Shell Oil Company.

Contributed by the Industrial Instruments and Regulators Division of THE AMERICAN SOCIETY OF MECHANICAL ENGINEERS and presented at The Seventh National Instrument Conference, Cleveland, Ohio, September 9–10, 1952.

NOTE: Statements and opinions advanced in papers are to be understood as individual expressions of their authors and not those of the Society. Manuscript received at ASME Headquarters, December 31, 1952.

Definitions

The early studies of the effects of combined stresses, including Bridgman's "pinching-off effect," as well as the discovery by metallurgists of creep phenomena at high temperature, have indicated that the ordinary terms used in describing the mechanical properties of materials such as "elastic limit" and "ultimate strength," can be very ambiguous if the stress is not uniaxial, if the temperature is elevated, or if long times are involved. The following terms will be used in the discussion:

1 "Creep" is the slow deformation of rocks under relatively small constant loads applied for long periods of time.

2 "Flow" signifies any deformation which is not instantly recoverable, except fracture. (The term "plastic" is avoided because it often implies slip in the case of metals or idealized behavior in the case of mathematical theory.)

(*a*) "Transient flow" is creep at a decelerating rate which is largely recoverable upon release of load.

(*b*) "Pseudoviscous" flow is flow at a constant rate, not a linear function, however, of applied shear stress.

3 "Fracture" is deformation with loss of cohesion.

4 "Strength" is a meaningless term unless all environmental conditions are specified. For short-time tests "yield strength" or "ultimate strength" or the stress at a given strain are used when pressure, temperature, and chemical environment are stated. It is better to avoid the term altogether for tests of long duration, since there is no obvious connection between rigidity and creep. (There is some evidence that rocks deeply buried in the crust have little or no resistance to shear stresses of long duration.)

5 "Triaxial tests" are made on cylindrical specimens surrounded by a liquid under pressure. Thus the specimen is initially under hydrostatic pressure, and the three principal stresses are equal.

(*a*) Compression tests are made by applying a compressive stress parallel to the cylinder axis so that the specimen is under hydrostatic pressure with a superposed axial compression. Two of the principal stresses are equal, the third greater, Fig. 1.

(*b*) Extension tests are made by reducing the axial stress, the hydrostatic pressure remaining constant. Two of the principal stresses are equal, the third is smaller, but greater than zero, compressions taken positive, Fig. 1. Ductile specimens are found to elongate, neck, and finally fracture as in an ordinary tensile test, even though all the principal stresses are compressions. Such tests are more meaningful than true tensile tests in geophysics, since true tensions probably cannot exist below moderate depths in the crust.[2] Moreover, unconsolidated rocks which cannot transmit a tensile force do flow and fracture in extension, resulting in faults in the crust.[3]

Previous Work

From an early date in the history of their science, geologists had observed that rocks appeared to flow in the crust, although in

[2] "The Dynamics of Faulting," by E. M. Anderson, Oliver and Boyd, London, England, 1951, p. 158.

[3] "Mechanical Basis for Certain Familiar Geologic Structures," by M. K. Hubbert, Bulletin of the Geological Society of America, vol. 62, 1951, p. 367.

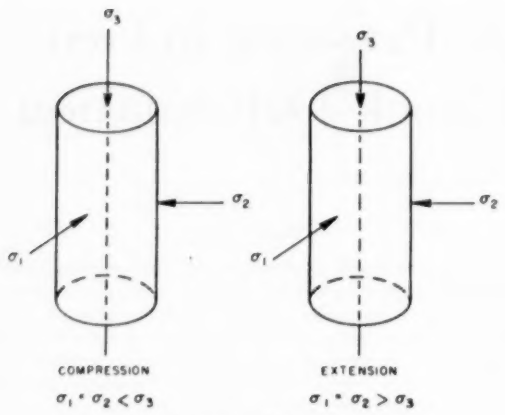

FIG. 1 STRESSES IN TRIAXIAL TESTING

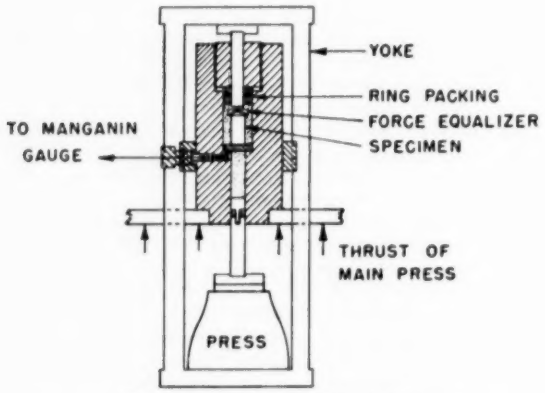

FIG. 2 GRIGGS' EARLY APPARATUS
(After Griggs, 1936, Fig. 2; see list of references at end of paper.)

ordinary laboratory tests the same rocks were found to be quite brittle. This striking difference was ascribed to the effect of one or more of four significant environmental factors—pressure, temperature, time, and the presence of solutions. Adams, 1901, first demonstrated the ductility of rock experimentally by compressing a small cylinder of marble under a confining pressure provided by the walls of a steel vessel. The nature of the experiments was such that only qualitative results were obtainable, but the findings were later verified quantitatively by von Kármán, 1911, and Böker, 1915, who obtained accurate stress-strain relations indicating that marble under high confining pressure was behaving much like a ductile metal with a well-defined yield point, work-hardening, and elastic afterworking. With increased pressure the inclination of fracture surfaces departed more from 45 deg to the direction of applied load.

In 1936 Griggs published the first of a series of most important contributions to the problem of rock deformation. Indeed, we are indebted to him for most of the knowledge of the inelastic behavior of rocks in the laboratory. Griggs's early apparatus designed for use to 13,000 atm is shown diagrammatically in Fig. 2. Yoked pistons of the same diameter entered the pressure vessel from either end. The lower piston with a conventional Bridgman packing compressed the fluid in the lower chamber under the action of a small hydraulic press. The upper piston with a new ring packing of the unsupported-area type applied differential pressure to the specimen through a force equalizer as the yoke was moved upward by a commercial hydraulic press. Since both pistons moved together a like amount, the confining pressure remained constant. Hydrostatic pressure was measured by a manganin gage, piston displacement by a dial gage, and differential force by a gage on the main press. Tests were made on unjacketed $^1/_2$-in. cylinders at room temperature.

Among the significant results of this work on marble and limestone are the following:

1 The elastic limit was raised only about 10 per cent for a 10,000-fold increase in confining pressure, but the ultimate compressive strength of marble increased 1400 per cent, Fig. 3.

2 Ultimate strength decreased with time, appearing to become asymptotic to a certain value at infinite time, Fig. 4.

3 At high confining pressure limestone was observed to creep, and the longer the test, the less the ductility, Fig. 5.

4 Rocks appeared to have a fundamental strength defined as "the differential pressure a body can support under given conditions without fracturing or deforming continuously."

Previous work coupled with geological observations had indicated that confining pressure alone is not sufficient to explain natural rock deformation. For example, using the 50,000-atm apparatus of Bridgman, 1935, Griggs, 1938, found that quartz

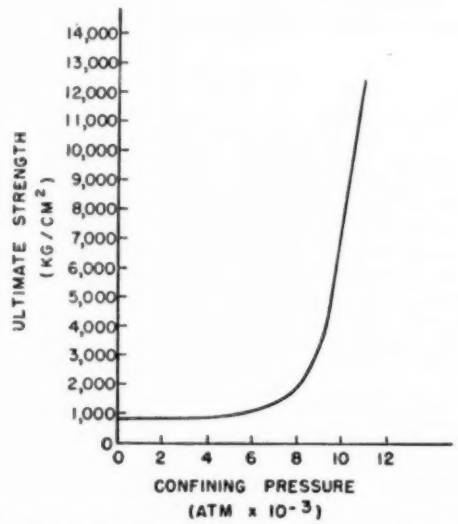

FIG. 3 ULTIMATE STRENGTH OF MARBLE AS A FUNCTION OF CONFINING PRESSURE
(After Griggs, 1936, Fig. 6.)

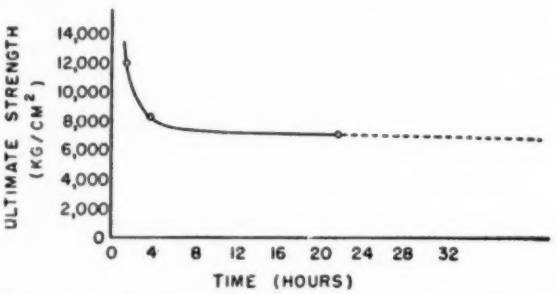

FIG. 4 ULTIMATE STRENGTH OF LIMESTONE AS A FUNCTION OF DURATION OF TEST AT 10,000-ATM CONFINING PRESSURE
(After Griggs, 1936, Fig. 8.)

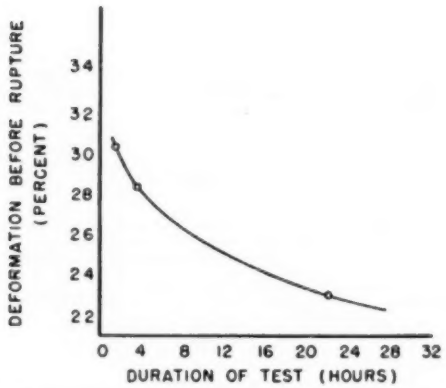

FIG. 5 DUCTILITY OF LIMESTONE AS A FUNCTION OF DURATION OF TEST AT 10,000-ATM CONFINING PRESSURE
(After Griggs, 1936, Fig. 11.)

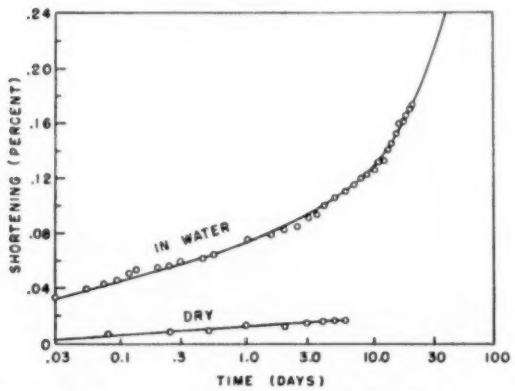

FIG. 6 CREEP OF GYPSUM LOADED TO 100 KG PER SQ CM AT ROOM TEMPERATURE, ATMOSPHERIC PRESSURE
(After Griggs, 1939, Fig. 12.)

would not flow even under a compression of nearly 150,000 kg per sq cm. Griggs (1938, 1939, 1940), therefore, took up the study of the effects of time, temperature, and chemical environment. Since most of the work was done at atmospheric pressure or at moderate confining pressure, time will not be taken to describe the apparatus, but some findings of fundamental interest should be mentioned. These are as follows:

1 Creep was observed in rocks loaded well below their ordinary crushing strength at room temperature, and the creep could be described by an equation identical to that used by engineers for metals, including terms for transient and pseudoviscous flow.

2 No pseudoviscous flow could be detected in limestone loaded to one half its crushing strength, although at high confining pressure such flow had occurred (Griggs, 1936).

3 Dry gypsum exhibited only transient flow, but in the presence of solutions pseudoviscous flow predominated, Fig. 6.

4 The effect of moderate confining pressure was to increase the creep rate and decrease the amount of deformation before fracture occurred.

5 The stress required to fracture gypsum depended on the duration of the test, fracture occurring at about the same strain irrespective of the magnitude of the stress.

Griggs, 1941, had begun work on experimental dynamothermal metamorphism combining all of the environmental factors: confining pressures up to 2000 atm, temperatures up to 500 C, variable chemical environment, superposed compressive and shearing stresses, and time up to several hundred hours. Unfortunately, this work was interrupted by the war.

STUDIES AT UNIVERSITY OF CALIFORNIA

At a time shortly after the war when it became possible to resume rock-deformation studies, a good deal, then, was known about the macroscopic behavior of rocks in the laboratory. We did not know much about the actual deformation mechanisms involved, nor had we gone far enough toward realization of an adequate simulation of natural environmental conditions. The natural environment is, of course, exceedingly complex, so that the only realistic approach to the problem was to gain an adequate understanding of the processes for a simple situation which could serve as a foundation for future work with the addition of new variables. These considerations led to the initiation at the Institute of Geophysics of the University of California of a project comprising three phases, namely, experimental (Griggs and Miller, 1951), analytical (Handin and Griggs, 1951), and observational (Turner and Ch'ih, 1951). The rock selected for study was Yule marble because of its homogeneity, suitable grain size, purity, and preferred orientation, and because previous work of Turner, 1949, Knopf, 1949, Balsley, 1941, and Griggs already had made available much information about it. For simplicity the dry rock was deformed at room temperature under a constant confining pressure of 10,000 atm, so that the only variable was the orientation of a specimen with respect to the applied stress.

Cylindrical specimens 1 in. long and $^1/_2$ in. diam were cored from an oriented block of marble, were jacketed in thin-walled annealed-copper tubes, and were subjected to hydrostatic pressure in the apparatus designed by Griggs, shown diagrammatically in Fig. 7. Pressure was generated by compressing the confining fluid with a hydraulic jack bearing against the lower piston, and measured with a manganin-wire resistance gage in a self-balancing bridge circuit using a servoamplifier and Helipot. Differential load was applied by moving the upper piston attached to the specimen in or out of the cylinder. The two pistons were coupled so that the confining pressure remained essentially constant during a test. The force on the upper piston was determined by measuring the elastic distortion of a steel ring with a Statham strain gage whose output was recorded by a Brown potentiometer calibrated in pounds. This force is that exerted by the confining liquid plus or minus the differential force on the piston, and must be corrected for friction. A special packing retained by a small press was employed to reduce friction on the upper piston. The true differential stress on the specimen was computed on the assumptions that the deformation is homogeneous and that there is no volume change during permanent straining; hence cross sections can be calculated from the original dimensions and the length changes. The motion of the piston was measured by a dial gage coupled to a one-turn Helipot, the voltage output of which was recorded on a Brown potentiometer calibrated in 0.001 in. Corrections were made for the elastic distortion of the apparatus in computing the strain of the specimen. The strain rate, nearly constant, was about 1.5 per cent per min.

Previous work on the marble along with concurrent work on calcite single crystals suggested that the important mechanism of deformation under the stated conditions was a combination of twin and translation-gliding. Moreover, the two sorts of gliding occurred on the same crystallographic plane in the same direction, but in opposite senses. In single crystals, compression parallel to the *c*-axis produced translation; extension produced twinning. Fig. 8 shows that the stress required for translation is several times that for twinning. Since in nature the Yule marble already has a strong preferred orientation in which the *c*-axes of the calcite grains tend to lie perpendicular to the foliation plane.

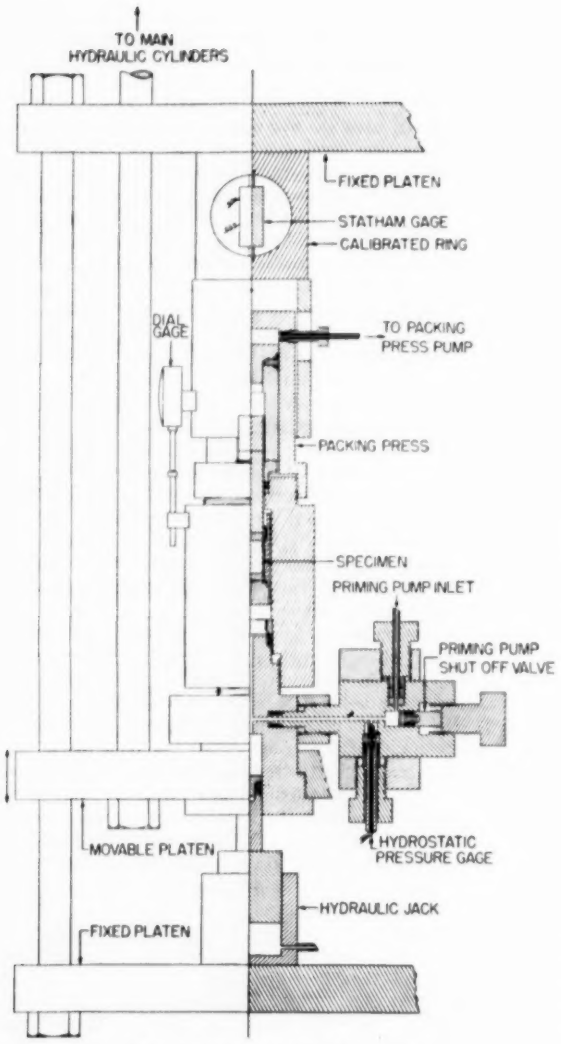

FIG. 7 GRIGGS' LATER APPARATUS
(After Griggs and Miller, 1951, Fig. 1.)

we anticipated that the stress-strain curves would indicate a strength anisotropy. That this was indeed the case is shown in Fig. 9 in which Q denotes a direction perpendicular and R a direction parallel to the foliation of the rock.

In an effort to explain the quantitative differences in these curves, we computed the resolved shear-stress coefficients in a representative sample of grains of known orientation in the undeformed rock. From a consideration of the average coefficients in the several orientations, the differences in strength at a given strain can be determined rather closely if one assumes that the deformation of the aggregate is "homogeneous" in accordance with Taylor's hypothesis[4] that "each grain suffers exactly the same strain as the surrounding material in bulk," but not if one assumes that it is "heterogeneous;" that is, each grain deforms preferentially in response to the applied stress with no restriction by surrounding grains.

[4] "Plastic Strain in Metals," by G. I. Taylor, *Journal of the Institute of Metals*, vol. 62, 1938, p. 319.

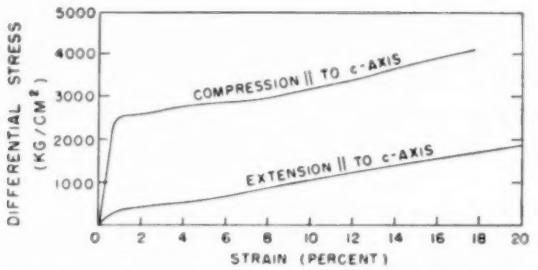

FIG. 8 STRESS-STRAIN CURVES OF CALCITE SINGLE CRYSTALS IN COMPRESSION AND EXTENSION PARALLEL TO c-AXIS AT 10,000-ATM CONFINING PRESSURE; ROOM TEMPERATURE
(After Griggs and Miller, 1951, Fig. 4.)

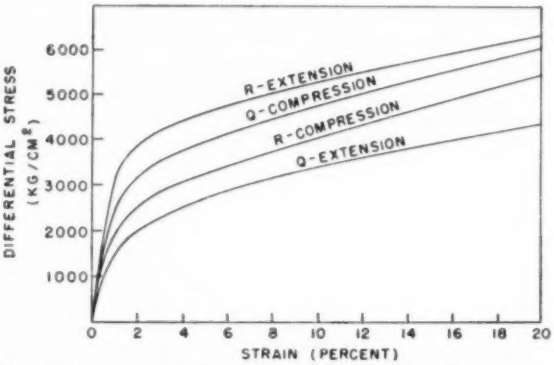

FIG. 9 STRESS-STRAIN CURVES OF YULE MARBLE IN COMPRESSION AND EXTENSION AT 10,000-ATM CONFINING PRESSURE; ROOM TEMPERATURE
(After Griggs and Miller, 1951, Fig 3.)

Another approach to a solution of the problem was to predict the fabric changes to be expected and to compare them with the actual observed changes accompanying deformation. We derived the predicted fabrics by determining the reaction of each of the representative grains to the postulated deformation using methods developed in the study of metals.[5] We first supposed that the deformation was heterogeneous. Then assuming the maximum resolved shear-stress law to hold, we constructed fabrics for the cases of twinning alone and translation alone for several values of strain and for various orientations. Compared with observed fabrics for the same deformation, the predictions indicated that translation alone could not account for the actual change and that twinning alone produced too large a change for small deformations. The procedure was then repeated for the case of homogeneous deformation, which involves both twin and translation-gliding. Fig. 10 shows examples of fabric diagrams (pole figures of metallurgists) of about 100 calcite c-axes for undeformed and deformed Yule marble and the corresponding predicted fabric. The agreement is rather good.

With a fair understanding of the processes involved in the flow of dry marble at room temperature, one could investigate profitably the effect of new variables (Griggs, et al, 1951). Fig. 11 shows the influence of temperature on the stress-strain curve of calcite single crystals, other conditions remaining the same. At only 150 C there is a drastic reduction in the shear stress for translation (compression parallel to c-axis), but the stress for twinning (compression perpendicular to c-axis) is about the same as that at

[5] "Kristallplastizität," by E. Schmid and W. Boas, Berlin, Germany 1935, pp. 61–67.

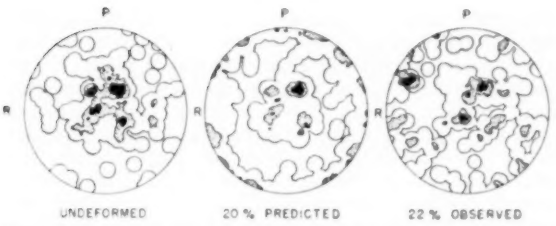

FIG. 10 FABRIC DIAGRAMS OF YULE MARBLE. ABOUT 100 *c*-AXES; CONTOUR INTERVAL 1, 3, 5 PER CENT. DEFORMATION IN EXTENSION PERPENDICULAR TO FOLIATION
(After Handin and Griggs, 1951, plate 2; Turner and Ch'ih, 1951, Fig. 4*b*.)

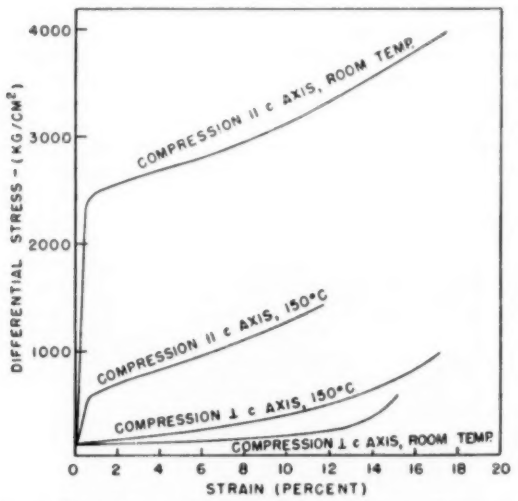

FIG. 11 STRESS-STRAIN CURVES OF CALCITE SINGLE CRYSTALS IN COMPRESSION AT 10,000-ATM CONFINING PRESSURE
(After Griggs, et al., 1951, Fig. 2.)

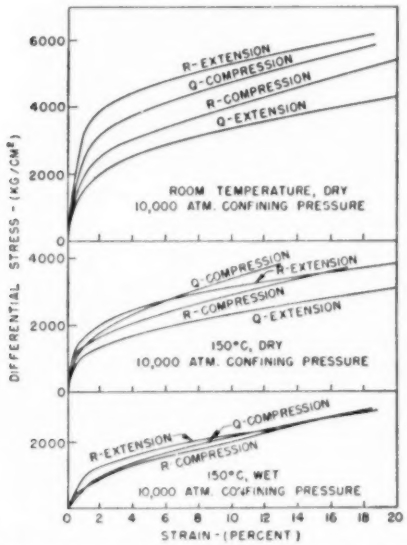

FIG 12 STRESS-STRAIN CURVES OF YULE MARBLE IN COMPRESSION AND EXTENSION AT 10,000-ATM CONFINING PRESSURE
(After Griggs et al., 1951, Fig. 1.)

room temperature. At 150 C the strength of the marble is reduced about 40 per cent (Fig. 12, compare upper and middle sets of curves). The relative strengths in the four orientations are different, consistent with the fact that individual crystals can translate more easily. The addition of small amounts of interstitial water lowered the strength about another 40 per cent (Fig. 12, compare upper and lower sets of curves). Computed relative strengths for the several orientations, based on the same assumptions used previously, as well as observed fabric changes, indicate that the deformation mechanism is essentially the same. There was no evidence of recrystallization even in one experiment of 7 hr duration on wet marble at 150 C.

Experiments are now under way in which the environment more closely approximates the natural one. Temperatures will be raised to 400 C, and a more complex chemistry introduced. An improved apparatus will be used.

STUDIES AT SHELL LABORATORY

High-pressure research is of course expensive, but more than that it is very time-consuming. In spite of the fine work accomplished so far in the few high-pressure laboratories of the world, the surface has barely been scratched, and this is especially true of rock-deformation studies. The number of fundamental geophysical and geochemical problems to be attacked is almost limitless. For this reason the author's company deemed it desirable to undertake work in this field. Now completed is an apparatus to be used for tests of relatively short duration with confining pressure to 10,000 atm and temperature to 400 C. Creep-testing equipment providing for runs of several hundred hours at confining pressures to 3500 atm and temperatures to 500 C is being constructed.

Apparatus. In describing the present apparatus, it will be convenient to divide the equipment into three categories; the pressure vessel and specimen assembly, the press with load and strain-measuring instruments, and the pressure-generating and measuring devices. Fig. 13 shows an over-all view of the recording and control panels.

The high-pressure cylinder, Fig. 14, with a 5 to 1 wall ratio is constructed of Carpenter 883 steel drawn to 40 Rockwell C. Of conventional design, it was built to our specifications by Harwood Engineering Company except for the piston packing, the scheme for which had been used for the first time at very high pressure by Harwood in a free-piston gage (Johnson and Newhall, 1953). A lapped piston of Carpenter Speed Star steel drawn to 65 Rockwell C passes into the vessel through a thin-walled steel sleeve which is subjected to external pressure suitably packed off and isolated from the confining pressure. The radial elastic deformation of the

FIG. 13 RECORDING AND CONTROL PANELS

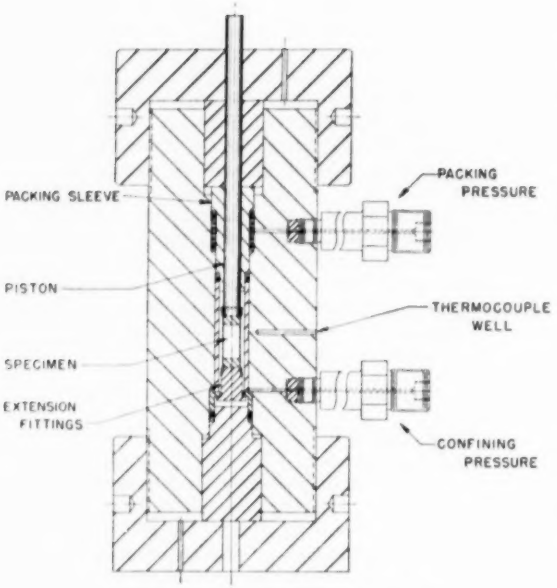

FIG. 14 TRIAXIAL TESTING CYLINDER

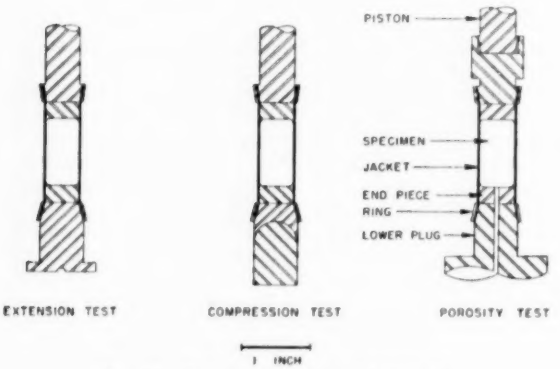

FIG. 15 DETAILS OF SPECIMEN ASSEMBLY

sleeve controls the clearance around the piston. This clearance is maintained at a very small value, but a slow leak is deliberately permitted to provide lubrication. With this arrangement we find the friction of the moving piston to be only about 1 per cent of the load.

Cylindrical rock specimens are held between the piston and special extension or compression fittings, whose function is to impart differential force to the specimen. In an extension test (set-up shown in Fig. 14) the bomb and piston are fixed initially and the extension fitting rests against the lower closure plug while confining pressure is built up. The bomb is then allowed to move down. Until the flange on the fitting comes up against the shoulder of the packing retractor ring, the only resistance to motion is piston friction which can then be measured during this free travel as the difference between the force exerted by the constant confining pressure and the indicated force on the piston. Thereafter there is a differential force on the specimen; it elongates with further downward movement of the bomb. In compression tests the bomb is moved upward against a ball-and-socket compression fitting, Fig. 15, shortening the specimen. The bomb can be heated externally by a resistance-wire furnace regulated by a thermocouple in the wall of the vessel and a Foxboro potentiometer controller. For high-temperature testing, a low-viscosity silicone rather than kerosene is used as the confining fluid.

Details of specimen assembly, worked out mostly at the University of California, are shown in Fig. 15. To prevent entry of the confining fluid into the specimen, the sample is enclosed in a thin annealed-copper tube of negligible strength which slips over the tapered ends of the piston and special fittings. Mild-steel rings are forced into the tapers over the copper jacket, forming a leak-proof seal. The specimen is separated from the hardened-steel piston and fittings by carefully fitted shaped copper or mild-steel end pieces, whose function is to reduce the tendency of the jacket to break because of discontinuity of deformation between the steel and the weaker rock and to insure uniform deformation near the ends of the specimen. The arrangement on the right of Fig. 15 is used to permit liquids to enter the specimen when the fluid pressure in porous rocks is to be controlled independently of confining pressure.

The 40-ton hydraulic press, Figs. 16, 17, consists of a 10-in. ram and a simple superstructure designed to support the test bomb. The press is locked while confining pressure is being built up by placing blocks under the movable platen.

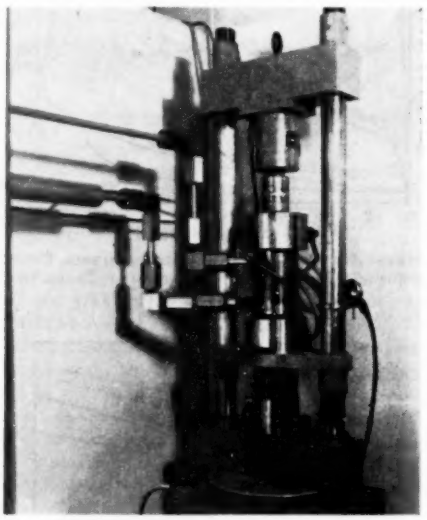

FIG. 16 PRESS WITH TEST CYLINDER IN PLACE

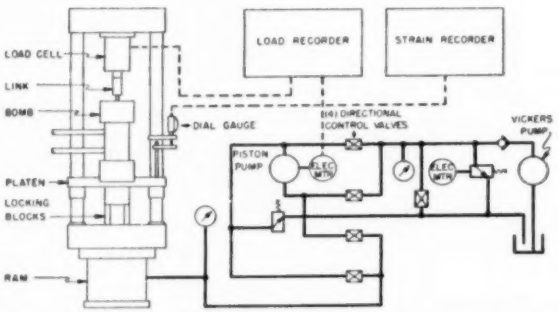

FIG. 17 SCHEMATIC DIAGRAM OF PRESS AND ASSOCIATED MEASURING EQUIPMENT

Force on the bomb piston is measured by a Baldwin SR-4 load cell bolted to the upper press platen and separated from the hot piston by a water-cooled link. Output of the cell is recorded on a Brown potentiometer calibrated in pounds. Force measurements have an accuracy of $^1/_4$ per cent and a sensitivity of $^1/_{10}$ per cent. The recorded differential force is corrected for friction and converted to true stress on the specimen. Displacement of the piston relative to the bomb is measured in a manner similar to that of Griggs. The accuracy is $^1/_4$ per cent, the sensitivity, $^1/_{10}$ per cent or 0.001 in. for 1-in. full scale on the recorder. In computing the strain of the specimen, a correction is made for elastic distortion of the apparatus.

Ram pressure is furnished by a Vickers pump and controlled by a motorized relief valve. To obtain very low constant strain rates with the single-acting ram, a low-capacity variable-stroke Milton-Roy piston pump is placed in series with the Vickers pump. Directional-control valves can be set for the following:

Fast Motion. With the highest pressure on the suction side of the piston pump, flow is by-passed, and the Vickers pump operates the press.

Slow Compression Tests. The Vickers pump provides a constant supply pressure for the piston pump which in turn imparts a slow motion at constant rate to the press.

Slow Extension Tests. The piston pump works against a relief valve to pump the press down.

Auxiliary switches in the load recorder can be made to actuate the pump for testing at any desired constant load. Strain rates can be changed by varying the speed of the direct-current motor driving the piston pump.

The pressure-generating equipment, Fig. 18, includes two systems—one to provide confining pressure, the other packing pressure. Confining pressure is generated in a large Harwood intensifier driven by a Gerotor 1500-psi pump unit. Low pressure is controlled by a motorized relief valve and directed by a solenoid-operated four-way valve. A Seco pump is used to drive the intensifier down for a new stroke and to prime the system so that the intensifier need only compress the confining fluid. A separator charged by a Blackhawk pump permits the use of confining fluids which cannot be handled by the Seco pump. High pressure is measured by a manganin gage, recorded by a Brown potentiometer, and held constant at a desired value by actuation of the four-way valve by auxiliary switches in the recorder. Pressure measurements have an accuracy of $^1/_4$ per cent and a sensitivity of $^1/_{10}$ per cent, and can be held constant to within 1 per cent.

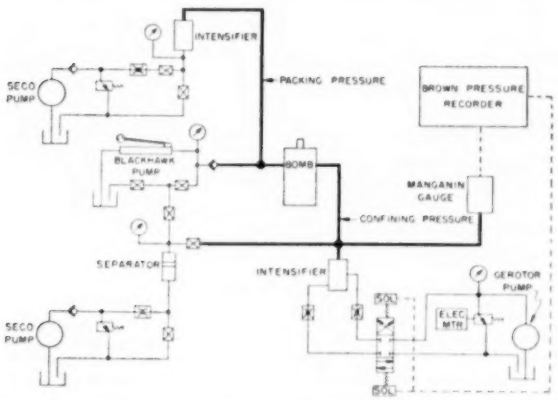

FIG. 18 SCHEMATIC DIAGRAM OF PRESSURE-GENERATING EQUIPMENT

Packing pressure is generated by a small intensifier driven by a 10,000-psi Seco pump. This intensifier is filled and driven down by the Blackhawk pump. High pressure is indicated approximately by measuring low pressure and multiplying by the ratio of the piston areas. We find that the packing pressure required to maintain the desired clearance for the piston of the test bomb is about one half the confining pressure.

Experimental Procedure. Briefly, the procedure is as follows: The test cylinder with an assembled specimen is placed in the locked press. The packing and confining-pressure systems are primed, and the measuring instruments are adjusted. If the run is to be made at high temperature, the bomb is heated and the temperature allowed to come to equilibrium. Confining pressure is then applied while the packing pressure is increased from time to time to prevent excessive leakage. To apply differential force, the directional-control valves are set for compression; the press pump is started. If the system were frictionless, the press would move upward when the force of the ram just balanced the force exerted by the confining pressure on the bomb piston. In an extension test it is necessary to remove the locking blocks, reverse the directional-control valves, and pump the press down. During free travel of the piston, before the specimen is loaded, the packing pressure is adjusted for minimum leak and friction. The specimen is then loaded to rupture or until some desired strain is achieved.

During a run the confining pressure (nearly constant), the piston displacement, and the force on the piston are being recorded simultaneously. To construct a stress-strain curve, the three records are matched as shown in Fig. 19. Corresponding points are taken at arbitrary time intervals and the three values are read off. Pressure is converted to force on the piston. During free travel the difference between this force and that read from the load record is the friction force for which further readings are corrected, assuming the friction does not change during the run. Once the specimen is loaded the differential force increases rapidly (on the record the load increases in compression, decreases in extension). Initially, the load-time curve is linear, indicating elastic deformation. Soon the curve steepens; the specimen is flowing. The force is converted to true differential stress on the specimen by dividing by the cross-sectional area determined from the original area and measured change in length, assuming no volume change. This procedure probably leads to no appreciable error until the strain becomes very large and the specimen necks down or assumes a barrel shape.

Zero on the displacement curve is taken at the point where the specimen is first loaded. Displacements are corrected for elastic distortion of the apparatus, previously determined by a run on steel, and converted to strain, per cent of change of length of original length. The displacement curve is a straight line, indicating that the strain rate is constant.

Some Results. Our first experiments were made mostly to test the functioning of the apparatus and to check the effectiveness of the specimen-jacketing technique. Some representative extension stress-strain curves are shown in Fig. 20. The brass is somewhat stronger and more ductile than at atmospheric pressure. The curve for Yule marble is found to agree remarkably well with that of Griggs[6] for a test under the same conditions. The specimens of brass and unconsolidated beach sand (still in the jacket) for which the curves were obtained are shown in Fig. 21. The brass has elongated, necked down, and broken like a typical ductile metal subjected to an ordinary tensile test. Indeed, in spite of Bridgman's well-known work on metals under multiaxial stress, the question is almost always asked: "Where are the tension grips?" The enigma of strain and fracture under triaxial stress

[6] "Deformation of Yule Marble. Part 4. Effects at 150° C," by D. T. Griggs, F. J. Turner, I. Borg, and J. Sosoka, Bulletin of the Geological Society of American, vol. 62, 1951, p. 1392.

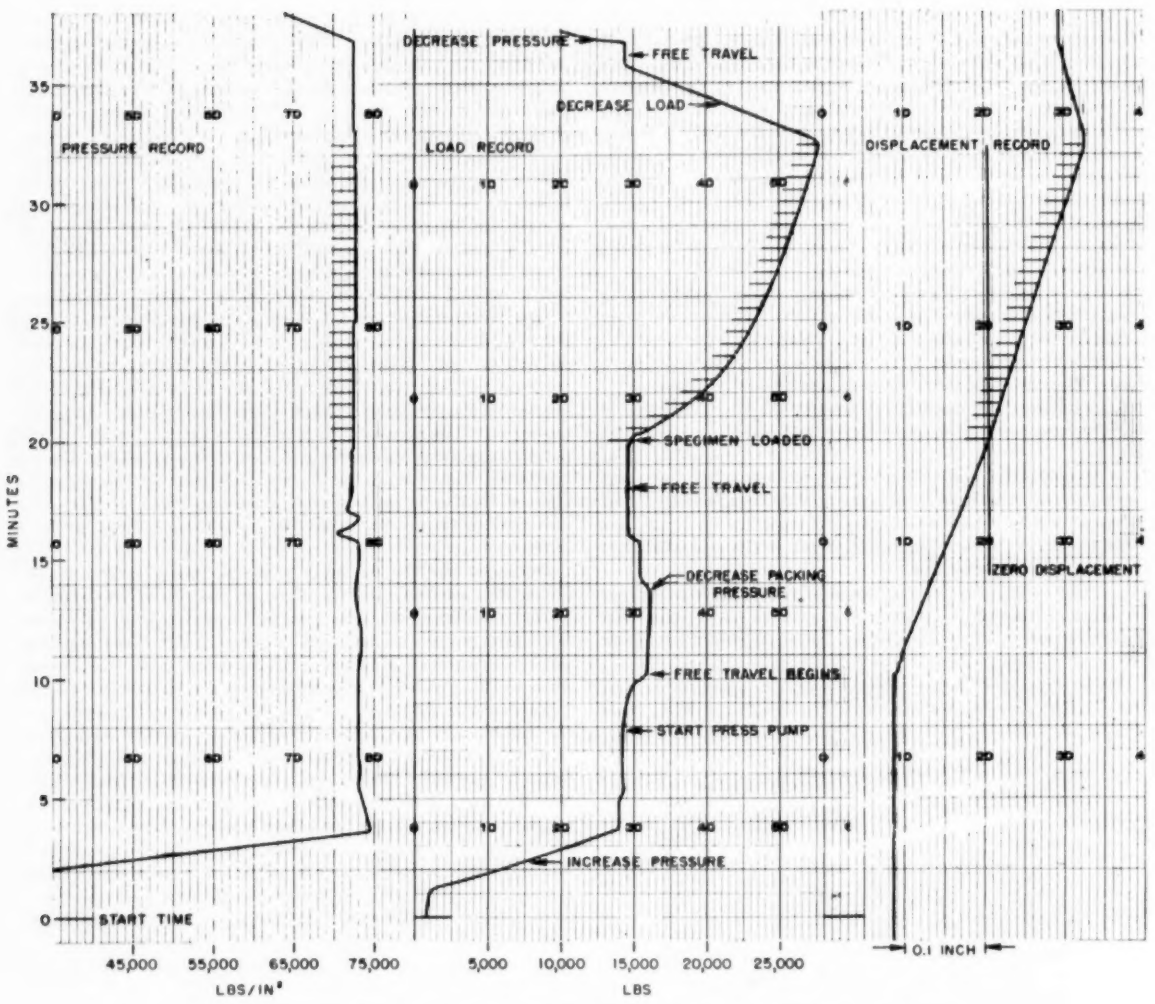

FIG. 19 MATCHED PRESSURE, FORCE, AND DISPLACEMENT RECORDS FOR TYPICAL EXPERIMENT

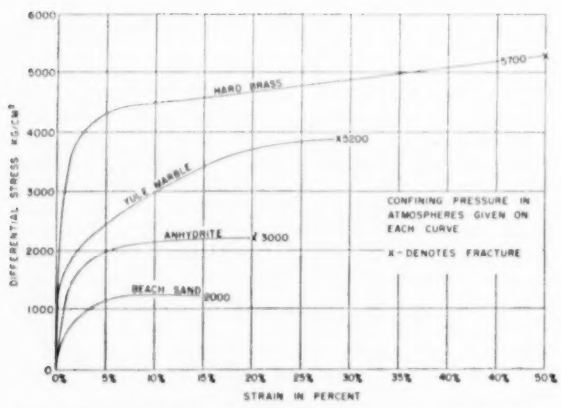

FIG. 20 STRESS-STRAIN CURVES OF VARIOUS MATERIALS DEFORMED IN EXTENSION

tempts one to look for a tension, but this is most difficult in the case of the beach sand which has been elongated some 20 per cent and has begun to neck in spite of the improbability of transmitting a tensile force through loose unconsolidated material.

A number of runs have been made on rock salt at room temperature. Schmidt, 1937, and Goguel, 1948, made triaxial tests on salt, but their confining pressures were less than 1000 atm, and the maximum strain achieved was only a few per cent. We have deformed natural rock salt from the Hockley mine, Texas, under confining pressures to 5100 atm and have obtained strains of nearly 75 per cent at a strain rate of about 2 per cent per min. The stress-strain curves in Figs. 22, 23, and 24 have been carried to only 40 per cent because of the uncertainty of computing the true stress for greater strains. The actual mechanism of deformation of salt under these conditions is still being investigated, but a number of interesting observations can be made from a knowledge of the stress-strain relationships:

1 The salt has remarkable ductility in compression even at very low confining pressures. At 1200 atm in compression, Fig.

FIG. 21 *At left,* UNDEFORMED BRASS CYLINDER AND BRASS SPECIMEN RUPTURED IN EXTENSION. *At right,* UNCONSOLIDATED BEACH SAND—WITHIN JACKET—ELONGATED IN EXTENSION

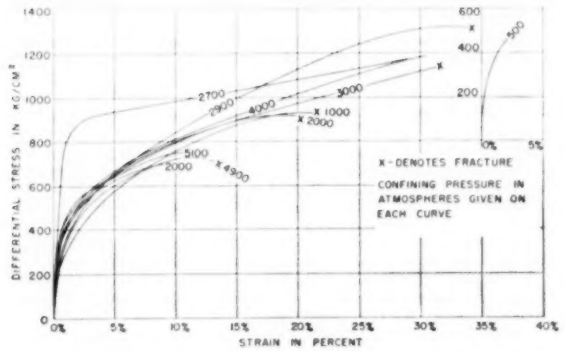

FIG. 22 STRESS-STRAIN CURVES OF ROCK SALT DEFORMED IN EXTENSION

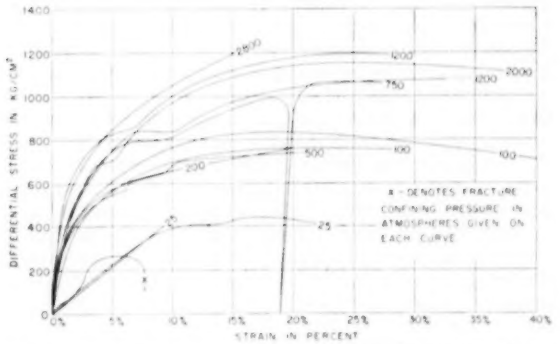

FIG. 23 STRESS-STRAIN CURVES OF ROCK SALT DEFORMED IN COMPRESSION

23, a specimen was shortened nearly 75 per cent before fracture (and it is probable that the jacket failed first). Fig. 25 shows two deformed samples and an undeformed cylinder for comparison. On the right one can see that the salt has flowed so as to surround the sides of the end pieces almost completely.

2 Initially, there is either no elastic limit or yield point, or it is too low to be detected with measuring devices employed, which were designed primarily for determining large stresses and strains.

3 Deformation results in work-hardening and the appearance of an elastic limit, as evidenced by the 750-atm curve, Fig. 23, obtained by unloading and reloading the specimen.

4 The increase of strength and ductility with confining pressure, so striking with many rocks, is much less pronounced in the case of salt, and much of the effect is observed in the first few hundred atmospheres.

5 The extension and compression curves are very similar. The ductility in extension appears to be lower, but it seems proba-

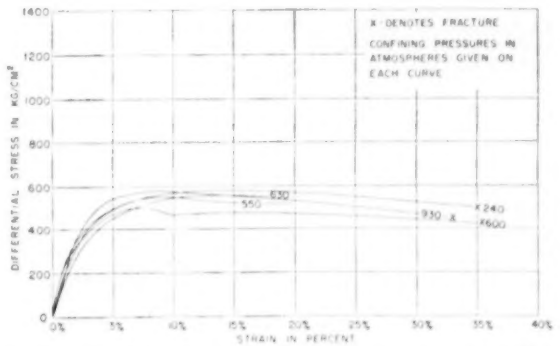

FIG. 24 STRESS-STRAIN CURVES OF ROCK SALT DEFORMED IN COMPRESSION WITH SPECIMENS EXPOSED TO CONFINING LIQUID; I.E., KEROSENE

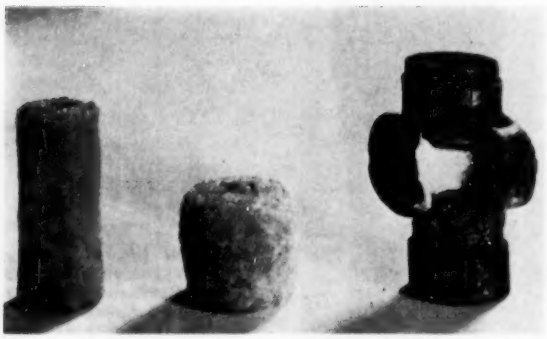

FIG. 25 *At left*, UNDEFORMED CYLINDER OF ROCK SALT; *Center*, SALT COMPRESSED 50 PER CENT; *At right*, SALT, STILL IN JACKET, COMPRESSED NEARLY 75 PER CENT

ble that the jackets broke first resulting in immediate separation of the specimens. (It is difficult to determine whether the jacket or the specimen failed first.)

6 Fig. 24 shows the behavior of the salt is radically different when exposed to the confining liquid, in this case kerosene.

7 The 2700-atm curve in Fig. 22 was obtained from a specimen which had first been compressed 10 per cent. The effect of the previous deformation was to increase the strength in extension, the opposite of what would be expected from the Bauschinger effect.

CONCLUSIONS

Because of the great importance of carbonate rocks to the petroleum industry—about 50 per cent of current oil production is from carbonate reservoirs—the planned testing program with the present apparatus includes studies of dolomite deformation and the calcite-dolomite reaction. Later we plan to look into clay compaction and sandstone cementation. With the creep-testing equipment being built we hope more realistically to simulate the natural environment with regard to the time factor.

Although only one aspect of geophysical high-pressure research has been discussed, it is not implied that this—inelastic rock deformation—is the only problem being investigated. There is an ever-increasing fund of information about the electromagnetic, thermal, elastic, and geochemical properties of rocks at high temperature and pressure. It is, nevertheless, true that an enormous amount of work remains to be done in high-pressure research, and it is to be hoped that discussions of this kind will provoke interest leading new workers into the field.

REFERENCES

"An Experimental Investigation Into the Flow of Marble," by F. D. Adams and J. T. Nicholson, Proceedings of the Royal Society of London, series A, vol. 195, 1901, pp. 363–401.

"Deformation of Marble Under Tension at High Pressure," by J. R. Balsley, Trans. American Geophysical Union, part 2, 1941, pp. 519–525.

"Die Mechanik der bleibenden Formänderungen in kristallinische aufgebauten Körpern," by R. Böker, *Mitteilungen über dem Vereines deutscher Ingenieure*, vol. 175, 1915, p. 1.

"Polymorphism, Principally of the Elements, Up to 50,000 Kg/cm²," by P. W. Bridgman, *Physical Review*, vol. 48, 1935, pp. 893–906.

"The Physics of High Pressure," by P. W. Bridgman, Bell and Sons, London, England, 1949.

"Some Implications for Geophysics of High-Pressure Phenomena," by P. W. Bridgman, Bulletin of the Geological Society of America, vol. 62, 1951, pp. 533–536.

"Introduction à l'étude mécanique des déformations de l'éncore terrestre," by J. Goguel, Imprimerie Nationale, Paris, France, 1948.

"Deformation of Rocks Under High Confining Pressure," by D. T. Griggs, *Journal of Geology*, vol. 44, 1936, pp. 541–577.

"Experiments Bearing on the Orientation of Quartz in Deformed Rocks," by D. T. Griggs and J. F. Bell, Bulletin of the Geological Society of America, vol. 49, 1938, pp. 1723–1746.

"Creep of Rocks," by D. T. Griggs, *Journal of Geology*, vol. 47, 1939, pp. 225–251.

"Experimental Flow of Rocks Under Conditions Favoring Recrystallization," by D. T. Griggs, Bulletin of the Geological Society of America, vol. 51, 1940, pp. 1001–1022.

"An Experimental Approach to Dynamic Metamorphism," by D. T. Griggs, Trans. American Geophysical Union, 1941, p 526.

"Deformation of Yule Marble. Part I. Compression and Extension Experiments on Dry Yule Marble at 10,000 Atmospheres Confining Pressure, Room Temperature," by D. T. Griggs and W. B. Miller, Bulletin of the Geological Society of America, vol. 62, 1951, pp. 853–862.

"Deformation of Yule Marble. Part 2. Predicted Fabric Changes," by J. W. Handin and D. T. Griggs, Bulletin of the Geological Society of America, vol. 62, 1951, pp. 863–885.

"The Piston Gage as a Precise Pressure Measuring Instrument," by D. Johnson and D. H. Newhall. Published in this issue, pp. 301–310.

"Festigkeitsversuche unter allseitigem Druck," by T. von Kármán, *Zeitschrift des Vereines deutscher Ingenieure*, vol. 55, 1911, pp. 1749–1757.

"Fabric Changes in Yule Marble After Deformation in Compression," by E. B. Knopf, *American Journal of Science*, vol. 247, 1949, pp. 433–461.

"Experimental Attempt to Solve the Problem of Failure in Materials—Nonmetallic Materials,— by H. C. Ros and A. Eichinger, U. S. Bureau of Reclamation, Technical Memo No. 635. (Translation of Report No. 28, Federal Materials Testing Laboratory, ETH, Zurich.)

"Festigkeit und Verfestingung von Steinsalz," by W. Schmidt *Zeitschrif für angewandte Mineralogie*, vol. 1, 1937, pp. 1–29.

"Preferred Orientation of Calcite in Yule Marble," by F. J. Turner, *American Journal of Science*, vol. 247, 1949, pp. 593–621.

"Deformation of Yule Marble. Part 3. Observed Fabric Changes Due to Deformation at 10,000 Atmospheres Confining Pressure, Room Temperature, Dry," by F. J. Turner and C. S. Ch'ih, Bulletin of the Geological Society of America, vol. 62, 1951, pp. 887–905.

"Tensile and Triaxial Compression Tests of Rock Cores From the Passage Way to Penstock Tunnel N-4 at Boulder Dam," U. S. Bureau of Reclamation, Basic Structural Report No. SP-6, 1946.

Techniques and Equipment for Generation of Dynamic High Pressures

By E. J. MICKEVICZ,[1] WHITE OAK, SILVER SPRING, MD.

An apparatus has been developed at the Naval Ordnance Laboratory which will reproduce characteristic pressure-time pulses, simulating ballistic pressures, for use in the design and evaluation of ordnance. Details of the apparatus and results obtained are given.

IN the course of developmental work at the Naval Ordnance Laboratory a need arose for the simulation of ballistic pressure pulses in the design and evaluation of ordnance. Hydraulic pulse-generation techniques were investigated but were discarded in favor of propellant powders as the pressure-generating medium.

The basic objective of this method was to develop a laboratory apparatus which would subject the components being tested to a pressure-time curve or "signature" of the general characteristic shape shown in Fig. 1. Such a signature may have a peak of 40,000 psi and a duration of 10 millisec. It was required that this apparatus reproduce the pressure pulse described, provide facilities for subjecting a captive test vehicle to this pressure signature, permit adequate instrumentation so that the various parameters of interest might be recorded and insure a very high degree of safety and ease of handling in the final design.

A schematic diagram of this apparatus is shown in Fig. 2. It consists of a firing chamber closed off at one end by a gasketed test vehicle, at the other by a heavy diaphragm; it is loaded with a powder charge fired through lead wires. The assembly is held together by bolts which firmly clamp the lid and baseplate to the firing chamber. In the side of the firing chamber is mounted a pressure gage and a bleed-off valve which is not shown.

The actual process of firing is as follows: A suitable component is placed in the test vehicle and the entire unit is put into the firing chamber which is resting on the baseplate, next a powder charge is placed in the chamber, firing leads are connected to external wires, the diaphragm is inserted closing the firing chamber and the lid is tightly clamped by the bolts which are threaded securely into the baseplate.

When the firing switch is closed the circuit is energized and an electric primer buried in the powder charge is ignited. Gases, liberated by the burning powder, cause the pressure in the chamber to rise; when the pressure has reached a predetermined magnitude the diaphragm ruptures through the aperture in the lid, venting the propellant gases into the atmosphere.

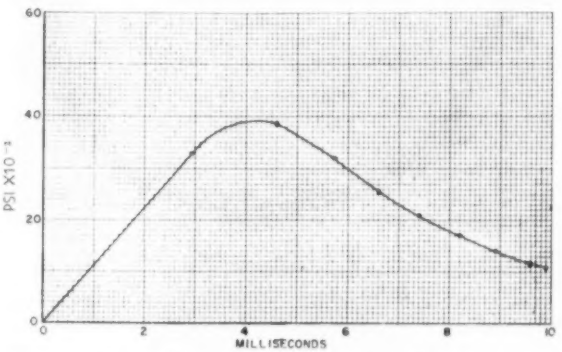

FIG. 1 TYPICAL DYNAMIC PRESSURE PULSE

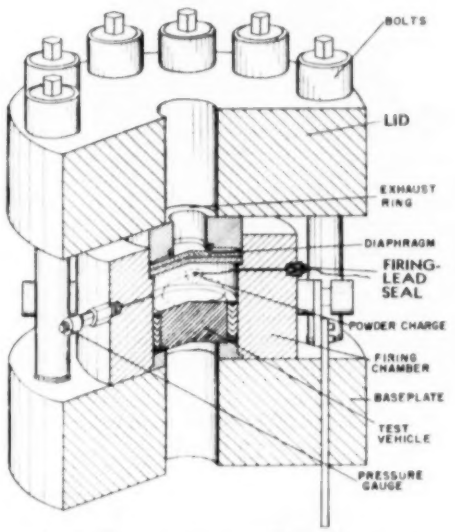

FIG. 2 DYNAMIC PRESSURE-PULSE GENERATOR

DESIGN CONSIDERATIONS

This equipment is designed to operate safely as a dynamic pressure-pulse simulator up to 50,000 psi. One of the more important design features is the series of 10 bolts which hold the lid and baseplate in contact with the firing chamber and seal the vessel against premature pressure leakage. These bolts are designed with a shank of reduced diameter equal to the root diameter of the threaded end and with a stress-relieving groove of 1/8 in. radius under the head of each bolt. By incorporating both of these features a bolt is obtained in which the stress-concentration effects of the threads and the junction of the head and shank are reduced materially, and although the bolts are of reduced cross-sectional area and total weight they nevertheless can absorb 10 per cent more energy elastically than bolts of conventional design.

The diaphragms will be discussed at further length under the subject of pressure control; at the moment it will suffice to say that they are of Naval brass stock 6 in. diam and of a thickness determined by the conditions of the experiment.

---

[1] Materials Engineer, Chief, Experimental Stress Analysis Unit, U. S. Naval Ordnance Laboratory. Jun. ASME.

Contributed by the Industrial Instruments and Regulators Division of THE AMERICAN SOCIETY OF MECHANICAL ENGINEERS and presented at the Seventh National Instrument Conference, Cleveland, Ohio, September 9–10, 1952.

NOTE: Statements and opinions advanced in papers are to be understood as individual expressions of their authors and not those of the Society. Manuscript received at ASME Headquarters, June 19, 1952. Paper No. 52—IIRD-6.

FIG. 3 "O" RING AFTER FIRING TEST

One of the more difficult phases was the design of the pressure seals required to eliminate even the most minute leakage paths and thereby prevent the attendant erosion. The diaphragm was made pressure-tight by means of two neoprene O-rings, one on each side of the diaphragm. The clamping load applied by the bolts is sufficient to extrude the O-rings and cause initial sealing. The appearance of these O-rings after a single test is shown in Fig. 3.

The test vehicle itself was sealed successfully through the use of a series of five neoprene V-rings. The customary aluminum-alloy female support ring which deteriorated very rapidly has been replaced by one of stainless steel which has functioned satisfactorily.

Considerable difficulty was encountered in the development of electrical firing-lead seals which would neither short-circuit the leads nor release the pressure. The design of these seals required that both seals must be insulated electrically from the firing chamber proper so the current required to initiate the primer would not be dissipated resulting in a misfire and also that not even the most minute leakage path to the atmosphere could be tolerated because of the extremely erosive effect of the hot gases.

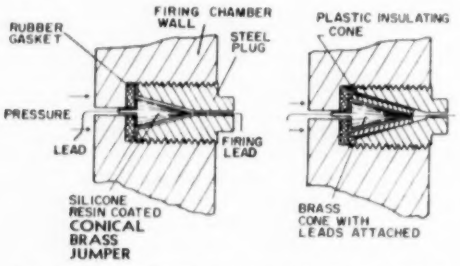

FIG. 4 COATED BRASS CONICAL FIRING-LEAD SEALS

An attempt was made to build firing-lead seals by using a cone-within-a-cone design as shown at the right in Fig. 4. In this unit a hollow plastic cone was inserted in a mating recess in the retaining plug; the firing lead having a conical mid-section was then inserted into the plastic member and the whole assembly was screwed into the firing chamber against a rubber gasket. Although this design initially failed because of the decomposition of the plastic cone caused by the high temperature and pressure, a slight modification made it successful.

The left-hand sketch in Fig. 4, illustrates the successful seal design. In this unit a baked silicone-resin coating is applied to the conical brass jumper which is then assembled into the mating retaining plug and the complete unit is then screwed into the firing-chamber wall.

TEST RESULTS

The parameters of the test are recorded with a Naval Ordnance Laboratory 6 trace recording oscillograph. With this apparatus 6 channels are recorded simultaneously on 35-mm film either on a continuous length or on a sweep synchronized 10-in. strip which represents some 160 millisec of recording time. Two typical records are shown in Fig. 5. The pulse seen at the left edge of the firing-voltage trace is the firing-condenser discharge occurring some 40 millisec before the pressure rise commences. A calibrating step is seen at the left end of the pressure-pulse traces.

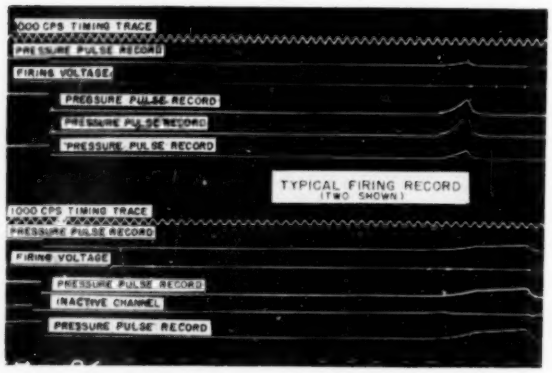

FIG. 5 TYPICAL FIRING RECORDS (Two shown.)

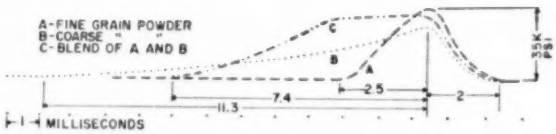

FIG. 6 EFFECT OF POWDER-GRAIN SIZE ON DURATION OF PRESSURE PULSE

The developed pressure actually is determined by the interaction of several dependent factors. They are the powder-charge weight and grain size, and the diaphragm thickness. Obviously a thicker diaphragm and a greater powder charge will produce a higher pressure pulse. To a limited extent, for a given weight of powder, the small grain, faster burning powders will give a slight increase in pressure. Not only is the magnitude of the pressure pulse subject to the experimenter's wishes, but also the pulse duration is subject to control. To understand pulse time-control techniques most clearly they must be analyzed in two parts depending on whether the pulse-rise rate or its decay rate is being considered. The pulse-rise rate is most effectively and reproducibly controlled by varying the powder-grain sizes in the firing charge as shown in Fig. 6. It is evident that a small grain-size rapid-burning powder produces a sharper pressure pulse than a slower burning powder. The fast-burning powder as shown in this figure develops a pressure rise rate of 14,000,000 psi per sec, the slow powder a rate of 2,500,000 psi per sec, while a given blend of the two produces an intermediate rate

of 4,300,000 psi per sec. Both faster and slower burning powders are available.

Originally the pressure-decay rate was to be controlled by means of a water-filled exhaust stack through which the exhaust gases would escape. However, the degree of control obtainable with practical exhaust stack lengths was found insufficient and therefore attention was turned to the exhaust aperture for control purposes. By varying the aperture through which the exhaust gases escape a greater latitude of control of the decay rate is obtained. Approximate relationships for the decay rate as a function of aperture area have been derived and are shown in Fig. 7. The dashed experimental curves are in fairly close agreement with the calculated decay rates.

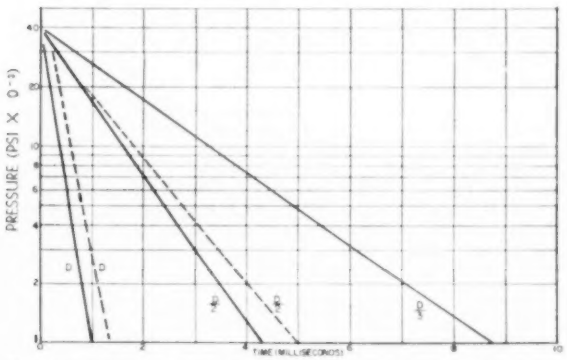

FIG. 7 PRESSURE-PULSE DECAY RATE VERSUS EXHAUST-APERTURE DIAMETER

—— Calculated; - - - Experimental; Full aperature diameter $D = 2.75$

GENERATOR USEFUL IN EXPERIMENTAL WORK

With the degree of control available the dynamic pressure-pulse generator lends itself to a variety of experimental purposes. It is directly applicable to an economical investigation of powder compositions and configurations and the effect of variations in these parameters on the characteristics of the pressure-time curve. The apparatus also may be used to subject ordnance items of a limited range of sizes to the environmental conditions which they would experience in actual service. Ballistic pressure-pulse-erosion effects caused by the combination of high pressures and temperatures of approximately 4000 F also may be studied. Dynamic calibration of pressure gages can be accomplished with this apparatus by comparing the response of the unknown gage with that of a calibrated, high-frequency response gage.

CONCLUSION

In conclusion it may be said that the basic objectives of the design have been fulfilled. A versatile apparatus, Fig. 8, has been developed which will reproduce characteristic pressure-time pulses, permit adequate parameter recording during this pulse, and will permit some degree of manipulation of the pulse shape and duration so that its applicable range is extended.

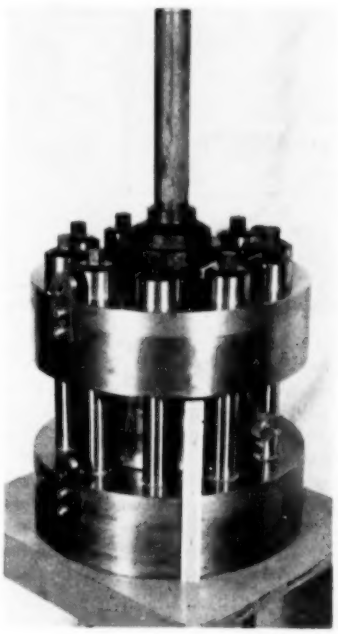

FIG. 8 DYNAMIC PRESSURE-PULSE GENERATOR

A Sensitive Pressure Controller for High-Pressure Service

By P. L. GOLDEN[1] and A. F. HEADRICK,[2] BRUCETON, PA.

An automatic, sensitive, pneumatic pressure controller has been developed for regulating the flow of hydrogen to a bench-scale, high-pressure, hydrogenation unit. It utilizes a 20-turn helical Bourdon tube which is connected to the flapper of a nozzle-flapper combination. When the nozzle is closed, air pressure in the controller acts through a system of bellows and cylinders on a rack which drives a gear connected to the regulating valve. The controller prevents slow drifts of pressure and has operated satisfactorily at 9000 psig pressure.

AN automatic, sensitive, pneumatic pressure controller has been developed for regulating the flow of hydrogen to a bench-scale, high-pressure, hydrogenation unit.[3] Previously, the hydrogen (stored at 12,000 psig) had been throttled manually to the reactor pressure of 9000 psig. However, the uncertainties of manual operation, combined with the relatively coarse graduations of the 20,000-psig gage and slack in the gage movement, resulted in small pressure variations which materially affected both the reactor temperature and the oil-feed rate. As no drastic or sudden changes in pressure were expected but only slow drifts from any set pressure a simple on-off control was considered sufficient. A schematic diagram of the controller is shown in Fig. 1.[4]

The sensing element is a helical tube manufactured by the Foxboro Company, having 20 turns and being rated at 20,000 psig. This tube gives much more movement than the conventional Bourdon tube. It is made of type 316 stainless steel which is suitable for use with hydrogen. The flapper of a nozzle-flapper combination is attached directly to the Bourdon tube, eliminating friction and drag in linkages, gears, and levers which are the chief causes of lack of sensitivity in pressure controllers. The air nozzle (1) is small and therefore can be located close to the flapper for maximum sensitivity. The nozzle position is adjustable for controlling any pressure between 0 and 20,000 psig.

As the hydrogen pressure rises, the flapper approaches the nozzle (1) and induces a back pressure of air in the controller,

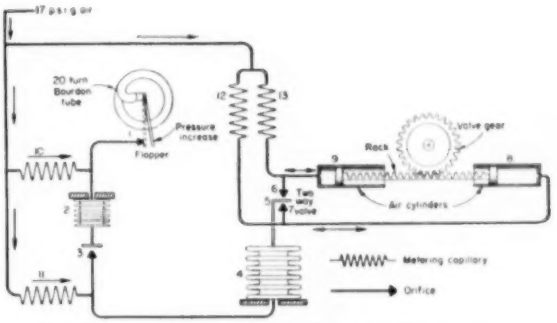

FIG. 1 SCHEMATIC DIAGRAM OF PRESSURE CONTROLLER

thus expanding a light bellows (2); this in turn shuts off an appreciably greater air leak (3) and thus pressurizes a larger and sturdier bellows (4). Attached to this bellows is a double-coned needle (5) which is moved between two closely spaced escape orifices (6) and (7) connected to opposed air-drive cylinders (8) and (9). The cylinders are sealed by leather cups which are attached to a rack extending between the cylinders. Air pressure in either cylinder pushes the rack which drives a gear connected directly to the stem of the throttling valve. At the center position of needle (5) the pressure on the cylinders is equal and the valve remains motionless until the large bellows (4) contracts or expands.

The usual air pressure of 17 psig may be changed by metering capillaries (10) to (13) when necessary. The rack contains two adjustable mechanical stops. One is set so that the throttling valve cannot be shut completely, thus preventing damage to the needle and seat. Manually operated valves, in series with it, are used for complete shutoff. The other stop, for maximum valve opening, is set for approximately twice the necessary flow.

With the original controller, a variation of 1.5 psi from the control point was sufficient to induce on-and-off action. However, the control point tended to drift slightly. In the final design, some sensitivity was sacrificed for greater stability. The present instrument, which was checked up to 10,000 psig on a gage tester, has a sensitivity of ± 10 psi. Air is metered to the cylinders through capillary tubing, giving a rather slow and deliberate action to prevent overshooting and cycling. One minor drawback is that close control of the air supply is necessary since a pressure change of 1.5 or 2 psi would inactivate the controller. Therefore a warning system is incorporated in the instrument to notify operators if such a deviation should ever occur.

This controller has been used in eleven operations which lasted from 1 to 4 weeks. It has given completely satisfactory and trouble-free service. At no time was there any pressure variation large enough to be registered on the reactor gage. If necessary, the instrument could be modified to give continuous rather than the intermittent flow which is satisfactory for the present application.

[1] Mechanical Engineer, Synthetic Fuels Research Branch, Fuels-Technology Division, U. S. Bureau of Mines, Region VIII.

[2] Laboratory Mechanic, Synthetic Fuels Research Branch, Fuels-Technology Division, U. S. Bureau of Mines, Region VIII.

[3] "Vapor-Phase Hydrogenation of Light and Heavy Oils," by M. L. Wolfson, M. G. Pelipetz, A. D. Damick, and E. L. Clark, *Industrial and Engineering Chemistry*, vol. 43, 1951, pp. 536–540.

[4] Detailed drawing of the controller may be obtained from the Synthetic Fuels Research Branch, U. S. Bureau of Mines, Region VIII, Bruceton, Pa.

Contributed by the Industrial Instruments and Regulators Division of THE AMERICAN SOCIETY OF MECHANICAL ENGINEERS and presented at The Seventh National Instrument Conference, Cleveland, Ohio, September 9–10, 1952.

NOTE: Statements and opinions advanced in papers are to be understood as individual expressions of their authors and not those of the Society. Manuscript received at ASME Headquarters, June 19, 1952. Paper No. 52—IIRD-4.

High-Pressure Research in Chemical Engineering Department of Yale University

By BARNETT F. DODGE,[1] NEW HAVEN, CONN.

This paper reviews only the "high lights" of research in this field which has been conducted since 1925 in our chemical engineering laboratory under the author's direction. Work carried out prior to 1947 is given only passing mention and most of the paper is devoted to an outline of current work and some researches completed in the past 5 years.

History and Present Status of High-Pressure Investigations

THE research in this field which was initiated by the author in 1925, has been carried on continuously since that year, except for the war years 1940–1946, with the aid of graduate students working for the Doctor's degree under the direction either of the author or Prof. H. Bliss. The results of the work have been published in 18 papers which are listed at the end of this paper. An outline of the investigations up to the year 1947 is as follows:

1 Methanol and formaldehyde synthesis
   (*a*) Catalyst studies
   (*b*) Chemical equilibria
2 Vapor-phase hydration of ethylene
   Catalysts and equilibria
3 Reaction of CO with ethyl alcohol
4 Phase equilibria
   (*a*) System: N_2–C_6H_6
   (*b*) System: CO_2–C_6H_6
   (*c*) System: N_2–CH_3OH
   (*d*) Methane-isopentane
   (*e*) Hexane-toluene
5 P-V-T relations of N_2–CO_2 mixtures.

The maximum pressure used was 1000 atm, but most of these investigations were conducted at considerably lower pressures.

Research problems either completed since 1947, or currently under investigation or under consideration for initiation of work in the near future may be stated briefly as follows:

1 Carbon monoxide reactions
   (*a*) CO + dihydric alcohols
   (*b*) CO + cyclohexanol
   (*c*) CO + phenol, aniline, and some halogenated benzenes
2 P-V-T relations of gases
   (*a*) System: N_2–H_2
   (*b*) System: N_2–H_2–NH_3
3 Action of hydrogen on tensile properties of metals
   (*a*) Chemical action at elevated temperatures
   (*b*) Physical action at room temperature
4 Permeability of metals to hydrogen
5 The ammonia synthesis equilibrium at pressures above 1000 atm
6 Phase equilibrium in system: N_2–NH_3
7 Catalytic oxidation of benzene
8 Equilibrium in hydration of C_2H_4 in presence of both vapor and liquid phases
9 Exploratory investigations of some reactions of butadiene
10 Kinetics of heterogeneous hydrogenation (system not yet chosen)
11 Chemical equilibrium in the water-gas reaction at high pressures
12 Reactions of carbon monoxide with ketones, diols, and some halogenated naphthenes
13 Problems under consideration but no work yet started
   (*a*) Polymerization of unsaturated hydrocarbons
   (*b*) Methanol-synthesis equilibrium
   (*c*) Effect of pressure on diffusivity and thermal conductivity of gases
   (*d*) Action of mercury on steels

The High-Pressure Research Laboratory

Up to 1947 the research work was carried out in a very small, overcrowded, and ill-adapted space in the main chemical engineering laboratory. In 1947 the one-story, cinder-block building with 4000 sq ft of floor area shown in Fig. 1 was completed and is now used to house all the high-pressure work. Various interior

Fig. 1 Exterior View of Chemical Engineering Laboratory for Research at High Pressures

views of the laboratory are shown in Figs. 2 to 7 inclusive. Fig. 2 gives a general view of the main room showing on the right the seven steel-barricaded cells inside of which the experimental setups are mounted. Control valves are mounted so that they may be operated from the outside and most instruments such as pressure gages and thermometers are read from the outside. Fig. 3 shows a piston gage for measuring pressures to 4000 atm and some of the low-pressure equipment outside of a barricaded cell used for *pvt* measurements. Fig. 4 is a view of the pump and compressor room, and Fig. 5 shows an assembly of apparatus for investigating rate of absorption of gases in liquids in a packed tower at pressures up to about 500 psi. Figs. 6 and 7 show some of the apparatus inside the steel cells.

The main items of equipment in the laboratory for the production, measurement, and control of pressures up to 150,000 psi (10,000 atm) are listed in Table 1.

In addition there are many storage cylinders for gas at 2000, 3000, and 7500 psi, valves, fittings, and tubing for pressures up to 150,000 psi, relief valves, blowout-disk assemblies, and miscellaneous Bourdon-type pressure gages. The laboratory also has lathes, drill press, bench grinder and other shop equipment and

[1] Professor of Chemical Engineering and Chairman of Department of Chemical Engineering, Yale University.

Contributed by the Industrial Instruments and Regulators Division of The American Society of Mechanical Engineers and presented at The Seventh National Instrument Conference, Cleveland, Ohio, September 9–10, 1952.

Note: Statements and opinions advanced in papers are to be understood as individual expressions of their authors and not those of the Society. Manuscript received at ASME Headquarters, January 6, 1953.

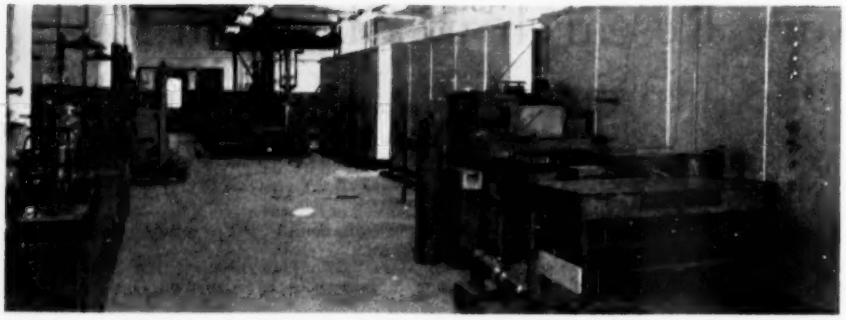

FIG. 2 GENERAL VIEW OF INTERIOR OF LABORATORY, SHOWING STEEL-WALLED CELLS AT RIGHT FOR PROTECTION OF PERSONNEL

equipment for catalytic reactions, *pvt* measurement, temperature measurement, and control and gas analysis.

REVIEW OF CURRENT PROBLEMS AND WORK RECENTLY COMPLETED

Action of Gases on Metals. Certain gases, notably hydrogen, nitrogen, oxygen, and carbon monoxide, have a deleterious effect on metals at elevated pressures and temperatures and a knowledge of these effects is important from the standpoint of safe design of equipment to handle gases under these conditions. We are particularly interested at the present time in hydrogen, and all the work to date in this laboratory has been with this gas.

This is by no means a new problem. It has been under study by many investigators over a period stretching from 1830 to the present time. A recent circular of the National Bureau of Standards (1)[2] lists 1191 papers and books written up to about October, 1949. This includes, however, not only publications which deal directly with the embrittlement of steel by hydrogen but many that are concerned only indirectly with this specific subject. For example, it also covers such things as the chemistry of the iron-hydrogen system, diffusion of hydrogen, solubility, removal of hydrogen, and various others. Three books which deal with the general subject and one with a chapter devoted to it are important enough to deserve separate mention (2, 3, 4, 5). In view of this voluminous literature one may wonder why anyone should wish to undertake further work and why there should be any need for it.

We were led to undertake work in this field for a number of reasons which seemed valid. In general, there is a great deal of conflicting information and it is exceedingly difficult to predict what the result of exposure to hydrogen would be under a given set of specific conditions. Also, the effect of pressure as a variable has been studied to only a small extent and there is almost no information for the effect of pressures above 200 atm. Many new alloys have appeared since some of the studies were made and just to extend the work to include these new metals is a worth-while objective in itself. Finally, much remains to be done to elucidate the mechanism of the action and, until this is more clearly understood, most of the facts that have been collected from all the painstaking research of many years will remain as unrelated observations incapable of being generalized. For an excellent review of the broad subject of the action of gases on metals and for further justification of the need of additional work, the paper by Schuyten (6) is recommended.

Although somewhat of an oversimplification it has been found useful to divide the problem into the four following aspects:

1 The chemical reaction between hydrogen and the various elements that are present in small amounts in metals, especially carbon.

[2] Numbers in parentheses refer to the Bibliography at the end of the paper.

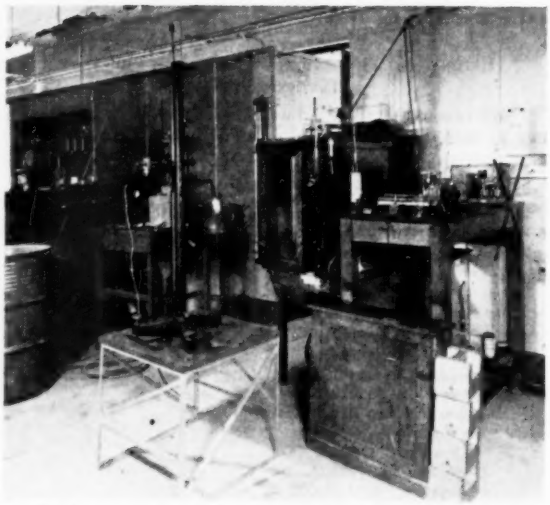

FIG. 3 APPARATUS FOR MEASUREMENT OF PRESSURE AND OF GAS COMPRESSIBILITY

FIG. 4 COMPRESSOR AND PUMP ROOM

2 A purely physical action involving a penetration of the gas into the crystal lattice with consequent disruptive effects.

3 The rate of diffusion or permeation of gases through metals.

4 The solubility or occlusion of hydrogen by metals.

Let us consider each of these very briefly.

TABLE 1 PRINCIPAL EQUIPMENT IN HIGH-PRESSURE LABORATORY

Single-stage, double-acting, Gardner-Denver horizontal compressor, size 9 × 12; maximum pressure 125 psig; displacement at 225 rpm = 166 cfm
Two-stage, duplex, vertical, Gardner-Denver compressor; maximum pressure 500 psig; displacement 75 cfm at 720 rpm
Three-stage, vertical, Rix compressor; 4500 psig; displacement = 5.3 cfm at 400 rpm
Five-stage, horizontal, duplex tandem, Norwalk compressor; maximum pressure 1000 atm; displacement = 15.0 cfm at 250 rpm
Dunning and Boschert, triplex hydraulic pump; 1000 atm pressure; displacement = 0.47 gpm at 80 rpm
Harwood intensifier; maximum pressure = 60,000 psi; ratio of cylinder areas = 64; displacement of high-pressure cylinder per stroke = 160 cc
Harwood intensifier; maximum pressure = 150,000 psi; ratio of cylinder areas = 175; displacement of high-pressure cylinder per stroke = 43 cc
Gerotor rotary oil pump for operating low-pressure cylinders of intensifiers; 1.5 gpm at 800 psi; maximum pressure = 1500 psi
Two Black hawk, hand-operated, oil pumps for 10,000 psi
Two dead-weight piston pressure gages with pistons of $^3/_{32}$, $^9/_{16}$, $^3/_8$, and $^{17}/_{32}$ in. diam with oil-injector pump for 1000 atm and small intensifier to inject oil at 4000 atm; maximum pressure = 4000 atm
Foxboro Bourdon-type pressure gage with stainless-steel helical element for maximum pressure of 60,000 psi
Manganin resistance pressure cell for 150,000 psi with auxiliary equipment for resistance measurement
Several Bourdon-spring pressure gages with maximum scale reading to 100,000 psi
Struthers-Wells $^1/_4$-gal autoclave with rotating stirrer for maximum pressure of 10,000 psi
Aminco $4^1/_2$-in. series shaking mechanism with autoclave for 15,000 psi
Aminco micro series shaking mechanism with reaction vessels for 13,000 psi at 100 F
Three storage vessels for gas at 1000 atm; one of 0.26 cu ft volume, one of 0.17 cu ft volume, one of 0.89 cu ft volume
Three gas holders for atmospheric-pressure storage; one of 50 cu ft and two of 100 cu ft capacity
Seven steel pressure cells (barricades) 7 ft × $8^1/_2$ ft × 8 ft high of $^1/_4$-in. steel plate

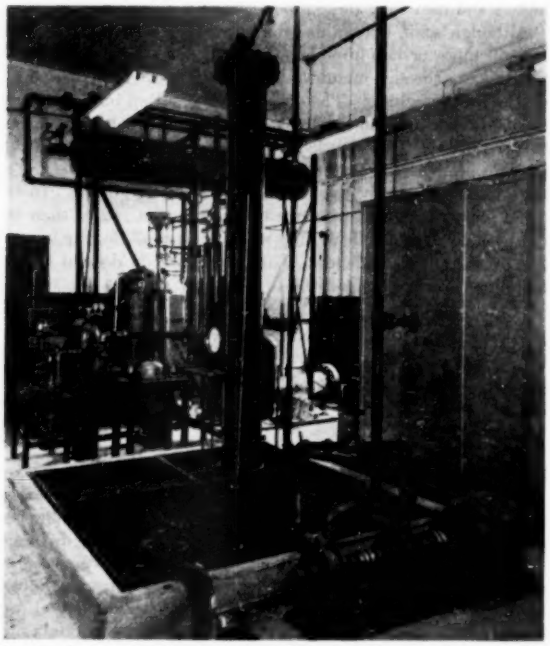

FIG. 5 APPARATUS ASSEMBLY FOR INVESTIGATION OF RATE OF ABSORPTION OF GASES BY LIQUIDS AT ELEVATED PRESSURE IN PACKED TOWERS

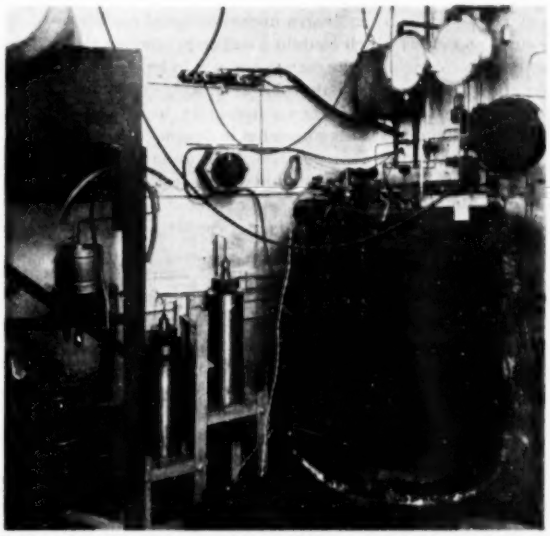

FIG. 6 APPARATUS INSIDE ONE OF PRESSURE CELLS, FOR INVESTIGATION OF PHASE EQUILIBRIA AT HIGH PRESSURES

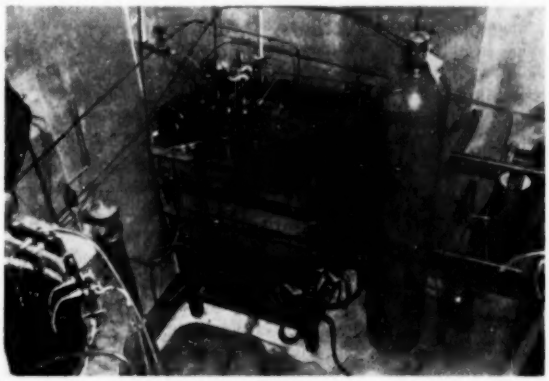

FIG. 7 APPARATUS INSIDE OF A PRESSURE CELL, FOR INVESTIGATION OF COMPRESSIBILITY OF GASES AT HIGH PRESSURES

1 The main chemical reaction in the case of steels is believed to be the reaction with carbon to form methane and much, if not all, of the damage to the metal is caused by the trapped methane which is unable to diffuse out of the metal with the result that very high localized gas pressures are developed which cause fissuring. Even if no methane were formed the removal of the carbon itself would alter the structure and presumably change the tensile properties. This action takes place at elevated temperatures, i.e., at 300 C or higher and, since chemical reaction rates are, in general, greatly accelerated by temperature, it is to be expected that the action would be negligible at room temperature.

The pressure is a less important variable than the temperature and its main effect is probably to speed up the attack or to cause it to take place at an appreciable rate at somewhat lower temperatures. According to Schuyten (6) there is a leveling off in attack with pressure at about 10,000 psi but it should be noted that this is based on very little evidence since almost no work has been done at pressures above 10,000 psi. To distinguish this chemical action from the purely physical action to be discussed next we have employed the word "attack" as a general term for the action of hydrogen on metals at elevated temperatures. The term "decarburization" also is used extensively in the literature, but this implies that the only reaction is that with carbon. Severe attack occurs in some alloys with low carbon content and it is possible that other reactions such as hydride formation or reduction of oxide inclusions may be important. In general, though, it is known that steels of high carbon content are more susceptible to attack than those of low carbon content.

Certain alloying elements used in steel such as chromium, molybdenum, vanadium, tungsten, and possibly titanium, zirconium, and a few others, form carbides that are relatively stable

(i.e., nonreducible by hydrogen under the usual conditions of exposure) and steels which contain a sufficient amount of these elements to combine with the carbon are said to be quite resistant to hydrogen attack. Elements such as nickel, silicon, and copper form no carbides and confer no immunity to hydrogen attack. The effect of manganese is somewhat in doubt.

It should be noted that the theory that immunity to hydrogen attack is only a question of stability of the carbides has been disputed by some investigators. As a matter of fact, little is known about any of the carbides except possibly those of iron and chromium.

2 This purely physical action that can occur at approximately room temperature is what we choose to describe by the word "embrittlement." It occurs at low pressures when hydrogen is liberated at the surface of the metal in the so-called "nascent" form (presumably atomic hydrogen) as, for instance, by electrolysis or by chemical reaction or when the metal is exposed to the gas through which a high potential electrical discharge is passed. Ordinary molecular hydrogen is apparently without appreciable effect at pressures below 1000 atm (except possibly over very long periods of time). A few isolated and not very systematic observations of Bridgman (7) and of Poulter and Uffelman (8) comprise the entire literature for the action when the hydrogen pressure is greater than 1000 atm.[3]

Bridgman found that a Cr-V steel vessel used to contain hydrogen at 9000 atm developed submicroscopic fissures which later developed into cracks visible to the eye. The same vessels withstood liquids at 25,000 atm with no damage. Even when the vessel was separated from the hydrogen by kerosene, it ruptured, presumably because of solution of hydrogen in the liquid. He found somewhat the same result with air but to a lesser degree.

Poulter and Uffelman observed rapid penetration of hydrogen through steel at 6000 atm though there was no similar effect at 4000 atm. However, when the hydrogen was generated by the action of acid on zinc, a rapid penetration of hydrogen took place at 4000 atm.

In an interesting paper on "Mechanism of Cavitation Erosion," Poulter (9) points out the fundamental similarity of the following apparently unrelated phenomena: Corrosion, caustic embrittlement, steam erosion, cavitation erosion, gun-barrel erosion, wire-drawing, creep of metals, fatigue, and the penetration of gases and liquids into metals. In this paper he gives a few observations on the effect of high-pressure hydrogen but the exact conditions of exposure are not described clearly. For example, he refers to cracks in a cylinder wall forming in only a few minutes at 30,000 psi but it is not certain whether the exposure was to ordinary molecular hydrogen or to hydrogen generated in situ from zinc and acid.

Various investigators have studied the properties of hydrogen and hydrogen-containing gases at pressures of 3000 atm and even 5000 atm without making any observations on damage to their equipment.

From a study of this very meager amount of information it did not seem to us likely that we would encounter any serious trouble if we compressed hydrogen in an ordinary alloy-steel vessel to 3000 atm but we were wrong. An intensifier which had been used repeatedly to pump oil at 4000 atm and several times to compress nitrogen to the same pressure, failed within a matter of minutes when used to compress hydrogen at not over 3000 atm. The failure consisted in the development of very fine cracks barely visible to the naked eye but easily seen when special techniques were used to develop them. They were sufficiently large to render the intensifier completely useless even with oil only. This sad experience brought home to us very forcibly the need for more work on the effect of high-pressure hydrogen.

3 The rate at which hydrogen and other gases permeate metals has been studied by a great number of investigators but there are so many variables influencing it that the picture is far from complete and many of the results are conflicting and hard to explain. Consider the effect of pressure. It has been fairly well established that the rate is proportional to $\sqrt{p}$ indicating that it is only atomic hydrogen which actually penetrates the metal and permeates through it. With many steels the rate becomes constant at about 100 atm and no further increase occurs as the pressure is increased. This is surprising and apparently no satisfactory explanation of it has been found. In the case of nickel the leveling off occurs at a pressure of only 20 atm (10). Further work is indicated. For example, it would be of interest to increase the pressure to 1000 atm and beyond and to study different metals and also vary the temperature and other factors.

Although some writers use the terms "permeation" and "diffusion" more or less interchangeably in describing the penetration of gases through metal walls, it is better to make a distinction on the following basis: The over-all process from bulk gas phase on one side of the wall to gas phase on the other is best described as permeation. This consists of interactions at the metal surfaces as well as the actual transport through the metal. The term diffusion strictly applies just to the latter process. In the usual experiment one measures the permeation rather than the diffusion because one deals only with the over-all driving force of gas pressure. A coefficient of diffusivity D, is defined by the equation (for linear, steady-state diffusion)

$$J = -D \frac{c_1 - c_2}{\Delta x} \quad [1]$$

whereas the permeability P is usually defined by

$$J = \frac{-P}{\Delta x} \quad [2]$$

where J is the diffusion current per unit of area and $(c_1 - c_2)/(\Delta x)$ is the concentration gradient in the metal wall of thickness Δx. It is clear that P will depend on the gas pressure difference on the two sides of the wall. One could define a permeation coefficient by basing it on a pressure gradient. The usual values of P have been obtained with a 1-atm pressure difference. If one assumes that the concentration in the metal is proportional to the square root of the pressure, the permeability might be defined by

$$J = -P \frac{\sqrt{p_1} - \sqrt{p_2}}{\Delta x} \quad [3]$$

That the penetration of a gas into a metal is not simply along crystal boundaries but directly through the lattice is quite well established by the work on single crystals which has shown that the rate of diffusion through the latter is just as rapid as through polycrystalline material.

It also has been fairly well established that the diffusion of a gas occurs only when it is in the form of atoms dissociated from the molecule. Molecular hydrogen does not diffuse nor do any of the monatomic gases. One of the chief bits of evidence sup-

[3] Since this statement was written, a brief note (*Chemical Engineering News*, vol. 30, 1952, p. 2942) has come to our attention in which mention is made of failure in laboratories of the du Pont Company of small equipment using hydrogen at room temperature and pressures above 2000 atm. Mention also is made, but no details given, of bursting tests on pressure vessels using both oil and hydrogen to develop the pressure. Vessels that withstood oil pressures of 7000 atm failed in very short periods of time when pressured by hydrogen at only 2000 atm. The best solution to this problem was found to be the use of stainless-type 316 steel liners in the vessels and the use of grooves and leakage holes in the walls of the latter to prevent build-up of pressure between the liner and the vessel.

porting this conclusion is the fact that the rate of permeation of a diatomic gas is generally proportional to the square root of the pressure. This would be expected if the diffusion were due solely to atoms, in view of the equilibrium relation

$$K = \frac{p_H}{\sqrt{p_{H_2}}} \quad \ldots\ldots\ldots\ldots\ldots\ldots [4]$$

where K is the equilibrium constant of the dissociation reaction and p_H and p_{H_2} are partial pressures of atomic and molecular hydrogen, respectively.

The importance of dissociation into atoms is also indicated by the exponential effect of temperature which is the effect that would be expected if the rate controlling the permeation were an activated adsorption on the surface resulting in some dissociation. Another bit of evidence is the fact that nascent hydrogen will diffuse in a metal against a high pressure of hydrogen.

The equation that is usually accepted as expressing the effect of pressure and temperature is as follows

$$J = \frac{K}{L} (p_1^{1/2} - p_2^{1/2}) e^{-E/RT} \quad \ldots\ldots\ldots\ldots [5]$$

where

J = rate of permeation per unit of area
K = constant depending on metal and probably on several factors related to state of metal
L = thickness of metal membrane through which gas is permeating
p_1 = pressure on high-pressure side of membrane
p_2 = pressure on low-pressure side
E = an activation energy
R = gas constant
T = absolute temperature

Although this law of pressure and temperature dependence is supposedly general, the limits within which it applies are not well known and the effect of variables on K is not at all established.

The relation between rate of permeability and practical effects on the properties of the metals is not clear but we are hoping that further work along this line may lead to some useful correlations. Even if it doesn't, the data on the permeability will have some value in indicating which metals are best for applications where no leakage of gas through a metal wall can be tolerated. It also will have application to the selection of liners for steel vessels.

4 The retention or occlusion of gases by metals may be of importance in some applications but as yet we have not had an opportunity to study the considerable literature on the subject. It is mentioned here only to call attention to a part of the general subject of interaction between gases and metals which may bear study and which may have an important relation to the other three aspects that we have considered.

In passing, it may be worth mentioning that the retention of gases by metals once they have penetrated beyond the surface is generally believed to involve not only solid solution, i.e., a penetration of the crystal lattice by atoms of the gas, but also an accumulation of gas at grain boundaries and in imperfections or rifts within the crystals.

Experiments on Hydrogen Attack. Our work in this field will now be reviewed briefly. The question of hydrogen attack by decarburization or other chemical reaction could be approached from a fundamental angle. The two basic factors in dealing with any chemical reaction are (*a*) chemical equilibrium and (*b*) rate of reaction. One could investigate the equilibrium and kinetics of the reduction of various metal carbides by hydrogen but the situation in an actual metal is probably far more complex and it seems doubtful if such information would be useful in predicting the practical effect of hydrogen on the tensile properties of a given metal under a given set of conditions. For this reason we have chosen a practical and not particularly fundamental approach to the problem. Briefly it is this: Hollow pieces of metal in the form of a tensile test specimen are subjected to internal hydrogen pressure while being held in a furnace for some time at a constant temperature. A control sample is subjected to the same temperature but without the hydrogen pressure. At the end of a certain period of time the samples are removed from the furnaces and tested in a standard tensile testing machine to determine the ultimate tensile strength, the elongation and the reduction in area. For comparison, the same tests were made on untreated samples from the same lot of material. Sections of exposed and unexposed specimens also are examined microscopically by the standard metallographic procedures. A drawing of the test specimen used is shown in Fig. 8, and Fig. 9 gives a schematic representation of the assembly for exposing the specimens.

To date tests have been made on 26 different metals under test conditions which may be summarized as follows:

Temperatures of 300 to 500 C
Pressures of 1000 and 2000 atm
Time of exposure varied from 4 to 10 weeks

In a paper of this broad scope it is not possible to present the results in any detail but a few general conclusions of the work so far accomplished may be interesting and will be enumerated. Before doing this, however, it is desirable to explain the basis for them. If the specimen exposed to hydrogen had, within reasonable limits of reproducibility, the same tensile properties as the unexposed control sample, it was concluded not to have been attacked. If these properties have been lowered in value but the microscope reveals no fissuring or if heating in the absence of hydrogen restores to a considerable extent the original properties, the sample is concluded to have been embrittled but not attacked. Finally, if the tensile properties have deteriorated and fissuring is clearly revealed by the microscopic examination, it is concluded that the metal has been attacked:

1 Plain-carbon steels, even those of low carbon content, were severely attacked at 400 C in a relatively short time. This, of course, was to be expected from the literature. At 300 C the attack was inappreciable.

2 Some alloy steels were attacked severely, others were embrittled, and others not appreciably affected. Not enough results are available to establish any definite pattern but contrary to expectations some Cr-Mo steels with as much as 5 per cent Cr were definitely attacked at 2000 atm even though they were low in carbon (about 0.10 per cent). There was some evidence, but not conclusive, of attack on a Cr-Mo steel containing 10 per cent Cr.

3 High-nickel alloys such as K-Monel, Inconel, and Hastelloy B were either attacked or embrittled.

4 Some embrittled samples had their original properties restored by heating to somewhat higher temperatures in the absence of hydrogen.

5 Results on high-chromium alloys such as chromax, nichrome, and nichrome V are somewhat inconclusive in that specimens of nichrome and chromax were unaffected but nichrome V was attacked severely.

6 Tentatively it appears that 2000 atm was a considerably more severe condition than 1000 atm. Some metals that were not affected appreciably at 1000 atm were attacked severely or embrittled at 2000 atm.

7 No effect was observed on any stainless steels either of the 300 or the 400 series (only one of the latter was tested).

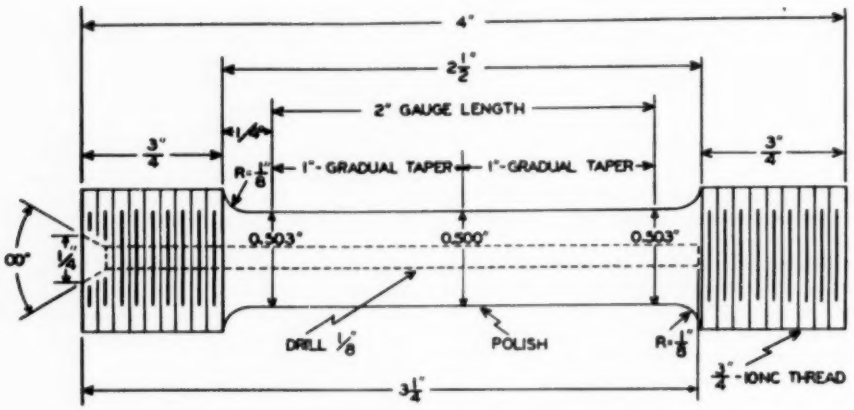

FIG. 8 TENSILE TEST SPECIMEN FOR EXPOSURE TO HYDROGEN

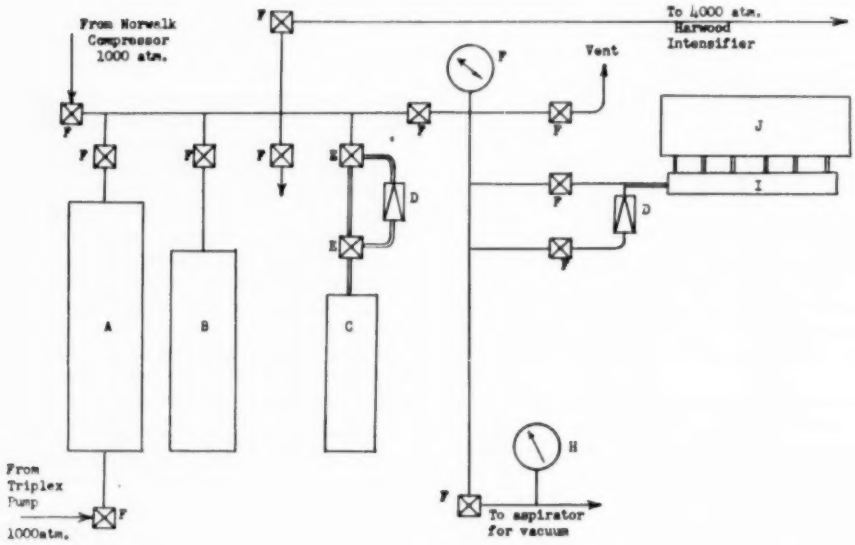

FIG. 9 DIAGRAM OF APPARATUS FOR EXPOSING TENSILE SPECIMENS TO GAS AT ELEVATED PRESSURE AND TEMPERATURE

A, 1/4 cu ft, 1000 atm storage
B, 1/4 cu ft, 1000 atm storage
C, 200 cc, 4000 atm storage
D, Check valves
E, Harwood 3-way 100,000 psi valves
F, Aminco 60,000 psi valves
H, Vacuum gage
I, Manifold
J, Furnace
——— Aminco 1/4 × 1/16 in. 60,000 psi tubing
═══ Harwood 3/16 × 1/16 in. 100,000 psi tubing

Experiments on Embrittlement at Room Temperature. In addition to the tests at elevated temperature, other tests were made at room temperature on specimens consisting of strips 1/2 in. × 4 in. × 16 gage, designed to yield information on the second aspect of the general problem. The strips were exposed to the gas in a vessel shown diagrammatically in Fig. 10. This is so constructed that the outer vessel of alloy steel which withstands the pressure is not exposed to hydrogen under pressure. The specimens rest on a shelf inside the inner stainless-steel vessel, above the level of the oil which is used to compress the gas from 1000 atm to higher pressures. Since the head of the vessel will be indirectly in contact with high-pressure hydrogen though its solubility in the oil, it was constructed of beryllium copper which was believed to be unaffected by hydrogen and could be heat-treated to give a yield strength of the order of 150,000 psi. The outer vessel and the intensifier could only be exposed to high-pressure hydrogen by virtue of diffusion of dissolved hydrogen through the oil. This is a very slow process and could never proceed very far in short-time tests because the process is interrupted frequently by venting the dissolved hydrogen to the atmosphere.

The exposed specimens were given a bending test in a simple, homemade, hand-operated bending device designed to give 180-deg bending. Several specimens of a given metal were exposed together and then tested to obtain an average number of bends before breakage. This figure then could be compared with a similar average obtained with unexposed specimens.

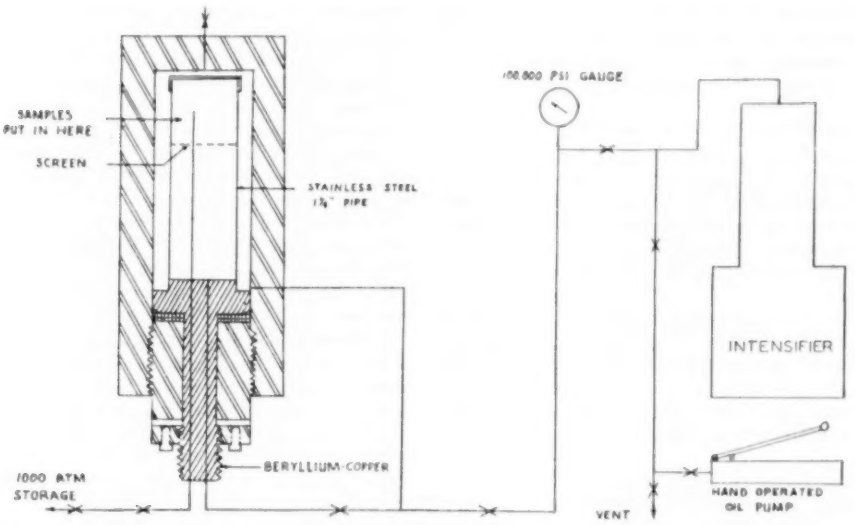

FIG. 10 DIAGRAM OF APPARATUS FOR TESTS OF HYDROGEN EMBRITTLEMENT AT ROOM TEMPERATURE

Only a very few tests have been made with this apparatus so that no results can be reported at this time. All we can say is that it works in the sense that relatively short exposures (a matter of hours) cause a very considerable effect on some samples when pressures of the order of 4000 atm are used.

Experiments on Permeability. The work on permeability is still in the stage of apparatus design and test. We have learned a few things about how not to build it but we have still to develop and prove a suitable design.

It is recognized that it may be exceedingly difficult to obtain reproducible results in these experiments because of the many variables which may affect the rate and because some of them will be difficult to control. For example, there are numerous variables connected with the previous history of the specimen such as its heat-treatment and the amount of cold-working it received which may be important. The nature of the surface may be significant. It is known that there is an "aging" effect which manifests itself in a decreasing rate of permeation with time. There may be flaws in the specimen which will give spurious results. What this means is that we cannot expect results of high precision but this is probably not too important since only gross differences are likely to be of interest and have practical application. It is planned to investigate a number of variables among which are the following:

(*a*) Nature of the gas; various pure gases and also gas mixtures.
(*b*) Pressure.
(*c*) Temperature.
(*d*) Composition of the metal.
(*e*) Previous history of the metal; cold-working, heat-treatment, etc.
(*f*) Condition of the surface.
(*g*) Strained versus unstrained metal.

The apparatus as now envisaged will consist of a tubular specimen surrounded by a jacket which can be evacuated and the whole assembly placed in an electric-tube furnace for temperature control. The rate of permeation will be measured by the rate of rise of pressure in the evacuated jacket.

Some thought has been given to the use of tritium, the radioactive isotope of hydrogen, as a tracer in these experiments.[4] It might be used simply as a sensitive means of determining how much hydrogen has permeated through a metallic membrane. A very sensitive means of measurement would have some advantages since the amount of gas permeating in any short interval of time is very small indeed and the problem of determining rate of permeation is a difficult one especially at the lower temperatures. We also had in mind the use of tritium to shed some light on the mechanism of permeation. Suppose one used tubular specimens and placed hydrogen containing tritium under pressure inside the tube. The amount of hydrogen retained in the specimen and its radial distribution conceivably might be measured by cutting off successive layers of the tube, dissolving each cut in acid and measuring the radioactivity. The radioactivity measurements would be a means of distinguishing the hydrogen that originated from the acid from that which permeated the metal.

In studying the effect of pressure on permeability, one usually increases the pressure on one side of the metal wall and maintains a low pressure on the other side. This results in an increase both in the total pressure and in the pressure gradient. For some purposes it would be desirable to increase the total pressure at constant pressure difference. It would be difficult in this case to measure the rate of permeation by the usual techniques but the use of a radioactive tracer offers a possible method.

When the pressure is not the same on the two sides of the diffusion membrane it will be strained. It might be of interest to measure also the permeability under a condition of no strain. This might be done by using an inert, i.e., nondiffusing gas, such as helium or argon, to equalize the total pressures while still maintaining a partial-pressure difference of hydrogen. In such a case the use of tritium to "tag" the hydrogen molecules in order to measure those which penetrate the wall of the metal, would be most useful.

One difficulty that arises in the use of tritium to trace hydrogen is the fact that these two isotopes are quite different in atomic weight and may have appreciably different rates of diffusion. However, it should not be too difficult to measure the relative permeation rates of hydrogen and tritium (actually the latter

[4] This was first suggested by Dr. S. W. Wan, formerly Research Associate in Chemical Engineering at Yale.

will be present almost entirely as HT molecules) by measurement of the total hydrogen (i.e., radioactive and nonradioactive) permeating by chemical or purely physical means and then to determine the tritium diffusing by radioactive measurement.

Compressibility of Gas Mixtures

Data on the volume (or density) of gases as a function of pressure, temperature and composition have many uses in engineering and particularly in the design of process equipment. Such data also are needed for the calculation of many thermodynamic properties. There is a dearth of data at pressures above 1000 atm even on pure gases and there is practically nothing on mixtures.

An investigation of nitrogen-hydrogen mixtures was completed and the results recently published (11). This particular system was chosen because of the industrial importance of the two gases and their use in the high-pressure synthesis of ammonia and also because of the availability of good data on the pure gases. The range of variables covered was as follows:

Temperature: 30 C to 125 C
Pressure: 1000 to 3500 atm
Composition: 25, 50, and 75 mole per cent nitrogen

The method of measurement used was the one commonly called the constant-volume method. It consists in isolating the gas in a vessel of fixed and known volume held at constant temperature in a thermostat, measuring its pressure, and then determining the mass by expanding the contents of the pressure vessel, or piezometer, into another known volume where the pressure will be approximately atmospheric. An accurate measurement of the pressure and temperature of the expanded gas gives the mass if the *pvt* relation for the gas is known at low pressure. Usually this is known with sufficient accuracy. Both volumes must be calibrated which is usually accomplished by filling them with a fluid whose density is accurately known at some specified condition. We used nitrogen gas to calibrate the high-pressure vessel and water for the low-pressure volume.

A schematic diagram of the apparatus is shown in Fig. 11.

The results may be presented in various ways but we have chosen to present them in Fig. 12 as Amagat factors A. This factor is the ratio of the pv product to the pv product of the same mass of gas at standard conditions (0 C and 760 mm). The figure shows clearly the extent of the deviation from the concept of the ideal gas since for such a gas the factors would all fall on a horizontal line at approximately $A = 1.072$. At the top

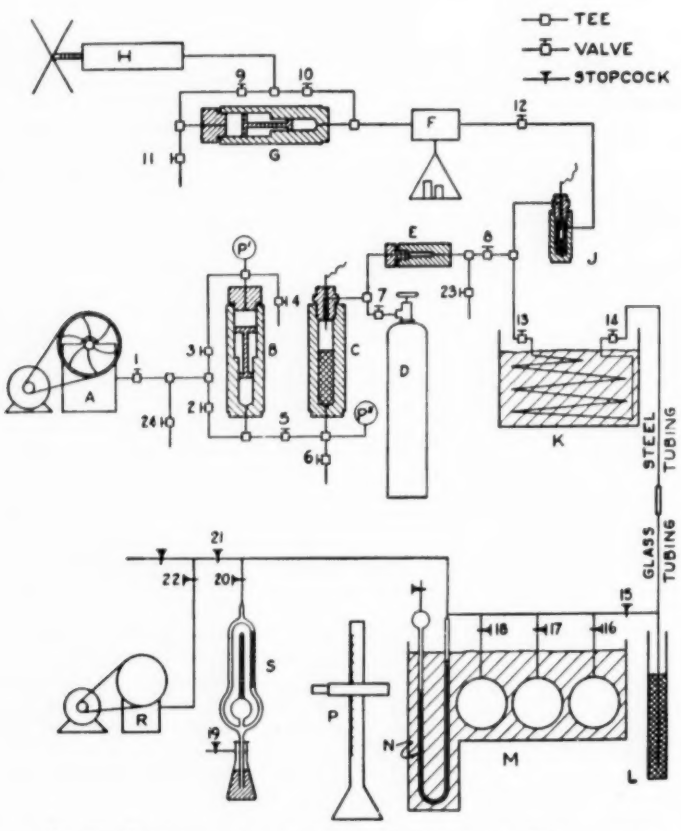

Fig. 11 Diagram of Apparatus for Compressibility Measurement

A	Triplex hydraulic pump	J	Mercury U-tube
B	Aminco intensifier	K	Constant-temperature oil bath
C	Gas-compression chamber	L	Safety tube
D	Gas-storage cylinder	M	Constant-temperature water bath
E	Drier	N	Mercury manometer
F	Dead-weight piston gage	P	Cathetometer
G	Small intensifier for piston gage	R	Vacuum pump
H	Cailletet pump	S	McLeod gage

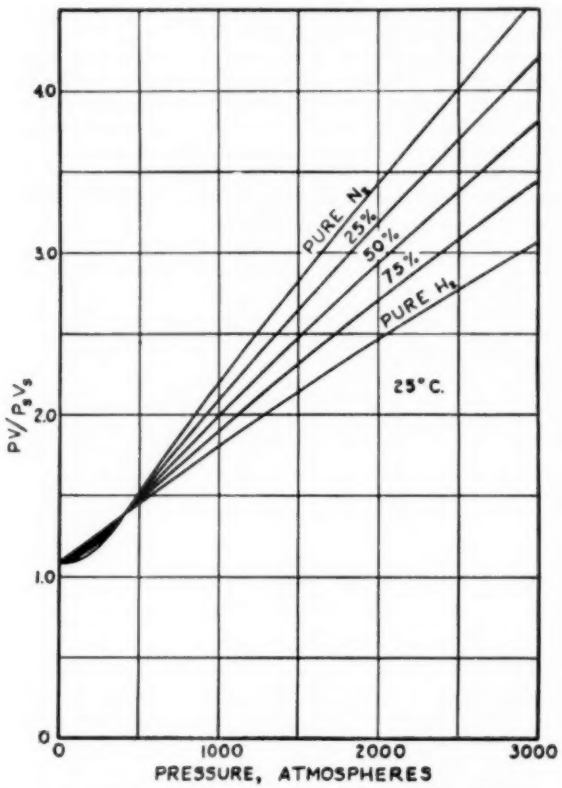

FIG. 12 AMAGAT COMPRESSIBILITY FACTORS FOR NITROGEN-HYDROGEN MIXTURES

pressure of 3000 atm it may be noted that the specific volume of nitrogen is over 4.5 times what it would be if the gas were ideal. Another interesting fact is that at these high pressures all the gas mixtures obey the ideal solution law (volumes are additive at constant pressure and temperature) within about the experimental error of the measurement (0.2 per cent).

Another investigation in this field is now in progress which involves *pvt* measurement on the ternary system: Nitrogen-hydrogen-ammonia over the temperature range 300-500 C and at pressures up to 3000 atm. One of the main objectives of this study is the prediction of the ammonia-synthesis equilibrium at pressures above 1000 atm. The qualitative effect of pressure on chemical equilibrium is well known from Le Chatelier's principle. The quantitative effect can be obtained from either of the following approaches: (*a*) Direct experimental measurement of the concentrations of the three gases under equilibrium conditions; or (*b*) calculation of the equilibrium constant at zero pressure from the free-energy change of the reaction followed by calculation of the effect of pressure on this constant with the aid of *pvt* data on the ternary system. There are advantages and disadvantages in both methods. Method (*a*) requires that the reaction be carried out and equilibrium established at all the pressures and temperatures for which the equilibrium conversion is desired. Among other things this involves establishment of equilibrium by use of an active catalyst and accurate sampling and analysis of the equilibrium mixture—two things that are not easy to accomplish. Method (*b*) is attractive in that it does not require that chemical equilibrium be established at all. The calculation of the zero-pressure equilibrium constant by means of thermal data is well known and treated in most texts on thermodynamics applied to chemistry and chemical engineering. The relation between the constant at any pressure and that at zero pressure is given by the equation

$$\ln \frac{K_p}{K_{p0}} = -\Sigma\nu \left[\frac{1}{RT} \int_0^p \left(V_i - \frac{RT}{p} \right) dp \right] \quad [6]$$

where K_p = equilibrium constant defined by the function

$$\frac{(x_L)^l (x_M)^m \ldots}{(x_A)^a (x_B)^b \ldots} p^{\Sigma\nu}$$

for the generalized reaction

$aA + bB + \ldots = lL + mM + \ldots$

K_{p0} is its value at $p = 0$

x_A, x_B, etc., are mole fractions of components A, B, etc.

p is total pressure

a, b, etc., are the stoichiometric numbers

$\Sigma\nu = l + m + \ldots - a - b \ldots$.

V_i is partial volume, $\left(\frac{\partial V}{\partial n_i} \right)_{p, T, n}$

where i refers to any component and n = number of moles.

The integral in Equation [6] can be evaluated with the aid of *pvt* data on the mixture. With the values of K_p obtained in this way, one is in a position to calculate the equilibrium conversion at any pressure and temperature and initial gas composition covered by the *pvt* data. For further details on such calculations a number of sources may be consulted (12, 13, 14).

The experimental method being used in this investigation is the same in principle as the one previously used but the presence of ammonia and the higher temperature range necessitated certain changes in detail which may be outlined as follows:

1 The long tubular constant-volume piezometer used in the measurements on the binary system was replaced by a thin-walled cylindrical vessel so disposed inside a heavy-walled vessel that the gas pressures inside and out would be approximately equalized. This was done to minimize hydrogen permeation through the metal wall which, it was feared, might be serious at these conditions. The differential pressure across the wall of the piezometer is indicated by an electric strain gage fastened to a diaphragm separating the two compartments and roughly controlled manually within about 200 atm.

2 A fused salt bath instead of an oil bath is used for temperature control.

3 Parts of the assembly outside of the thermostat are located in an air bath maintained at 140 C to prevent any condensation of liquid ammonia.

The apparatus assembly is practically complete at the present writing but no runs have yet been made. Most of the individual units have been tested and calibrated but unexpected difficulties keep cropping up to delay the operation of the entire setup as a functioning unit. It is of interest to note that an apparatus assembly of this character takes an inexperienced investigator, such as a graduate student, from 2 to 3 years to set up and put into operation. Once it is set up it should in theory be used for the study of a number of systems but, unfortunately, in university research this is seldom possible.

CHEMICAL REACTIONS AT HIGH PRESSURE

Pressure is an important variable in carrying out many reactions. It has an important effect both on the equilibrium and hence the maximum possible degree of conversion and on the reaction rate. Many important products of industry are now made by chemical reactions operating at high pressure which

would not be at all feasible at low pressures. The production of ammonia, methanol, urea, synthetic fuels, higher alcohols, and polyethylene are only a few of the many examples that could be cited. Several pressure reactions have been studied recently in this laboratory and some are now in progress.

In a university laboratory the investigation of a chemical reaction should be from as fundamental a standpoint as possible. Ideally, this means that one should study the equilibrium in the reaction and its kinetics. When these two factors have been investigated fully one presumably has a complete knowledge of the course of the reaction under all important conditions. In actual practice the problem is seldom as simple as that. In a simple reaction such as the synthesis of ammonia (simple in the sense that only one reaction is possible between the reactants) one can take this fundamental approach, but even in this case the kinetics are complex and still not well understood. This is probably true of all catalytic reactions in which the reaction occurs on the surface of a solid. In the case of most organic reactions the situation is further complicated by the many possible reactions that can occur with a given set of reactants. It is not very fruitful to study reaction rate or equilibrium until one knows just what reactions he is dealing with and under what conditions they will proceed to a measurable extent. For this reason much of the initial work in this field has to be of an exploratory character. It is not concerned with precise physicochemical measurements to "pin-point" an effect but rather with rough, order-of-magnitude studies designed to sketch the broad outlines of the problem and locate those areas which later may be investigated more minutely.

Ammonia-Synthesis Equilibrium. An investigation of the ammonia-synthesis equilibrium by the direct method (in contrast to the indirect one as previously discussed) was completed a few years ago but the results have not heretofore been published. Although this is a reaction of great industrial importance and is now conducted at pressures as high as 1000 atm, it is doubtful if higher pressures are of more than academic interest. The equilibrium was investigated at 400 C and 450 C over the pressure range 1000–3500 atm. The results obtained are shown in Fig. 13 in the form of mole per cent ammonia in the equilibrium mixture when starting with pure gases in stoichiometric ratio or when starting with ammonia. It is of interest to note that at 3500 atm the conversion to ammonia is nearly 100 per cent complete. This may be compared to the maximum conversion of 27 per cent which is obtained at 450 C and 200 atm, a condition commonly used in present industrial processes.

Before publishing this work in detail we are waiting for a confirmation of the results by the indirect method utilizing *pvt* data.

Hydration of Ethylene. Another reaction now under study in this laboratory is the ethylene-hydration reaction

$$C_2H_4 + H_2O = C_2H_5OH \quad [7]$$

which requires elevated pressures for appreciable yields. Along with this reaction the following one occurring simultaneously also must be considered

$$2C_2H_5OH = (C_2H_5)_2O + H_2O \quad [8]$$

Investigations of catalysts for Reaction [7] carried out in the vapor phase and of the equilibrium, completed some years ago in this laboratory, were among the first in this field. The results were published in two papers (15, 16). The present investigation is concerned with the heterogeneous system, i.e., both liquid and vapor phases present. We are particularly interested in the two-phase system because the available data on it are very meager and it appears, from approximate calculations we have made, that a more concentrated alcohol solution might be made in this way than with vapor-phase hydration.

One should, of course, be able to calculate the effect of pressure on this reaction from *pvt*- and phase-equilibrium data given the free-energy change at low pressure. Such calculations were attempted but the data available are so incomplete and so many assumptions had to be made that no faith whatever can be placed in the results. As in the case of ammonia synthesis one can either establish chemical equilibrium and determine equilibrium concentrations by sampling and analysis or one can measure *pvt*- and phase-equilibrium compositions and calculate the chemical equilibrium. In this case we chose the direct method.

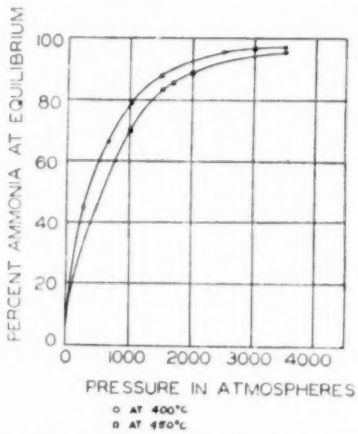

FIG. 13 EQUILIBRIUM CONCENTRATION OF AMMONIA AS FUNCTION OF PRESSURE AT TWO TEMPERATURES, FOR AMMONIA SYNTHESIS REACTION STARTING WITH INITIAL REACTANTS IN STOICHIOMETRIC RATIO

During the planning of the attack two major problems presented themselves. These were (*a*) the development of an accurate and reliable analytical method for determining ethanol and ethyl ether in the presence of each other in dilute aqueous solutions, and (*b*) the development of a suitable liner for the autoclave (Aminco shaking autoclave) to withstand the corrosive action of dilute mineral acids, particularly sulphuric acid, at temperatures of 300–350 C. The solution to (*a*) has been developed and thoroughly tested but it required much time and effort. Problem (*b*) enters because some of the best catalysts for this reaction are dilute mineral acids. Glass could be used as a liner for the high-pressure autoclave but because of the need for a thermocouple well and for gas and liquid-phase sampling tubes, the design of a suitable glass liner appeared out of the question and besides, its fragility is against it. We decided to try and design a metal liner. Very little information is available either in the literature or from manufacturers of metals on corrosion resistance to sulphuric acid at temperatures this high. Several metals seemed a possibility, particularly one or two of the stainless steels, titanium, tantalum, and some of the Hastelloys. After considerable study of the matter, Hastelloy B was chosen and a liner was designed and fabricated with the aid of the Haynes-Stellite Company. It has not yet been tested.

The question of a suitable catalyst is a very important one for this reaction. In addition to dilute solutions of various mineral acids we intend to try a sulphonic acid and a solid catalyst consisting of tungstic oxide supported on silica. During the war the Germans did considerable work on ethylene hydration in the presence of a liquid phase, some of which has been published in the FIAT reports. Various solid catalysts were tried but tung-

stic oxide appeared to be the best. It is doubtful in our minds if any solid catalyst will be as good as the mineral acids. We are not interested in the catalyst per se but must have a reasonably active one to approach equilibrium.

Water-Gas Reaction at High Pressure. Another reaction on which work has just been started is the water-gas reaction

$$CO + H_2O = CO_2 + H_2 \quad [9]$$

This is a very important industrial reaction usually carried out at about atmospheric pressure but there has been some recent industrial interest in the use of higher pressures. Since there is no change in number of moles in the reaction one is apt to conclude at first thought that pressure has no effect on the equilibrium. This would be true for ideal gases but for actual gases there is an effect though it may not be great. Although the reaction has been extensively studied at atmospheric pressure there appears to be only one published paper dealing with the effect of pressure on the equilibrium. Sartori and Newitt (17) found that the equilibrium constant, K_p, decreased about 20 per cent as the pressure increased from 1 to 100 atm. Our present plans call for investigating the reaction in the temperature range 380 to 450 C and the pressure range from 100 to 2000 atm with some variation also in initial reactant composition.

Other reactions such as

$$CO + 3H_2 = CH_4 + H_2O \quad [10]$$

and

$$CO_2 + C = 2CO \quad [11]$$

are also possible in this system, and one of the useful pieces of information that may come out of the investigation is something about the conditions which tend to favor or suppress these side reactions.

Reactions of Butadiene. We have started an investigation of certain reactions of butadiene that might be favored by pressure. This is very much of an exploratory research as so little is known about any such reactions that one cannot take the fundamental approach of studying equilibrium or reaction kinetics. Here we are simply trying to find out under what combination of conditions—temperature, pressure, concentration, catalyst, and so on—the proposed reaction will proceed to a measureable extent and what the side reactions will be. Butadiene was chosen because it is a reactive organic chemical which, almost a laboratory curiosity only 10 to 15 years ago, suddenly became available in very large quantities as a result of the synthetic-rubber program.

The reactions under consideration may be listed as follows:

1 With sulphur dioxide to yield cyclic sulphones.
2 With HCN to give nitriles and also possibly pyridine.
3 Diels-Alder reaction with ethylene to form cyclohexene.
4 Dimerization to 4-vinyl cyclohexene or to cyclo-octadiene.
5 With formaldehyde to produce a variety of possible compounds including alcohols, adipaldehyde, cyclic formals, and a dioxane.
6 The oxo reaction—hydrogen, carbon monoxide, and an olefin reacting to yield an aldehyde.
7 Hydration to tetrahydrofuran, possibly in two steps with 1, 4 butane diol as the intermediate.
8 With hypochlorous acid to give the isomeric chlorobutene-ols which could probably be converted to tetrahydrofuran.
9 Reaction with cyanogen and nitriles to give various products such as 2-cyanopyridine and 2-ethyl pyridine.
10 With sulphur or hydrogen sulphide to make thiophene.
11 With ammonia to produce pyrrole or acetonitrile and higher nitriles.
12 Reaction with steam to yield furan and hydrogen.

Most of the products of these reactions are either substances of industrial importance or of potential importance if they could be produced in good yields. Not all of the reactions would need to be carried out at elevated pressures or be favored by pressure but pressure certainly would be an important factor in some of them.

The experimental work has been started with a study of the reaction with hypochlorous acid (No. 8) the latter being produced in situ by bubbling CO_2 through a suspension containing calcium hypochlorite and butadiene and sometimes chloroform as a solvent. Most of the runs were made under pressure in a rocking autoclave with a glass liner. The product has been found to consist of a mixture of the 1, 2 and the 1, 4 monochlorohydrins and the dichlorohydrin. The relative amount varied with the conditions but the dichloro and the 1, 2 mono isomer predominated. Low temperatures, around 4–5 C, gave the best yields. The work is being continued to find the best conditions for good yields of the chlorohydrins, after which some of the other reactions will be studied.

Reactions of Carbon Monoxide. A number of interesting and important possible reactions may be mentioned such as the following:

1 with dihydric alcohols to give dibasic acids
  CO + 1,4 butane diol → adipic acid is just one example
2 with cyclohexanol to give the corresponding carboxylic acid
3 with phenol to give benzoic acid or salicylaldehyde
4 with anilin to form benzamide
5 with chlorobenzene (also the bromo- and iodo-benzenes) and water to yield acids
  Typical reactions are
  chlorobenzene + CO + H_2O → benzoic acid + HCl
  dichlorobenzene + CO + H_2O → terephthalic acid + HCl
6 with tetrahydrofuran and water to give adipic acid
7 with acetone to yield methacrylic acid
8 with cyclohexyl chloride and water to form cyclohexane carboxylic acid

Reactions 1 through 5 have been tried in this laboratory and the others are about to be tried. Catalysts used are nickel carbonyl, boron trifluoride, and benzoyl peroxide. Pressures vary from 1000 psi to 5000 psi and in the future work it is proposed to work at pressures up to 15,000 psi and possibly higher. Some work was done on reaction 7 using boron trifluoride as the catalyst and no methacrylic acid obtained, but in the proposed work use will be made of nickel carbonyl whose remarkable catalytic properties came to light only after the war. The possibility of obtaining the desired product hinges on the postulate that the acetone is an equilibrium mixture of the keto and enol forms. Work on reaction 1 using the butane diol and on reaction 6 was started in this laboratory but the experiments had to be stopped before any results of value were obtained.

Reaction 2 took place with yields up to 65 per cent.

Reaction 3 gave the aldehyde rather than the acid.

Reaction 4 took place but with very small yield.

Several of the reactions of series 5 gave appreciable yields. For example, paradichlorobenzene yielded 33 per cent of mixed p-chlorobenzoic and terephthalic acids.

Partial Oxidation of Aromatic Hydrocarbons. The possibility of partial vapor-phase oxidation of benzene to phenol by oxygen gas and of many related reactions has intrigued researchers for many years. In spite of all the work that has been done very little has been accomplished toward achieving the partial oxidation. In some cases investigators claimed high yields of phenol but the conversions per pass were very low. Most of the work had been performed at low pressures and the motivating factor behind our work was the thought that elevated pressures might favor the survival of the intermediate products of oxidation. It was felt that increased pressure would increase reaction rates

and thereby make possible the use of lower temperatures. At lower temperatures the relative rates of the partial and the complete oxidation reactions might be so altered that appreciably higher yields of intermediates would be obtained.

The experimental data obtained were rather meager. So much time was devoted to overcoming troubles with the apparatus that little time was available to the student to vary many of the conditions. Runs were made under a limited set of conditions at a maximum pressure of about 200 atm. About the only conclusion we are justified in drawing is the very general one that conversions to phenol were very low under all conditions tried. Although a number of the important conditions such as pressure, temperature, ratio of air to benzene, and contact time were varied, the results are not conclusive enough to give the effect of any one of them. Further work on benzene at higher pressures and on other aromatic hydrocarbons as well as on naphthenic hydrocarbon appears desirable.

Phase Equilibria at High Pressures

This is a very wide and largely uncultivated field of investigation. Some years ago we completed an investigation of the pressure-temperature-composition (*ptx*) relations in the liquid-vapor systems: nitrogen-benzene, carbon dioxide-benzene, and nitrogen-methanol. The conditions under which these binary systems were studied are given in Table 2.

TABLE 2 CONDITIONS FOR STUDY OF BINARY SYSTEMS

System	Temperature deg C	Pressure, atm
CO_2-benzene	10–60	1–95
N_2-benzene	30–125	60–300
N_2-benzene	50–150	100–1000
N_2-methanol	50	200–500

The first two sets of results have been published (18, 19) but those on nitrogen-benzene at the higher pressures and on nitrogen-methanol are still unpublished (20). The most recent work, just published (21), is that on the system nitrogen-ammonia at pressures up to 3000 atm which was concerned primarily with the critical phenomena and the immiscibility phenomena that occur when the system is composed of two substances whose critical temperatures differ widely. In this case we have nitrogen with a critical temperature of —146 C and ammonia with a critical temperature of +132 C. We chose this particular system for three main reasons:

1 The composition was easily determined by chemical analysis.

2 Data were already available up to 1000 atm and this was a logical extension to a higher pressure.

3 Recent work of Russian investigators on this and a few other systems revealed some interesting and unusual phenomena. One of these is the existence of a gas-gas equilibrium or immiscibility in phases ordinarily regarded as both gaseous, at pressures higher than those at which the usual gas-liquid equilibria are observed. The other is the so-called "barotropic phenomenon" which consists in the fact that the initially more dense of the two phases becomes the less dense phase as the pressure is increased. This is something like saying that in the case of a liquid and gas phase in equilibrium the liquid changes to the gas and the gas to a liquid as pressure is increased.

Neither of these phenomena is very new; the gas-gas immiscibility was predicted by Van der Waals (22) nearly 60 years ago and discussed in some detail from a theoretical viewpoint by Onnes and Keesom (23). No experimental observation was reported, however, until the appearance of the paper by Krichevsky and Bolshakov in 1941 (24). The barotropic phenomenon was first discovered in 1906 by Onnes (25) while working with mixtures of hydrogen and helium at liquid-hydrogen temperatures. He observed visually that when two phases were in co-existence at a pressure a little below 49 atm and then the pressure increased, the helium-rich lighter phase became the heavier phase. In other words a "gas" phase sank as a bubble through the "liquid" phase. By alternate lowering and raising of the pressure he could cause the bubble to rise or sink at will.

A search of the literature revealed only 12 systems whose phase equilibria have been investigated at pressures above 1000 atm and the highest pressure used was 9650 atm. A complete list of these literature references is given in the paper by Lindroos and Dodge (21). It may be noted that two other systems besides the N_2–NH_3 one, namely, ammonia-methane and nitrogen-sulphur oxide, were found by Russian investigators to exhibit limited miscibility in a region that would normally be regarded as a homogenous gas-phase region.

A discussion of this so-called "gas-gas" equilibrium in the light of the various types of critical locus curves of binary systems is given by Lindroos and Dodge (21) and their paper should be consulted for further details on this phenomenon and on the experimental methods used.

The results, presented in tabular form, and also as *px*, *tx*, and *pt* curves for the system, are in qualitative agreement with those of the Russian investigators but there is considerable disagreement in the quantitative data.

Since the work of Lindroos and Dodge on the one system, N_2-NH_3, no further work has been done at this laboratory. Much more remains to be done even with this system to explore fully the critical locus curve. At the highest pressure reached by the Russians (9650 atm) the system is still heterogeneous and one wonders whether at still higher pressures another critical point will be reached and the system become homogeneous once more. It would be of interest to replace the ammonia by many other substances whose critical temperatures are far removed from that of nitrogen and likewise to replace the nitrogen by other gases of low critical temperature such as oxygen, carbon monoxide, argon, neon, helium, and hydrogen. Unfortunately for progress in this field, it involves difficult techniques so that results are very slow to accumulate and as far as we can see at present are purely of scientific interest with no practical bearing whatever.

BIBLIOGRAPHY

1 "Hydrogen Embrittlement of Steel. Review of the Literature," by R. W. Buzzard and H. E. Cleaves, U. S. Bureau of Standards, Circular No. 511, September 24, 1951.

2 "Hydrogen in Metals," by D. P. Smith, University of Chicago Press, Chicago, Ill., 1948.

3 "Diffusion in and Through Solids," by R. M. Barrer, Cambridge University Press, Cambridge, England, 1941.

4 "Gases and Metals," by C. J. Smithells, John Wiley & Sons, Inc., New York, N. Y., 1937.

5 "Atom Movements," American Society for Metals, Cleveland, Ohio, chapter 4, 1951.

6 "Hydrogen Attack on Metals at High Temperatures and Pressures," by J. Schuyten, *Corrosion and Material Protection*, vol. 4, September–October, 1947, pp. 13–18.

7 "The Compressibility of Five Gases to High Pressures," by P. W. Bridgman, Proceedings of the American Academy of Arts and Sciences, vol. 59, 1924, pp. 173–211. (Mainly on page 175.)

8 "The Penetration of Hydrogen Through Steel at Four Thousand Atmospheres," by T. C. Poulter and Lester Uffelman, *Physics*, vol. 3, 1932, pp. 147–148.

9 "The Mechanism of Cavitation Erosion," by T. C. Poulter, *Journal of Applied Mechanics*, Trans. ASME, vol. 64, 1942, pp. A-31 to 37.

10 "Wasserstoffdurchlässigkeit und Wasserstoffentkohlung von Stählen, Armco-Eisen, Kupfer, Nickel und Aluminum bei höheren Drücken," by W. Baukloh and H. Guthmann, *Zeitschrift für Metallkunde*, vol. 28, 1936, pp. 34–40.

11 "Compressibilities of Mixtures of Hydrogen and Nitrogen Above 1000 Atmospheres," by C. O. Bennett and B. F. Dodge, *Industrial and Engineering Chemistry*, vol. 44, 1952, pp. 180–185.

12 "Chemical Engineering Thermodynamics," by B. F. Dodge, McGraw-Hill Book Company, Inc., New York, N. Y., 1944.

13 "The Computation of the Thermodynamic Properties of Real Gases and Mixtures of Real Gases," by J. A. Beattie, *Chemical Reviews*, vol. 44, 1949, pp. 141–192.

14 "The Empirical Calculation of the Fugacities in Gaseous Mixtures. II. Its Relation to the Tangents on Certain Thermodynamic Diagrams. Approximate Equations for Some Important Thermodynamic Properties of Gas Mixtures," by L. J. Gillespie, *Physical Review*, vol. 34, 1929, pp. 1605–1614.

15 "Catalytic Vapor-Phase Hydration of Ethylene," by F. J. Sanders and B. F. Dodge, *Industrial and Engineering Chemistry*, vol. 26, 1934, p. 208.

16 "Vapor-Phase Hydration of Ethylene," by R. H. Bliss and B. F. Dodge, *Industrial and Engineering Chemistry*, vol. 29, 1937, p. 19.

17 Publication No. 222/92 of the Institution of Gas Engineers, Sartori and Newitt, London, England, 1952.

18 "Solubility of Carbon Dioxide in Benzene at Elevated Pressure," by S. W. Wan and B. F. Dodge, *Industrial and Engineering Chemistry*, vol. 32, 1940, p. 95.

19 "The System Benzene-Nitrogen," by Philip Miller and B. F. Dodge, *Industrial and Engineering Chemistry*, vol. 32, 1940, p. 434.

20 Dissertation presented to Faculty of the Yale School of Engineering, by E. Groth, 1941.

21 "Phase Equilibria at High Pressures," The System: Nitrogen-Ammonia at Pressures Above 1000 Atm, by A. E. Lindroos and B. F. Dodge, *Chemical Engineering Progress*, Symposium Series No. 3, vol. 48, 1952, pp. 10–17.

22 "Over de afwezigheid van of wijziging in de kritische verschijnselen voor een mengsel, ten gevolge van het bestaan der lengteplooi op het ψ-vlak bij hoogere temperaturen," by J. D. van der Waals, Verslagen der Zittingen van de Wis- en Natuurkundige Afdeeling der Koninklijke Akademie van Wetenschappen, Amsterdam, Holland, 1894–1895, pp. 133–137.

23 "Contributions to the Knowledge of the ψ-surface of Van der Waals. XV. The case that one component is a gas without cohesion with molecules that have extension. Limited miscibility of two gases," H. Kamerlingh Onnes and W. H. Keesom, Proceedings of the Koninklijke Akademie van Wetenschappen, Amsterdam, Holland, vol. 9, 1906, pp. 786–798, vol. 10, 1907, pp. 231–237.

24 "Heterogeneous Equilibria in the Ammonia-Nitrogen System at High Pressures," by I. R. Krichevsky and P. Bolshakov, *Acta Physicochim*, USSR, vol. 14, 1941, pp. 353–364.

25 "A Gas That Sinks in a Liquid," by H. Kamerlingh Onnes, Proceedings of the Koninklijke Akademie van Wetenschappen, Amsterdam, Holland, vol. 9, 1906, pp. 459–460.

Additional References

In addition to the foregoing the following papers on high pressure and related subjects from the Chemical Engineering Department, Yale University, are cited:

"Decomposition of Methanol Over Catalysts Composed of Oxides of Zinc and Chromium," by J. R. Huffman and B. F. Dodge, *Industrial and Engineering Chemistry*, vol. 21, 1929, p. 1056.

"Note on the Methanol Equilibrium," by B. F. Dodge, *Industrial and Engineering Chemistry*, vol. 22, 1930, p. 89.

"The Methanol Equilibrium," by E. F. von Wettberg, Jr., and B. F. Dodge, *Industrial and Engineering Chemistry*, vol. 22, 1930, p. 1040.

"Designing Equipment for High Pressures," by B. F. Dodge, *Chemical and Metallurgical Engineering*, vol. 38, 1931, pp. 241–243.

"Physico-Chemical Factors in High-Pressure Design," by B. F. Dodge, *Industrial and Engineering Chemistry*, vol. 24, 1932, p. 1353.

"The Equilibrium Between Carbon Monoxide, Hydrogen, Formaldehyde and Methanol," I. The Reactions $CO + H_2 = HCOH$ and $H_2 + HCOH = CH_3OH$, by R. H. Newton and B. F. Dodge, *Journal of the American Chemical Society*, vol. 55, 1933, p. 4747.

"The Equilibrium Between Carbon Monoxide, Hydrogen, Formaldehyde and Methanol," II. The Reaction $CO + 2H_2 = CH_3OH$, by R. H. Newton and B. F. Dodge, *Journal of the American Chemical Society*, vol. 56, 1934, p. 1287.

"Zinc Oxide—Chromium Oxide Catalysts for Methanol Synthesis," by M. C. Molstad and B. F. Dodge, *Industrial and Engineering Chemistry*, vol. 27, 1935, p. 134.

"Calculation of Pressure Effect on Liquid-Vapor Equilibrium in Binary Systems," by R. H. Newton and B. F. Dodge, *Industrial and Engineering Chemistry*, vol. 29, 1937, p. 718.

"Compressibilities of Nitrogen-Carbon Dioxide Mixtures," by R. E. D. Haney and Harding Bliss, *Industrial and Engineering Chemistry*, vol. 36, 1944, pp. 985–987.

"The P-V-T-X Relationships for the System: Methane-Isopentane," by E. H. Amick, W. B. Johnson, and B. F. Dodge, *Chemical Engineering Progress*, Symposium Series No. 3, vol. 48, 1952, pp. 65–71.

"The P-V-T-X Relations of the Toluene-n-Hexane System," by L. M. Watson and B. F. Dodge, *Chemical Engineering Progress*, Symposium Series No. 3, vol. 48, 1952, pp. 73–81.

Influence of Residual Stress on Behavior of Thick-Wall Closed-End Cylinders

By J. H. FAUPEL[1] AND A. R. FURBECK,[1] WILMINGTON, DEL.

Results obtained from macro residual-stress tests, internal-pressure tests, and mechanical property tests on Cr-Ni-Mo-V steel, SAE 3320, SAE 4340, and SAE 1045 steel cylinders[2] are presented. The presence of macro residual stresses appears to influence only initial yielding at the bore of cylinders; the effect of this residual stress can be allowed for in the formula used to predict the internal pressure at initial yielding at the bore. Methods also are presented for predicting, approximately, the internal pressures at full wall yielding (overstrain) and bursting. Finally a method is suggested for predicting the pressure-strain curve for heavy-wall cylinders from an analysis of tensile-test data.

Nomenclature

The following nomenclature is used in the paper:

A_0 = initial cross-sectional area,[3] sq in.
A = cross-sectional area[3] (variable), sq in.
E = Young's modulus (taken as 30×10^6 psi for steel)
R = wall ratio of hollow cylinder (OD/ID)
a = bore radius of hollow cylinder, in.
b = radius to outside of hollow cylinder, in.
d = differential sign
ln = symbol for natural logarithms
p = internal pressure, psi
p_b = bursting pressure of cylinder, psi
$(p_b)_i$ = lower limit of bursting pressure of cylinder, psi
$(p_b)_s$ = upper limit of bursting pressure of cylinder, psi
p_o = pressure at overstrain through wall of cylinder, psi
p_y = elastic breakdown pressure at bore of cylinder, psi
r = radius (variable), in.
$\alpha = (\epsilon_z + \mu\epsilon_h)$, in/in
$\beta = \epsilon_z/\epsilon_h$
$\theta = (\epsilon_h + \mu\epsilon_z)$, in/in
μ = Poisson's ratio
ϵ_h = hoop strain in cylinder, in/in
$(\epsilon_h)_b$ = hoop strain in cylinder at bursting pressure, in/in
$(\epsilon_h)_{bi}$ = hoop strain in cylinder at bore at bursting pressure, in/in
$(\epsilon_h)_{bs}$ = hoop strain in cylinder at surface at bursting pressure, in/in
$(\epsilon_h)_o$ = hoop strain in cylinder at overstrain pressure, in/in
$(\epsilon_h)_{oi}$ = hoop strain in cylinder at bore at overstrain pressure, in/in
$(\epsilon_h)_{os}$ = hoop strain in cylinder at surface at overstrain pressure, in/in
$(\epsilon_h)_y$ = hoop strain in cylinder at elastic breakdown pressure, in/in
$(\epsilon_h)_{yi}$ = hoop strain in cylinder at bore at elastic breakdown pressure, in/in
$(\epsilon_h)_{ys}$ = hoop strain in cylinder at surface at elastic breakdown in/in
ϵ_r = radial strain in cylinder, in/in
ϵ_u = strain in tension at ultimate strength, in/in
ϵ_y = strain in tension at 0.01 per cent offset yield strength, in/in
ϵ_z = longitudinal strain in cylinder, in/in
σ_h = hoop stress in cylinder, psi
σ_h' = residual hoop stress in cylinder, psi
σ_r = radial stress in cylinder, psi
σ_r' = residual radial stress in cylinder, psi
σ_u = ultimate tensile strength, psi
σ_y = yield strength in tension at 0.01 per cent strain offset, psi
σ_z = longitudinal stress in cylinder, psi
σ_z' = residual longitudinal stress in cylinder, psi

Introduction

During the course of research work on the behavior of heavy-wall cylinders under internal pressure it became evident that macro-residual stresses (1)[4] introduced by heat-treatment could have a significant effect on dilation characteristics of these cylinders. These residual stresses can be as high as the yield strength of the material and also frequently act in the same direction as the stresses induced by internal pressure. Consequently, it was desirable to study the effects of residual stress and to determine how such stresses can be allowed for in engineering work.

Although some work on autofrettage (2) has been reported in the literature, correlation of dilation characteristics of heavy-wall cylinders subjected to internal pressure with the residual stresses in the cylinder wall apparently has not been studied. Consequently, research work was undertaken for this purpose and the present paper is a brief account of the results obtained.

When a steel cylinder is quenched from the austenitizing temperature there are two opposing stress effects which are responsible for the final distribution of the macro residual heat-treatment stress in the material (3, 4, 5). The cooling produces a stress effect as illustrated in Fig. 1 (4), and this is opposed by the stress effect associated with the transformation from austenite to martensite.[5] For a material like Type 304 stainless steel, which is "annealed" by quenching from 2000 F, the final distribution of residual stress is determined by cooling alone since this material undergoes no phase transformation.

---

[1] Engineering Research Laboratory, E. I. du Pont de Nemours and Company, Inc. (Mr. Fraupel is a member of ASME.)

[2] Most of the cylinders tested were approximately 4.125 in. OD, with a wall thickness of 1.30 in.

[3] In the Sachs equations, [1], [2], [3], A_0 given later, is the initial cross-sectional area of the cylinder including the bore. A is the cross-sectional area of the bore following a machine cut.

Contributed by the Industrial Instruments and Regulators Division of The American Society of Mechanical Engineers and presented at The Seventh National Instrument Conference, Cleveland, Ohio, September 9–10, 1952.

Note: Statements and opinions advanced in papers are to be understood as individual expressions of their authors and not those of the Society. Manuscript received at ASME Headquarters, June 19, 1952. Paper No. 52—IIRD-9.

[4] Numbers in parentheses refer to Bibliography at end of paper.

[5] The only phase transformation considered in this paper is the austenite to martensite reaction which is accompanied by an increase in volume. Micro residual stresses involved as a result of transformation, and which may be determined by x-ray means, are not considered in this paper.

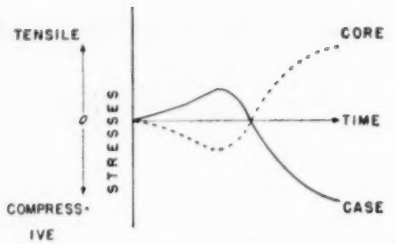

FIG. 1 SCHEIL'S REPRESENTATION OF STRESS VARIATION DURING COOLING OF A CYLINDER OF STEEL WITHOUT PHASE TRANSFORMATION (4)

EXPERIMENTAL PROCEDURE

Material Tested. The steels employed and their heat-treatments are listed in Table 1. In the selection of materials for investigation it was desired to test a range of composition and strength levels.

In the heat-treatment, three cylinders of each material were treated under identical conditions. One cylinder was then used for the residual-stress test, the second for the static internal-pressure test, and the third one was used to determine the mechanical properties resulting from heat-treatment as well as to provide material for microscopic examination. For each material used, several different heat-treatment conditions were employed; that is, some were heat-treated as hollow cylinders while others were treated as solid cylinders. The details of these treatments are given in column 3 of Table 2.

In general, the mechanical properties of the heat-treated materials were obtained on four specimens at the bore zone in the transverse direction, Table 2. These properties are considered critical since the peak elastic-range stresses in a cylinder under internal pressure are in the transverse direction at the bore (6).

Internal-Pressure Testing. The cylinders for internal-pressure testing were processed in accordance with the procedure outlined in the following:

The $1^1/_2$-in-ID × 36-in-long test cylinder was made up as shown in Fig. 2, and was tested under hydrostatic pressure after attaching 20 SR-4 strain gages to the outside of the cylinder (arranged as shown in Fig. 3), to measure the increase in diameter

TABLE 1 OUTLINE OF THERMAL TREATMENTS

Item	Material applied to	Thermal treatments
1	Cr-Ni-Mo-V steel (0.35 C; 0.73 Mn; 0.48 Ni; 1.39 Cr; 0.13 V; 0.52 Mo; 0.20 Si)	Heated at 1525 F; cooled to 750 F at rate of 30 F/hr, and from 750 F to room temperature in air at uncontrolled rate
2	Cr-Ni-Mo-V steel	Heated at 1600 F for 3 hr, quenched in oil, drawn at 1000 F for 3 hr and quenched in water
3	SAE 3320 steel (0.23 C; 0.35 Mn; 3.60 Ni; 1.62 Cr; 0.03 Mo; 0.49 Si)	Heated at 1580 F for 4 hr, quenched in oil, drawn at 970 F for 4 hr, air-cooled, redrawn at later date at 1200 F for 4 hr, and quenched in water
4	SAE 4340 steel (0.40 C; 0.75 Mn; 1.87 Ni; 0.77 Cr; 0.26 Mo; 0.27 Si)	Heated at 1600 F, quenched in oil, drawn at 1200 F, and furnace-cooled
5	SAE 4340 steel	Heated at 1650 F, air-cooled, drawn at 1200 F, and quenched in water
6	SAE 4340 steel	Heated at 1650 F, air-cooled, drawn at 1200 F, and furnace-cooled
7	SAE 1045 steel (0.45 C; 0.70 Mn; 0.23 Si)	Heated at 1600 F, quenched in oil, drawn at 800 F, and furnace-cooled

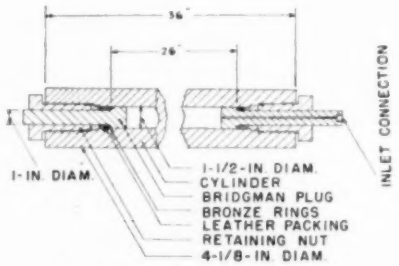

FIG. 2 TEST-CYLINDER ASSEMBLY

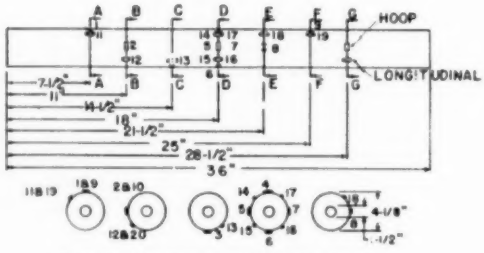

FIG. 3 LOCATION OF STRAIN GAGES ON TEST CYLINDER

TABLE 2 SUMMARY OF TRANSVERSE MECHANICAL PROPERTIES AT BORE ZONE OF CYLINDERS

1	2	3	4	5	6	7	8
Cylinder no.	Material	Processing treatment[a]	Yield strength, psi, 0.01% offset	Yield strength, psi, 0.20% offset	Ultimate strength, psi	Elongation in 1 in., per cent	Reduction in area, per cent
1	Cr-Ni-Mo-V steel	Item 1, Table 1, treated as solid 3-in-OD bar and machined to 1.00 in. ID × 2.75 in. OD	47000	47800	93100	16	23
2	Cr-Ni-Mo-V steel	Item 2, Table 1, same processing as preceding	141200	159800	177500	9	20
3	SAE 3320	Item 3, Table 1, treated as solid 4.5-in-OD bar and machined to 1.50 in. ID × 4.125 in. OD	74300	79500	105400	24	51
4	SAE 4340	Item 4, Table 1, same processing as SAE 3320 (cylinder No. 3)	99400	103900	124100	16	31
5	SAE 4340	Item 6, Table 1, same processing as cylinder No. 3	83400	86500	115300	17	33
6	SAE 4340	Item 5, Table 1, treated as solid 2-in. OD bar and machined to 0.50 in. ID × 1.25 in. OD	119600	115600[b]	124600	22	50
7	SAE 1045	Item 7, Table 1, treated as plugged-end hollow cylinder 1.25 in. ID × 4.5 in. OD, machined to 1.50 in. ID × 4.125 in. OD	57500	60900	101800	18	28
8	SAE 1045	Item 7, Table 1, treated as hollow cylinder 1.25 in. ID × 4.5 in. OD, quenching done by immersing bar in oil and simultaneously inserting a perforated pipe through bore for bore quenching by oil under pressure. Machined to 1.50 in. ID × 4.125 in. OD	76800	81600	122200	13	28

[a] In descriptions that follow, OD is outside diameter and ID is inside, or bore diameter.
[b] Lower yield point—used in calculations for data in other tables.

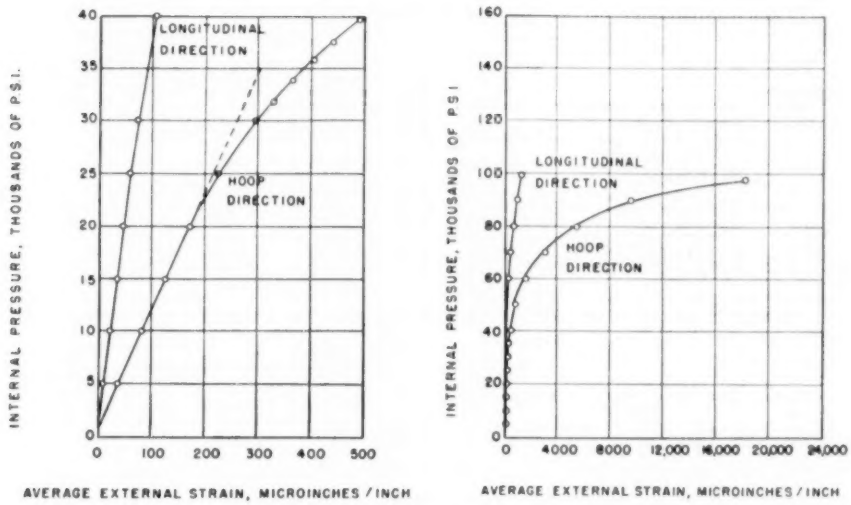

FIG. 4 PRESSURE-STRAIN CHARACTERISTICS OF ANNEALED CR-NI-MO-V STEEL

and length as pressure was increased. Strains were recorded for small increments of pressure. Pressures at initial yielding of the material at the bore, at overstrain through the wall, and bursting were determined. Initial yielding of the bore of the cylinder was taken as the end of the straight-line portion of the pressure-strain curve. The pressure at which overstrain through the wall occurred was determined from the same plot by using an analysis described later in the paper. The bursting pressure recorded is the maximum pressure reached within the cylinder before failure.

Testing of the cylinders was done by raising the pressure to a predetermined level and holding it constant while recording the data from the 20 strain gages. Strain data were recorded at 2000-psi intervals in the elastic range and at 1000-psi intervals in the plastic range.

When testing cylinders in the plastic range, it was necessary to increase the time between readings in order to allow the material to work-harden and reach equilibrium at each pressure for which strain data were recorded. At increments of 1000 psi, $^1/_2$ to $^3/_4$ hr was required between readings. This rate of strain is much lower than that used in the tensile tests, where a rate of 20,000 microin/min was used. For a ductile cylinder, approximately 6 to 8 hr were required to complete a test after initial yielding at the bore.

Internal pressure-external strain curves were plotted from the data recorded. Fig. 4 shows a typical set of curves obtained. Only one set of curves is included in this paper, but the external hoop strains corresponding to initial yielding at the bore, overstrain through the wall, and bursting are recorded in Tables 3, 4, and 5, respectively, for all cylinders tested.

Residual-Stress Determination. Each of the cylinders used for residual-stress measurements was provided with twelve resistance-wire strain gages placed in the central 10-in. section of the 15-in-long cylinder, six in the longitudinal direction, and six in the hoop direction, Fig. 5. These gages were spaced equally

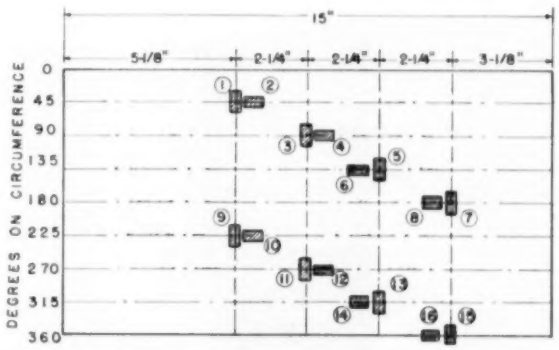

FIG. 5 DEVELOPED SURFACE OF CYLINDER FOR RESIDUAL STRESS TEST, SHOWING ARRANGEMENT OF SR-4 TYPE A-1 ELECTRIC STRAIN GAGES

TABLE 3 SUMMARY OF OBSERVED AND CALCULATED ELASTIC BREAKDOWN PRESSURES

1	2	3	4		5	6	7	8	9	10
			Residual stress at bore, psi		External hoop strain at elastic breakdown,	Elastic breakdown pressure, psi			Error based on observed value, per cent	
Cylinder no.	Material and treatment (see Table 2)	Wall ratio	Longitudinal	Hoop	microinches/in.	Observed[a]	Calculated Equation [7]	Calculated Equation [4]	Equation [7]	Equation [4]
1	Annealed Cr-Ni-Mo-V steel	2.74	0	0	180	21000	23500	23500	12	12
2	Quenched-and-tempered and quenched Cr-Ni-Mo-V steel	2.74	0	0	620	70000	70800	70800	1	1
3	Quenched-and-tempered and quenched SAE 3320	2.74	45000	35000	185	21000	19400	37150	−8	77
4	Quenched-and-tempered SAE 4340	2.75	0	0	400	45000	49800	49800	11	11
5	Normalized-and-tempered SAE 4340	2.75	0	0	390	43700	41800	41800	−4	−4
6	Quenched-and-tempered and quenched SAE 4340	2.50	32000	26000	450	42500	44500	56000	10	31
7	Quenched-and-tempered SAE 1045	2.75	20000	20000	195	21300	20300	28800	−5	35
8	Bore-surface quenched-and-tempered SAE 1045	2.75	−37000	−34000	490	57500	55300	38500	−4	−33

[a] The observed elastic breakdown pressures are taken as that pressure on the pressure-external hoop strain curve where departure from linearity occurs.

TABLE 4 SUMMARY OF OBSERVED AND CALCULATED OVERSTRAIN PRESSURES

Cylinder no.	Material and treatment (see Table 2)	Wall ratio	Eternal hoop strain at overstrain, microinches/in.	Observed overstrain pressure, psi	Calculated overstrain pressure psi Equation [27]	Error based on observed value, per cent
1	Annealed Cr-Ni-Mo-V steel	2.74	1550	58000	54400	−7
2	Quenched-and-tempered and quenched Cr-Ni-Mo-V steel	2.74	>4000	200000	163800	−18
3	Quenched-and-tempered and quenched SAE 3320	2.74	2200	84000	86200	3
4	Quenched-and-tempered SAE 4340	2.75	3600	117000	115200	−2
5	Normalized-and-tempered SAE 4340	2.75	2950	99000	97200	−2
6	Quenched-and-tempered and quenched SAE 4340	2.50	3335	111000	122100	10
7	Quenched-and-tempered SAE 1045	2.75	2025	66500	67000	1
8	Bore-surface quenched-and-tempered SAE 1045	2.75	2335	87750	89500	2

TABLE 5 SUMMARY OF OBSERVED AND CALCULATED BURSTING PRESSURES

Cylinder no.	Material and treatment (see Table 2)	Wall ratio	$\frac{\sigma_y}{\sigma_u}$	Approx. external hoop strain at bursting, microinches/in.	Bursting pressure, psi		Error, based on observed value, per cent
					Observed	Calculated	
1	Annealed Cr-Ni-Mo-V steel	2.74	0.505	19000	100000	81500	−19
2	Quenched-and-tempered and quenched Cr-Ni-Mo-V steel	2.74	0.796	...	>200000	192200	...
3	Quenched-and-tempered and quenched SAE 3320	2.74	0.700	15000	106000	111800	5
4	Quenched-and-tempered SAE 4340	2.75	0.800	17000	133000	138500	4
5	Normalized-and-tempered SAE 4340	2.75	0.720	16000	120000	124200	4
6	Quenched-and-tempered and quenched SAE 4340	2.50	0.940	9000	117000	129400	11
7	Normalized-and-tempered SAE 1045	2.75	0.564	20000	107000	96100	−10
8	Bore surface quenched-and-tempered SAE 1045	2.75	0.630	19000	119000	122700	3

around the periphery of the cylinder and along its length and were connected to binding posts on a plastic ring as shown in Fig. 6. The final strains recorded for the two directions were averages of the individual gage readings.

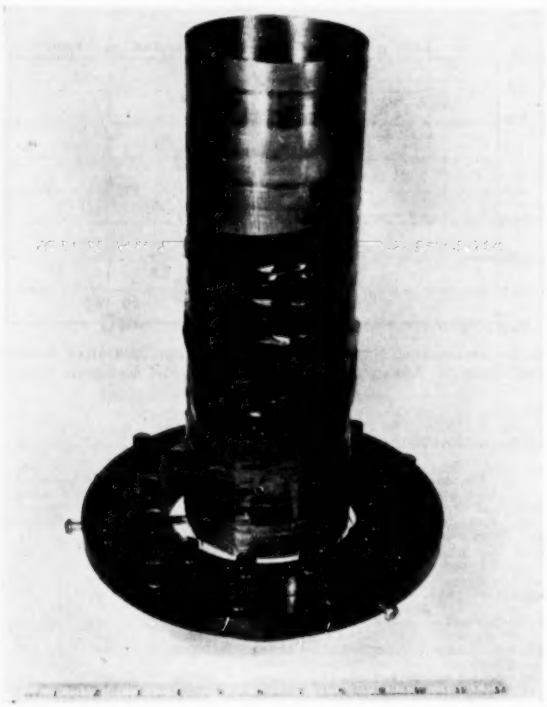

FIG. 6 RESIDUAL-STRESS TEST CYLINDER

Residual-stress determinations were made in the conventional manner by the procedure developed by Sachs (7). The cylinders were aligned in a lathe and concentric layers of metal were removed from the bore in successive steps. The hoop and longitudinal strains accompanying each machine cut, which was generally 0.05 in., on the diameter, were recorded. Throughout the test, flush-cooling was provided in order to keep heating of the cylinders to a minimum. This precaution, plus the use of temperature-compensating gages, permitted almost continuous testing so that a complete test could be performed in about 24 hr. Following each cut the new bore diameter was measured to 0.0001 in. The strains and bore areas recorded were then substituted into the Sachs equations (7), which follow. The residual-stress distributions thus obtained were as in Figs. 7 to 11, inclusive.

$$\sigma_z' = \frac{E}{1-\mu^2}\left[(A_o - A)\frac{d\alpha}{dA} - \alpha\right] \quad \ldots\ldots [1]$$

$$\sigma_h' = \frac{E}{1-\mu^2}\left[(A_o - A)\frac{d\theta}{dA} - \frac{A_o + A}{2A}\theta\right] \quad \ldots\ldots [2]$$

$$\sigma_r' = \frac{E}{1-\mu^2}\left[\frac{A_o - A}{2A}\theta\right] \quad \ldots\ldots [3]$$

RESULTS OF INVESTIGATION

Correlation of Residual Stresses With Initial Yielding[6] of Bore. One of the methods used for predicting the elastic breakdown pressure is to assume the von Mises condition of yielding (8) and express the predicted elastic breakdown pressure in terms of the tensile-test yield strength of the material and the cylinder-wall ratio. According to this theory the elastic breakdown internal pressure is given by the relation

$$p_y = \frac{\sigma_y}{\sqrt{3}}\left[\frac{R^2 - 1}{R^2}\right] \quad \ldots\ldots [4]$$

Equation [4] is satisfactory for predicting the elastic breakdown

[6] Hereinafter called "Elastic Breakdown."

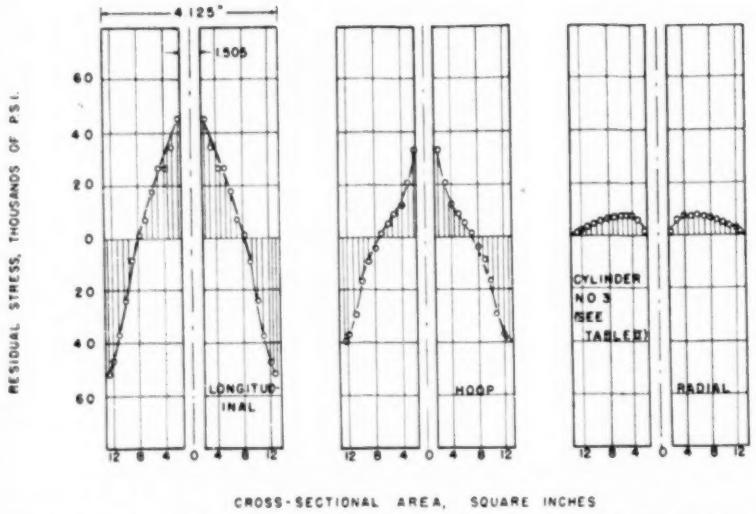

FIG. 7 DISTRIBUTIONS OF RESIDUAL STRESS IN QUENCHED-AND-TEMPERED AND QUENCHED SAE 3320 STEEL

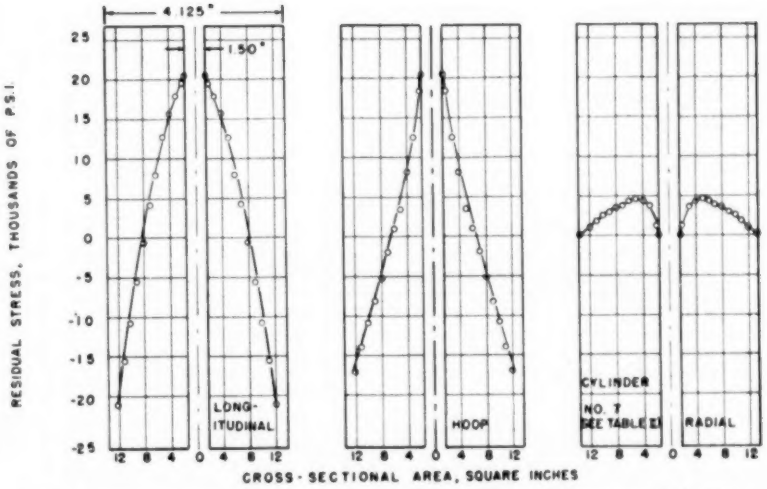

FIG. 8 DISTRIBUTIONS OF RESIDUAL STRESS IN QUENCHED-AND-TEMPERED SAE 1045 STEEL

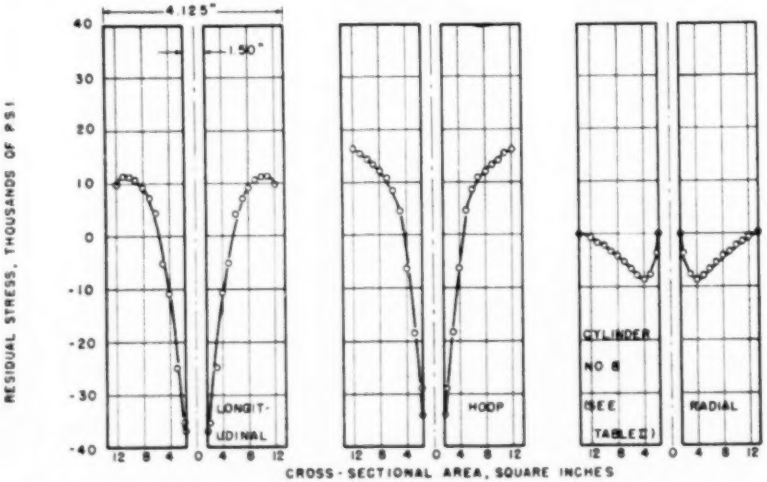

FIG. 9 DISTRIBUTIONS OF RESIDUAL STRESS IN SURFACE BORE QUENCHED-AND-TEMPERED SAE 1045 STEEL

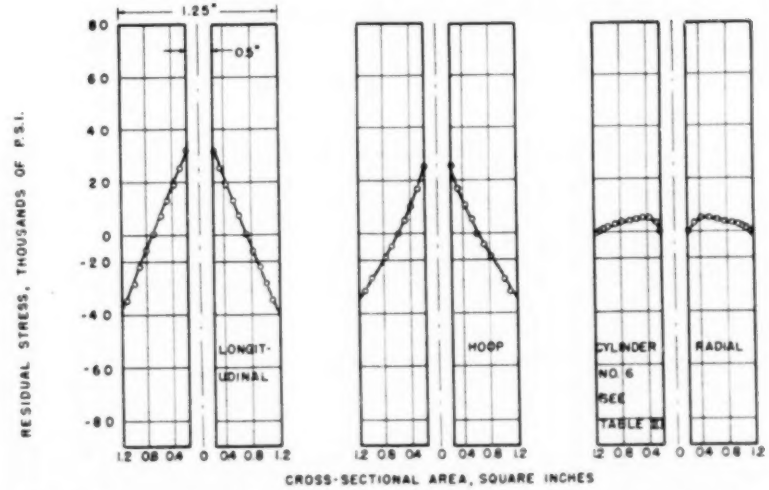

FIG. 10 DISTRIBUTIONS OF RESIDUAL STRESS IN QUENCHED-AND-TEMPERED AND QUENCHED SAE 4340 STEEL

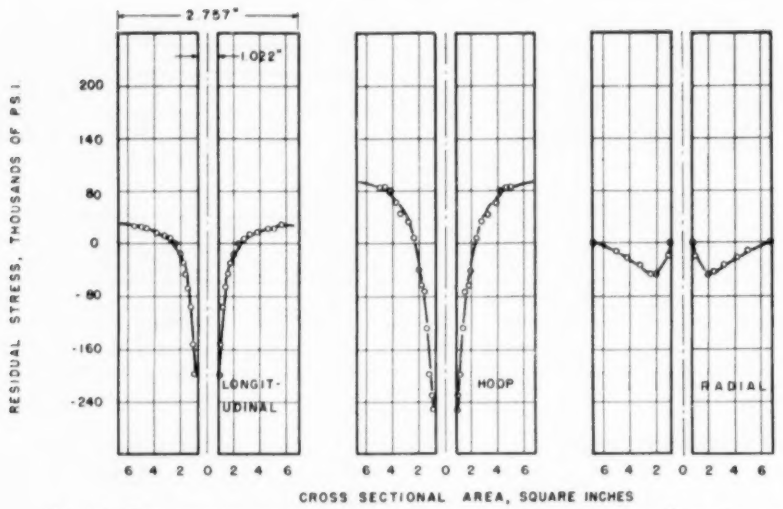

FIG. 11 DISTRIBUTIONS OF RESIDUAL STRESS IN AUTOFRETTAGED HEAT-TREATED CR-NI-MO-V STEEL

pressure in heavy-wall closed-end cylinders that contain no macro-residual stresses. However, if macro residual stresses are present at the bore they either increase or decrease the breakdown pressure, depending on whether they are of the tension or compression type.

The effect of macro residual stresses on elastic breakdown pressure can be accounted for by using the von Mises yield condition in the form

$$\sigma_y = \sqrt{\frac{1}{2}\left[(\sigma_h - \sigma_r)^2 + (\sigma_r - \sigma_z)^2 + (\sigma_z - \sigma_h)^2\right]} \quad \ldots [5]$$

and introducing the appropriate terms for the residual stresses present at the bore in a heavy-wall cylinder. There is no radial residual stress at the bore of a cylinder; consequently, only hoop and longitudinal residual stresses have to be considered; thus, in terms of elastic breakdown at the bore, Equation [5] can be rewritten in the following form

$$\sigma_y = \sqrt{\frac{1}{2}\left\{[\sigma_h + \sigma_h' - \sigma_r]^2 + [\sigma_r - (\sigma_z + \sigma_z')]^2 + [\sigma_z + \sigma_z' - (\sigma_h + \sigma_h')]^2\right\}} \ldots [6]$$

For the case of internal pressure in a closed-end cylinder the stresses σ_h, σ_r, and σ_z in Equation [6] become (7)

$$p\left(\frac{R^2+1}{R^2-1}\right);\ -p, \text{ and } \frac{p}{R^2-1}$$

respectively, at the bore; consequently, Equation [6], expressed in terms of both applied and residual bore stresses, takes the form

$$p_y^2\left[\frac{R^2}{R^2-1}\right]^2 + p_y\left[\frac{R^2}{R^2-1}\right]\sigma_h' + \frac{1}{3}\left[(\sigma_z')^2 + (\sigma_h')^2 - \sigma_z'\sigma_h' - \sigma_y^2\right] = 0 \ldots [7]$$

Equation [7] is a quadratic in p_y, and the predicted bore yield pressure is solved by application of the binomial theorem.

Equation [7] is a generalization of Equation [4]; consequently, if no residual stress is present at the bore of the cylinder, the terms σ_h' and σ_z' in Equation [7] vanish and the general equation reduces to Equation [4].

The experimental results on elastic breakdown obtained on several heavy-wall cylinders are presented in Table 3. The values of the residual stresses at the bore of the cylinders are listed in column 4 of Table 3.

The residual stresses listed in column 4 of Table 3, together with the tensile yield strength of the material listed in column 4 of Table 2 were placed in Equation [7] to give the values of calculated elastic breakdown pressure given in column 6 of Table 3. In all cases, if residual bore stresses are allowed for in the formula, agreement to within ±15 per cent of the experimentally observed elastic breakdown pressure (column 5 of Table 3) is obtained. When residual stresses are not allowed for, Equation [4], errors of over 50 per cent can be obtained as shown by column 10 of Table 3. It is evident, therefore, that allowance should be made for residual stresses in the design of heavy-wall cylinders where elastic breakdown at the bore is critical.

The experimentally observed values of residual stress are generally as would be expected except for cylinder 2. It was thought that quenching from the temper at 1000 F would impart macro residual cooling stresses to the wall of the cylinder. The fact that no residual stresses were found means that either the quench from 1000 F was not drastic enough to produce thermal stress, or that residual austenite transformed during tempering which caused an expansion and thus canceled any effect of contraction caused by quenching.

Residual Stresses Induced by Autofrettage of Closed-End Cylinder. In view of the fact that the cylinder of the Cr-Ni-Mo-V steel, heat-treated to a hardness of 42 Rockwell C, contained no residual stresses (cylinder No. 2) it was decided to autofrettage a cylinder of this material in order to determine what advantage, stress-wise, could be obtained by such processing on a high-strength steel. This cylinder is described under item 2 of Table 1 and also in Table 2. The cylinder was autofrettaged by applying an internal pressure of 200,000 psi for 4.5 hr. Following the pressurizing the cylinder was given a stabilizing heat-treatment by holding for 3 hr at 650 F. Recycling four times to 200,000 psi established that the cylinder was stable and operated elastically up to the autofrettage pressure. Following the autofrettage treatment,

the distribution of residual stress was determined by the Sachs method. The results are shown in Figs. 11 and 12. At the bore, compression, residual, longitudinal, and hoop stresses of 200,000 and 250,000 psi, respectively, were found. These values of

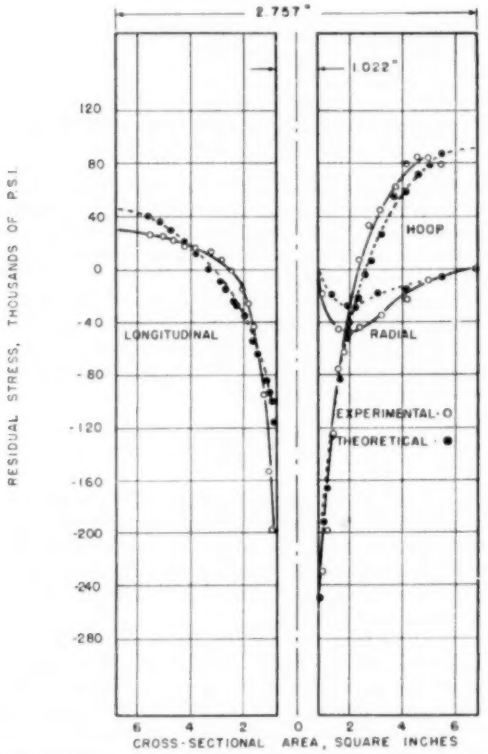

FIG. 12 COMPARISON OF THEORETICAL AND EXPERIMENTAL RESIDUAL-STRESS DISTRIBUTIONS IN AUTOFRETTAGED HEAT-TREATED CR-NI-MO-V CYLINDER

residual bore stress, together with a transverse yield strength of approximately 160,000 psi substituted into Equation [7] give a predicted elastic breakdown pressure of approximately 215,000 psi. This value is more than 200 per cent higher than the elastic breakdown pressure obtained without autofrettage, which was approximately 71,000 psi.

The theoretical analysis of stress distributions obtained in autofrettage is not on a universally accepted basis (2, 8). Many theories have been advanced over the past several years to rationalize residual stresses imparted to cylinders by autofrettage. All theories, however, must utilize stress equations in the plastic range of strain for pressurized cylinders, and it is this requirement that apparently precludes the general acceptance of any particular theory. One of the oldest of the theories assumes plane strain, and the von Mises condition of yielding. The plastic-range stresses due to internal pressure in a thick-wall cylinder are thus

$$\sigma_h = \frac{2\,\sigma_y}{\sqrt{3}}\left(1 + \ln\frac{r}{b}\right) \quad [8]$$

$$\sigma_z = \frac{2\,\sigma_y}{\sqrt{3}}\left(\frac{1}{2} + \ln\frac{r}{b}\right) \quad [9]$$

$$\sigma_r = \frac{2\,\sigma_y}{\sqrt{3}}\ln\frac{r}{b} \quad [10]$$

The theoretical residual-stress distribution is obtained by calculating the plastic-range stresses from the foregoing equations and subtracting the stresses that would be present if the cylinder were elastic at the autofrettage pressure. These hypothetical elastic-range stresses are obtained from the theory of elasticity for a closed-end cylinder (6) and are

$$\sigma_h = \frac{p}{R^2 - 1}\left(1 + \frac{b^2}{r^2}\right) \quad [11]$$

$$\sigma_z = \frac{p}{R^2 - 1} \quad [12]$$

$$\sigma_r = \frac{p}{R^2 - 1}\left(1 - \frac{b^2}{r^2}\right) \quad [13]$$

In these equations[7] p is the pressure for full wall yielding (autofrettage pressure) and has the form

$$p = \frac{2\,\sigma_y}{\sqrt{3}}\ln R$$

Thus the residual stresses in a cylinder wall after autofrettage are

$$\sigma_h' = \frac{2\,\sigma_y}{\sqrt{3}}\left(1 + \ln\frac{r}{b}\right) - \frac{p}{R^2 - 1}\left(1 + \frac{b^2}{r^2}\right) \quad [14]$$

$$\sigma_z' = \frac{2\,\sigma_y}{\sqrt{3}}\left(\frac{1}{2} + \ln\frac{r}{b}\right) - \frac{p}{R^2 - 1} \quad [15]$$

$$\sigma_r' = \frac{2\,\sigma_y}{\sqrt{3}}\ln\frac{r}{b} - \frac{p}{R^2 - 1}\left(1 - \frac{b^2}{r^2}\right) \quad [16]$$

In the procedure outlined, it is assumed that relaxation is linear and that reyielding does not occur on unloading due to release of the internal pressure.

Included in Fig. 12 is the theoretically calculated residual-stress distribution for comparison with experiment. It is seen that agreement between theory and experiment is good except for the longitudinal residual stress at the bore. This disagreement probably is due to the inability of the theory to express the longitudinal stress in a precise way. However, for high-strength materials it is seen in Equation [7] that the contribution of the longitudinal stress is small so that a discrepancy such as shown in Fig. 12 probably is not serious. For low-strength materials the longitudinal stress would be more important. In addition, the cylinder was given a stabilizing heat-treatment at 650 F which undoubtedly had some effect on the residual-stress distribution. However, just how this heat-treatment influences the residual stresses induced by autofrettage is not at present known, and allowance for this influence is not made in the theory.

Method for Determining Overstrain Through Wall. An important characteristic of heavy-wall cylinders is the internal pressure sustained at the moment when the outside fibers reach the yield strength of the metal. This pressure is called the overstrain pressure.

Unlike the elastic breakdown pressure (the pressure at which

[7] Equations [8] and [10] are independent of the end conditions. However, an expression for σ_z can only be simply obtained by assuming plane strain. The expression for σ_z in Equation [12] is based on closed-end conditions, which is more realistic in the elastic range.

the bore fibers start to yield) and the bursting pressure (the maximum internal pressure sustained by the cylinder), the overstrain cannot be read directly from the experimental pressure-strain curve for comparison with theoretically predicted values; the problem then, is to define the "observed" value of overstrain pressure. This situation has been examined in the present work and a method for defining the observed overstrain pressure has been worked out. The proposed method utilizes the usual assumptions of elastic and plastic behavior of materials. The observed values obtained by the method agree fairly well with the values predicted by the von Mises theory, which for overstrain of heavy-wall cylinders has the form

$$p_o = \frac{2\,\sigma_y}{\sqrt{3}} \ln R \quad [17]$$

Since there is no characteristic "jog" in the cylinder pressure-strain curve at the overstrain pressure, it is necessary to indicate the observed overstrain pressure on the curve by means of some theory. Thus when the observed and experimental values are compared, the situation is one in which two theories are checked against each other rather than one of checking theory against fact. Inasmuch as the radial stress is zero at the outside surface, only two stresses are involved and the problem is statically determinate. If the von Mises condition of yielding is utilized, the cylinder strain at the overstrain pressure can be determined from the strain obtained in the tension test at the yield point in accordance with the following method.

Since strain measurements are made in two directions at the outside surface of the cylinder the method used to predict overstrain must utilize these measurements. In addition, it is known that at the outside surface the radial stress is zero. Also, at the instant of full wall yielding the sum of the three principal strains must be zero, i.e., Poisson's ratio $\mu = 0.5$.

Within the elastic range at the outside surface of the cylinder

$$\epsilon_h = \frac{1}{E}\left[\sigma_h - \mu\sigma_z\right] \quad [18]$$

$$\epsilon_z = \frac{1}{E}\left[\sigma_z - \mu\sigma_h\right] \quad [19]$$

$$\epsilon_r = \frac{-\mu}{E}\left[\sigma_h + \sigma_z\right] \quad [20]$$

By using the condition of constancy of volume, which is a good approximation in both the elastic and plastic ranges, it is seen from the foregoing equations that

$$\sigma_h = \frac{E\,(\epsilon_h + \mu\epsilon_z)}{1 - \mu^2} \quad [21]$$

$$\sigma_z = \frac{E\,(\epsilon_z + \mu\epsilon_h)}{1 - \mu^2} \quad [22]$$

At the time of yielding of the outer surface the von Mises yield condition is considered valid; consequently, when Equations [21] and [22] are substituted into the von Mises relation

$$\sigma_y^2 = \sigma_h^2 + \sigma_z^2 - \sigma_h\,\sigma_z \quad [23]$$

the following equation results

$$\sigma_y^2 = \frac{4E^2}{3}\left(\epsilon_z^2 + \epsilon_h^2 + \epsilon_h\,\epsilon_z\right) \quad [24]$$

However, σ_y, taken as the yield strength at 0.01 per cent offset, can be expressed approximately as

$$(E\,\epsilon_y)^2 = \sigma_y^2 \quad [25]$$

Therefore, using this relation, Equation [24] becomes

$$(\epsilon_h)_o = \frac{\epsilon_y\sqrt{3}}{2}\left[\frac{1}{\sqrt{\left(\frac{\epsilon_z}{\epsilon_h}\right)^2 + \left(\frac{\epsilon_z}{\epsilon_h}\right) + 1}}\right] \quad [26]$$

or[8]

$$(\epsilon_h)_o = \frac{\epsilon_y\sqrt{3}}{2}\left[\frac{1}{\sqrt{\beta^2 + \beta + 1}}\right] \approx 0.866\,\epsilon_y \quad [27]$$

The value of $(\epsilon_h)_o$ thus obtained is a point along the abscissa of the pressure-strain curve. This strain point corresponds to some value of pressure as determined by the pressure-strain curve, and this value of pressure is defined as the observed or experimental overstrain pressure.

The observed overstrain pressure is thus obtained by calculating ϵ_h, the outside hoop strain on the cylinder, and drawing a perpendicular from this value to the pressure-strain curve. The point of intersection gives the overstrain pressure which is compared with the "theoretical" value

$$p_o = \frac{2\,\sigma_y}{\sqrt{3}} \ln R \quad [28]$$

Comparison of observed overstrain pressures thus obtained with corresponding values predicted by the von Mises theory is made in Table 4. Data from 30 other cylinders not specifically studied in this investigation also were analyzed and it was found that about two thirds of the values were in agreement to approximately 15 per cent or better.

The precise influence of macro residual stresses due to heat-treatment on the overstrain characteristics of a heavy-wall cylinder is not known. Since the stress distribution throughout the wall changes continuously from the instant of initial yielding at the bore a reasonably simple analysis appears to be an impossibility. However, since initial residual stresses are eradicated by yielding of the material it is believed that any effect of initial heat-treatment residual stresses on overstrain through the wall would be small.[9] This item needs further investigation since the good agreement found in the present work is only agreement between two theoretical values.

Method for Predicting Bursting Pressure. As in the case of overstrain through the wall, macro residual heat-treatment stresses initially present in the cylinder wall apparently do not influence bursting pressure. The theoretical prediction of bursting pressure has received considerable attention in the literature and has been rationalized by several methods (9, 10). In this investigation a formula has been developed for predicting the bursting pressure which is consistent with the assumptions previously used for predicting elastic breakdown and overstrain through the wall.

It is postulated that, if the cylinder yields at constant stress, as stated by classical plasticity theory, it will burst at the pressure required to overstrain the wall; that is, the lower limit will be

$$(p_b)_i = \frac{2\,\sigma_y}{\sqrt{3}} \ln R \quad [29]$$

[8] For many cases $\sqrt{\beta^2 + \beta + 1}$ becomes very close to 1.0; consequently it cancels out, leaving $(\epsilon_h)_o = 0.866\,\epsilon_y$. The same result is obtained by considering the equilibrium of stresses and the closed-end condition (2).

[9] This may not be true for work-hardened materials.

Now, if the ratio of the tensile yield strength σ_y, to the tensile ultimate strength σ_u, were unity, bursting would occur at a pressure defined by the relation[10]

$$(p_b)_1 = \frac{2\,\sigma_u}{\sqrt{3}} \ln R \quad \ldots\ldots [30]$$

However, for yield-ultimate ratios less than unity the bursting pressure will be somewhere between the pressures defined by Equations [29] and [30]. Consequently, it is postulated that the bursting pressure will be a function of both the overstrain pressure, Equation [29], and the pressure defined by Equation [30]. Thus, assuming direct proportionality

$$p_b = \frac{\sigma_y}{\sigma_u}\left(\frac{2\sigma_u}{\sqrt{3}} \ln R\right) + \left(1 - \frac{\sigma_y}{\sigma_u}\right)\left(\frac{2\sigma_y}{\sqrt{3}} \ln R\right)$$

which reduces to

$$p_b = \frac{2\,\sigma_y}{\sqrt{3}} \ln R \left(2 - \frac{\sigma_y}{\sigma_u}\right) \quad \ldots\ldots [31]$$

Thus, according to Equation [31], if σ_y/σ_u were unity, then $\sigma_y = \sigma_u$ and

$$p_b = \frac{2\,\sigma_u}{\sqrt{3}} \ln R$$

which is consistent with the foregoing reasoning.

The results of predicted bursting pressure using Equation [31] are given in Table 5. Data from 30 additional cylinders which were not studied specifically in this investigation also were analyzed and it was found that an over-all absolute accuracy of 8 per cent was obtained.

Prediction of Total Pressure-Strain Curve. In the preceding paragraphs, methods have been outlined for predicting elastic breakdown, overstrain, and bursting pressure for heavy-wall cylinders. The corresponding hoop strains also are of interest since, having them, it would be possible to estimate the total pressure-strain curve for a cylinder. Methods have been worked out for obtaining these strains and are included in the discussion which follows.

Elastic breakdown: The elastic breakdown at the bore is defined in this paper as the termination of the straight-line portion of the pressure-strain curve. Therefore, at the elastic breakdown pressure, elastic theory can be used to define the strain values. In the hoop direction at the outside surface of the cylinder by the theory of elasticity

$$\epsilon_h = \frac{1}{E}\left[\sigma_h - \mu\,(\sigma_r + \sigma_z)\right] \quad \ldots\ldots [32]$$

In this equation

$$\sigma_r = 0 \quad \ldots\ldots [33]$$

$$\sigma_z = \frac{p}{R^2 - 1} \quad \ldots\ldots [34]$$

$$\sigma_h = \frac{p}{R^2 - 1}\left(1 + \frac{b^2}{r^2}\right) \quad \ldots\ldots [35]$$

Consequently, Equation [32] may be rewritten as follows

$$(\epsilon_h)_{ys} = \frac{p_y\,(2 - \mu)}{E\,(R^2 - 1)} \quad \ldots\ldots [36]$$

[10] Same formula as for overstrain by classical plasticity theory except ultimate strength σ_u, substituted for yield strength σ_y.

At the bore of the cylinder the radial stress is equal to $-p$; consequently, Equation [32] has the form

$$(\epsilon_h)_{yi} = \frac{p_y}{E\,(R^2 - 1)}\left[(R^2 + 1) + \mu\,(R^2 - 2)\right] \quad \ldots\ldots [37]$$

Equations [36] and [37] thus define the surface and bore hoop strains corresponding to the elastic breakdown pressure p_y.

Overstrain: It already has been shown that the external hoop strain at the overstrain pressure is given by the relation

$$(\epsilon_h)_{os} \cong 0.866\,\epsilon_y \quad \ldots\ldots [27]$$

The corresponding hoop strain at the bore is easily obtained from the geometry of the deformation in the plastic range. Geometrically, it can be shown that the bore and surface hoop strains are related as follows

$$\epsilon_h\,(\text{bore}) = R^2\,\epsilon_h\,(\text{surface}) \quad \ldots\ldots [38]$$

Therefore, utilizing Equations [27] and [38], the hoop strain at the bore corresponding to the overstrain pressure is given by the relation

$$(\epsilon_h)_{oi} = 0.866\,\epsilon_y\,R^2 \quad \ldots\ldots [39]$$

Bursting: In determining the external hoop strains corresponding to elastic breakdown and overstrain through the wall the problem was simplified by the fact that the strain equations of elastic theory could be used. For bursting, however, these equations cannot be used because the entire cylinder wall has yielded and is in the plastic condition.

Consequently, the definition of strain at the bursting pressure becomes a complex problem unless some simplifying assumptions are made.

From the symmetry of the deformation, however, the bore and surface hoop strains are related in accordance with Equation [38]. This equation shows that the bore strains are greater than the surface strains; consequently, as an approximation it is assumed that failure will initiate at this location. Thus, in terms of a theory of failure, it can be postulated that failure will occur in the cylinder when the bore strain reaches the value of the strain at the ultimate stress in tension. Therefore the bore hoop strain at failure is given by the relation

$$(\epsilon_h)_{bi} = \epsilon_u \quad \ldots\ldots [40]$$

At the outside of the cylinder, the hoop strain at failure by virtue of Equation [38] is defined by the relation

$$(\epsilon_h)_{bs} = \frac{\epsilon_u}{R^2} \quad \ldots\ldots [41]$$

Equations [40] and [41] thus define the bore and surface hoop strains corresponding to the bursting pressure.

The external hoop strains defined by Equations [36], [27], and [41], were combined with the corresponding pressure values for four cylinders (Table 6) for which total stress-strain curves in tension were available, and the results are shown in Fig. 13.[11] Similar results using Equations [37], [39], and [40] for the bore strains also could be plotted. It is seen that a fairly good estimate of the total pressure-strain curve can be obtained. The practical utility of the result lies in the ability of the method to indicate the course of straining, for example, in autofrettage, and to show roughly the degree of strain that can be expected before complete failure of a cylinder. More precise methods have been advanced by MacGregor (11); however, from an engineering point of view

[11] With the exception of cylinder No. 3 in Fig. 13, all cylinders were free from macro residual stress.

TABLE 6 TREATMENT AND PROPERTIES OF CYLINDERS

Cylinder no.	Material and treatment	Wall ratio	—Properties in transverse direction at bore of cylinder— Yield strength, psi— 0.01% offset	0.2% offset	Ultimate strength, psi	Elongation in 1 in., per cent	Reduction in area, per cent
3	Quenched-and-tempered and quenched SAE 3320	2.74	74300	79500	105400	24	50
9	Annealed SAE 1035	2.75	39950	38600	73100	25	32
10	Annealed SAE 3320	2.75	58100	68500	112600	20	41
11	Annealed Cr-Ni-Mo-V	2.75	45100	45300	83300	25	37

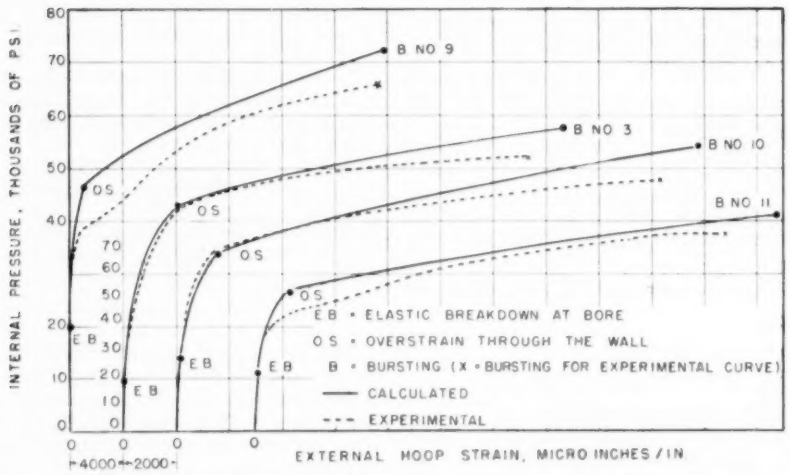
INTERNAL PRESSURE, THOUSANDS OF PSI
EXTERNAL HOOP STRAIN, MICRO INCHES / IN
B NO 9
B NO 3
B NO 10
B NO 11
O S
E B
E B = ELASTIC BREAKDOWN AT BORE
O S = OVERSTRAIN THROUGH THE WALL
B = BURSTING (X = BURSTING FOR EXPERIMENTAL CURVE)
CALCULATED
EXPERIMENTAL

FIG. 13 PRESSURE-STRAIN CURVES FOR HEAVY-WALL CYLINDERS UNDER INTERNAL PRESSURE

the method outlined in this paper appears to have promise. A conclusive generalization of the method is not possible since the data do not include a wide enough range of materials. Also, until an experimental method is devised which can be used to denote the overstrain point precisely it is not possible to try and account for residual stresses in terms of overstrain.

CONCLUSIONS

1 High macro residual stresses at the bore of a cylinder before application of internal pressure may change the elastic breakdown pressure by a factor of one half or more as compared to an initially stress-free cylinder.

2 Knowing the magnitude and sign of the bore residual stresses in a cylinder it is possible to allow analytically for these stresses in the design formula and to obtain agreement between theory and practice to within, and generally less than, ±15 per cent.

3 Steel cylinders heat-treated to high-hardness levels do not necessarily contain high residual stresses.

4 Residual stresses in cylinders due to heat-treatment do not appear to influence overstrain or bursting pressures.

5 The total pressure-strain curve of a cylinder can be approximated by an analysis of tensile-test data.

6 The state of residual stress in an item of equipment should be known if operation within the elastic range is required.

BIBLIOGRAPHY

1 "Classification and Nomenclature of Internal Stresses," by E. Orowan, Symposium on Internal Stresses in Metals and Alloys, The Institute of Metals, London, England, 1948, pp. 47–59.

2 "The Mathematical Theory of Plasticity," by R. Hill, first edition, Clarendon Press, London, England, 1950 (see chapter 5 on solution of plastic-elastic problems).

3 "Eigenspannungen bei der Wärmebehandlung von Stahl," by H. Bühler, H. Buchholtz, and E. H. Schulz, *Archiv für das Eisenhüttenwesen*, vol. 5, 1932, pp. 413–418.

4 "Entstehung von Rissen in Stahl bei der Wärmebehandlung," by E. Scheil, *Archiv für das Eisenhüttenwesen*, vol. 8, 1935, pp. 309–314.

5 "Zusammenwirken von Wärme und Umwandlungsspannungen in abgeschreckten Stählen," by H. Bühler and E. Scheil, *Archiv für Eisenhüttenwesen*, vol. 6, 1933, pp. 283–288.

6 "The Theory of Elasticity," by S. Timoshenko, first edition, McGraw-Hill Book Company, Inc., New York, N. Y., 1934.

7 "Residual Stresses, Their Measurement and Their Effects on Structural Parts," by G. Sachs, Symposium on the Failure of Metals by Fatigue, Melbourne University Press, Melbourne, Australia, 1947, pp. 237–247.

8 "Plasticity—A Mechanics of the Plastic State of Matter," by A. Nadai, first edition, McGraw-Hill Book Company, Inc., New York, N. Y., 1931.

9 "The Overstrain of Tubes by Internal Pressure," by W. R. D. Manning, *Engineering*, London, England, vol. 159, 1945, pp. 101–102; 183–184.

10 "Plasticity in Engineering," by F. K. Th. van Iterson, first edition, Blackie and Son, Ltd., Glasgow, Scotland, 1947.

11 "The Plastic Flow of Thick-Walled Tubes With Large Strains," by C. W. MacGregor, L. F. Coffin, Jr., and J. C. Fisher, *Journal of Applied Physics*, vol. 19, March 1948, pp. 291–297.

Rupture-Disk Design Evaluation and Bursting Tests

By G. R. PRESCOTT,[1] CHARLESTON, WEST VA.

The use of rupture disks as a quick-acting pressure-relief device in the chemical industry is well established. High-pressure synthesis units must be protected adequately against abnormal pressure surges caused by malfunctioning of equipment and chemical decompositions and reactions which may occur with explosive violence. The results of a recent investigation into the design and application of rupture disks at du Pont's Belle Works in West Virginia constitute the basis of this paper.

Description of Disks

TWO variations of a shear-type disk are used as illustrated in Fig. 1. The materials used for fabrication of disks are commercial bronze (90 Cu, 10 Zn) and AISI Type 329 stainless steel (25.5 Cr, 3.7 Ni, 1.5 Mo). The commercial bronze single-hub disk is employed in applications where corrosion is a factor. The disk is protected on the process side by the addition of a thin disk of a highly corrosion-resistant material, usually fine silver. All Type 329 disks are of the single-hub type. A thin disk of copper or bronze is used with this relatively hard material in order to obtain a seal. In application, the shear-type disks are placed in a disk holder, a shear block is placed over the disk, and the assembly is tightened with a retaining nut. A typical assembly is shown in Fig. 2.

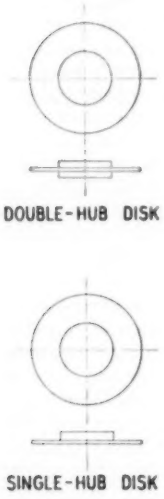

Fig. 1 Types of Rupture Disks

Specification of Material, Fabrication, and Control

The two alloys are purchased as 1/2 hard plate stock. Disks are machined from the as-received stock, and the finished disks are annealed. Commercial-bronze disks are held at 420 C for 30 min and air-cooled. Type 329 disks are given a full anneal at 920 C and water-quenched. Approximately 10 per cent of each batch of disks are tested in an Aminco dead-weight tester. The test disks must rupture in the range specified for the individual disks before the batch is approved for plant service. Frequent difficulties have been encountered in fabricating disks which would rupture in the desired range, although specifications of material, fabrication, and heat-treatment were met. The specified rupture ranges apparently did not have a sound basis. Accordingly, the effect of machine tolerance, shear-strength variation, and size of disk was investigated.

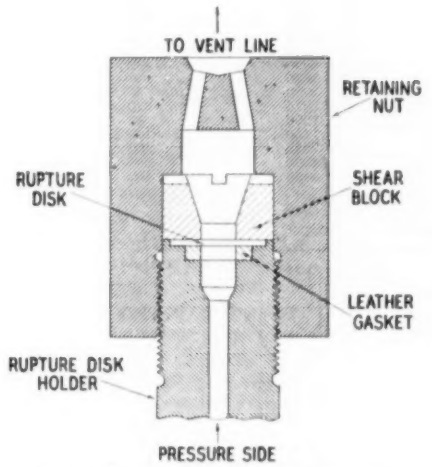

Fig. 2 Typical Rupture-Disk Assembly

The rupture pressure of the shear-type disk is determined by the shear strength of the material, shear area, and the area on which the pressure acts as shown by the equation

$$R = \frac{sdt\pi}{\frac{d^2\pi}{4}}$$

where

R = rupture pressure
d = diameter of shear block
t = thickness of disk web, in.
s = shear strength

The equation simplifies to

$$R = \frac{4st}{d} \qquad [1]$$

Tolerance
$t \pm 0.0003$
$d \pm 0.001$

The machine tolerances shown are standard for all disks. The equation shows that the rupture pressure will be a maximum value when t is on the high side of the tolerance specification and d is on the low side. Conversely, the rupture pressure will be minimum when t is low and d is high. The difference between the maximum and minimum rupture pressure is the rupture range resulting from machine tolerances. This range was calculated for each disk and Table 1 shows a comparison between machine-tolerance range and the specified range. Six of the twenty-one disks have specified ranges narrower than the machine-tolerance range. The J-disk, for example, has a machine-tolerance range of 380 psi and a specified range of 200 psi.

[1] E. I. du Pont de Nemours & Company, Inc., Belle Works.

Contributed by the Industrial Instruments and Regulators Division of The American Society of Mechanical Engineers and presented at The Seventh National Instrument Conference, Cleveland, Ohio, September 9–10, 1952.

Note: Statements and opinions advanced in papers are to be understood as individual expressions of their authors and not those of the Society. Manuscript received at ASME Headquarters, June 19, 1952. Paper No. 52—IIRD-8.

TABLE 1 RUPTURE-DISK DESIGN EVALUATION AND BURSTING TESTS; COMPARISON OF SPECIFIED RANGES TO MACHINE-TOLERANCE RANGES

Disk designation	Nominal design rupture pressure, psi	Rupture range due to machine tolerances, psi	Specified rupture range, psi
A	22080	930	2000
B	4070	150	100
C	9230	385	400
D	19200	885	1000
E	6650	225	200
F	15080	555	1000
G	7120	230	200
H	1800	45	100
J	8460	380	200
K	900	40	40
L	11800	410	400
M	10800	305	400
N	6990	80	200
P	1920	50	200
Q	2290	60	200
R	7075	220	200
S	1200	40	40
T	7150	105	200
V	7025	105	200
W	14300	665	1000
Y	4150	150	100

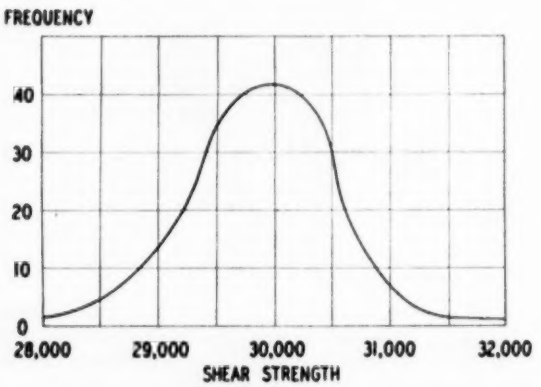

FIG. 3 SHEAR-STRENGTH DISTRIBUTION OF COMMERCIAL BRONZE

The comparison shows further that no allowance is made for variation in shear strength. This variation is influenced by the prior working and thermal history of the alloy and variations in chemical composition. Disks were designed on the basis of 30,000-psi shear strength for commercial bronze and 83,000 psi for Type 329. No allowance was made for variation in shear strength or the rupture range which results from this variation.

Statistical data on the shear-strength variation of commercial bronze and Type 329 stainless were not available. Accumulated data were available, however, from the numerous commercial-bronze test disks which were burst over a period of years. A frequency-distribution curve of the commercial-bronze shear-strength data is shown in Fig. 3. The standard deviation is approximately 800 psi which means that a shear strength of 30,000 ± 800 psi is necessary to include 70 per cent of the commercial-bronze stock. It should be noted that base dimensions were assumed when calculating the shear strengths of the test disks. This is a reasonable assumption, however, since the majority of disks in a representative batch will be machined very close to the base dimensions. A critical examination of the data indicates that the minimum practical design value of shear strength should be taken as 30,000 ± 500 psi.

The rupture range resulting from the ±500-psi variation is significant as shown in Table 2. The rupture ranges resulting from machine tolerances and shear-strength variation are additive in the finished disk, and the sum of the two ranges is compared to the specified ranges. In this comparison, eighteen of the twenty-one disks have specified ranges narrower than the sum

TABLE 2 RUPTURE-DISK DESIGN EVALUATION AND BURSTING TESTS; REVISED SPECIFIED RANGES

Disk designation	1 Rupture range based on 30,500 ± 500 psi shear strength	2 Machine-tolerance range, psi	3 Sum of columns 1 and 2	4 Present specified range, psi
A	740	930	1670	2000
B	135	150	285	100
C	310	385	695	400
D	640	885	1525	1000
E	220	225	445	200
F	505	555	1060	1000
G	235	230	465	200
H	60	45	105	100
J	280	380	660	200
K	30	40	70	40
L	390	410	800	400
M	360	305	665	400
N	230	80	310	200
P	60	50	110	200
Q	80	60	140	200
R	225	220	445	200
S	40	40	80	40
T	225	105	330	200
V	235	105	340	200
W	470	665	1135	1000
Y	125	150	275	100

of the machine tolerance and shear-strength ranges. The specified ranges of the eighteen disks should be revised to values more consistent with actual conditions.

The data in Table 1 show a definite lack of correlation between the nominal design rupture pressure and the machine-tolerance rupture range. For example, consider the G and the V-disks. Although both are designed to rupture at the 7100-psi level, the G-disk has a machine-tolerance rupture range of 230 psi as compared to 105 psi for the V-disk. Since the machine tolerances specified are the same for both disks, the difference is due to the relative sizes of the disks. The rupture range which is produced by a constant set of machine tolerances will be diminished as the size of the disk increases. Another example is the C and M-disks. The C-disk has a design rupture pressure of 9230 psi and a machine-tolerance range of 385 psi. The M-disk has a design rupture pressure of 10,800 psi and a machine-tolerance range of 305 psi. It is inconsistent for the C-disk, which has a lower design rupture pressure than the M-disk, to have a larger machine-tolerance range than the M-disk.

From the equation used to calculate design rupture pressures, Equation [1], it is apparent that any combination of values for d and t can be used to design a rupture disk for a given pressure level, provided the ratio of t to d remains constant. The designer merely selects a value of either d or t and the other dimension becomes fixed. The disk can be made large or small. The resulting machine-tolerance range can be determined by calculating the maximum and minimum rupture pressures and obtaining the difference between the two values. An equation for this relation can be set up as follows

$$R = \frac{4s(t + 0.0003)}{d - 0.001} - \frac{4s(t - 0.0003)}{d + 0.001}$$

where

R = machine-tolerance rupture range
s = shear strength
t = thickness of rupture-disk web
d = diameter of shear block

By expanding and simplifying the foregoing equation, the following relation is obtained

$$R = \frac{0.0024sd + 0.008st}{d^2}$$

Substituting for t from Equation [1] and the value of 30,000 psi as the shear strength of commercial bronze for s

$$R = \frac{72 + 0.002P}{d} \quad \ldots\ldots\ldots\ldots\ldots\ldots [2]$$

This relation shows that the machine-tolerance range is an inverse function of d at a given rupture pressure level. If the diameter of the shear block of the disk is doubled, the machine-tolerance-range rupture is decreased to one half its value. The variation of rupture range as a function of d at rupture pressures of 1000, 12,000, and 24,000 psi is shown in Fig. 4. This set of curves will permit the designer to determine the approximate

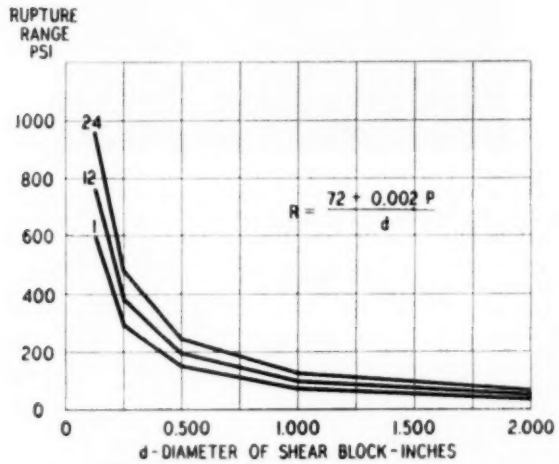

Fig. 4 Commercial-Bronze Machine-Tolerance Rupture Range Versus Size of Disk at Design Rupture Pressures of 1000, 12,000, and 24,000 Psi

range corresponding to values of d. Having selected a value for d, the exact range can be calculated by using Equation [2]. The value obtained for d would in turn fix the thickness t. The machine-tolerance rupture range is narrowed by using the maximum-size disk within practical limits.

Protection Against Internal Explosions

Protection of high-pressure synthesis equipment containing combustible mixtures of gases or vapors is a difficult problem. The design of rupture disks which will protect the equipment adequately is hampered by the lack of available data. A recent publication[3] on the effect of internal explosions on rupture disks at relatively low initial pressures shows the important variables are (1) ratio of length of vessel to diameter; (2) initial pressure; and (3) ratio of vent area to volume. In the reference cited, the authors found that the maximum explosion pressure recorded in a vessel protected by rupture disks was determined almost solely by the vent area per unit volume. The rapid rate of pressure rise resulting from an explosion must be countered by sufficient vent area in order to protect the equipment. The vent area is determined by the size of the rupture disk and can be one large disk or several smaller ones. Application of the data presented in the paper is limited to a maximum initial pressure of 60 psi between 50 and 90 F.

An example of successful protection at an initial pressure of 18,000 psi was afforded by a violent reaction which occurred in the vessel shown in Fig. 5. Note that two rupture disks are used and are located in the top and bottom heads. The vent area in square feet per hundred cubic feet of volume is 0.21. The vessel has a relatively low length-to-diameter ratio which is in the range of sizes tested by Cousins and Cotton. The rate of pressure rise from the reaction is comparable to a hydrogen-air mixture of maximum explosiveness. The vessel was not damaged by the rapid pressure pulse.

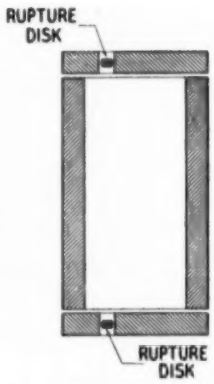

Fig. 5 Sketch Showing Location of Rupture Disks in Vessel Which Was Protected Adequately From Effects of Violent Reaction

Designing for Actual Service Conditions

The use of rupture disks to protect equipment operating at elevated temperatures requires special precautions. The temperature of the disk is determined by the operating temperature of the vessel and the geometry of the installation. The line between the vessel and the disk may be from 1 to 20 ft in length. The line may be lagged, unlagged, and in some cases jacketed with steam, depending on service requirements. Where elevated temperature conditions are known to exist at the disk, the actual temperature must be measured before the disk can be designed properly.

The installation shown in Fig. 5 represents an extreme case where the disks are located in the heads of the vessel. The temperature of the disk is the same as the 240 C operating temperature in the vessel. The original disks designed for this vessel were based on the shear strength at room temperature instead of the shear strength at 240 C. Several disks failed at pressures considerably below the design rupture pressure. Experimental bursting tests made at elevated temperatures showed that the shear strength of Type 329 stainless at 240 C is approximately 10,000 psi lower than the shear strength at 28 C. The disk was redesigned on this basis and is operating satisfactorily.

Experimental Bursting Tests at Elevated Temperatures

The effect of temperature on the shear strength of commercial bronze was determined since equipment operating as high as 300 C is protected with this type of disk. A single-hub and a double-hub disk were selected for the tests in an effort to determine also the effect of the design. The dimensions of the two types of disks differed only in the web thickness, the double-hub disk being 0.003 in. thicker. In plant service a 0.003-in. fine silver disk is used with this single-hub disk. In designing this disk, the rupture pressure of the composite disk is based on the sum of the bursting strengths of the two components. The validity of this design procedure at elevated temperatures was tested by bursting the single-hub disk with and without the silver.

The bursting tests were made in an Aminco dead-weight tester over a temperature range of 30 to 300 C. All dimensions were measured to the nearest 0.0001 in., temperature to ±2 C, and bursting pressures to ±25 psi.

The results of the tests are shown graphically in Fig. 6. The shear strength of the double-hub disk is consistently higher than the single-hub disk, without the silver, over the entire temperature range. Some deviation in the rate of decrease is also apparent from the two curves. Since all disks were machined from the same plate and heat-treated under the same conditions, the difference must be largely due to difference in design. Difference in grain

[3] "Design Closed Vessels to Withstand Internal Explosions," by E. W. Cousins and P. E. Cotton, *Chemical Engineering*, vol. 58, 1951, p. 133.

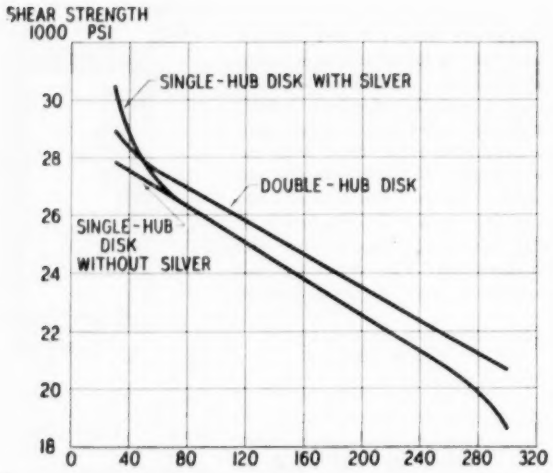

FIG. 6 COMMERCIAL BRONZE—SHEAR STRENGTH VERSUS TEMPERATURE

size between a web thickness of 0.020 and 0.023 in. is not likely to be a factor. There is some indication that actual shear area is less than the calculated shear area used in the design of the disks, and the deviation is greater in the single-hub-type disk.

The variation of shear strength with temperature of the single-hub-type disk with and without the silver is also compared in Fig. 6. At room temperature the difference between the two curves is 2800 psi, which compares closely to the shear strength of the silver disk. The shear strength of the composite bronze and silver disk drops sharply between 30 and 60 C. Above 60 C the two curves obtained with and without the silver disk coincide. The low yield strength of fine silver at moderately elevated temperatures probably accounts for the coincidence of the two curves. The decrease in rupture pressure of the composite disk between 30 and 60 C amounts to 1800 psi in a disk originally designed to burst at 13,500 psi. Allowance must be made for the 13 per cent decrease n bursting pressure as a result of being warmed to 60 C.

MECHANICAL PROPERTIES OF RUPTURE-DISK MATERIAL

The mechanical requirements of an ideal rupture-disk material appear to be a small plastic range, stability at elevated temperatures, reproducibility, and high creep strength. The relation between the yield strength (shear yield) and shear strength is important. If the plastic range is large, the yield strength is considerably lower than the shear strength, and the disk will yield at pressure well below the design rupture pressure. Yielding may occur as the result of intermittent pressure surges or may be continuous as in creep. Both effects will produce dimensional changes and strain-hardening which will alter the original design of the disk. An example of this is shown in Fig. 7. The original web thickness has been decreased by 12.5 per cent as a result of being in service at 18,000 psi and 240 C for a relatively short time. The 12.5 per cent decrease in web thickness corresponds to a 2700-psi drop in the calculated rupture pressure. Bursting of similar disks from the same service, however, shows no drop in rupture pressure of the disks, indicating that the amount of strain hardening has offset the reduced web thickness.

The shear-strength variation of 30,000 ± 800 psi determined for commercial bronze is considered to be a wide variation for rupture-disk material. The corresponding tensile-strength variation is 37,000 ± 2400 psi. The reproducibility of rupture disks fabricated from this material is necessarily difficult unless the

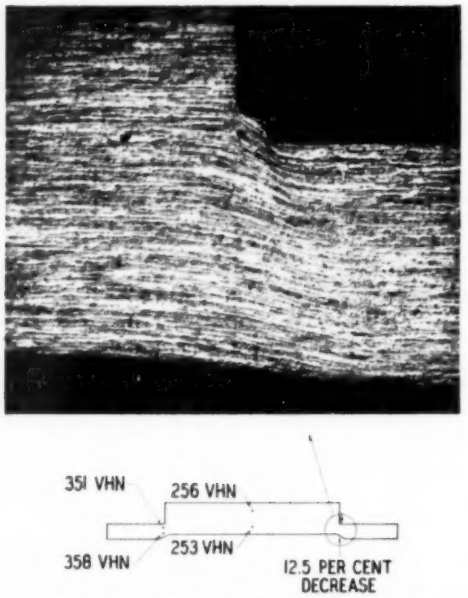

FIG. 7 *(Top)* CROSS SECTION OF TYPE 329 DISK WHICH HAS YIELDED IN SERVICE. *Below,* DIAGRAM SHOWS EXTENT OF DIMENSIONAL CHANGES AND STRAIN-HARDENING

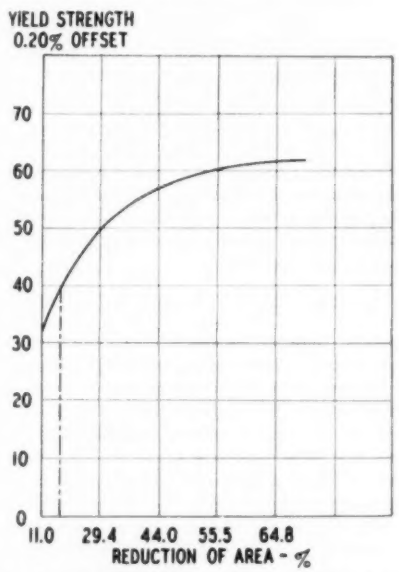

FIG. 8 COMMERCIAL BRONZE—EFFECT OF COLD-ROLLING

specified ranges are extended greatly. Probable reasons for the wide variation are the hardness specification and heat-treatment. Fig. 8 shows the variation of yield strength as a function of the amount of cold reduction in area. Half-hard material corresponds approximately to 15 per cent reduction in area. The slope of the curve at this point is very high and a small deviation in the amount of cold reduction will produce a large deviation in mechanical properties. Further, this relatively small amount of cold work will not produce homogeneity throughout the thickness of the plate. Subsequent recrystallization at 420 C will occur to a

greater extent at the surface as compared to the center. The web of the finished disk utilizes a thin section, from 0.01 to 0.06 in. thick, out of the center of the original $\frac{1}{4}$-in. stock. A specification of 60 per cent cold reduction of area would minimize greatly the variation of mechanical properties which in turn would permit narrower specified ranges compatible with the material. The material could be used in the "as-rolled" state or annealed to a specified grain size.

A small plastic range can be obtained either by cold-rolling or heat-treatment, provided the alloy is heat-treatable. Cold-rolled material has an economic advantage and should be entirely satisfactory for general applications where only moderate temperatures are encountered. The use of highly stable heat-treated alloys should be reserved for application of unusual severity.

Discussion and Conclusions

The conclusions which are drawn from the results of this investigation are limited to the particular group of disks under discussion. While some of the specific conclusions possibly could be translated into generalities applicable to any group of disks, such translations will be left to the reader. It should be noted that the shear-strength data contained herein are applicable only to commercial-bronze rupture disks having identical material and heat-treatment specifications. Comparison with published data indicates that the rate of decrease of shear strength with increasing temperature is greater than the rate obtained with standard shear specimens. This may be due to the stress-raising of the sharp corners created by the intersection of the web and the button.

The present specified ranges should be revised to include the sum of the ranges resulting from machine tolerances and shear-strength variation, as shown in Table 2. The shear-strength variation of 30,000 $\pm$ 500 psi for commercial bronze represents a practical compromise as shown by the frequency distribution in Fig. 3. For this reason, the fabrication of a large number of a given-type disk should be limited to a single plate of stock. If it is necessary to use different plates the disks made from each plate should be segregated and tested independently.

In some cases the suggested revised range is considerably larger than the present range. Consideration should be given to the possibility of redesigning the disk in order to decrease the range resulting from machine tolerances. The curves shown in Fig. 4 and Equation [2] will facilitate redesign of the disks.

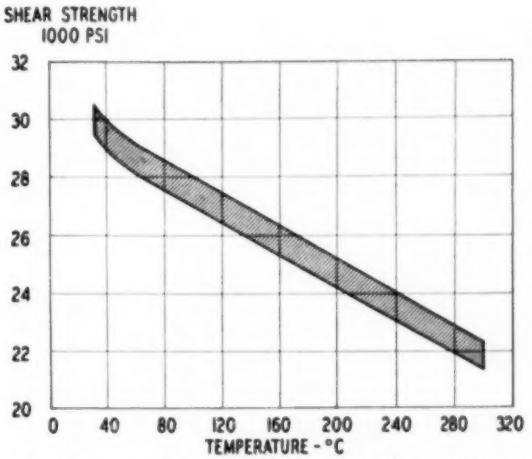

Fig. 9 Commercial Bronze—Shear Strength Versus Temperature

The sharp decrease of the shear strength of commercial bronze at moderately elevated temperatures requires that rupture disks of this material be designed on the basis of both operating pressure and temperature. For design purposes, the shear-strength variation and the rate of decrease of shear strength can be combined to yield a curve showing the relation of shear strength to temperature up to 300 C. The resulting curve is shown in Fig. 9.

The design of a bronze-and-silver composite disk based on the sum of the bursting strengths of the components is not a sound procedure. Control of this composite disk is difficult owing to the sharp decrease in the rupture pressure which occurs between 30 and 60 C. Above 60 C the silver contributes nothing to the total rupture pressure.

Design and Application of Controlled-Volume Pumps for High Pressure in the Range of 10,000 to 30,000 Psi

By D. H. JONES,[1] PHILADELPHIA, PA.

Any thorough examination of current trends in process development should include consideration of the steady move toward higher operating pressures in various fields. Certain reactions which are favored at higher pressures are being investigated not only in the laboratory, but now are being expanded into semiworks and even into full commercial scale. Reactions formerly undertaken only at lower pressures are being developed for use at high pressures because of higher efficiencies and better yields. Equipment manufacturers certainly have felt the impact of this trend in that high-pressure specifications are definitely increasing. Controlled-volume pumps are required for many developments in this high-pressure field and this paper is an examination of their design and application in the range of 10,000 to 30,000 psi.

Development of Controlled-Volume Pumps

CONTROLLED-volume pumps are reciprocating-plunger, positive-displacement-type pumps specifically designed to deliver accurately a metered quantity, a controlled volume, to a point of application. During the past 15 years this classification of pumps has developed from a mere adaptation of inaccurate forced-feed lubricators to the point where they are now considered precision instruments for the process industries. Previous papers (1)[2] have described their versatility in handling quantities from a few milliliters per hour to 45 gallons per minute accurately, in metering difficult materials such as slurries and those with varying viscosity, and their use in automatic pH-control and concentration-control systems.

Basically, these pumps consist of a plunger reciprocating in a specifically designed displacement chamber with check valves on suction and discharge sides. Properly designed, the displacement chamber, or liquid end, permits a controlled volume to be delivered for each plunger stroke—a quantity determined by the plunger diameter and plunger-stroke length. A typical liquid end for a controlled-volume pump, Fig. 1, employs double check valves on both the suction and discharge sides to assure the continuance of accurate pumping should one check temporarily be held off its seat. The checks are so arranged as automatically to discharge any entrained air or gas which could impair volumetric efficiency.

Capacity Adjustment

Capacity is adjusted by changing the plunger displacement.

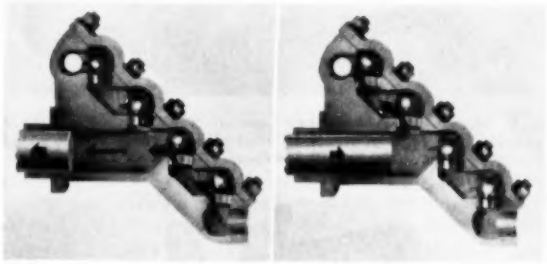

Fig. 1 Typical Liquid End of Low-Pressure Controlled-Volume Pump

Two methods of plunger stroke-length adjustment are generally available on motor-driven controlled-volume pumps. Stroke adjustment while the pump is stopped is made by adjusting the throw of the connecting rod through turning the crank screw as shown on this simplex high-pressure pump, Fig. 2. Frequently, however, it is not possible to stop operation in order to make capacity adjustments. Adjustment while the pump is in operation can be accomplished by using a mechanism, Fig. 3, capable of varying the relative positions of a fixed connecting rod and a variable-drive rod as shown on this duplex high-pressure pump. Capacity regulation also can be made by adjustment of the stroke speed, or frequency of plunger strokes made per minute while the pump is operating. Various means of speed regulation have been employed, including those permitting automatic regulation by process variables. Continuous operation makes automatic lubrication desirable as shown on this high-pressure duplex pump, Fig. 4. Liquid ends are jacketed on this unit to permit brine cooling when handling a liquefied hydrocarbon at low temperatures. This is also desirable to prevent temperature rise resulting from the heat of compression.

In addition to motor drivers, controlled-volume pumps are available powered by double-acting fluid cylinders as shown on the high-pressure pump, Fig. 5. Fluid pressures such as plant air pressures are employed in the cylinder to obtain desired pump-discharge pressures. The straight-through stroking action makes this design desirable for future higher-pressure developments since the crank mechanism required on the motor-driven types has been eliminated. Capacity adjustment is again made by regulation of the plunger-stroke length, or by control of the number of strokes per minute. Stroke-length adjustment on fluid-powered pumps differs from that on motor-driven pumps where adjustment is made around the center of the crank. In the fluid-powered pumps, adjustment of the stroke length is made by limiting the return stroke of the plunger. The forward position of the plunger is always the same regardless of stroke length, permitting maximum scavenging of the liquid end at all times and reducing the effect of compressibility on capacity delivered. Self-reciprocating, fluid-powered, controlled-volume pumps are employed as self-balancing hydrostatic-pressure generators, automatically building up the pressure in the system, or chamber

---

[1] Mechanical Engineer, Milton Roy Company.

[2] Numbers in parentheses refer to the Bibliography at the end of the paper.

Contributed by the Industrial Instruments and Regulators Division of The American Society of Mechanical Engineers and presented at the Seventh National Instrument Conference, Cleveland, Ohio, September 9-10, 1952.

Note: Statements and opinions advanced in papers are to be understood as individual expressions of their authors and not those of the Society. Manuscript received at ASME Headquarters, June 30, 1952. Paper No. 52—IIRD-3.

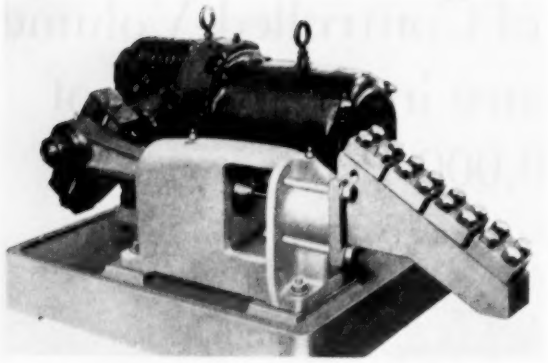

FIG. 2 SIMPLEX HIGH-PRESSURE CONTROLLED-VOLUME PUMP WITH CAPACITY CONTROLS BY STROKE-LENGTH ADJUSTMENT WHILE PUMP IS STOPPED

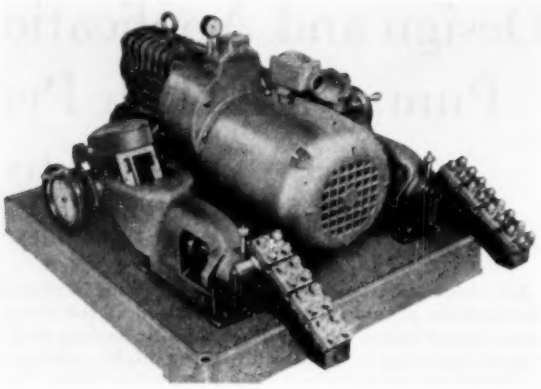

FIG. 3 DUPLEX HIGH-PRESSURE CONTROLLED-VOLUME PUMP WITH CAPACITY CONTROL BY STROKE-LENGTH ADJUSTMENT WHILE PUMP IS IN OPERATION

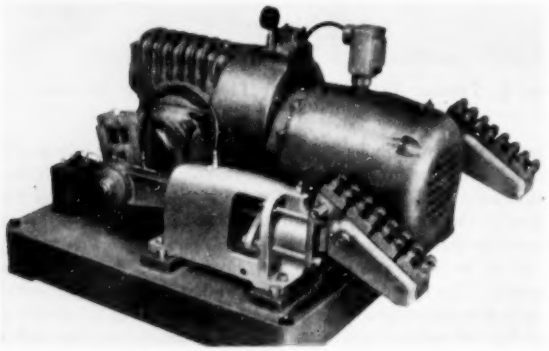

FIG. 4 DUPLEX HIGH-PRESSURE CONTROLLED-VOLUME PUMP WITH JACKETED LIQUID ENDS AND AUTOMATIC LUBRICATION

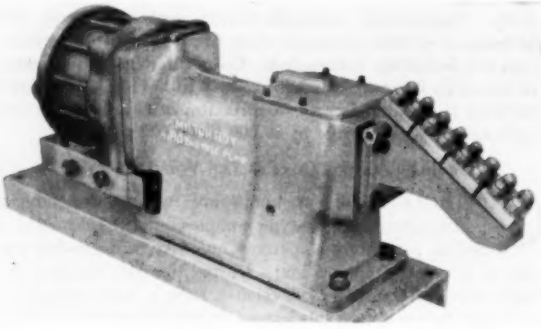

FIG. 5 AIR-POWERED HIGH-PRESSURE CONTROLLED-VOLUME PUMP

to be tested, until the fluid pressure acting on the piston area is balanced by the hydrostatic pressure acting on the plunger area. At this point the hydrostatic pressure is maintained at the desired value. If there is a small leak in the system, the plunger will move slowly forward to take up leakage and maintain pressure.

DESIGN OF HIGH-PRESSURE LIQUID ENDS

As research into high-pressure reactions increased, the manufacturers of controlled-volume pumps designed special high-pressure liquid ends in order that the equipment would meet the requirements for service in the range of 10,000 to 30,000 psi. Much of the design of the reciprocating mechanism used in the lower-pressure pumps is used, Fig. 6, by enlarging parts, increasing bearing areas, strengthening parts by changing materials of construction, and redesigning members such as the plunger where column action must be considered. The major changes are in the liquid end, or displacement chamber, where the higher pressures are encountered. A solid forging is required, with the passages connecting suction and discharge openings, and between one check valve and another, being machined rather than cast. It is necessary to maintain a similar arrangement of the check valves as on liquid ends for lower-pressure units in order to achieve controlled-volume pumping. An additional requirement is the necessity of keeping the total internal volume of the liquid end as small as possible because of the compressibility effect on liquids at these higher pressures. These factors are all considered in the present design, Fig. 7. Liquid ends of this type are ma-

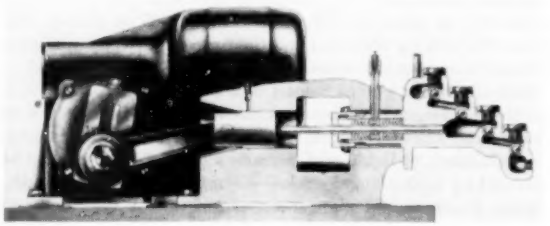

FIG. 6 CROSS SECTION OF TYPICAL LOW-PRESSURE CONTROLLED-VOLUME PUMP

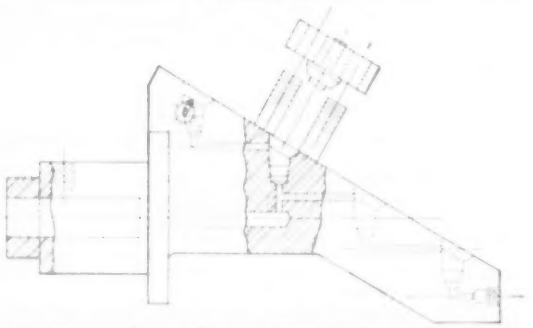

FIG. 7 TYPICAL LIQUID END OF HIGH-PRESSURE CONTROLLED-VOLUME PUMP

chined from forgings of stainless steel as well as from carbon steel.

The major problem facing any designer of high-pressure equipment is the development of methods of sealing the pressure within a given volume. Such sealing involves the use of joints, gaskets, and packing of one form or another. In the high-pressure liquid end described, three types of seals are employed. The liquid-end discharge outlet which is connected to the high-pressure system must be sealed and this is readily accomplished by using various tubing adapters available, so that standard high-pressure tubing is utilized. The openings over the check valves which permit individual inspection of each check valve must be sealed, and this is done by using mushroom-type plugs so machined as to give a tight metal-to-metal seal with the sockets machined in the liquid end body. Such an arrangement has been found satisfactory for pressures up to 25,000 psi. For pressures from 25,000 to 30,000 psi, it is necessary to incorporate a soft metal gasket between the mushroom plug and the socket, a successful method on which the limiting pressure has not yet been reached.

The third and most difficult problem involves the sealing of the reciprocating plunger. Many methods have been attempted to develop a special stuffing-box design suitable for use with plungers reciprocating at speeds up to 100 strokes per min on 3 to 4-in. maximum stroke lengths. It was hoped that some form of "unsupported-area" packing might be employed but as Bridgman has pointed out (2) this is not readily adaptable to a reciprocating plunger. The most successful plunger-stuffing-box combination found thus far, Fig. 8, includes the use of a hardened plunger superfinished to 3 to 5 microinches, with a special packing arrangement consisting of soft metallic-foil packing combined with other packing materials. Such a combination has proved satisfactory up to a maximum pressure of 30,000 psi.

Compressibility Effects

One of the most interesting effects of high pressure is the resulting compressibility of liquids. While investigators have been successful in measuring the compressibility of materials under pressures over 1,000,000 psi (3), the average engineer has little concept of the magnitude of this effect even in the lower high-pressure range from 10,000 to 30,000 psi. Compressibility is of even greater importance in this range, for the compressibility, of necessity, decreases greatly with increasing pressure—so much so that the average compressibility factor of a liquid at atmospheric pressure decreases to about one half of this value when measured at approximately 15,000 psi (4). Therefore the importance of compressibility in this range is such as to suggest most careful consideration by the engineer, particularly as this is the range in which most problems are being investigated today.

How this compressibility affects the design of high-pressure pumps was initially described by Schmoyer (5). Fig. 9 clearly illustrates the effect of the ratio R, on the theoretical volumetric efficiency with increasing pressure, where R is the ratio of the total internal volume of the liquid end of a pump to the displacement of its plunger or piston. These curves were obtained from calculations based on the formula

$$\text{Theoretical volumetric efficiency} = 100 - \beta\,(R\text{-}1)\,p$$

where β is the compressibility factor—the contraction in unit volume per atmosphere of pressure—R is the ratio just described, and p is the operating pressure in atmospheres. The formula itself is derived from the observation that not merely the volume displaced by the plunger, but the total internal volume between operating valve checks must be compressed to the operating pressure. The volume displaced per stroke, therefore, will be reduced by the amount the total internal volume has been compressed. The theoretical volumetric efficiency, the ratio of the plunger displacement accounting for compressibility to the actual plunger displacement, is also affected. For this graph, water, the liquid pumped, is assumed to be at a constant temperature and β the compressibility factor, is assumed to be an average value, 4.3×10^{-6}. No attempt has been made in this or other graphs used in this paper to compensate for slippage through the valve so as to show actual volumetric efficiencies rather than theoretical, since the slippage factor will vary depending on the fluid handled, liquid-end design, and valve check or valve-seat wear.

The graph clearly points out the necessity for consideration of the ratio R in the design of liquid ends for high-pressure pumps. Note that at 15,000 psi with $R = 13$, only half of the plunger displacement theoretically could be discharged.

In all calculations made for these graphs, the compressibility factors are based on a constant temperature and all compressions are assumed to be isothermal. In actual pumping there is a temperature rise due to the heat of compression. This heat of compression causes the volume of the liquid to expand which in some measure has an opposite effect to the compressibility.

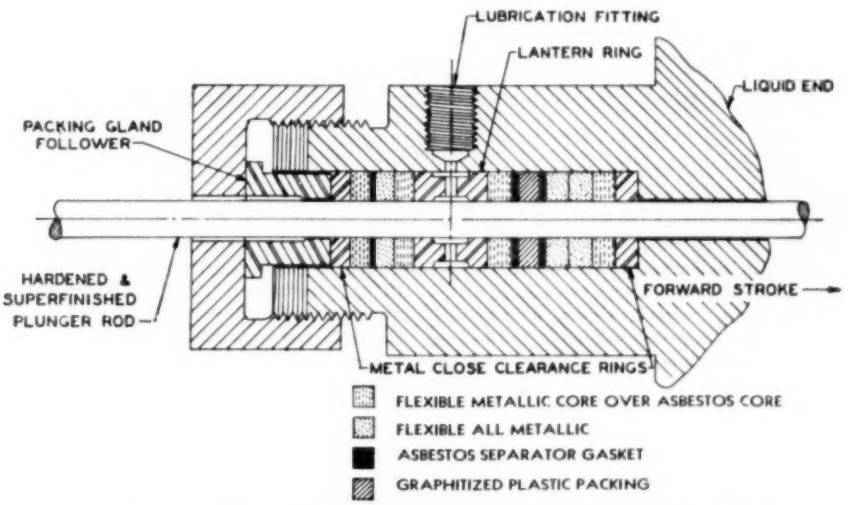

Fig. 8 Packing Arrangement for High-Pressure Controlled-Volume Pump

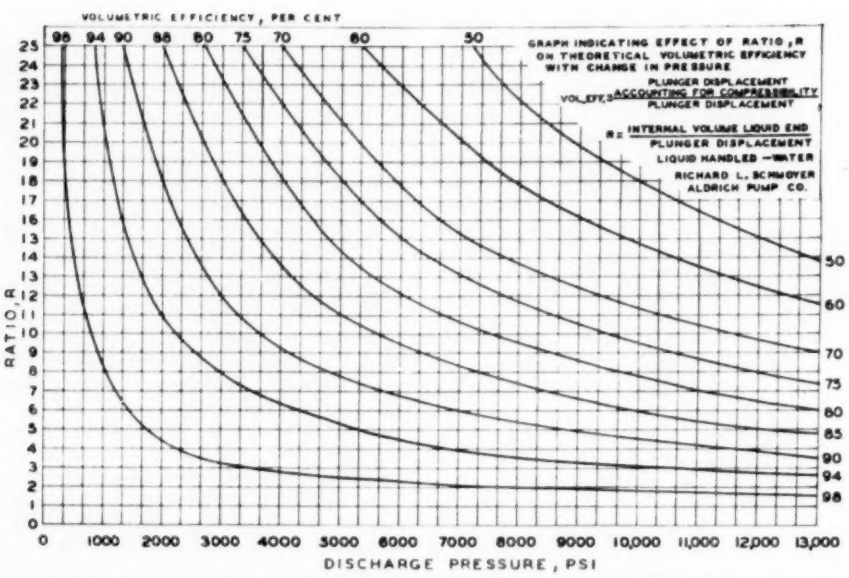
VOLUMETRIC EFFICIENCY, PER CENT
98 94 90 88 80 75 70 60 50
GRAPH INDICATING EFFECT OF RATIO, R ON THEORETICAL VOLUMETRIC EFFICIENCY WITH CHANGE IN PRESSURE
PLUNGER DISPLACEMENT
VOL. EFF. = ACCOUNTING FOR COMPRESSIBILITY
PLUNGER DISPLACEMENT
R = INTERNAL VOLUME LIQUID END
PLUNGER DISPLACEMENT
LIQUID HANDLED — WATER
RICHARD L. SCHNOVER
ALDRICH PUMP CO.
RATIO, R
DISCHARGE PRESSURE, PSI
0 1000 2000 3000 4000 5000 6000 7000 8000 9000 10,000 11,000 12,000 13,000
50 60 70 75 80 85 90 94 98

FIG. 9 GRAPH INDICATING EFFECT OF RATIO R, ON THEORETICAL EFFICIENCY WITH RANGE IN PRESSURE
(As reproduced from reference 5.)

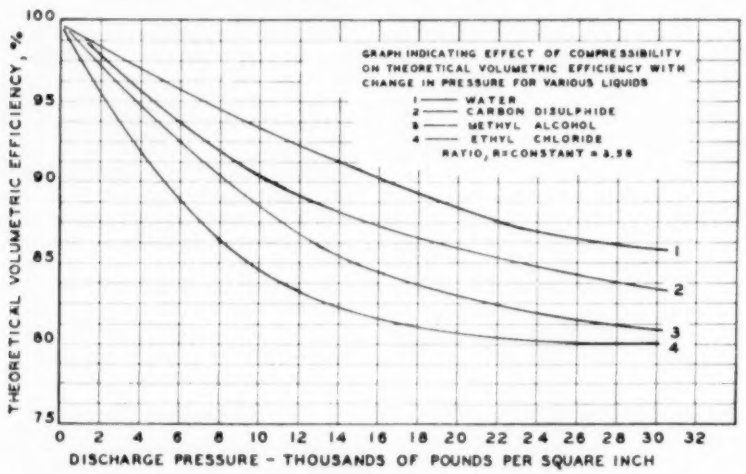
GRAPH INDICATING EFFECT OF COMPRESSIBILITY ON THEORETICAL VOLUMETRIC EFFICIENCY WITH CHANGE IN PRESSURE FOR VARIOUS LIQUIDS
1 —— WATER
2 —— CARBON DISULPHIDE
3 —— METHYL ALCOHOL
4 —— ETHYL CHLORIDE
RATIO, R=CONSTANT = 3.58
THEORETICAL VOLUMETRIC EFFICIENCY, %
100 95 90 85 80 75
0 2 4 6 8 10 12 14 16 18 20 22 24 26 28 30 32
DISCHARGE PRESSURE - THOUSANDS OF POUNDS PER SQUARE INCH
1 2 3 4

FIG. 10 GRAPH INDICATING EFFECT OF COMPRESSIBILITY ON THEORETICAL VOLUMETRIC EFFICIENCY WITH CHANGE IN PRESSURE FOR VARIOUS LIQUIDS

Since many liquids other than water are now being employed in high-pressure work, a graph showing the comparison of several of these with water is given in Fig. 10. The ratio R in this case is considered to be constant, as it would be for any given set of conditions. Also, a controlled-volume pump was selected with a capacity range of 0 to 4 gph, a range frequently used in high-pressure applications. With an internal volume of 1.615 cu in. and with a $^{7}/_{16}$-in-diam plunger on a full 3-in. maximum stroke length having a displacement of 0.451 cu in., the liquid end of this pump has an R of 3.58, the constant value used. The values for β (6, 7, 8) were not taken as average values over a wide pressure range, but were corrected values for various pressures.

The graph shows how, with a specific pump having a constant R, the theoretical volumetric efficiency will decrease at different rates for different liquids, indicating that the designer must consider carefully the liquid to be pumped and its individual compressibility.

Since controlled-volume pumps have adjustable plunger-stroke lengths to permit capacity adjustment, it follows that R will change when the stroke length is changed. The ratio R increases as the stroke length decreases, since the internal volume remains the same, while the plunger displacement decreases. Assuming the previously selected pump was handling methyl alcohol, the effect on theoretical volumetric efficiency of changing stroke length from 3 in. to 2 in. to 1 in., and therefore the effect of a change in R, can be seen on the graph, Fig. 11.

Fluid-powered controlled-volume pumps have a definite advantage over motor-driven units in regard to stroke-length adjustment and its effect on volumetric efficiency. Stroke-length adjustment is made around the center of the crank on motor-

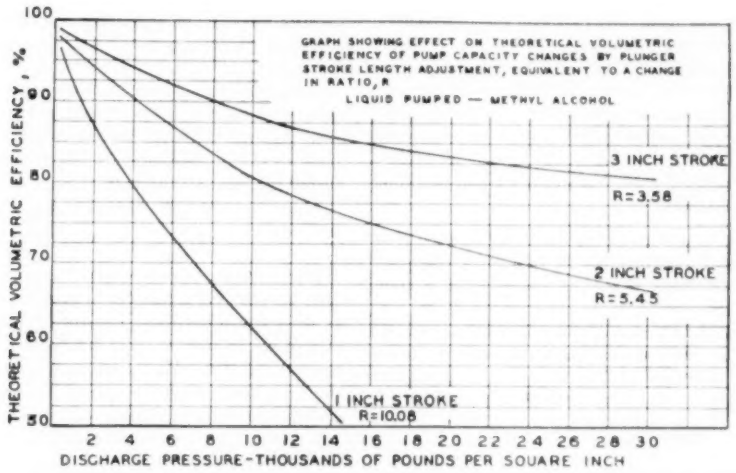
GRAPH SHOWING EFFECT ON THEORETICAL VOLUMETRIC EFFICIENCY OF PUMP CAPACITY CHANGES BY PLUNGER STROKE LENGTH ADJUSTMENT, EQUIVALENT TO A CHANGE IN RATIO, R
LIQUID PUMPED — METHYL ALCOHOL
3 INCH STROKE
R=3.58
2 INCH STROKE
R=5.45
1 INCH STROKE
R=10.08
THEORETICAL VOLUMETRIC EFFICIENCY, %
100
90
80
70
60
50
2 4 6 8 10 12 14 16 18 20 22 24 26 28 30
DISCHARGE PRESSURE-THOUSANDS OF POUNDS PER SQUARE INCH

FIG. 11 GRAPH SHOWING EFFECT ON THEORETICAL VOLUMETRIC EFFICIENCY OF PUMP-CAPACITY CHANGES BY PLUNGER STROKE-LENGTH ADJUSTMENT, EQUIVALENT TO A CHANGE IN RATIO R

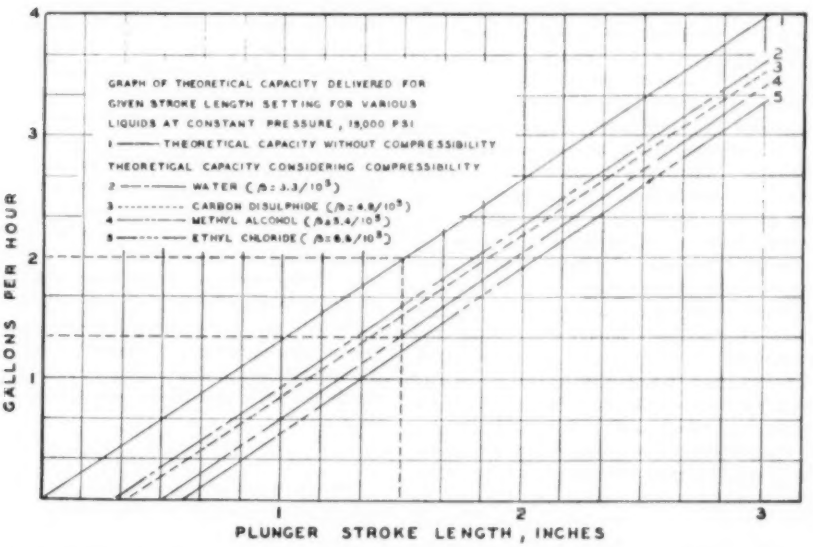
GRAPH OF THEORETICAL CAPACITY DELIVERED FOR GIVEN STROKE LENGTH SETTING FOR VARIOUS LIQUIDS AT CONSTANT PRESSURE, 15,000 PSI
1 ——— THEORETICAL CAPACITY WITHOUT COMPRESSIBILITY
THEORETICAL CAPACITY CONSIDERING COMPRESSIBILITY
2 ——— WATER (β = 3.3/10⁶)
3 ---------- CARBON DISULPHIDE (β = 4.8/10⁶)
4 ——— METHYL ALCOHOL (β = 5.4/10⁶)
5 ----- ETHYL CHLORIDE (β = 6.6/10⁶)
GALLONS PER HOUR
4
3
2
1
1
2
3
PLUNGER STROKE LENGTH, INCHES

FIG. 12 GRAPH OF THEORETICAL CAPACITY DELIVERED FOR GIVEN STROKE-LENGTH SETTING FOR VARIOUS LIQUIDS AT CONSTANT PRESSURE, 15,000 PSI

driven pumps, while adjustment by limiting the return stroke of the plunger is used on fluid-powered pumps. Using C as the displaceable volume in any liquid end and D as the displacement of the plunger on maximum stroke length, the ratio R equals $(C + D)/(D)$. Decreasing the stroke length to half its maximum the ratio R for a fluid-powered pump equals $(C + D/2)/(D/2)$. When the stroke length is reduced to half its maximum on motor-driven pumps the ratio R equals $[(C + D/4) + D/2]/(D/2)$. Therefore C is increased by $D/4$ because the plunger does not return to the same forward position. This increase in C on motor-driven pumps further increases the ratio R which in turn further decreases the volumetric efficiency. A comparison of the two illustrates the definite advantage of the fluid-powered controlled-volume pumps in this respect.

Using the same controlled-volume pump as used for the previous graph, Fig. 11, for operation at a constant pressure of 15,000 psi—most applications will involve constant pressures—the effect of compressibility on theoretical capacity delivered is illustrated in Fig. 12 when pumping various liquids. While the theoretical capacity delivered for a certain stroke-length setting at 15,000 psi is always less than the displacement of the plunger, the reduction in capacity differs with different liquids, depending on the compressibility factor, which at 15,000 psi is 6.6×10^{-6} for ethyl chloride; 5.4×10^{-6} for methyl alcohol; 3.3×10^{-6} for water; and 4.8×10^{-6} for carbon disulphide. An example of the appreciable effect of compressibility on capacity of controlled-volume pumps is given, showing that when a capacity of 2 gph of methyl alcohol might be expected from the displacement, only 1.4 gph theoretically will be delivered. Another point to note is that the capacity range through stroke-length adjustment is reduced materially. Under normal operating conditions at lower pressures a capacity range from 100 to 10 per cent of maxi-

mum or 10 to 1 is easily and accurately obtained through stroke-length adjustment. At 15,000 psi this capacity range is reduced to approximately 6 to 1 as a theoretical maximum, due solely to compressibility, and indicating that speed adjustment be employed if wide capacity adjustment is required. In addition, the pump must be calibrated for each liquid handled, since compressibility affects each differently.

The effects of compressibility on controlled-volume pumping point up the following factors:

1 The designer of the liquid end should attempt to keep R as small as practical in order to reduce loss in volumetric efficiency and also reduce the horsepower wasted in excess work of compression.

2 The manufacturer and the user of controlled-volume pumps for high-pressure service must work closely together in order to make the proper selection of the unit for a particular application, since compressibility so greatly affects capacity.

Application

Controlled-volume pumps are employed successfully to meter liquids under high pressures, to compress hydraulically a gas to a high pressure, and in hydrostatic-pressure testing. With the advent of petrochemicals, the petroleum and chemical industries have intensified their research programs in high-pressure synthesis. The word "petrochemical" is self-explanatory—a chemical derived from petroleum. A primary petrochemical would be a petroleum hydrocarbon. Rossini (9) has shown that 72 hydrocarbons have been isolated from petroleum. Many of these hydrocarbons are in the gaseous state at room temperature and atmospheric pressure. The research investigator and the manufacturer of chemical and petroleum products frequently desire to handle these gaseous hydrocarbons in the liquid state, which necessitates high pressures. Many times he is concerned with the maintenance of a continuous process. To introduce these hydrocarbons into such a system and maintain their concentration at a fixed amount, a controlled-volume pump is required.

The hydrocarbon that has in all probability given the greatest impetus to the development of new products is ethylene. Ethylene lends itself well to the alkylation of other hydrocarbons with the production of a carbon to carbon alkylate. Such an alkylation is obtained by a number of methods and furnishes such products as intermediates in the preparation of antioxidants, detergents, and dyes. Ethylene also polymerizes with itself to produce intermediates for polyethylene resins and plastics, and alkylate for high-octane gasolines. Liquid ethylene has been handled successfully by controlled-volume pumps in the investigation and production of petrochemical intermediates.

The partial list which follows represents some of the materials handled by controlled-volume pumps at high pressures:

1 Aliphatic hydrocarbons.

(*a*) Saturated compounds such as propane.

(*b*) Unsaturated compounds other than ethylene, such as propylene and butylene.

2 Aromatic hydrocarbon compounds such as benzene.

3 Miscellaneous materials such as solutions of various organic and inorganic compounds.

As previously mentioned, controlled-volume pumps are used to compress a gas to a high pressure hydraulically. This pressure generator, as it is called, maintains a constant pressure of gas over the liquid in a closed cylinder containing the gas and liquid by the introduction of more liquid into the cylinder causing the gas to be compressed. The compressed gas is then used for investigating various chemical reactions, the effect of high pressures on decomposition rates of such materials as explosives, and the burning velocity of propellant powders. Fluid-powered, self-balancing pressure generators are particularly well adapted for this service.

A third field of application is the use of these pumps for hydrostatic pressure testing. They are used by high-pressure equipment manufacturers for pressure testing, by the aircraft and steel industries for testing forgings and castings, and by the rubber industry for burst test on high-pressure hose. Oil, water, and glycerine are the hydraulic fluids employed in such testing.

Safety and New Development

The use of controlled-volume pumps in high-pressure service has been proved over a number of years in many applications. Just as with any other high-pressure equipment, such high-pressure pumps are as safe as those for lower pressures by using certain precautions (10). High-pressure tubing specifically designed for the operating range is required. A positive relief valve is installed on the discharge side of the liquid end to protect the pump and system from overpressure due to accidental blocking or closure in the discharge line. The relief valve is piped to a safe point of discharge, possibly back to the suction side of the pump, and the pipe employed must be of sufficient size to permit quick discharge and relief of the pressure. Fluid-powered pumps are protected by placing a relief valve in the fluid-pressure line, since limiting the fluid pressure automatically limits the discharge pressure against which the pump can operate. High-pressure liquid ends should be given hydrostatic tests, initially by the manufacturer and then periodically by the user. Even with these precautions, some users of controlled-volume pumps have placed them behind heavy barriers for protection of the operators, although this is usually due to the explosive nature of the materials handled rather than the high pressure itself. However, caution must always be exercised, for there are some phenomena experienced at high pressure which are not clearly understood at this time. The report of Russell and Mueller describing the explosive decomposition of propylene, ethylene, and actylene is an example (11). Under certain pressure-temperature conditions these may decompose spontaneously with a sudden violent rise in pressure and temperature. The use of jacketed liquid ends is desirable on many applications where it is essential to limit temperature rise.

Conclusion

This discussion of high-pressure pumps has given the history of this type equipment as it has been developed to date. The future of the controlled-volume pump in the high-pressure field has been established in its utility in the applications outlined. Already scientific personnel in industry and in our universities are considering pressures beyond the present range. The necessary tools for such investigations will be available to them with the development of new controlled-volume pumps for higher pressures. The responsibility for this development does not rest solely with the manufacturer. Only through the co-operation of both the equipment manufacturer and the personnel concerned with the utilization of such equipment can these goals be achieved to their mutual satisfaction. The challenge is certainly an interesting one.

BIBLIOGRAPHY

1 "Electronics in Automatic Chemical Feed Systems," by R. T. Sheen, Trans. American Institute of Chemical Engineers, vol. 42, 1946, pp. 725–739; and Paper No. 48-4-3, Conference of Instrument Society of America, Philadelphia, Pa., 1948.

2 "The Physics of High Pressure," by P. W. Bridgman, George Bell & Sons, London, England, 1949, p. 49.

3 Ibid., p. 402.

4 Ibid., p. 132.

5 "Compressibility of Liquids," by R. L. Schmoyer, *Machine Design*, vol. 19, August, 1947, pp. 134–137.

6 "Smithsonian Physical Tables," eighth edition, Smithsonian Institution, Washington, D. C., 1934, Table 106; also "Chemical Engineers' Handbook," by J. H. Perry, third edition, McGraw-Hill Book Company, Inc., New York, N. Y., 1950, p. 209.

7 "International Critical Tables," McGraw-Hill Book Company, Inc., New York, N. Y., vol. 3, 1928, pp. 35, 40, 41.

8 Reference (2), pp. 128–230.

9 "Hydrocarbons in Petroleum," by F. D. Rossini, *Chemical and Engineering News*, vol. 25, 1947, pp. 230–233.

10 "Chemical Engineers' Handbook," by J. H. Perry, third edition, McGraw-Hill Book Company, Inc., New York, N.Y., 1950, p. 1261.

11 Paper presented by F. R. Russell and R. H. Mueller before Fuel, Gas and Petroleum Chemistry Section of the 12th International Congress of Pure and Applied Chemistry, New York, N. Y., Sept. 9–13, 1951.

Seals to Minimize Leakage at Higher Pressure

By B. A. NIEMEIER,[1] RICHMOND, VA.

Fixed and moving seals to be used in the super-pressure range, 10,000 to 100,000 psi, as classified by the author, are studied and evaluated. A general discussion of the theoretical problems in confining pressures of great magnitude precedes methods for designing seals for such pressures. A method and device for evaluating seals has been developed to provide confirmation of theories. Practical seal problems and applications are shown.

Introduction

A CONCERN exists for the strength-of-material problem in the design of pressure vessels, valves, piping, and all such devices which subjugate fluids to specific zones; however, the mechanical design of joints and auxiliary members whose purpose is to close the connections is a problem of paramount importance. In developing mechanical devices, engineers and designers are faced constantly with the problem of preventing leakage. For simple cases at ordinary pressures, techniques are available to retain lubricating oils, hot gases, and similar substances. In many other instances gases, oils, or chemical liquids must be confined with an effective and trouble-free seal under pressures of great magnitude.

The purpose of the work discussed in this paper has been the analysis and development of seals for use in the super-pressure range. Super pressure, high pressure, and low pressure are admittedly relative, but for a somewhat parallel classification to the velocity subdivisions the following has been suggested:

Classification	Range
Low pressure	1–1000 psi
High pressure	1000–10000 psi
Super pressure	10000–100000 psi

A brief look at the problem of super-pressure seals suggests that the interrelation of the mechanics of the fluid being sealed and the mechanical device making the final closure of the confined space is of prime importance. Moreover, when super pressures exist, the elastic displacement of the pressure vessel as well as the motion of the seal device must be studied. Correlation of all the factors of importance in sealing ordinary fluids at super pressures and the analysis of several specific seal configurations is the primary purpose of this investigation.

Theoretical and Engineering Considerations

Fixed-Point Seals. A juncture void of any seal member, as shown in Fig. 1, has an unclosed area which is the product of the gap and a periphery of the volume contained; furthermore, the gap as a measure of the relative position of the two members is the principal factor which causes the loss of fluid at any given pressure. Within the super-pressure range the gap created at the

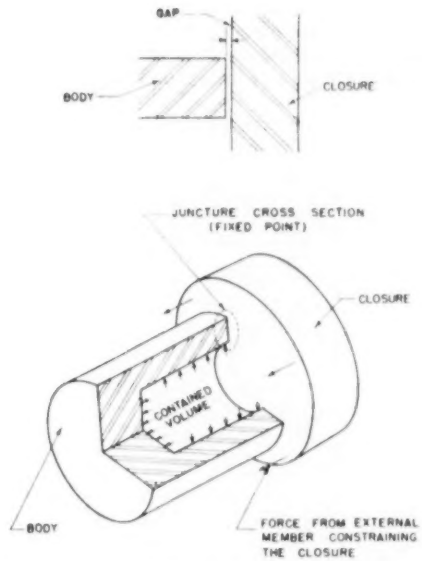

Fig. 1 Generalized Fixed-Point and Related Parts

closure due to elastic deformation of the mated members and those members constraining the joint will be of primary importance. Brkich (1)[2] has shown the quantity of leakage at low pressure to be expected from a constant axial gap. This clearance or gap between two parts forming the junction is recognized to be important whether intended from design or expected from strain displacements of the members.

No leakage occurs when two adjacent parts are in contact in such a manner that the pressure of contact is greater than the pressure of the sealed liquid or gas. Professor Bridgman (2) arrived at this conclusion in discussing the fully enclosed packing used by Amagat. Such contact pressures are obtained directly from the pressure in the vessel when the seal area exposed to pressure is greater than the area upon which the constraints act to maintain the seal in the cavity. The important criteria by which high contact pressures are attained are the seal, cavity, and the surfaces at the contact points.

The contact-pressure effects can be visualized from inspection of Fig. 2. In this diagram various types of geometric surfaces are maintained against a flat surface by a constant force. Rigid-body assumption for the members would suggest immediately that the knife-edge, type C-1, would seal best. All the geometric contacts, in theory at least, might be expected to seal the pressure so long as the pressure at contact is made greater than the confined pressure. However, elastic changes in the body and closure will induce effects at the seal point that may create a gap and leakage path of considerable importance.

A series of plausible seal-ring cross sections which may have

[1] Senior Engineer, Experiment Incorporated, Deepwater Terminal. Mem. ASME.

Contributed by the Industrial Instruments and Regulators Division of The American Society of Mechanical Engineers and presented at The Seventh National Instrument Conference, Cleveland, Ohio, September 9–10, 1952.

Note: Statements and opinions advanced in papers are to be understood as individual expressions of their authors and not those of the Society. Manuscript received at ASME Headquarters, July 14, 1952. Paper No. 52—IIRD-11.

[2] Numbers in parentheses refer to the Bibliography at the end of the paper.

the following recommended characteristics for super-pressure seals are shown in Fig. 3:

1 Unsupported area configuration.
2 Seal-ring material of steel or a substance of similar high modulus of elasticity and strength.
3 Compensation for elastic changes of body and closure.
4 Seal action is only a minor function of the bolt load.

In general, means for utilizing the inner pressure of a pressure vessel for actuating the seal are in themselves universally recognized (3, 4, 5). The mechanics of particular arrangements are not fully understood, as there are reported (6) to be hundreds of closure designs differing very little in principle.

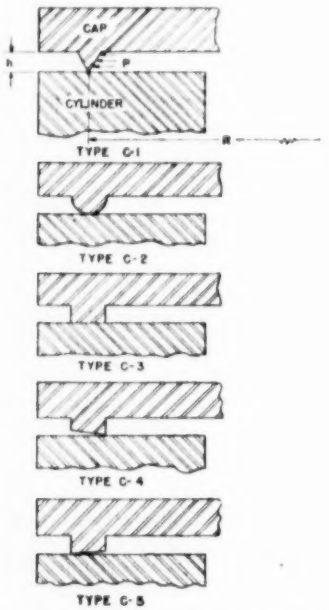

FIG. 2 CONTACT-GEOMETRY CONFIGURATIONS

The unsupported area configuration refers to a cross section of the seal ring and cavity wherein the area over which the pressure force acts is greater than the area upon which the other forces external to the cross section act. In such an arrangement an intensification of the unit load of the internal pressure occurs. If this intensified unit load, i.e., the contact pressure, is not derived from the internal pressure, then the force must come from the external members constraining the closure. Two general classifications of unsupported-area-type rings have been found to exist—the axial and radial types. The axial types, which include the Bridgman and all its modifications, are the more complex and require longitudinal stresses in the rings to resolve themselves into lateral pressure by Poisson's effect, and thereby produce the contact pressure required. The radial types, rectangular, triangular, circular, lens, wave ring, cross sections, to mention a few, consist of a single item and directly resolve the radial pressure into radial contact pressure by a slight stretch of the ring which should be designed to have more elastic deformation than the related cylinder and cap.

The two classes mentioned, illustrated in Fig. 3, have the following principal features:

S-1 Ring of triangular cross section (delta ring, reference 7) whose sealing is effected by a wedge action between the cap and cylinder.

S-2 Modification of S-1 to provide for increased area of contact and thereby lower the contact pressure such that plastic flow of the gasket need not occur.

S-3 Ring of rectangular cross section, arranged with orientation to give wedge action but less contact pressure than S-1 and have greater internal restraint, i.e., resistance to expulsion into the gap.

S-4 Ring of circular cross section providing equal contact pressure on the cap and cylinder and eliminating points of stress concentration.

S-5 Similar to S-4, but arranged to permit simple cap design and further reduction of stress concentration.

S-6 The double-coned design found in principle (8) in German high-pressure autoclave practice.

S-7 Lens type (6), which is essentially a wedge type, wherein the orientation of the wedge is fixed, or this may be a ring type basically with a radius placed on the ring at the contact points.

S-8 A three-point restraining ring of irregular cross section.

S-9 Bridgman type which has a floating head for pressure intensification.

Wedge-Type Seals. The type S-1 rings undergo action in sealing as shown in Fig. 4. Essentially, the ring is a wedge that the pressure drives into a cavity provided by the cap and body. The reported galling (6) does not happen when the cap-cylinder angle is less than the ring angle by an amount only slightly

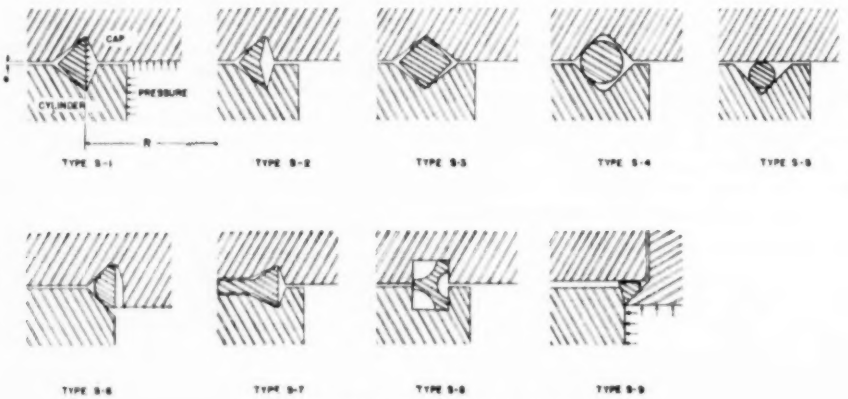

FIG. 3 FIXED-POINT SEAL CONFIGURATIONS

less than the angle of repose, and the following formula is used to determine the width of the ring

$$L = \sqrt{\frac{d^2 p}{E\,[\tan\,(45 + {}^1/_2 \arctan f) - 1]}} \quad \ldots\ldots [1]$$

where

L = axial length of ring, in.
d = diameter of ring, in.
E = modulus of elasticity
f = coefficient of friction between ring and cavity
p = internal pressure, psi

The triangular ring stretches similar to a thin-wall cylinder

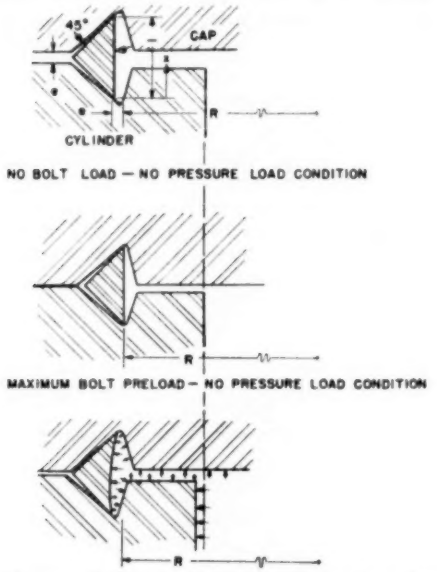

FIG. 4 MAXIMUM BOLT LOAD-MAXIMUM PRESSURE LOAD CONDITION

for as the pressure is applied the cap lifts away. The outer cavity angle may be defined in terms of the radial increase in the gasket

$$\tan\,(45 + {}^1/_2 \arctan f) = \frac{\Delta R + x}{x} \quad \ldots\ldots [2]$$

The radial displacement for a thin vessel, such as this ring, depends on the internal pressure and takes the form

$$\Delta R = \frac{pR^2}{Et} \quad \ldots\ldots [3]$$

The thickness t, of the axial element x-units long has a value $x/2$, but one end, $x = 0$, remains fixed and thus we can write

$$2\,\Delta R = \frac{2pR^2}{Ex} \quad \ldots\ldots [4]$$

Equation [4] combined with [2] gives

$$\tan\,(45 + {}^1/_2 \arctan f) = \frac{pR^2}{Ex^2} + 1 \quad \ldots\ldots [5]$$

The maximum value x is, by the limits imposed by Equation [2], $L/2$. With this value Equation [5] can be transformed to give the axial length of Equation [1].

Nonwedge-Type Seals. The type S-8 ring functions differently from the prior types. This ring is an expansion type which increases in axial length under load and does not decrease as do the other types. As shown schematically in Fig. 3, the ring cross section seals at four points. Radially, the ring must undergo the same deformation as the cylinder and cap. In order to compensate for cap displacement under load, the cross section must extend axially.

The contact pressures from this type seal, Fig. 5, depend more

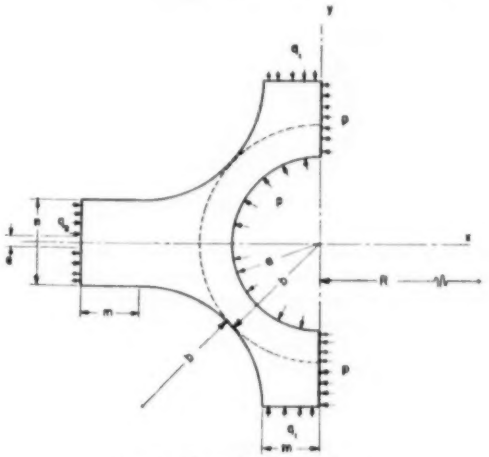

FIG. 5 TYPE S-8 STATIC SEAL

on the internal restraints than do those of the wedge type. When these restraints are not significant, the contact pressures as a maximum depend on the following ratios

$$q_2 = \frac{p(2b + n)}{n - e} \quad \ldots\ldots [6]$$

$$q_1 = \frac{pa}{m} \quad \ldots\ldots [7]$$

Moving Seals. These devices or means which close the clearance between members translated relative to each other have been termed moving seals. In contrast with sealing between members which are essentially fixed, the elimination of leakage requires the study of more complex phenomena, e.g., the case of a piston within a cylinder. As in the problem statement for fixed-point seals, the unclosed area, created in this case by design clearance and manufacturing tolerances, must be made zero if no leakage is to be tolerated.

When super pressures are bounded by a moving seal, we must expect contact pressures in excess of 10,000 psi. Fluids in contact and moving over a surface at such pressures do not create the same problems as when solid materials are rubbed over the same surface at similar pressures.

In a series of accounts efforts have been made to explain the proper design parameters for a specific seal or packing. Among these in the low-pressure and high-pressure ranges, Beacham (9) has shown the important arrangements for rotating and moving seals. The theory and design criteria (1) for mechanical seals exclude the effects created by elastic changes of the basic related members, i.e., piston and cylinder. Rothrock and Marsh (10) used a dimensionless-analysis technique to predict the leakage in fuel-injection units, but assumed, when taking into account elastic changes, that the pressure was constant along the leakage path.

The parameters which must be studied in order to produce a good moving seal can best be had by considering a simple piston and cylinder void of any seal, Fig. 6. Functionwise, the contained

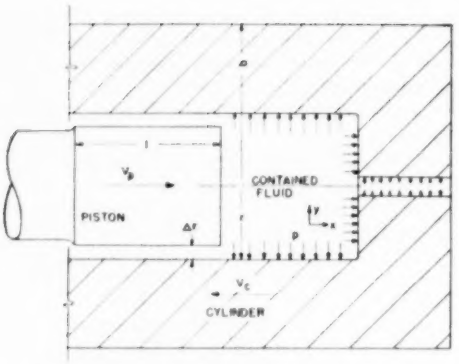

FIG. 6 GENERALIZED PISTON-AND-CYLINDER COMBINATION

fluid may be displaced by either moving the piston or the cylinder. The leakage through the clearance between the piston and cylinder interface is obtained by studying the fluid flow in this zone. Since the clearance is small, a combination of parabolic laminar and linear laminar flow exists. Elementary fluid-flow considerations relate the leakage to other physical quantities as follows

$$Q_L = 2\pi r \Delta r v_{avg} \quad [8]$$

The solution to this equation depends on proper assignment of the average velocity and radial clearance.

The velocity in a particular lamina is the sum of the relative components. For the parabolic leakage profile

$$v_1 = v_{max}\left[1 - 4\left(\frac{\Delta r - 2y}{2\,\Delta r}\right)^2\right] \quad [9]$$

For the linear leakage profile resulting from the piston

$$v_2 = v_p \frac{y}{\Delta r} \quad [10]$$

and from the cylinder

$$v_3 = v_c\left(1 - \frac{y}{\Delta r}\right) \quad [11]$$

The average velocity of flow in the clearance will be the sum of the average values obtained for Equations [9], [10], and [11].

The average velocity of the parabolic profile is $^2/_3$ the maximum. The average for the linear profiles is $^1/_2$ the maximum. The average velocity is written as follows

$$v_{avg} = \frac{2}{3}\frac{(\Delta r)^2}{8\mu}\left(-\frac{dp}{dx}\right) - \frac{v_p}{2} + \frac{v_c}{2} \quad [12]$$

This result in Equation [8] gives the leakage

$$Q_L = \frac{\pi r(\Delta r)^3}{6\mu}\left(-\frac{dp}{dx}\right) - \pi r(\Delta r)(v_p - v_c) \quad [13]$$

Equation [13] is a basic expression for leakage applicable to any moving cylindrical seal, and is not restricted to the limitations in Fig. 6.

In the super-pressure range Δr is a function of pressure sufficient to alter the pressure gradient. A more complex result is obtained when with Equation [13] an integration is performed using the dynamic clearance.

$$\Delta r = \Delta r_1 - \frac{rvp'}{E} + \frac{r}{E}\left(\frac{2b^2}{b^2 - r^2}\right)p \quad [14]$$

where

p' = maximum value of p
E = modulus of elasticity of piston and cylinder
ν = Poisson's ratio
b = outside radius of cylinder
r = inside radius of cylinder

The elastic changes produce a radial clearance which is not constant along the length of seal and is dependent on the pressure at the point being studied. As a result the laminar-leakage profile will be affected by these elastic changes through the pressure-gradient term.

Equation [14], which was obtained by summing the individual clearance terms, shows that the dynamic clearance is a linear function of pressure in the clearance volume. The solution to Equation [13] must be made simultaneous with Equation [14] as follows

$$\Delta r = K_1 + K_2 p \quad [15]$$

$$-\frac{dp}{dx} = \left[\frac{Q_L + \Delta r \pi r(v_p - v_c)}{\pi(\Delta r)^3 r}\right]6\mu \quad [16]$$

This theoretical formulation is restricted, of course, to the simple piston-cylinder combination where laminar flow of the leakage occurs. The best form for the result is to solve for the length of seal. At $x = 0$, $p = p'$ and $x = X$, $p = 0$

$$X = \frac{(K_1 + K_2 p')^3 - K_1^3}{18\,\mu K_2(v_p - v_c)} - \frac{Q_L(K_1 + K_2 p')^2 - Q_L K_1^2}{12\,\mu K_2 \pi r(v_p - v_c)^2} + \frac{Q_L^2(K_2 p')}{6\mu K_2 \pi^2 r^2 (v_p - v_c)^3} - \frac{Q_L^3 \log\left(1 + \frac{K_2}{K_1}p'\right)}{6\mu K_2 \pi^3 r^3 (v_p - v_c)^4}$$

where

$$K_1 = \Delta r - \frac{rv}{E}p' \text{ and } K_2 = \frac{r}{E}\left(\frac{2b^2}{b^2 - r^2}\right) \quad [17]$$

Equation [17] contains refinements not used by Rothrock and Marsh (10), and is felt to be more nearly representative of the actual leakage. When the motion of the piston and cylinder does not exist, i.e. zero, the integration from Equation [16] to obtain [17] is not proper. The expression obtained after integration is meaningless if zero piston and cylinder velocity is assigned. The moving seal under static conditions has the following length of seal corresponding to a certain leakage and cylinder-piston configuration

$$X = \frac{\pi r}{24 Q_L K_2}[(K_1 + K_2 p')^4 - K_1^4] \quad [18]$$

A number of methods for reduction of leakage, Fig. 7, have been proposed for study. Moving pistons with and without auxiliary members are described and cataloged as follows:

M-1 Ordinary closely fitted piston, the assumed practical counterpart of the previously described theoretical piston-cylinder combination.

M-2A A grooved piston intended to be self-aligning and to create turbulence in the flow path.

M-2B Same as type 2A, but with a different groove configuration.

M-3 Standard (11) Society of Automotive Engineers piston ring.

M-4 Continuous rectangular ring in a two-part piston.

M-5 Combination split and continuous rings in a one-piece piston.

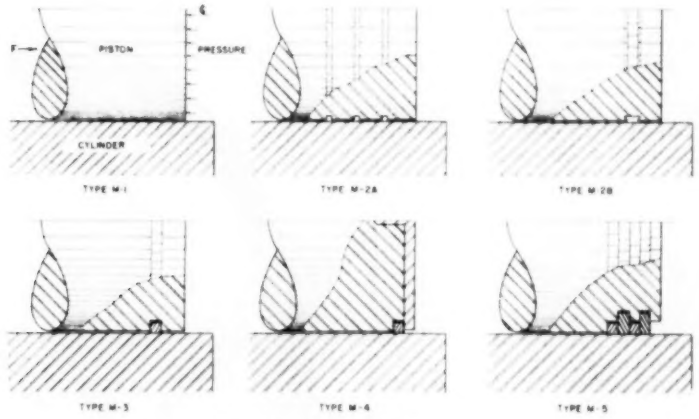

FIG. 7(*a*) MOVING-SEAL TYPES

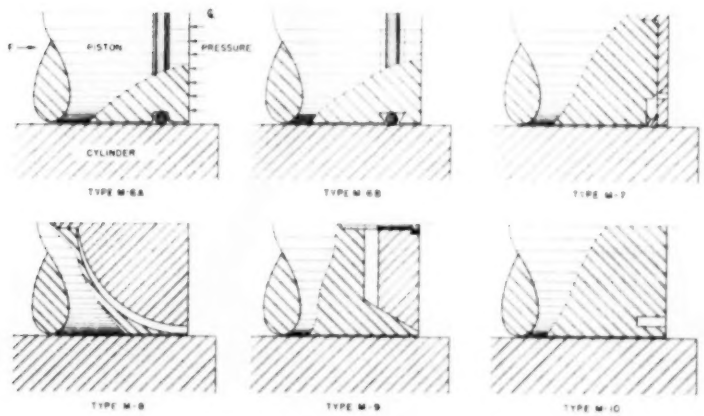

FIG. 7(*b*) MOVING-SEAL TYPES

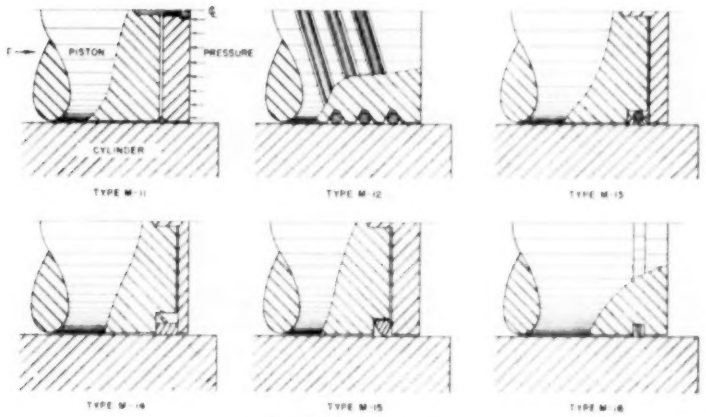

FIG. 7(*c*) MOVING-SEAL TYPES

M-6A Normal O-ring seal.
M-6B O-ring in a nonstandard cavity.
M-7 Continuous ring with pressure-actuated side-sealing lips.
M-8 Sealing action by deformation of the piston component.
M-9 Similar to M-8 except for a mechanical advantage imposed by a secondary moving member.
M-10 Similar to M-8, but with a straight lip proposed in a one-piece piston.
M-11 A continuous ring similar to the K-ring (11), but with a mechanical advantage member.
M-12 A helical sealing ring of circular cross section.
M-13 Metal shrouded O-ring, where the O-ring acts as a static seal behind the sliding metal surfaces.
M-14 Spring-loaded continuous ring with the spring action derived from the shape of the ring.
M-15 A triangular ring with sealing affected at the apexes.
M-16 A grooved piston with the groove filled with a viscoelastic material.

Eccentric Conditions. A lapped and closely fitted piston as represented by type M-1 does not practically represent the theoretical piston-and-cylinder combination, Fig. 6, because the radial clearance is not constant due to eccentricity of the piston in the cylinder. The eccentric piston leakage is important in comparison with the concentric piston previously analyzed.

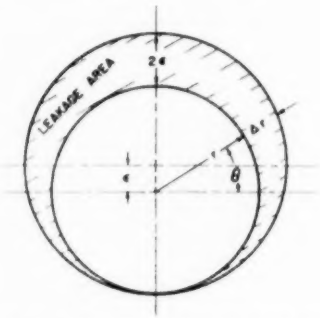

FIG. 8 ECCENTRIC-PISTON LEAKAGE AREA

Fig. 8 shows the geometry of eccentricity, and the clearance is written

$$\Delta r = \epsilon + \epsilon \sin \theta \quad \ldots\ldots [19]$$

Equation [13] takes the form for the eccentric case as

$$Q_L = \frac{r}{12\,\mu} \int_0^{2\pi} \frac{dp}{dx} (\Delta r)^3\, d\theta - \frac{r(v_p - v_c)}{2} \int_0^{2\pi} \Delta r\, d\theta \quad \ldots\ldots [20]$$

If $(dp)/(dx)$ is considered independent of θ, Equation [20] can be solved simultaneously with Equation [19], and the result is as follows

$$Q_L = \frac{2.5\,\pi r \epsilon^3}{6\,\mu} \left(- \frac{dp}{dx} \right) - \pi r \epsilon (v_p - v_c) \quad \ldots\ldots [21]$$

The mean clearance ϵ, in Equation [21] corresponds to Δr in Equation [13]. Comparison of the equations shows that the leakage from an eccentric piston will be two and one-half times that for the concentric piston.

Many explanations have been proposed as to why grooves in a lapped piston, type M-2, tend to reduce the leakage. The foregoing seems the best basis to show that the groove actually channels the leakage to a θ-position where the pressure in the leakage path is low caused by a small radial clearance. This circular flow lifts the piston into proper alignment and thereby reduces the leakage.

FIG. 9 NEOPRENE O-RING FAILURE

The O-ring, type M-6, made of rubber and rubberlike material has in the high and low pressures recently solved many seal problems. The efficacy is explained by Equation [13]. While the clearance remains unchanged and the pressure gradient becomes greater, the viscosity μ, of the rubberlike material which must leak before the sealed fluid can be lost, has a very high value compared with the usual fluids. Eccentricity of the piston and any rotation tends to shred the usual O-ring materials at super pressures as shown in Fig. 9.

TEST RESULTS

Geometry Plates. Two groups of geometry plates were tested,[3] and Figs. 10(*a*) and 10(*b*), in comparison reflect the improvement obtained in the results. The best contrast between these plates was provided by a gradual and uniform application of the preload. In the first group, loads were applied in a somewhat random manner; in fact, C-2 was deformed to a useless configuration by a

[3] Equipment used and technique described in a companion paper, "Static-Dynamic Load Machine for High Pressure," by E. T. Fleischhauer and E. G. Dorsey, Jr., published in this issue, pp. 381–383.

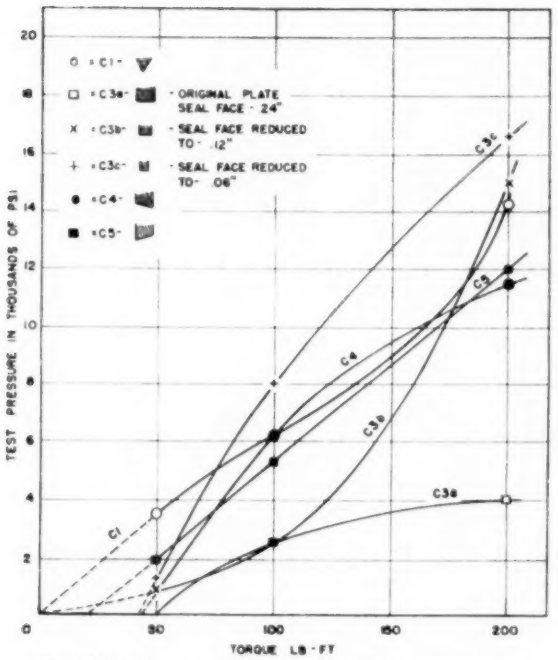

FIG. 10(a) GEOMETRY PLATE-LEAKAGE CHARACTERISTICS

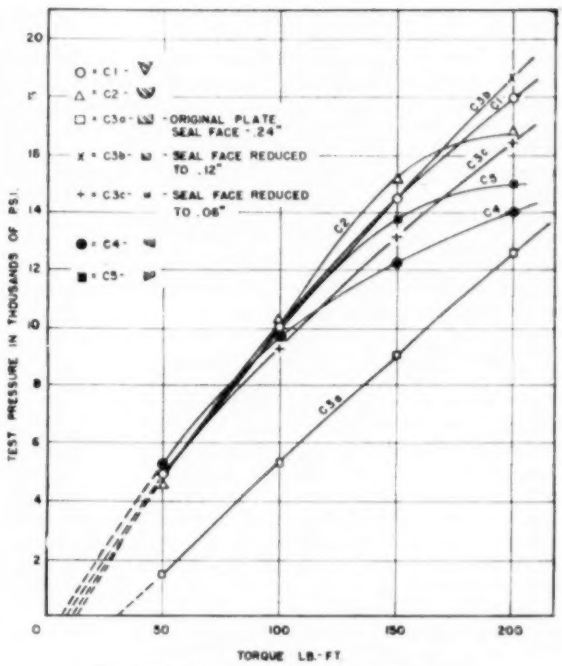

FIG. 10(b) GEOMETRY PLATE-SEAL CAPACITY

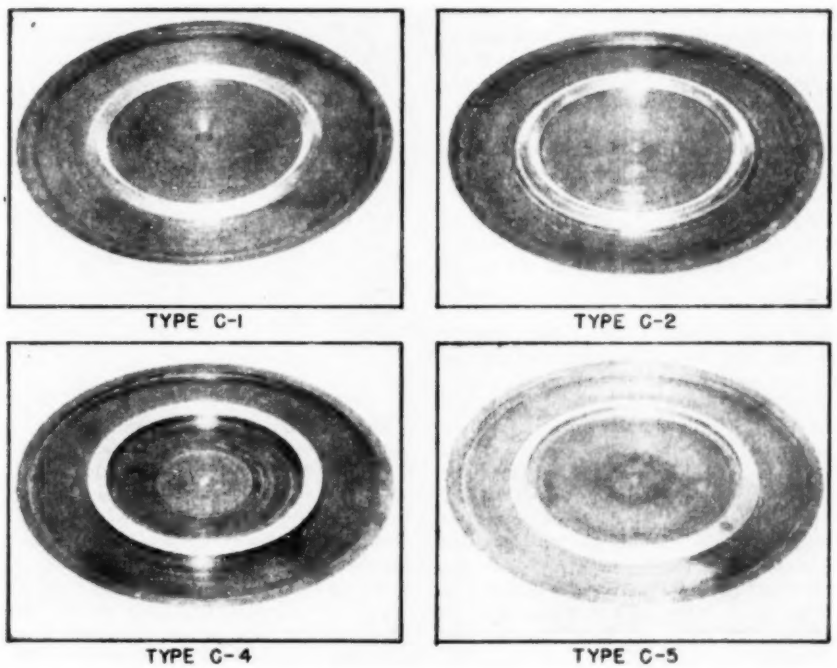

FIG. 11 CONTACT-GEOMETRY PLATES

small amount of eccentric loading, and thus no data occur for the C-2 plate. Plates 3-b and 3-c were obtained by modifying the basic C-3 form to give a smaller contact area. It is quite clear that this technique for increasing the contact pressure, as earlier described, does represent a vast improvement in inherent ability to contain the fluid. Of further interest is that up to 10,000 psi, within the high-pressure range, all of the shapes, Fig. 11, can be made equally effective. Containing liquid in the super-pressure range becomes more dependent on the shape with the preload effects less noticeable.

Fixed-Point Seals. Tests with the type S-1, S-2, and S-3 static seals gave no leakage at pressures in excess of 40,000 psi. Experimentally, the effect of incorrect design dimensioning was observed on the radial unsupported-area types. The triangular, square, or vee sections leaked within certain pressure ranges if the dimensions were such as to induce motion of the ring from the steep slope of the cavity to contact across the apex to the outer slope. However, when the basic dimensions and tolerances were such that the ring always remained in contact with the outer surface, no leakage could be produced. It was noted that the S-2, designed with a surface to mate the cavity by having the same angle on the ring, had zero leakage with less assembly technique. This fact demonstrated in an actual seal ring the observations made with the contact geometry plates. The better action may be ascribed to overcoming of surface-finish effects, which are likely to be pronounced when a line contact over a surface contact is attempted at the contact zone.

Even though the first configurations, Fig. 12, produced excellent sealing characteristics, tests on the others are desired in furtherance of these studies.

Moving Seals. The moving seals were tested under essentially nonmoving conditions; i.e., the motion was only that due to leakage. The results of these tests are given in Table 1. Water was used as the test fluid above the nominal 2-in-diam pistons, and the chamber, having an outside diameter of 8 in., held about 200 cc. The rate of leakage for most of the configurations was such that developing pressure into the super-pressure range was difficult. A valuable initial screening resulted from the tests; moreover, methods to improve the functioning of certain types are evident since the correlation between theory and experiment is very good.

With the experimental data in Table 1, Table 2 was constructed to show an experimental order of merit for these types as indexed by the item numbers. These results, however, must be taken as preliminary, and of course will be altered and improved as further testing is accomplished.

If higher pressures are to be reached, it seems evident that the ordinary split piston ring, M-3, Fig. 13, will not play a major role. The same ring cross section made continuous, M-4, has a pressure leakage rate of $^1/_{38}$ the split section. The continuous ring made of plastic, M-16, has about the same leakage characteristic as a steel ring, M-4. The advisability of increasing the contact pressure as discussed in the section, Theoretical and Engineering Considerations, is verified from the high rating achieved by the M-11 through axial intensification and M-13 through radial intensification. In general, one concludes that in these tests the deformable pistons were not the most favorable, and while split rings are better, any sort of continuous ring is the most effective seal for use in the super-pressure range.

A comparison between experiment and theory for the basic leakage phenomena is available from Table 3. Since the motion of the pistons was very small, Equation [18] was used to compute the theoretical values. The correction for eccentricity (2.5 times the concentric leakage), as written in Equation [21], was made for the plain piston, M-1. A similar correction for the grooved piston M-2B is clearly not necessary.

TABLE 1 EXPERIMENTAL RESULTS ON MOVING SEALS

Type seal	Piston diam, in.	Cylinder diam, in.	Time of leakage, sec	Quantity of leakage, cc	Test pressure, psi	Temperature of water deg C
M-1	1.9994	1.9997	390	194	1500	27
M-1			64	194	3250	27
M-1			24	194	5000	27
M-1			11	194	7500	27
M-2B	1.9993	1.9997	170	194	2500	23
M-2B			47	194	5000	23
M-2B			30	194	5750	23
M-2B			15	194	7500	23
M-3	1.9992	1.9998	30	100	1250	27.6
M-4	1.9993	1.9998	77	75	13730	30
M-6A	1.9993	2.0003	330	0	45750	35.1
M-6A			300	0	41000	35.5
M-6B	1.9991	2.0003	27	0	5000	32.8
M-6B			345	0	35500	33.0
M-6B			300	0	37500	32.9
M-8	1.9995	1.9998	10	200	2500	32.0
M-9[a]	1.9994	1.9998	13	100	2500	28.0
M-9			15	100	3500	28.0
M-10	1.9994	1.9998	10	200	2500	32.0
M-11	1.9992	1.9998	60	5.5	2500	29
M-11			90	5.5	2500	29
M-11			250	5.5	21000	29
M-12	1.9996	1.9998	17	100	2500	30.8
M-13	1.9992	2.0003	98	0.1	18750	31.6
M-13			330	2.0	39000	32.0
M-13			90	0.2	2500	28.6
M-13			210	0.2	2500	28.6
M-13			105	1.5	24320	28.6
M-13			255	1.5	24500	28.6
M-15	1.9992	2.0003	12	100	5000	28.9
M-16	1.9993	2.0003	77	75	13730	30.0

[a] Expander omitted.

TABLE 2 COMPARISON OF MOVING SEALS UNDER STATIC CONDITIONS; MERIT RATING

Item no.	Seal designation	Average leakage (cc/sec-psi) Experiment
1	M-6A	0
2	M-6B	0
3	M-13	0.23×10^{-6}
4	M-11	0.62×10^{-6}
5	M-4	71×10^{-6}
6	M-16	71×10^{-6}
7	M-2B	1033×10^{-6}
8	M-1	1310×10^{-6}
9	M-15	1668×10^{-6}
10	M-9	1905×10^{-6}
11	M-12	2353×10^{-6}
12	M-3	2667×10^{-6}
13	M-9[a]	3077×10^{-6}
14	M-8	8000×10^{-6}
15	M-10	8000×10^{-6}

[a] Expander omitted.

TABLE 3 THEORETICAL AND EXPERIMENTAL LEAKAGE

Type seal	Test pressure, psi	Experiment cc per sec	Theoretical cc per sec	Theoretical corrected for eccentricity cc per sec
M-1	1500	0.5	0.161	0.402
M-1	3250	3.03	0.757	1.9
M-1	5000	8.08	2.24	5.6
M-1	7500	17.6	7.16	17.9
M-2B	2500	1.14	0.84	
M-2B	5000	4.13	3.7	
M-2B	5750	6.46	4.0	
M-2B	7500	12.9	10.8	

Practical Applications

The triangular-cross-section ring has been used by others, in particular the Bureau of Mines (7), with a constant axial length of 0.72 in., regardless of the pressure being sealed. Diameters up to $33^1/_4$ in. were sealed against a pressure of 10,300 psi. The least trouble was reported in private correspondence on the $13^1/_4$-in. diam at this pressure, and it is interesting to note that by coincidence the conditions and configuration agree very nearly to that suggested by the formula developed in this paper.

Typical designs, shown in Fig. 14, were used at the author's laboratory and were for diameters from 2 in. to 8 in., with the axial length for the smallest about $^1/_8$ in. These types were applied to the chamber in Fig. 15 where pressures were recorded in excess of 50,000 psi.

The triangular seal has contained pressures well beyond its rated value. The bolt load necessary to preload the ring needs to be only about 10 per cent of the expected load due to the pressure.

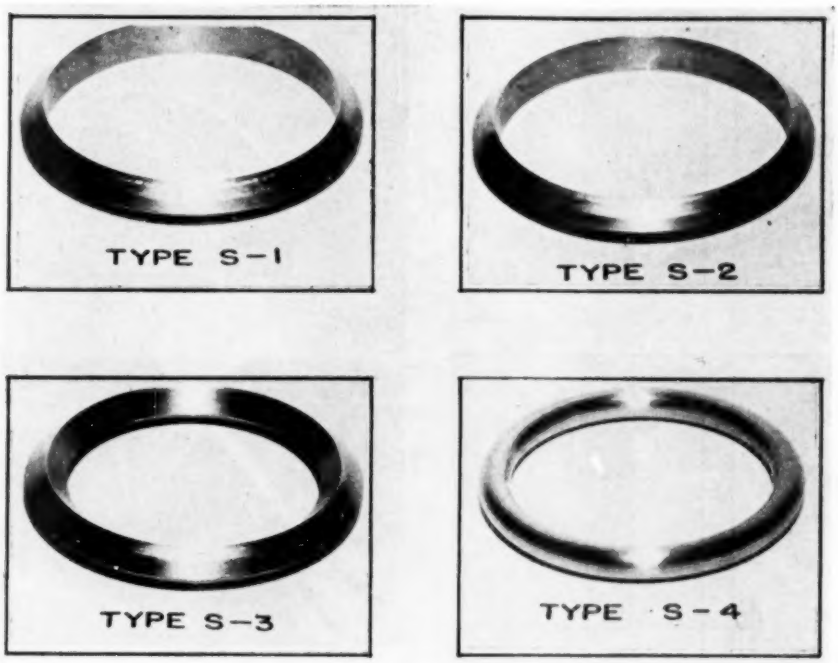

FIG. 12(*a*) FIXED-POINT SEAL DESIGNS

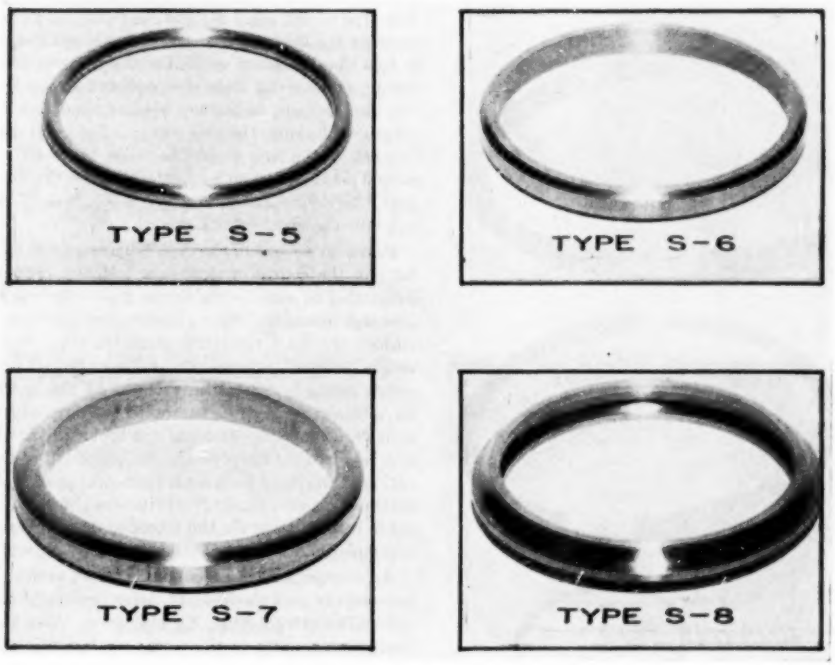

FIG. 12(*b*) FIXED-POINT SEAL DESIGNS

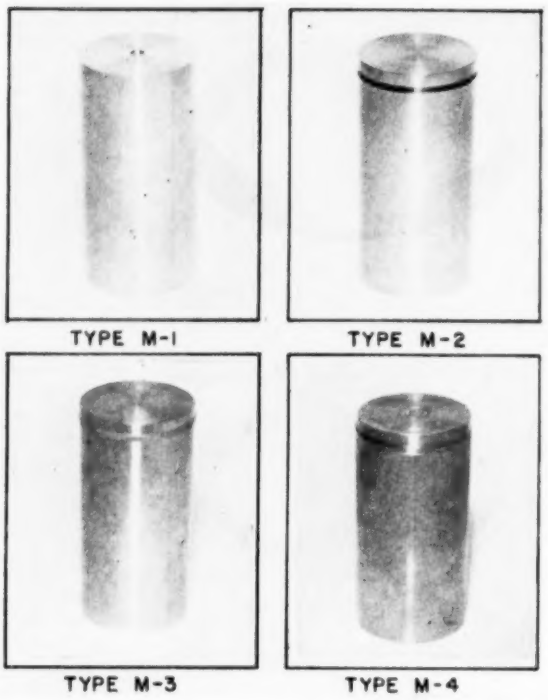

FIG. 13 TYPICAL TEST-PISTON DESIGNS

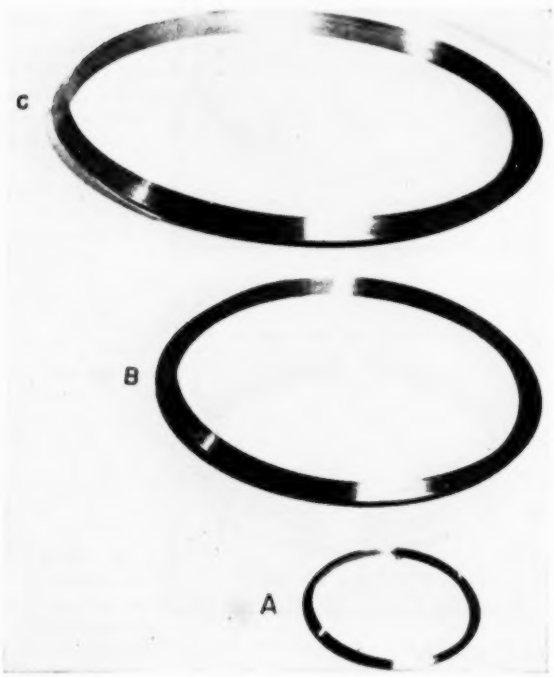

FIG. 14 TYPICAL TRIANGULAR-SECTION RING SEALS

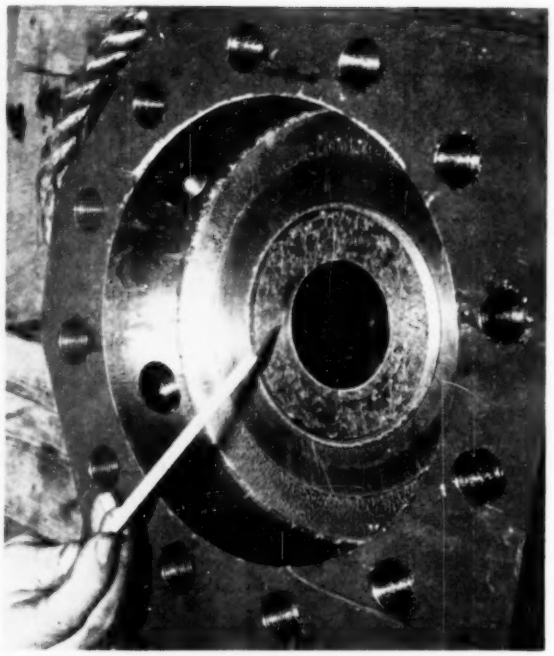

FIG. 15 A REACTION CHAMBER FOR 50,000 PSI

Strain-gage tests have shown that the wedge action of the ring produces no added load on the bolts. Some designers believe that this type of seal must deform plastically to a considerable degree in order to effect a good seal, but this has not been verified. It is true that pressures applied to the rings in excess of the design value permanently alter the configurations. For the S-1, when the displacement of the cap became almost as great as the axial length of the ring, the ring was expelled from the cavity and segmented as the ring passed between the bolts. For this failure 86,000 psi occurred on a ring designed for 50,000 psi. In another case, the double-coned ring, type S-6, was extruded into a gap one half the width of the ring.

Practical designs of the type S-9 never have been made successfully in the course of this work. Heavy preloads are generally demanded to achieve the initial seal. Since it is difficult to design this form for a rated pressure, trial-and-error techniques are employed. As a result the rings are often overloaded, and the ring is "frozen" in the cavity and must be jacked out. A nitrogen weigh bottle hydrostatically tested by the author was found to have this class of ring constructed of pure silver (the reason for which is unknown). One seal ring broke during the sledging operation required for the preload. Replacement of the ring and fabrication of the rings from SAE 1020 steel produced a seal up to the 6000-psi design value. The brittleness of the silver-cast ring had made it unsuitable for the intended use, and was a clear case of incomplete knowledge of the function of the seal ring.

As an expedient the O-ring made from neoprene will work most successfully as a static seal. After prolonged use the ring material will be extruded into the clearance. Also, the ring may shape itself permanently to the cavity configuration, but still it functions satisfactorily. For general laboratory use, and commercial short-time unit processes at high pressure as well as moderate temperatures, this ring should be used. A neoprene O-ring with proper shielding by labyrinth construction was found to be still

in good condition and sealing after 25 applications of pressures between 40,000 and 60,000 psi.

The practical applications of the moving seals studied have been somewhat limited at the time of this writing. In the applied work, resistance to corrosion and high temperature have been coupled with the pressure problem. Fig. 16 demonstrates an attempt to shield the O-ring with a plain piston ring. In this case coating of the neoprene with a high-temperature inert lubricant improved the life of the ring.

At the present time the laboratory testing and theoretical thinking for seals is ahead of the applied work within the author's domain. The problems of sealing higher pressures are still present, but means exist for their solution.

Conclusions

1 A means for laboratory evaluation of fixed-point and moving seals under various conditions of loading has been developed.

2 Seals for higher pressures must compensate for elastic changes due to pressure acting on the mated parts.

3 The effects of the geometry of contact become pronounced above 10,000 psi.

4 The best fixed-point seals are those of the radial unsupported-area class.

5 A theoretical treatment of the leakage phenomena provides a basis to analyze and improve the action of certain mechanical seals.

6 The grooved piston will leak less than a plain piston because of the aligning action provided by the fluid flowing in the groove.

7 O-rings made from neoprene and similar materials are not satisfactory for prolonged use at super pressures.

8 Continued work along the lines developed will be fruitful in improving the characteristics of any type or method of sealing.

Acknowledgment

This work was performed under the auspices of the Department of the Army Ordnance Corps, to which organization we wish to express our thanks for permission to publish the foregoing material.

BIBLIOGRAPHY

1 "Mechanical Seals, Theory and Criteria for Their Design, by A. Brkich, *Product Engineering*, vol. 21, April, 1950, pp. 85–89.

2 "The Physics of High Pressure," by P. W. Bridgman, G. Bell & Sons, 1949.

3 "Letters Patent No. 1,617,451," by W. H. Knisker, February 5, 1927

4 "Letters Patent No. 2,029,606," by K. Bredtschneider, February 4, 1936.

5 "Letters Patent No. 2,180,795," by N. A. Christensen, November 21, 1939.

6 "High Pressure," anonymous staff report, *Chemical Engineering*, vol. 56, August, 1949, pp. 107–123.

7 "Coal Hydrogenation," by J. A. Markovits, *Mechanical Engineering*, vol. 71, 1949, pp. 553–560.

8 "Special Equipment in the Coal-Hydrogenation," by J. A. Markovits, et al., Bureau of Mines Report No. 4584, January, 1950.

9 "Hydraulic Seals," by T. E. Beacham and F. H. Towler, Trans. of The Institution of Mechanical Engineers, London, England, vol. 160, 1949, pp. 532–540.

10 "Effect of Viscosity on Fuel Leakage Between Lapped Plungers and Sleeves and on the Discharge From a Pump Injection System," by A. M. Rothrock and E. T. Marsh, NACA Report No. 477, 1934.

11 Society of Automotive Engineers Handbook, 1951 (SAE).

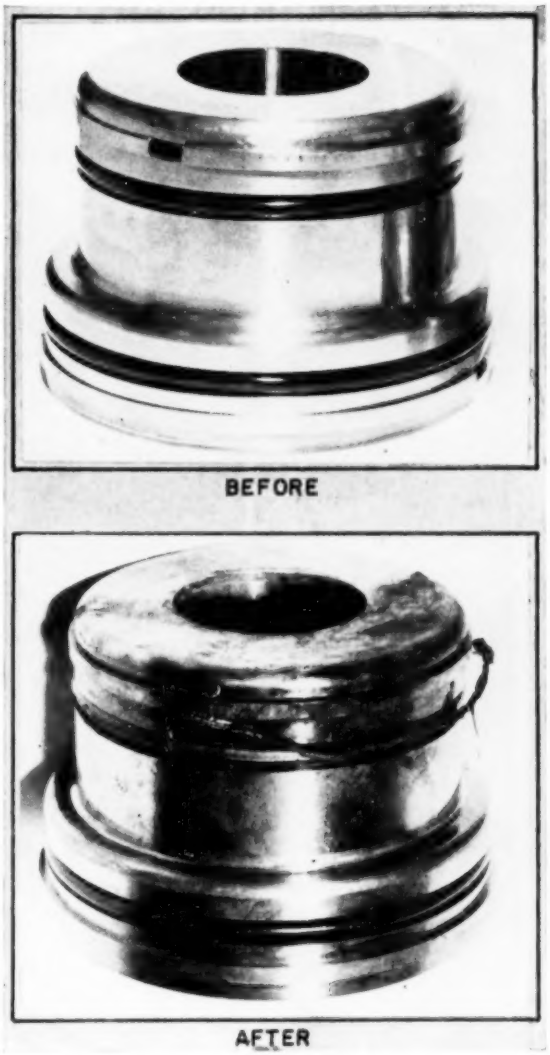

Fig. 16 Piston Ring—O-Ring Combination

Static-Dynamic Load Machine for High Pressure

By E. T. FLEISCHHAUER[1] and E. G. DORSEY, JR.,[2] RICHMOND, VA.

During the course of a particular machine-design program it was found that experimental difficulties with fluid seals and impact loads were hindering the proper solution of the design problem. There was a clear need for auxiliary apparatus which would permit systematic exploration of fixed-point fluid seals, moving fluid seals, and impact loads created by arrestation of rapidly moving machine elements. The "static-dynamic load machine," that is presently employed in an investigation of all three problems, is described in the paper. The basic design configuration of this machine was determined by the required accessibility of the test devices and the method employed for rapid load delivery.

General Design

ALL performance specifications for the static-dynamic load machine, Fig. 1, were based upon a need for a wide range of fluid pressures, impact loads, and seal velocities if the machine were to be truly versatile in its application to design problems. A final design had to be capable of producing fluid pressures up to 50,000 psi, impact loads ranging upward to 10,000 ft-lb, and seal velocities from 0 to 90 fps.

A further requirement implicit in the ultimate application of the test devices was that these phenomena would occur in rather short time intervals, possibly as low as three to ten millisec.

By reference to Fig. 2, the action of the machine in meeting these requirements may be clarified. Chamber B serves as a primary source of energy within the machine. Commercially available inert-gas cylinders at pressures up to 2000 psi are connected to this chamber through a piping arrangement which is not shown. Thus a simple intensifier principle provides the high fluid pressures necessary for seal testing.

A modified procedure is employed to obtain the proper seal velocities or impact loads. Chambers A and B are pressurized so that the forces acting on the transfer rod and piston are in balance. A slight increase of pressure in chamber B will upset the balance sufficiently to permit an upward motion of the transfer rod, thereby exposing a large port in the cylinder cap. The resulting rapid gas flow through the port permits a sudden expansion of the gas in chamber B producing a high acceleration of the piston and transfer rod.

Fig. 2, furthermore, illustrates the manner of attachment of a test cylinder and piston, and the provisions made for vertical stroke adjustment, the intention here being to permit rapid alteration of test items or conditions. It is apparent that all machine components are readily accessible for any special instrumentation required during seal or impact tests.

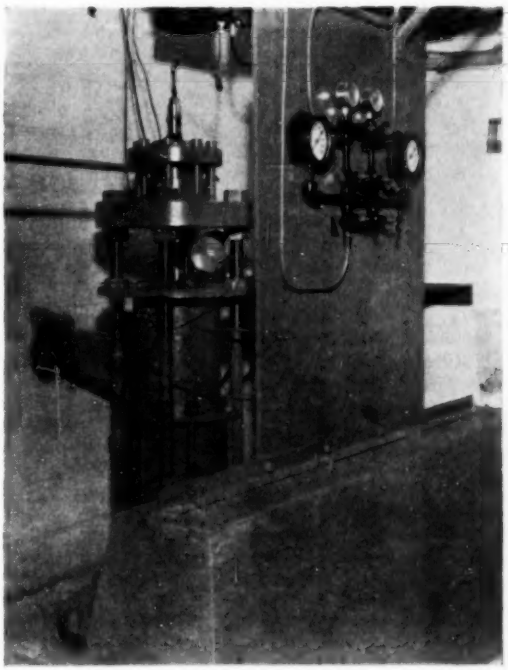

Fig. 1 Static-Dynamic Loading-Machine Installation

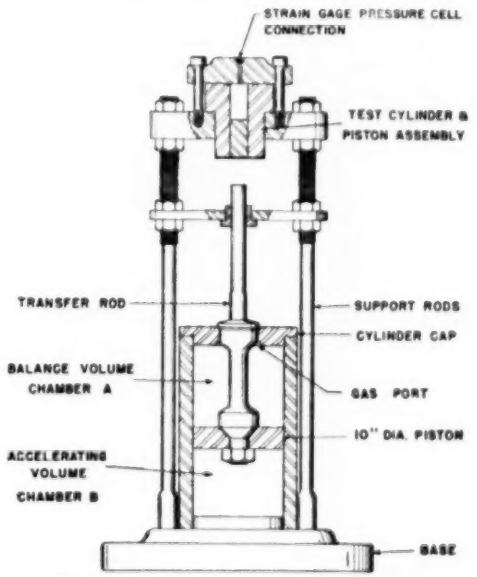

Fig. 2 Static-Dynamic Loading Machine

[1] Experiment Incorporated, Deepwater Terminal.

[2] Experiment Incorporated, Deepwater Terminal.

Contributed by the Industrial Instruments and Regulators Division of The American Society of Mechanical Engineers and presented at The Seventh National Instrument Conference, Cleveland, Ohio, September 9–10, 1952.

Note: Statements and opinions advanced in papers are to be understood as individual expressions of their authors and not those of the Society. Manuscript received at ASME Headquarters, July 3, 1952. Paper No. 52—IRD-10.

Theoretical Performance Characteristics

The static performance characteristics of the testing machine were estimated theoretically in terms of maximum pressure upon a 2-in-diam test piston. The nominal gas-supply pressure of 2000 psi acts directly upon the transfer piston which is 10 in. diam. The test pressure available from this area ratio and supply pressure is 50,000 psi.

Dynamic performance was not readily obtainable by a direct analytical solution, so an approximate numerical solution was obtained by a process of iteration using the following relations

$$pV = WRT \quad [1]$$

$$pV^{\gamma} = \text{const} \quad [2]$$

$$\frac{p_t}{p} = \frac{(2)}{(\gamma + 1)}^{\frac{\gamma}{\gamma - 1}} \quad [3]$$

$$C = \sqrt{\frac{\gamma RT}{M}} \quad [4]$$

$$p_B A_B + p_A A_O - p_A A_A = M_p a \quad [5]$$

Equations [1] and [2] are the conventional thermodynamic relationships for ideal gases; Equation [3] is the ratio of throat and inlet pressure for sonic-velocity gas flow; Equation [4] permits the calculation of sonic velocity in the gas port; and Equation [5] is a force equation for the piston of the machine, neglecting friction, in which

p_B = pressure in accelerating chamber
p_A = pressure in balance chamber
A_B = area of piston on accelerating-chamber side
A_A = effective area of piston on balance-chamber side
A_O = effective area of quick-release valve orifice
M_P = mass of piston
a = acceleration of piston

To begin a solution for piston displacement as a function of time, the initial pressures, volumes, and temperature are noted, and the weight of gas in the balance chamber is calculated from Equation [1]. At $t = 0$, the valve is assumed to open fully, allowing gas to escape for an assumed increment of time. The weight increment of gas that escapes is computed using Equations [1] through [4] and is subtracted from the initial weight of gas in the balance chamber. The new chamber pressure is computed with Equation [1] using the remaining weight of gas. This is applied in Equation [5] from which the velocity and displacement are determined using the assumed increment of time. After a significant change in displacement is found by repeating the foregoing process, the pressure is recomputed in the accelerating chamber using Equation [2] and is applied in Equation [5]. The process is repeated for the full stroke of the machine. Fig. 3 shows the curves of the velocity as a function of piston displacement determined by this method for several accelerating pressures.

Performance Results

Dynamic results compared with the calculated results are shown by the curves in Fig. 3. The experimental curve for the machine is in the low-pressure range since high-velocity trials have been held in abeyance until impact-absorption apparatus is applied in the current testing program.

Static test pressure results were found to conform within experimental accuracy to the pressure calculated from the intensification ratio and pressure acting upon the main piston.

Auxiliary Equipment

Needle valves are used to control the flow of nitrogen from the supply cylinders to each side of the piston, and Bourdon-type

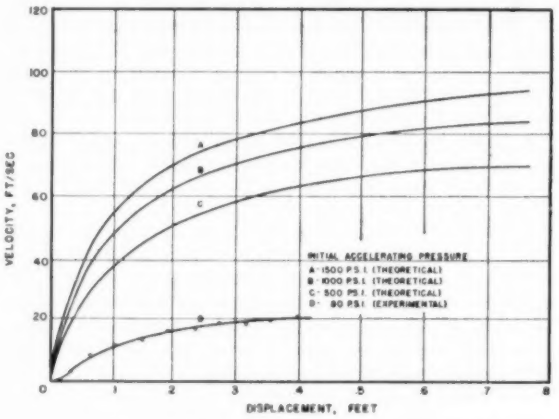

Fig. 3 Transfer Rod Velocity Versus Displacement

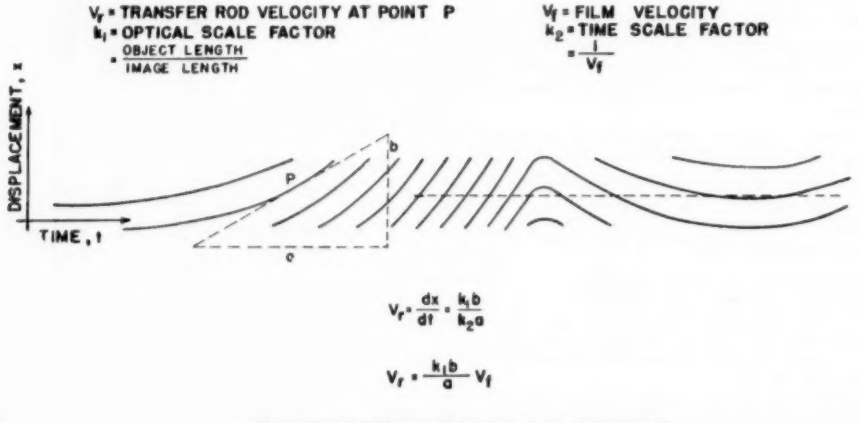
V_f = TRANSFER ROD VELOCITY AT POINT P
k_1 = OPTICAL SCALE FACTOR = OBJECT LENGTH / IMAGE LENGTH
V_f = FILM VELOCITY
k_2 = TIME SCALE FACTOR = 1 / V_f
DISPLACEMENT, x
TIME, t
P
b
a
$V_r = \frac{dx}{dt} = \frac{k_1 b}{k_2 a}$
$V_r = \frac{k_1 b}{a} V_f$
VELOCITY DETERMINATION FROM FILM RECORD

Fig. 4 Transfer Rod Displacement—Time Record

gages indicate the pressures existing in the balance and accelerating chambers. A bonded-wire strain-gage type of pressure cell attached to the test cylinder, Fig. 1, picks up test pressure and its output is amplified and displayed upon a cathode-ray oscilloscope for photographic recording. Strain gages may be applied to the support rods to pick up strain as a function of time during impact-absorption tests.

A strip-film camera (shown mounted in position in Fig. 5), of novel design is used to record piston displacement as a function of time directly upon a strip of 35-mm motion-picture film. The camera is triggered through mechanical linkage by a small initial displacement of the piston. The photographic record is the resultant of images of equally spaced lines engraved on the piston rod at right angles to the rod axis passing through a slit (between the moving film and rod) parallel to the rod axis. This intersection produces a transverse moving spot upon the film which is proportional to the piston-rod displacement, and the film acts as a time base resulting in a displacement-time record as shown in Fig. 4. Records of this type were employed in plotting the experimental curves in Fig. 3.

The mechanical arrangement of the camera is such that a strip of film 3 to 5 ft in length, and consequently of very small mass, is accelerated by a synchronous motor coupled through a gear train to a flywheel-film drive of high inertia. The film-drive system is rotating at its predetermined constant angular velocity while the strip of film is at rest prior to initiation of a velocity record. A clutch plate brings the film into contact with the drive wheel at the instant of record initiation, causing the strip to assume the tangential velocity of the drive wheel almost simultaneously.

The camera has a film-speed range of 100, 200, and 400 ips made possible by a quick-change gear train. A marker pulse light is contained within the camera allowing a pulse to come from the 60-cps motor circuit or from an external source through a two-position switch. The camera was checked prior to use by photographing the oscilloscope trace of a 1000-cps signal. The film velocities, absence of slip, and constancy of velocity conformed to design expectations.

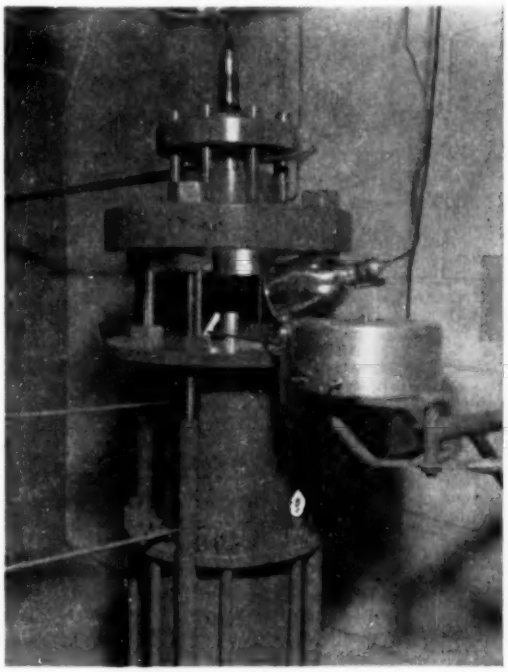

Fig. 5 Strip-Film Camera Installation

Conclusions

A static-dynamic load machine has been described, which, with the available specialized instrumentation, will permit a systematic exploration of problems associated with fixed-point and moving seals and impact loads. Performance curves and test records have been presented to indicate the adequacy of the machine in fulfilling design specifications.

Several allied physical phenomena are within the capabilities of the machine, and deserve consideration for future test programs. Among these may be mentioned material, equipment, and instrument testing at high pressures and under shock-loading conditions. A fundamental program aimed at an understanding of pressure waves or stress waves may prove to be of long-range importance to the fluid-power industry. Finally, the adaptability of the machine to investigation of rapid compression processes in gases suggests its use in this important and promising field of study.

Acknowledgment

This work was performed under the auspices of the Department of the Army-Ordnance Corps, to which organization we wish to express our thanks for permission to publish the foregoing material.

Local Coefficients of Mass Transfer by Evaporation of Water Into an Air Jet

By MAURICE SPIELMAN[1] and MAX JAKOB,[2] CHICAGO, ILL.

A previous paper dealt with the heat transfer in the flow of an air jet parallel to a plane plate. The present paper reports on experiments on evaporation from wet porous plates to such a jet. A satisfactory correlation of a modified Nusselt number with a Reynolds number and a starting-length function is presented. The influence of the starting points of hydrodynamic, thermal, and diffusional boundary layers is discussed, with reference to previous work on this subject.

Nomenclature

The following nomenclature is used in the paper:

$b = \dot{m}''RT_f/(p_s - p_j)$ = local coefficient of mass transfer, fph

$\dot{m}''$ = local rate of mass flow per unit area (see note at end of nomenclature), $lb_m/hr\ ft^2$

$(N_{Nu})_{mod} = bx/\delta$ = modified Nusselt number

$N_{Re} = vx/\nu$ = Reynolds number

$N_{Sc} = \nu/\delta$ = Schmidt number

p = total atmospheric pressure, psf

p_a = mean partial pressure of the inert gas (air), psf

p_s = partial pressure of water vapor in environment air (room air), psf

p_j = smallest observed partial pressure of water vapor measured in jet at distance x from nozzle outlet, psf

p_{jy} = partial pressure of water vapor in jet at distance x from nozzle outlet and at height y above plate, psf

p_o = partial pressure of water vapor in air at nozzle outlet, psf

p_s = partial pressure of water vapor at plate surface, psf

$R = 85.66$ = individual gas constant for water vapor, ft lb_f/lb_m F

t_d = dew-point temperature, deg F

t_s = temperature of environment air, deg F

$t_f = (t_s + t_o)/2$ = air-film temperature, deg F

T_f = absolute temperature of air film, deg R

t_{jy} = jet temperature at distance x from nozzle outlet and at height y above surface, deg F

t_o = nozzle-outlet air temperature, deg F

t_s = surface temperature of plate at distance x, deg F

v = air velocity (used with subscript j for local maximum jet velocity and with subscript o for air velocity at nozzle outlet), fph

x = horizontal distance from the nozzle outlet, ft

x_{st} = starting length (total length of dry or unheated plates), ft

y = vertical distance from test surface, ft

δ = mechanical (mass) diffusivity, ft^2/hr

ν = kinematic viscosity of air, ft^2/hr

Φ, Ψ, Ψ_o = starting-length functions

Note: The double-prime sign in the symbol refers to unit area and the dot refers to unit time.

Introduction

In pressurized cabins of airplanes, condensation or freezing of water vapor on the inside of windshields has to be prevented. This is particularly necessary for military aircraft. The practical purpose of the present investigation was to find criteria for the design of hot-air drying or defrosting of the inside surfaces of such windshields. The work was performed for the United States Air Force[3] as a continuation of research work previously published (1).[4] In principle, the studied method of drying or defrosting consists in discharging a plane jet of hot dry air parallel to the surface to be protected. In the present part of the work, an unheated jet at room temperature was used and the evaporation of water on a wet plane surface was studied, considering the simultaneous entrainment of humid air from the room.[5]

A test method was devised so that the results would not be restricted to the practical purpose just mentioned, but also would contribute to the knowledge of the following fundamental items:

1 Local coefficients of mass transfer by evaporation.
2 Effect of dry starting lengths on mass transfer.
3 Mass-transfer characteristics of an expanding air jet.

The experimental technique of the mass-flow meter method is straightforward; it is based upon measurement of the steady-state rate of evaporation from the surface of a wetted porous plate. It differs from previous investigations of evaporation by several major improvements.

Regarding the results, this investigation seems to be the first in which mass transfer to a flat air jet has been represented by dimensionless groups in a reliable way.

Equipment and Operation

General. The duct system for supplying a heated jet of dried air to the wet test surface has been described in reference (1). Major components of the air-duct system are a centrifugal blower, a refrigerating dehumidifier, a bank of electrical heating elements, and a rectangular-slot nozzle. The system produced air jets 17.5 in. wide and 0.25 in. thick, having velocities from 50 to 230 fps, and dew-point temperatures as low as 40 deg F. Low-pressure steam could be bled through the transom of the laboratory door-

[1] Formerly, Associate Research Engineer, Illinois Institute of Technology. Jun. ASME; now, Serafon Resinous Chemicals Corporation, Telaviv, Israel.

[2] Research Professor of Mechanical Engineering, Illinois Institute of Technology. Mem. ASME.

Contributed by the Heat Transfer and Power Divisions and presented at the Semi-Annual Meeting, Cincinnati, Ohio, June 15–19, 1952, of The American Society of Mechanical Engineers.

Note: Statements and opinions advanced in papers are to be understood as individual expressions of their authors and not those of the Society. Manuscript received at ASME Headquarters, January 22, 1952. Paper No. 52—SA-1.

[3] This investigation was carried out under a contract between Wright-Patterson Air Force Base and Illinois Institute of Technology.

[4] Numbers in parentheses refer to the Bibliography at the end of the paper.

[5] The present paper is essentially based upon a thesis submitted by Maurice Spielman to the Graduate School of Illinois Institute of Technology in partial fulfillment of the requirements for the degree of Doctor of Philosophy in Chemical Engineering.

way into the room, thus bringing the relative humidity close to 90 per cent.

Measuring Instruments. The instrumentation consisted of devices for measuring velocity, temperature, and humidity. The key instrument of this group was a shiftable, rakelike frame containing impact tubes and thermocouples, which was used to traverse the jet air stream over the mass-flow meter, Fig. 1. The thermocouples give the local air temperature, and the impact tubes permit determination of the local velocity, or, alternatively, local values of the dew-point temperature of the jet. Thermocouple voltages were measured by a portable precision potentiometer, impact heads by draft gages, and dew-point temperatures by a dew-point meter. Room-air humidity was determined by means of a sling psychrometer. See also Fig. 1 (1).

Equipment for Evaporation. Two mass-flow meters were constructed and used in place of the heat-flow meter of the previous investigation. Each of the mass-flow meters consisted of twelve porous plates, 15 in. × 3 in. × 1 in. These were mounted separately in a compartmented frame, and so arranged that a smooth, plane surface, 15 in. wide and 36 in. long was formed. Thin plates of Johns-Manville asbestos ebony were added along the 36-in. sides to avoid discontinuities on the edges of the test surface. The porous plates were identified by the letters A to L, taken in the flow direction. Fig. 1 shows the first meter in position for testing. Each porous plate formed the top of an otherwise watertight sheet-copper box which had a water inlet at one side.

Water was supplied from a float-operated device which served to hold a constant hydrostatic head on the water reservoir. Hence the plate surface could be maintained smoothly wet without any flooding or appearance of dry spots. The float controls were supplied by a series of burettes. This apparatus is sensitive to $^1/_{32}$ in. change of the water level in the float chamber. The rate of evaporation into the air stream was obtained by measuring the height of water in the burettes as a function of time. A steady state of evaporation could be achieved and maintained easily.

The twelve compartments in the mass-flow meter allowed determination of local coefficients, as did the rows of surface thermocouples of the heat-flow meter (1). However, only average coefficients over the width of each plate could be measured. Alundum[6] porous plates of medium porosity were used. Each plate had three lap-soldered thermocouples cemented into shallow grooves cut in the upper surface. The thermocouple junctions were spaced 5 in. apart along the mid-line of the plate, with one junction located at the geometric center of the surface. Every thermocouple was calibrated at the steam point in a hypsometer. Slight variations in the surface areas of the porous plates were found and taken into account.

Scope of Experiments

Experimentation comprised 17 runs with the first mass-flow meter and 21 with the second one.[7] They were identified by the meter number I or II and a serial number. Of these runs, 31 were performed under the natural humidity of the laboratory air and 7 with the laboratory air humidified and the duct air dried. The two series will be distinguished as "Runs With Environment of Low Humidity" and "Runs With Environment of High Humidity."

The nozzle-outlet air temperatures were adjusted to correspond closely to the temperature of the laboratory environment. The pertinent conditions for each test are listed in Tables 1 and 2.

During a run, the rate of evaporation for every porous plate was determined as the average of numerous observations of burette levels and elapsed time. Fig. 2 shows these rates for one run. As expected, the rates decreased with distance from the nozzle outlet.

The air velocities at the nozzle outlet and over the test plate were obtained from the static pressure in the duct, the impact pressure on the traverse rake, and the barometric pressure. The humidity of the room air was measured with the sling psychrome-

[6] These plates of the type produced as false floors in filtration and sewage-aeration installations were manufactured by the Norton Company. According to a catalog of the company, medium-porosity plates have an average pore diameter of 0.20 mm.

[7] The experimental data are tabulated in reference (2).

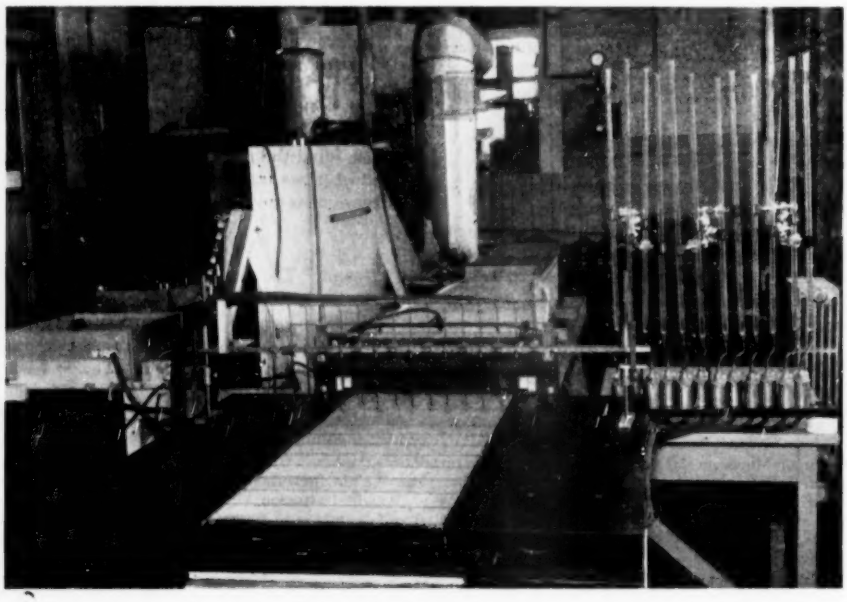

Fig. 1 Mass-Flow Meter Arrangement

TABLE 1 SUMMARY OF RUNS WITH ENVIRONMENT OF LOW HUMIDITY

(Laboratory and jet air of the same humidity)

Run no.	Number of dry plates	Initial flow velocity, fps, v_o	Initial flow temp deg F, t_o	Initial flow dewpoint, deg F, t_{do}	Average temp of wet plates, deg F, t_s
I-3	1	118	80.0	38.8	59.4
II-1	1	122	81.1	53.2	63.9
II-2	1	122	81.2	49.8	63.2
I-5	1	150	80.1	43.1	60.7
I-4	1	151	80.1	42.6	60.3
I-6	1	165	75.8	33.7	56.3
II-3	2	122	81.4	51.4	62.9
II-4	3	122	81.7	53.4	64.2
II-12	3	214	84.2	55.5	66.7
II-21	4	48.3	82.3	61.6	70.0
I-17	4	98.5	74.5	41.8	56.7
I-7	4	113	67.6	25.4	51.2
II-5	4	122	81.4	54.2	64.2
I-1	4	126	83.5	56.8	67.4
I-2	4	127	83.0	57.7	68.1
I-8	4	133	68.3	23.5	50.6
I-16	4	138	74.8	41.7	55.4
I-9	4	145	77.0	27.3	55.6
I-10	4	159	77.5	28.3	55.2
I-11	4	172	78.0	28.9	55.6
I-14	4	198	96.7	55.4	70.5
II-13	4	216	85.2	56.2	67.5
I-15	4	226	98.7	58.9	72.6
II-16	5	62.3	85.7	43.4	65.3
II-6	5	122	80.5	52.0	63.4
II-15	5	229	92.7	44.8	67.5
II-17	6	61.3	86.6	48.8	66.6
II-7	6	122	81.0	55.0	64.8
II-19	6	174	88.6	55.0	69.2
II-18	6	230	93.9	51.5	68.6
II-8	7	122	80.7	57.4	66.0

TABLE 2 SUMMARY OF RUNS WITH ENVIRONMENT OF HIGH HUMIDITY

(Laboratory air humidified and jet air dried)

Run no.	Number of dry plates	Initial flow velocity, fps, v_o	Initial flow temp deg F, t_o	Initial flow dewpoint, deg F, t_{do}	Average temp of wet plates, deg F, t_s
II-10	3	189	80.0	52.2	68.2
II-11	3	214	78.5	52.8	67.0
I-12	4	125	87.7	56.6	71.1
I-13	4	150	91.7	57.9	73.0
II-14	5	214	77.7	52.2	67.5
II-9	6	122	80.1	53.0	68.2
II-20	6	152	78.5	50.6	68.2

ter, while the jet humidity was determined by means of the dewpoint meter.

In every run the average surface temperature of each plate was determined. It was found generally that the dry plates assumed the temperature of the jet air, while the wet plates dropped 10 to 25 F below ambient temperature, independent of the distance from the nozzle. Fig. 3 shows the experimental data for four runs. The lowering of the surface temperature of that dry plate which adjoins the first wet plate (indicated by arrows) may be due to conduction, for the alundum material has a fairly high thermal conductivity.

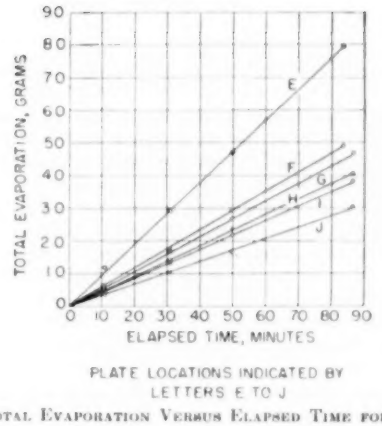

FIG. 2 TOTAL EVAPORATION VERSUS ELAPSED TIME FOR RUN I-1

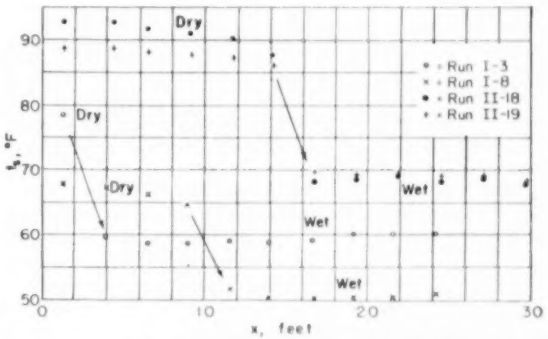

FIG. 3 SURFACE TEMPERATURE VERSUS DISTANCE FROM NOZZLE FOR RUNS I-3, I-8, II-18, II-19

DATA TAKEN FROM VELOCITY, TEMPERATURE, AND PARTIAL PRESSURE TRAVERSES

Velocity Traverses. Velocity profiles over the test plate at various distances from the nozzle outlet were determined for 12 runs. Representative profiles of velocity distribution are shown in Fig. 4. The letters D/E, F/G, and so on, indicate that the

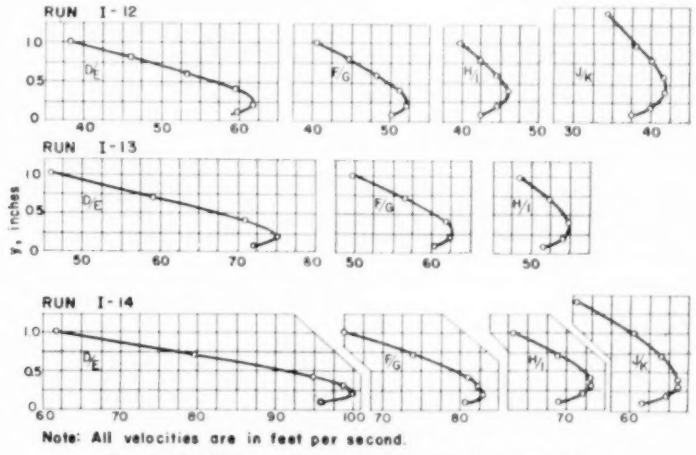

FIG. 4 JET-VELOCITY PROFILES FOR RUNS I-12, I-13, I-14

traverse was made above the interface between the named porous plates.

Near the nozzle outlet the velocity profiles are "sharp." The high-velocity region of the air stream is relatively narrow and quite close to the plate. A steep gradient of velocity exists between the jet and the room air and also between the jet and the test surface. At greater distance from the nozzle the jet expands, its maximum velocity diminishes, and an increasing amount of room air is entrained into the jet. The air stream also rises from the plate, for the points of maximum velocity are found at increasing elevations. The jet becomes more "blunt."

The ratios of local maximum jet velocity v_j to the nozzle-outlet velocity v_o, for the entire test surface were needed in some correlations. These ratios were obtained from the jet-profile graphs. Fig. 5 shows averages of many experiments as points, and separate lines for the two mass-flow meters. These lines differ somewhat for reasons not understood.

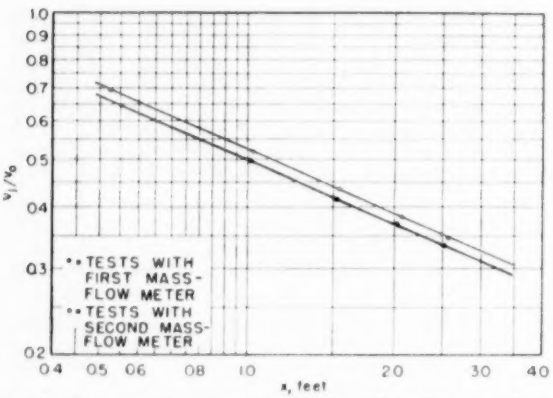

FIG. 5 DECAY OF MAXIMUM JET VELOCITY WITH DISTANCE FROM NOZZLE OUTLET
(Local values of v_j/v_o for two mass-flow meters.)

Temperature Traverses. Jet-temperature traverses were taken for 8 runs. The shiftable rake was used with the center 5 thermocouples connected in series. The thermocouples were of the twisted-wire type and were positioned so as to face into the air flow. Recovery factors for just such an arrangement were presented by Hottel and Kalitinsky in an earlier paper (3). Corrections varied from 0 F at 28 fps to —1.5 F at 150 fps.

Some temperature profiles are shown in Fig. 6. In general, they are isothermal; however, part of the air stream is lowered in temperature by passage over the evaporating surface. This lowering occurs only over a very small vertical distance from the wet surface, and does not extend to the elevation of maximum jet velocity shown in Fig. 4.

Partial-Pressure Traverses. Dew-point traverses were made for 7 runs with environment of high humidity. The test rake was used again; the center 4 impact tubes were manifolded together in parallel and connected to the dew-point meter. Partial pressures corresponding to the observed dew-point temperatures were taken from the steam tables. Representative values of partial pressure are plotted[8] in Fig. 7. Most of the curves have a shape predicted by Fig. 18 of reference (1).

Some of the traverses were made over the dry plates which served as starting length. These traverses are entirely similar to those obtained previously with the plane-plate heat-flow meter [see Fig. 11 of reference (1)]. Since no mass was transferred, no partial-pressure gradient appeared at the surface, while a gradient from the "wet" environment into the "dry" jet was observed. The traverses taken over the wetted plates show clearly

[8] In this figure the symbol × represents the partial pressure of the nozzle outlet air, and the arrows indicate the partial pressure of the environmental air at great distance from the test plate. The symbol + on the axis of abscissas indicates the partial pressure of water vapor at the evaporating surface.

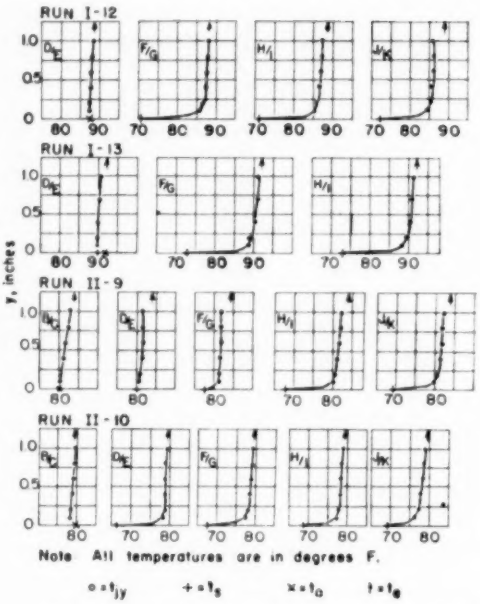

FIG. 6 JET-TEMPERATURE PROFILES FOR RUNS I-12, I-13, II-9, AND II-10

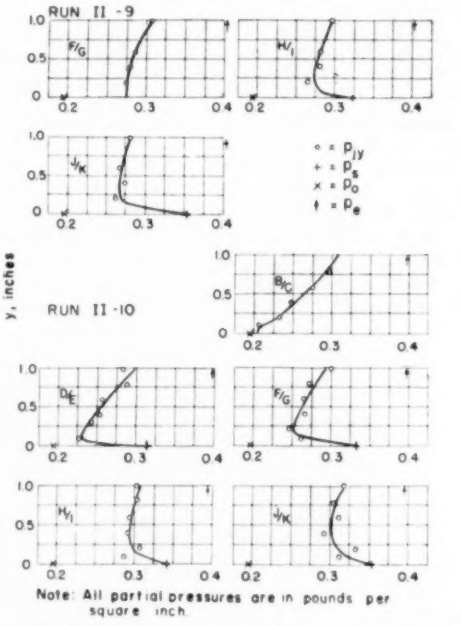

FIG. 7 PROFILES OF PARTIAL PRESSURE IN THE JET FOR RUNS II-9, AND II-10

partial-pressure gradients from the surface and from the environment into the jet.

Values of the local minimum jet partial pressure p_j, which were needed for some correlations, were taken from the profile graphs. Some of them are shown in Fig. 8. As expected, the local minima increase with distance from the nozzle outlet. This is analogous to the decrease of maximum velocity with that distance; the air jet decays and the properties of the stream approach those of the environment.

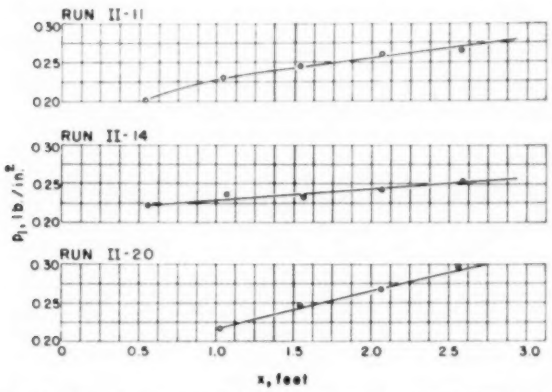

FIG. 8 PARTIAL-PRESSURE MINIMA IN AIR JET FOR RUNS II-11, II-14, II-20

It seems that profiles of partial pressure above a well-defined bounded air jet have not been obtained before the present studies.

CORRELATIONS

Definition of Local Coefficients. From the test data coefficients of mass transfer can be calculated. For molecular or convective diffusion, a coefficient of mass transfer b, may be defined by the relation

$$\dot{m}'' = \frac{b}{RT_f}(p_s - p_j) \quad \ldots\ldots [1]$$

where

$\dot{m}''$ = time rate of mass transfer, $lb_m/hr\ ft^2$
b = mass transfer coefficient, ft/hr
R = individual gas constant of the diffusing substance, ft lb_f/lb_m F = 85.66 for water vapor
T_f = average absolute temperature of "film," deg F abs
p_s = partial pressure of water vapor at evaporating surface, lb/ft^2
p_j = partial pressure of water vapor in jet, lb/ft^2

(see reference (4), page 590).

Influence of Reynolds Number. The local coefficients of mass transfer were put into modified Nusselt numbers for mass transfer, as follows

$$(N_{Nu})_{mod} = bx/\delta \quad \ldots\ldots [2]$$

where

x = characteristic length, measured from nozzle outlet, ft
δ = mechanical diffusivity, ft^2/hr

In the present work the physical properties were evaluated at the film temperature $t_f = (t_o + t_s)/2$, and the characteristic length was taken to be the distance from the nozzle outlet to the center line of the porous plate under consideration.

The Reynolds number was calculated according to

$$N_{Re} = vx/\nu \quad \ldots\ldots [3]$$

where ν is the kinematic viscosity, arbitrarily evaluated at the nozzle outlet temperature.

To correlate the experimental data for the runs with environment of low humidity, bx/δ was plotted against $v_x x/\nu$. It was found that for each fixed value of x_{st}/x (x_{st} is the "starting" length, that is, the length of the dry plates in the flow direction)

$$(N_{Nu})_{mod} \sim N_{Re}^{0.8}$$

No regular variation with x_{st}/x was found.

Local values of v_j were then incorporated into a Reynolds number, $v_j x/\nu$, and bx/δ was plotted versus that group. Again, for fixed x_{st}/x it was found that

$$(N_{Nu})_{mod} \sim N_{Re}^{0.8}$$

and a regular variation with x_{st}/x was observed.

This variation with x_{st}/x will be discussed in the following sections.

Influence of Starting Length. By varying the number of dry plates preceding the wet plates, it was possible to change the starting point of the "mass-transfer boundary layer" while keeping the "flow boundary layer" unchanged. It was found that the evaporation from a plate depends upon its relative location among the wet plates, as well as upon the distance from the nozzle outlet.

It was not possible to have the mass transfer and flow begin at the same location, for the first porous plate of each mass-flow meter could not be used for evaporation because even at very low velocities, water was sucked from the first plate into the air stream. Therefore this plate had to be kept dry.

As mentioned previously, values of the modified Nusselt number were seen to vary as the 0.8 power of the Reynolds number for fixed x_{st}/x. It also was found that the correlating lines of 0.8 slope shifted regularly with x_{st}/x.

Correlation of the experimental data was started, holding $N_{Re} = 10^6$, and tabulating the modified Nusselt number with the corresponding values of x_{st}/x. The circles in Fig. 9 show the averaged data. They are compared with an empirical starting-

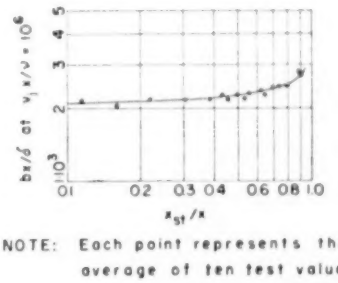

FIG. 9 EXPERIMENTALLY DETERMINED EFFECT OF STARTING LENGTH COMPARED WITH EMPIRICAL STARTING-LENGTH FUNCTION GIVEN BY MAISEL AND SHERWOOD

length function (shown as the solid line) given by Maisel and Sherwood, which will be discussed later.

In general, the relationship can be expressed in the form of

$$(N_{Nu})_{mod} = C\, N_{Re}^{0.8}\, \Psi(x_{st}/x) \quad \ldots\ldots [4]$$

where $\Psi(x_{st}/x)$ is a starting-length function.

FINAL RESULTS

Runs With Environment of Low Humidity. The experimental points of mass transfer for the tests in which the laboratory was at low humidity are presented in Fig. 10. The equation of the line shown is

$$(N_{Nu})_{mod}\,[1 - (x_{st}/x)^{0.8}]^{0.11} = 0.032\,N_{Re}^{0.8} \quad \ldots\ldots [5]$$

where the modified Nusselt number is based on the partial-pressure difference $p_s - p_o$.

With slightly less accuracy, these results also can be presented as

$$(N_{Nu})_{mod}\,[1 + 0.40(x_{st}/x)^{2.75}]^{-1} = 0.032\,N_{Re}^{0.8} \quad \ldots\ldots [6]$$

With a satisfactory correlation for these tests established, attention was then directed to the other series of runs.

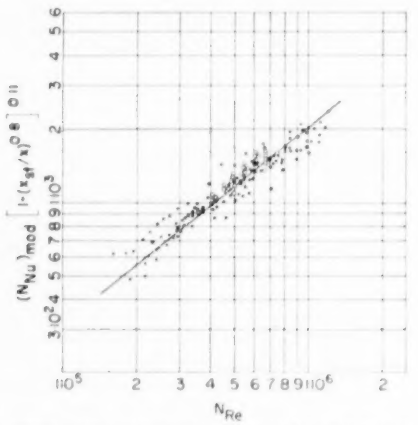

NOTE: Dots represent one experimental point; circles represent two experimental points

FIG. 10 MASS-TRANSFER CORRELATION, RUNS WITH ENVIRONMENT OF LOW HUMIDITY

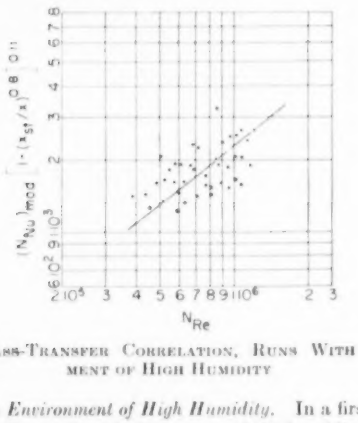

FIG. 11 MASS-TRANSFER CORRELATION, RUNS WITH ENVIRONMENT OF HIGH HUMIDITY

Runs With Environment of High Humidity. In a first attempt to correlate the results of the tests at high-humidity environment, the modified Nusselt number was based on the partial-pressure difference $p_s - p_o$. This did not work at all. A correlation based on the difference $p_s - p_j$ was possible, as shown in Fig. 11, the correlating line corresponding to the equation

$$(N_{Nu})_{mod}\,[1 - (x_{st}/x)^{0.8}]^{0.11} = 0.036\,N_{Re}^{0.8} \quad \ldots\ldots [7]$$

The individual points do scatter, largely because of the uncertainty in the values of p_j, the profiles of partial pressure by no means being as well defined as the corresponding profiles of velocity or temperature. (Compare Figs. 4, 6, and 7.)

Again, with little loss in accuracy, the results also can be expressed by

$$(N_{Nu})_{mod}\,[1 + 0.40(x_{st}/x)^{2.75}]^{-1} = 0.036\,N_{Re}^{0.8} \quad \ldots\ldots [8]$$

It should be mentioned again that this paper is concerned with local coefficients. Much of the scatter observed in the experimental correlations would have been eliminated if average coefficients had been employed, but the effect of starting length probably would have been masked.

Extension of Results. Introducing average values of p/p_a, where p is the total atmospheric pressure and p_a is the mean partial pressure of the inert gas (air), Equations [5] and [7], respectively, become[9]

$$(N_{Nu})_{mod} = 0.031\,(p/p_a)\,N_{Re}^{0.8}\,[1 - (x_{st}/x)^{0.8}]^{-0.11} \quad \ldots [9]$$

$$(N_{Nu})_{mod} = 0.035\,(p/p_a)\,N_{Re}^{0.8}\,[1 - (x_{st}/x)^{0.8}]^{-0.11} \quad \ldots [10]$$

It is thought that Equations [5] and [7] could be extended to other substances by introducing the Schmidt number. Assuming that its influence can be expressed by the 0.4 power, the two equations mentioned become

$$(N_{Nu})_{mod} = 0.039\,N_{Re}^{0.8}N_{Sc}^{0.4}\,[1 - (x_{st}/x)^{0.8}]^{-0.11} \quad \ldots [11]$$

$$(N_{Nu})_{mod} = 0.045\,N_{Re}^{0.8}\,N_{Sc}^{0.4}\,[1 - (x_{st}/x)^{0.8}]^{-0.11} \quad \ldots [12]$$

COMPARISON WITH OTHER INVESTIGATIONS

We know only of one investigation in which the mass transfer has been measured in a way directly comparable to our experiments, that is, the work of Maisel and Sherwood. Relatively few investigators have considered what happens if the hydrodynamic, thermal, and diffusional boundary layers start at different points. In reports on the project which formed the basis of the present paper (5), the influence of dry starting sections of different lengths was dealt with.[10] Maisel and Sherwood also considered this effect (6, 7); these authors also refer to the work of Jakob and Dow (8), in which a similar effect for heat transfer had been dealt with.

Jakob and Dow performed experiments with a heated cylinder, 1.3 in. diam, 8 in. long, provided with wooden nosepieces 0.9 to 12.5 in. in length. The correlation of their results in the turbulent range includes the following empirical starting-length function

$$\Phi(x_{st}/x) = 1 + 0.40(x_{st}/x)^{2.75} \quad \ldots\ldots [13]$$

with values of x_{st}/x ranging from 0.61 to 0.10 in a correlation where the dimensionless groups are based on average coefficients of heat transfer. By differentiation, they obtained the following expression for local coefficients of heat transfer

$$\Psi_0(x_{st}/x) = 0.8 + 0.2(x_{st}/x) - 0.78(x_{st}/x)^{2.75} + 1.18(x_{st}/x)^{3.75} \quad \ldots\ldots [14]$$

Concerning this equation, the authors mention that "since differentiation of an empirical equation is a delicate matter, the accuracy of the result should not be overestimated." The equation shows that because of the exponent 0.8 of the Reynolds number, the local coefficient is 0.8 of the mean coefficient when[11] $x_{st} = 0$. Dividing the starting function Ψ_0 by 0.8, the same basis for a comparison is obtained, that is

[9] It will be seen that Equation [10] is identical with the equation by which Maisel and Sherwood represented their results on mean transfer.

[10] In report No. 6 (dated November 29, 1948), the arrangement of dry starting lengths was described, and in report No. 7 (dated February 28, 1949) a first correlation with starting lengths was presented. These reports are signed by M. Jakob, who directed the entire project; the experimentation on mass transfer by evaporation was performed by M. Spielman.

[11] This means that Jakob and Dow, by definition, used $C/0.8$ instead of C, and $\Psi_0 = 0.8\Psi$ instead of Ψ in their equation corresponding to Equation [4] of this paper.

$$\Psi\,(x_{st}/x) = 1.0 + 0.25(x_{st}/x) - 0.975(x_{st}/x)^{2.75} + 1.47\,(x_{st}/x)^{3.75} \quad [15]$$

Theoretical treatments are due to Eckert (9) and Rubesin (10). These may be considered now. Eckert studied the heat transfer on a plane plate in longitudinal laminar flow. He dealt with the hydrodynamic and thermal boundary layers on the plate, assuming parabolic distributions of velocity and temperature. Employing von Kármán's momentum balance for the boundary layer, he obtained the following expression for the local heat transfer

$$N_{Nu} = 0.331\,N_{Re}^{1/2}\,N_{Pr}^{1/3}\,\Psi(x_{st}/x) \quad [16]$$

where

$$\Psi\,(x_{st}/x) = [1 - (x_{st}/x)^{0.75}]^{-1/3} \quad [17]$$

The symbol Ψ will be used for any of the starting-length functions to be considered, when the dimensionless groups in the main equation are based on local coefficients.

Eckert also derived boundary-layer equations of mass transfer without considering the effect of starting lengths.

Rubesin likewise presented Equation [16] but with a constant of 0.304. He further dealt with turbulent boundary layers, assuming the "1/7-power" rule for the velocity and temperature distributions, and arrived at

$$N_{Nu} = 0.0286\,N_{Re}^{0.8}\,N_{Pr}^{1/3}\,\Psi(x_{st}/x) \quad [18]$$

with

$$\Psi\,(x_{st}/x) = [1 - (x_{st}/x)^{39/40}]^{-7/39} \quad [19]$$

Again the Nusselt number was based on a local coefficient of heat transfer.

To correlate mass-transfer data, Maisel and Sherwood used an empirical starting-length function. They investigated the evaporation of water from an apparatus similar to the mass-flow meters used in the present study, using three porous plates, each 2 in. long in the flow direction, 5 in. wide, and 3/4 in. thick. Different wooden starting sections were attached, and the entire assembly placed in a 6-in-wide duct. Values of x_{st}/x ranging from 0.95 to 0.46 were used. The authors represented their results on mean mass transfer by the equation

$$(N_{Sh})_{mod,m} = 0.035(p/p_a)N_{Re}^{0.8}\Psi_m \quad [20]$$

in which

$$\Psi_m = [1 - (x_{st}/x)^{0.8}]^{-0.11}$$

and the subscript m refers to a mean value of the coefficient of mass transfer b, taken over the wetted portion of the exposed surface.

In the same way in which Equation [15] was derived from Equation [13] by Jakob and Dow (8), Equation [20] can be converted to

$$(N_{Sh})_{mod} = 0.8(N_{Sh})_{mod,m}(1.25\psi) = 0.028(p/p_a)N_{Re}^{0.8}\Psi_m\cdot(1.25\psi) = 0.028(p/p_a)N_{Re}^{0.8}\Psi \quad [21]$$

where

$$\psi = (x_{st}/x) + 0.888(1 - x_{st}/x) - \frac{0.088(1 - x_{st}/x)}{1 - (x_{st}/x)^{0.8}}$$

and

$$\Psi = \Psi_m(1.25\psi)$$

Herewith the values of Table 3 are obtained.

TABLE 3

(Conversion of Maisel and Sherwood's mean values into local values of heat transfer)

x_{st}/x	0	0.6	0.8	0.9	0.99	1
Ψ_m	1	1.128	1.209	1.319	1.701	∞
1.25ψ	1	1.063	1.096	1.101	1.111	1.111
Ψ	1	1.198	1.323	1.451	1.893	∞
$\frac{(N_{Sh})_{mod}}{(N_{Sh})_{mod,m}} = \frac{0.8\Psi}{\Psi_m}$	0.8	0.850	0.875	0.881	0.889	0.889

Hence, in the range $x_{st}/x = 0$ to 1, the local modified Nusselt number is 20 to 11 per cent smaller than the mean values obtained by Maisel and Sherwood and represented by Equation [20]. In other words, replacing the constant 0.035 in this equation by values increasing from 0.028 to 0.031 between $x_{st}/x = 0$ and 1, local values of the modified Nusselt number are obtained. These factors are to be compared with an average value 0.032, which follows from our Equations [9] and [10], when double weight is given to the low-humidity measurements. Considering the differences in the conditions of experimentation (jet flow and flow in a wind tunnel), the agreement is very satisfactory.

It is obvious that some source of heat energy is necessary in order to supply the latent-heat requirements of the evaporating water. The major portion of this heat energy was supplied by convection from the air jet to the wet plates at the expense of a substantial drop in surface temperature, Fig. 3. If this were the only source, then the calculation of local heat transfer in the same field and occurring simultaneously with the mass transfer would be simple, and knowledge about a complex case of similarity would be obtained.

Unfortunately, many other influences enter. For example, an induced convective effect due to a net flow of mass (water vapor) normal to the surface has to be considered. Radiation to the surface, as well as heat energy brought with the supplied water have to be taken into account. In addition, heat leakages to the apparatus from the side extensions and along the unexposed lower surfaces also must be included in the consideration.

Quantitative evaluation of all these influences is difficult. However, by estimating some of them, it was possible to obtain a rough correlation of the local coefficients of heat transfer which showed that the correlations for heat transfer and for mass transfer were not greatly dissimilar. In particular, the same exponent

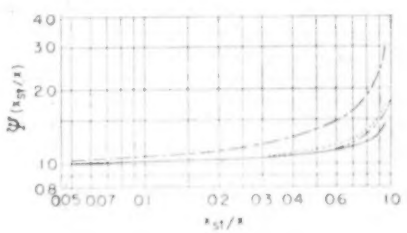

— — — Theoretical, laminar boundary layer (Equation 17)

------ Theoretical, turbulent boundary layer (Equation 19)

—·— Empirical, turbulent heat transfer (Equation 15)

——— Empirical, turbulent mass transfer (Equations 4 to 6)

FIG. 12 COMPARISON OF STARTING-LENGTH FUNCTIONS

of the Reynolds number and the same starting-length function appeared. However, the experimental data are not exact enough to establish definitely the relationship and to determine whether the correlations are identical.

In Fig. 12 values of the various functions of starting length are plotted versus x_{st}/x. The agreement between the theoretical and empirical results and between mass and heat transfer in turbulent flow is very satisfactory. The shape of a curve which would represent Equation [21] is shown in Fig. 9 only, not to overcrowd Fig. 12. Table 3 indicates that values of Ψ according to this equation would be 0 to 11 per cent higher than those of the lowest curve in Fig. 12. For comparison the theoretical starting-length function for laminar flow is also shown.

Summary and Conclusions

1 This paper describes an investigation of the evaporation of water from wetted plane surfaces to an expanding flat air jet.

2 Local rates of evaporation were obtained by means of a mass-flow meter, consisting of horizontal porous plates which formed the covers of individual compartments. Each compartment was supplied separately with water; the total evaporating porous surface was nearly 36 in. long and 15 in. wide. Dry "starting sections" could be obtained at will.

3 The air stream was discharged parallel to the system of porous plates from a horizontal rectangular-slot nozzle of $^1/_4$-in. gap. Initial velocities were varied from 50 to 230 fps.

4 Two types of tests were carried out. In the first the air of the jet and of the environment were of the same moderate humidity; in the second type the laboratory air was humidified artificially and the nozzle-outlet air dried. In this way concentration gradients from the wet surface to the jet and from the environment to the jet were established.

5 Distributions of velocity, temperature, and humidity at various heights above the evaporating surface were investigated. A traverse rake containing thermocouples and impact tubes was used to explore the jet, as was a dew-point meter of special design. It does not seem that humidity traverses above a surface evaporating into an expanding air stream have been performed in any previous investigation.

6 Distribution of local surface temperature was measured over the entire test plate.

7 A satisfactory correlation was obtained, showing that a modified Nusselt number, based on local coefficients, is proportional to the 0.8 power of a Reynolds number based on local maximum jet velocity and distance from the nozzle outlet. The range of Reynolds number was 0.16×10^6 to 1.3×10^6.

8 A strong influence of the ratio of dry starting length x_{st}, to total length, x, was observed and incorporated into the correlation.

9 Various theoretical and empirical formulas which account for the influence of (x_{st}/x) on mass transfer and heat transfer were discussed and compared with the experimental data.

10 Our final correlation is in good agreement with Maisel and Sherwood's empirical representation of their evaporation data, notwithstanding considerable differences in configuration and type of flow.

11 Some heat-transfer measurements were performed in the same field as those of evaporation. They led to a correlation which is not greatly different from that of the mass transfer; however, further experimentation will be necessary to obtain a quantitative comparison.

Acknowledgment

The authors wish to express their appreciation to the Air Force Wright Air Development Center for permission to publish this paper.

Bibliography

1 "Heat Transfer From an Air Jet to a Plane Plate With Entrainment of Water Vapor From the Environment," by M. Jakob, R. L. Rose, and M. Spielman, Trans. ASME, vol. 72, 1950, pp. 859.

2 "Local Coefficients of Mass Transfer by Evaporation of Water Into an Air Jet," by M. Spielman, unpublished PhD thesis, Illinois Institute of Technology, Chicago, Ill., 1951.

3 "Temperature Measurements in High-Velocity Air Streams," by H. C. Hottel and A. Kalitinsky, *Journal of Applied Mechanics*, Trans. ASME, vol. 67, 1945, p. A-25.

4 "Heat Transfer," by M. Jakob, John Wiley & Sons, Inc., New York, N. Y., vol. I, 1949.

5 "Defrosting and Ice Prevention," by M. Jakob, Ten unpublished reports to the United States Air Force, Illinois Institute of Technology, 1947, 1948, 1949, and 1950.

6 "Evaporation of Liquids Into Turbulent Gas Streams," by D. S. Maisel and T. K. Sherwood, *Chemical Engineering Progress*, vol. 46, 1950, p. 131.

7 "Mass Transfer Effects in Turbulent Streams," by D. S. Maisel, unpublished PhD thesis, Massachusetts Institute of Technology, 1949.

8 "Heat Transfer From a Cylindrical Surface to Air in Parallel Flow With and Without Unheated Starting Sections," by M. Jakob and W. M. Dow, Trans. ASME, vol. 68, 1946, p. 123.

9 "Introduction to the Transfer of Heat and Mass," by E. R. G. Eckert, McGraw-Hill Book Company, Inc., New York, N. Y., 1950.

10 "An Analytical Investigation of Convective Heat Transfer From a Flat Plate Having a Stepwise Discontinuous Surface Temperature," by M. W. Rubesin, unpublished ASME Paper No. 48—A-43, 1948.

11 "Influence of Curvature Upon the Heat Transfer From Cylinders to Gas Streams Parallel to the Axis," by W. Tessin, unpublished PhD thesis, Illinois Institute of Technology, 1951.

Discussion

D. S. Maisel[12] and T. K. Sherwood.[13] The authors have measured the rate of evaporation of water from a series of successive plane strips into a jet of air flowing parallel to the surface. These data, together with similar information obtained by the writers, confirm the fact that mass and heat-transfer rates are influenced by the presence of a "starting length," i.e., an initial length of plane over which momentum transfer without heat or mass transfer occurs. In addition, the present data are correlated excellently by an expression developed from our earlier data. While this is pleasing, there appear, at first glance, several differences in experimental conditions which should be noted.

1 Conditions of flow are quite different. The authors used an air jet resulting in an inverted form of velocity profile over the transfer surface. This is compared to our earlier work wherein the plane surface was suspended in the center of the air stream in a tunnel drier.

2 In some experiments by the authors an inverted humidity gradient was obtained by steam injection into ambient air.

3 We used average coefficients for 1, 2, and 3 planes, each 2 in. in downstream length, with the Reynolds number determined by the distance to the downstream edge of the wet surface. The authors calculate the Reynolds number based on the downstream distance to the center of the 3-in. section.

It may be helpful to dwell briefly on the conditions of flow at a plane boundary to help understand the mechanism of mass and momentum transfer. As shown in Fig. 13, herewith, a velocity and a concentration gradient exist at the interphase boundary. The conditions at this point can be expressed rigorously by means of a material balance. Note that momentum and heat balances may be similarly derived for these cases if desired. The crux of the situation lies, therefore, in determining the partial

[12] Esso Laboratories, Development Division, Standard Oil Development Company, Linden, N. J.

[13] Massachusetts Institute of Technology, Cambridge, Mass.

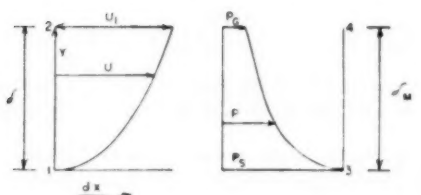

$$\frac{d}{dx}\int_0^{\delta_M}(P - P_G)\,U\,dY = \left(\frac{dP}{dY}\right)_W$$

δ_M = mass-transfer boundary layer
δ = momentum-transfer boundary layer must determine
(1) $P = F(Y)$ (2) $U = F(Y)$

FIG. 13 GENERAL BOUNDARY-LAYER EQUATION FOR MASS TRANSFER

pressure, velocity, and/or thermal gradients as a function of distance from the transfer surface. Several solutions for the mass-transfer case have been described. The results are generally quite similar and differ only to the extent that different functions were assumed in each for velocity and partial-pressure functions.

The authors, for example, cite the work of Eckert in deriving a relationship based on a parabolic velocity distribution. His relationship is shown in Fig. 14, together with the results from two other theoretical derivations. The first and the second, based on simple power series, obviously apply to conditions for laminar flow in the boundary which is characterized by the 0.5 power of the Reynolds number.

ECKERT (1950)
$$(N_{Nu})_{MT} = 0.331\,(R_E)^{1/2}\,(P_R)^{1/3}\left[1 - \left(\frac{x_{ST}}{x}\right)^{0.75}\right]^{-1/3}$$

MAISEL - SHERWOOD (1949)
$$(N_{Nu})_{MT} = 0.323\,(R_E)^{1/2}\,(S_C)^{1/3}\left[1 - \left(\frac{x_{ST}}{x}\right)^{0.75}\right]^{-1/3}$$

SEBAN (1951)
$$(N_{Nu})_{MT} = 0.0289\,(R_E)^{0.8}\,(P_R)^{1/3}\left[(P_R)^{1/3}\left[1 - \left(\frac{x_{ST}}{x}\right)^{0.9}\right]^{-0.111}\right]$$

FIG. 14

We have included the Seban relation, which was brought to our attention only recently, because it is so similar to the empirical expression which has been shown to apply to mass transfer from plane surfaces. This expression, incidentally, was derived for a turbulent boundary layer over an isothermal section preceded by an unheated section.

The point which has been troubling the writers is evident from these expressions. We believe x_{st} and x are independent, and it does not seem likely that a correlation based solely on the ratio x_{st}/x can be complete. For a given air speed the laminar boundary layer breaks to a turbulent layer at some definite distance from the leading edge of the plate, and the position of the wet test surface relative to this break point is important; the rate of vaporization certainly will depend on whether the wet surface is under the laminar or the turbulent boundary layer, or under both. It seems evident, therefore, that both x_{st} and x must enter the correlation; the ratio x_{st}/x is insufficient.

M. W. RUBESIN.[14] It is gratifying that the authors chose to emphasize the role played by boundary layers of momentum, heat transfer, and mass transfer which do not all begin at the same place. The point that the surface-temperature distribution in the case of heat transfer and surface partial-pressure distribution in the case of mass transfer are important factors in controlling the amount of heat or mass transfer cannot be overemphasized. Even after a fair amount of work dealing with these effects has been published (see Bibliography of paper) one may still find articles in the literature which ignore the effects of the surface temperature or partial-pressure discontinuity.

One aspect of this paper should be clarified. The end results of the paper are given in terms of dimensionless groups which implies their application to more general cases. The agreement of the data with Maisel and Sherwood's work seems to substantiate this general character. To determine the values of the local Reynolds number and local partial-pressure potential, however, it is necessary to know v_f and p_j. As a designer is much more likely to know the values of the velocity and partial pressure at the exit of his nozzle, some means of relating v_j and v_∞ or p_j and p_∞ for various shaped nozzles and various free-stream partial pressures, if known, should be included.

MYRON TRIBUS.[15] The writer believes that the method of accounting for the unheated starting length used by Rubesin[16] and by Maisel and Sherwood, is more realistic than the authors' Equation [13] or [15]. The boundary conditions require that the equation have a singularity at the point where the temperature or vapor discontinuity occurs. Scesa[17] credits Seban with the development of a starting-length function of the form

$$\left[1 - \left(\frac{X_{st}}{X}\right)^{9/10}\right]^{-1/9}$$

This agrees fairly closely with the empirical equation of Maisel and Sherwood. A good test of these equations cannot be made unless the measurements are reduced to point measurements rather than averages over a short length of the plate. A method of comparing the various functions which are proposed to take into account starting length is to provide several steps in vapor pressure in order to accentuate the discontinuities in the region where $(X_{st}/X) = 1$. The important differences in these expressions, which are all approximations, is in the neighborhood of the singularity.

The authors do not draw any conclusions concerning heat transfer. The data of run II-9 show that if one uses the minimum jet vapor pressure at each station to compute the "equivalent free-stream dew point" (by definition) and the local maximum dry-bulb temperature (61.5 F and 84 F, respectively) the wet-bulb temperature is computed as 67.5 F. The plate temperature was measured at 68.2 F; hence the heat and mass-transfer rates must have been in almost the same ratio as over a wet-bulb thermometer.

The effect of starting length on heat transfer, if the foregoing result is typical, is the same as on mass transfer. Unfortunately, other runs could not be analyzed in this fashion as the other data are not given.

AUTHORS' CLOSURE[18]

It is gratifying that Messrs. Maisel and Sherwood start their comments with elaborating item 10 of the Summary in the

[14] Ames Aero Works, Moffett Field, Calif

[15] Director, Icing Research, Engineering Research Institute, University of Michigan, Ann Arbor, Mich. Mem. ASME.

[16] See Authors' bibliography, reference (10).

[17] "Experimental Investigation of Convective Heat Transfer to Air From a Flat Plate With a Stepwise Discontinuous Surface Temperature," by Steve Scesa, MS thesis, University of California, 1951.

[18] In the absence of Mr. Spielman, this closure was prepared by Max Jakob, with confidence that he would agree with it.

paper, and add Seban's equation, which we had not known, to those discussed in the paper. Their next point is that the term x_{st}/x occurring in all correlations, including theirs and ours, does not cover the whole mechanism of development of the boundary layers. However, it seems that not using an additional term, as, for instance, x_{cr}/x where the subscript cr refers to the critical distance at which turbulence starts, does not seriously affect the correlation. This would mean that the separate influences of x and x_{st}, which Maisel and Sherwood would like to have considered, actually are taken care of by the two independent functions of vx/ν and x_{st}/x which occur in the various correlations. One might solve each of the correlating equations with respect to x, keeping x_{st} constant, or with respect to x_{st} with x as parameter. Of course, as usual in similarity treatments, the relationship between the dimensionless groups used is a very simplified form which may be far from the form of an analytical solution of the differential equations.

Referring to the last item of Maisel and Sherwood's discussion, this author agrees with their statement that starting of the mass transfer in the laminar or turbulent section of the momentum boundary layer should yield different rates of evaporation. Hence, if a correlation should cover both cases, a third independent variable, for instance, x_{cr}/x_{st} or x_{cr}/x, would have to be added.[19] However, because of the flow conditions past our nozzle,[20] it is quite unlikely that in any of our tests the boundary layer was in laminar flow at the start of evaporation; therefore the two independent variables used are sufficient.

Mr. Rubesin's remark that, for practical purposes, v_o and p_o should be used is also well justified. The velocity v_o can be taken from Fig. 5 of the paper. As an average of the two lines in this figure

$$v_o = 1.97x^{0.438}\, v_j$$

with x in foot-units.

The pressure p_o, on the other hand, can be calculated from the equation

$$N_p = 0.045\left(\frac{x}{a} - 14.4\right)^{0.80}$$

where a = vertical width of our nozzle, and

$$N_p = \frac{p_o - p_j}{p_j - p_s}$$

This equation is based on Fig. 17 of reference (1); however, it is more exact than Equation [13] of that paper, for a reason given there.[21]

Mr. Tribus in his discussion seems to have overlooked the fact that Equations [13] and [15] of the paper are not those recommended in the present paper but are taken from reference (8) for comparison with our Equations [5] and [7], in which we used the starting-length function of Maisel and Sherwood. We did this because their function can be extrapolated to $x_{st}/x = 1$, while Jakob and Dow's empirical function, though perfectly representing the observed data, is not fit for extrapolation to the largest values of x_{st}/x. Hence our equations satisfy Tribus' requirement. We also agree with him concerning the importance of the crucial check in the neighborhood of $x_{st}/x = 1$.

In an example from our tests, Tribus demonstrates the agreement between heat and mass transfer. As mentioned already in the paper, we correlated the data of heat transfer occurring in the same field as mass transfer, and we found the form of our Equations [11] and [12] confirmed with not more scattering in the heat-transfer case than in the corresponding Fig. 10, and less scattering than in Fig. 11. However, the constant factors were 28 and 26 per cent larger than those in Equations [11] and [12], respectively.

Half of this difference might have been expected, according to an equation of Gamson, Thodos, and Hougen,[22] which can be converted to the form

$$\frac{N_{Nu}}{(N_{Nu})_{mod}} = 1.076\sqrt[3]{\frac{N_{Pr}}{N_{Sc}}} = 1.076\sqrt[3]{\frac{0.71}{0.59}} = 1.143$$

The other half may come from inaccuracies of the heat balance, because our apparatus had not been designed for measuring the heat exchange with the environment exactly, except for the upper surfaces of the test plates. Therefore we postponed publishing this part of the results.

Summarizing, it is a pleasure to feel oneself in agreement with the elucidating comments of four noted experts in the field under consideration.

[19] Fig. 15 in reference (8), however, shows that for different values of x_{cr}/x the relationship in the fully developed turbulent range may be independent of x_{cr}/x.

[20] See second paragraph in section, Influence of Starting Length.

[21] See reference (1), p. 865, footnote 9.

[22] "Heat, Mass and Momentum Transfer in Flow of Gases Through Granular Solids," Trans. American Institute of Chemical Engineers, vol. 39, 1943, p. 1.

Design and Development of a Broad-Range, High-Efficiency Centrifugal Compressor for a Small Gas-Turbine-Compressor Unit

By IVAN E. SPEER,[1] LOS ANGELES, CALIF.

The compressor requirements for a small gas-turbine-compressor unit imposes factors with regard to broad flow range and efficiency that form the basic objectives for the design and development. Highly backwardly curved impellers, designed according to the reasoning presented, are shown to evidence the required characteristics. Results of the development program show that the objectives can be met and exceeded.

Nomenclature

W_c = Air flow, compressor, lb/sec
H_{ad_c} = Adiabatic head, compressor, ft-lb/lb
η_c = Adiabatic efficiency, compressor, per cent
W_t = Air flow, turbine, lb/sec
H_{ad_t} = Adiabatic head, turbine, ft-lb/lb
η_t = Adiabatic efficiency, turbine, per cent
η_m = Mechanical efficiency, complete machine, per cent
W_b = air flow, bleed, lb/sec
U = Tip speed, ft/sec
C = Air velocity, absolute, ft/sec
C_m = Air velocity, meridianal, ft/sec
C_t = Air velocity, tangential, ft/sec
H_t = Total head, ft-lb/lb
H_{st} = Static head, ft-lb/lb
V = Air velocity, relative, ft/sec
ϕ = Impeller discharge angle, degrees
β = Discharge angle of relative velocity, degrees
R = Reaction, dimensionless
η_I = Efficiency, impeller, per cent
η_D = Efficiency, diffuser, per cent
η_{s1} = Adiabatic efficiency, stage, first, per cent
η_{s2} = Adiabatic efficiency, stage, second, per cent

Introduction

Work on auxiliary power units of the gas-turbine type was started by the author's company in June, 1946, under the sponsorship of BuAer. At first it was thought that the only type needed was the constant-speed shaft-power machine, originally for 50 hp output and later increased to adequate power to handle a 40-kva alternator. However, the problem of starting turbojet and turboprop engines became more important as the starting power requirements began to get higher than could be handled by electric starters of reasonable size and weight. This led to interest in the pneumatic starter which the company also undertook to develop under BuAer contracts. To make the air starter practical it was necessary to have a small and lightweight source of compressed air. For this reason, emphasis was put on the development of a gas-turbine-driven compressor (designated GTC) from which all of the useful output was taken in the form of compressed air from the compressor of the base machine. Both the gas-turbine compressor (GTC) and the gas-turbine power (GTP) versions of the unit developed for BuAer have now gone into production.

In May, 1948, the Equipment Laboratory of AMC became interested in the GTC type units as ground, air transportable, support equipment for aircraft. The type of equipment required by AMC took a variety of configurations and variants of purpose, but their studies indicated that most if not all needs could be satisfied by one GTC, to be used singularly or in multiples as required. Review of the equipment in the field showed that there was no unit available that fitted ideally into the line of equipment contemplated. The early GTC unit developed for BuAer appeared to be too small, but was utilized as interim equipment for a large-capacity ground heater (Model GH4) which delivers 4,000,000 Btu per hr at —65 F and is currently in production. Accordingly, AMC sponsored a development for a unit design to meet their projected needs more satisfactorily. This GTC not only was to have a somewhat higher through-flow rate but also was specified so as to require considerably higher performance components than were available in this class of equipment at that time. This development was undertaken by the author's company, and the compressor, developed as a component for the Air Force Type F2 Gas Turbine-Compressor Unit (Model GTC85), is the subject of this paper.

Requirements of Compressor

The operating characteristics of a gas turbine which produces all of its useful output in the form of compressed air imposes several requirements on the compressor component that are ordinarily not considered of prime importance on a shaft-power or thrust-producing gas turbine. In order to appreciate these special demands it is necessary to investigate the locus of the operating points of the unit in the compressor chart. Fig. 1 shows in stylized form an example of a typical compressor-performance characteristic. Superimposed on Fig. 1(*a*) is the locus of compressor operating points for a GTC, while Fig. 1(*b*) shows the locus of operating points for a GTP, both cases assuming a constant-speed control. It may be noted that the operating point for the GTC moves in the opposite direction on the compressor chart from the GTP as the unit is loaded from no-load to full output. In the case of the GTP, the compressor characteristic shown is probably acceptable since at full load nearly peak efficiency and head are obtained with both efficiency and head dropping as the unit is operated toward no-load, where these factors are perhaps of lesser importance. However, in the case of the GTC, the compressor characteristic shown is not desirable. It can be seen that the full-bleed (full-load) point occurs at a point of low efficiency and head on the compressor if the operating range is located so as to avoid pulsation at zero

[1] Assistant Project Engineer, Gas-Turbine Project, AiResearch Manufacturing Company.

Contributed by the Hydraulic and Gas Turbine Power Divisions and presented at the Semi-Annual Meeting, Cincinnati, Ohio, June 15–19, 1952, of The American Society of Mechanical Engineers.

Note: Statements and opinions advanced in papers are to be understood as individual expressions of their authors and not those of the Society. Manuscript received at ASME Headquarters on March 24, 1952. Paper No. 52—SA-14.

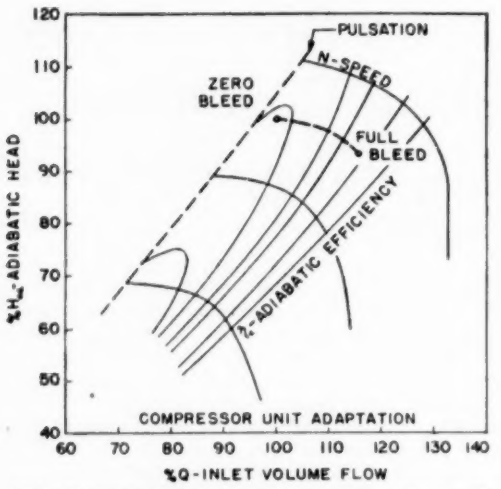

FIG. 1(*a*) COMPRESSOR OPERATING CHARACTERISTICS IN A BLEED AIR-GAS TURBINE UNIT

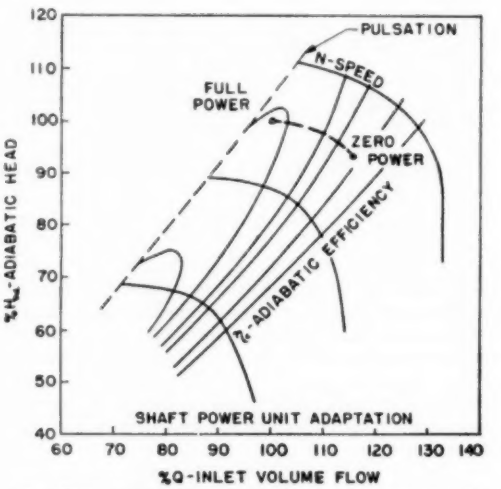

FIG. 1(*b*) COMPRESSOR OPERATING CHARACTERISTICS IN A SHAFT POWER-GAS TURBINE UNIT

bleed (no-load) operation. Examination of the basic energy-balance equation for a GTC

$$\frac{W_c\, H_{ad(c)}}{\eta_c} = W_t\, H_{ad(t)}\, \eta_t\, \eta_m$$

where $W_t = W_c - W_B$. Substituting and rearranging terms

$$\frac{W_B}{W_c} = 1 - \frac{H_{ad(c)}}{H_{ad(t)}(\eta_c \eta_t \eta_m)}$$

shows that, with a given through-flow rate, turbine-inlet temperature (thus determining $H_{ad(t)}$ as function of $H_{ad(c)}$),[2] turbine efficiency, and mechanical efficiency, the maximum bleed airflow output of a machine with compressor characteristics as shown in Fig. 1(*a*), necessarily will be low for its size. In addition, it is desirable that the bleed air head (or pressure ratio at a given inlet temperature) remain essentially constant over the full bleed-flow loading range. This characteristic is usually favorable for the equipment which is to utilize the compressed air produced. This objective can be approached by utilizing a constant-head control in place of the constant-speed control assumed. Thus it may be concluded that a compressor suitable for a GTC should have a broad compressor characteristic that will allow operation at through-flow rates less than that corresponding to peak efficiency without pulsation difficulty, and a flat enough head delivery that essentially constant head can be maintained over the full bleed-flow loading range either with a constant-speed control or with a constant-head control without demanding excessive operating speed range.

The approximate flow range required on the compressor for a constant-head delivery from a GTC with a fixed turbine-nozzle area can be expressed by the following relation:

$$\frac{W_{c(\text{zero bleed})}}{W_{c(\text{full bleed})}} = \left[\frac{H_{ad(c)(\text{full bleed})}}{H_{ad(t)(\text{full bleed})}}\right]^{1/2} \times \frac{\left[\eta_{m(\text{zero bleed})}\, \eta_{t(\text{zero bleed})}\, \eta_{c(\text{zero bleed})}\right]^{1/2}}{\eta_{m(\text{full bleed})}\, \eta_{t(\text{full bleed})}\, \eta_{c(\text{full bleed})}}$$

Thus it can be seen that as the component efficiencies of a GTC are raised generally, inherently more flow range will be demanded of the compressor. This factor necessarily must enter the design considerations as a compromise to the usual tendency of compressor developments to increase the peak efficiency at the expense of flow range.

With the foregoing thoughts in mind, it was possible to set up several objectives for the compressor to be developed. Noting the desirability of operation on both sides of peak efficiency on the compressor chart, the objectives were established at a mid-loading point. For the turbine and mechanical efficiencies known to be obtainable, it was established that the compressor should be developed for approximately 2.5 lb per sec through-flow rate at a head of 40,000 ft-lb/lb (3.36:1 pressure ratio on a standard day) with an adiabatic efficiency of at least 80 per cent. Under these objectives the operating flow range required on the compressor was approximately 32 per cent, with respect to the compressor flow at zero bleed, without pulsation and as small a variation in efficiency as possible.

BASIC COMPRESSOR CONSIDERATIONS

Since flow range was of prime importance, it was evident that this requirement should represent a basic objective. The most suitable way to obtain increased flow range on a centrifugal compressor for the purpose established is to be able to operate at flow rates less than that at peak efficiency. To be able to accomplish this it is necessary to utilize an impeller with an increasing head delivery as flow is reduced. Furthermore, it is logical that the rate of input-head increase must be greater than the rate of adiabatic-efficiency drop as flow is reduced so as to obtain a rising delivered-head characteristic and thus avoid pulsation.

The characteristics just discussed can be illustrated better by a curve such as Fig. 2 which is similar to the type of curves plotted for centrifugal pumps, but in this case has been adapted to be applicable to a compressible fluid. Two types of impeller characteristic are shown, namely, a 90-deg discharge straight-radial impeller and a rather highly backwardly curved impeller with a discharge angle of 35 deg, plotted as total-head input as a function of per cent inlet-volume flow. In addition, lines for impeller and diffuser efficiency are shown as a function of per cent inlet-volume flow, where it is presumed that the same efficiencies would apply to either type impeller. It is necessary, however, to plot a different line of over-all adiabatic efficiency for each impeller

[2] $H_{ad(c)} = 778\, C_p T_1 \left(\frac{P_2}{P_1}^{\frac{\gamma-1}{\gamma}} - 1\right)$

where for air, $\gamma = 1.395$.

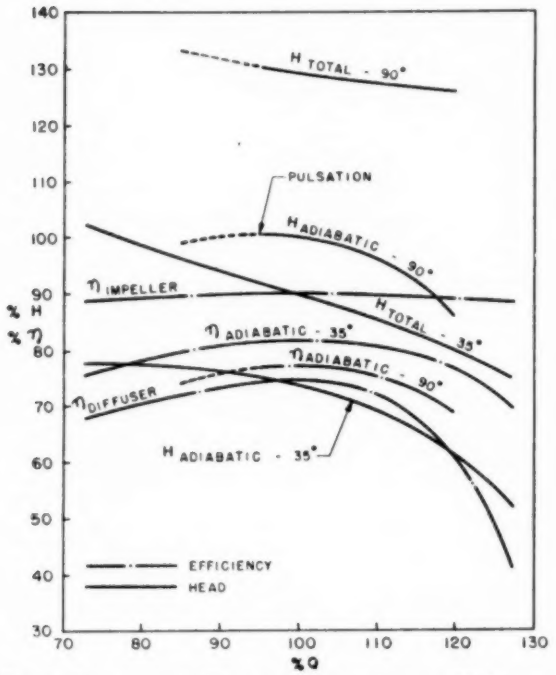

FIG. 2 COMPARISON OF HEAD AND EFFICIENCIES FOR 90-DEG AND 35-DEG COMPRESSORS

type for reasons that will be pointed out later. Combining the efficiency curves and the total-head curves results in the adiabatic-head (or pressure-delivery) characteristics as shown.

Thus it can be seen from Fig. 2 that the 90-deg impeller has a relatively flat total-head curve while the backwardly curved impeller has a considerably steeper rising total-head characteristic with decreasing inlet-volume flow. For this reason the compressor with the 90-deg impeller shows a drop in adiabatic head at flows only slightly less than at peak efficiency whereas the compressor with the backwardly curved impeller shows a gradual rise in adiabatic head at inlet-volume flows considerably less than at peak efficiency. Since pulsation normally occurs at the point where the delivered head begins to drop, it can be seen that the backwardly curved impeller should allow stable operation at flows considerably less than the 90-deg impeller. Thus it can be concluded that, to meet the objective of broad range for operation at flows both above and below that corresponding to peak efficiency, the backwardly curved impeller has the desired characteristic and should be utilized.

A legitimate objection to the highly backwardly curved impeller does exist in that for a given tip speed a lower total head will be produced than with a 90-deg-discharge impeller. This discrepancy in total head can be minimized by the following reasoning:

Assume for comparison of a 90-deg with a backwardly curved impeller that two impellers have the same inlet eye-flow capacity, same diameter ratio, and same tip speed. These assumptions make it possible to consider only the conditions that occur at the discharge of the two impellers. Let it be assumed further that each impeller has the proper number of blades for equivalent cascaded influence so that slip can be considered as a constant 10 per cent of the theoretical absolute tangential velocity. If both have the same blade depth at the discharge, which means that the two impellers are geometrically similar except for discharge angle, then, as shown in Fig. 3, the discharge-velocity triangle (A), represents the 90-deg case while (B) represents the conditions for the backwardly curved impeller. Figs. 3(A) and (B) are to scale for a 90-deg and a 30-deg impeller, respectively, having a tip speed (U) of 1150 fps and a meridional velocity (C_m) of 277 fps. By means of the Euler equation with no whirl at the inlet

$$H_t = \frac{1}{g}(UC_t)$$

where C_t = tangential velocity; the total head may be solved for in each case. From Fig. 3(A), it may be determined that for the 90-deg impeller

$$U = 1150 \text{ fps}$$
$$C_t = 1035 \text{ fps}$$

therefore

$$H_t = \frac{(1150)(1035)}{32.2} = 37{,}000 \text{ ft-lb/lb}$$

Similarly, in the 30-deg case represented by Fig. 3(B)

$$U = 1150 \text{ fps}$$
$$C_t = 600 \text{ fps}$$

and

$$H_t = \frac{(1150)(600)}{32.2} = 21{,}400 \text{ ft-lb/lb}$$

In other words, the 30-deg-discharge impeller shows only 57.8 per cent as much total head as the 90-deg type for the same tip speed. This is too low and is not acceptable in this application if the required delivered head is to be developed in a reasonable number of stages.

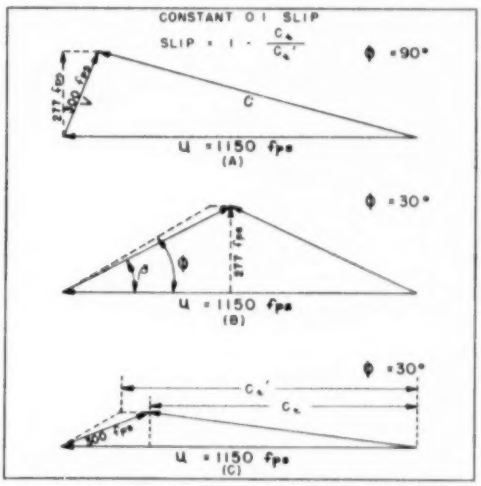

FIG. 3 COMPRESSOR DISCHARGE-VELOCITY RELATIONSHIPS WITH VARYING BLADE ANGLE AND AREA GEOMETRIES

Now let it be assumed that the 90-deg design shown is known to be a good one from the standpoint of impeller efficiency and has no detrimental flow separation. Let it further be reasoned that if such is the case the relative velocity distribution through the impeller must have a significant influence on the results obtained. If this reasoning is correct it appears logical that the same relative velocity distribution also should be acceptable in the backwardly curved impeller. Now, the inlet-eye relative

velocities in both cases have been established as the same by the initial assumptions, and the discharge relative velocities also can be made equal by increasing the blade depth at the tip on the backwardly curved impeller. If this similitude is carried throughout the impeller design, then again only the tip-discharge conditions need be considered. These latter conditions are shown by triangle (C) in Fig. 3. The 30-deg impeller so changed has

$$U = 1150 \text{ fps}$$
$$C_t = 865 \text{ fps}$$

and

$$H_i = \frac{(1150)(865)}{32.2} = 30{,}900 \text{ ft-lb/lb}$$

or the 30-deg impeller with the tip depth increased shows 83.5 per cent as much total head as the 90-deg type for the same tip speed, which is a much more favorable comparison.

Not only can the total head of a backwardly curved impeller be increased by the line of reasoning just given, but certain other inherent advantages also result. To show these advantages, and since the foregoing comparison can be handled in terms of tip speed, relative velocity at the discharge, and discharge angle, it is necessary to establish several useful expressions in terms of these variables.

The following relation may be derived (refer to the Appendix) for the theoretical static head (H_{st}) developed in the impeller

$$H_{st} = \frac{U^2 - V^2}{2g}$$

where V = relative velocity at impeller discharge. This indicates that the theoretical static head is independent of the discharge angle; and, therefore, the 90-deg and 30-deg impellers compared in Fig. 3 which have equal tip speed and discharge relative velocity also will develop equal static head. Now, the reaction of the impeller in a compressor stage can be written

$$R = \frac{H_{st}}{H_i}$$

This can then be written in terms of the variables desired (refer to Appendix)

$$R = \frac{1 - \dfrac{V^2}{U^2}}{2 - \dfrac{2\,V\cos\beta}{U}}$$

where β = discharge angle of relative velocity.

Thus it can be seen that the reaction of the impeller increases with decreasing discharge angle if tip speed and relative discharge velocity are held constant. Finally, an expression can be developed (refer to Appendix) which approximates closely the adiabatic stage efficiency (η_c) in terms of the reaction (R) impeller efficiency (η_I) and diffuser efficiency (η_D)

$$\eta_c = R - (1 - \eta_I) + \eta_D\,(1 - R)$$

Fig. 4 shows a plot of the solution of this expression for the possible range of the variables. Hence it can be stated, as shown in Fig. 4, that with equal impeller and diffuser efficiencies in each case, the stage with the higher reaction impeller inherently will have a higher stage efficiency.

Continuing with the comparison shown in Fig. 3 (A) and (C), the reaction for the conditions of tip speed and relative velocity considered is plotted as a function of discharge angle in Fig. 5. From Fig. 5 the reaction of the 90-deg impeller is 0.519 and for

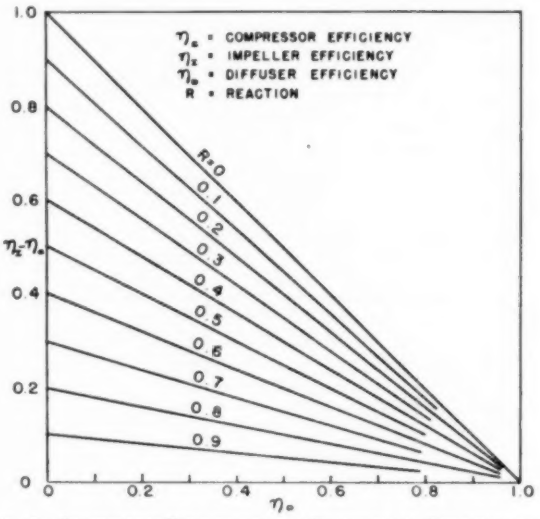

FIG. 4 COMPRESSOR EFFICIENCY AS A FUNCTION OF REACTION AND COMPONENT EFFICIENCIES

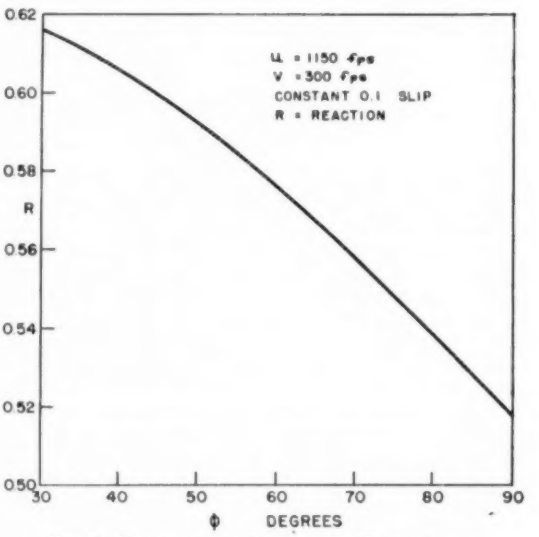

FIG. 5 REACTION AS A FUNCTION OF BLADE ANGLE

the 30-deg case in Fig. 3(C) is 0.616. If an impeller efficiency of 90 per cent and a diffuser efficiency of 75 per cent are assumed as representative of obtainable values in either case, then for the 90-deg case

$$\eta_c = 0.519 - 0.10 + 0.75\,(0.481) = 0.779$$

and similarly, for the 30-deg case

$$\eta_c = 0.616 - 0.10 + 0.75\,(0.384) = 0.804$$

Now, since the actual pressure delivery head (H_{ad}) determines the acceptability of the design, the final comparison can be made.

Since $H_{ad} = H_i\eta_c$, for the 90-deg case

$$H_{ad} = 0.779\,(37{,}000) = 28{,}800 \text{ ft-lb/lb}$$

and for the 30-deg case

$$H_{ad} = 0.804\ (30{,}900) = 24{,}800\ \text{ft-lb/lb}$$

or in the final analysis for equal development level of the component efficiencies and equal tip speeds, the 30-deg impeller in the case considered would develop 86.1 per cent as much delivered head as the straight-radial and would do it with 2.5 per cent higher efficiency. Consideration of all of these factors led to the conclusion that highly backwardly curved impellers would develop the required characteristics and should be used in the subject compressor.

Compressor Arrangement

The required delivered head of 40,000 ft-lb/lb as established previously indicated that two stages of compression would be required. This conclusion was based on the known allowable tip speeds from a structural standpoint for highly backwardly curved impellers. If it is assumed that the head is to be divided essentially equally between the two stages, then the influence of stage efficiency on compressor efficiency can be shown as plotted in Fig. 6. Thus, it may be seen that to obtain a compressor

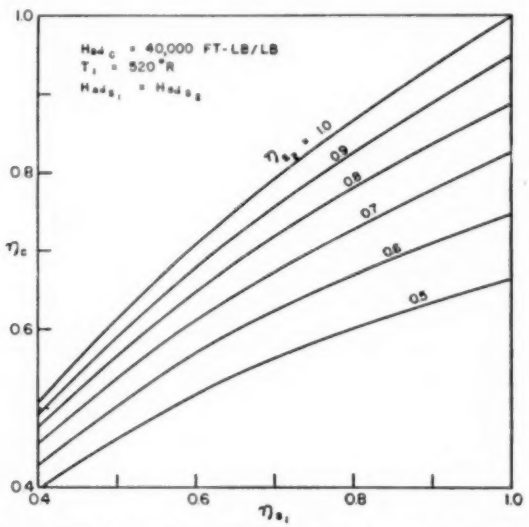

Fig. 6 Two-Stage Compressor Efficiency as a Function of Stage Efficiencies

efficiency (η_c) of 80 per cent requires a stage efficiency of at least 81.7 per cent each if stage efficiencies are identical. It should be pointed out that the interstage system must be charged to one of the stages and its influence considered in the development objectives of that stage to obtain the results shown in Fig. 6. Since the stage-performance requirement appeared rather severe, it follows that full advantage of the reasoning presented in the preceding section should be taken to assure success of the compressor meeting the objectives established. Accordingly, it was decided that fully shrouded impellers with discharge angles of 30 to 35 deg, operating at approximately 1130 fps tip speed, should be used to meet the requirements.

The GTC, for which the subject compressor was to be utilized, contemplated the use of an inward radial turbine which set certain limitations on the allowable speed range. Since the tip speed of the turbine should be approximately 40 per cent higher than that of the compressor for the operating conditions of this particular GTC, a relatively high speed, 38,000 to 40,000 rpm, was favorable for the turbine in terms of weight and space considerations. If the simplicity of running the compressor and turbine at the same speed were maintained, it was evident that a single-inlet first-stage impeller would result in an impractical impeller geometry for a through-flow rate of 2.5 lb per sec. However, a double-entry first-stage impeller for the speed, tip speed, and through-flow rate required, would result in an impeller geometry the proportions of which were well known and considered to be favorable. With the head divided almost equally between the two stages, the double-sided first-stage design presented an additional advantage in that the second-stage impeller could be similar to a single side of the first stage.

Since it was desirable to assemble the two impellers in line on a common shaft, the interstage system with a double-sided first-stage impeller departed from usual practice. It can be appreciated that the air must be taken from the first-stage discharge across one of the first-stage inlets to the second-stage inlet. This was accomplished by utilizing a multiplicity of ducts which for the subject compressor have been called "crossover ducts." Factors such as diffusing efficiency, interference of air entry to the one inlet, and assembly considerations together with over-all envelope diameter had the greatest influence on the design geometry chosen. It was concluded from information presented by Cheshire[3] that diffusion could be accomplished more efficiently and with greater stability if carried out in a linear path. This was applied to the crossover ducts as well as to the outlet casings from the first stage. Thus a considerable portion of the diffusion for the first stage was accomplished in linear paths in the crossover ducts. No diffusion was attempted in either of the two elbows that are necessary in the transfer of air from the first to second stage. The elbows were vaned, however, in accordance with methods presented previously.[4] Divergence in only one plane was used in the crossover ducts with the degree of divergence based on information presented by Young and Green.[5] Consideration of the additional factors mentioned led to the conclusion to utilize seven crossover ducts in the final design.

A cross section of the compressor is shown in Fig. 7 in which the basic design features discussed are evident.

Stage Development

Utilization of existing test facilities together with the relatively short-time schedule established for the development made it highly desirable to be able to conduct individual stage development simultaneously. Accordingly, the second-stage development was carried out on an electric dynamometer-driven test rig while the first-stage development was carried out on a so-called "back-to-back" stand. The back-to-back arrangement consisted of a compressor rig driven by the turbine-and-combustion-chamber section of an available GTC operated from plant compressed-air supply. This arrangement has proved to be quite flexible and reliable for compressor developments.

The first series of tests on the first-stage rig were started in December, 1949. A single-entry impeller which consisted of one half of the double-sided design was used to limit the power required and to utilize an existing rig. This series of tests were carried out to establish basic impeller characteristics and to a lesser degree to establish diffuser requirements. For this purpose a very much oversized scroll was used on the rig primarily to serve

[3] "The Design and Development of Centrifugal Compressors for Aircraft Gas Turbines," by L. S. Cheshire, Proceedings of The Institution of Mechanical Engineers, London, England, vol. 153, 1945, pp. 426–440.

[4] "Airplane Heating and Ventilating Equipment Engineering Data," SAE Aeronautical Information Report No. 2, prepared by Committee A-9, Aircraft Air Conditioning Equipment, January 1, 1943.

[5] "Tests of High-Speed Flow in Diffusers of Rectangular Cross-Section," by A. D. Young and C. L. Green, Reports and Memoranda No. 2201, ARC Technical Report, July, 1944.

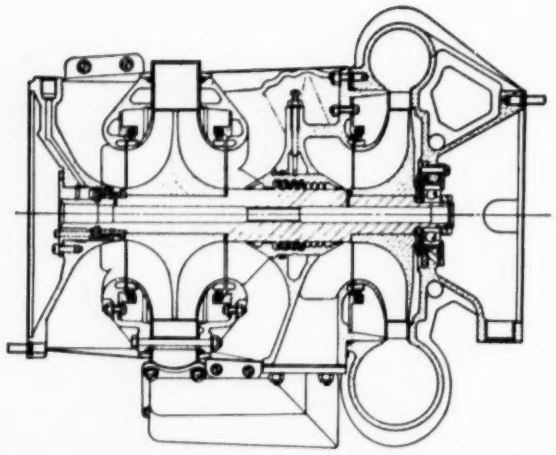

FIG. 7 CROSS SECTION OF FINAL COMPRESSOR CONFIGURATION

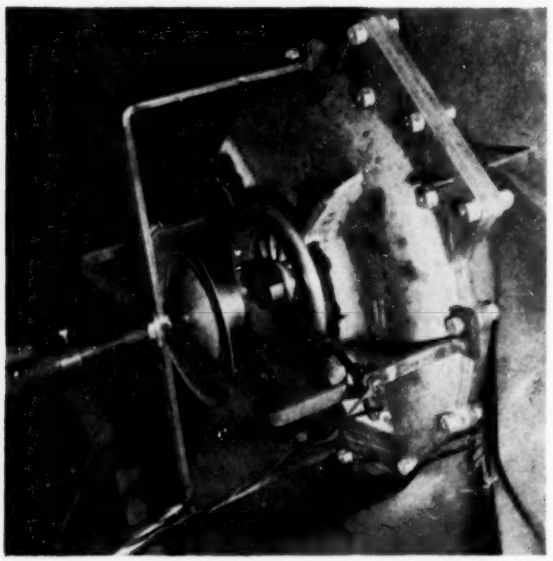

FIG. 8 FIRST-STAGE TEST RIG WITH PERIPHERAL INLET MOUNTED

as an air collector with instrumentation so located as to minimize the influence of the scroll in the interpretation of the results obtained. The results obtained in this first series of tests showed that the characteristics of the impeller chosen were satisfactory and further tests were limited to investigations applicable to the final compressor.

As may be noted in Fig. 7, it was contemplated to use an entry of the full peripheral type on both sides of the first stage. Accordingly, a test series was run to determine the influence of such an air entry with the objective of obtaining the shortest axial length possible. For these tests a contoured spun sheet-metal part simulating the air entry was mounted at the inlet of the first-stage rig so that it could be moved axially, thus allowing calibration of the stage as a function of axial length of the inlet. The test rig with the peripheral inlet mounted is shown in Fig. 8. The results of this test series showed that as axial length was decreased the performance was affected only slightly up to a minimum point at which further decrease resulted in a sharp reduction in performance. For the setup tested this minimum axial dimension, for practically no loss in performance, was approximately 20 per cent of the impeller diameter. This ratio held even when a relatively sharp radius was used on the entry shroud at the outside diameter of the impeller-inlet eye.

As was pointed out in the preceding section, the interstage system should be charged against one of the stages and was so developed. With a design utilizing crossover ducts from the first stage in which a considerable portion of the diffusion was to be done, it appeared logical to develop this phase as a part of the first stage. Since double-sided impellers were not yet available at this point in the development, the first-stage rig was modified to simulate the interstage system with the single-entry impeller.

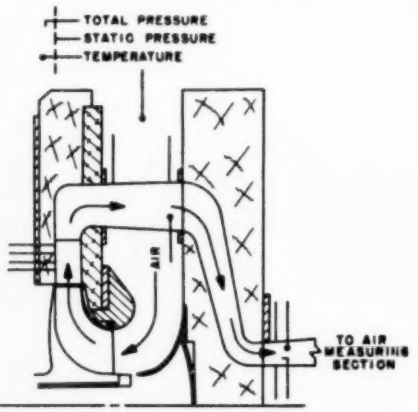

FIG. 9 INSTRUMENTATION AND TEST SETUP FOR INTERSTAGE TESTS

The test rig is shown schematically in Fig. 9. As may be noted, the rig was set up to simulate the conditions that would occur for the entry drawing air past the crossover ducts. In this manner it was felt that the most unfavorable conditions would be investigated. For this phase of testing the results were compared at the point which represented the second-stage entry. The first runs were made with a seven-vane diffuser matched to the seven outlets on the casing and crossover ducts. The results showed 7.5 per cent less efficiency than had been obtained on the rig with conventional diffuser and collector arrangement. Analysis of the data showed that most of this loss was occurring in the early portion of diffusion before the air entered the outlet casings. Accordingly, a 14-vane diffuser was designed which effectively added a splitter vane ahead of each outlet casing. This configuration resulted in only 2 per cent less efficiency, including interstage system, than the best that had been obtained with the earlier rig. These results were considered good, particularly when it was considered that the final unit would have considerably less wetted-surface area per unit of flow and therefore should be better.

The testing with the simulated interstage system showed an additional result, of perhaps just as much significance as the performance, in that no loss of range was observed over that which had been obtained with the earlier rig. For clarification it should be pointed out that all of the tests were conducted down to very low inlet-volume flows at each speed. In none of the tests was pulsation encountered of the type that could result in mechanical destruction. On the contrary, the criterion for the limit of stable range was strictly on the basis of observation of fluctuations on the manometers to a degree that the base accuracy of the readings could not be maintained.

While the first-stage testing was being conducted, development was being carried out on the second stage on the dynamometer-driven rig. Basic impeller characteristics were determined in a manner similar to that of the first stage, except in this case the testing was done on the actual impeller to be used in the complete compressor. A conventional diffuser and scroll arrangement was to be used in the second stage, but it was desirable to develop as short a diffusion length as possible in order to minimize the over-all diameter of the stage. Thus most of the development testing on the second stage was concerned with diffuser and scroll variants.

The second-stage rig was designed to be particularly adaptable for testing various diffuser and scroll designs with minimum cost and time expenditure. The rig housing consisted of two large circular steel halves into which wooden scrolls were inserted. One half of the housing and wooden scroll with the rotating group in place is shown in Fig. 10. These wooden scrolls worked quite satisfactorily after certain techniques were developed. The scrolls were made in sections by a patternmaker, out of mahogany, the sections being glued together with a high temperature-resistant glue. It was found that a new scroll would open up at the seams after a relatively short time of operation. To correct this, the scrolls were baked in an oven for about 1 hr at 250 to 300 F while clamped in place in the heavy steel housing, thus preventing warpage. After the baking the seams were calked and sanded and the scroll given two coats of high-temperature lacquer of a type used for impregnation of electric-motor armatures. The lacquer provided a smooth surface and protected the wood from the high-temperature air while the initial baking prevented any further tendency of the scrolls to open up at the seams during operation.

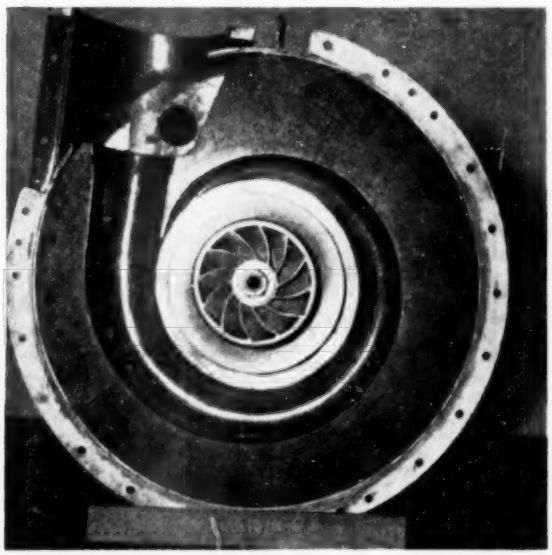

FIG. 10 SECOND-STAGE TEST RIG WITH ONE HALF OF HOUSING REMOVED

Several combinations of diffusers and scrolls were built and tested during this phase of the development. The scrolls were of the diffusing type, the design of which was based on information presented by NACA.[5] It was determined that the best combination for the purpose resulted when the scroll and diffuser were matched for a flow approximately 15 per cent higher than that for which peak efficiency was developed by the impeller. This combination resulted in a peak efficiency only slightly less than that obtainable by ideally matching with the impeller while giving higher efficiency at the higher flows, thus effectively increasing the range of the stage and providing a better match for the two-stage compressor. Further, it was determined that the design objectives for the stage could be met with extremely short diffusion length, namely, with the ratio of outside diameter to inside diameter of the diffuser as low as 1.185.

The complete performance charts resulting from the stage-development phase are shown in Fig. 11, plotted in a manner

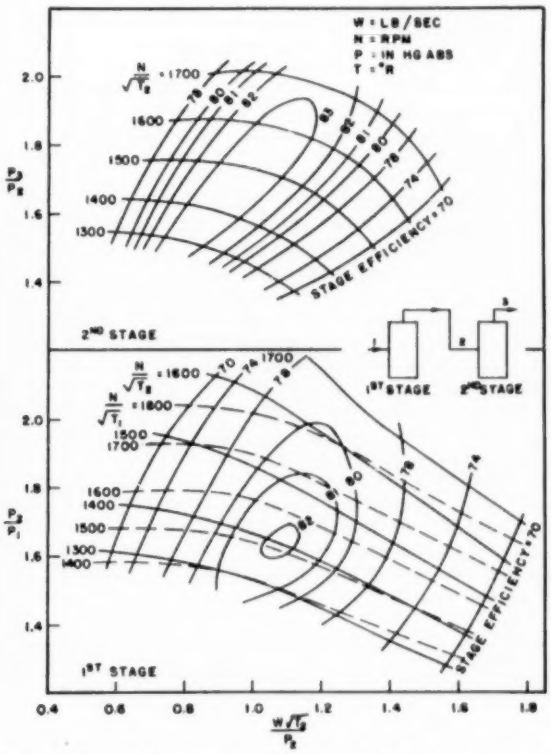

FIG. 11 STAGE-PERFORMANCE CHARTS FOR MATCHING ANALYSIS

which allows quick evaluation of the expected two-stage performance as well as giving a visual presentation of match of the two stages for any given point of investigation. In Fig. 11 the corrected air flow for discharge conditions of the first stage, and inlet conditions for the second stage is plotted as the common abscissa as a function of pressure ratio for each of the stages separately. Thus any given operating point for the two-stage compressor must fall on a vertical line drawn through the two performance charts. Lines of constant corrected speed for both inlet and discharge temperature are plotted for the first stage to facilitate use of the charts. Thus, for a given set of inlet conditions, the first-stage chart may be entered at the desired pressure ratio, move right to the corrected speed line for inlet temperature, read the corrected speed for discharge temperature, move vertically to the same corrected speed line on the second stage, and read the corresponding pressure ratio and efficiency on the second stage. The over-all pressure ratio for the two-stage compressor will be the product of the stage pressure ratios, and the over-all

[5] "Design and Performance of a Family of Diffusing Scrolls With Mixed-Flow Impellers and Vaneless Diffusers," by W. B. Brown and G. R. Bradshaw, NACA TN1568, May, 1948.

adiabatic efficiency can be determined by the following relation

$$\eta_c = \frac{\eta_{s1}\eta_{s2}(Y_{1-3})}{(\eta_{s1} + Y_{1-2}(\eta_{s2} + Y_{2-3}) - \eta_{s1}\eta_{s2}}$$

where

$$Y_{1-4} = (P_3/P_1)^{\frac{\gamma-1}{\gamma}} - 1$$

$$Y_{1-2} = (P_2/P_1)^{\frac{\gamma-1}{\gamma}} - 1$$

$$Y_{2-4} = (P_3/P_2)^{\frac{\gamma-1}{\gamma}} - 1$$

Complete Compressor Development

The final compressor development was carried out on the back-to-back stand used during the first-stage development which was capable of the rather high power demands of the complete compressor. Since it was desired to be able quantitatively to compare the results obtained on the compressor with those obtained on the rigs, the compressor was completely instrumented to duplicate the instrumentation points used on the rigs. The first calibration of the compressor showed that the second-stage performance was low. Tests were then run on the second stage with the first stage removed to determine if the geometry of the final unit was the cause of the low performance. Comparison of the results thus obtained proved that the second stage was 3.5 per cent lower in efficiency than that obtained on the rig. By comparing the pressure recovery at the same points of instrumentation on the compressor to the rig it was determined that all of the differences were occurring after the air left the impeller. The greatest change noted was in the first 45 deg of the scroll where actually static pressure went down instead of up, indicating acceleration instead of diffusion. Careful inspection of the scroll revealed that a casting-pattern error had been made in this region, resulting in the areas being undersize and nonuniform in rate of change. Correction of the scroll casting, together with closer tolerance control on the diffuser itself when tested again in the same manner, resulted in 2 per cent higher efficiency than had been obtained on the rig.

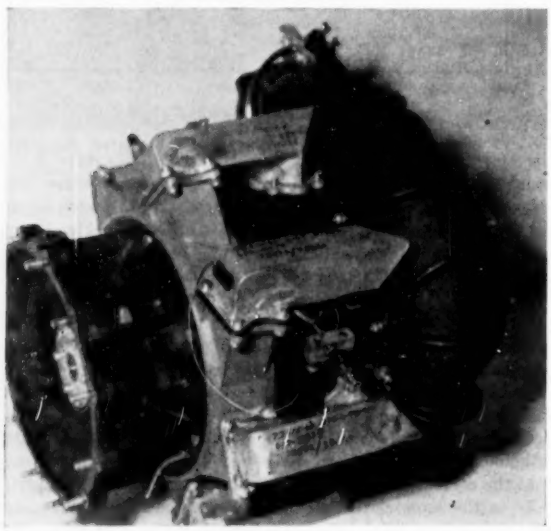

Fig. 12 Completely Assembled and Instrumented Compressor for Calibration

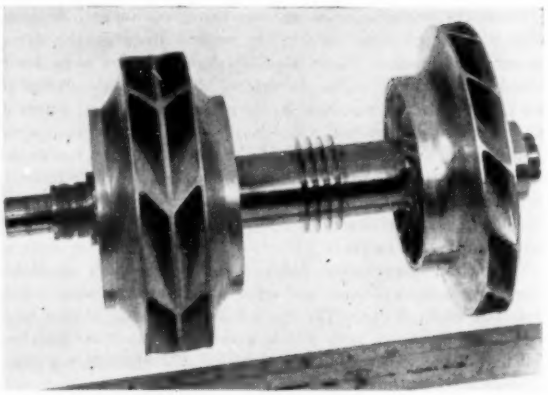

Fig. 13 Rotating Group for Compressor Used for Final Calibration

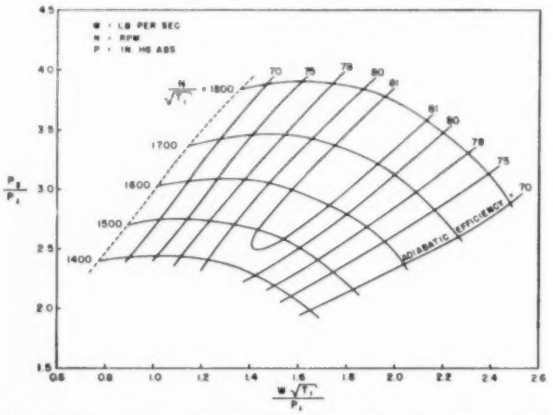

Fig. 14 Compressor Chart Resulting From Calibration of Final Compressor Configuration

With the performance deficiency eliminated, the compressor was again assembled for calibration. The instrumented assembled compressor is shown in Fig. 12, while the rotating group for this compressor is shown in Fig. 13. The calibration of the compressor was completed in April, 1951, and the final over-all performance is shown in Fig. 14. As may be noted, the compressor-performance characteristic is plotted in the general form of corrected air flow as a function of pressure ratio with lines of constant corrected speed and adiabatic efficiency. Again the criterion for pulsation was that of fluctuations in the manometers to a point that the base accuracy of readings could not be maintained, although the unit could be operated at lower air flows with no evidence of the type of pulsation that could cause mechanical failure. The chart as presented was verified by checking the over-all performance with the stage performance, repeating the calibration on different days with different ambient conditions, and by repeating the calibration after disassembly. In addition, the performance has been checked by testing of two other compressor assemblies operating on the complete GTC where close power-balance checks are possible. Therefore it is felt that the chart shown in Fig. 14 has been amply verified and represents repeatable production performance.

The design point established for the compressor in the section Requirements of Compressor, may be found in Fig. 14 at a corrected air flow of 1.9, a pressure ratio of 3.36, and a corrected

speed of 1710. The objective was to obtain an efficiency of 80 per cent at this point. From the stage performance obtained on the rigs, an efficiency of 80.2 per cent was predicted, while the efficiency actually obtained was 81.2 per cent at the design point. This performance was obtained because the first stage, including interstage in the double-sided configuration, gave approximately 1.5 per cent better efficiency than the rig (probably as a result of the less wetted surface per unit of flow) and the second stage gave approximately 2 per cent higher efficiency than the rig as discussed previously. The objective for broad range is self-evident as having been met by reference to Fig. 14.

Thus concluded the aerodynamic phase of the development of a compressor which weighs 33 lb and encompasses maximum envelope dimensions of 16 in. diam × 13.5 in. length. The performance that had been set up as objectives had been met and exceeded and the development was accomplished in a total elapsed time of 16 months. To the best of the author's knowledge, the performance characteristics as shown for the second stage in Fig. 11 and for the complete compressor in Fig. 14 are the best that have been obtained to date on this size class of equipment.

Appendix

Derivation of Expression for Static Head in a Centrifugal Impeller

Assume any general case such as those illustrated in Fig. 3. Then by Euler equation for zero inlet whirl

$$H_t = \frac{1}{g} UC_t \quad [1]$$

which may be written in terms of the impeller static head and the velocity head with respect to stagnation conditions at the impeller inlet

$$H_t = H_{st} + \frac{C_{s_1}^2}{2g} + \frac{C_1^2}{2g} \quad [2]$$

or

$$H_t = H_{st} + \frac{C^2}{2g} \quad [3]$$

From the discharge velocity diagram

$$C_t = U - V\cos\beta \quad [4]$$

and

$$C^2 = V^2\sin^2\beta + [U - V\cos\beta]^2 \quad [5]$$

Substitute Equation [4] into [1]

$$H_t = \frac{1}{g} U[U - V\cos\beta] \quad [6]$$

Solve for static head in Equation [3]

$$H_{st} = H_t - \frac{C^2}{2g} \quad [7]$$

Substitute Equations [6] and [5] into [7]

$$H_{st} = \frac{U[U - V\cos\beta]}{g} - \frac{V^2\sin^2\beta + [V - V\cos\beta]^2}{2g} \quad [8]$$

Combine terms in Equation [8]

$$H_{st} = \frac{2U[U - V\cos\beta] - V^2\sin^2\beta - [U - V\cos\beta]^2}{2g} \quad [9]$$

Expand Equation [9]

$$H_{st} = \frac{2U^2 - 2UV\cos\beta - V^2\sin^2\beta - U^2 + 2UV\cos\beta - V^2\cos^2\beta}{2g} \quad [10]$$

Simplify Equation [10]

$$H_{st} = \frac{U^2 - V^2\sin^2\beta - V^2\cos^2\beta}{2g} \quad [11]$$

Rearrange Equation [11]

$$H_{st} = \frac{U^2 - V^2[\sin^2\beta + \cos^2\beta]}{2g} \quad [12]$$

Now since

$$\sin^2\beta + \cos^2\beta = 1$$

Equation [12] simplifies to

$$H_{st} = \frac{U^2 - V^2}{2g} \quad [13]$$

Derivation of Expression for Reaction

By definition let

$$R = \frac{H_{st}}{H_t} \quad [14]$$

Substitute Equations [13] and [6] into [14]

$$R = \frac{\dfrac{U^2 - V^2}{2g}}{\dfrac{U[U - V\cos\beta]}{g}} \quad [15]$$

Expand Equation [15]

$$R = \frac{U^2 - V^2}{2U^2 - 2UV\cos\beta} \quad [16]$$

Rearrange Equation [16]

$$R = \frac{1 - \dfrac{V^2}{U^2}}{2 - \dfrac{2V\cos\beta}{U}} \quad [17]$$

Derivation of Expression for Compressor Efficiency

Let impeller efficiency be defined in terms of Equation [3]

$$\eta_I H_t = \left(H_{st} + \frac{C^2}{2g}\right)\eta_I \quad [18]$$

which merely says that in the definition of impeller efficiency it is assumed that all of the velocity head produced is recovered without loss. Let it be reasoned, however, that all of the impeller loss must be subtracted from the theoretical static head and that diffusion efficiency applies only to the velocity head produced.

Then, since adiabatic head is the actual pressure head delivered, from Equation [18]

$$H_{ad} = H_{st} - (1 - \eta_I)H_t + \eta_D\frac{C_1^2}{2g} \quad [19]$$

where C_1 is used in place of C since the impeller losses must appear as a change in velocity head. The value of C_1 may be either larger or smaller than C depending on the impeller geometry and discharge angles. Usually the magnitude of C_1 is only slightly

different from C and may be neglected without introducing serious error. Then Equation [19] becomes

$$H_{ad} = H_{st} - (1 - \eta_I) H_t + \eta_D \frac{C^2}{2g} \quad [20]$$

By definition

$$\eta_c = \frac{H_{ad}}{H_t} \quad [21]$$

Divide Equation [20] by H_t; then by Equation [21]

$$\eta_c = \frac{H_{st}}{H_t} - \frac{(1 - \eta_I) H_t}{H_t} + \frac{\eta_D C^2}{H_t 2g} \quad [22]$$

Substitute Equation [14] into [22] and simplify

$$\eta_c = R - (1 - \eta_I) + \frac{\eta_D C^2}{H_t 2g} \quad [23]$$

Divide Equation [7] by H_t, then

$$\frac{H_{st}}{H_t} = 1 - \frac{C^2}{H_t 2g} \quad [24]$$

Again substitute Equation [14] in [24] and rearrange terms

$$\frac{C^2}{H_t 2g} = 1 - R \quad [25]$$

Finally, substitute Equation [25] in [23]

$$\eta_c = R - (1 - \eta_I) + \eta_D (1 - R) \quad [26]$$

Discussion

CHARLES HILL.[7] The compressors described in the paper have exceptionally high efficiency. The paper indicates that most of the author's attention was given to the impeller. What are the individual impeller and diffuser efficiencies?

The NACA has found from tests that the curvature of the inducer portion of an impeller has considerable influence on performance. Was any special consideration given this feature in the impellers described in the paper?

ROGER LAPP.[8] The author has presented a fine paper on the aerodynamic features of a very successful compressor-design program.

He states that the relative velocity distribution through the impeller has considerable bearing upon the efficiency of the impeller. A discussion of the relative velocity and acceleration schedules through the impeller would be desirable.

Emphasis is placed on the fact that pulsation was not severe in this compressor, at least not of the type that could cause mechanical failure. If the author has experience with pulsation severe enough to cause mechanical failure would he comment on the type of failure encountered and at what tip speed?

It has been the writer's experience with 90-deg-discharge compressors that a performance over 80 per cent requires close tolerances throughout the machine. In this case what is the size of the casting error involved in the second-stage scroll and diffuser to effect a 5½ per cent change in the over-all efficiency?

The cross-section view of the final compressor shows two outboard bearings and the use of inlet-guide walls for each stage. Is any change in the performance of a centrifugal compressor caused by the introduction of a shaft through the eye as compared to the overhung type without any shaft protruding through the eye?

J. D. STANITZ.[9] The author and his company are to be congratulated on the development of a centrifugal compressor with exceptionally high efficiency, especially in view of its relatively small size. The broad range of this compressor is also noteworthy, and the author has given an interesting discussion of the design considerations leading to this range. In the opinion of the writer, one of the important factors leading to the excellent performance of the compressor is the apparently well-designed interstage ducting.

The author has developed a convenient approximate Equation [26] for the compressor efficiency in terms of the reaction R and and the impeller and diffuser efficiencies. As pointed out by the author, this equation indicates that the compressor efficiency increases with reaction R, provided the impeller and diffuser efficiencies remain unchanged. It is further shown, Equation [17], that, for a given ratio of exit relative velocity to impeller-tip speed V/U, the reaction R increases with decreasing relative exit flow angle β. In addition, it might be pointed out that, for a given angle β, there is an optimum value of V/U for which the reaction R is a maximum. This optimum value of V/U is obtained from Equation [17], if the derivative of R with respect to V/U is set equal to zero. The result is

$$\left(\frac{V}{U}\right)_{opt} = \frac{1 - \sin \beta}{\cos \beta} \quad [27]$$

A plot of this equation over the range of β is shown in Fig. 15 of this discussion, and indicates that, as β increases from 0 to 90 deg, $(V/U)_{opt}$ decreases from 1.0 to zero. For an angle β of 22 deg, such as required in Fig. 5 of the paper, for a blade angle Φ of 30 deg, the optimum value of V/U is 0.674 compared to a value of 0.261 used in the design.

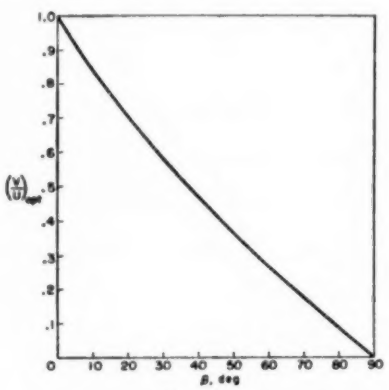

FIG. 15

If Equation [27] of this discussion is combined with Equation [17] of the paper, the maximum value of the reaction R for a given angle β is obtained. The result is

$$R_{max} = \frac{1 - \sin \beta}{\cos^2 \beta} = \frac{1}{1 + \sin \beta} \quad [28]$$

A plot of this equation over the range of β is shown in Fig. 16, herewith, and indicates that, as β increases from 0 to 90 deg, R_{max} decreases from 1.0 to 0.5. For β equal to 22 deg, the

[7] Ford Motor Company, Scientific Laboratory, Dearborn, Mich.
[8] Ford Motor Company, Scientific Laboratory, Dearborn, Mich.
[9] Head, Centrifugal Compressor Research Section, National Advisory Committee for Aeronautics, Cleveland, Ohio. Jun. ASME.

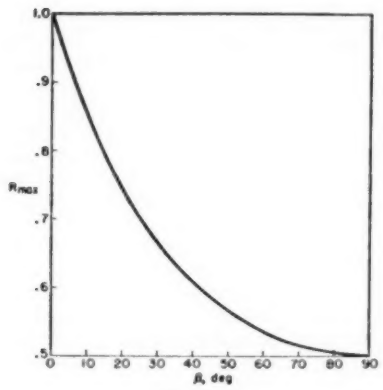

FIG. 16

maximum value of R is 0.727, compared to the value of 0.616 obtained in the paper for the same value of β. For the higher value of R the compressor efficiency becomes 0.832, compared to 0.804 obtained in the paper, and this higher figure assumes that the impeller and diffuser efficiencies remain unchanged.

It should be noted that the optimum value of V/U required to achieve the 0.832 efficiency is high (0.727), and compared to a design with lower value for V/U, would result in a relatively large decrease in total head H_t for only a moderate increase in compressor efficiency. It is easily shown that the ratio λ of the work input with backward curved blades and with optimum V/U to the work input with radial discharge ($\beta = 90$ deg) is

$$\lambda = \sin \beta \ldots\ldots\ldots\ldots\ldots\ldots\ldots\ldots [29]$$

Thus, if high total heads are desired, it is not advisable to use the optimum value of U/V for low values of β. However, the same total head as achieved in the paper for β equal to 22 deg (blade angle Φ equal to 30 deg) can be achieved for β equal to 48°46′ with the optimum value of V/U equal to 0.376. For this condition, the value of R_{max} is 0.571 so that, if the impeller and diffuser efficiencies remain unchanged, the compressor efficiency is slightly reduced to 0.793, but the blades are not curved backward so greatly, and, therefore, for some applications might be more desirable structurally.

N. VAN LE.[10] The writer wishes to discuss the possibility of having the same relative velocity distribution for radial impeller (ri) and backwardly curved impeller (bci) as stated by the author in the section of the paper, Basic Compressor Considerations. The discussion is centered around the following analysis which also can be found in a more complicated form:[11]

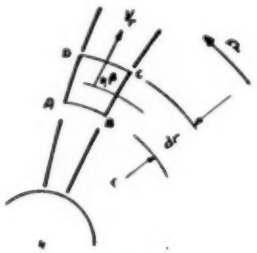

FIG. 17

Consider an element A-B-C-D in the blade passage of a "bci," Fig. 17. The following assumptions are made: Two-dimensional flow; the relative velocity V_r makes an angle β with the tangential direction, β being the mean blade angle at the radius considered; the absolute flow is irrotational. Then the circulation Γ along the path A-B-C-D is

$$\Gamma_{AB} \quad -(r\Omega - V_u)\, rd\theta; \quad V_u = V_r \cos \beta$$

$$\Gamma_{CD} \quad +(r\Omega - V_u)\, rd\theta + \frac{\partial}{\partial r}(r\Omega - V_u)\, rd\theta\, dr$$

$$\Gamma_{BC} \quad V_r\, dr/\sin \beta$$

$$\Gamma_{DA} \quad -\left(V_r \frac{dr}{\sin \beta}\right) - \frac{\partial}{\partial \theta}\left(V_r \frac{dr}{\sin \beta}\right) d\theta$$

$$\Sigma\Gamma = 0$$

$$\frac{\partial}{\partial \theta}\left(\frac{V_r}{\sin \beta}\right) = 2r\Omega - \frac{\partial}{\partial r}(r\, V_u) \ldots\ldots\ldots\ldots [30]$$

This gives a good approximation of the distribution of V_r in the tangential direction.

For radial impeller

$$\beta = 90 \text{ deg}, \sin \beta = 1, V_u = V_r \cos \beta = 0$$

Equation [30] becomes

$$\frac{\partial}{\partial \theta} V_r = 2r\Omega$$

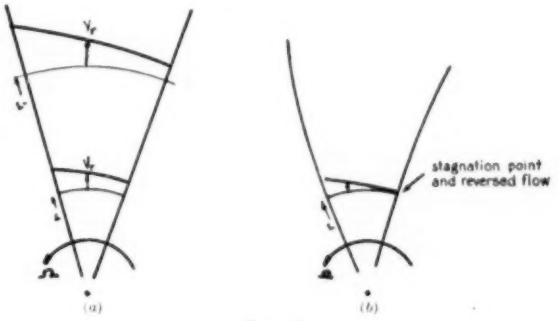

FIG. 18

1 At a radius r_1, the distribution V_r of a radial impeller in the tangential direction is as shown, Fig. 18(a), herewith. By compromising between the ri and the bci to obtain a higher whirl, the author has reduced the radial component of the relative velocity as shown in Fig. 3(c) of the text. If, furthermore, the area at the section r_1 of the blade passage is kept the same for both types of impellers, the mass flow is smaller in the bci and a tangential distribution of V_r can appear as shown in Fig. 18(b) of this discussion. Existence of a stagnant region and reversed flow is obvious. Now if the mass flow is increased by increasing the width (measured in the axial direction) of the blade passage, one still wonders whether such a distribution, as shown in Fig. 18(b), disappears.

2 Assume now that there is a common radial distribution of the mean relative velocity for both types of impeller. For a bci, geometric consideration shows that V_u may increase with the radius, the slope

$$\frac{\partial}{\partial \theta} \frac{V_r}{\sin \beta}$$

[10] Research Assistant in Mechanical Engineering, Gas Turbine Laboratory, Massachusetts Institute of Technology, Cambridge, Mass.

[11] "All NACA reports on Two Dimensional Compressible Flow in Centrifugal Compressors," by J. D. Stanitz.

from Equation [30] is smaller for a bci. As a result, the relative velocity may decrease faster on the trailing face of a bci. This rate of deceleration is to be controlled to avoid separation. Probably owing to the complicated calculation (though possible[11]) one has to use the mean relative velocity to control the possibilities of separation.

This discussion is valid only if the assumptions hold. This is true for radii up to $r/r_{op} = 0.85$ according to Stanitz.[11]

F. C. Gilman.[12] The author and his associates are to be congratulated for having achieved the broad range and high efficiency reported in so small a compressor and especially in so short a time. The machine Reynolds number as defined by Davis, Kottas, and Moody[13] would be 3,670,000 using kinematic viscosity of air at 80 F and 1 atm, and 4,700,000 using the viscosity of air under conditions of entrance into the second stage. Efficiencies of centrifugal compressors reported by the authors mentioned[13] seemed to be between 78 and 79 per cent in this range of machine Reynolds number.

The language of the paper gives the impression that the author felt the impeller design selected was a novel one to fulfill the requirements of a broad stable range while maintaining a high stage head. Actually, this type of impeller was used by manufacturers of centrifugal refrigeration compressors at least 13 years ago and has been used in pumps for years before that.

The technique described for the successful application of wood components under high air-temperature conditions no doubt will prove helpful to experimenters in this field, and the writer, for one, wishes to thank the author and his company for disclosing this kind of useful information.

The author's analysis of the beneficial effect of a high degree of reaction on the compressor adiabatic-stage efficiency is based on the assumption of constant impeller and diffuser efficiencies regardless of impeller-discharge angle. Such an assumption may be found true to fact down to angles of 30 deg as used in the subject compressor but readers should not be led to the conclusion that even smaller angles would yield still higher stage efficiencies. It must be remembered that with constant impeller-tip speed and constant-discharge relative velocity, increased reaction is realized only by reduced total head, since static head is constant. At constant tip speed, impeller-disk friction losses will be unchanged and with smaller exit angle the "wetted surface" within the impeller will increase. Under these conditions both impeller efficiency and compressor efficiency are likely to fall off. There is a general rule which, while not true in every instance, is believed to be worth bearing in mind. This says that for best efficiency one should try to get maximum useful output from a given size of machine. Of course flow separation, shock fronts, choking, and cavitation in liquids are limiting factors.

The paper refers to the adiabatic head as the actual pressure-delivery head. This may be true to the extent that the adiabatic or preferably isentropic efficiency used in determining the adiabatic head is based on the actual pressure delivered. But the adiabatic head is not the actual mechanical work put into the gas. That is the polytropic head. The adiabatic head of a single stage cannot be multiplied by the number of similar stages in series to find the over-all head of a machine. This can be done with the polytropic-stage head. Let us reserve the word actual for polytropic head and polytropic efficiency. They indicate the true worth of the aerodynamic design.

H. E. Sheets.[14] The author's paper presents some interesting and basic information relating to the development of highly efficient centrifugal compressors with backwardly curved blades having a high-compression ratio. The efficiency and performance shown are outstanding. The basic considerations for analysis presented in this paper are, however, primarily of a simplified nature. The assumption of constant impeller efficiencies for radially ending vanes and backwardly curved vanes does not always exist and the additional assumption of constant slip does not necessarily hold true. The basic conclusions derived from these simplified assumptions are essentially correct.

This writer disagrees with the author's assumption that pulsation for compressors with radially ending vanes normally occurs at the point where the delivery head begins to drop. Pulsation can be analyzed and, if required, compressors with radially ending vanes can be designed for a wide range of operation, particularly if the compression ratio is on the same order as for the compressor with the backwardly curved vanes. The writer has published some data[15] on compressors with a wide range of operation in "Nondimensional Compressor Performance for a Range of Mach Numbers and Molecular Weights," ASME Paper No. 51—SA-19. That paper also contains performance curves of compressors with backwardly curved blades which have a range of operation over the entire range of flow. This shows the ultimate in development which can be achieved in operation for compressors with backwardly curved blades.

Author's Closure

The author wishes to express his appreciation to Messrs. Hill, Lapp, Stanitz, Van Le, Gilman, and Sheets for the time and effort spent in reviewing and commenting on this paper. The worth of this paper has been greatly increased by the considered opinions and additional thoughts presented by the discussers. Since space will not permit detailed comment on all of the discussions, the author will attempt to cover only those points which appear to warrant amplification or clarification.

The reasoning presented by Mr. Stanitz is very interesting, and certainly well worth consideration during the design phase of any new compressor. As pointed out, if the optimum V/U is used at low-discharge angles, total head is materially reduced. Since any design must usually embody a system of compromises, it still would appear to the author that in this design it was better to depart from the optimum V/U. In this manner it was possible to use a lower-discharge angle while maintaining an acceptable total head, thus obtaining increased stability and flow range, which was a primary objective of the development.

From the reasoning presented by Mr. Van Le utilizing the circulation theory, it would appear that the same relative velocity distribution in a radial and backwardly curved impeller would not be possible. Perhaps in a strict sense this is true. However, as pointed out in the section Basic Compressor Considerations, the static head at any given radius in the impeller is independent of the flow angle. Thus, in the cases compared, the air density at any given radius is the same. Therefore, if the flow areas normal to the flow direction are equal, the mean relative velocities along the mean flow path are also equal. This simplification of reasoning may not lead to any greater error than the simplification of assuming two-dimensional flow, which led to the mathematical results shown by Mr. Van Le.

If the conditions suggested by Fig. 18 were serious, one could expect a poor flow distribution at the discharge between any two adjacent blades. Our test seemed to show that, if anything, the flow distribution at the discharge on a backwardly curved impel-

[12] Research Engineer, Worthington Corporation, Harrison, N. J.

[13] "The Influence of Reynolds Number on the Performance of Turbomachinery," by H. Davis, H. Kottas, and A. M. G. Moody, Trans. ASME, vol. 73, 1951, pp. 499–509.

[14] Goodyear Aircraft Corporation, Akron, Ohio. Mem. ASME.

[15] "Nondimensional Compressor Performance for a Range of Mach Numbers and Molecular Weights," by H. E. Sheets, Trans. ASME, vol. 74, 1952, pp. 93–102.

ler is somewhat better than on a radial impeller. Detrimental flow separation appears to be of very much the same type on a backwardly curved impeller as on a radial impeller when it occurs; namely, the flow pattern at the tip leaves the impeller at the back disk and re-enters at the front face. The limitation as to the amount of deceleration that can be tolerated (based on the mean relative velocity) to avoid the type of separation mentioned has been very much the same for either backwardly curved or radial impellers in the experience of the author.

The remarks of Messrs. Gillman and Sheets with respect to the assumption of constant impeller efficiency would appear to need some clarification. It was the intent of the author to utilize this assumption only to simplify the illustration of a point for this paper. Since the question has been raised, actually the impeller efficiency for discharge angles as low as thirty degrees (in well-developed impellers) is very comparable to that attained with radial-discharge impellers. It is true that the path length in a backwardly curved impeller is somewhat longer and should lead to greater surface friction loss. However, due to the longer-path length, fewer blades are required for equivalent cascade effect which tends to be a compensating influence. The author agrees with Mr. Gilman that with discharge angles much below thirty degrees, some loss in efficiency could be expected, since the compensating effect of reduced number of blades has a diminishing influence at still lower-discharge angles. Although not mentioned by any of the discussers, the assumption of constant diffuser efficiency is also subject to some suspect. In this case, however, the assumption is conservative with respect to the backwardly curved impeller system, since the discharge absolute velocity (which is the entering relative velocity in the diffuser) is always less for comparable conditions with the backwardly curved impeller than for the radial impeller. For this reason, in a conventional design in which Mach-number considerations may be a limiting factor, it is feasible that a backwardly curved impeller could produce a total head equivalent to or even higher than that obtainable with a radial impeller.

The remarks of Mr. Sheets with respect to pulsation and flow range are interesting, although somewhat in variance with the opinions of the author. The point at which the delivered head begins to drop is the lowest flow for which conditions for stability are satisfied, and as such usually represents the lowest usable flow delivery. This is true regardless of the discharge angle of the impeller. Perhaps pulsation can be analyzed for any given set of conditions, but it would appear that the analysis would be for the purpose of determining the flow at which conditions for stability were no longer satisfied. Actually, the characteristics of either backwardly curved or radial impellers are stable over an extremely broad flow range. It is the geometry of the diffusing system that usually determines the usable flow range and the severity of the instability. It has been the author's experience that some loss in efficiency is associated with diffusing geometries that lead to a broad and stable flow range with radial-discharge impellers. This, then, becomes a matter of designer's choice for a given application. In the application discussed in this paper, high efficiency was of extreme importance—thus the reasoning as presented led to the configuration shown.

Some Investigations With Wet Compression

By J. T. HAMRICK[1] AND W. L. BEEDE,[1] CLEVELAND, OHIO

This paper presents the results of some experimental investigations on several centrifugal-flow compressors using water injection. In addition, mechanical considerations, special instrumentation, and theoretical aspects are discussed and a method of computing adiabatic efficiency with wet compression is presented.

Introduction

WATER injection in both jet and reciprocating engines has achieved varying degrees of attention over the past two decades and has been applied successfully in specific cases in both the United States and foreign countries. The written literature has been somewhat vague in the treatment of the theoretical aspects of water injection as applied to compressors and, in the case of reciprocating engines, the main effort has been concentrated on elimination of knock (1, 2, 3,[2] for example) rather than upon improvement in supercharger performance.

With both types of engines, water injection has been used for augmentation of normal power over short periods and not in a continuous application, one of the primary reasons being the requirement of a large quantity of water. This factor can be appreciated if we consider a turbojet engine into which water equal to 5 per cent of the air weight flow is injected. For an engine using 100 lb of air per sec the amount of water required would be 18,000 lb per hr or a weight approximately equal to that of an aircraft which would use such an engine. Recovery of the water in the exhaust gases is discussed in reference (3) and, although the use of the required equipment appears impractical for aircraft, its application to stationary gas-turbine engines might be feasible.

Liquids of injection other than water such as alcohol and conventional fuels have been proposed and in many cases alcohol-water mixtures have been used. Dilution of the water with enough alcohol to prevent freezing and to augment the normal fuel supply to the burners is quite advantageous in some cases.

Volatile fuels, in general, have a latent heat of vaporization only 10 to 15 per cent of that for water; therefore a fuel-air mixture which would effect a significant amount of evaporative cooling would result in excessive turbine-inlet temperatures. Even if operation at high turbine-inlet temperatures could be achieved (with turbine-blade cooling, for example) the fire hazards involved might be too great.

Water or water-alcohol mixtures have been injected into both centrifugal-flow and axial-flow types of turbojet engines with varying degrees of success. A somewhat complex problem is presented for injection of water into an axial-flow compressor because of the large number of stages. A substantial amount of evaporative cooling at the inlet stages easily could cause severe mismatching in the later stages. In general, the increase in pressure ratio with water injection has been somewhat less for the axial-flow than for the centrifugal-flow-type compressor, a situation which probably could be corrected with design modifications for wet compression.

In general, there are many problems associated with wet compression; however, the potentially large increase in compression ratio which may be obtained with little or no increase in work input to the compressor makes the use of wet compression quite attractive.

It is the purpose of this paper to present the results of some experimental investigations on several centrifugal-flow compressors using water injection. In addition, mechanical considerations, special instrumentation, and theoretical aspects are discussed and a method of computing adiabatic efficiency is presented. The results presented in this paper were obtained from investigations conducted at the Lewis Flight Propulsion Laboratory of the National Advisory Committee for Aeronautics and are partially reported in references (4) and (5).

Experimental Results

Several different compressors were operated with water injection in order to determine the effect of a 0.05 water-air ratio upon over-all performance. During the first tests conducted, difficulty was encountered from mineral deposits upon the instruments and in the passages and from the impingement of entrained water droplets upon the thermocouples in the compressor exit. Fig. 1 shows the results of an investigation for a compressor on which the foregoing difficulties had been eliminated and vapor-sampling devices installed in the outlet ducts.

In the discussion of these results it should be kept in mind that many of the changes in performance were encountered upon the injection of water because the compressors used in these investigations were designed for dry compression. Therefore the results presented do not indicate a fair picture of the potential benefits of wet compression; however, they do serve to point out some of the technical difficulties which may be encountered.

Performance—Pressure Ratio. The primary advantage of injecting water into the compressor inlet is the increase in pressure ratio obtained. The manner in which the pressure increase is affected is somewhat analogous to the effect of using refrigerated air at the compressor inlet which increases the compression ratio for a given work input. However, precooling of the air is not necessary to effect a pressure increase inasmuch as cooling of the air stream in the impeller or the diffuser would produce a similar result. In fact, a scheme for a wind tunnel employing no mechanical equipment and using evaporative cooling of the air stream to effect a pressure rise has been devised (6).

In Fig. 1(*a*) maximum pressure ratio is plotted against water-air ratio for operation at one tip speed over a range of weight flows. The leveling off at 0.04 water-air ratio agrees in trend with theory.

For a compressor operating as a component of an engine it is not always possible to operate the compressor at maximum pressure ratio. For example, it may be necessary to operate the engine along line 1-1 in Fig. 1(*b*), in which case the pressure-ratio increase upon the injection of water would be greater than the increase at the peak conditions shown in Fig. 1(*a*). Thus the practicality of the injection of water into a particular engine may depend to a great extent on its effect upon the engine operating line.

Maximum Weight Flow. In the centrifugal compressors tested

[1] Aeronautical Research Scientist, Lewis Flight Propulsion Laboratory, National Advisory Committee for Aeronautics.

[2] Numbers in parentheses refer to the Bibliography at the end of the paper.

Contributed by the Hydraulic and Gas Turbine Power Divisions and presented at the Semi-Annual Meeting, Cincinnati, Ohio, June 15–19, 1952, of The American Society of Mechanical Engineers.

Note: Statements and opinions advanced in papers are to be understood as individual expressions of their authors and not those of the Society. Manuscript received at ASME Headquarters, March 24, 1952. Paper No. 52—SA-15.

the maximum flow was limited by choking in the vaned diffuser. This choking may be relieved by evaporative cooling with a resulting increase in maximum weight flow which in itself would allow an increase in thrust. However, the engine is usually so designed that the maximum air flow is fixed by the critical pressure ratio in the turbine stator or the turbine blades. Therefore, for a fixed turbine-inlet temperature the increase in weight flow could not be realized without an increase in compression ratio. In the event that the weight flow is limited by choking at the impeller inlet, which is often the case where vaneless diffusers are used, no increase in air weight flow resulting from evaporative cooling within the impeller could result.

Choking occurred in the entrance to the vaned diffuser of the compressor of Fig. 1; therefore an increase in weight flow was obtained as shown in Fig. 1(*c*). Above a water-air ratio of 0.02 the increase in weight flow is due solely to the increase in water injected which indicates that above that ratio any increased evaporation took place downstream of the choke point.

Minimum Weight Flow (Surge). The minimum weight flow or, more correctly, the minimum volume flow rate through a compressor is generally limited by the severe mechanical vibrations which accompany surge. Investigations thus far concerning surge have resulted in a somewhat superficial knowledge of its cause (reference 7, for example). On all compressors investigated, an increase in air weight flow at surge was obtained with water injection, and with one exception was of the order of increase shown for the impeller in Fig. 1(*d*). Such an increase could be very detrimental to the engine operation if the engine operating line fell, for example, along 2-2 in Fig. 1(*b*).

The effect of wet compression upon surge is not always as mild as that shown in Fig. 1(*b*). With the injection of water into the compressor in Fig. 2 there was an increase of 17 per cent in total weight flow at surge with an increase in maximum pressure ratio of less than 5 per cent, a condition which probably would prevent the use of water injection on an engine employing the compressor. An analysis of flow within this compressor indicated that the formation of an unstable eddy on the driving face of the impeller blades may have been the exciting force for surge as suggested in reference (8). This eddy formation, an example of which is shown in Fig. 3, grows in size as the volume flow rate per unit area is decreased, but may be reduced in size or eliminated for any given flow rate by increasing the number of blades in the impeller. Whether or not surge was caused by the unstable eddy could not be verified; however, increasing the number of blades in the impeller did improve the range, especially for wet compression. Fig. 2(*b*) shows the performance of a compressor identical to the one in Fig. 2(*a*), except for an increase in the number of blades in the impeller.

Power Requirements. The specific power per pound of mixture per second is given in Fig. 1(*e*). Inasmuch as the tip speed remains constant, the changes in power supplied are a function of slip factor and disk friction. The slip factor remains fairly near

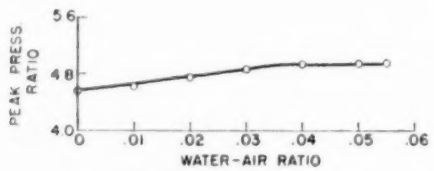

(*a*) Peak total-pressure ratio

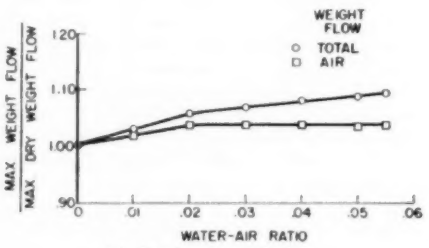

(*c*) Maximum weight flow

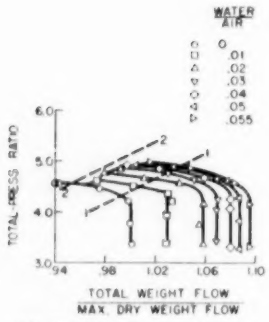

(*b*) Total-pressure ratio over range of weight flows

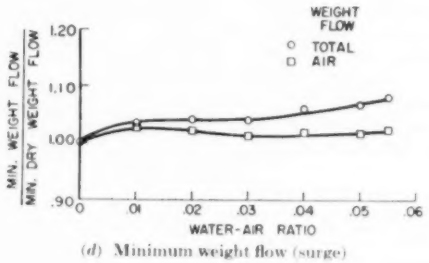

(*d*) Minimum weight flow (surge)

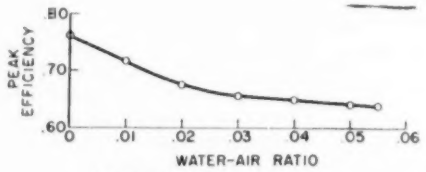

(*f*) Peak adiabatic efficiency

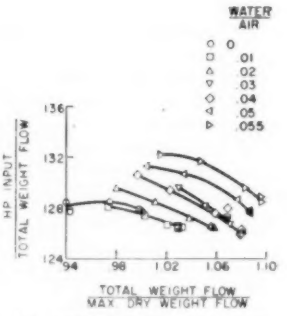

(*e*) Specific power input over range of weight flows

FIG. 1 PERFORMANCE OF CENTRIFUGAL COMPRESSOR WITH WATER INJECTION AT CONSTANT IMPELLER SPEED, CONSTANT INLET PRESSURE OF 14 IN. HG ABS, AMBIENT INLET-AIR TEMPERATURE, AND WATER-AIR RATIOS FROM 0 TO 0.055

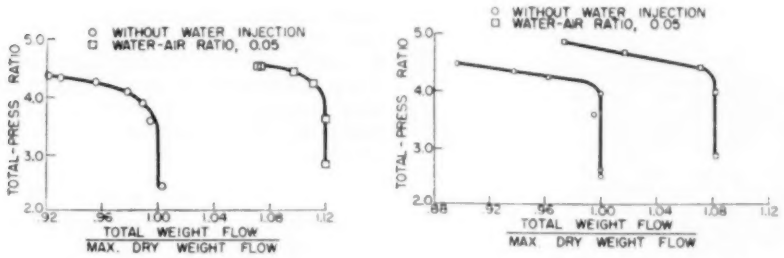

(*a*) Original blading (*b*) Number of blades increased

FIG. 2 PERFORMANCE OF CENTRIFUGAL COMPRESSOR WITH WATER INJECTION AT CONSTANT IMPELLER SPEED, CONSTANT INLET PRESSURE OF 14 IN. HG ABS, AND AMBIENT INLET-AIR TEMPERATURE

constant as indicated by the specific power over the range of weight flows for dry compression which agrees with the theoretical findings of reference (8). However, there is a variation in slip factor with the injection of water as indicated by the decreasing power required with increasing weight flow. Centrifuging of the water to the stationary shroud may have caused increased disk friction between the rotating impeller and the shroud which would account for the over-all increase in required power. For this compressor the maximum difference in power required in going from dry to wet compression is of the order of 3 per cent. However, this is not always the case. A difference as high as 8 per cent was observed on one compressor.

Efficiency. Upon increasing the water-air ratio from 0 to 0.055 there is a 12-point decrease in adiabatic efficiency as shown in Fig. 1(*f*), with a greater part of the decrease having taken place below a water-air ratio of 0.03. There are numerous factors which may contribute to this decrease in efficiency in addition to the possible increase in disk friction. They include mismatching of components, boundary-layer separation, and thermodynamic losses associated with the evaporative cooling. Although mismatching of compressor components is not as critical in the centrifugal compressor as in the axial-flow type, the angle of flow into a vaned diffuser can be changed sufficiently by the injection of water to cause substantial losses in the diffuser, and further, efficient designs for dry compression are not necessarily good designs for wet compression because of changes in over-all flow configuration. A theoretical analysis of flow through a mixed-flow centrifugal impeller of conventional design (9) showed velocity decelerations which appear excessive from the standpoint of boundary-layer build-up and separation. With evaporative cooling these decelerations would be even more pronounced because of the progressive nature of the cooling process.

Instability of the mixture of water droplets, water vapor, and air may be the source of sizable thermodynamic losses in the compressor, the probable sources of loss being the evaporation of water into an unsaturated mixture and heat transfer from the air to the droplets across a temperature difference.

Per Cent Evaporation. The per cent of water evaporated varied greatly over all conditions of operation and seemed to be a function of no one parameter. A plot of per cent evaporated against total weight flow for water-air ratios from 0.02 to 0.05 are shown in Fig. 4. The scatter of the data may result from both limitations of instrumentation and the nonhomogeneous nature of the water-air mixture.

Mechanical Considerations. A compressor typical of those used in these investigations with the location of water-spray nozzles and outlet instrumentation station is shown in Fig. 5.

Water-Spray Nozzles. The nozzles used in these investigations did not produce fine droplets but ejected the water in a conical

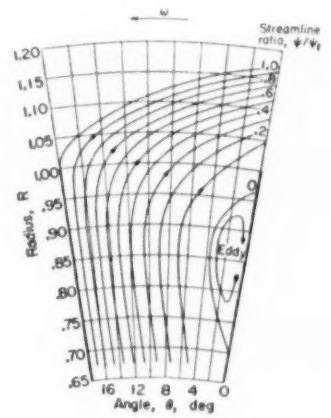

FIG. 3 RELATIVE STREAMLINES FOR FLOW THROUGH CENTRIFUGAL COMPRESSOR
(From solutions of reference 8.)

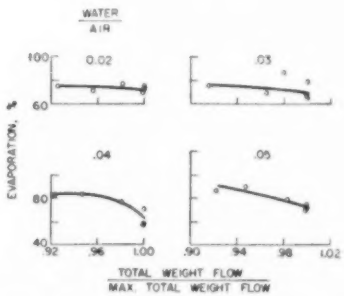

FIG. 4 PER CENT EVAPORATION OF WATER INJECTED FOR CENTRIFUGAL COMPRESSOR IN FIG. 1
(Identical operating conditions prevail.)

sheet. From the standpoint of heat transfer to entrained water droplets from the surrounding air the droplet sizes should have been much smaller. For evaporation from the wetted surfaces of the shroud and diffuser and rotating impeller passages, the droplet size probably would not be too important. The theoretical calculations of reference (10) indicate that droplets as small as 20 microns would be required to evaporate all the water entrained in air moving at low relative velocities through a compressor. These theoretical results seem quite reasonable in view of the fact that the residence time for an entrained droplet in the

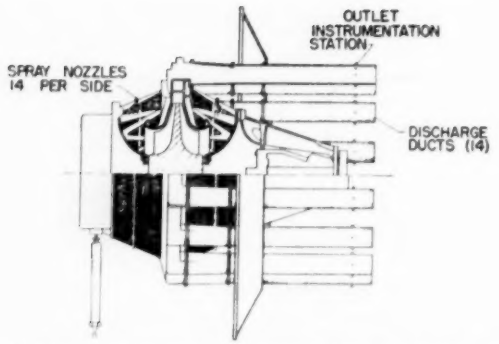

FIG. 5 TYPICAL CENTRIFUGAL COMPRESSOR USED IN INVESTIGATION OF WATER INJECTION

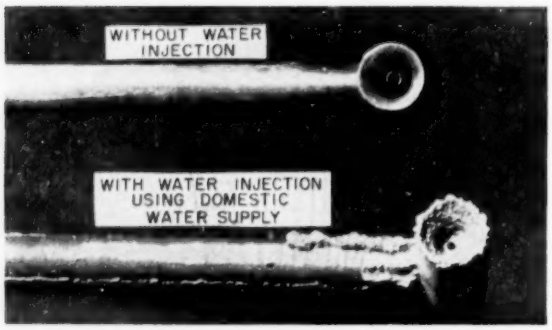

FIG. 6 OUTLET TOTAL-PRESSURE PROBE SHOWING DEPOSITS AFTER 6 HR OF OPERATION

FIG. 7 DRIVING FACE OF BLADE SHOWING PITTED BLADE SURFACE AFTER 6 HR OF WET OPERATION

compressor tested was of the order of 0.01 sec. Inasmuch as 60 to 90 per cent of the water was evaporated as determined by the outlet instrumentation in the experimental investigations it appears that a major portion of the water was evaporated from the wetted surfaces.

Mineral Deposits. In the initial investigations with water injection, water from the domestic water supply was injected without treatment into the compressor inlet. After approximately 6 hr of operation, the diffuser walls, outlet ducts, and instruments were coated with mineral deposits, a typical example of which is shown in Fig. 6. Water-softening equipment was used in subsequent tests to eliminate the problem.

Erosion. Erosion of the impeller blades and diffuser vanes is a factor to be considered with the use of water injection in continuous operation. Fig. 7 shows the pitted driving face of an aluminum-alloy impeller blade after 6 hr of operation with water injection.

SPECIAL INSTRUMENTS

Computations of work input based upon the assumption of complete evaporation and measurements from conventional unshielded thermocouples were in error as much as 40 per cent when compared with measured shaft input. A shielded thermocouple and a sampling probe were designed and developed at the NACA Lewis laboratory for use in these investigations.

Sampling Probe. The details of the sampling probe are shown in Fig. 8(*a*). The direction of air flow is indicated by the arrow.

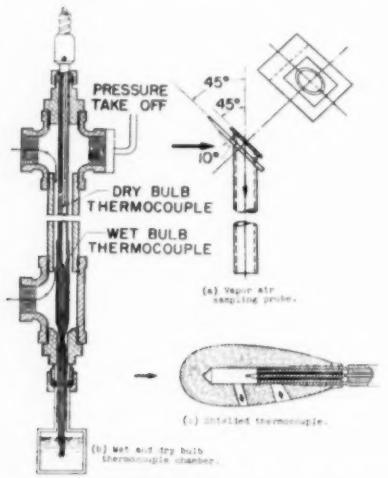

FIG. 8 INSTRUMENTS FOR USE IN AIR STREAMS CONTAINING ENTRAINED DROPLETS

Droplet-free samples of air-vapor mixture are drawn off and cooled to a temperature below the boiling point of the water in the wet-bulb well. The mixture is then passed through the wet- and dry-bulb thermocouple chamber in Fig. 8(*b*). From the specific humidity of the sample mixture the quantity of droplets remaining in the stream may be determined.

Shielded Thermocouple. The shielded thermocouple is shown in Fig. 8(*c*). The nonmetallic shielding is so designed that droplet-free air is forced to circulate around the thermocouple as shown by the small arrows in the passages. The main airstream is directed as shown by the large arrow. Thermocouples shielded in this manner have the functional disadvantage of being restricted to use in passages relatively much larger than the shield which has a practical minimum diameter of approximately $\frac{1}{2}$ in.

Accuracy. These instruments were designed primarily with the object of finding the work input from the state of the mixture at the exit; therefore a comparison of work input as obtained from the enthalpy rise with that from the measured shaft input was used as a check on their accuracy. The enthalpy change through the compressor was determined by the method given in the Appendix. The work thus determined was compared to the shaft work input as measured with a high-speed strain-gage torquemeter (11). The accuracy decreased as the number of entrained droplets increased as shown in Fig. 9. The possible error

for the air weight flow used in computing work input from enthalpy rise plus the error in torquemeter measurements represent an accumulation of ±2 per cent. The scatter of data at droplet-air ratios higher than about 0.011 indicates that for computation of work input the instruments should be placed as far downstream in the compressor outlet as possible where maximum evaporation will have taken place. Droplet-air ratios above 0.011 were obtained only where the water-air ratios of injection were 0.04 or greater.

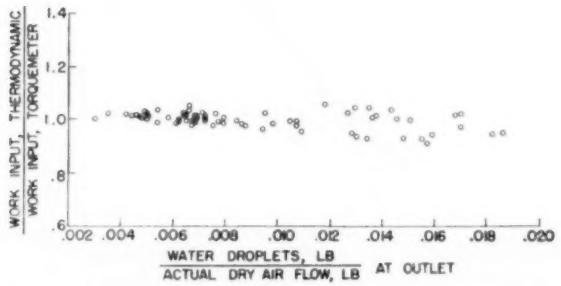
WORK INPUT, THERMODYNAMIC / WORK INPUT, TORQUEMETER
1.4
1.2
1.0
.8
.6
.002 .004 .006 .008 .010 .012 .014 .016 .018 .020
WATER DROPLETS, LB / ACTUAL DRY AIR FLOW, LB AT OUTLET

FIG. 9 CORRELATION BETWEEN COMPRESSOR WORK INPUT AS DETERMINED FROM ENTHALPY RISE AND FROM TORQUEMETER MEASUREMENTS

THEORETICAL ASPECTS

The prospect of obtaining substantial increases in compression ratio with little or no increase in work input to the compressor is highly attractive from the standpoint of the compressor alone. Also, for momentary augmentation of thrust where specific fuel consumption is of secondary importance, liquid injection is highly practical. However, for continuous operation of a gas turbine the over-all effect upon cycle efficiency is a matter of concern. In order to maintain a given turbine-inlet temperature it is necessary to increase the fuel supplied to the burners when water is injected because of the evaporative cooling of the air. In addition, the combustion efficiency may be affected adversely (12). These effects together with a lowered compressor efficiency may be enough to offset the benefits of increased pressure ratio or even result in increased specific fuel consumption.

Difficulty in evaluating the properties of the vapor-air mixture complicates the analysis of the gas-turbine cycle and especially the computation of the isentropic compressor work when liquids are injected into the compressor inlet. The variation in latent heat of vaporization and in specific heats may best be handled by use of tables of properties, such as references (13) and (14). The method by which these tables were used in computing the compressor work is discussed in the Appendix.

The method was used to compute isentropic enthalpy change and isentropic outlet temperatures over a range of pressure ratios and water-air ratios for a given set of inlet conditions. The results are shown in Figs. 10 and 11. From these curves it can be seen that relatively few points are required to plot a functional curve of isentropic enthalpy change for any set of inlet conditions.

The effect of varying the inlet pressure and temperature upon the outlet temperature and enthalpy change are shown in Figs. 12 and 13, respectively. For Fig. 14 a given work input was specified and the curves in Fig. 10 were used to determine the pressure ratios that would be obtained over a range of adiabatic efficiencies. From these curves it can be seen that substantial increases in pressure ratio can be obtained if the efficiency for wet compression can be maintained near that for dry compression

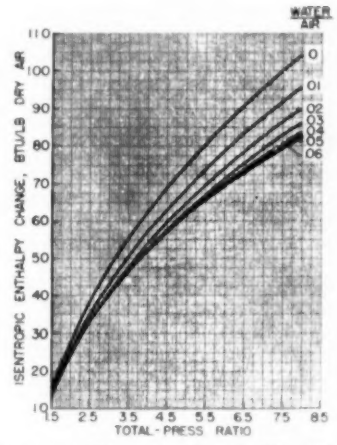

FIG. 10 VARIATION OF ENTHALPY CHANGE WITH PRESSURE RATIO FOR ISENTROPIC COMPRESSION

(Compressor-inlet conditions: Pressure, 14 in. Hg abs; temperature, 77 F; specific humidity = 0.)

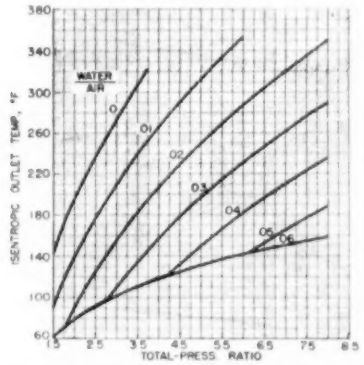

FIG. 11 VARIATION OF OUTLET TEMPERATURE WITH PRESSURE RATIO FOR ISENTROPIC COMPRESSION

(Compressor-inlet conditions: Pressure, 14 in. Hg abs; temperature, 77 F; specific humidity = 0.)

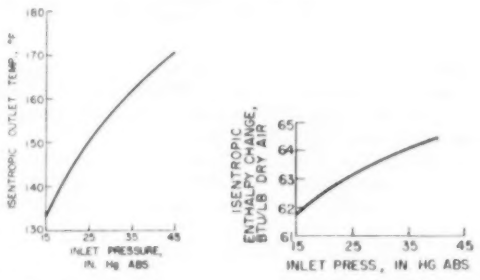

(*a*) Isentropic outlet temperature

(*b*) Enthalpy change

FIG. 12 VARIATION OF OUTLET TEMPERATURE AND ENTHALPY CHANGE WITH INLET-AIR PRESSURE

(Compressor-inlet temperature, 77 deg F; water-air ratio, 0.05; humidity = 0; compressor pressure ratio, 5.)

and that water-air ratios above 0.05 are relatively ineffective for the work input specified.

The method of the Appendix has been applied using water as

the liquid of injection because of the large amount of information available on the properties of water vapor; however, the method may be applied to any liquid of injection for which similar data are available. Further, it may be applied to any type of compressor.

Summary of Results and Conclusions

1 In general, the injection of liquids at the inlet to a compressor shows promise of increasing the pressure ratio obtainable for a given work input. However, the increase in pressure ratio may be offset by a decrease in cycle efficiency with a consequent increase in specific fuel consumption.

2 For momentary augmentation of normal power, liquid injection is practical on engines using compressors designed for dry compression, but for continuous operation with wet compression specially designed compressors are necessary.

3 It appears from the evidence available that the main source

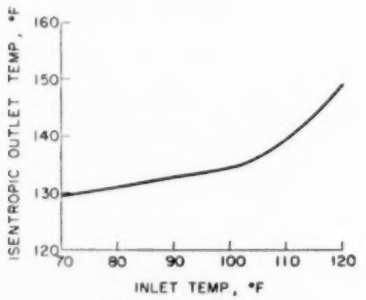

(*a*) Outlet temperature

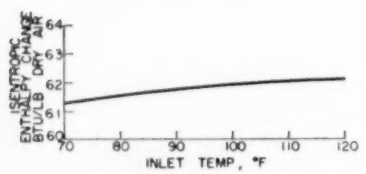

(*b*) Enthalpy change

Fig. 13 Variation of Outlet Temperature and Enthalpy Change With Inlet-Air Temperature

(Compressor-inlet pressure, 14 in. Hg abs; water-air ratio, 0.05; humidity = 0; compressor pressure ratio, 5.)

of evaporation of the injected liquid was from the wetted surfaces in the compressors investigated. It is probable that the adiabatic efficiency could be increased if vaporization from droplets homogeneously mixed with the air could be achieved.

4 Generally, when water is injected into a compressor, increases in both maximum and minimum (surge) weight flows are obtained. It is possible to render an engine inoperable with the injection of water due to the shifting of the compressor surge point.

5 Excessive pitting of aluminum-alloy blades occurs for continuous operation with water injection.

6 When hard water is injected into a compressor, a heavy layer of minerals is deposited rapidly on compressor-outlet surfaces.

7 Theoretical calculations show that for pressure ratios less than 8, water-air ratios greater than 0.05 are relatively ineffective.

BIBLIOGRAPHY

1 "Effect of Internal Coolants on the Knock-Limited Performance of a Liquid-Cooled Multi-Cylinder Aircraft Engine With a Compression Ratio of 6.0," by R. Lee Nelson, M. L. Harries, and R. J. Brun, NACA MR No. E5F30, E-260, 1945.

2 "End-Zone Injection as a Means of Suppressing Knock in a Spark-Ignition Engine," by R. J. Brun, H. Lowell Olsen, and C. D. Miller, NACA MR E4I27, E-72, September, 1944.

3 "Summary Report on the Induction of Water to the Inlet Air as a Means of Internal Cooling in Aircraft Engine Cylinders," by A. M. Rothrock, Alois Krsek, Jr., and A. W. Jones, NACA ARR E-79, August, 1942.

4 "Method of Determining Centrifugal-Flow-Compressor Performance With Water Injection," by J. T. Hamrick and W. L. Beede, NACA RM E9G12, September 7, 1949.

5 "Experimental Evaluation by Thermodynamic Methods of Work Input to a Centrifugal Compressor Operating With Water Injection," by Karl Kovach, W. L. Beede, and J. T. Hamrick, NACA RM E50J31, October, 1950.

6 "The Mechanics and Thermodynamics of Steady One-Dimensional Gas Flow," by A. H. Shapiro and W. R. Hawthorne, *Journal of Applied Mechanics*, Trans. ASME, vol. 69, 1947, p. A-329.

7 "Compressor Surge Investigated by NACA." "Surging in Centrifugal and Axial Flow Compressors," by R. O. Bullock and H. B. Finger, abridged form, *SAE Journal*, vol. 59, September, 1951, pp. 42–45. (Complete paper available in multilithograph form from SAE special publications department.)

8 "Some Theoretical Aerodynamic Investigations of Impellers in Radial and Mixed-Flow Centrifugal Compressors," by J. D. Stanitz, Trans. ASME, vol. 74, May, 1952, pp. 473–497.

9 "Method of Analysis for Compressible Flow Through Mixed-Flow Centrifugal Impellers of Arbitrary Design," by J. T. Hamrick, Ambrose Ginsburg, and W. M. Osborn, NACA TN 2165.

10 "Wet Compression in an Axial-Flow Compressor," by Shao-Lee Soo, Trans. ASME, vol. 74, July, 1952, pp. 879–886.

11 "Investigation of an NACA High-Speed Strain-Gage Torquemeter," by J. J. Rebeske, Jr., NACA TN 2003, 1950.

12 "Effect of Combustor Inlet Conditions on Performance of an Annular Turbojet Combustor," by J. H. Childs, R. J. McCafferty, and O. W. Surine, NACA Report No. 881.

13 "Thermodynamic Properties of Steam," by J. H. Keenan and F. G. Keyes, John Wiley & Sons, Inc., New York, N. Y., 1936.

14 "Thermodynamic Properties of Air," by J. H. Keenan and Joseph Kaye, John Wiley & Sons, Inc., New York, N. Y., 1945.

15 "The Refrigerating Data Book." American Society of Refrigerating Engineers, New York, N. Y., fifth edition, 1942, p. 428.

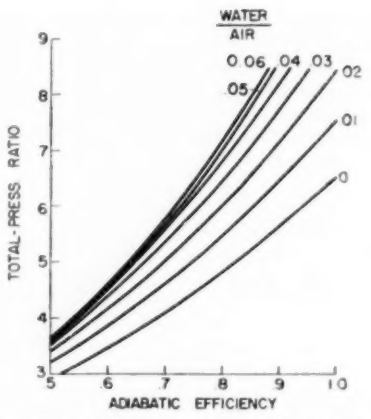

Fig. 14 Variation of Pressure Ratio With Adiabatic Efficiency for Compressor Work Input of 129.3 Hp Per Lb Per Sec

(Compressor-inlet conditions: Pressure, 14 in. Hg abs; temperature, 77 F; specific humidity = 0.)

Appendix

Method of Computing Compressor Efficiency With Water Injection at Compressor Inlet

The adiabatic efficiency of a compressor is defined as the ratio of the isentropic (reversible adiabatic) compression work to the actual compression work. In computing the isentropic work, only the end points need be considered inasmuch as the second law of

thermodynamics precludes the possibility of any change in entropy during the process.

In the computations, the mixture of water particles, vapor, and air are treated in the following manner: From the Gibbs-Dalton law it may be deduced that the entropy and enthalpy of a mixture of gases and vapors can be regarded as the sum of the individual entropies and enthalpies of the constituents when each occupies the same space as the mixture at the temperatures of the mixture. This law is not extended to liquid particles suspended in a gas. For the method presented herein, however, the liquid water particles are assumed to be distributed homogeneously throughout the mixture but to exert no pressure. The entropy and the enthalpy for the particles are calculated in the same manner as for gases.

Evaluation of the entropy of the mixture at the inlet is difficult because an increase in entropy due to adiabatic saturation of the air at inlet generally cannot be avoided. Only if the air is saturated before the water is injected and is at the same temperature as the injected water can the process conceivably be ideally reversible. Nevertheless, the process must be charged with this inefficiency; therefore the entropy of the water particles is taken as that of the water before injection in computing the entropy of the mixture at inlet. All values of entropy are taken from the steam and air tables of references (13) and (14), respectively. The entropy of each constituent in the mixture is based on 1 lb of dry air, with the result that the sum of all the entropies gives the entropy of the mixture per pound of dry air. The enthalpy of the mixture at the inlet is determined by the same procedure.

For a fixed set of inlet conditions and given compression ratio, the pressure at outlet is fixed. The temperature at outlet, therefore, will determine not only the state of the injected liquid at that point but also the entropy. A temperature that will give an entropy at outlet equal to that at inlet, therefore must be found by trial and error. With an assumed outlet temperature, the outlet entropy is computed in the same manner as the inlet entropy except that complete equilibrium is specified. When the isentropic outlet temperature is found, either of two sets of conditions may prevail depending upon the quantity of water injected: the air may be saturated with or without droplets being present, or the vapor may be in the superheated condition, in which case no droplets will be present. In the case of saturation with or without water droplets, the entropy can be found easily because these properties are the same as those for saturation temperature. With the superheated vapor, the exact temperature at which saturation occurs must be determined. The pressure corresponding to the temperature of saturation is the same as that which the vapor exerts at any higher temperature, the pressure of the mixture remaining constant. When this pressure is determined, the entropy of the vapor can be obtained from the superheated vapor tables of reference (13). The enthalpy of the mixture at the outlet is determined by the same procedure.

Numerical Example

A numerical example is presented to show the method of computing isentropic enthalpy rise, actual enthalpy rise, and adiabatic efficiency of a compressor for a given set of conditions. In each case where a temperature is assumed for trial-and-error solution, only the calculations resulting in the correct temperature are shown. The following conditions from actual experimental data prevail:

Water injected, lb per sec	2.175
Air weight flow, lb per sec	43.97
Water temperature, deg F	55
Air temperature, deg F	77.4
Inlet pressure, psi	6.870
in. Hg abs	14.00
Outlet pressure, psi	19.998
in. Hg abs	40.73
Outlet temperature, deg F	264
Specific humidity,[a] lb water per lb air	0.01025
Water-vapor pressure (humidity[a]), psi	0.1110

[a] The specific humidity and the pressure of water vapor at the inlet are calculated from an assumed wet-bulb temperature by means of the empirical equations of reference (15).

Nomenclature

The following nomenclature is used in the numerical examples:

c_p = specific heat at constant pressure, Btu/(lb) (deg F)
h = enthalpy, Btu/lb
N = ratio of actual pressure to base pressure
P = total pressure, psi or in. Hg abs
q = specific humidity, lb water per lb air
R = universal gas constant for air, 53.35 ft-lb/(lb) (deg F)
s = entropy, Btu/(lb) (deg F)
T = temperature (459.7 + t), deg R
t = temperature, deg F
v = specific volume, cu ft per lb
W = air weight, lb
w/a = water-air ratio due to water injection
η_{ad} = adiabatic efficiency
$\varphi = \int_{T_0}^{T} \frac{c_p}{T}\,dT$, Btu/(lb) (deg F)

The following subscripts refer to states of working fluid through the compressor:

0 = NACA standard sea-level conditions
1 = compressor inlet before injection of water
2 = compressor outlet
a = constituent of mixture based on 1 lb of dry air
d = dry air
f = saturated liquid
g = saturated vapor
m = mixture
s = superheated vapor
t = stagnation

Entropy of Mixture at Inlet

1 *Water-Air Ratio Due to Injection:*
Pounds water contained in inlet air

$$(0.01025)\,(43.97) = 0.4507 \text{ lb water per sec}$$

Pounds dry air supplied

$$43.97 - 0.4507 = 43.52 \text{ lb per sec}$$

Water-air ratio due to injection

$$w/a = 2.175/43.52 = 0.04997$$

2 *Entropy Due to Injected Liquid:*
Entropy of saturated liquid at inlet

$$s_{f,1} \text{ at } 55 \text{ F} = 0.0459 \text{ Btu/(lb) (deg F)}$$

Entropy of saturated liquid per pound of dry air at inlet

$$s_{f,a,1} = s_{f,1} w/a = (0.0459)\,(0.04997) = 0.002294 \text{ Btu/(lb) (deg F)}$$

3 *Entropy Due to Superheated Vapor in Incoming Air.* Although the Mollier diagram for steam does not include values of entropy for a pressure of 0.1110 psi, the low-pressure region near saturation indicates an entropy increase of 0.018 Btu per lb per

deg F for each temperature rise of 20 deg F along an isobaric line. By using the entropy at saturation for a pressure of 0.1110 psi and correcting for temperature difference from saturation temperature to 77.4 F, an entropy value $s_{s,1}$ of 2.204 Btu per lb per deg F was obtained.

Entropy of superheated vapor per pound of dry air at inlet

$$\begin{aligned} s_{v,a,1} &= s_{s,1}\, q_1 \\ &= (2.204)\,(0.01025) \\ &= 0.02259 \text{ Btu/(lb) (deg F)} \end{aligned}$$

4 *Entropy Due to Dry Air:*

Pressure of dry air

$$\begin{aligned} P_{d,1} &= P_1 - P_{s,1} \\ &= 6.870 - 0.1110 \\ &= 6.759 \text{ psi} \end{aligned}$$

$$\begin{aligned} \frac{1}{N} &= \frac{P_0}{P_{d,1}} \\ &= 14.70/6.759 \\ &= 2.175 \end{aligned}$$

$$R \log_e N = -R \log_e \frac{1}{N} = -0.05326$$

where

$$R = 53.35 \text{ ft-lb/(lb) (deg F)}$$

The temperature function at the inlet $\varphi_{t,1}$ is 0.07067, from Table 1 of reference (14).

Entropy of dry air at inlet

$$\begin{aligned} s_{d,1} &= \varphi_{t,1} - R \log_e N \\ &= 0.07067 + 0.05326 \\ &= 0.1239 \text{ Btu/(lb) (deg F)} \end{aligned}$$

5 *Entropy of Mixture at Inlet.* Because ratios of the quantities remain unchanged, the use of tables having different temperature bases (13) and (14) is valid. The entropy of mixture per pound of dry air equals the entropy of saturated liquid per pound of dry air plus the entropy of superheated vapor per pound of dry air plus the entropy of dry air

$$\begin{aligned} s_{m,a,1} &= s_{f,a,1} + s_{v,a,1} + s_{d,1} \\ &= 0.002294 + 0.02259 + 0.1239 \\ &= 0.1488 \text{ Btu/(lb) (deg F)} \end{aligned}$$

Isentropic Outlet Temperature

1 *Outlet Temperature.* An outlet temperature $t_{t,2}$ of 108.1 F is assumed for computing an entropy at the outlet equal to that at the inlet by trial-and-error solution.

2 *Specific Humidity at Outlet:*

$P_{g,2}$ at $t_{t,2}$ of 108.1 F

$$= 1.206 \text{ psi (from Table 1, reference 13)}$$

$P_2 = 19.998$ psi (original conditions)

$$\begin{aligned} P_{d,2} &= P_2 - P_{g,2} \\ &= 19.998 - 1.206 \\ &= 18.79 \text{ psi} \end{aligned}$$

$v_{g,2}$ at $t_{t,2}$ of 108.1 F

$$= 279.5 \text{ (cu ft per lb) (from Table 1, reference 13)}$$

$$T_{t,2} = 567.8 \text{ deg R}$$

$$R = 53.35 \text{ ft-lb/(lb) (deg F)}$$

$$\begin{aligned} W &= \frac{P_{d,2}\, v_{g,2}}{R(T_{t,2})} \\ &= \frac{(144)\,(18.79)\,(279.5)}{(53.35)\,(567.8)} \\ &= 24.97 \text{ lb} \end{aligned}$$

where W = weight of air that would occupy same volume as $v_{g,2}$.

Specific humidity at outlet

$$\begin{aligned} q_2 &= \frac{1}{W} \\ &= \frac{1}{24.97} \\ &= 0.04005 \text{ lb water per lb air} \end{aligned}$$

3 *Quantity of Liquid Water Present at Outlet.* The total water-air ratio equals the water-air ratio due to water injected plus the water-air ratio due to humidity at inlet

$$\begin{aligned} \text{Total water-air ratio} &= w/a + q_1 \\ &= 0.04997 + 0.01025 \\ &= 0.06022 \end{aligned}$$

$$\frac{\text{Pound liquid water at outlet}}{\text{Pound dry air}} = \text{total water-air ratio} - \text{specific humidity at outlet}$$

$$\begin{aligned} &= 0.06022 - 0.04005 \\ &= 0.02017 \end{aligned}$$

4 *Entropy Due to Liquid Water:*

Entropy of saturated liquid at outlet

$s_{f,2}$ at $t_{t,2}$ of 108.1 F

$$= 0.1438 \text{ Btu/(lb) (deg F) (Table 1, reference 13)}$$

Entropy of saturated liquid per pound of dry air at outlet

$$\begin{aligned} s_{f,a,2} &= s_{f,2}\left(\frac{\text{lb liquid water}}{\text{lb dry air}}\right) \\ &= (0.1438)\,(0.02017) \\ &= 0.002900 \text{ Btu/(lb) (deg F)} \end{aligned}$$

5 *Entropy Due to Saturated Vapor:*

Entropy of saturated vapor at outlet

$s_{g,2}$ at $t_{t,2}$ of 108.1 F

$$= 1.962 \text{ Btu/(lb) (deg F) (Table 1, reference 14)}$$

Entropy of saturated vapor per pound of dry air at outlet

$$\begin{aligned} s_{g,a,2} &= s_{g,2}\, q_2 \\ &= (1.962)\,(0.04005) \\ &= 0.07859 \text{ Btu/(lb) (deg F)} \end{aligned}$$

$$N = \frac{P_{d,2}}{P_0} = \frac{18.79}{14.70} = 1.278$$

$$R \log_e N = 0.01681$$

Temperature function at outlet

$\varphi_{t,2} = 0.08403$ Btu/(lb) (deg F) (from Table 1, reference 13)

Entropy of dry air at outlet

$$\begin{aligned} s_{d,2} &= \varphi_{t,2} - R \log_e N \\ &= 0.08403 - 0.01681 \\ &= 0.06722 \text{ Btu/(lb) (deg F)} \end{aligned}$$

6 *Entropy of Mixture at Outlet.* The entropy of mixture per pound of dry air at the outlet equals the entropy of saturated

liquid per pound of dry air plus the entropy of saturated vapor per pound of dry air plus the entropy of dry air

$$\begin{aligned} s_{m\,a,2} &= s_{f,a,2} + s_{g,a,2} + s_{d,2} \\ &= 0.002900 + 0.07859 + 0.06722 \\ &= 0.1487 \text{ Btu/(lb) (deg F)} \end{aligned}$$

When $s_{m,a,1}$ and $s_{m,a,2}$ are equal, the assumed temperature is that for isentropic compression. If they are unequal, a new temperature $t_{t,2}$ must be selected until equality is attained. The entropy value as computed is sufficiently close to that at the inlet to assume an isentropic process.

Enthalpy Change Through Compressor

1 *Enthalpy at Inlet:*

Enthalpy of saturated liquid at inlet

$h_{f,1}$ at $t_{f,1}$ of 55 deg F = 23.07 Btu per lb

Enthalpy of saturated liquid per pound of dry air at inlet

$$\begin{aligned} h_{f,a,1} &= h_{f,1}\, w/a \\ &= (23.07)\,(0.04997) \\ &= 1.153 \text{ Btu per lb} \end{aligned}$$

Enthalpy of saturated vapor at inlet

$h_{g,1}$ = 1096 Btu per lb at $p_{s,1}$ of 0.1110 and $t_{t,1}$ of 77.4 deg F

Pressure effect on enthalpy is negligible in this region of pressure. Enthalpy of saturated vapor per pound of dry air at inlet

$$\begin{aligned} h_{g,a,1} &= h_{g,1}\, q_1 \\ &= (1096)\,(0.01025) \\ &= 11.23 \text{ Btu per lb} \end{aligned}$$

Enthalpy of dry air at inlet

$h_{d,1}$ at $T_{t,1}$ of 537.1 deg R = 32.87 Btu per lb

The enthalpy of mixture per pound of dry air at the inlet equals the enthalpy of saturated liquid per pound of dry air plus the enthalpy of saturated vapor per pound of dry air plus the enthalpy of dry air

$$\begin{aligned} h_{m,a,1} &= h_{f,a,1} + h_{g,a,1} + h_{d,1} \\ &= 1.153 + 11.23 + 32.87 \\ &= 45.25 \text{ Btu per lb} \end{aligned}$$

2 *Enthalpy at Outlet:*

Enthalpy of saturated liquid at outlet

$h_{f,2}$ at $t_{t,2}$ of 108.1 deg F = 76.05 Btu per lb

Enthalpy of saturated liquid per pound of dry air at outlet

$$\begin{aligned} h_{f,a,2} &= h_{f,2}\left(\frac{\text{lb liquid water}}{\text{lb dry air}}\right) \\ &= (76.05)\,(0.02017) \\ &= 1.534 \text{ Btu per lb} \end{aligned}$$

Enthalpy of saturated vapor at outlet

$h_{g,2}$ at $t_{t,2}$ of 108.1 deg F = 1108.6 Btu per lb

Enthalpy of saturated vapor per pound of dry air at outlet

$$\begin{aligned} h_{g,a,2} &= h_{g,2}\, q_2 \\ &= (1108.6)\,(0.04005) \\ &= 44.40 \text{ Btu per lb} \end{aligned}$$

Enthalpy of dry air at outlet

$h_{d,2}$ at $T_{t,2}$ = 40.25 Btu per lb

The enthalpy of mixture per pound of dry air at the outlet equals the enthalpy of saturated liquid per pound of dry air plus the enthalpy of saturated vapor per pound of dry air plus the enthalpy of dry air.

$$\begin{aligned} h_{m,a,2} &= h_{f,a,2} + h_{g,a,2} + h_{d,2} \\ &= 1.534 + 44.40 + 40.25 \\ &= 86.18 \text{ Btu per lb} \end{aligned}$$

3 *Enthalpy Change from Inlet to Outlet:*

$$\begin{aligned} \Delta h_{m,a} &= h_{m,a,2} - h_{m,a,1} \\ &= 86.18 - 45.25 \\ &= 40.93 \text{ Btu per lb} \end{aligned}$$

If the vapor at the outlet is in the superheat region, the entropy and the enthalpy are computed for the assumed temperature in the same manner as the enthalpy or the actual work in the next section.

Actual Work Determined From Total Temperature at Outlet

Temperature at outlet = 264 deg F (assumed)

For this temperature, the vapor contained in the air is in the superheated condition. Therefore the pressure exerted by the vapor in the mixture will be equal to that exerted at saturation. The following method is used to determine the temperature at which saturation occurs: By assuming values of saturation temperature t and using the corresponding values of specific volume v_g found in Table 1 of reference (13), a value of specific humidity equal to the total water-air ratio at the outlet is obtained.

From the section Isentropic-Outlet Temperature, item 3, the total water-air ratio is 0.06022. Assume the temperature t of saturation to be 121.3 F. The pressure $P_{g,2}$ corresponding to 121.3 F is 1.755 psi in the steam tables (Table 1, reference 13).

1 *Pressure of Superheated Vapor:*

$$\begin{aligned} P_{d,2} &= P_2 - P_{g,2} \\ &= 19.998 - 1.755 \\ &= 18.24 \text{ psi} \end{aligned}$$

The volume occupied by 1 lb of vapor at saturation v_g for 121.3 F is 196.5 cu ft per lb from Table 1, reference (13).

The weight of air that would occupy the same volume as v_g at $P_{d,2}$ is

$$\begin{aligned} W &= \frac{P_{d,2}\, v_g}{R(t + 459.7)} \\ &= \frac{(144)\,(18.24)\,(196.5)}{(53.35)\,(581.0)} \\ &= 16.65 \text{ lb} \end{aligned}$$

Water-air ratio

$$\frac{1}{W} = \frac{1}{16.65} = 0.0601$$

Inasmuch as the actual $q_{m,2}$ is 0.06022 lb water per lb of air, the assumed temperature is acceptable; the pressure exerted by the vapor in the superheat region $P_{s,2}$ is therefore 1.755 psi.

2 *Enthalpy of Mixture:*

Enthalpy of vapor h_s at 264 F = 1179 Btu/lb (reference 13, Fig. 10).

Enthalpy of vapor per pound of dry air at outlet

$$h_{s,a,2} = (0.0601)\,(1179) = 70.86 \text{ Btu per lb}$$

Enthalpy of dry air

$$h_{d,2} \text{ at } 264 \text{ F} = 77.85 \text{ Btu per lb}$$

Enthalpy of mixture per pound of dry air at outlet

$$\begin{aligned} h_{m,a,2} &= h_{s,a,2} + h_{d,2} \\ &= 70.86 + 77.85 \\ &= 148.7 \text{ Btu per lb} \end{aligned}$$

$h_{m,a,1} = 45.25$ Btu per lb from preceding section

3 *Enthalpy Change Equivalent to Actual Work*

$$\begin{aligned} \Delta h_{m,a} &= h_{m,a,2} - h_{m,a,1} \\ &= 148.7 - 45.25 \\ &= 103.5 \text{ Btu per lb} \end{aligned}$$

Adiabatic Efficiency

$$\eta_{ad} = \frac{\text{isentropic } \Delta h_{m,a}}{\text{actual } \Delta h_{m,a}}$$

$$= \frac{40.93}{103.5} = 0.395$$

Discussion

W. S. Bowen.[3] This paper has particular merit for the lucidity of its presentation.

In the writer's opinion the sprays should have been located on the hot rather than the cold side of the compressor. This would have reduced greatly the difficulty with wet surfaces and the consequent irregularity of the friction effects noted. On the hot side, evaporation would have taken place so fast that friction with water films and droplets would have diminished greatly. This would have increased the efficiency materially. It also would have reduced losses due to impingement.

As the authors point out, finer atomization also would have helped. It is a fundamental principle of "spray-drying" (of which this is a special case) that fineness and uniformity of atomization are basic to good operation. It is the large particles that govern the throughput of a spray drier and it is the big particles that produce the wet surfaces and large drip at the edges. These in turn produce irregularity of operation.

Also, the capacity of cold air for evaporation is very low as compared with hot air. Hence the place to spray is in the hot air, after it has passed through the rotor, not before.

The authors are quite correct in saying that for continuous operation the compressor should be designed for the wet mixture to be used because the specific gravity of the mixture is utterly different and upsets the design for air only. In spray-drying all passages are designed specifically for the specific gravity or volume of the mixture flowing. The problem is no different for a compressor.

In Fig. 3 of the paper the suggested cause of a surge point is indicated. Might it not always be well to make that point in the vane structure of a Venturi shape? The writer has used this in designs upon which he is working. Such a structure in the vane side of a compressor might help with this problem.

The hard-water effects are not surprising. The writer often has observed spray-dried city water make a beautiful white deposit. Consequently, the use of water in a centrifugal compressor involves softening the water. It also means condensing the vapor formed in the compressor so it can be re-used. The increased weight has to be set against the increased power available from the fuel, not only because of the increased pressure ratio, but also because of the saving of heat normally lost through the cooling-jacket walls. The compressed air is cooled without removing the heat of compression from the working space. The air-and-vapor mixture under compression is a power mixture at lower temperature.

Another factor not mentioned in the paper is the fact that the proper use of water reduces the amount of critical materials now required for furnace and turbine. These facts should be brought into the evaluation of the use of distilled and recirculated water in centrifugal compressors for use with gas turbines.

It is quite possible to set up automatic control over the amount of water sprayed so that at the outlet of each stage the air-saturation temperature will be reached. If that were done carefully and the spray entered into the hot air so all surfaces were reasonably dry, would not the data for the optimum mixture weight as against air weight conceivably be considerably higher with a higher efficiency, at the same time giving greater power?

It would seem that such a concept might make it worth while doing these very fine tests over again on this new base.

For continuous operation the assumption is made of very large weights of water. This does not seem to be justified. The increased weight should be the condenser and not the relatively small amount of water recirculating.

G. M. Dusinberre.[4] A paper[5] by R. V. Kleinschmidt, and a discussion[6] of that paper by the writer perhaps did not come to the authors' attention.

Ideal calculations and certain practical calculations on wet compression are somewhat simplified by the use of a chart described in the reference discussion.

In the first paragraph of the authors' Appendix, it may be noted that it is the definition of the process (adiabatic) which insures that the work can be calculated from the end states. The second law has nothing to do with this. It merely furnishes a rule for computing an end state when the process is also reversible.

F. C. Gilman.[7] The paper is based on experimental work with single-stage radial-flow aircraft-jet-engine compressors and the outlook is principally that of the jet-engine designer or analyst. In view of this it would seem that the title might well have indicated the type of compressors investigated.

The primary advantage of water injection for a jet engine is the temporary increase in thrust resulting from increased compressor mass flow, pressure ratio, and fuel-air ratio. In commercial applications the principal advantage may be increased pressure ratio to one customer, temperature limitation to another, power savings to a third and quantity control at constant speed and pressure to a fourth. In tests made recently by the writer's company on a six-stage centrifugal compressor a 15 per cent increase in air capacity was achieved by spraying $3\frac{1}{2}$ per cent of water into the interstage passage between the third and fourth stage while holding speed and discharge pressure constant. Evaporation was complete.

The authors state that a maximum of 0.02 lb of water per lb of air was evaporated upstream of the diffuser throats even when 0.055 lb per lb was being introduced. If the pressure ratio at the entrance to the diffusers is 3.4, the water-air ratio for adiabatic saturation under the same inlet and efficiency conditions would

[3] President, Bowen Engineering, Inc., Westfield, N. J. Mem. ASME.

[4] Professor of Mechanical Engineering, The Pennsylvania State College, State College, Pa. Mem. ASME.

[5] "Value of Wet Compression in Gas-Turbine Cycles," by R. V. Kleinschmidt, *Mechanical Engineering*, vol. 69, 1947, pp. 115–116.

[6] *Mechanical Engineering*, vol. 69, 1947, pp. 684–685.

[7] Research Engineer, Worthington Corporation, Harrison, N. J.

be 0.06. With only one third of the equilibrium quantity being evaporated up to this point, much of the cooling took place after the compression, yielding little saving in compression work and adding to the mass load.

That minimum weight flow or surge will be somewhat increased in percentage of maximum weight flow by the injection of water may be unavoidable if mismatching of angle at the diffuser vanes is a controlling factor for the onset of surge. This is because with wet compression, volume reduction due to reduced mass flow is compensated to a lesser extent by increased temperature. However, the authors' suggestion that flow conditions within the impeller may be the most important factor is borne out by the effect of increasing the number of impeller blades. Fig. 2(*b*) of the paper shows essentially equal percentage range between maximum flow and minimum flow for dry compression and with 0.05 water-air ratio. The writer would expect the trailing face of the blades rather than the driving face to be the place where flow breaks down since that has been shown by Prian and Michel[8] to be where poorest conditions exist even with dry operation. The tangential acceleration of the air in the impeller passage is of the order of 35,000 grams. Thus not only will the water drops be quickly concentrated on the driving face of the blades but also the denser cooled air-vapor mixture, resulting in a stratification of densities. This will leave the normally poorer side of the passage operating with a lower-density fluid thus compounding the inequality. A number of shallow corrugations in line with the flow to serve as water collection channels together with series of small holes through the blades spaced along the troughs would feed water to the air stream from the trailing face of the blades. If a closer approach to saturation equilibrium could be achieved by some such means not only would the surge characteristics be improved but the over-all performance as well. Fig. 14 of the paper shows that only a small part of the potential increase in pressure ratio was realized by the method of water injection used. Further work on this phase of the problem seems justified.

The authors use the term "slip factor." For completeness it would seem desirable to define this term somewhere in the paper. The shape of the curves in Fig. 1(*c*) leads the writer to doubt that increased disk friction resulting from the presence of water in the clearance space was primarily responsible for increased specific horsepower input under maximum pressure conditions with water injection. However, if this were the case a raised edge on the driving face of the blades adjacent to the stationary shroud should remedy the situation. A more likely explanation of the increased specific horsepower would seem to be the re-entry into the impeller periphery of the lighter air strata displaced inward by the denser moist strata.

It should be made clear that the efficiency base used by the authors is constantly shifting since the work for wet adiabatic or isentropic compression is less than the work required for dry isentropic compression. There is considerable evidence that the polytropic or hydrodynamic efficiency of the compressor reported did deteriorate as water was added. This probably was due mainly to density stratification. Tests made on multistage centrifugal compressors by the writer's company have shown lower horsepowers per pound of dry air handled when operating at constant speed and constant pressure ratio.

The writer concurs wholeheartedly with the conclusion that improvements in adiabatic efficiency probably depend on achieving greater homogeneity of the fluid mixture. Reducing the size of droplets fed to the inlet of the compressor no doubt will show some improvement but greater benefit would be expected from an injection system such as suggested.

As has been pointed out previously by Kleinschmidt[8] the authors warn that water for injection must be demineralized if troublesome deposits are to be avoided. This is particularly important in commercial installations using continuous water injection.

Erosion would not likely be a problem in aircraft compressors because the accumulated time of water injection would be so short. For stationary compressors the use of a more erosion-resistant material might be necessary. It should be remembered that liquid drops in a noncondensable gas stream such as air are less destructive than drops of a liquid in the vapor of the same substance. In the latter case there is no gas cushion. Erosion within a compressor provided with water injection should not be as severe as that found in the final stages of a condensing steam turbine. The extent of erosion reported in this paper may have resulted mainly from the coarse nature of the injection spray and to hydrolysis of the aluminum alloy.

The description of thermocouple probe and sampling tube design to eliminate liquid droplets will be helpful to all who wish to test compressors operating with liquid injection.

The Appendix describes a painstaking method of computing compressor efficiency with water injection at the inlet but strangely makes no reference to available charts[9] which simplify such determinations.

It is my hope that neither the NACA nor industrial engineers will be discouraged by the rather disappointing performance realized with the units tested.

D. C. Prince, Jr.[10] The use of wet compression is attractive because of the potential gain in pressure ratio for a given work input to the compressor. Figs. 1(*a*) and (*b*) of the paper show a compressor which delivers 4.4:1 pressure ratio at an adiabatic efficiency of 76 per cent. According to Fig. 14, the pressure ratio could be raised to 6.6:1 by addition of water in wet compression. The available energy in the turbine for a given pressure ratio will be increased if there is any change due to the addition of water vapor. Hence it would seem that there is a clear gain of 1.5:1 pressure ratio available to increase jet kinetic energy and thrust.

If the pressure-ratio increase in practice were only half as much as the potential, to a pressure ratio of 5.5:1, there would still be a large clear gain. The actual observed increase, as reported in Fig. 1(*a*), is to 4.7:1 pressure ratio, which seems too small to be attractive as an augmentation device. The writer would like to know what minimum pressure increase the authors feel would be attractive, in view of all the difficulties mentioned, and whether they feel such an increase can be attained.

Authors' Closure

Mr. Bowen's opinion that all of the water should be introduced into the diffuser is not shared by the authors. For a given work input the compression ratio increases greatly as the inlet temperature is decreased; therefore it is desirable to cool the air as early as possible in the compression process.

The use of a Venturi shape on the impeller blade to displace the eddy might be of value at minimum weight flow; however, it might cause unnecessary losses at design weight flow and other weight flows at which the eddy does not appear. Addition of short vanes

[8] "An Analysis of Flow in Rotating Passage of Large Radial-Inlet Centrifugal Compressor at Tip Speed of 700 Feet Per Second," by Prian and Michel, NACA TN 2584.

[9] "Theoretical Turbojet Thrust Augmentation by Evaporation of Water During Compression as Determined by Use of a Mollier Diagram," by A. M. Trout, NACA TN 2104.

[10] Aircraft Gas Turbine Department, General Electric Co., West Lynn, Mass.

which extend from a point just upstream of the eddy to the impeller exit appears more practical.

Providing enough water to saturate the air at outlet may be desirable for intercooling between stages, however, it is doubtful that it would be beneficial to saturate the outlet of the final stage of a compressor which is used on a turbojet engine. The experimental data indicate that above a water air ratio of 0.04, which is below that for saturation, no increase in pressure is obtained. Therefore, in this case, any further cooling of the air by evaporation would needlessly increase the amount of fuel required to bring the mixture up to the required turbine-inlet temperature. That part of the heat from the additional fuel which goes into the latent heat of vaporization is for all practical purposes not recoverable as useful work.

Mr. Gilman is correct in indicating that the requirements for a jet engine may be different from other commercial applications as regards water injection. For example, in the compression of air which is to be cooled to atmospheric temperature any increase in compression ratio for a given amount of work is a saving, assuming that drying of the air does not offset the gain. With a gas-turbine engine where the air must be heated to the turbine-inlet temperature, increased specific fuel consumption may result from evaporative cooling in the compressor even though an increase in pressure ratio is obtained.

The indication of a maximum of 0.02 lb of water per pound of air evaporating upstream of the diffuser refers only to maximum weight flow. This ratio may be higher at lower weight flows where the average stream velocity is lower. In any event, increases in pressure ratio may be obtained in both the impeller and diffuser inasmuch as compression takes place in both, even though the compression work is determined by the tip speed of the impeller only for a given slip factor. Of course with other than radial blades the change in slip factor with change in flow conditions at exit may be considerable. Slip factor is defined as the ratio of the actual compressor work to that which is required to give all particles a tangential component of velocity equal to the impeller tip speed.

It may be possible that flow breakdown on the trailing face causes the instability mentioned; however, in the work of Messrs. Prian and Michel there seems to be an accumulation of low-energy air on the trailing face due to secondary flows rather than a flow breakdown. In fact, it appears that this collection of low-energy air serves to increase the volume flow per unit area and delay the appearance of the eddy on the driving face as predicted by theory.

The reference to a constantly shifting efficiency base is not clear. Each value of efficiency shown is for a fixed set of conditions at inlet and a given water-air mixture. It should be pointed out that each mixture is a separate medium with its own potential pressure ratio for a given work input. As is shown by Fig. 1, it is possible with a given power input to have a higher-pressure ratio for a mixture than for dry air alone and yet show a lower efficiency for the mixture. This occurs because the potential pressure ratio for any water-air mixture is higher than for air alone.

With the injection of all of the water at the compressor inlet which is generally the case with turbojet engines, water droplets are present in the mixture. At the outlet the mixture is in most cases either saturated with water droplets present or is in the superheated condition depending upon the pressure ratio for which the isentropic work is being computed. A mixture in which the air is saturated with no droplets present represents a singularity. With droplets present in the mixture or with superheated vapor the Mollier charts of Messrs. Dusinberre or Trout do not apply. However, with vapor in the superheated condition at exit, time may be saved by using either of these charts to obtain the temperature at which saturation occurs.

Unfortunately Fig. 1(*a*) in the advance copy from which Mr. Prince obtained the pressure ratios of 4.4:1 and 4.7:1 was in error. These should have been, as can be seen in the corrected figure, 4.6:1 and 4.9:1 respectively. However, this does not change the point of the discussion. In general, water injection has proved to be a valuable device for augmentation because any increase in specific fuel consumption for the short augmentation period is unimportant. This paper was pointed toward the problems which might be encountered in continuous injection rather than for augmentation. The minimum-pressure-ratio increase which would be attractive for an engine would depend upon the effect upon the complete cycle which would be determined ultimately by engine tests. The authors could not venture a guess as to the minimum figure. The reader was cautioned in the discussion of the experimental results that the compressors upon which the investigations were made were designed for dry compression and that the results do not present a fair picture. It is felt that only from compressors designed and developed specifically for wet compression can a fair picture be obtained. This applies not only to the aerodynamic design but also to the injection methods.

Transient and Steady-State Heat Transfer in Irradiated Citrus Fruit[1]

By H. F. POPPENDIEK,[2] OAK RIDGE, TENN.

This paper presents an analytical study of the thermal structure within citrus fruits that are artificially heated by radiant orchard heaters; this analysis may be utilized to establish more firmly orchard heating-design criteria. Transient and steady-state temperature solutions are derived for an ideal heat-transfer system consisting of a homogeneous sphere which suddenly receives radiant energy from a point source and loses energy by convection and reradiation to the surroundings. These solutions are compared to a set of experimental temperature measurements within an orange which was transiently irradiated in an orchard.

Nomenclature

The following nomenclature is used in the paper:

a = thermal diffusivity of the sphere, $\frac{k}{wC_p}$, sq ft per hr
A_n = constants in Equation [19]
b = barometric pressure, mm Hg
C_p = heat capacity of sphere, Btu/lb deg F
D = distance between heater stack and orange, ft
E_H = emissive power of heater stack, Btu/hr ft²
$F(\varphi)$ = function which when multiplied by parallel ray source radiation yields existing nonuniform irradiation on periphery of sphere
$F(\varphi) = \cos\varphi$ for $0 \leqq \varphi \leqq \pi/2$ and $-\pi/2 \leqq \varphi \leqq 0$
$F(\varphi) = 0$ for $\pi/2 \leqq \varphi \leqq \pi$ and $-\pi \leqq \varphi \leqq -\pi/2$
h_c = unit thermal convective conductance of sphere, Btu/hr ft² deg F
h_r = unit thermal radiative conductance of sphere, Btu/hr ft² deg F
G = parallel ray radiation from point source, Btu/hr ft²
H = height of heater stack, ft
I = modified Bessel function of first kind
J = Bessel function of first kind
k = thermal conductivity of sphere, Btu/hr ft² (deg F/ft)
k_a = thermal conductivity of air, Btu/hr ft² (deg F/ft)
L_s^{-1} = inverse Laplace transformation
m = positive integer
n = zero or positive integer
$P_n(x)$ = Legendre polynomial
r = radial distance denoted in Fig. 1, ft
r_0 = radius of sphere, ft
Re = Reynolds modulus of sphere
s = defined by $t(s) = {}_0\int^\infty e^{-s\theta}T(\theta)d\theta$ where $T(\theta)$ is object function and $t(s)$ is result function
$t(s)$ = Laplace transform of T with respect to θ
T = temperature above initial sphere temperature, deg F
W = half-width of rectangular radiating area which represents heater stack, ft
w = weight density of sphere, pcf
Z = variable of integration in Equation [22]
α = gray-body emissivity or absorptivity of sphere
β = arises in inversion integral; integration takes place along abscissa γ from point $\gamma - i\beta$ to $\gamma + i\beta$
β_m = the roots of $(Br_0 - n - 1)J_{(n+1/2)}(z) + zJ_{(n-1/2)}(z)$
γ = abscissa along which inversion integral integration takes place
θ = time, hr
σ = Stefan-Boltzmann constant, 17.3×10^{-10} Btu/hr ft² deg R⁴
τ = temperature, deg F
τ_a = air temperature, deg F
τ_H = heater stack temperature, deg F
τ_0 = initial sphere temperature, deg F
$\bar{\tau}_{r0}$ = mean sphere surface temperature, deg F
τ_s = temperature of surroundings, deg F
φ = co-ordinate angle denoted in Fig. 1

Terms:

$$A = \frac{\alpha G}{k} \qquad F = C_1 I_{(n+1/2)}\left(\sqrt{\frac{Z}{a}}\, r_0\right) + C_2 \frac{d}{dr}\left[I_{(n+1/2)}\left(\sqrt{\frac{Z}{a}}\, r\right)\right]_{r_0}$$

$$B = \frac{(h_c + h_r)}{k} \qquad x = \cos\varphi \qquad z = i\sqrt{\frac{Z}{a}}\, r_0$$

$$C_1 = \left(\frac{B}{r_0^{1/2}} - \frac{1}{2r_0^{3/2}}\right) \qquad r_1 = \sqrt{D^2 + H^2 + W^2}$$

$$C_2 = \frac{1}{r_0^{1/2}} \qquad \tau_m = \frac{\bar{\tau}_{r0} + \tau_a}{2}$$

Introduction

The heat-transfer mechanism which controls the thermal structure of artificially heated citrus fruit in an orchard is briefly reviewed. When ambient air and, consequently, fruit temperatures in an orchard are near the freezing temperature, orchard heaters are kindled. The common oil-burning types of orchard heaters yield heat in the form of convective and radiative energy. The convective heat is released in the form of a rising jet of combustion gases and entrained air, and the radiant heat is emitted from the surface of a long vertical exhaust stack. Because normally only a small part of the convective heat issuing from the conventional orchard heater is added to the air layers into which the citrus trees extend, the fruit is largely heated by radiation. One fraction of the fruit of a tree receives direct heater radiation, another fraction receives some direct and some reradiated radiation, and the remaining fraction of the fruit, which is totally shielded, receives only reradiated radiation. The heat lost from the surface of the fruit is in the form of convective and radiative energy. The heat being conducted into or out of the fruit

[1] This paper is a summary of Part I of a Ph.D. thesis (consisting of three parts) prepared by the author at the University of California in 1949.

[2] Oak Ridge National Laboratory.

Contributed by the Heat Transfer Division of The American Society of Mechanical Engineers and presented at the Heat Transfer and Fluid Mechanics Institute, June 20–22, 1951, Stanford, Calif.

Note: Statements and opinions advanced in papers are to be understood as individual expressions of their authors and not those of the Society.

through a differential area on the fruit surface is equal to the difference between the absorbed portion of the incident radiation and the heat lost by convection and radiation.

Analytical Study

It is proposed that the following ideal system be used to predict transient and steady-state temperature distributions within irradiated fruit located in the outer tree foliage region. A homogeneous sphere receives radiant heat from a point source located at a great distance from the sphere. That portion of the radiant energy which is absorbed at the surface of the sphere is partially convected to the surrounding air, partially radiated to the surroundings, and partially conducted into the sphere; within the sphere heat is transferred by conduction only. The convective and radiative heat-transfer conductances of the sphere are postulated to be uniform and constant. The heat capacity, thermal conductivity, and density of the sphere do not vary with time or temperature. The radiation characteristics of the surface of the sphere are those of a gray body (the monochromatic emissivity or absorptivity is less than unity but uniform with wave length). Fig. 1 illustrates the co-ordinate system which

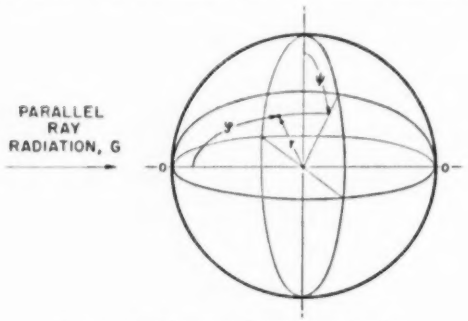

Fig. 1 Co-Ordinate System for Sphere

will be used for the sphere. The temperature distribution within the sphere is a function of r and φ but not a function of ψ, because of symmetry (the convective and radiative heat-transfer conductances have been postulated to be uniform over the surface of the sphere). The initial condition imposed on this system is that at time equal to zero, just before the sphere is irradiated by the point source, the sphere is at some uniform initial temperature (an equilibrium temperature lying between the air and surrounding temperatures both of which are postulated to be uniform and constant).

The differential equation that describes the transient heat-conduction mechanism within the sphere is (1)[a]

$$\frac{\partial T}{\partial \theta} = a\left[\frac{\partial^2 T}{\partial r^2} + \frac{2}{r}\frac{\partial T}{\partial r} + \frac{\cot\varphi}{r^2}\frac{\partial T}{\partial \varphi} + \frac{1}{r^2}\frac{\partial^2 T}{\partial \varphi^2}\right] \quad [1]$$

The initial condition imposed on the system is

$$T(r, \varphi, 0) = 0 \quad [2]$$

Because the sphere temperature distributions are symmetrical about the axis 0-0, the following two boundary conditions exist

$$\frac{\partial T}{\partial \varphi}(r, 0, \theta) = 0 \quad [3]$$

$$\frac{\partial T}{\partial \varphi}(r, \pi, \theta) = 0 \quad [4]$$

A third boundary condition consisting essentially of a heat balance on a differential area on the surface of the sphere is (see Appendix I)

$$\frac{\partial T}{\partial r}(r_0, \varphi, \theta) = AF(\varphi) - BT(r_0, \varphi, \theta) \quad [5]$$

The author has obtained a solution to the boundary-value problem described by Equations [1] to [5] by two independent methods, namely, the Laplace transform technique and the separation of variables technique. The former method will be presented here. The Laplace transforms of the foregoing differential and boundary equations with respect to time yield the following equations

$$st(r, \varphi, s) = a\left[\frac{\partial^2 t}{\partial r^2}(r, \varphi, s) + \frac{2}{r}\frac{\partial t}{\partial r}(r, \varphi, s) + \frac{\cot\varphi}{r^2}\frac{\partial t}{\partial \varphi}(r, \varphi, s) + \frac{1}{r^2}\frac{\partial^2 t}{\partial \varphi^2}(r, \varphi, s)\right] \quad [6]$$

$$\frac{\partial t}{\partial \varphi}(r, 0, s) = 0 \quad [7]$$

$$\frac{\partial t}{\partial \varphi}(r, \pi, s) = 0 \quad [8]$$

$$\frac{\partial t}{\partial r}(r_0, \varphi, s) = \frac{AF(\varphi)}{s} - Bt(r_0, \varphi, s) \quad [9]$$

where $t(r, \varphi, s)$ denotes the Laplace transform of $T(r, \varphi, \theta)$ with respect to θ. The transformed heat-conduction equation now possesses derivatives with respect to only two variables rather than three; the third variable now appears only as a parameter. Equation [6] can be solved by the separation of variables technique. Let

$$t(r, \varphi) = R(r)\,\Phi(\varphi) \quad [10]$$

where $R(r)$ and $\Phi(\varphi)$ are functions of r and φ, respectively. Upon substituting Equation [10] into Equation [6], simplifying, and grouping terms involving the same variable, one obtains

$$r^2\frac{\frac{d^2R}{dr^2}}{R} + 2r\frac{\frac{dR}{dr}}{R} - \frac{s}{a}r^2 = -\cot\varphi\frac{\frac{d\Phi}{d\varphi}}{\Phi} - \frac{\frac{d^2\Phi}{d\varphi^2}}{\Phi} \quad [11]$$

Because both sides of Equation [11] are functions of a single different variable, each side can be set equal to a constant λ. Thus the following two ordinary differential equations result

$$r^2\frac{d^2R}{dr^2} + 2r\frac{dR}{dr} - \left(\lambda + \frac{s}{a}r^2\right)R = 0 \quad [12]$$

$$\frac{d^2\Phi}{d\varphi^2} + \cot\varphi\frac{d\Phi}{d\varphi} + \lambda\Phi = 0 \quad [13]$$

Equation [13] can be transformed to a Legendre equation if the change of variable $x = \cos\varphi$ is made

$$(1 - x^2)\frac{d^2\Phi}{dx^2} - 2x\frac{d\Phi}{dx} + \lambda\Phi = 0 \quad [14]$$

If the constant λ is related to a new constant n by the expression $\lambda = n(n + 1)$, Equation [14] becomes the Legendre differential equation

$$(1 - x^2)\frac{d^2\Phi}{dx^2} - 2x\frac{d\Phi}{dx} + n(n + 1)\Phi = 0 \quad [15]$$

It can be shown that one solution of Equation [15] is the first

[a] Numbers in parentheses refer to the Bibliography at the end of the paper.

Legendre function of order n. Another solution of this differential equation is the second Legendre function of order n. If the value of n is zero or a positive integer, it can be shown that the Legendre function of the first kind is continuous in the interval $-1 \leqq x \leqq 1$ or $0 \leqq \varphi \leqq \pi$ (reference 2) and will satisfy the boundary Equations [7] and [8]. The Legendre functions of the second kind become infinite at $x = \pm 1$ (reference 3) and are therefore not solutions for this specific problem. Thus the solutions of Equation [15] are the Legendre polynomials

$$\Phi = P_n(x) = P_n(\cos \varphi) \quad [16]$$

It can be shown that the solution of Equation [12] is

$$R = \frac{b_1}{r} I_{(n+1/2)}\left(\sqrt{\frac{s}{a}}\, r\right) + \frac{b_2}{r^{1/2}} I_{-(n+1/2)}\left(\sqrt{\frac{s}{a}}\, r\right) \quad [17]$$

where b_1 and b_2 are constants.

The $\lim_{r \to 0} I_{(n+1/2)}\left(\sqrt{\frac{s}{a}}\, r\right) \Big/ r^{1/2}$ is finite but the

$\lim_{r \to 0} I_{-(n+1/2)}\left(\sqrt{\frac{s}{a}}\, r\right) \Big/ r^{1/2}$ is ∞. Because the temperature transform t, and thus the function R, must always be finite, the constant b_2 must be equal to zero. Thus the proposed solution, Equation [10], is

$$t = R\,\Phi = \sum_{n=0}^{\infty} \frac{c_n I_{(n+1/2)}\left(\sqrt{\frac{s}{a}}\, r\right)}{r^{1/2}} P_n(\cos \varphi) \quad [18]$$

Equation [18] satisfies the boundary conditions denoted by Equations [7] and [8]. The constants c_n in Equation [18] can be determined from the last boundary condition (Equation [9])

$$\frac{\partial t}{\partial r}(r_0, \varphi, s) = \frac{AF(\varphi)}{s} - Bt(r_0, \varphi, s) \quad [9]$$

The function $AF(\varphi)$ is an even function and can be expressed in terms of a series of Legendre polynomials (4)

$$AF(\varphi) = \sum_{n=0}^{\infty} A_n P_n(\cos \varphi) \quad [19]$$

where

$$A_n = \frac{2n+1}{2} \int_0^{\pi} AF(\varphi) P_n(\cos \varphi) \sin \varphi \, d\varphi, \quad n = 0, 1, 2, \ldots$$

The coefficients $A_0, A_1, A_2, \ldots$ for this particular system are tabulated in Appendix 2. Upon the substitution of Equations [18] and [19] into Equation [9], the constants c_n can be determined.

$$c_n = \frac{\frac{A_n}{s}}{\left(\frac{B}{r_0^{1/2}} - \frac{1}{2r_0^{3/2}}\right) I_{(n+1/2)}\left(\sqrt{\frac{s}{a}}\, r_0\right) + \frac{1}{r_0^{1/2}} \frac{d}{dr}\left[I_{(n+1/2)}\left(\sqrt{\frac{s}{a}}\, r\right)\right]_{r_0}} \quad [20]$$

Thus the temperature transform $t(s)$, is

$$t(s) = \sum_{n=0}^{\infty} A_n P_n \frac{1}{r^{1/2} s} \frac{I_{(n+1/2)}\left(\sqrt{\frac{s}{a}}\, r\right)}{c_1 I_{(n+1/2)}\left(\sqrt{\frac{s}{a}}\, r_0\right) + c_2 \frac{d}{dr}\left(I_{(n+1/2)}\left(\sqrt{\frac{s}{a}}\, r\right)\right)_{r_0}} \quad [21]$$

where

$$c_1 = \left(\frac{B}{r_0^{1/2}} - \frac{1}{2r_0^{3/2}}\right), \quad c_2 = \frac{1}{r_0^{1/2}}$$

The inverse Laplace transform can be expressed in terms of inversion integrals or residues (5)

$$T(\theta) = L_\theta^{-1}(t(s)) = \frac{1}{2\pi i} \lim_{\beta \to \infty} \int_{\gamma - i\beta}^{\gamma + i\beta} e^{Z\theta} t(Z)\, dZ$$

$$= \Sigma \text{ residues of } e^{Z\theta} t(Z) \quad [22]$$

The quantity Z is the variable of integration. Integration takes place along a straight line parallel to the axis of imaginaries (abscissa = γ). The integrand in Equation [22] is single-valued and has poles at $Z = 0$ and at the zeros of

$$C_1 I_{(n+1/2)}\left(\sqrt{\frac{Z}{a}}\, r_0\right) + C_2 \frac{d}{dr}\left(I_{(n+1/2)}\left(\sqrt{\frac{Z}{a}}\, r\right)\right)_{r_0}$$

The term

$$C_1 I_{(n+1/2)}\left(\sqrt{\frac{Z}{a}}\, r_0\right) + C_2 \frac{d}{dr}\left(I_{(n+1/2)}\left(\sqrt{\frac{Z}{a}}\, r\right)\right)_{r_0}$$

is denoted as F.

The residue of $e^{Z\theta} t(Z)$ at $Z = 0$ is

$$\lim_{Z \to 0} [Z e^{Z\theta} t(Z)] = \sum_{n=0}^{\infty} A_n P_n(\cos \varphi) \frac{r^n}{Br_0^n + nr_0^{n-1}} \quad [23]$$

The residues of $e^{Z\theta} t(Z)$ at the zeros of term F are

$$\left\{ \sum_{m=1}^{\infty} e^{Z\theta} \sum_{n=0}^{\infty} A_n P_n(\cos \varphi) \frac{1}{r^{1/2} Z} \frac{I_{(n+1/2)}\left(\sqrt{\frac{Z}{a}}\, r\right)}{\frac{d}{dZ}\left[C_1 I_{(n+1/2)}\left(\sqrt{\frac{Z}{a}}\, r_0\right) + C_2 \frac{d}{dr}\left(I_{(n+1/2)}\left(\sqrt{\frac{Z}{a}}\, r\right)\right)_{r_0}\right]} \right\}_{Z \text{ at zeros of } F} \quad [24]$$

where m refers to the zeros of F. Upon expressing the modified Bessel functions in terms of the J Bessel functions, making a substitution for the derivative with respect to r, and making the substitution, $z = i\sqrt{\frac{Z}{a}}\, r_0$, Relation [24] becomes

$$\left\{\sum_{m=1}^{\infty} e^{-\frac{a\beta^2}{r_0^2}\theta} \sum_{n=0}^{\infty} \frac{2r_0^{3/2} A_n P_n(\cos\varphi)}{r^{1/2} z} \frac{J_{(n+1/2)}\left(z\frac{r}{r_0}\right)}{\frac{d}{dz}\left[(Br_0 - n - 1)J_{(n+1/2)}(z) + zJ_{(n-1/2)}(z)\right]}\right\}_{z \text{ at zeros of } F}$$

$$= \sum_{n=0}^{\infty}\sum_{m=1}^{\infty} \frac{2r_0^{3/2} A_n P_n(\cos\varphi)}{r^{1/2}\beta_m} \frac{J_{(n+1/2)}\left(\beta_m\frac{r}{r_0}\right)}{\frac{d}{dz}\left[(Br_0 - n - 1)J_{(n+1/2)}(z) + zJ_{(n-1/2)}(z)\right]_{\beta_m}} e^{-\frac{a\beta_m^2}{r_0^2}\theta} \quad [25]$$

Note that term F is now expressed as

$$(Br_0 - n - 1)J_{(n+1/2)}(z) + zJ_{(n-1/2)}(z)$$

and its roots are β_m.

The substitution of Equations [23] and [25] into Equation [22] yields the desired transient-temperature solution

$$T(r, \varphi, \theta) = \frac{A_0}{B} + \sum_{n=1}^{\infty} A_n P_n(\cos\varphi) \frac{r^n}{Br_0^n + nr_0^{n-1}}$$

$$+ \sum_{n=0}^{\infty}\sum_{m=1}^{\infty} \frac{2r_0^{3/2} A_n P_n(\cos\varphi)}{r^{1/2}\beta_m} \frac{J_{(n+1/2)}\left(\beta_m\frac{r}{r_0}\right)}{\frac{d}{dz}\left[(Br_0 - n - 1)J_{(n+1/2)}(z) + zJ_{(n-1/2)}(z)\right]_{\beta_m}} e^{-\frac{a\beta_m^2}{r_0^2}\theta} \quad [26]$$

A Comparison of Predicted and Actual Transient-Temperature Distributions Within an Irradiated Orange

Transient-temperature distributions within a navel orange which was suddenly irradiated by an orchard heater have been measured by C. Lorenzen (6). The orange was located in the outermost zone of the tree foliage. Eight thermocouples were threaded through the orange in such a fashion that the junctions were positioned along the orange diameter which was parallel to the parallel ray heater radiation.

Before a comparison of analytical and experimental orange temperature distributions was made, it was necessary to evaluate the various system parameters that influence the analytical temperature distribution (see Equation [26]). The results of such an evaluation are presented in Appendix 3.

Fig. 2 reveals a comparison of the predicted and actual transient-temperature histories at three points within the orange along diameter 0-0. The experimental orange temperature histories were predicted within an accuracy of ±25 per cent; those experimental points falling below $T = 0.5$ deg F were not included in this percentage because (*a*) the initial orange temperature distribution was only uniform within about 0.5 deg F, and (*b*) the scatter of the experimental data was of the order of 0.5 deg F. Under the specific weather conditions that existed and for the particular kind of orchard heater used, the maximum and minimum steady-state orange temperature rises (at the intersection of axis 0-0 and the surface of the orange) were about 8 and 1 deg F, respectively; also, 2 hr after the orange began to receive heater radiation, the orange temperature distribution was within about 10 per cent of the steady-state temperature distribution.

Discussion

Uniform and constant convective and radiative heat-transfer conductances were postulated in the ideal system. A study of the actual local conductance distributions was made. Local free and forced convection-conductance distributions were estimated from local free and forced convection-cylinder data, respectively (7, 8). It was indicated that the maximum difference between the total local conductances and the total average or uniform conductance was of the order of 20 to 30 per cent. The forced-convection and radiative conductances are nearly constant (not functions of time) because they are insensitive to orange surface temperatures. The free-convection conductance is not very uniform because it is a function of the orange surface temperature; however, this conductance is only about one quarter as large as the total conductance.

The orange has been treated as a homogeneous sphere with uniform and constant properties. Actually the orange is composed of a thin peel which covers the inner pulp.

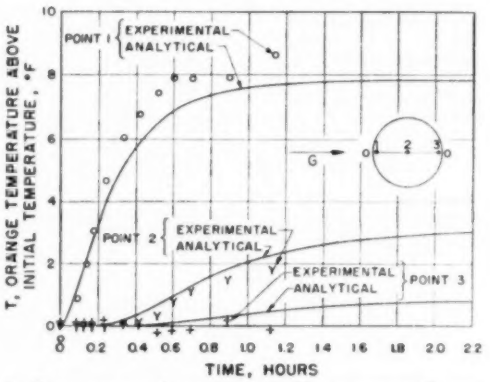

Fig. 2 Comparison of Analytical and Experimental Transient-Temperature Distributions Within an Orange

Equation [26] can be used to estimate the amount of radiant energy that is required to obtain any specified orange temperature rise above a given temperature datum for any particular set of meteorological conditions. Knowledge of such radiant-energy requirements will facilitate (*a*) the design of orchard-heater stack sizes and temperatures, and (*b*) the planning of orchard-heater spacing.

BIBLIOGRAPHY

1 "Heat Transfer Notes," by L. M. K. Boelter, V. H. Cherry, H. A. Johnson, and R. C. Martinelli, University of California Press, Berkeley and Los Angeles, Calif., 1946, pp. III—14.

2 "Fourier Series and Boundary Value Problems," by R. V. Churchill, McGraw-Hill Book Company, Inc., New York, N. Y., 1941, p. 186.

3 "Tables of Functions," by E. Jahnke and F. Emde, Dover Publications, New York, N. Y., 1943, p. 110.

4 "Fourier Series and Boundary Value Problems," by R. V. Churchill, McGraw-Hill Book Company, Inc., New York, N. Y., 1941, p. 192.

5 "Modern Operational Mathematics in Engineering," by R. V.

Churchill, McGraw-Hill Book Company, Inc., New York, N. Y., 1944, p. 157.

6 "A Report on the Experimental Temperature Distributions Within Irradiated Oranges on File at the University of California," by C. Lorenzen, Davis, Calif.

7 "Temperature Distribution and Heat Flux in Air by Interferometry," by R. B. Kennard, in "Temperature, Its Measurement and Control in Science and Industry," Reinhold Publishing Company, New York, N. Y., 1941, p. 685.

8 "Heat Transfer Over the Circumference of a Heated Cylinder in Transverse Flow," by E. Schmidt and K. Wenner, Technical Memorandum, NACA No. 1050, 1943.

9 "The Scientific Basis of Illuminating Engineering," by R. Moon, McGraw-Hill Book Company, Inc., New York, N. Y., 1936, p. 267.

10 "Heat Transmission," by W. H. McAdams, McGraw-Hill Book Company, Inc., New York, N. Y., 1942, p. 237.

11 "Surface Heat Transmission," by R. H. Heilman, Trans. ASME, vol. 51, 1929, paper FSP-51-41, pp. 287–302.

Appendix 1

A heat balance at the sphere interface is

$$\alpha GF(\varphi) = k\frac{\partial \tau}{\partial r}(r_0, \varphi, \theta) + h_c(\tau(r_0, \varphi, \theta) - \tau_a) + h_r(\tau(r_0, \varphi, \theta) - \tau_a)$$

where τ is the temperature in degrees Fahrenheit. Upon substituting $\tau(r_0, \varphi, \theta) = T(r_0, \varphi, \theta) + \tau_0$, and the heat-balance equation at time equal to zero, $h_c(\tau_a - \tau_0) = h_r(\tau_0 - \tau_r)$, into the foregoing equation there results

$$\frac{\partial T}{\partial r}(r_0, \varphi, \theta) = \frac{\alpha GF(\varphi)}{k} - \frac{(h_c + h_r)}{k} T(r_0, \varphi, \theta)$$

Appendix 2

$$A_n = \frac{2n+1}{2}\int_0^{\pi} AF(\varphi)\, P_n(\cos\varphi)\sin\varphi\, d\varphi, \quad n = 0, 1, 2, \ldots$$

where

$AF(\varphi) = A\cos\varphi$ for $0 \leq \varphi \leq \pi/2$ and

$AF(\varphi) = 0$ for $\pi/2 \leq \varphi \leq \pi$

For $n = 0$

$$A_0 = \frac{1}{2}\int_0^{\pi/2} A\cos\varphi\, P_0(\cos\varphi)\sin\varphi\, d\varphi + \frac{1}{2}\int_{\pi/2}^{\pi} 0 \cdot P_0(\cos\varphi)\sin\varphi\, d\varphi = \frac{A}{4}$$

Similarly, it can be shown that $A_1 = A/2$, $A_2 = 5A/16$, $A_3 = 0$, $A_4 = -3A/32$ and $A_5 = 0$. The series $\sum_{n=0}^{\infty} A_n P_n(\cos\varphi)$ converges rapidly.

Appendix 3

The results of an evaluation of the parameters appearing in Equation [26] follow:

Orchard-Heater Radiation, G. The radiation from a rectangular radiating area (idealized orchard-heater stack) on an area parallel to the radiating area and at a point that lies on a perpendicular erected at the center of the bottom edge of the radiating area given by (9)

$$G = \frac{E_H}{\pi}\left(\frac{H}{\sqrt{D^2 + W^2}}\sin^{-1}\frac{W}{r_1} + \frac{W}{\sqrt{D^2 + W^2}}\sin^{-1}\frac{H}{r_1}\right)$$

was found to be 51 Btu/hr ft².

Forced-Convection Conductance, $h_{c\,forced}$. The forced-convection conductance for a sphere in air expressed as (10)

$$h_{c\,forced} = 0.33\frac{k_a}{2r_0}(\mathrm{Re})^{0.6} \quad \text{for} \quad 20 < \mathrm{Re} < 10^5$$

was found to be 1.65 Btu/hr ft² deg F.

Radiation Conductance. The radiation conductance given by

$$h_r = \frac{\alpha\sigma[(\bar{\tau}_{r0} + 460)^4 - (\tau_a + 460)^4]}{(\bar{\tau}_{r0} - \tau_a)}$$

was found to be 0.68 Btu/hr ft² deg F. The gray-body emissivity was determined from the monochromatic reflectivity data for orange peel shown in Fig. 3. These reflectivity data were obtained for the author by Mr. L. Possner of the Thermal Radiation Project of the Engineering Department of the University of California, Berkeley. The evaluation of h_r is technically a trial-and-error process because this conductance is a function of the orange temperature distribution itself. However, the term h_r can be determined satisfactorily without trial and error because it is not a very sensitive function of surface temperature over the temperature range involved (less than a 2 per cent variation in h_r).

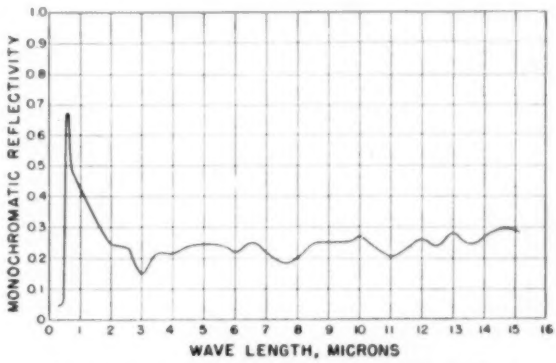

FIG. 3 MONOCHROMATIC REFLECTIVITY OF ORANGE PEEL

Free-Convection Conductance, $h_{c\,free}$. The free-convection conductance for a sphere in air is expressed as (11)

$$h_{c\,free} = 1.82\left(\frac{1}{24\,r_0}\right)^{0.2}\left(\frac{b}{760}\right)^{0.52}\left(\frac{1}{\tau_m + 460}\right)^{0.181}(\bar{\tau}_{r0} - \tau_a)^{0.266}$$

Although the evaluation of this conductance is a trial-and-error process, it can be accomplished satisfactorily in one or two trials. The term $h_{c\,free}$ was found to be 0.80 Btu/hr ft² deg F for a mean air-surface temperature difference of 5 deg F.

Total Heat-Transfer Conductance. The total heat-transfer conductance (a sum of the three given in the foregoing) was 3.1 Btu/hr ft² deg F.

Thermal Conductivity, Heat Capacity, and Weight Density of Oranges. The author has conducted some limited experiments for the purpose of determining mean values of the thermal conductivity, heat capacity, and weight density of navel oranges. Mean values of thermal conductivity were obtained (*a*) by transient heating or cooling of oranges, and (*b*) steady-state heating of oranges by means of central heating sources. A mean heat-capacity value was determined with the aid of a calorimeter, and a mean weight-density value was obtained by the water-displacement technique. These experiments indicated that $k = 0.25$ Btu/hr ft² (deg F/ft), $C_p = 0.71$ Btu/lb deg F, and $w = 58$ pcf.

Operation of Sunbury Steam-Electric Station Using Pulverized-Anthracite Fuel

By T. B. RICHARDS,[1] SUNBURY, PA.

The largest deposits of anthracite in the United States are located in north and central eastern Pennsylvania. Only a few central stations burn this type of fuel, and prior to World War II those stations able economically to justify its use, were relatively small in size. Pennsylvania Power & Light Company, whose service area includes a large segment of the anthracite region, is a pioneer in the burning of anthracite and is the largest single consumer of this fuel in the United States, having burned 2,325,500 net tons in 1951. During 1949 this company completed the installation of four 400,000 lb per hr steam generators at Sunbury Steam Electric Station located between Shamokin Dam and Hummels Wharf on the Susquehanna River near Sunbury, Pa. This paper presents the design features peculiar to the handling, pulverizing, and burning of anthracite, as well as some of the problems encountered during the first 3 years of operation. Reference is also made to a third unit, placed in service in 1951, which burns a mixture of anthracite and bituminous coal and a fourth unit, in the process of construction, which will employ the reheat cycle and also will burn an anthracite-bituminous coal mixture.

General

ELECTRICAL energy for commercial use was produced for the first time at the Sunbury Steam Electric Station on September 19, 1949, when the first unit was placed in regular operation. On November 17, 1949, the second unit was placed in commercial operation thus completing the largest anthracite-fired generating station in the world and the first two units of an ultimate six-unit station. Rapid load growth in the company's service area made it necessary to install unit No. 3 which was placed in regular operation on April 18, 1951, and unit No. 4, which is to be placed in service in 1953.

The plant site covers 259 acres with 30 per cent of this area devoted to coal-handling and storage facilities, 50 per cent to active and future ash disposal, and the remainder for switchyards and the main station.

Table 1 lists the principal design features of units Nos. 1, 2, and 3 turbine generators and steam generators. These units are interconnected through steam and feedwater ties to provide operating flexibility. Figs. 1 and 2 are cross-section elevation drawings of the two types of boilers now in service. They are direct-fired rather than the bin-and-feeder system previously employed by Pennsylvania Power & Light Company on pulverized-anthracite installations. No. 4 unit will be a single steam generator-and-turbine generator unit of 125,000 kw capacity incorporating the reheat cycle and operating with throttle conditions of 1450 psig and 1000 F with 1000 F reheat.

TABLE 1 DESIGN FEATURES

	Units 1 and 2	Unit 3
Turbine generators:		
Number of units	2	1
Manufacturer	General Electric Co.	Westinghouse Corp
Rating, kw	75000	100000
Speed, rpm	3600	3600
Throttle steam pressure, psig	1250	1250
Throttle steam temperature, deg F	950	950
Turbine stages	21	31
Number of bleed points	5	5
Back pressure, in. Hg	1.5	1.5
Type blading	Impulse	Impulse-reaction
Note: All three are tandem-compound, double-flow condensing.		
Boilers:		
Number of units	4	1
Manufacturer	Foster Wheeler	Foster Wheeler
Rating, lb per hr	400000	800000
Steam pressure superheater outlet, psig	1350	1350
Steam temperature superheater outlet, deg F	955	955
Primary fuel	Anthracite	Mixture anthracite and bituminous coal
Type firing	Vertical	Horizontal

Coal-handling facilities include a coal-storage area, thaw sheds for thawing 20 cars of coal at one time, a rotary car dumper and car-shakeout facilities for unloading coal by truck, two fireless steam locomotives, six tractors, three carry-all scrapers, and 26 conveyer units (active transport distances total over 1 mile). Except for the storage and reclaiming belts, the conveyer system is completely enclosed.

The ash-handling system includes mechanical and electrostatic dust collectors, a hydropneumatic dust-removal system, and a hydraulic ash-transport system which pumps a mixture of 10 per cent ash and 90 per cent water through 2500 ft of 8-in. steel pipe to the ash-storage area.

Operation of these units has been highly satisfactory in spite of numerous difficulties normally encountered in operating a station incorporating new developments or developments previously tried only on smaller installations.

Since features peculiar to the handling and burning of anthracite have been incorporated in the equipment at Sunbury, this paper will deal with the difficulties encountered with this equipment and the operation of the station as an anthracite-fired installation.

Anthracite

Pennsylvania Power & Light Company and its predecessor companies have played an active part in designing equipment to burn the smaller sizes of anthracite. For the past 40 years, No. 3 and No. 4 buckwheat coal have been burned successfully on traveling-grate stokers, and for over 30 years smaller sizes have been burned in pulverized-fired boilers. At Sunbury, No. 4 and No. 5 buckwheat coal are burned. This mixture is called "prepared anthracite" to differentiate between the prepared product and "silt" or unprepared product obtained from settling or silt basins. The company's specifications for the purchase of prepared sizes of anthracite are given in Table 2.

The amount of anthracite produced in the smaller sizes is dependent upon the domestic market. If the supply of small-size, fresh-mined anthracite becomes limited, provisions have been made at Sunbury to blend silt with prepared anthracite and bi-

[1] Superintendent of Plant, Sunbury Steam Electric Station, Pennsylvania Power & Light Company. Mem. ASME.

Contributed by the Fuels Division of The American Society of Mechanical Engineers and presented at the ASME-AIME Fuel Conference, Philadelphia, Pa., October 30–31, 1952.

Note: Statements and opinions advanced in papers are to be understood as individual expressions of their authors, and not those of the Society. Manuscript received at ASME Headquarters, October 2, 1952. Paper No. 52—Fu-3.

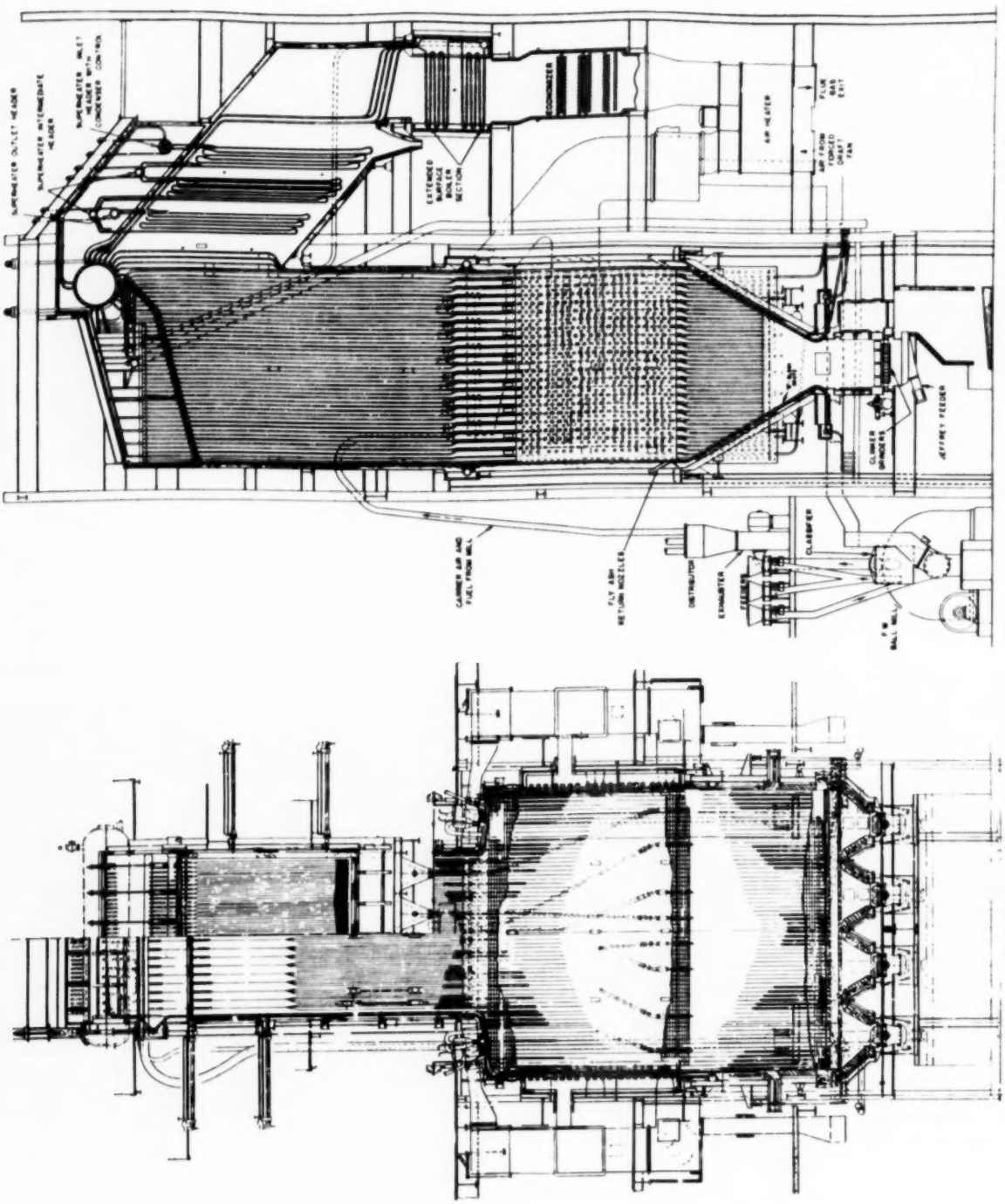

FIG. 1 STEAM-GENERATOR UNITS NOS. 1 AND 2, ANTHRACITE, PENNSYLVANIA POWER & LIGHT COMPANY, SUNBURY STEAM ELECTRIC STATION

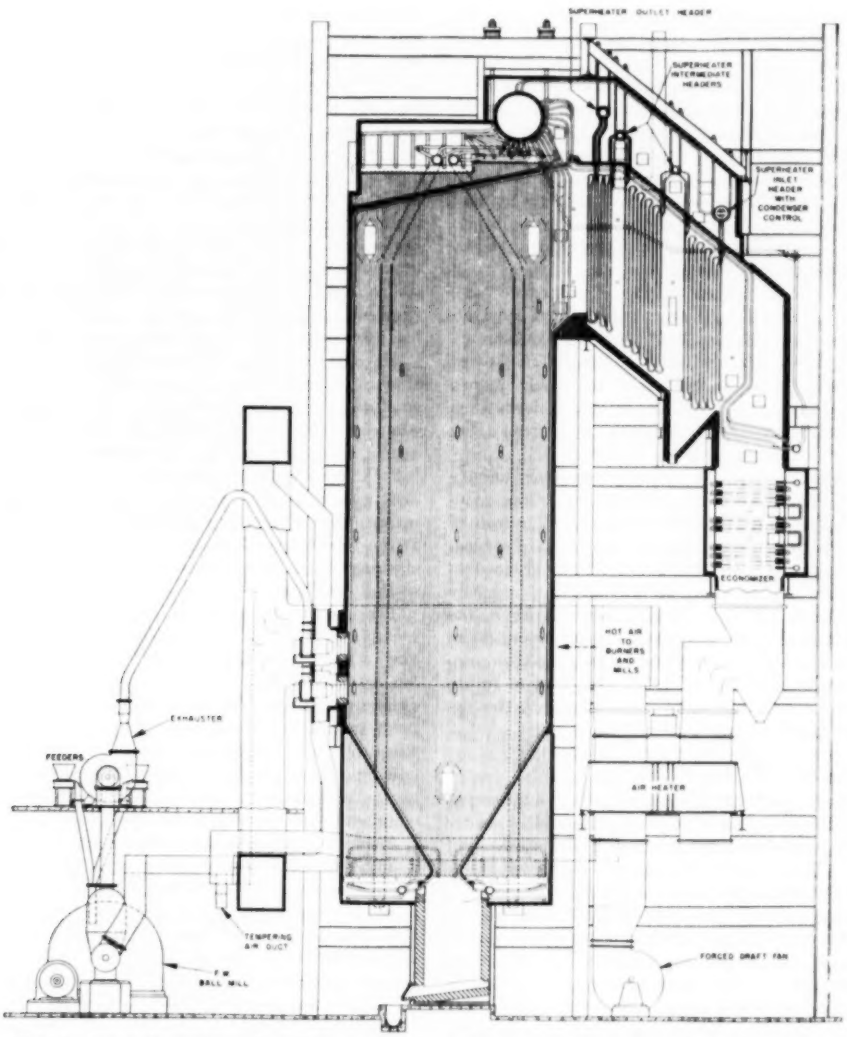

FIG. 2 STEAM-GENERATOR UNIT NO. 3, ANTHRACITE-BITUMINOUS COAL MIXTURE, PENNSYLVANIA POWER & LIGHT COMPANY, SUNBURY STEAM ELECTRIC STATION

TABLE 2 SIZE SPECIFICATIONS FOR PURCHASE OF PREPARED SIZES OF ANTHRACITE

No. 3 Buckwheat (Barley): Shall be of such size that not more than 20 per cent by weight will pass through a $^{3}/_{32}$-in. round-hole screen.
No. 4 Buckwheat: Shall be of such size that not more than 20 per cent by weight, will pass through a $^{5}/_{64}$-in. round-hole screen.
No. 5 Buckwheat: Shall be of such size and condition that it will not require any unusual additional labor to unload and transport it through any of the coal-handling equipment, in excess of that required for No. 4 buckwheat, in the plant in question.

tuminous coal. Silt contains ash in quantities varying from 12 to 50 per cent and most of it requires blending with a better-quality fuel.

Table 3 compares the characteristics of prepared anthracite, silt, and bituminous coal. Three items in this table are of particular interest since they influence the design of an anthracite-fired station:

High Moisture Content. A station designed to burn high-moisture anthracite coal requires (*a*) facilities to thaw frozen coal, (*b*) coal-handling facilities designed to minimize blockages, (*c*) adequate pulverizing-mill capacity to dry and pulverize the

TABLE 3 TYPICAL ANALYSES AND HEATING VALUES OF THREE TYPES OF FUEL

	Prepared anthracite	Unprepared anthracite silt	Bituminous coal
Heating value as fired, Btu/lb	10970	8900	13433
Ash-fusion temperature, deg F	2600–2700	2600–2700	2400–2500
Grindability, Hardgrove scale	40	48.5	56.8
Proximate analysis, dry basis, percentage by weight:			
Volatile matter, per cent	5.5	5.4	38.6
Fixed carbon, per cent	79.5	68.8	53.9
Ash, per cent	15.0	25.8	7.5
Total	100.0	100.0	100.0
Sulphur, separate determination on dry basis, per cent	0.65	0.41	1.47
Moisture as fired, per cent	12.5	15.0	3.0

coal, and (*d*) facilities to blend bituminous coal with extremely wet anthracite coal.

Low-Volatile Content. The design of a furnace to burn anthracite with its slow-burning characteristics requires (*a*) coal burners capable of providing a rich coal-air mixture, (*b*) a vertically downward-fired furnace having a large furnace volume, (*c*) re-

fractory-covered waterwalls in the ignition zone, and (*d*) a secondary-air supply capable of scrubbing the flame along its entire downward path.

High Ash Content. A fuel having a high ash content requires (*a*) large dust precipitators and ash-handling facilities, (*b*) furnaces designed to reduce slag formation, and (*c*) a boiler arrangement designed to minimize erosion.

Two additional items, not readily apparent from the table but indicated by its low grindability index and high moisture content, are its severe abrasive and corrosive properties. Corrosion presumably is caused by a dilute solution of sulphuric acid formed by the moisture and sulphur in the coal.

Thus far, only the adverse characteristics of anthracite have been discussed. A fuel with these characteristics offers some advantages. For example, Pennsylvania Power & Light Company does not experience fires with small-size anthracite in storage banks or explosions in confined areas such as bunker rooms, storage bins, mills, or furnaces; it need not be wetted down when dumped from railroad cars and high coal-air temperatures leaving pulverizing mills are permissible.

The mines from which most of the coal is procured for Sunbury are within the first freight-rate zone and this condition largely influenced the choice of anthracite for units Nos. 1 and 2 in spite of the larger capital investment required as compared to a bituminous-coal installation. Units Nos. 3 and 4 were designed to burn a 30 per cent portion of anthracite with facilities primarily designed to burn bituminous coal. With this arrangement, the capital investment was reduced as compared to an all-anthracite unit and a slight decrease in operating costs was realized as compared to an all-bituminous unit. Careful projection of future operating costs and coal availability also influenced the decision to use the bituminous-type steam generator.

Operating Experiences Units Nos. 1 and 2

Raw-Coal Handling. (*a*) *Thaw Sheds:* A four-bay, five cars per bay, concrete-block thaw-shed structure was designed to shelter the cars completely while hot water is sprayed on the sides and bottom of the cars. The recirculated spray water is heated by reduced steam from the main plant by a mixing-type heater.

Generally, coal cars are not exposed to freezing weather for any great length of time owing to the proximity of the station to the coal company's preparation plants. Rarely does the depth of the frozen coal exceed 12 in. To thaw completely coal frozen to this extent, the cars are placed in the thaw sheds overnight for a period of 15 to 16 hr. Hot water is sprayed on the cars for the first 8 hr followed by 7 to 8 hr of "soaking" to utilize the heat remaining in the sheds and to permit the moisture to drain from the cars.

(*b*) *Coal Storage:* Tractors and carry-all scrapers are used in moving coal to and from storage. The smaller sizes of anthracite pack well and track-laying-type vehicles with wide track shoes are effective on this type of coal.

(*c*) *Conveyers:* Coal containing moisture less than 14 per cent and fines (particles passing through a 200-mesh sieve) less than 5 per cent are handled conveniently by the conveyer system. Blockages frequently occur in chutes at transfer points when these limits are exceeded. The chutes originally were coated with rubber to resist abrasion which for this purpose proved to be successful but was found to be mainly responsible for blockages. Stainless steel, although less resistant to abrasion, was installed and improved the condition.

(*d*) *Mill Feeders:* The first problem encountered after starting the station was blockages at the pulverizing-mill coal feeders resulting in ignition instability. Two things were mainly responsible for this difficulty:

1 The coal suppliers pack excelsior in the bottom of coal cars to prevent leakage of the fine coal through the hopper doors. When the car is emptied on the car dumper, the excelsior mixes with the coal and is difficult to remove. A large portion of it is removed by the cleaning screens, provided it remains in bulk form, but this requires the attention of one man to prevent blockage of the screens when excessive quantities of excelsior are encountered. The strands of excelsior pass through the screens and removal thereafter is impossible.

When this condition was first encountered, the excelsior collected behind the shear blades of the mill feeders just as if the blades were designed to do so but unfortunately, when a sufficient amount was collected, the flow of coal to the mills was interrupted thus upsetting boiler operation.

The feeder shear blades were redesigned to prevent the excelsior from collecting behind the blade. This was an improvement but has been only partially successful under extreme conditions.

The coal companies were requested to reduce to a minimum the amount of excelsior placed in coal cars. When this was done, the condition improved considerably. The co-operation of the coal companies has been gratifying and they are looking for a more satisfactory packing method to replace the excelsior.

2 There are three feeders on each end of each pulverizing mill and originally two feeder-discharge pipes were joined together before entering the pulverizing-mill classifier. Blockages occurred at the junction point of these two pipes and frequently required cleaning. This problem was solved by relocating the coal pipes so that each pipe entered the classifier separately.

The most troublesome coal-handling problem, and one which remains to be solved, is blockages in the raw-coal transport system due to wet coal. Freezing weather (explained previously) and long periods of rainy weather increase the normal "as-received" moisture content of the coal to such an extent that it becomes difficult to handle. Some progress has been made toward solving this problem. Stainless steel has been used as liner material for coal pipes from the mill feeders to the mills and for inlet funnels on the mill feeders. This by no means has solved the problem completely but is a step in the right direction.

Blockage of the cleaning screens due to wet coal also presented a problem. This was partially remedied by (1) reversing the operation of the screens so that the coal passing over the screen would be thrown backward against the incoming coal and (2) redesigning the screens so that the long axis of the rectangular holes was parallel to the flow on the top half of the screen and perpendicular to the flow on the bottom half. (Originally the holes were all parallel to the flow of coal.)

Pulverized-Coal Handling. (*a*) *Mills:* The pulverizing mills were guaranteed to produce pulverized coal of a fineness of at least 85 per cent through a 200-mesh sieve when supplied with 20 per cent ash and 15 per cent moisture coal. In operation, the mills produced a fineness of 92 to 95 per cent through a 200-mesh sieve with lower ash and moisture coal and an average boiler load slightly less than 400,000 lb per hr.

Mill maintenance has not been excessive. Spiral conveyers have required occasional repairs and air tubes have become worn and damaged necessitating repairs and in some cases replacement. None of the eight mills installed has required replacement of the liners to date.

Mill-ball replacements are made on a monthly schedule. Two of the mills were charged with copper-molybdenum-alloy steel grinding balls and six with forged-steel grinding balls to obtain data to determine the type of ball which would be the most economical to use in these mills. The mill-ball consumption rate to date for forged-steel grinding balls has been 0.299 lb per ton of anthracite and 0.284 lb per ton of anthracite for copper-molybdenum-alloy steel grinding balls. No definite conclusion has been reached pending an evaluation of the effect of each type of ball on the mill liners.

(*b*) *Exhausters:* The mill exhausters are simple paddle-wheel fans fitted with replaceable liners and fan blades to facilitate maintenance. The liners and fan blades are subjected to severe erosion from the impingement of high-velocity coal-air mixtures on their surfaces.

To obtain service-life data of various types of fan-blade materials, two fans were fitted with carbon-steel blades coated with an abrasion-resistant paste, two with carbon-steel blades coated with an abrasion-resistant metal, two with stainless-steel-clad steel blades and the remainder with the manufacturer's standard carbon-steel blades. Replacement blades, fabricated from diamond floor plate, were tested and found to be an inexpensive, readily attainable, and very satisfactory material for this type of service.

Exhauster liners have been replaced or worn spots repaired each time an exhauster has been taken out of service for periodic inspection. Originally, welding rods were used to build up the worn spots on the liners but this procedure proved to be expensive and required considerable outage time. For the past 18 months satisfactory results have been attained by filling the worn spots in the liners with a plastic-chrome cement. This material is easy to apply and holds up remarkably well between inspections.

(*c*) *Coal Pipes:* After 3 years of operation, none of the coal pipes from the exhausters to the burners has required replacement. Examination of these pipes has indicated that very little erosion has taken place.

The burner riffles, located between the coal pipes and the burners to divide the coal equally to the twin-cyclone anthracite burners, are subjected to very severe service and must be replaced when they become worn.

Steam Generators. (*a*) *Design Features:* Furnaces for anthracite steam generators previously were designed for heat-release rates as high as 21,000 Btu per hr per cu ft of furnace volume. The Sunbury units Nos. 1 and 2 steam generators are designed for a a heat-release rate of 8520 Btu per hr per cu ft of furnace volume at rated capacity to minimize combustion and slag-accumulation problems.

These units are designed for vertically downward firing from two rows of burners on opposite sides of the furnace. In this manner the tails of the two flames impinge on each other rather than on a cooled surface. This feature contributes to more nearly complete combustion of the carbon particles and eliminates slagging of the rear wall.

By contrast, No. 3 steam generator, designed to burn a mixture of anthracite and bituminous coal, is horizontally fired from two rows of burners along one wall. Horizontal firing has limited the amount of anthracite that can be burned on this unit. In fact, it is necessary to feed most of the anthracite to the upper row of burners to reduce the unburned carbon loss and to stabilize ignition. On units Nos. 1 and 2 the waterwall tubes below the burner arch were covered with refractory to aid in maintaining stable ignition. Above the burner arch the tubes are bare.

The air required for best pulverization and drying of anthracite is greater than that required to maintain stable ignition at the burner. In the unit system, the air in excess of the amount required at the burner must be removed. This can be accomplished with a cyclone-type burner which separates the coal from the air and vents the excess air to the furnace through the top of the burner. The amount of excess air vented is controlled by a damper in the vent line. The pulverized-anthracite-coal burners on these units are of this type.

Examination of Fig. 1 shows the secondary-air ports, indicated by small holes and arranged in a belt across the full width of the furnace and extending vertically from a point just below the burner arch to a point just above the sloping section of the furnace bottom. Tertiary air is supplied around the outside of the burners and also serves to cool the burner.

The furnace bottom and ash-removal equipment were designed to facilitate the removal of slag and clinkers when burning coal having 20 per cent ash with a fusion temperature of 2400 F. The furnace bottom was designed to retain 10 to 15 ft of ashes to allow sufficient time for the carbon in the ash to be reduced before removal from the furnace. Access doors were provided to reduce large pieces of slag with hand tools. Clinker grinders were provided to crush the ash to a size easily handled by the ash-sluicing system and the ash-disposal pumps. With the type of coal now being burned, no difficulty is experienced with slagging conditions but when it becomes necessary to burn lower grades of anthracite, slagging may become a serious problem.

(*b*) *Combustion Problems:* Originally, the burner nozzles contained an adjustable helical-shaped vane to give turbulence to the coal-air mixture. With this arrangement the flame length was too short and the full volume of the furnace was not being utilized to the greatest advantage. Studies also revealed stratification of the gases as indicated by nonuniform CO_2 readings across the furnace above the burners. Heavy slagging of the furnace walls below the burners also prevailed.

Various combinations of adjustments to primary, secondary, and tertiary air were tried but only mediocre success was achieved. Considerable effort was exerted to obtain a distribution of secondary air which would provide a uniform CO_2 across the furnace outlet.

Originally, all of the secondary-air ports in the furnace walls were open and the velocity through the ports was comparatively low. By blocking off a number of these ports, the velocity was increased and, through the process of trial and error, a pattern was determined which provided the desired amount of turbulence and almost completely eliminated stratification. The flame length was increased by removing the helical-shaped vanes in the burner nozzles and installing straightening vanes.

With these changes, combustion has been improved and slag and dust accumulations on the walls have been reduced to a satisfactory degree. Dust accumulations are readily removed by occasional air-lancing and daily use of wall blowers.

Ash Handling. Superheater dust hoppers: Originally a 4-in. discharge line was provided to drain the superheater dust hoppers to the furnace bottom. Shortly after the steam generators were placed in service, these hoppers became blocked and dust built up above the hoppers to a point where the lower part of the superheater tubes became embedded in it. Clinkers were formed and occasionally would drop on top of the extended-surface boiler section, the economizer, and the air heater. Air-heater blockage was the most serious difficulty. Larger ash pipes and flapper valves, 8 in. in size, corrected this problem.

Auxiliary Equipment. Induced-Draft Fans: Exceptionally good service life has been obtained with the induced-draft fans. After 3 years of service, none of the eight fans installed has required blade replacements. Past experience on other anthracite-fired installations indicated that the induced-draft fans were very weak spots in the system since in some cases blade replacements were necessary as frequently as once a month. For this reason the induced-draft fans selected for Sunbury are large, low-speed fans of a simple paddle-wheel design and equipped with magnetic couplings for variable-speed control. The extreme fineness of the dust particles due to finer pulverized coal has been a factor helping to extend the service life of these fans.

Operating Procedure. Firing up an anthracite steam generator is accomplished by lighting off with four fuel-oil torches and increasing the number of torches as required until such time as the gas temperature leaving the economizer section reaches 275 F. Two coal burners fed with anthracite are lighted off and additional burners are placed in service as required until the boiler is brought up to rated capacity. The fuel-oil torches are removed

as quickly as possible after stable ignition has been attained. Originally it was believed that bituminous coal would be required to fire up a boiler but early attempts to omit the firing of bituminous coal were highly successful and the procedure as outlined was adopted.

The coal-air temperature leaving the mills is maintained at 180 F. A high coal-air temperature is desirable when firing anthracite for good ignition stability. Even at this comparatively high temperature there is no danger of fire starting in the mills.

The anthracite steam generators are operated with a 13.8 per cent CO_2 at the air-heater inlet which is equivalent to 40 per cent excess air.

Occasionally abnormally wet anthracite must be burned in the boilers. Under such conditions ignition becomes unstable as a result of low coal-air temperatures leaving the mills and it is necessary to blend bituminous coal with the anthracite. As much as 13 per cent bituminous coal has been required to stabilize ignition on days when the anthracite is exceptionally wet.

Fuel oil is used primarily to fire up boilers but, occasionally, in an emergency such as a loss of an auxiliary unit or a sudden heavy load drop, fuel oil is injected as quickly as possible to prevent loss of the unit.

Soot blowers are installed in the air heaters but are rarely used. The abrasive action of the ash keeps the heat-transfer surfaces clean. Operation of an air-side by-pass damper is occasionally required during severe cold weather to prevent condensation of moisture on the heat-transfer surfaces.

Operating Results. Performance data which is based on three years of operating experience with these units are given in Table 4.

TABLE 4 PERFORMANCE DATA

Boiler efficiency, per cent	85
Flue-gas loss, per cent	6
Combustible in refuse loss, per cent	2.5
Heat release, Btu/hr/cu ft furnace volume	7500
Evaporation rate, lb steam/lb of coal	8.90
Average boiler steam rate, lb/hr	350000
Station coal rate, lb coal/kwhr output	1.02
Station heat rate, Btu/kwhr output	11800
Station make-up, per cent	2.0
Station water rate, lb steam/kwhr output	9.1
Turbine water rate, lb steam/kwhr generated	8.3

NOTE: This anthracite-burning plant presently has the lowest average incremental fuel cost on the interconnection system (area 5) of which our company is a member.

CONCLUSION

Operation of Sunbury as an anthracite-fired installation in most respects has exceeded the expectations of the designers. Problems remain to be solved, particularly with respect to the handling of small-size anthracite in a modern high-capacity station. Economic factors in some cases prevent the complete solution of some of these problems from the standpoint of both the coal user and the coal producer. At Sunbury every effort has been made to improve equipment design to handle anthracite and studies are continually being made toward further improvement. This paper has presented the problems of the user in an attempt to better acquaint the many coal producers with these problems and with the hope that the anthracite industry will be able to further improve its product for this important industrial use.

Cyclone Dust Collectors for Boilers

By A. J. TER LINDEN,[1] DELFT, HOLLAND

A laboratory analysis is given of various cyclone dust collectors according to requirements prevailing in Holland. The author describes the experimental studies, theoretical considerations, and efficiencies of different types. Suggestions are given of cyclones suitable for grate-fired and pulverized-fuel-fired boilers in various locations.

Inconveniences Caused by Boiler Plants

THE nuisance caused in the neighborhood of a boiler plant depends on the quantity of the gases and dust particles leaving the stacks, the size of these particles, the height of the stacks, the nature of the surroundings, and on some less important factors.

Theoretically speaking, it may be possible to construct installations capable of protecting the surroundings of the boilerhouse from all nuisances. These installations, however, are so expensive that very seldom would one be justified in putting them into practice. Therefore one has to make a compromise between the hygienic and the economic demands and to look for a solution which will obtain a reasonable protection of the environment of the boilerhouse at a reasonable cost.

First of all, the stacks should be of sufficient height, and rise above the disturbed and turbulent layer of the wind near the earth's surface, so that the flue gases leaving the stacks will be free from the influence of eddy winds. In Holland a minimum height of $1^1/_2$ times the height of the highest building in the neighborhood is prescribed. For large industrial installations this height certainly would be insufficient.

Experimental investigations in a wind tunnel have shown that, depending on the nature of the surroundings, the stack should be about 2 to 3 times as high as the highest building. For large boilers the height of the stack should be at least 300 ft.

The cheerless outlook of some of the older industrial areas and the permanent hazy atmosphere which the people of these districts have to endure, result principally from the insufficient height of the stacks. A high stack not only provides good protection against the nuisance caused by sulphuric stack gases, but lessens considerably the inconveniences created by the settling of dust particles.

A simple reasoning may prove this fact. If by a horizontal wind (velocity w) a dust particle (rate of settling V_g) leaves a stack (height H), the settling time t_v of the particle on buildings (height h) will amount to

$$t_v = \frac{H - h}{V_g}$$

During this time t_v, the particle will be conveyed a distance s_h

$$s_h = wt_v = \frac{w(H - h)}{V_g}$$

in the direction of the blowing wind.

Even if the average velocity and the average direction of the wind should remain constant for some time, all dust particles V_g leaving the stack will not settle on the same spot, but will be spread over an area with a radius s_r owing to the deviations of the wind from its general direction

$$s_r = c_1 s_h = c_1 \frac{w(H - h)}{V_g}$$

(c_1 = proportionality constant of wind deviation.) From this we presume that the deviation s_r will be proportional to the settling time t_v of the particle.

If the weight of the dust particles leaving the stack in a certain time amounts to G lb, the average deposit on the exposed area will be

$$A = \frac{G}{\pi s_r^2} = \frac{GV_g^2}{(H - h)^2} \frac{1}{\pi c_1^2} \frac{1}{w^2} \quad [1]$$

This weight A of the deposit might be expressed in grains per square foot per day and considered as a measure of the nuisances in the exposed region.

If this measure is accepted, the nuisance will be proportional to the weight G, the square of the rate of settling V_g, and inversely proportional to the square of the height $(H - h)$ of the stack above the surrounding buildings. In reality the favorable influence of a high stack is still more prominent than according to Equation [1], as the velocity of the wind will increase on higher levels above the ground

$$\frac{dw}{dH} > 0$$

so the average velocity w of the wind will increase with H. Furthermore, the eddy winds near the ground will influence the path of the falling dust particle over a smaller portion of its total way.

The rate of settling of a globular dust particle following Stokes' law (Reynolds number $Re < 1$) will be proportional to the square of the diameter δ

$$V_g = \frac{1}{18} \frac{\delta^2(\gamma_s - \gamma_L)}{\eta_L} = c_2\delta^2$$

if γ_s, γ_L, and η_L are constant. Therefore the nuisance caused by the particle will be proportional to δ^4 (see Equation [1]).

However, the supposition that the weight of the dust settled on a square foot per day should be a measure of the nuisance may be argued. Strong arguments can be put forward to prove that not the weight, but the surface of the dust deposit will determine the nuisance. In that case the nuisance will be proportional to δ^2 and not to δ^4. Even so, it will be clear that the inconveniences caused by coarse dust particles leaving the stacks will be more serious than those caused by the same weight of fine particles. Not the over-all collecting efficiency alone, but also the size distribution of the dust particles escaping the dust separator is essential for the evaluation of the collector. The separator should be selective, and should extract particles with a settling rate of 1 cm per sec or more ($\delta \cong 25$ microns) almost completely.

Mechanical dust collectors working on the principle of separating by centrifugal forces are generally very selective. In com-

---

[1] Professor of Mechanical Engineering, Delft University.

Contributed by the Fuels Division of The American Society of Mechanical Engineers and presented at the Fifteenth Annual ASME-AIME Fuels Conference, Philadelphia, Pa., October 30–31, 1952.

Note: Statements and opinions advanced in papers are to be understood as individual expressions of their authors and not those of the Society. Manuscript received at ASME Headquarters, September 10, 1952. Paper No. 52—FU-1.

bination with a high stack these collectors may give good results in many cases.

In several countries rules are prescribed in order to keep the inconveniences caused by boiler plants within bounds. In some of these countries it is prescribed that the dust content of the flue gases should not exceed 1 gram/nm³.

This prescription is insufficient as no account is taken of the total amount of the dust leaving the stack, the size of the particles, the height of the stack, or the nature of the surroundings.

In Holland a dust content of 1 gram/nm³ is permitted for stacks 50 m in height. For other heights the dust content may vary in proportion to the square of the height H of the stack. Thus for a height of 100 m the dust content may rise to 4 grams/nm³. Furthermore, it is prescribed that the weight of the coarse dust particles ($\delta > 50\mu$) should be limited to 2½ per cent of the total dust quantity leaving the stack. For large boiler plants these rules are not sufficient and special prescriptions will be required.

It may be observed that, although the deposit A, Equation [1], will be small for fine dust particles, the area (πs_r^2) of this deposit will be much larger than for coarse particles. The nuisance will be limited, but the exposed region will be larger.

Experience has proved, however, that no complaints will arise if the deposit A is kept within certain bounds.

Different Types of Cyclone Dust Collectors

The cyclone is one of the oldest and most efficient mechanical dust collectors in use for the cleaning of flue gases. Many different types of cyclones have been constructed for this purpose.

In this paper only a few types of cyclones tested or developed in the author's laboratory at the Technical University at Delft will be discussed.

Fig. 1 shows types of cyclones composed of a cylindrical upper portion with a concentrically placed exhaust pipe, and a conical under portion connected to the dust bunker. We may call these cyclones "complete cyclones" to distinguish them from the cyclone constructions shown in Figs. 2 and 3.

In the cyclones, Fig. 1, the dust-laden gases enter more or less tangentially into the cylinder and rotate around the exhaust pipe. The rotation is continued in the exhaust pipe and even in the dust bunker. In order to obtain a strong centrifugal field in the cyclone and a high collecting efficiency, the rotation of the gases nowhere should be hindered by guiding vanes, spiral ducts, or regulating devices of any kind. Even the checking of the rotation inside the gas-exhaust pipe and the dust bunker has an unfavorable influence on the efficiency. The dust bunker should be emptied in time and its size should be so great that the gases may rotate freely inside the bunker.

The cyclone type A, Fig. 1, is an example of the well-known orthodox cyclone design. The gases entering the cyclone cylinder meet the rotating gases with a shock at the point P. By this shock the entering dust particles may be thrown to the center and to the exhaust. The unfavorable influence of the shock can be lessened by increasing the height h of the cylinder and the length S of the exhaust pipe.

Better cyclone constructions are represented by the types B and C in Fig. 1. Here the gases enter without severe shocks on the rotating mass of gas.

If the distribution of the dust particles over the inlet surface of the cyclone is even, a portion of these particles will enter into the cyclone cylinder near the center and near the exhaust at a spot where the separating efficiency is low. To avoid this, the cyclone type D, Fig. 1, is shaped for a gradual entry of the gases at the circumference of the rotating gas mass inside the cyclone.

The cyclones A, B, C, and D require a large space. To

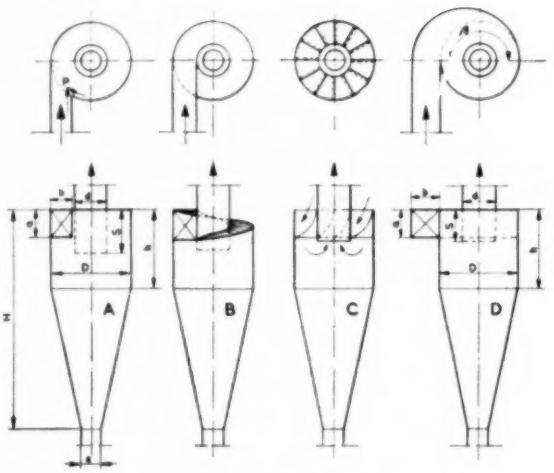

Fig. 1 Different Types of Cyclones

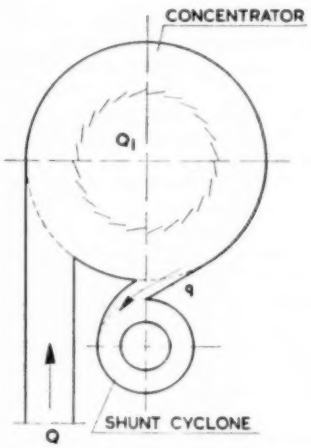

Fig. 2 Cyclone With a Shunt Cyclone

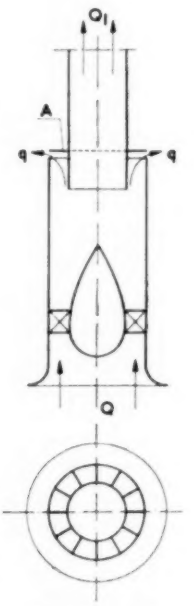

Fig. 3 Cyclone of the Straight-Through Type

economize on space and initial costs the cyclone constructions in Figs. 2 and 3 have been designed. In a dust-laden vortex the dust particles will be centrifuged to the circumference, whereas in the center the dust content of the gases will be considerably lower. In these cyclones, Figs. 2 and 3, the gas flow Q is split into a large portion Q_1 with a low dust content and a small portion q with a high dust content. The portion q passes an efficient shunt cyclone, whereas Q_1 is carried off to the stack. Generally the collecting efficiency of the small shunt cyclone will be much higher than that of the first-stage cyclones in Figs. 2 and 3; therefore the over-all efficiency η of the whole installation will increase with an increasing proportion q/Q, Fig. 4.

Although the collecting efficiency is lower than that of a

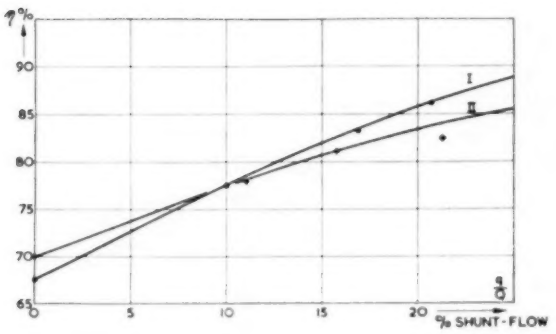

FIG. 4 EFFICIENCY η OF A STRAIGHT-THROUGH CYCLONE IN RELATION TO THE PERCENTAGE q/Q OF THE SHUNT FLOW

(Curve I holds good for a cyclone without deflector ring A, curve II for a cyclone with deflector ring; see Fig. 3.)

complete cyclone with the same exhaust diameter, the space required is so small that the straight-through cyclone has provided satisfactory solutions for many industrial dust problems.

For this and most of the other tests mentioned in this paper pulverized clay dust was used with an almost constant size distribution, as follows:

Microns	Per cent
0– 5	30
5–10	12
10–20	18
20–50	28
50	12

NOTE: Specific weight $\gamma_s = 2.15$.

EXPERIMENTAL INVESTIGATIONS ON CYCLONES

Experimental investigations on a rather large scale were carried out in the Delft Laboratory in order to determine the most efficient shape for a cyclone and to attain a better insight into the flow pattern of gas and dust particles inside the cyclone. For this purpose the effect of a change in each of the principal dimensions (D, d, H, h, S, and β, Fig. 1), on the efficiency η was measured in succession on a series of cyclone models.

From these measurements it appeared that a gradual entry of the gases into the cyclone cylinder was essential to obtain a high efficiency. Good results were obtained with an inlet angle $\beta = 180$ deg; a further increase of β did not raise the efficiency.

The influence of the length S of the exhaust pipe is shown in Fig. 5. It is noteworthy that too small a dimension S spoils the effect completely. A dimension $S \cong d$, or $S \cong a$ when $a > d$, Fig. 1, may be recommended. The values for $\beta = 180$ deg and $S \cong d$ belong together, and are characteristic for all cyclones developed in the author's laboratory and for nearly all cyclones which have been designed by the author for industrial purposes.

Furthermore, the experiments showed an improvement of the efficiency η by increased proportions D/d and H/d; the space required and the initial cost, however, are also raised.

The height of the cylindrical portion may be made equal to the diameter D. A square inlet surface ($a = b$) is recommended for cyclones with a gradual inlet (type D), whereas for the orthodox cyclone, A in Fig. 1, a high and narrow inlet surface ($a > b$) will be preferable. In both cases the dust particles are led as far as possible from the center.

The centrifugal forces working on the rotating dust particles are predominant in comparison to gravitational forces, so the separation will be almost independent of the position of the cyclone. Even in an upside-down position with the cleaned gases leaving in a downward direction and the dust exhaust directed vertically upward, a good cyclone will still separate satisfactorily. Difficulties may arise, however, with the coarse particles, which will keep rotating in the conical portion and cannot reach the dust-outlet opening. One may overcome this difficulty by bending the cyclone axis so that the dust outlet will be directed downward.

Fig. 6 shows a curved cyclone with a horizontal cylinder and a downward-directed dust outlet.

Experiments have shown that the collecting efficiency of the

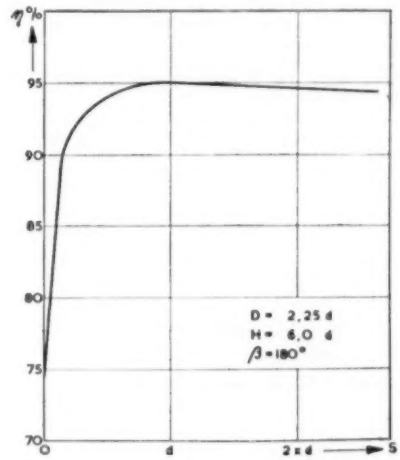

FIG. 5 INFLUENCE OF LENGTH S OF EXHAUST PIPE INSIDE CYCLONE ON COLLECTING EFFICIENCY

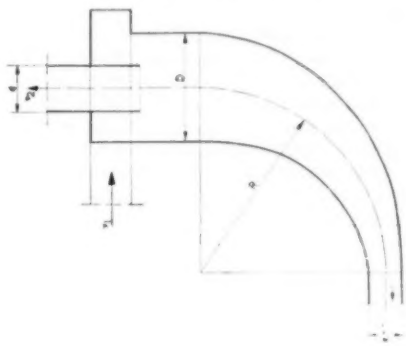

FIG. 6 HORIZONTAL CYCLONE WITH CURVED AXIS

curved cyclone is equal to that of a straight cyclone under the same conditions. In many cases it might be preferable to install a curved cyclone in view of the available space and in order to avoid curves in the gas ducts.

The gas flow in a cyclone is three-dimensional and of a very complicated nature. Without the knowledge of the course of the gases and dust particles it is useless to try to deduce theoretical formulas for the calculation of the collecting efficiency or the pressure loss of a cyclone.

In the laboratory at Delft the gas flow in a cyclone type D has been measured with the use of a Globe Pitot meter of Dr. van der Hegge Zijnen, an instrument designed to determine the gas velocity and its tangential, radial, and vertical components (v_t, v_r, v_h), as well as the total pressure p_t, and the static pressure

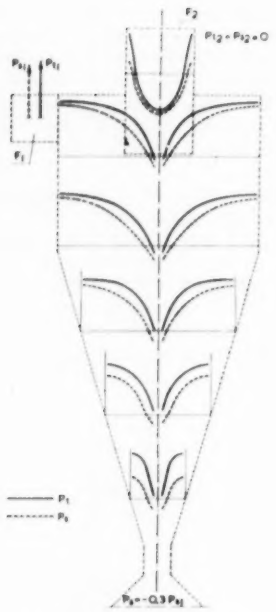

FIG. 7 TOTAL AND STATIC PRESSURES OF GASES AT DIFFERENT POINTS IN CYCLONE

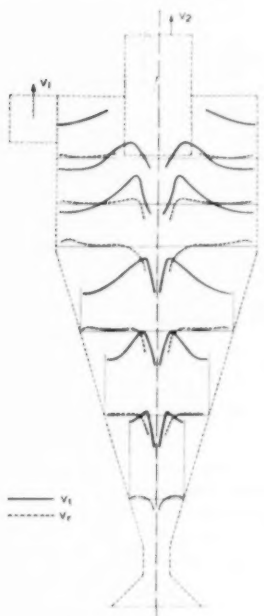

FIG. 8 TANGENTIAL VELOCITY v_t AND RADIAL VELOCITY v_r OF GASES AT DIFFERENT POINTS IN CYCLONE

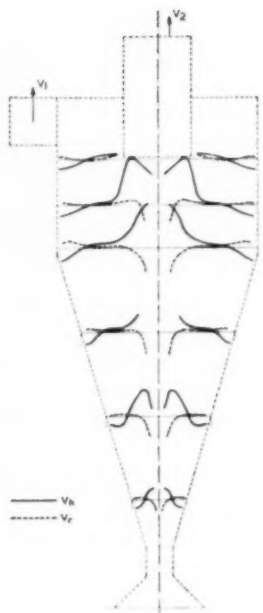

FIG. 9 RADIAL VELOCITY v_r AND VERTICAL VELOCITY v_h OF GASES AT DIFFERENT POINTS IN CYCLONE

p_s at various points inside the cyclone, without disturbing the course of the gases noticeably.

During the tests the cyclone type D had a free exhaust to the atmosphere.

The results of the measurements are shown in the Figs. 7, 8, and 9. Fig. 7 gives the variation of the total and static pressures p_t and p_s in different points in relation to the pressures p_{t1} and p_{s1} at the inlet surface of the cyclone. With the exception of the highly turbulent core in the center, the pressure is above the atmospheric pressure throughout the entire cyclone. The core of low pressure extends the full height of the cyclone and is continued into the exhaust pipe and the dust bunker, in which it causes a vacuum. If the bunker is not closed hermetically, air from outside will be drawn into the bunker and will carry the dust, which already has separated, back to the cyclone and to the exhaust. In the exhaust pipe the low pressure in the center may cause a downward flow, especially for cyclones with a relatively large exhaust in proportion to the cyclone diameter D.

It must be stated that in the unstable and highly turbulent core in the center no accurate measurements can be taken, so Figs. 7, 8, and 9 can show only approximate values in this region.

Fig. 8 shows the variations in the components v_t and v_r at various points inside the cyclone. The tangential velocity v_t is predominant in the entire cyclone, with the exception of the turbulent core in the center; v_t deviates only slightly from the total velocity v at the point. In the cylindrical portion of the cyclone, v_t increases from the circumference to the center. At a radius r, v_t can be calculated approximately by the formula

$$v_t = v_{t0}\left(\frac{D}{2r}\right)^n \qquad [2]$$

if v_{t0} represents the tangential velocity at the circumference. This tangential velocity at the circumference does not deviate much from the velocity v_1 at the inlet, ($v_{t0} \cong v_1$), as might be expected for a cyclone with a gradual gas inlet.

At a radius $r_s \cong 0.65\, d/2$, v_t attains a maximum, after which its value decreases quickly. The values of v_t in the unstable core are uncertain.

In the conical portion of the cyclone, v_t increases as the cone becomes narrower; therefore, at the same radius r, v_t is greater in the conical portion than in the cylinder.

The exponent n in Equation [2] depends on the shape of the cyclone but deviates not very much from $n = 0.5$.

The radial velocity v_r, with the exception of the turbulent core, is directed to the center. This component tries to carry the rotating dust particles to the center and to the exhaust. A low value of v_r in combination with a high value of v_t will produce a good efficiency.

Fig. 9 shows the components v_h and v_r for various points inside the cyclone. The vertical component v_h is directed downward along the outer walls, and upward in the center. The downward flow is favorable and assures that the particles which have been centrifuged to the circumference are carried off to the dust bunker. Thanks to this flow of gas a cyclone can function in an upside-down position. The upward flow in the center is unfavorable for the efficiency and will carry dust particles from the under portion of the cyclone to the exhaust. A long cone will diminish this unfavorable effect. It is clear that a cyclone with a short cone, or worse, with a flat bottom, cannot show a high collecting efficiency.

The measurements were carried out for a cyclone type D as this type showed the highest efficiency. We may assume, however, that the nature of the gas flow for the other cyclone types in Fig. 1 will not differ essentially from that of cyclone D.

By combining v_r and v_h one may get an insight into the secondary gas flow apart from the rotation round the exhaust, Fig. 10.

From Figs. 8 and 9 it may be deduced that the region in the center of the cyclone will be very unfavorable for separation.

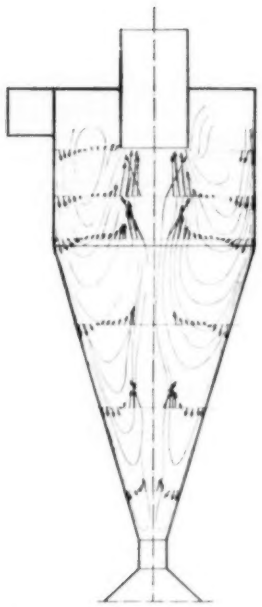

FIG. 10 SECONDARY STREAM-LINES OF GASES IN CYCLONE

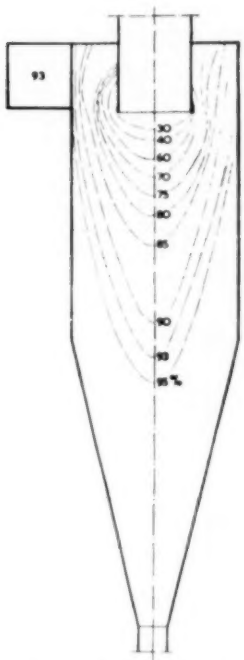

FIG. 11 VALUE OF COLLECTING EFFICIENCY AT DIFFERENT POINTS IN CYCLONE

Therefore the aim should be to keep the dust particles outside this area as much as possible.

In accordance with this conclusion are the results of the measurements shown in Fig. 11. This figure gives the collecting efficiency η at various points inside the cyclone. For this purpose dust was injected at different points by a small tube without disturbing noticeably the flow of the gases. As could be expected, a poor efficiency in the central region under the gas exhaust and a good efficiency in the area near the outer walls was obtained.

The efficiency at each point is determined fully by the extent of the three components v_t, v_r, and v_h of the gas velocity.

Although the flow pattern of gases and particles is too complicated for exact calculations, by using the results of the preceding investigations it is possible to explain most of the properties of a cyclone and to obtain information for the construction of efficient cyclones.

THEORY OF THE CYCLONE

Several authors have tried to calculate the collecting efficiency and the pressure loss of a cyclone—among others P. Rosin, E. Rammler, and W. Intelmann.[2] According to this well-known theory a dust particle could be considered as separated if it should reach the outer wall of the cyclone before reaching the bottom of the exit duct. In order to calculate the path of the particle, Rosin assumes that the gas flow, which enters the cyclone, should remain in it as a whole, and should reach the exhaust opening after n-revolutions around the exhaust in time t.

During this time t the dust particles will move in the radial direction under the influence of the centrifugal force and the viscous resistance.

[2] "Grundlagen und Grenzen der Zyklonentstaubung," by P. Rosin, E. Rammler, and W. Intelmann, *Zeitschrift des Vereines deutscher Ingenieure*, vol. 76, 1932, pp. 433–437.

The simplified flow pattern of Rosin's theory differs considerably from the real one, so it is no wonder that the conclusions do not correspond with the results of the experiments shown in Figs. 5 and 12.

Although in the author's opinion it will not be possible to deduce accurate formulas to calculate the efficiency, some simple calculations may be useful.

At every point P inside a cyclone a dust particle (rate of settling V_g) is submitted to the opposing forces of centrifugal action and resistance to the relative motion with regard to the flowing gases. The gravity may be neglected in comparison to these forces. If the centrifugal forces are predominant the particle will move to the outer walls of the cyclone and finally be separated. If, on the contrary, the viscous-gas resistance predominates, the particle will be carried away by the gases to the exhaust.

The centrifugal force working on a particle (V_g, mass m) on a radius r, tangential velocity v_t, amounts to

$$C = \frac{m v_t^2}{r}$$

The opposing resistance F working on the particle at a relative radial velocity v_r in accordance with Stokes' law amounts to

$$F = \frac{v_r}{V_g} mg$$

If $C = F$ both forces will be in balance and the particle will move at a constant distance r from the center. If this case holds good, then

$$\frac{v_t^2}{r} = \frac{v_r g}{V_g} \quad \text{or} \quad V_g = \frac{v_r r g}{v_t^2} \qquad [3]$$

For every point P in the cyclone the rate of settling V_g of a particle with $C = F$ may be calculated. At this point P dust particles with a larger rate of settling $V_{ga} > V_g$ will be separated, whereas smaller particles with $V_{ga} < V_g$ will be carried off by the gases.

If a sample of dust particles of different sizes is injected cautiously at the point P, we may observe a fan-shaped flow of the particles. The coarse particles will show streamlines directed to the outer walls, whereas the finer particles will flow to the center.

The value

$$V_g = \frac{v_r r g}{v_t^2}$$

may be considered as a measure for the "separating capacity" of the cyclone at the point P. A low value of V_g indicates a good separating capacity. V_g determines the diameter of the smallest dust particle which still will be separated at the point P.

The separating capacity varies considerably at different spots inside the cyclone as shown in Fig. 11. In the region beneath the exhaust opening the separating efficiency will be a minimum; we may call this region the "danger zone" of the cyclone. Even coarse dust particles will be carried away with the gases if these particles reach this area.

If u represents the radius of the danger zone a dust particle with a rate of settling V_{gu}

$$V_{gu} = \frac{u v_t g}{v_t^2}$$

will be in balance on the radius u and will determine the smallest particles that will be separated completely (η = 100 per cent). Smaller particles will be separated only if these can avoid the danger zone on their path through the cyclone.

The danger zone is situated under the exhaust opening, so the radius u will be nearly proportional to the radius $d/2$ of the exhaust pipe

$$u = c_3 \frac{d}{2}$$

If we assume that $c_3 = 1$ or $u = d/2$, the cyclone will separate all particles with a rate of settling

$$V_g \geq V_{ge}$$

For the smaller particles $V_g < V_{ge}$ the efficiency η cannot be calculated. The efficiency decreases quickly with a decreasing rate of settling V_g.

Although the foregoing considerations are not exact and not complete, they may be useful for the construction of cyclones. It will be clear that a good efficiency may be attained by the following means:

1 Reducing the danger zone as much as possible by increasing the tangential velocity v_t and by decreasing the exhaust diameter d and the radial velocity v_r of the gases.

2 Keeping the dust particles in so far as possible outside the danger zone by arranging a gradual admission of the dust-laden gases into the cyclone cylinder and by increasing the proportions D/d and H/d of the cyclone.

Pressure Drop in Cyclones

The gases leaving the cyclone keep on rotating in the exhaust pipe. Therefore the pressure in this pipe will be higher at the circumference than in the center. If we consider the pressure drop Δp of the cyclone, it will be necessary to know at which spot in the exhaust the pressure has been estimated. In this paper the pressure losses are all estimated for cyclones with a free exhaust into the atmosphere. The pressure drop is expressed as the drop in total, i.e., static pressure between the inlet of the cyclone and the atmosphere (p_{i1} and p_{a1} in Fig. 7).

If guide vanes are fitted in the exhaust the pressure drop may be diminished considerably, likewise the pressure differences in the exit surface. A considerable amount of the kinetic energy of the rotating gases can be recovered by these vanes, but only at the cost of the efficiency.

The pressure drop depends on the shape of the cyclone, especially on the proportion m

$$m = \frac{F_2}{F_1} = \frac{\text{exhaust surface}}{\text{inlet surface}}$$

It depends further on the proportions D/d and H/d and on the specific weight γ of the gases. The pressure drop is approximately proportional to the velocity head

$$\frac{v_1^2}{2g} \gamma$$

of the gases at the inlet, and thus to the square of the gas velocity at the inlet. The dust content of the gases has a slight influence on the pressure loss. A high dust content decreases the pressure loss, probably by reducing the turbulence of the gas flow.

It is tempting to try to calculate the pressure drop for a cyclone with given dimensions and load conditions, or to publish practical formulas estimating the pressure drop. Only by assuming considerable simplifications can results be attained. It is doubtful, however, if these results will be of much practical value.

In the usual range for the inlet velocity v_1, 20 to 80 fps, the pressure drop may be expressed by the formula

$$\Delta p = \xi \frac{v_1^2}{2g}$$

The factor ξ depends on the shape of the cyclone, is only slightly dependent on the size of the cyclone and the load, and may be determined experimentally on a smaller cyclone model of the same form. Although ξ for a large cyclone differs a little from that measured on a small model, the results of the measurements are still more accurate than those obtained by a pure theoretical calculation.

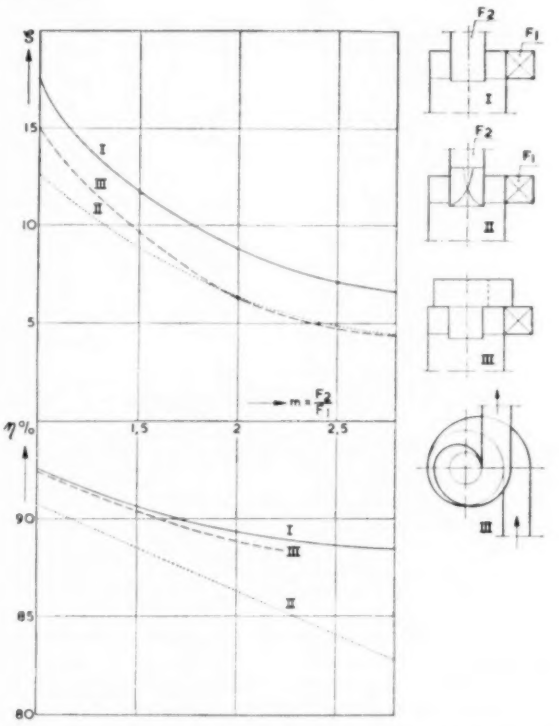

Fig. 12 Coefficient of Static Pressure Loss ξ and Efficiency η in Relation to Different Proportions $m = F_2/F_1$

In Fig. 12 the factor ξ is represented for different values $m = F_2/F_1$; the dimensions D, H, S, a, and b are the same in all cases shown in Fig. 12.

The curve I shows the relation between ξ and m for a cyclone (type D) with a straight exhaust into the atmosphere.

The curve II in this figure shows the relation between ξ and m for a cyclone with a straight exhaust fitted with guiding vanes.

The curve III holds good for a cyclone with a scroll outlet. The inlet velocity v_1 = 35 fps for all measurements in Fig. 12. For the three cyclones the efficiency is indicated also in relation to m. Considering both the pressure losses and the efficiency, the cyclone type with the scroll outlet seems to give the best results.

Efficiency in Relation to Load of Cyclone

The opinion that a cyclone needs high gas velocities in order to obtain a good efficiency is widespread but not correct. A well-proportioned cyclone will show a good collecting efficiency for

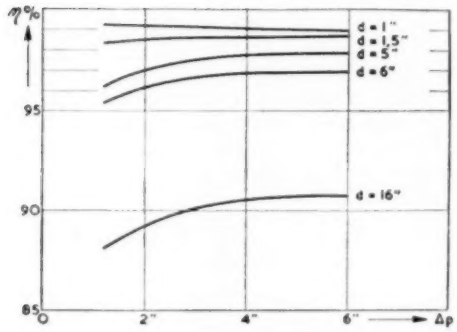

FIG. 13 EFFICIENCY η IN RELATION TO STATIC PRESSURE DROP Δp FOR CYCLONES OF DIFFERENT SIZES

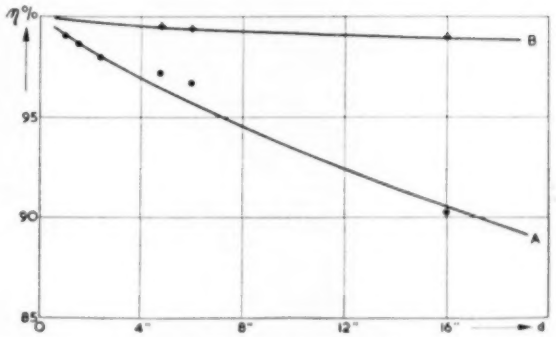

FIG. 14 EFFICIENCY η IN RELATION TO SIZE OF EXHAUST DIAMETER d FOR CYCLONES OF TYPE D, FIG. 1

the whole velocity range that may occur in practical use. Regulating devices are generally superfluous and often harmful.

Fig. 13 shows the efficiency in relation to the pressure drop in the cyclone (type D). The efficiency curves are rather level. For the smallest cyclone (exhaust diameter d = 1 in.) the efficiency is highest for the lowest load, whereas for the larger cyclones, η increases a bit for higher loads. The differences are small, however.

For boilers the dust content of the flue gases depends on the load of the boiler; at a low load the dust content is generally small, so in this case one need not trouble about a few per cent lower efficiency of the separator.

According to Equation [3] one would expect an increasing proportion v_t^2/v_r at higher loads and thus a more prominent increase of the efficiency than shown in Fig. 13. It may be that v_r increases more quickly than v_t; or perhaps the flow pattern at a low load will be less influenced by harmful turbulent secondary currents.

INFLUENCE OF SIZE OF CYCLONE ON EFFICIENCY

From Equation [3] we may conclude that a cyclone with a small exit diameter will show a higher efficiency than a cyclone with a large exhaust under similar conditions. If a high efficiency should be required, small cyclones should be used. This will lead to the application of multicyclones containing a number of small cyclone units in parallel.

Fig. 14 shows the collecting efficiency in relation to the exhaust diameter d for a set of cyclones of different sizes. Curve A holds good for the pulverized-clay dust (fine dust), curve B for fly ash (coarse dust) with the following size distribution:

Microns	Per cent
0 – 50	52
50 – 75	24
75 –100	6
100	18

The curves in Fig. 14 are in accordance with expectations, and account for the construction of multicyclones. In many cases these multicyclones will give a good solution for a dust problem.

Nevertheless, it is advisable to be careful with the application of multicyclones with a common dust bunker for all unit cyclones, as the efficiency of the multicyclone may be considerably lower than that of the small cyclones of which it is composed. This drop in efficiency may be caused by slight irregularities in the distribution of the gases over the cyclones. There may be differences in pressure in the dust-outlet openings of the unit cyclones which will cause vertical gas currents in these openings. These currents may spoil the efficiency completely by carrying the already separated dust particles from the bunker to the gas exhaust.

To avoid these upward currents, in some installations gases are sucked out of the dust bunker by a special fan, in order to obtain a downward gas flow in every dust outlet. The gases sucked out of the bunker have to be cleaned in a shunt cyclone. This solution is rather complicated and in the author's experience does not always meet expectations.

Another solution of this problem may be found by producing automatically an even distribution of the gases over the cyclone units. This may be attained by fitting the units in a large casing, where the velocity v and the kinetic energy of the flowing gases will be small. The gas-exhaust pipes, too, should discharge into a large room with low gas velocities.

Figs. 15 and 16 show multicyclone constructions for stoker-fired boilers in accordance with the foregoing specifications.

Fig. 15 shows a multicyclone composed of cyclone units like

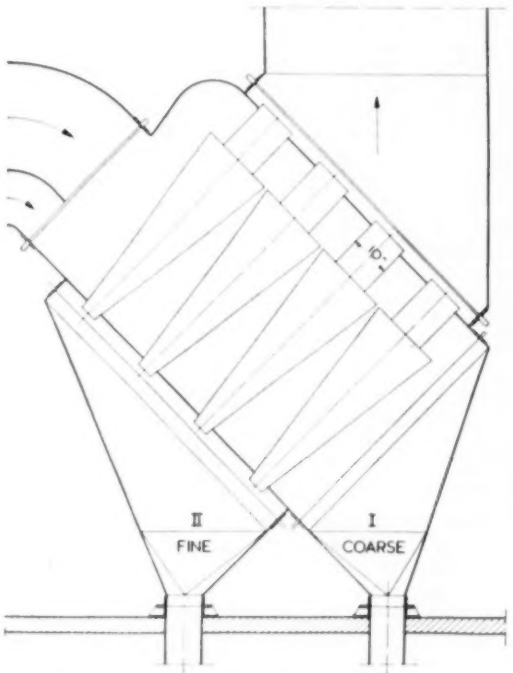

FIG. 15 MULTICYCLONE FOR STOKER-FIRED BOILER COMPOSED OF CYCLONES OF TYPE C, FIG. 1

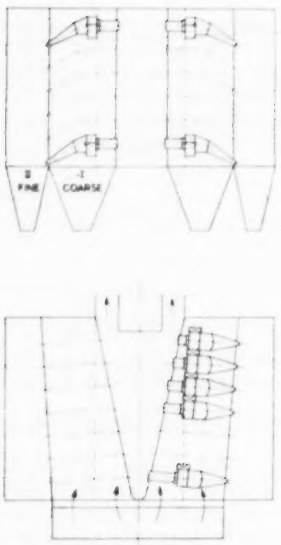

FIG. 16 MULTICYCLONE FOR STOKER-FIRED BOILER COMPOSED OF CYCLONES WITH CURVED AXIS

type C; Fig. 16 is a multicyclone with curved cyclones. In both separators the coarse dust particles will settle in the large casing and not enter the unit cyclones. This will reduce the wear of these cyclones considerably.

CONCLUSIONS

The following systems of dust collectors may be recommended:

1 For small grate-fired boilers with a maximum capacity of about 30 ton per hr, one or two complete cyclones in parallel. The exhaust should not exceed 5 ft.

2 For larger grate-fired boilers, a highly efficient multicyclone. To prevent the blocking up of the small passages the exhaust diameter d of the cyclones should not be less than 5 in.

3 For pulverized-fuel boilers, in an industrial or rural district, a highly efficient multicyclone or a multicyclone of simple design in combination with an electrostatic precipitator.

4 For pulverized-fuel boilers in a residential district, a multicyclone in combination with a highly efficient electrostatic precipitator.

In all these cases a high stack is necessary in order to avoid creating a nuisance to the surroundings.

Discussion

T. A. PIERSON, 3RD.[3] Mr. ter Linden's paper is an interesting one. His attack of the problem seems quite logical in studying the internal-flow characteristics in order to evaluate the probable efficiencies. The plotting of the velocity and pressure measurements does much to clarify the operation of these units.

[3] Research Corporation, Bound Brook, N. J. Jun. ASME.

In this country the type C design is more generally used on present-day large installations of 300,000 cfm and up because it can be more easily integrated with the flue arrangements of large equipment. The writer's company has used this type of collection in series with electrical precipitators on occasion with advantage. This size is smaller than suggested by ter Linden, being only a 9-in. outside tube diam. Volumes of about 500 cfm per tube can be handled at pressure drops of 2 to 3 in. and will provide efficiency about 75 per cent depending on the dust analysis. The test dust used by ter Linden is similar but somewhat coarser than the average fly ash produced in generating stations in this country as is noticed in the following comparison.

Microns	ter Linden, per cent	Avg. U. S. fly ash, per cent
0–5	30	35.8
5–10	12	22.3
10–20	18	21.4
20–50	28	14.1
50	12	6.5

In relation to the discussion on stack design it might be pointed out that the practical factors of gas temperature and velocity and major turbulence materially contribute to actual gas dispersion. Sometimes generating stations are located in the vicinity of major airports and the stack height is necessarily limited. Considerable study has been made in this country to determine methods of increasing the effective height of the stack without increasing its actual height. Gas velocities up to 120 fps or four times the probable wind speed have been found necessary to prevent the discharge plume from being carried down to the ground. Proper shaping of the stack itself has been found to increase the effective stack height as much as 25 per cent for the same gas velocity. Considerable use of gas-flow models has been found necessary for studies of this nature.

AUTHOR'S CLOSURE

The author agrees that the cyclones of the B and C types require less space, and therefore will be easier to install than the cyclones of the D type. The collecting efficiency, however, of these cyclones will be considerably lower than that of the D type.

In the case mentioned by Mr. Pierson, where the multicyclone is installed in series with an electrical precipitator, this lower efficiency may not be serious. Otherwise, if the multicyclone has to do the work alone, without the help of an expensive electrofilter, it may be necessary to choose the most effective type of cyclone (D).

Apart from the blocking up of the passages to be feared when very small units are installed, a thin layer of dust or soot deposited on the surfaces of the gas inlet will cause irregularities in the gas distribution over the cyclones and spoil the collecting efficiency. So, in the author's opinion, very small units with a gas exhaust of less than 5 in. are not advisable. Finally, the difference in size between a cyclone with an exhaust of 5 in. and the cyclone mentioned by Mr. Pierson with a diameter of 9 in. will be small.

According to Equation [1], increasing the effective height (H-h) of a stack by increasing the gas velocity will certainly ameliorate the nuisance in the neighbourhood of a boilerhouse. This measure will be most effective for stacks with a large diameter dealing with large quantities of gas.

FIG. 1 GENERAL VIEW OF OIL-SHALE DEMONSTRATION BRANCH PLANT, RIFLE, COLO.

Mechanical Design in Oil-Shale Retorting Plants

BY L. H. BRAKEL,[1] RIFLE, COLO.

For retorting of oil shale, the primary elements are handling of large quantities of crushed shale, in a satisfactory manner for good heat exchange, through a suitable retorting vessel; generation of the necessary heat at the temperatures required for retorting; controlled exchange of heat to the shale in the amount required for retorting; passage of a carrier fluid through the retorting shale to pick up the retorted oil; and further passage of this carrier fluid with the retorted oil through suitable equipment to separate and recover the oil from the fluid stream. Of the processes tested experimentally by the Bureau of Mines at Rifle, Colo., the gas-combustion process is most efficient and most economical in operation. No water is required. The simplicity of the design, the gravity flow of shale through the retort, the heat-exchange zones to keep all practicable heat within the retort, and the few simple mechanical devices make this retort both low in construction cost and most economical in operation.

INTRODUCTION

OIL shale is not a shale but a marlstone containing very little oil as such. It contains a solid organic substance, commonly termed "kerogen," which is only slightly soluble at ordinary temperatures.

The production of synthetic liquid fuels from oil shale involves four distinct operational phases; namely, mining, ore preparation, retorting or conversion of the kerogen to a crude liquid hydrocarbon, and refining of crude shale oil into products in commercial demand, similar to those obtained from petroleum.

Although oil-shale industries have existed in foreign countries since the middle of the past century, the technology as practiced elsewhere is, for the major part, not applicable to American oil shales. To develop the technology for the successful utilization of American shales, oil-shale research laboratories were established at Laramie, Wyo.; and an experimental oil-shale mine, pilot plants for developing new processes, and demonstration retorting and refining plants were established at Rifle, Colo., Fig. 1.

The Rifle project is actively engaged in technical development work on the four operational phases of mining, ore preparation, retorting, and refining. Considerable progress has been made in developing mining techniques and machines for producing large quantities of ore at low cost. These techniques include development of large, unsupported underground openings and development of bits and shot-hole patterns, as well as design and construction of specialized machines for mechanized gang drilling, rotary drilling, scaling, and shot-hole loading equipment. The technology of retorting and refining is not as far advanced as that of mining, primarily because of the complex chemical structure of

[1] Mechanical Engineer, Bureau of Mines.

Contributed by the Petroleum Division and presented at the Petroleum Mechanical Engineering Conference, Kansas City, Mo., September 22–24, 1952, of THE AMERICAN SOCIETY OF MECHANICAL ENGINEERS.

NOTE: Statements and opinions advanced in papers are to be understood as individual expressions of their authors and not those of the Society. Manuscript received at ASME Headquarters, June 10, 1952. Paper No. 52—PET-10.

kerogen and the crude oil obtained from it. Although both are hydrocarbons, the presence of sulphur, nitrogen, and oxygen in combination within the molecular structure presents problems that do not lend themselves to easy solution.

The most noteworthy mechanical design developments have been in mining machines and in retorting equipment. The mining machines have been described in Bureau of Mines articles (1)[1] and publications (2).

Crushing oil shale presents the problem of crushing several types of materials as a mixture. The Green River shale deposit is in mixed layers of comparatively rich and lean ore. It is mined as a mixture of these various ores. The leaner ore is a hard abrasive rock that fractures more readily across the grain. The richest ore is only mildly abrasive, very tough and springy, and fractures with the grain into long, thin flakes. Since it is not practicable to mine or crush the different grades separately, they must be handled as a mixture in the same crushing equipment.

The demonstration refinery became available during 1949 for refining-development work. The investigations made up to the present time have utilized simple refinery operations. These have been described in Bureau of Mines articles (3) and publications (4, 5).

Retorting and the latest design developments of retorting equipment are discussed in this paper.

Mechanism of Conversion of Solid to Liquid Hydrocarbon

Heating is the essential element for converting solid hydrocarbon in oil shale to liquid hydrocarbon. This conversion process by heating is called retorting.

The elementary requirements of a retorting apparatus are that it be a set of apparatus for the necessary handling of crushed shale, heating the shale throughout to the temperature required to accomplish retorting, and discharging the spent shale, preferably after recovery of its sensible heat; passing a carrier gas through the retorting shale to pick up the retorted products, then through the oil-recovery part of the apparatus to recover the oil.

It is apparent that during retorting, as the very small particles of kerogen reach retorting temperature, they spurt minute quantities of combined oil aerosols and gas into the surrounding carrier fluid. For the kerogen particles on the surface of the shale pieces a lower temperature probably causes the reaction, or a partial reaction, because little or no pressure is required to break down the particle enclosure. It seems reasonable to assume that more pressure is required for kerogen particles inside a piece of shale that would also require a higher temperature for retorting. Soaking time is required for heat flow from the surface of the shale lump to its interior against the outward flow of retorted products. The increasing rate of flow of retorted products, from the interior of the shale pieces with an increase in retorting rate, is probably the prime factor in limiting retorting rate. The oil aerosols and gas emitted in retorting are dispersed into the carrier fluid and carried out of the retort with the fluid. Coke from the kerogen is left on the spent-shale particles. If the hot, product-laden fluid is passed through cooler shale to heat the shale and cool the fluid, some gas condensation and oil-aerosol-particle precipitation will take place on the shale, the amount depending to a large extent upon the final temperature of the fluid. These deposited products will be distilled, and to some extent cracked, as the shale they rest on reaches the hot retorting zone. The carbon deposit in the spent shale is thereby increased, and probably the quality of the oil produced is slightly improved. In most recent Bureau of Mines retort designs this cracking is a rather small amount.

[1] Numbers in parentheses refer to the Bibliography at the end of the paper.

One of the important parts of the recovery system is an apparatus suitable for agglomerating and washing out the oil aerosol from the carrier-gas stream.

It is desirable to reduce the temperature of the spent shale before it leaves the retort unit (*a*) to recover heat from it, and (*b*) to facilitate handling spent shale, which is easier to handle when cool in the large quantities required for industry-scale operations.

An average of 16.8 per cent of Green River oil shale now considered for commercial development is organic material referred to as solid hydrocarbons or kerogen. This shale contains a relatively high percentage of carbonates, which, by their endothermic reaction, become important heat consumers if decomposed. Temperature and time together—time being required to bring all parts of the particle to a temperature—determine the amount of carbonate decomposition. Figs. 2 and 3 show this relationship for test conditions.

About one third of the carbonates are magnesium which begins to react appreciably at approximately 950 F. This temperature is below the maximum used in most retorting processes, thus becoming an unavoidable heat loss and source of CO_2 in the product gas. The 70-ft-thick mahogany ledge, which is the part of the Green River shale formation now considered for industry development, contains total mineral CO_2 averaging 18.9 per cent (6).

The heat content of raw shale is shown in Fig. 4. The retorting heat of shale under test conditions is shown in Fig. 5. The heat content of spent shale is shown in Fig. 6. The actual heat required for retorting the kerogen under precise retorting conditions has not yet been determined accurately. It is complicated by carbonate decomposition and other highly variable conditions that may depend upon several factors. The retorting of Green River shale is fully accomplished in a Fischer assay retort at 932 F, with a soaking time of 30 min (7). This is similar to, but is not the same condition as in a production retort.

The carbon residue on the retorted shale varies with the process. For the gas-combustion process, it is between 2 and $2^1/_2$ per cent.

Retorting Processes

The heat required for retorting is most frequently obtained by combustion of the carbon residue on the spent shale, combustion of the noncondensable gas from the retorting process, and recovery of the sensible heat in the spent shale and product gas[2] leaving the retort.

Heat may be transferred to the shale in the retort by many methods. Those more frequently used in retort designs are by the following:

(*a*) Transmission through an externally heated wall.

(*b*) A carrier fluid heated in an external heat exchanger.

(*c*) A carrier fluid heated by burning a part of the noncondensable gas in the fluid stream.

(*d*) A carrier fluid heated by burning carbon from the spent shale.

(*e*) Contact with hot solids, such as spent shale, which have been heated outside the retorting zone by burning residual carbon or by other means.

There are combinations of these methods of heating. In some foreign retorts, steam is used to increase the gas yield or aid in the recovery of by-products.

In processes using a carrier fluid, the contact with the shale may be by crossflow, concurrent flow, or countercurrent flow. Recent designs have favored gas as a carrier fluid and countercurrent-flow heat exchange.

[2] Product gas is any gas containing the products of retorting and includes make gas, the gas produced in the retorting reaction, combined with the carrier or recycle gas.

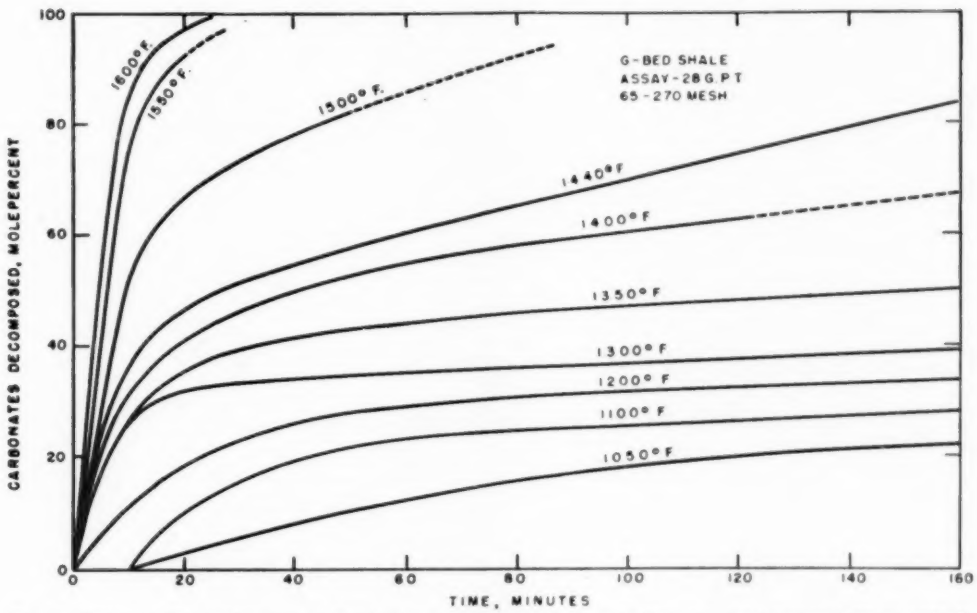

FIG. 2 THERMAL DECOMPOSITION OF CARBONATES IN OIL SHALE, CARBON-DIOXIDE ATMOSPHERE 1050 TO 1600 F

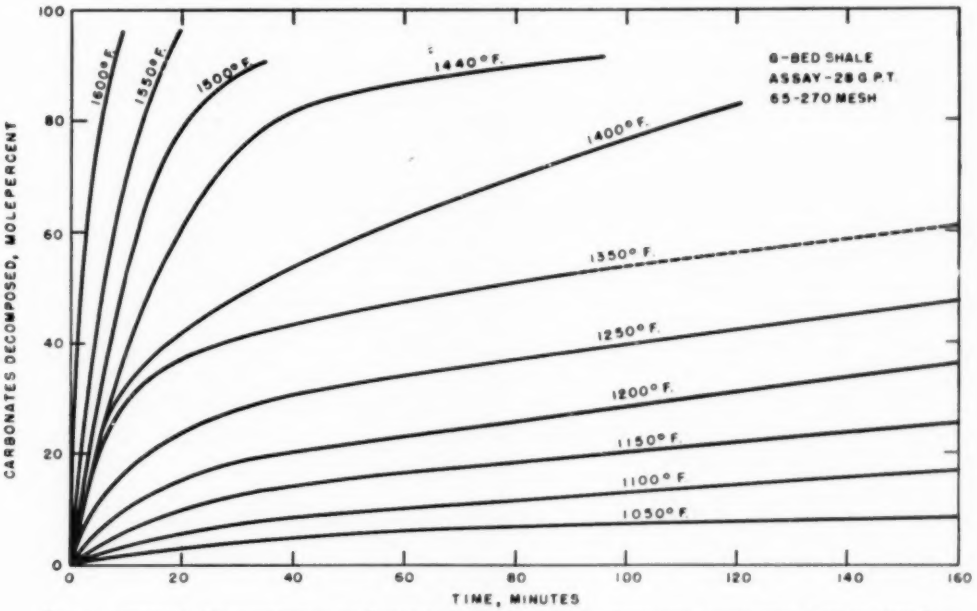

FIG. 3 THERMAL DECOMPOSITION OF CARBONATES IN OIL SHALE, NITROGEN ATMOSPHERE 1050 TO 1600 F

The Gas-Combustion Process

The Bureau's Oil-Shale Demonstration Branch at Rifle, Colo., has designed and pilot-plant-tested several retorting processes. These have gone through a continuing series of improvements and developments based on new designs and additional information obtained from laboratory and pilot-plant operation. These test results coupled with economic studies have shown that the gas-combustion process, recently invented and developed by the engineers at Rifle, is the most promising of all those yet studied.

This retorting process uses vertical, continuous, gravity shale flow and countercurrent flow of carrier gas in a simple lined retort shell. Carrier gas[4] is preheated by heat exchange with the spent shale and finally heated at the top of this lower heat-exchange zone by burning some carrier gas and a part of the re-

[4] Recycle gas is gas recycled to the retort for a heat-exchange medium and to carry the retorted products. Also called carrier gas.

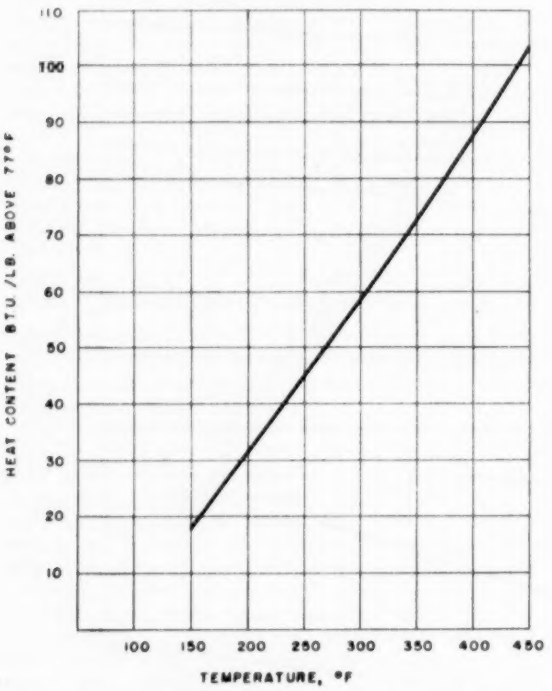

Fig. 4 Heat Content of 30 Gal Per Ton Colorado Oil Shale, Above 77 F

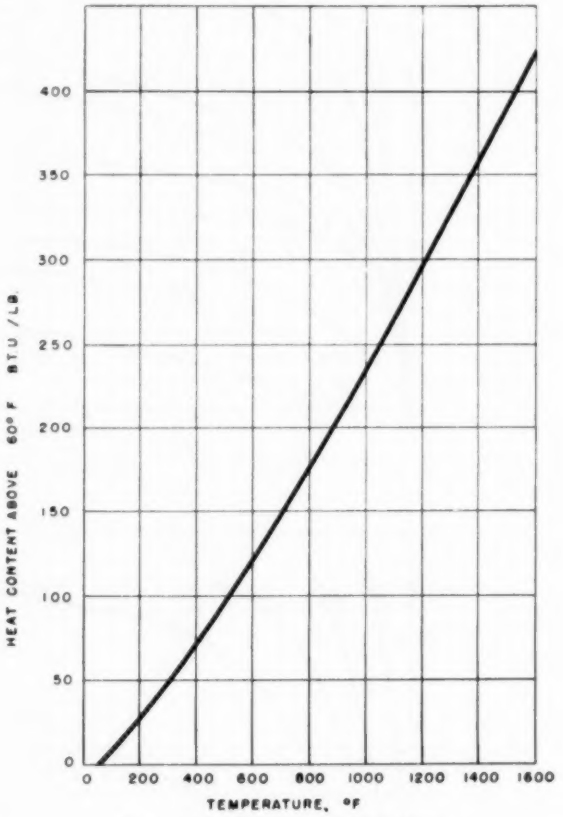

Fig. 6 Heat Content of Spent Shale

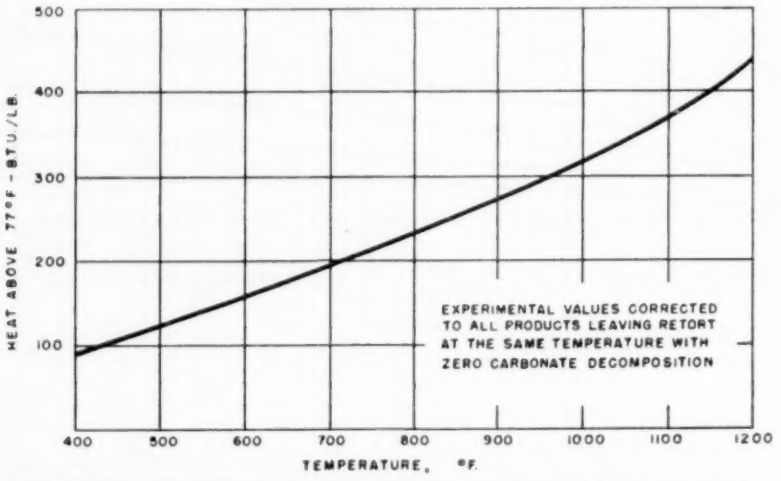
HEAT ABOVE 77°F - BTU/LB.
500
400
300
200
100
EXPERIMENTAL VALUES CORRECTED TO ALL PRODUCTS LEAVING RETORT AT THE SAME TEMPERATURE WITH ZERO CARBONATE DECOMPOSITION
400 500 600 700 800 900 1000 1100 1200
TEMPERATURE, °F

Fig. 5 Retorting Heat of Raw 30 Gal Per Ton Colorado Oil Shale, Above 77 F

sidual carbon within the shale bed, in a combustion zone,[5] at the top of this gas-preheating zone.[5] Shale is preheated by heat exchange with the product[3] gas in the upper heat-exchange zone[5] and finally heated and retorted by heat exchange with hot recycle gas[4] at, and just above, the combustion zone.[5] Typical temperatures in the retort for this process are shown in Fig. 7.

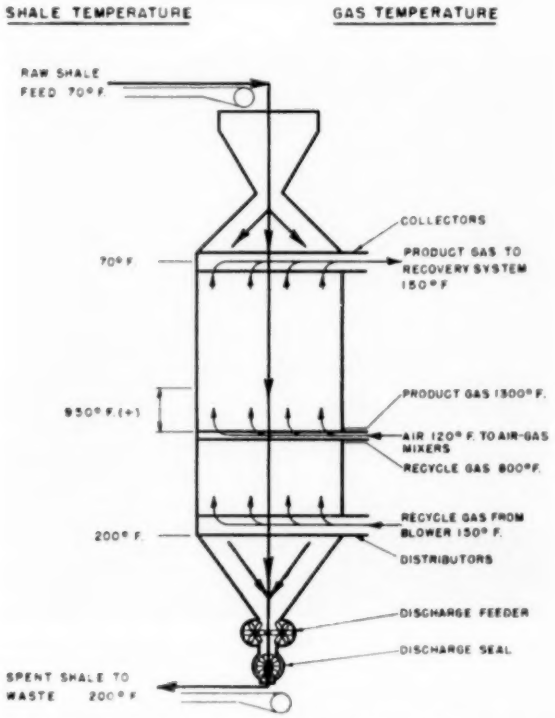

FIG. 7 GAS-COMBUSTION-PROCESS RETORT, TYPICAL TEMPERATURES

The shale is choke-fed by gravity from an open feed hopper attached to the retort, through the retort to the discharge feeder below, which controls the shale flow. From the discharge feeder through the rotary gas seal to the spent-shale disposal conveyer, the flow is free-falling. This permits the rotary seal to be oversized and reduce shale-particle shearing to a minimum.

At the bottom of the retort, the recycle gas enters through distributors to insure distribution over the area of the retort. The rotary gas seal in the shale discharge below the discharge feeder prevents the loss of significant amounts of recycle gas with the spent shale. As the recycle gas rises through the downward-moving hot spent shale, the shale is cooled to about 200 F, and the gas is heated to about 800 F by heat exchange when it reaches the air outlet from the air-gas mixers. An amount of air suited to the heat requirements, admitted to the recycle-gas stream at this level causes the combustion of some recycle gas and some carbon on the spent shale. This combustion raises the temperature of the recycle gas to about 1300 F. It is probable that the carbon combustion is a multiple reaction involving some of the water vapor included in the recycle gas.

Heat transfer from the 1300 F recycle gas to the shale is rapid, raising and holding the shale temperature above 950 F long enough for retorting to be completed. The product gas here formed includes the recycle gas, the products of combustion, the gases from carbonate decomposition, the oil vapors, and the make gas. This hot-product gas rises from the retorting zone through the descending cold raw shale to the product-gas collectors at the top of the retort. During its passage through the raw shale, the oil vapors are condensed into an aerosol and leave the retort at about 150 F and a pressure equal to atmospheric pressure. This eliminates need for sealing the retort top. The seal leg formed by the shale above the product-gas collectors is adequate for the slight variations in automatic control.

The stream of product gas is piped to the oil-recovery system. Here it passes through oil-wetted rotary washers, dry or oil-washed multiple-cell cyclone collectors, or entrainment separators. It then passes through pressurizing blowers, followed by separators, to remove any oil aerosol agglomerated in the blowers, which does not separate out in the blower casings. From here, the recycle gas is piped to the recycle-gas distributors in the bottom of the retort.

The excess gas in the recycle-gas stream is withdrawn from this stream on the discharge side of the pipe-line separators. This excess gas is sent to flare or is available for fuel. Any desired heating or cooling of the external gas stream may be accomplished by heating or cooling the wetting oil for the oil-wetted rotary washer. The liquid oil made in the process is withdrawn from the sumps of the oil-wetted rotary washer, the cyclone collector, and the blower casing.

Process information now available indicates that the most economical operation, crushing and retorting considered, will be effected when minus 3-in. crushed shale is used with half of the minus $^3/_{16}$-in. fines removed. These removed fines will be available for retorting by another process in an industry development. All the crushed shale, including fines, may be retorted together, but this would probably not be economical because of the increased power required for the recycle gas and air blowers.

The raw crushed shale weighs about 75 pcf. The spent shale weighs about 56 pcf. The process requires about 16,000 to 18,000 cu ft of recycle gas and about 4000 cu ft of air per ton of shale retorted. Approximately 6000 cu ft of 90-Btu gas per ton is excess from the process and available for fuel. Shale rate is a variable, depending upon recycle gas and air rates and the shale-bed depths above and below the air-gas mixers in the retort. Shale rates of 230 psf per hr have been maintained in extended test runs in the original pilot plant. Runs at higher rates have been made. There is every reason to believe that the 230-lb rate can be increased greatly when adequate retorts are available. For investigating operation over a wide range, a larger pilot plant and a demonstration gas-combustion retort are being built. It is expected that the most economical rate may be well over 400 psf per hr in these new plants.

DESIGN OF DEMONSTRATION-SCALE UNIT

A 300-ton per day demonstration-scale plant of this process has been designed and built. This experimental and development retorting-plant design differs from a production unit design principally in that it is designed to operate over a very wide range of conditions to provide data from which the optimum design and operation may be established. It follows that this plant must have more elaborate weighing, measuring, and sampling devices than are required for a production unit. The design must provide for several shale-bed operating depths, the maximum to be greater than the estimated maximum economical depth, to permit establishment of the optimum bed depths for set conditions. Shale flows, gas flows, and the generation of heat must be provided for in greater range than is believed to be most economical to establish the optimum values.

[5] The term "zone" used in connection with the gas-combustion retorting process is used to speak of function, as there is no separation within the retort cell.

Existing Facilities and Conditions. The size of the retorting unit was determined by the minimum size in which operating conditions could reasonably well parallel those in an industry-scale plant. These conditions resulted in a rather tall, slender retorting vessel as compared with an industry-scale plant. Existing facilities and conditions required some accommodation of the design to suit.

The site chosen for this plant was the location of the old N-T-U retorting demonstration plant. This site was in the most advantageous position with relation to other facilities. The existing structural framework for the N-T-U retorts could be used with only limited modifications, the existing shale-supply conveyer could be used, and the existing control house was suitable for reuse. The proximity to the canyon provided a location for economical spent-shale disposal. The existing oil run-down tanks could be used without change. The new instrument panel could be installed in the same location in the control house as the old control panel. The electric motor starters, previously in the control-house office, left too little office space; and the decision was made to move them to a suitable enclosure in the retort structural framework.

Basis for Design. It was decided that the basis for design would be 300 tons per calendar day at the rate of 450 psf per hr, or 5.4 tons per sq ft per day.

The design flows are shown in Table 1. A high-temperature allowance for spent shale is made because of no pilot-plant experience at the 5.4-ton per sq ft per day rate.

TABLE 1 DESIGN FLOWS AT 450 PSF PER HR

	Std. cfm	Lb/hr	Temp, deg F	Psia
Shale to retort		27200	60	12
Spent shale to waste dump		21400	300	12
Product gas from retort	5580	26200	150	12
Oil mist out of retort		3030	150	12
Gas out of precleaner	5580	26200		12 + 2 in. H_2O
Oil mist out of precleaner		910		
Gas to blower	5580	26200		
Gas from blower	5580	26200		14.5
Recycle gas to retort	4210	19800		14
Vent gas to stack	1370	6430	150	14.5
Air to blower	906		60	12
Air to retort	906		120	13.5

The design pressures and temperatures for the retort are given in Table 2.

TABLE 2 RETORT PRESSURES AND TEMPERATURES

	Working pressure, psig	Design pressure, psig
Retort top	0	5
Retort bottom	2	5
Maximum bed temperature, deg F	1500	1700
Maximum bare shell temperature, deg F	150	200

The design bed heights for three shale feeds are shown in Table 3.

TABLE 3 EXAMPLES OF SHALE-BED DEPTHS

Rate	Size, in.	Heat-exchange zone, ft	Retorting zone, ft
450	1/4 to 1	3.8	6.8
	1 to 3	8.8	16.3
	1/4 to 3	5.6	12.5

The design recycle-gas characteristics are given in Table 4. The design yield and oil characteristics are shown in Table 5.

Retorts of both round and rectangular shape were considered. The round retort offers some saving in material owing to its economical enclosing shell; however, it is not possible to design into it equal flow areas for the crushed shale through the three layers of internal fittings required in this retort design. The rectangular shape permits completely uniform distribution of the gases from

TABLE 4 RECYCLE-GAS CHARACTERISTICS

	Mol. per cent
CO_2	25.8
C_2H_4	1.2
O_2	0.2
CO	3.8
H_2	4.5
CH_4	1.6
C_2H_6	1.2
N_2	49.1
H_2O	12.6

TABLE 5 OIL YIELD AND CHARACTERISTICS

Yield, per cent	95
Specific gravity	0.938
Viscosity SUS at 150 F	147
Viscosity SUS at 210 F	51
Flash point, deg F	270
Pour point, deg F	85
Water, per cent vol	2.3
Ash, per cent wt	0.13

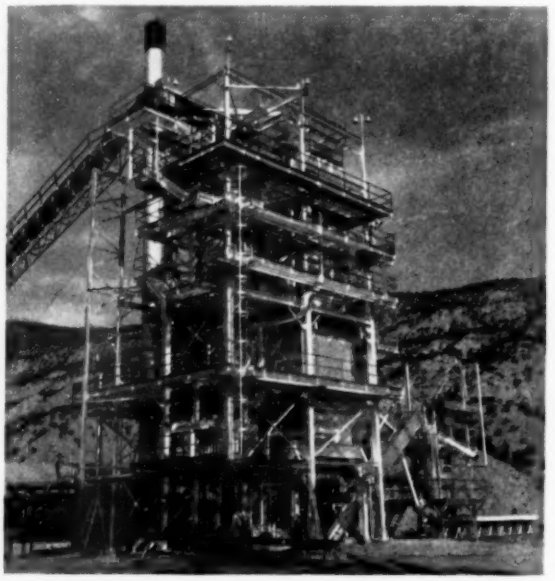

FIG. 8 GAS-COMBUSTION DEMONSTRATION RETORTING PLANT

and to these three required layers of fittings and yet allows evenly sized areas for shale flow through them. The rectangular shape also permits much simpler design of these fittings and much greater ease in making adjustments or changes to them. Since this is a test and development installation, the rectangular design had enough advantages to justify its acceptance for the installation. Fig. 8 is a view of the gas-combustion demonstration retorting plant. The existing supply conveyer limited the top height of the retort. A normal discharge would have required a pit below the retort. This was considered less desirable than a special discharge arrangement.

Meeting these requirements made it necessary to set the retort as far as practicable from the existing supply-conveyer terminal, install an inclined feed conveyer from the supply conveyer, and use a discharge arrangement somewhat different from similar equipment for an industry-size retort.

Retort and Shale-Handling Equipment. Fig. 9 is a diagram of the shale-handling system. The shale-handling system starts at the discharge of the existing supply conveyer, which is fed over a scale. A new inclined-belt charge conveyer running from this point to the location of the new retort is supported by the existing steel structure, with only minor additions. This conveyer discharges through a sampler to the retort hopper. A 3-point controller on the retort hopper maintains the shale surface level within narrow limits.

The retort shell is a vertical, rectangular, stayed-steel-plate tube 34 ft 4 in. high, with a 5-ft-high adapter section above it that supports the attached shale-feed hopper. The entire vessel is supported on two steel beams running lengthwise under the re-

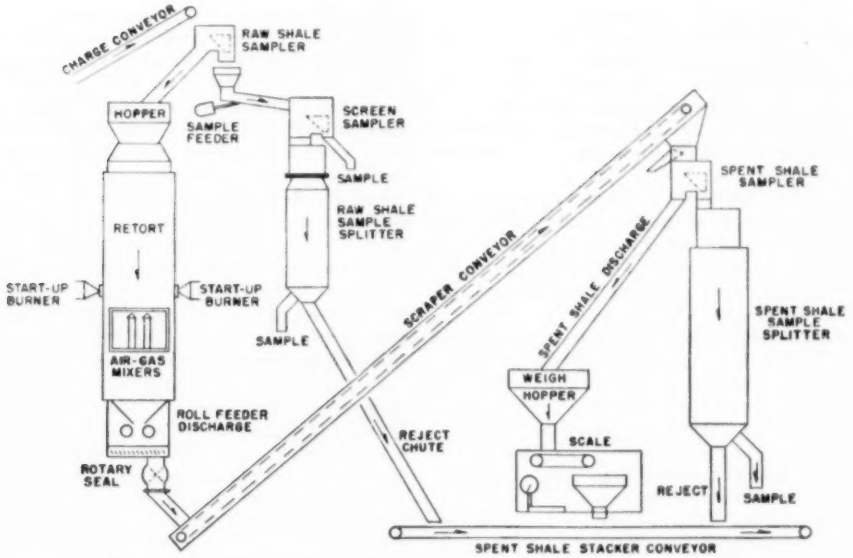

FIG. 9 GAS-COMBUSTION DEMONSTRATION PLANT, SHALE-HANDLING SYSTEM

tort. Removable side plates are provided to permit easy removal of the air-gas mixers. A 2-roll discharge feeder is mounted in an adapter section on the bottom of the retort, with the top of the rolls 11 in. below the bottom of the retort.

The relatively cool bottom 26½ in. of the retort has a steel-plate lining, faired into the refractory above, and forms part of the recycle-gas wind boxes. Above this, the retort is lined with 3 in. of hung refractory and about 3 in. of insulating material up to 12 in. above the air-gas mixers, and from this point to the top, with 3 in. of hung refractory and 3 in. to 9 in. of insulating material. The inside dimensions are 6 × 10 ft from the bottom to 12 in. above the air-gas mixers and tapering from this point to 5 × 9 ft at the top. The corners in the refractory lining are rounded. The taper and rounded corners are so designed as to promote freeness of shale flow in this relatively tall slender vessel. Removable refractory linings are installed in the sides at the air-gas mixers.

A telescoping feed chute is installed in the top adapter. This chute has a 21 × 72-in. outlet with a spreader baffle below. Its minimum length is 4 ft 5 in., and its maximum length 15 ft 8 in.

This variation in length permits varying the shale-bed depth correspondingly. The minimum normal shale bed-seal leg depth is 7 ft 6 in. above the bottom of the feed chute. This provides a cushioning seal for minor variations from zero gas pressure at the gas offtake. Two round-bottom inverted V-product gas collectors run lengthwise across the retort on 36-in. centers, at a minimum of 10 ft 10 in. below the normal bed top in the feed hopper. There are four positions in which these collectors may be installed, spaced 3 ft 4 in. vertically.

The original air-gas mixers are patterned from the type used in the January, 1952, test run of the pilot plant. They are installed on 26-in. centers with 4 full mixers, and with half units at each wall, across the short dimension of the retort, and at 15 ft 1¼ in. above the bottom of the retort. The removable side plates in line with these mixers, and trolley hoists provided, facilitate removal and adjustment of these mixers. Provision is made for changing their center-to-center distance and replacement with other designs.

At the retort bottom, a double louver is run lengthwise on each side of the retort. These louvers open continuously into recycle-gas wind boxes. The louvers are removable and adjustable if required to improve the recycle-gas distribution.

A mock-up of a rectangular retort discharge, complete with a 2-roll discharge feeder, was built in the pilot plant and tested. The results of these tests showed that, with vertical end plates and side plates sloping less than 30 deg from the vertical, such a 2-roll feeder would discharge the shale and cause the shale flow, over the area of the rectangular retort above, to be even and level. These conditions have been complied with in this design. The rolls of the 2-roll feeder are 18-in-diam cleated rolls, 9 ft 9½ in. long. This size was arrived at on the basis of shale-particle size and would not necessarily be larger for a larger retort.

The 2-roll feeder is driven by a 1:1 to 6:1 ratio, infinitely variable, a-c eddy-current brake, "Adjusto-Spede" drive. This unit will maintain the desired speed within plus or minus 0.5 per cent of the set speed. Additional feed variation is provided for by the adjustment of the roll center-to-center distance. Gasketed plate seals with clamp plates are provided where the shafts pass through the retort wall. A separate drive shaft is run on one side of the feeder, with a steel-roller chain drive to each end of both feeder rolls. A wide-range chain take-up permits adjustment of the roll.

To conserve headroom and insure breaking of any lumps in the spent shale, a 16-in. screw conveyer with breaker teeth at the discharge is provided to collect the discharge from the roll feeder for the rotary seal. Below the screw-conveyer discharge is a 16 × 16-in. 4-blade rotary seal, which seals the bottom of the retort against loss of recycle gas. The screw-conveyer, roll-feeder, and rotary-seal sizes were determined by the maximum particle size rather than by the capacity required. The screw conveyer and the roll feeder are driven from a single drive unit at a constant speed to maintain a constant gas loss through the pumping action of the rotary seal.

To gain the necessary height and distance from the retort, a 4 × 10-in. flight conveyer, with 17-in-wide enclosure and shoe-suspended flights, was provided to lift the spent shale to a height of 24 ft, 37 ft from the center of the retort. The shale is discharged through a spent-shale sampler at this point to a batch weigh scale. The scale discharges to a 16-in-belt waste conveyer,

which, in turn, discharges to the canyon about 22 ft away.

Electrical interlocks are provided to prevent damage to other equipment in case of unit failure and to prevent improper starting sequence. The only severe metal service in the retort construction is the high temperature and presence of oxygen prevailing in the air-gas mixers. The spent shale contains 2 to $2^1/_2$ per cent carbon, which helps to reduce the abrasion in the feeders, seals, and conveyers.

A dust-collector system, consisting of a dry blower and centrifugal collector, takes suction from the flight conveyer and the spent-shale scales to eliminate dust hazard and remove the leakage recycle gas from the retort rotary seal. The dust-collector vent discharge is up away from the working area, and the dust discharges to the waste conveyer.

Gas-Circulation and Oil-Recovery System. Fig. 10 shows a diagram of the oil-recovery system. A 12-in. pipe supplies recycle gas to the recycle-gas wind boxes at the bottom of the retort. The designed maximum velocity in this line is 6330 fpm. A 6-in. pipe to the air-gas mixer header along the side of the retort supplies combustion air to the air-gas mixers at a designed maximum velocity of 5370 fpm. Product gas leaves the retort through a 14-in. line on a nozzle in the top adapter section or through a 14-in. line from the two collectors with a designed maximum velocity of 8070 fpm. Low-pressure drops were designed into this experimental plant. The connection in the adapter section permits use of a void space above the shale for product-gas removal instead of the collectors within the shale bed. From this line the product gas is passed through two oil-wetted Roto-clones. These machines are designed for adding 6 in. water pressure to the gas stream and 12 psia at 150 F suction conditions.

No. 14 machine has a capacity of 4850 cfm, and No. 10 machine of 3250 cfm. They were purchased complete with vent-back piping. The two machine sizes were used to permit using three gas rates, plus the machine working range, for a wide range of operation. The product oil agglomerated and condensed in these machines joins with the wetting or spray oil in the machine sump. The product gas next passes through a Multiclone, size 40–5, type 61D, which is designed for maximum operation of 10,000 cfm at 12 psia, 150 F, and a pressure differential of 4 in. of water. The oil removed in this collector is collected in its sump. This oil and the make oil from the Roto-clones are drawn off to the run-down tanks. The gas stream next passes to two Spencer 50-in. 4-bearing blowers. These machines were each rated 3000 std cfm and 5 lb differential at 6000 ft elevation when equipped with 5 stages. Three stages are installed for this installation, since these were calculated to furnish the required pressure and volume. The pipe-line separators on the blower discharges are estimated to remove a very small amount of oil, which may be agglomerated in the blowers, but most of the blower-agglomerated oil can be drawn directly from the blower casings. A 12-in. recycle gas line runs from the blowers to the retort recycle-gas-distributor wind boxes. An 8-in. excess-gas vent line with a flow-control valve runs from the gas-blower discharge to the stack.

Air for combustion in the retort is supplied by two Spencer 36-in., 4-bearing blowers rated at 800 std cfm at 5 lb differential at 6000 ft elevation. A 6-in. line with a flow-control valve runs from the air blowers to the air-gas mixers in the retort.

Two propane start-up burners, rated at 500,000 Btu per hr each and equipped with flame-failure control, are set to enter the retort about 3 ft above the top of the air-gas mixers during start-up. The retort is filled with shale to about 30 in. above the air-gas mixers. The piping arrangement on one air blower permits it to circulate gas through the retort by taking suction from the bottom of the retort and discharging to the top of the retort, to draw the flame and heat into the start-up shale bed.

Standard-weight fittings are used in the piping system, and a pipe-wall thickness of $^1/_4$ in. is used. All oil lines and small lines that may have oil passing through or into them are electric-traced and provided with connections for steaming out and blowing out. All vessels and equipment that may contain oil have provision for steaming out and blowing out. There are no temperature or corrosion problems in the piping system.

Sampling. The raw-shale sampler at the discharge of the feeder conveyer is a 36-in., heavy-duty, Geary-Jennings unit with variable cutter size of 3 × 14 in. to 9 × 14 in. to permit desirable adjustments when the shale-feed size is changed. This sampler makes a 1 per cent cut. This 1 per cent cut passes over a feeder and conveyer to a second sampler of the same size and type, which makes a 5 per cent cut of the stream at this point for screen-analysis sample. The remainder of the stream[6] is crushed in a Jef-

[6] 95 per cent of the original 1 per cent cut or 0.95 per cent of the main feed stream.

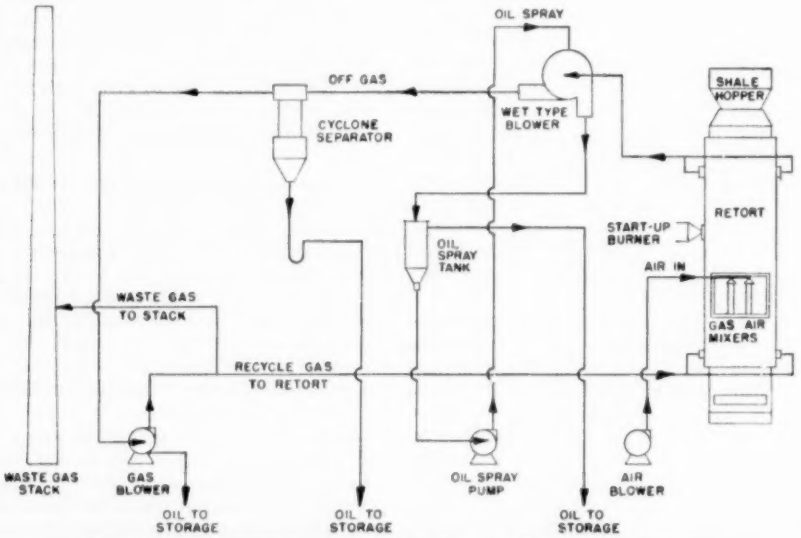

FIG. 10 GAS-COMBUSTION DEMONSTRATION PLANT, OIL-RECOVERY SYSTEM

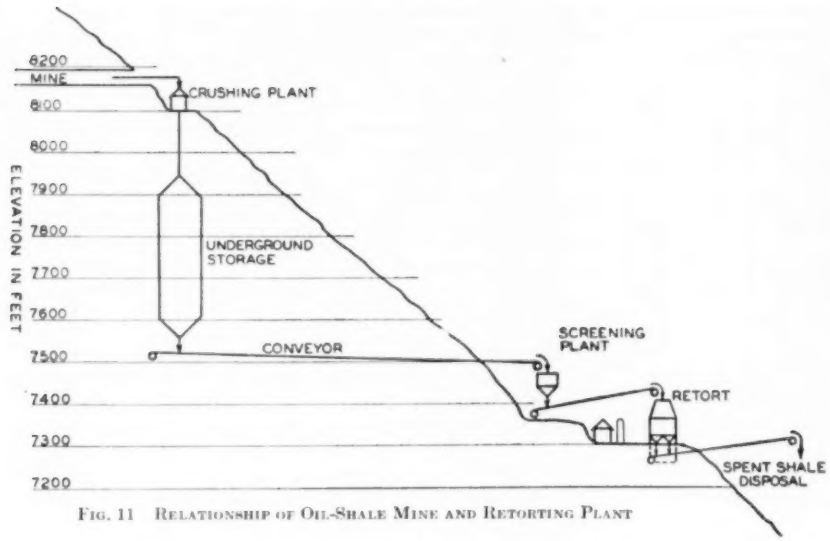

FIG. 11 RELATIONSHIP OF OIL-SHALE MINE AND RETORTING PLANT

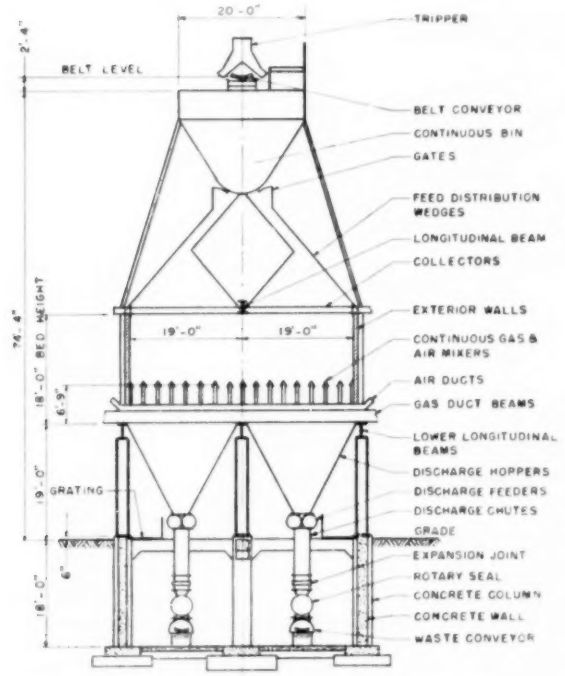

FIG. 12 CROSS-SECTIONAL ELEVATION THROUGH RETORT

frey, Jr., type "A" hammer mill and passed through a 7-multiple splitter, producing a final sample of about 45 lb per day. The splitter is similar to a Jones-type riffle. The waste from the splitter discharges directly to the waste conveyer. The spent-shale sampler at the discharge of the flight conveyer is the same as the raw-shale samplers, except that it has a 9 × 14 cutter. It makes a 1 per cent cut from the spent-shale stream and discharges the sample to a hammer-mill crusher and 7-multiple splitter, like those just noted, to produce a sample of about 40 lb per day. The waste from the splitter discharges directly to the waste conveyer.

Controls. The control board is mounted in the control house, adjacent to the retorting installation. Transmission is generally pneumatic. The principal controls are as follows:

1 A 3-unit shale-level controller on the feed hopper, which is combined pneumatic and electric. Step controls control the vibrating feeders at the shale supply to high feed rate, low feed rate, and off. The steps may be set at the desired values manually.

2 The retort-discharge roll feeder is controlled by a temperature-recorder controller in the product-gas line leaving the retort. This controller regulates the roll speed.

3 A pressure-recorder controller maintains zero psig at the product-gas off-take of the retort by controlling the amount of vent gas from the blower discharge to the stack.

4 A temperature-indicating controller on the temperature of the shale through the retort roll feeder stops the feeder if the spent-shale temperature exceeds a predetermined safe limit.

5 A flow-recorder controller on the air-blower discharge line controls the air flow to the retort at a predetermined set flow.

6 Temperature recorders are provided for 80 points on the retort and 16 points on the recovery and auxiliary equipment.

7 Pressure indicators are provided for side points on the retort, the wet blowers, the stack, the gas blowers, and the air blowers.

INDUSTRY-SCALE RETORT DESIGN

The size of an industry-scale retorting plant is determined by the size required to retort the output of one or more mine units, each producing 19,200 tons per day. General designs of retorts for several retorting processes have been made. The gas-combustion process retorting plant will retort 18,200 tons per day of the 19,200 tons, the balance being available for another process.

Designs have been made of multiple rectangular-cell retorts, with common walls between the cells of a retorting unit, with separate cell walls, and of round retort cells, all on an equal area basis. The rectangular-cell plant with separate cell walls has the net advantage over other types at this time. However, additional work is being done on the round-cell design to overcome some of its disadvantages.

In these large units having 700 to 800 sq ft per cell, the problems of even flows of shale and gases required to produce even retorting and permit high rates requires full consideration of the many elements affecting their flow. Thermal expansion becomes an important consideration, particularly in the internal fittings.

The weight of shale in the retort, the collection zone below, the distribution zone above, and the shale-feed bin make up most of the rather large loads on the supporting structure. These designs have been so made that no primary steel structural members are in the heated space.

The even shale flow and its satisfactory distribution are the more difficult problems. The interior gas distributor and collector ducts required by the gas-combustion process afford a ready means for designing flow resistance and equalizing grids across the area of the retort—at the top by the product gas collectors, at the bottom

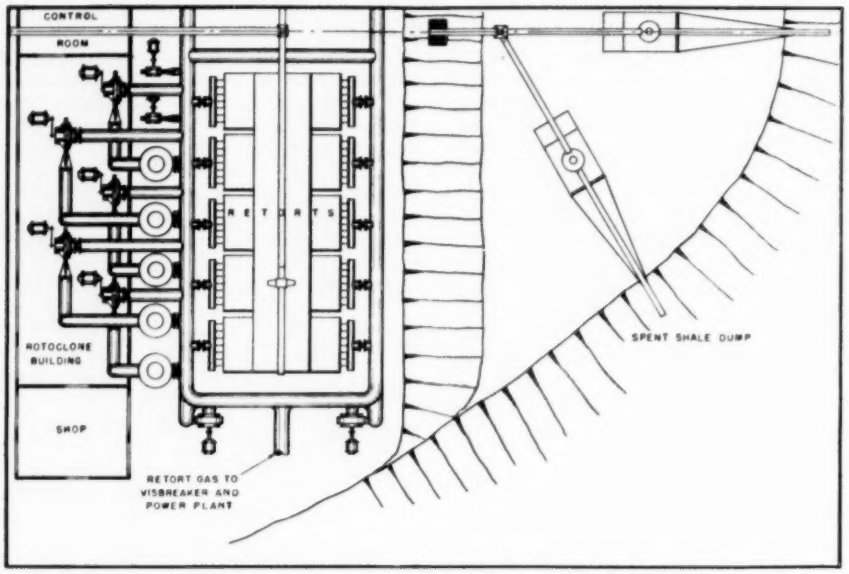

FIG. 13 PARTIAL PLAN OF RETORTING PLANT

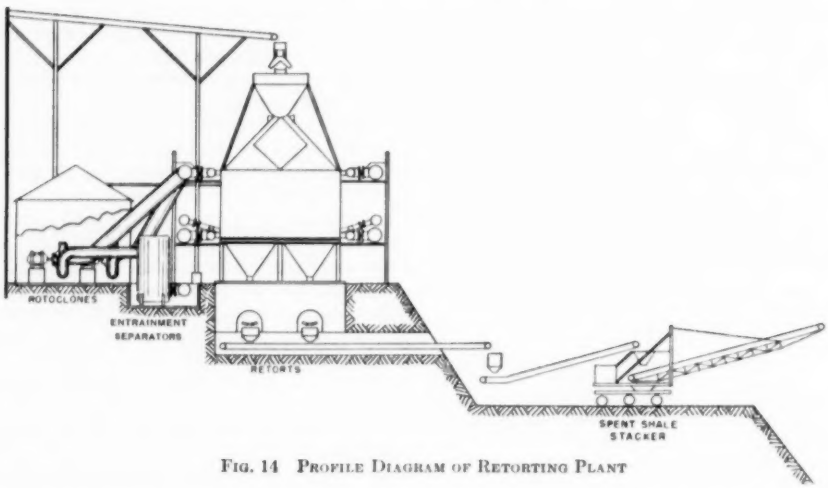

FIG. 14 PROFILE DIAGRAM OF RETORTING PLANT

of the retorting zone by the air-gas mixers, and at the bottom of the retort by the recycle gas distributors. These grids assist greatly in securing the desired uniform flow.

The design of the shale feed-stream distribution at the top, and the spent shale-stream concentration at the bottom, are most important in securing proper shale flows. The results of mock-up tests for the latter made at Rifle have been described. Experimental work at the University of Minnesota (8) shows that baffles may be installed in a broken-solids discharge, similar to that at the bottom of the rectangular retort cell, to produce uniform flow over the bed area above. These baffles are so arranged that they support the load of the broken solids above and permit the free flow under them of material farther from the opening. They form an inclined base upon which material supported on them moves to the discharge opening. The commercial retorts designed for the gas-combustion process permit the installation of such baffles, if required, without other change.

The design of the shale discharge below the recycle-gas distributors at the bottom of the retort is a shale-stream concentration section with sides sloping less than 30 deg from the vertical, then a 2-roll discharge feeder across the bottom width of the retort cell. Below the feeder, the spent-shale stream is concentrated to the rotary-seal feed size in a free-falling zone. The rotary seal is oversized sufficiently to prevent choke feed and consequent unnecessary particle shearing.

In the rectangular cells, all flows are controlled by half-cell areas. In the round cells only the gas flows are so controlled.

The rotary seal and waste conveyer are directly supported from below. All other parts are supported on the structural supports for the retort. This minimizes the expansion which must be taken in the expansion joint above the rotary seal. An 18-ft-deep pit is provided under the retorting unit to permit spent-shale conveyers to pass under ground-level operations and keep the plant height moderate.

A suspended feed bin is supported above the top of the multiple-cell retort with multiple gated-chutes to the top of each retort cell. These gates permit the closing down of any retort cell. The bin is filled from a belt conveyer equipped with a motor-driven tripper. The relationship of the oil-shale mine and retorting plant is shown in Fig. 11. The retort sectional elevation is shown in Fig. 12. A partial plan of the retorting plant is shown in Fig. 13 and a profile diagram in Fig. 14. Shale for such a plant is crushed at the mine, passed through a 24-hr storage, withdrawn from storage, and conveyed to a suspended surge hopper in the screening plant. Feeders remove the shale to screens where half the minus $^3/_{16}$-in. material is removed. The crushed shale is then conveyed to the feed-bin filling conveyer.

Acknowledgments

This study was made under the general supervision of Boyd Guthrie, Chief, Oil-Shale Demonstration Branch, Bureau of Mines, Rifle, Colo. The following members of the Bureau of Mines reviewed the manuscript and made helpful suggestions concerning its final form: R. J. Cameron, J. B. Mull, L. W. Schramm.

Special thanks are due to A. S. Houghton, J. R. Ruark, K. L. Berry, Carl Ellis, and John B. Jones for their assistance in supplying related information.

BIBLIOGRAPHY

1 "Oil-Shale Mining," by E. D. Gardner and E. M. Sipprelle, *Mechanical Engineering*, vol. 72, 1950, pp. 701–706.

2 "Development of a Rotary Test Drill," by F. D. Wright and L. H. Brakel, Bureau of Mines Report of Investigations 4864, April, 1952.

3 "Extraction and Refining of Shale Oil," by Boyd Guthrie and Lester Schramm, *Mechanical Engineering*, vol. 72, 1950, pp. 707–711.

4 "Synthetic Liquid Fuels, 1950 Annual Report of the Secretary of the Interior, Part II—Oil From Oil Shale," Bureau of Mines Report of Investigations 4771, February, 1951.

5 "Synthetic Liquid Fuels, 1951 Annual Report of the Secretary of the Interior, Part II—Oil From Shale," Bureau of Mines Report of Investigations 4866, July, 1952.

6 "Properties of Colorado Oil Shale," by K. E. Stanfield, I. C. Frost, W. S. McAuley, and H. N. Smith, Bureau of Mines Report of Investigations 4825, November, 1951.

7 "Method of Assaying Oil Shale by a Modified Fischer Retort," by K. E. Stanfield and I. C. Frost, Bureau of Mines Report of Investigations, June, 1948, fig. 5.

8 "Magnetic Roasting of Iron Ore," by E. W. Davis, Bulletin No. 13, University of Minnesota, May 10, 1947, pp. 46–47.

FIG. 1 PARACHUTE CREEK AREA OF COLORADO SHALE DEPOSIT

Engineering Features of the Union Oil-Shale Retort

BY H. C. REED[1] AND CLYDE BERG,[2] WILMINGTON, CALIF.

The retorting of shale requires an operation combining very good heat and fuel economy with low capital investment. In order to meet these demands the Union Oil Company developed its novel underfeed retorting method, which was publicly demonstrated in 1950 in a 50-ton per day unit. The retorting unit employs countercurrent flow of shale and air in a kiln utilizing bottom feed of solids. Ash and clinkers are removed overhead, and the oil drained from the bottom of the unit is cooled by countercurrent heat exchange with the incoming shale. No water is required for process operation. Movement of the shale through this unit is effected by a hydraulically operated underfeed mechanism. The shale kiln employs an external retorting section with cowling to direct air flow over the fins and to control shell temperature. Unlike conventional retorts, fusion of ash is not considered a problem in the operation of the Union retort since specially designed sodium-filled plows carry out a scraping action in the plastic ash-fusion zone, maintaining uniform bed porosity and size range of the discharged ash. It has been estimated that a typical commercial shale mine can produce approximately 20,000 tons per day of shale. The shale-retorting plant designed to handle this production would employ a battery of retorts, each having a capacity of 1000 tons per day, and centralized gas-handling and hydraulic power-supply systems.

[1] Chief Engineer, Union Oil Compsny of California. Mem. ASME.

[2] Manager, Union Oil Company of California. Mem. ASME.

Contributed by the Petroleum Division and presented at the Petroleum Mechanical Engineering Conference, Kansas City, Mo., September 22-24, 1952, of THE AMERICAN SOCIETY OF MECHANICAL ENGINEERS.

NOTE: Statements and opinions advanced in papers are to be understood as individual expressions of their authors and not those of the Society. Manuscript received at ASME Headquarters, August 5, 1952. Paper No. 52—PET-2.

OIL SHALE

OIL shale of the Green River formation in Colorado was formed in an ancient lake in which a gradual deposition of both organic and inorganic material occurred. The water in the lake during the period of deposition was in a reducing condition so that the organic material was not oxidized. Principally, the organic material consists of fossilized spore cases and algae, together with some leaves, stems, and animal material. The inorganic material in the Colorado deposition consists of magnesium marlstone. Fig. 1 shows the Parachute Creek area of the Colorado shale deposit. It will be noted that the shale formation is at an elevation of 5000 to 8000 ft and that the plateau in which the shale deposition is located is penetrated by deep ravines of considerable depth and length. These ravines expose the face of the shale deposit to form convenient locations for opening mining operations. Exploitation of this huge Colorado shale reserve depends upon the combined economic solution of mining, retorting, and refining of shale and shale oil.

MINING

The problem of mining shale constituted a major limitation in the economic possibilities for utilization of shale for many years. The Bureau of Mines has effected an important advance in the successful mining of shale in the demonstration shale mine near Rifle, Colo. (1, 2, 3).[3] By utilizing modern large-scale ore-han-

[3] Numbers in parentheses refer to the Bibliography at the end of the paper.

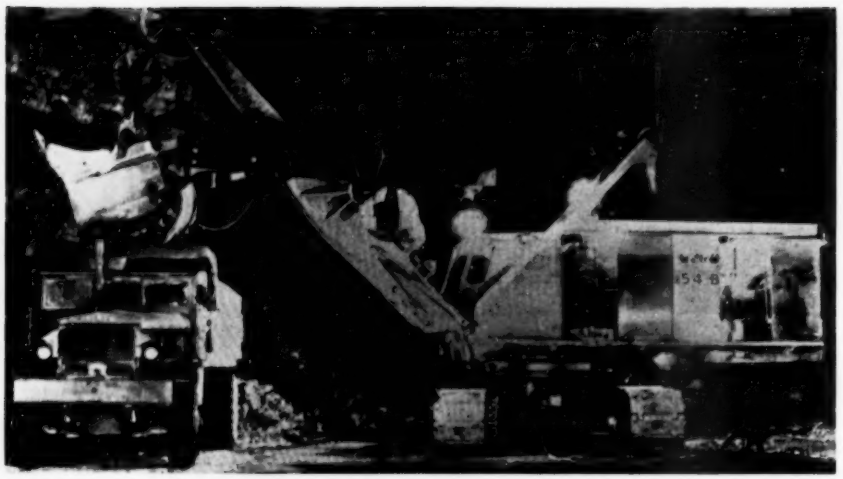

FIG. 2 INTERIOR OF BUREAU OF MINES DEMONSTRATION MINE

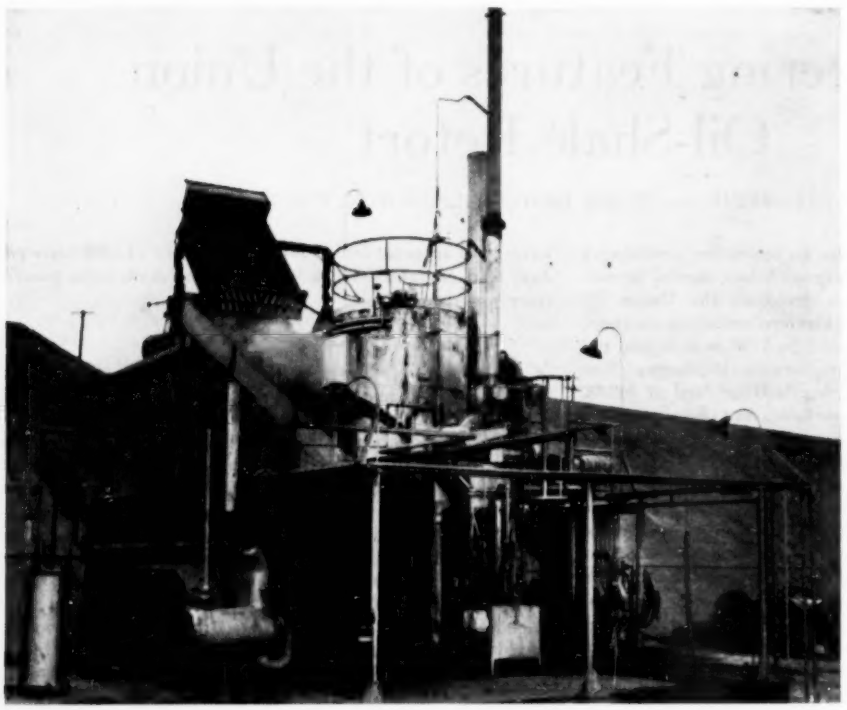

FIG. 3 FIFTY-TON PER DAY SHALE UNIT

dling equipment, the cost of mining has been reduced to the range of costs obtained in the most modern open-quarry operations. Since the strength of the Green River shale formation is two to three times that of concrete, large mining openings can be made without fear of roof failure, and rooms have been opened 70 × 100 ft in extent without the use of support beams. The most recent concept of the mining operation involves the room-and-pillar type of mining with approximately 75 per cent of the shale being removed, leaving only 25 per cent of the shale behind as support pillars. Fig. 2 shows the interior of the Bureau of Mines demonstration shale mine. In operation of the mine, drilling and blasting are employed to open the roof area, followed by drilling and blasting of the bench to break the shale, which is loaded by electric shovels into large Diesel-driven trucks and hauled from the mine.

RETORTING

Commercial shale retorts would be located at the mouth of the mine to permit minimum handling of the raw shale and ash refuse. Crushing facilities would consist of a one-stage breaking operation to reduce the run of the mine to an aggregate maximum 4-in. particle diameter. The flexibility of the retorting operation will permit adjustment of plant operations to meet fluctuations in shale supply, and only a minor installation of shale storage capacity is required.

Capacity of the ravines in the shale properties is sufficient to permit ready disposal of the ash discharge for an extended period of time and the transportation operation will be that of the retorted oil and the retort gas to the refinery site located within a few miles of the mouth of the mine.

UNION RETORTING PROCESS

The retorting of shale requires an operation combining very good heat and fuel economy with low capital investment. A variety of retorts for shale have been developed (3); however, in this particular area water is at a premium and should not be required for operation of the retorting units. The retorting operation also must be capable of handling a wide size range of shale particles as well as a wide range of shale characteristics in order to avoid screening and discard of appreciable quantities of shale. In order to meet these demands the authors' company developed its novel underfeed retorting method, which was publicly demonstrated in a 50-ton per day unit in 1950 (4, 5, 6). Fig. 3 is a photograph of this unit in action. This retorting unit employs countercurrent flow of shale and air in a kiln utilizing bottom feed of solids. The ash and clinkers are removed overhead and the oil drained from the bottom of the unit, cooled by countercurrent heat exchange by the incoming shale. The oil is distilled by downward flow

of heat furnished by combustion of the residual carbon on the shale clinker near the top of the kiln. The heat available from combustion of the stack gases far exceeds the power requirements of the plant. Almost perfect heat exchange is obtained in the units since the incoming air is preheated by the spent hot clinker and the products of distillation are condensed on the cool incoming shale.

General Construction of Shale Retort. The general construction of the continuous shale retort is diagrammed in Fig. 4. It will be noted that the unit employs a cylindrical kiln with a hydraulically operated underfeed mechanism. Movement of the granular shale is upward through the unit with overflow at the top. Clinkers are removed by a hydraulically actuated plow mechanism and fall into an ash-disposal chute. The sections of the kiln expand gradually upward, minimizing restriction to movement. The shale kiln employs an externally-finned retorting section with cowling to direct air flow over the fins and to control shell temperature. A secondary stack draws the air through the cowling section. Cooling of the shale by this arrangement is designed to effect a maximum metal temperature of 750 F at the burning zone. A conical slotted section below the retorting section effects the separation of the oil and gas from the shale bed. A cowling surrounds this section and the gas is withdrawn from this by a roto-clone blower.

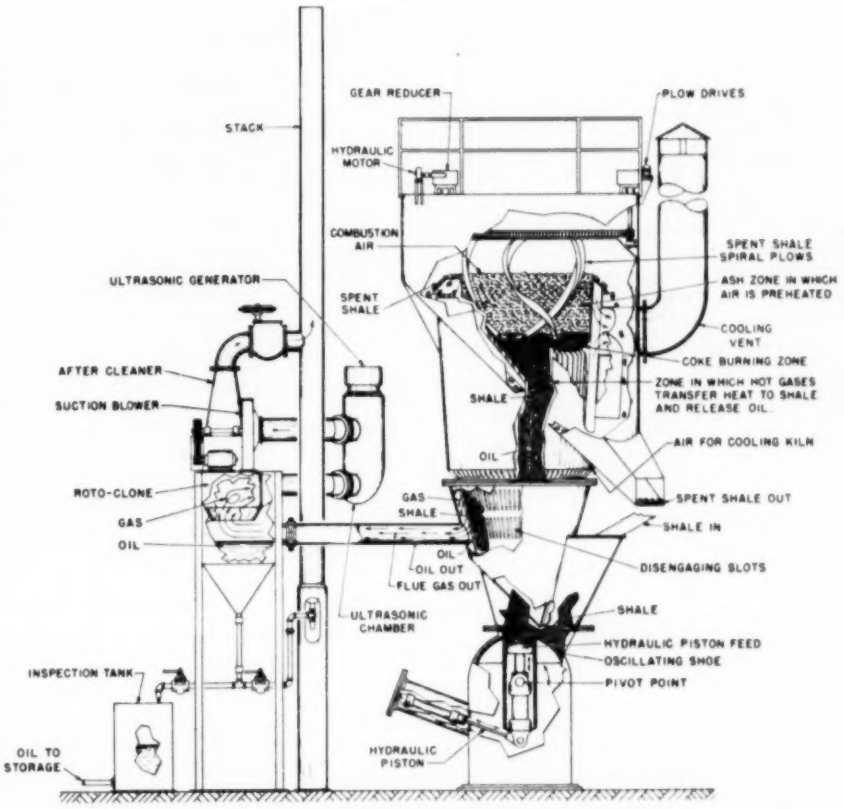

FIG. 4 UNION OIL SHALE RETORT

The feeding mechanism at the base of the unit is so constructed that any fines falling through the grate return to the feeding piston and are reintroduced into the unit. This prevents the gas-and-oil-collecting housing from plugging as a result of accumulation of fines. The feeding mechanism is filled with oil to a level just below the slot edges, providing a liquid seal which prevents the blower from pulling air in through the feed hopper.

20,000-TON PER DAY SHALE-RETORTING PLANT

It has been estimated that a typical commercial mine can produce approximately 20,000 tons per day of shale. The shale-retorting plant designed to handle this production will employ a battery of retorts, each having a capacity of 1000 tons per day of shale. In Fig. 5 is given a plot plan of a commercial retorting unit of this capacity. It will be noted that the gas-handling system of this unit is centralized as well as that of the hydraulic power-supply equipment.

1000-Ton Per Day Shale Retorts. Fig. 6 gives details of a 1000-ton per day shale retort. It will be noted that each retort is equipped with four feeding mechanisms which operate in unison and discharge the shale into four separate disengaging sections

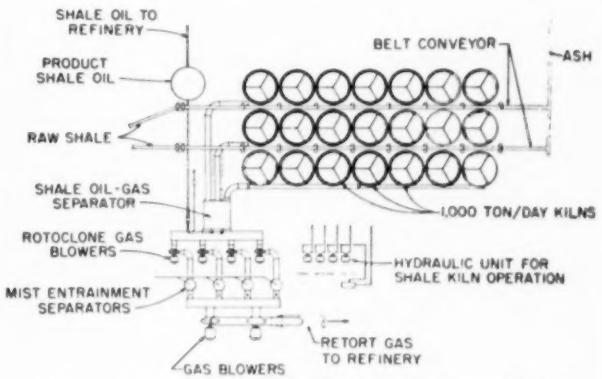

FIG. 5 PLAN OF 20,000-TON PER DAY SHALE-RETORTING PLANT

which in turn are combined into a single retorting section. The gas and oil from the disengaging sections enter a common collector from which the products are discharged into a main and gas-oil header handling a number of retorts.

Feeding Mechanism. The four feeding mechanisms for each retort are hydraulically operated with a common pilot-valve system which actuates the four feeders to discharge and fill simultaneously. In this manner uniform shale flow is maintained over the entire cross-sectional area of the retort. The feeding piston is actuated in filling and discharging by a hydraulic cylin-

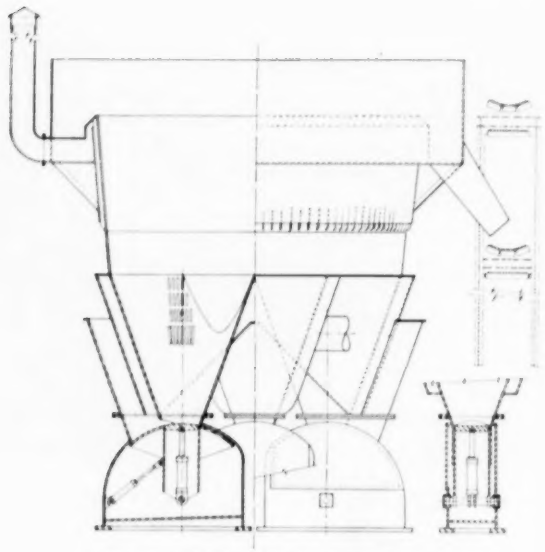

FIG. 6 1000-TON PER DAY SHALE UNIT

der mounted inside of the piston and free to oscillate by a trunnion mount. The feeding cylinder is oscillated between loading and discharge positions by a horizontal hydraulic cylinder which is actuated at the end of each of the filling and discharge operations. The feeding mechanism is constructed to provide free access to all the internals through an access door in the side of the case. The feeding cylinder can be installed through this access door as well as the shaft and bearings of the operating mechanism. The equipment can be checked for alignment and stroke before the access door is bolted into position.

Disengaging Section. The disengaging section of the 1000-ton per day retort consists of four 70-deg cones. These cones possess a substantial section of slots through which gas and oil are disengaged. The products of the shale-kiln discharge are collected in an annular section surrounding the slotted area. Solids which may drop through the slots fall down through the liquid seal and are reintroduced through the feeder.

Retorting Section. The retorting section is cooled by fins which cover the heated metal surface completely. These fins effectively maintain the temperature of the shale below 700 F. A cowling surrounds the fins and assures a constant flow of cooling air. The cooling air rises through the fin section and is collected in an annular ring located near the top of the retorting section. The draft for cooling-air flow is maintained by two stacks which exhaust the air from this collection ring.

The spent shale from the retort flows from the top of the retorting bed into the ash hopper and drops from the hopper through the ash chute into the ash-disposal conveyer.

Plows. During operation of the shale retort, uniform air distribution is achieved by the plow mechanism, which breaks up clinker formations and prevents restriction of air flow by fusion effects within the kiln. Three large plows are employed. They extend into the retorting bed to a depth of about one third of the retorting section. They enter the solids bed at an angle of 45 deg and maintain a spiral pattern so as to offer minimum resistance to solids motion. These plows are filled with metallic sodium. Convection of the metallic sodium effectively cools the tips and prevents temperatures in excess of 800 to 900 in spite of high temperatures in the burning zone. Heat removed from the plow tips is dissipated at the top of the plow tips by radiation. The plows are supported at the periphery by a ring which is restricted in its vertical and horizontal motion by a series of rollers. This ring is rotated slowly by the hydraulic mechanism.

Operation of Shale Retort. Operation of the shale kiln is entirely automatic. The flow of air is controlled by an automatic flow-control system. A temperature controller actuated by thermocouples located at the shell of the retort maintains the burning section approximately at the tip of the plows of the kiln by control of the feeding mechanism.

The retorting section may be divided into three zones. In the top zone heat exchange between incoming air and hot clinkers is effected. In the lower portion of this top zone combustion of the carbon residue on the clinker is effected, producing flue gas with a temperature near 2000 F. This flue gas progresses into the second zone, termed the retorting zone, wherein the oil is educted from the shale. The mixture of shale-oil vapors and flue gas progresses downward into the third zone, termed the condensation zone, where the incoming green shale is heated and the products of eduction are cooled and condensed. The temperature of the exit oil and gas from the kiln approaches within 20 F that of the shale being charged. A typical temperature profile of the shale kiln is illustrated graphically in Fig. 7.

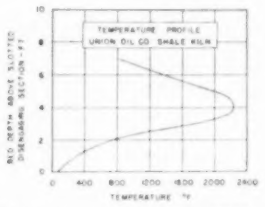

FIG. 7 TYPICAL TEMPERATURE PROFILE IN 50-TON PER DAY SHALE UNIT

RETORTING-PLANT PERFORMANCE

Table 1 presents yield data for a typical operation of a shale-retorting plant processing 20,000 tons per day of shale averaging 30 gal per ton.

TABLE 1 RETORTING-PLANT PERFORMANCE

Shale feed, tons/CD	20,000
Shale-oil product, bbl/CD	13,125
Gas production (dry, total), MSCF/CD	270,000
Shale ash, tons/CD	12,500
Air rate to kilns, MSCF/CD	203,000

The shale oil produced from the Union-type underfeed retort is characterized by relatively constant quality with little variation due to fluctuations in operating conditions. Typical properties of the shale oil are given in Table 2.

TABLE 2 PROPERTIES OF SHALE OIL

Gravity, °API at 60 F	20.7
Specific gravity at 60 F	0.930
Distillation (50 mm vac), deg F:	
Initial, per cent	402
10	536
20	622
30	692
40	764
50	814
60	836
70	865
80	889
90	Cracked
Water, per cent	0.1
Ash, weight, per cent	0.03
Conradson carbon, per cent	4.57
Viscosity, SSU at 100 F	223
Viscosity, SSU at 210 F	46
Pour point, deg F	90
Sulphur, weight, per cent	0.77
Nitrogen, weight, per cent	2.01

Of particular interest are the exceptionally low water and ash contents of this crude shale oil, averaging 0.2 weight per cent for

the former and 0.003 weight per cent for the latter. Gas produced in retorting of Colorado shale amounts to 13,490 SCF per ton and has the composition given in Table 3. The ash produced amounts to 62.8 weight per cent of the fresh shale. Heat efficiency of the retorting operation is very high and the total energy requirements for operation of the retort amounts to only 7 per cent of the gas yield and less than 2 per cent of the energy value of the total retort production.

TABLE 3 COMPOSITION OF GAS PRODUCED IN RETORTING OF SHALE

Component	Mol, per cent
Air	2.0
Nitrogen	57.5
Argon	0.6
Carbon monoxide	4.7
Carbon dioxide	29.7
Hydrogen	2.2
Hydrogen sulphide	0.1
Methane	1.0
Ethylene	0.6
Ethane	0.4
Propylene	0.5
Propane	0.2
Butylene	0.3
Butane	0.1
Pentenes	0.1
Total	100.0
Average molecular weight	32.44
Gross heating value, Btu/SCF	83.3

Location of Mines, Retorts, and Refineries

Fig. 8 is a map showing typical location of the shale mines, retorts, and refineries which could be employed in a practical scheme of operations of the production of shale oil and refined products. The retorting operation effects a hydrocarbon recovery of approximately 100 per cent, based on weight of oil and hydrocarbons from assay of the shale. An important consideration in the over-all retorting operation is the high energy quantities available from combustion of the retort gas, amounting to approximately 25 per cent of the total energy available from the retorting of shale. This gas is vital to the refining step on shale oil. Transmission of the gas through large-diameter low-pressure drop conduits is a fundamental step in the over-all economy in the refining of shale oil. Without this important fuel source, approximately 20 per cent of the crude shale oil would be destroyed to provide power requirements necessary for refining. Through utilization of the gases from retorting, very high over-all yields of refined products from crude shale oil are maintained.

BIBLIOGRAPHY

1 "Mining of Colorado Oil Shale," by Tell Ertl, *Mechanical Engineering*, vol. 71, 1949, pp. 478–480.

2 "Oil Shale Mining," by E. D. Gardner and E. M. Sipprelle, *Mechanical Engineering*, vol. 72, 1950, p. 701.

3 "Liquid Fuels From Shale," by W. Q. Hull, Boyd Guthrie, and E. M. Sipprelle, *Industrial and Engineering Chemistry*, vol. 43, 1951, p. 2.

4 "Continuous Shale Retorting Process," by Clyde Berg, *Petroleum Refiner*, vol. 27, September, 1948, p. 76.

5 "Development of Union Oil Retorting Method for Recovery of Shale Oil," by Homer Reed and Clyde Berg, *Mechanical Engineering*, vol. 71, 1949, p. 639.

6 "Retorting of Oil Shale," by Clyde Berg, Glasgow, Scotland, published in Proceedings of the Oil Shale and Cannel Coal Conference, Glasgow, Scotland, vol. 2, 1951, pp. 419–427.

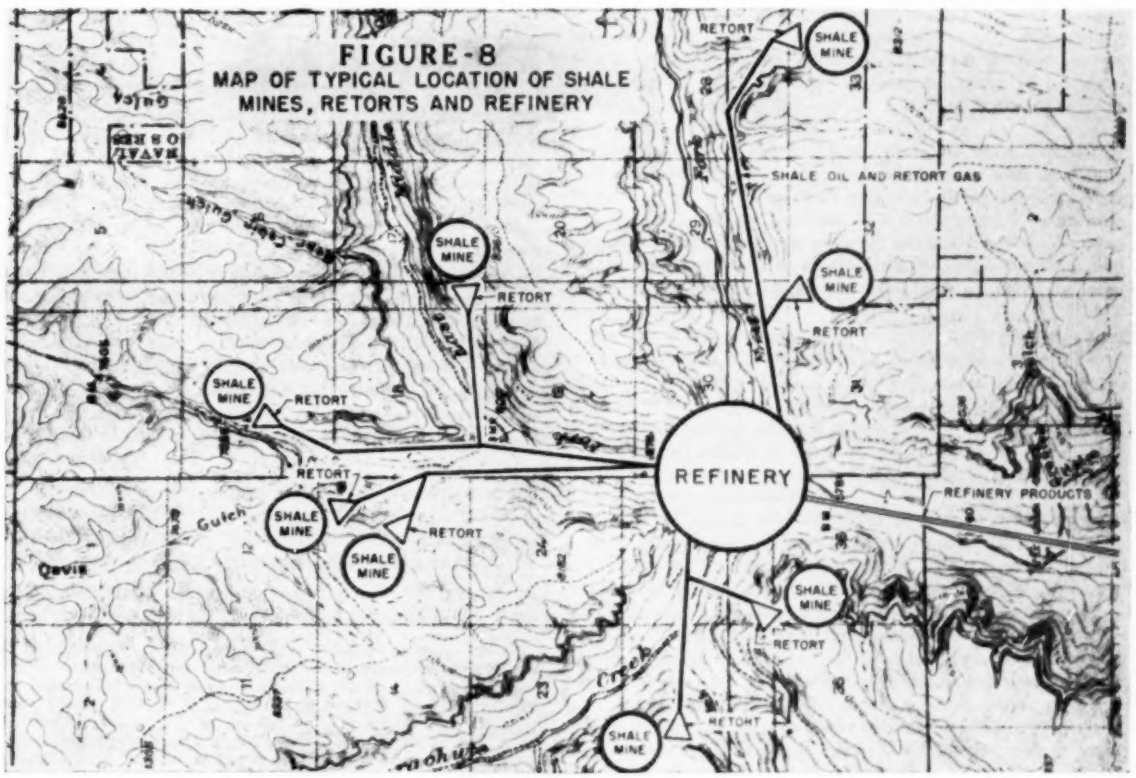

Fig. 8 Map of Typical Location of Shale Mines, Retorts, and Refinery

Low-Temperature Insulation for Refinery Service

By W. L. MARTIN,[1] BAYTOWN, TEXAS

The problem confronting the refinery engineer in the selection, application, and maintenance of an insulation for low-temperature service involves consideration of factors that are, in general, of only minor significance in the high-temperature field. The principal basic factor in any insulation is, of course, conductivity. However, water absorption, upper-temperature limit, fire resistance, coefficient of expansion, and so on, also must be considered in selecting an insulant for particular service conditions. This paper presents a discussion of the more common insulating materials and the relative importance of the various properties and characteristics of these materials for low-temperature service in petroleum refineries. In addition to the care exercised in obtaining the proper insulating material, considerable attention must be devoted to the selection of accessory materials such as adhesives, vapor sealers, water and fireproof coverings, mechanical securement devices, and the like. These materials also will be discussed since they have a pronounced effect on the over-all effectiveness and life of the insulation.

Introduction

THE trend in recent years has been toward the increased use of refining processes operating at subatmospheric temperatures. The high cost of obtaining and maintaining low temperatures demands the application of insulations that yield a maximum of dependable service and thermal efficiency. Low-temperature conditions necessitate special insulating materials; designers, contractors, and insulation manufacturers have done much to improve results that can be obtained in this field by research and experimentation. New insulation and accessory materials, better designs, and improved application techniques have been developed. The problem in each particular application is to obtain the insulation that will accomplish the desired results most effectively and economically. Fundamentally, the primary purpose of thermal insulation is to control the flow of heat. On this basis, conductivity is the most important property of an insulating material. However, requirements of the particular installation may indicate other properties to be of paramount importance. In order to make an intelligent analysis of an insulation problem, the following information must be developed:

1 Requirements, such as heat-transfer rate, resistance to fire, resistance to mechanical abuse, and so on.

2 Service conditions, such as maximum and minimum operating temperatures, weather exposure, humidity, and so on.

After these data are known, a satisfactory solution can be determined. The over-all efficiency and dependability of the insulation will be controlled by the five basic factors which follow:

1 Proper selection of materials based on requirements and service conditions.

2 Adequate design and specifications determined by materials selected, requirements, and service conditions.

3 Quality of the workmanship of the insulating craftsmen.

4 Careful inspection of materials and methods of application during installation.

5 Periodic inspection and maintenance of the insulation in service.

It is the purpose of this paper to present a general discussion of the foregoing factors to serve as an aid in analyzing low-temperature insulation problems encountered in petroleum refineries.

Types of Insulation

In the selection and design of an insulation for low-temperature service, the engineer has a wide range of thermal insulating materials from which to choose. Some materials are accidental discoveries, but, in general, they are the result of years of research, development, and practical experience. The selection of an insulating material for particular service conditions is determined primarily by properties and characteristics, comparative costs, and economics associated with application and maintenance of the material. Before entering a discussion of these factors, it is believed that the following brief discussion of the most widely used insulants will aid in better understanding their properties and characteristics.

Vegetable Cork. Cork is obtained from the outer bark of the cork oak tree. The bark has a cellular structure with more than 50 per cent of the volume in air cells, the still air trapped in cells acting as a barrier to heat flow. Cork insulation is made from granulated cork, molded, compressed, and baked into the required shape. It is available in blocks, sectional pipe covering, and shaped fitting covers. Granular cork also is available for loose fills.

Mineral Wool. Mineral wool is made by exposing a thin stream of molten blast-furnace slag or glass to a high-velocity steam jet. Primary product is a woolly mass of fine, pliant, vitreous fibers. As an insulation, it is available as loose wool which is the form in which it is first produced; granules which are loose wool refined and granulated; blankets or batts; and blocks or pipe coverings formed by compacting, felting, and adding a resin or asphaltic binder.

Rock Wool. Rock wool is similar to mineral wool—actually it is a mineral wool. It is made by exposing a thin stream of molten rock to a high-velocity steam jet. Physical qualities of the wool depend upon the type or class of rock used. Rock wool is available as loose or granulated material, in blankets or batts, and in molded blocks and pipe coverings.

Cellular Glass. Cellular glass is made from a mixture of pulverized glass and pure carbon which is baked in an oven at high temperatures. A reaction occurs in which carbon gases are formed causing cellulation of the molten mixture. The result is a product which contains more than 5,000,000 cells of inert hermatically sealed air per cubic foot. Cellular glass is available in blocks or as sectional pipe covering.

[1] Mechanical Engineer, Humble Oil & Refining Company.

Contributed by the Petroleum Division and presented at the Petroleum Mechanical Engineering Conference, Kansas City, Mo., September 22–24, 1952, of The American Society of Mechanical Engineers.

Note: Statements and opinions advanced in papers are to be understood as individual expressions of their authors and not those of the Society. Manuscript received at ASME Headquarters, June 10, 1952. Paper No. 52—PET-12.

Cellular Rubber. Several special processes are used to produce celltight and gastight cellular rubber. One type is made in molds under high pressure and sufficient heat for partial vulcanization. After removal from the mold, the rubber expands and is then vulcanized. Another type is an expanded synthetic rubber similar in appearance to sponge rubber with many small individual cells filled with nitrogen gas. Cellular rubber is generally available in sheets only.

Glass Fiber. Glass-fiber insulation is distinct from mineral wool in that glass fibers are made to definite formulation with a uniformity not found in mineral wool. Fibers are made by dropping molten glass through tiny orifices and blowing with air or steam to attenuate the fibers. Glass-fiber insulation can be obtained in boards or as formed pipe coverings both of which are made from fibers approximately 0.00055 in. diam compressed and treated with a thermosetting binder. It also can be obtained as loose fibers or in batts and blankets.

Plastic Foam. Plastic foam is an expanded high-molecular-weight polymer with a distinct cellular structure consisting of a multitude of unit sealed cells. Several base plastics are used, the more common being polystyrene and urea formaldehyde. Properties of foams will vary with the type of base plastic used. In general, foams are available in blocks only; however, one manufacturer markets a shredded material.

Various forms in which an insulation can be obtained will have a definite bearing on the selection for a specific application. There are essentially three basic forms, i.e., (*a*) rigid, (*b*) flexible, (*c*) granular.

Rigid insulation includes blocks, boards, beveled lags, curved segments, sectional or molded pipe coverings, molded fitting covers, and so on. This form has been used more widely than others because it is easy to install, support, and protect against weather and moisture entry. It is generally less subject to abuse and mechanical damage; hence does not require as much protection as other forms. If properly applied, maintenance generally can be accomplished with a minimum of expense.

Flexible insulation includes blankets, batts, felts, sheets, and the like. Insulation in this form has been highly successful in some fields but has been found to possess a number of disadvantages in refinery service. It is subject to mechanical damage and is generally quite absorbent; consequently, expensive protective weatherproof coverings are necessary. It is easily compressed so that it is difficult to know what actual thickness will be obtained upon installation. In addition, extensive supports and attachments are required to prevent sagging. The primary advantage is the ease with which it can be adapted to irregular shapes.

The granular form serves a special purpose in many installations and might be considered a supplement to other forms. For general insulating service, it is subject to many objections. It compacts or settles after installation, reducing thermal efficiency; and it must be totally supported and adequately encased to prevent moisture entry. However, it serves quite satisfactorily as a fill around irregular shapes and cavities enclosed by a rigid insulation, and provides the only practical means of insulating these surfaces.

Properties of Insulating Materials

All insulating materials possess certain inherent properties. These properties vary considerably in different materials and the relative importance of each generally will be determined by service conditions and results desired. The importance of analyzing these properties thoroughly with respect to service conditions cannot be overemphasized if a successful installation is to be obtained. Table 1 gives some of the more important properties of the insulating materials previously discussed.

The most important property of a thermal insulation is heat conductivity. This property is generally referred to as the K-factor which expresses the Btu per hour that will be passed through 1 sq ft of the material 1 in. thick for each deg F temperature difference between surfaces. The lower the K-factor, the greater is the resistance to heat flow. This factor is the basis used in calculating the amount or thickness of an insulation required for specified operating conditions. All other things being equal, the most economical selection obviously is the material with the lowest K-factor. Unfortunately, the selection of an insulating material is not this easy. For one thing, the published conductivity of a particular material is determined by laboratory tests of a dry sample. It is difficult to attain this value under service conditions due to application joints, moisture or water absorption, metal fastenings, and so on. It will be found in many cases that the material with the lowest conductivity will be the most expensive to apply and maintain or, for other reasons such as upper temperature limit, fire resistance, and the like, may be unsatisfactory for applied conditions. The most practical approach is to assign a relative weight to conductivity as with other properties, and to select the material that will accomplish desired results most economically.

Density or weight per cubic foot gives an indication of the rela-

TABLE 1 PROPERTIES OF VARIOUS INSULATING MATERIALS[a]

Property	Cork board	Mineral-wool board	Rock-wool board	Cellular glass block	Cellular rubber	Glass-fiber board	Plastic foam
Density, pcf	7.5 to 10	14 to 17	14 to 18	9 to 11	8	6 to 9	1.6
Specific heat	0.40	0.29	0.27	0.20	0.27	0.25	—
Upper temperature limit, deg F	200	150	150	800	150	200	150
Coefficient of expansion per deg F $\times 10^{-6}$	33.9	4.9	4.5	4.0	24	4.0	—
Compressive strength, psi, for 5 per cent compression	6	4.5	5.0	140	40	—	20
Water absorption, per cent volume 24 hr submerged	5.2	3.3	2.0	Negligible	0.2	—	1.5
Moisture absorption from air, 96 hr at 90 per cent RH, per cent volume	1.9	1.0	0.7	Negligible	0.1	—	Negligible
Water-vapor permeability, grains/sq ft/hr/in. Hg pressure differential	9.0	35	33	0.0	0.0	—	Negligible
Fire resistance, per cent combustible	94	27	29	0	100	—	100
Conductivity, Btu/hr/sq ft/deg F/in.:							
Mean temp, 60 F	0.27	0.31	0.32	0.43	0.22	0.27	0.28
0 F	0.25	0.28	0.285	0.41	0.21	0.22	0.25
—40 F	0.237	0.26	0.27	0.345	0.205	0.19	0.235

[a] Data from manufacturers' publications and Stone (5).

tive ease of handling which will have some bearing on installation costs. It also will determine the total dead load of an installation. Density multiplied by specific heat gives the heat capacity of an insulation. A high heat capacity is of value in cases where it is necessary to prevent a sudden or rapid temperature rise in the event of a refrigeration failure. Conversely, a low heat capacity is desirable in installations where there is a rapid cycling from hot to cold.

Upper temperature limit is the maximum temperature to which a material can be subjected without causing adverse effects such as breakdown of the binder, excessive shrinkage, and the like. This property is important since most refineries periodically steam out a large percentage of process vessels and piping for cleaning, inspection, or maintenance purposes. Insulation on such equipment, of course, is exposed to the maximum temperature reached during the steam-out period. In order to prevent premature failure of the insulation with resulting excessive maintenance or replacement costs, it is necessary to select a material that satisfactorily will withstand the maximum temperature which may be encountered.

The coefficient of expansion or linear change with temperature should approach closely that of the wall material over which the insulation is applied. Otherwise, excessive stress will be placed on the bonding agent and the insulation will part at joints, crack, or tear away from the wall. Most insulations are installed on equipment fabricated from carbon or alloy steels which have a coefficient of linear expansion in the range of 6 to 10 $\times$ 10^{-6} per deg F. No insulating material currently available has a figure equal to this; however, the wider the variation, particularly on equipment that is subject to cyclic operation or large temperature fluctuations, the greater the possibility of the insulation damage.

Compressive strength gives an indication of the amount of support required for a particular installation. On large towers, a material with high compressive strength will require fewer supports to prevent sagging; hence installation costs will be less. In addition, high compressive strength aids in reducing damage from mechanical shock or abuse, such as workmen climbing on or leaning ladders against the insulation. Compressive strength also gives some indication of handling properties of the material.

Water absorption is an important factor since a large percentage of refinery insulation is exposed to the weather. Any defect in the exterior protective or weatherproof covering presents the possibility of water entering the insulation. Water increases the thermal conductivity considerably and in many cases will cause rotting or disintegration of the material. Flexible and granular insulations generally are much more water-absorbent than the rigid form.

Moisture absorption and water-vapor permeability are closely associated properties that constitute two of the most important properties of low-temperature insulating materials. Moisture (water-vapor) penetration of various materials dictates the necessity of providing an effective vapor barrier on the warm side of low-temperature insulations. There is always some moisture present in the air as invisible vapor. The amount the air will hold without forming fog or dew—indicating a saturated atmosphere—varies sharply with the temperature. Water vapor moves independently of other constituents of air and tends to travel from regions of high temperature toward those of lower temperatures where its pressure is less. Vapor pressures at saturation for various temperatures are shown in Fig. 1. Under normal atmospheric conditions, saturation is seldom encountered and relative humidity is used to indicate the per cent of saturation. It is apparent from the curve that the vapor-pressure differential between the warm and cold sides of an insulation is the motivating force responsible for migration of water vapor through an insulation.

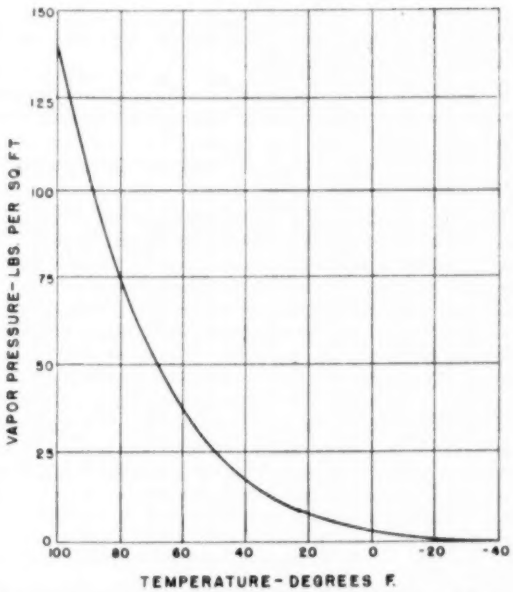

Fig. 1 Water-Vapor Pressure at Saturation Versus Temperature

It should be borne in mind that water vapor passes readily through many materials that are impervious to air or water. Any vapor that gets into an insulation through penetration or breaks in the vapor barrier will continue to migrate until the area of lowest temperature is reached or until it encounters an impermeable surface. This moisture would be of little consequence if it remained in the vapor phase; however, in most cases it condenses to form water or ice depending upon the temperature. Water in insulation is a problem for reasons previously mentioned, i.e., rotting or disintegration of the insulation, and also because of corrosion of any metal present.

The formation of ice is considerably more damaging than water since it usually forms at the vessel shell or wall forcing the insulation away from the wall. Cracks generally result permitting entrance of additional moisture; hence progressive damaging continues until the effectiveness of the insulation is destroyed. In any event, water or ice causes a considerable increase in conductivity. The total heat transmission of an insulation is the sum of the solid-phase conduction, gas-phase conduction, and radiation (1).[2] In general, transmission by the solid phase will increase in approximately direct proportion to the weight per cent of water or ice formed.

In some instances, cost studies may show that the most economical installation is a particular material with a high degree of moisture absorption protected by a suitable vapor barrier. It should be remembered that this material can pick up moisture from the air prior to application that will migrate to the cold surfaces when the insulation temperature is reduced. The quantity of moisture probably will not be sufficient to cause excessive damage; however, an increase in conductivity will occur which might result in troublesome surface-condensation problems.

---

[2] Numbers in parentheses refer to the Bibliography at the end of the paper.

The last property to be discussed, an important one in refinery service, is fire resistance or combustibility. Two basic requirements are considered important:

1 The insulation should add as little fuel to a fire as possible—complete incombustibility is desirable but not absolutely essential.

2 The material should be sufficiently fire-resistant to adequately protect the equipment it covers.

The latter requirement is probably the more important of the two. In the event of a fire at a process unit, an insulation that can protect the equipment it covers adequately, even though the insulation itself is destroyed as far as further use is concerned, will save many times the cost necessary to reinsulate. Some materials that support combustion to a limited extent still possess sufficient resistance to protect the equipment they cover. Others melt, spall, or burn readily under fire exposure and hence provide very little or no protection, or help in spreading fire (burning cork carried by wind). The cost of the insulation installed on a particular piece of equipment is generally only a small fraction of the cost of the equipment itself. Therefore it is desirable to select an insulation that affords protection even though it may not be the most economical in first cost.

Selecting an Insulant

Values assigned to various properties in Table 1 are indicative only. Mineral-wool board, for example, is marketed by several different companies. Each company uses different manufacturing techniques and, as a consequence, properties of final products vary considerably even though they may all come under the general class of mineral-wool board. In analyzing an insulation problem, accurate data on properties of specific materials being considered must be obtained to permit intelligent selection of a material that will accomplish desired results.

To review briefly, the success of an insulation job will depend largely on the selection of an insulant that is suitable for service conditions. If the equipment is to be steam-cleaned at temperatures around 250 F, limit the selection to materials that can withstand this temperature. If service conditions involve cyclic operation through a wide temperature range, keep the coefficient of linear expansion in mind. The material with the lowest thermal conductivity is desirable, but it may be highly permeable to water vapor and in a short time its conductivity may be higher than that of another material less subject to moisture penetration. It is apparent that a material should not be chosen on the basis of one or even two properties. Rather, each property should be assigned a relative weight depending upon particular requirements, and the material that most adequately and economically meets these requirements should be selected.

Accessory Materials

The application of an insulation requires a variety of accessory materials such as adhesives, vapor sealers, weatherproof and fireproof coverings, mechanical attachment devices, and so on. One accessory material is the protective coating applied for corrosion protection to the surface of the equipment to be insulated. There is disagreement as to whether this accessory is necessary since it is felt by some that a properly applied vapor seal will preclude the possibility of moisture reaching metal surfaces. This is an ideal condition but one seldom achieved in practice particularly in humid atmospheres. Even if a perfect vapor seal could be obtained and maintained, the moisture absorbed by some insulating materials prior to application will migrate to the surface of the equipment after the temperature is lowered and initiate corrosive action. Experience indicates that the expense required for application of a protective coating is well justified.

There are several types of adhesives available, some of which are better-suited for a particular application than others. The oldest and one of the most widely used adhesives is hot asphalt. It has several inherent disadvantages though, in that fired kettles required for melting the asphalt are prohibited by safety regulations in many refineries. Also, erection asphalt has a melting point or upper temperature limit of 125 F to 175 F. The upper temperature limit of the adhesive is equally as important as that of the insulant, and a material must be used that will maintain adhesive properties at the maximum anticipated temperature. Cold-application adhesives are generally of two basic types (*a*) asphalt cutback which is essentially petroleum asphalt dissolved in a petroleum solvent, and (*b*) asphalt emulsion which is petroleum asphalt dispersed in water. Some of these materials are available with an upper temperature limit of 300 F to 450 F which is obtained by the addition of mineral fillers to the asphaltic compounds. In addition to upper temperature limit, there are several other points to remember when using adhesives. A material should not be used that sets to brittle hardness if wide temperature differences are likely to be encountered, since the difference in expansion characteristics of the insulation and the vessel or pipe wall will break the adhesive bond. Further, joints should be as small as possible since the conductivity of the adhesive is usually high. Stone (2) points out that, other things being equal, joints only $^1/_{16}$ in. wide completely filled with adhesive will transmit enough heat to raise the total heat transfer of the insulation some 10 to 12 per cent.

Mechanical attachment or securement of the insulation is a necessity regardless of whether or not an adhesive is used. The most commonly used securement devices are bands, wires, welded studs, and welded hairpins. The latter two must be attached to the vessel or pipe wall; hence provide through metal paths for heat flow. The probability of moisture being present in any low-temperature insulation dictates the desirability of using corrosion-resistant materials. Monel and stainless steel are commonly used since they possess good tensile strength and excellent corrosion-resistant properties. Galvanized and copper-covered steel wire and bands are frequently used but their life is considerably less than either stainless steel or Monel.

Vapor sealers and weatherproof coverings are available in a variety of types, the particular material or materials selected generally being determined by job requirements. Some materials serve both as a vapor seal and weatherproof covering, whereas others installed as vapor barriers require protection from the weather. In a like manner, certain weatherproof coverings possess fire resistance while others require additional protection if fire resistance is a requirement. Factors affecting selection of these coverings are discussed in more detail under vapor-barrier design.

Design and Specifications

The second basic factor which determines the efficiency and dependability of an insulation is adequate design and specifications. Each low-temperature application must be analyzed individually and details of design and specifications prepared that will result in an insulation capable of satisfying specified requirements. The design, of course, will vary considerably with what is desired of the insulation. This may be simply a matter of obtaining the most economical thickness. On the other hand, operational requirements, such as accurate process control, refrigeration economy, and elimination of excessive condensation on exterior surfaces, may be of primary importance with economic considerations secondary. Other factors which affect the design are whether the equipment will be indoors or outdoors, anticipated life of the equipment, vibration or mechanical abuse that can be expected, fire hazard involved, maximum

and minimum temperature conditions, nature of operation (cyclic or constant), weather conditions with particular reference to humidity, deleterious effect of product spills, heat capacity necessary in event of refrigeration failure, and the number of hours' operation each year.

It is generally conceded that the most economical insulation thickness for a particular application is that thickness at which the sum of the costs of annual maintenance, refrigeration, and the amortization of the first cost is a minimum. This thickness, however, may not be enough to prevent excessive surface condensation in areas of high humidity or to permit accurate control of process temperatures. Calculations necessary to determine the required thickness for a particular application have been omitted from this paper; however, excellent reference material can be obtained from information prepared by Stone (2, 5), Bradley and Stone (3), and McMillan (4).

One of the most important phases of low-temperature-insulation design is the provision of an adequate vapor barrier on the warm side of the insulation. The extent of protection necessary will vary somewhat with operating conditions. Intermittent or cyclic operation requires less protection since during the off period or high-temperature part of the cycle, the vapor pressure of the normally cold side will rise, tending to force the moisture out of the insulation. However, if low temperatures are maintained over a long period of time, an effective vapor barrier must be provided to prevent loss of thermal efficiency and serious damage to the insulation. The most effective vapor seal is a metal sheathing with welded joints. This type of seal has several other advantages in that it is weather and fireproof, and resistant to mechanical damage. It has not proved attractive for refinery installations though, since it is expensive to install, makes inspection and maintenance of equipment difficult, and poses the problem of a pressure differential across the sheathing due to contraction of the entrapped air as the temperature is lowered.

A number of so-called vapor-barrier materials are currently available. Inasmuch as most of these are subject to moisture penetration when a vapor-pressure differential exists, they might more aptly be called vapor-resistive materials. Table 2, compiled by Stone (5), presents permeability values for some of the more commonly used vapor barriers. These should be considered indicative rather than specific values since they will vary considerably under applied conditions. The degree of impermeability required of the vapor barrier will depend to an extent on the insulating material selected. An insulant that is impermeable itself, such as cellular glass, will require protection from vapor penetration only at the joints. Use of a joint adhesive with low vapor permeability on this material will reduce exterior vapor-barrier requirements to a minimum. On the other hand, insulants with high permeability, particularly blankets or felts, require the maximum in exterior vapor resistance.

TABLE 2 WATER-VAPOR PERMEABILITY OF SOME WEATHERPROOFING MATERIALS[a]

	Material	Permeability[b]
1	1/16-in. film, rubber-emulsion adhesive	0.60 to 0.75
2	Approximately 1/8-in. emulsified asphalt, asbestos fiber and filler	1.8 to 4.5
3	Approximately 1/8-in. asphalt, fiber and filler (solvent-type plastic)	0.10 to 0.80
4	15-lb asphalt-saturated rag-felt roofing	4.0 to 20.0
5	15-lb asphalt-saturated asbestos-felt roofing	1.0 to 8.0
6	20-lb asphalt-saturated asbestos-felt roofing, coated	1.0 to 2.0
7	35-lb cold-application asbestos felt, coated two sides	0.0
8	1/4-in. asbestos-cement sheet	6.0 to 7.0
9	Paper-backed aluminum foil, 110 lb/3000 sq ft	0.40
10	1 1/2-in. stone concrete (1:2:4 mix)	2.9
11	1/2-in. Portland-cement plaster (1:2 mix)	12.0 to 20.0
12	Combination: 1/16 in. No. 3, 1 course No. 5, 1/8 in. No. 3	0.01 to 0.10
13	25/32-in. plain wood-fiber insulating board	30.0

[a] Data from publication by Stone (5).
[b] Water-vapor permeabilities expressed in grains per sq ft per hr with a pressure difference of 1-in. of Hg across sample.

A vapor barrier, to remain effective, must be protected adequately from mechanical abuse and from the weather, if the equipment is outdoors. It is desirable, of course, from the economical standpoint to use only one material for the final coat. The solvent plastic asphaltic compounds (cutbacks) possess relatively good vapor-resistant properties and at the same time provide adequate weather protection. A relatively low degree of abrasion resistance can be obtained by applying these coatings over a reinforcing membrane such as poultry netting or glass cloth. If fire resistance is a requirement of the insulation, compressed asbestos-cement sheets, metal, or fire-retardant felt covering are necessary. This, again, will depend to some extent on the insulant selected since certain materials will themselves provide adequate protection of equipment in event of fire exposure.

Another factor to consider is the necessity of protecting exterior finish materials from possible damage by product leaks, drips, or spills. Asphaltic compounds are soluble in most liquid hydrocarbons and if used as the final coat, must be protected by suitable metal shields at likely points of contact with process liquids.

In the design of a new process unit or an addition to an old unit, considerable care and conscientious attention must be devoted to the arrangement of towers, drums, exchangers, and piping to insure that ample space will be allowed for application and maintenance of insulation. If sufficient space is not provided installation costs will be increased, the optimum installation will not be obtained, and maintenance will be difficult and expensive. It is good practice to insulate each line separately rather than nesting two or more lines and insulating them as a unit. It is also desirable to install valves with stems looking down, wherever feasible, so that condensation on cold stems or packing-gland leaks will not drip on the insulation. Adequate supports should be provided even though an adhesive is used. In designing supports, care must be exercised to minimize through-metal paths for heat flow. The cost of extracting heat is considerably more than the cost of supplying heat and through-metal paths even though they may be small, can add appreciably to over-all refrigeration costs.

Specifications are essentially the connecting link between engineering design and field application. They should be sufficiently rigid and detailed to assure that desired results will be achieved. However, unnecessarily rigid or complicated specifications invite difficulties and incur unwarranted expense. Specifications should be prepared by someone familiar with the equipment to be insulated, operating and atmospheric conditions to which the insulation will be subjected, and physical properties and characteristics of the various materials to be used in the installation. Also, it will pay dividends to have specifications either prepared or reviewed by someone familiar with field application so that impractical details can be corrected before field problems arise.

Workmanship

Field application is the third basic factor affecting the efficiency and dependability of an insulation job. Regardless of how much care is exercised in the selection of materials and preparation of design details and specifications, over-all results will be no better than the quality of the workmanship obtained during installation. Some materials such as glass-fiber insulations or coal-tar compounds are irritating to the skin and eyes, and workmen will not devote as much conscientious effort to their application as to materials that do not cause physical discomfort. Certain materials are easier to handle than others. Weatherproofing compounds with equal vapor-and-weather-resistant proper-

ties will be found to vary widely in the ease of trowel or spray application. Materials that require highly skilled or specially trained craftsmen for application should be avoided as much as possible. Better results at less cost generally can be obtained if materials that can be simply and easily installed by semi-skilled craftsmen are specified. The average insulation crew probably will be composed of as many "green" men or apprentices as skilled men. For this reason, design details for flashings, supports, and the like, should be as simple as is consistent with results desired. Again, the necessity of providing ample space is mentioned to emphasize the importance of this point. Regardless of how skilled the craftsman may be, it is impossible to apply materials as effectively under crowded conditions as when adequate space is available.

Inspection

Field inspection will aid immeasurably in assuring that the installed insulation conforms to design and specifications in so far as the quality of materials and workmanship and the method of application are concerned. Each phase of the installation should be carefully checked as the work is being done. After the second layer of insulation is applied, it is too late to find out if the bands supporting the first layer were installed on 9-in. centers as specified. The field inspector is more concerned with characteristics affecting application than with properties such as conductivity or vapor resistance. For example, specifications may call for a weatherproofing material that should not be applied when the atmospheric temperature is 45 F or below or the relative humidity is 80 per cent or above. This type of information is of vital importance and the inspector should be completely familiar with limiting properties of all materials to be used in order to control application effectively.

Maintenance

Once the insulation is placed in service, prompt and adequate maintenance is the major factor affecting its life. Periodic inspection will aid in locating breaks in the exterior finish, loose or broken banding, places where product spills have affected the finish adversely, defective flashing, and so on. These damaged spots are generally of a minor nature when first detected and repairs can be made at small cost. However, if repairs are delayed, moisture or water penetration will cause progressive damage and eventually complete breakdown of large areas will occur. Repairs then become quite expensive not only because of the larger area involved but also because shutdown of the equipment is often required and process losses will be incurred.

Summary

The high costs associated with both the extraction of heat to secure low temperatures and the application and maintenance of low-temperature insulations dictate the necessity of obtaining the most efficient, dependable, and economical insulation for each particular low-temperature operation. It is believed that optimum results will be achieved if the following procedure is adopted in each insulation application:

1 Develop exact requirements.

2 Determine service conditions.

3 Obtain accurate data on properties and characteristics of materials being considered.

4 Judiciously select the material that will most adequately satisfy service conditions and requirements.

5 Calculate the thickness to be installed based on requirements.

6 Select accessory materials as determined by requirements, service conditions, and the insulating material.

7 Prepare details of design and specifications that will result in a suitable application for conditions, requirements, and materials selected.

8 Carefully and thoroughly inspect materials and application techniques during installation.

9 Periodically inspect and effectively maintain the insulation after it is in service.

Bibliography

1 "Low Temperature Insulation: Problems and Developments," by J. F. White, *Chemical Engineering Progress*, vol. 44, 1948, pp. 647–651.

2 "Analysis of Thermal Insulation Problems in Respect to Refrigerated Equipment," by J. F. Stone, *Petroleum Engineer*, vol. 22, 1950, p. C37.

3 "Thermal Insulation for Low-Temperature Application," by C. B. Bradley and J. F. Stone, *Chemical Engineering Progress*, vol. 44, 1948, pp. 723–726.

4 "Heat Transfer Through Insulation in the Moderate and High Temperature Fields," by L. B. McMillan, Trans. ASME, vol. 48, 1926, pp. 1269–1317.

5 "Thermal Insulation in Refineries," by J. F. Stone, *Petroleum Engineer*, vol. 22, January, 1950, p. C11.

Discussion

Clyde Berg.[3] The author has made an excellent review of the materials available and the factors of significance in the selection of low-temperature insulation for refinery service. His tabulation of properties of various materials over a range of characteristics such as density, conductivity, fire resistance, and water absorption, will be useful to refinery engineers in setting up specifications for insulation of low-temperature units. The problem of proper vapor-barrier insulation over materials utilized in low-temperature insulation is surely important. It is thought that the author has listed the relative merits of various materials available for this service in a very useful manner. His tabulation of the water-vapor permeability of various waterproofing materials, together with his outline of factors to be considered in the application of these materials, should aid refinery engineers in setting up proper specifications for low-temperature plant installations.

Those who have installed low-temperature units no doubt will be conscious of specific problems which have been encountered in the application of installation for this service, and it certainly would be helpful if the author would include in his closure an analysis of some of the more common problems. For example: (1) What is the best way to insulate a low-temperature valve of which there is a variety of types which are operated, particularly in regard to the problems of icing of the stem and handwheel and exposed portions? (2) What is good technique in the insulation of removable manhole covers and the like?

J. R. Cratin.[4] The paper gives a comprehensive and excellent treatment of the factors peculiar to the field of low-temperature insulation. Factors such as conductivity, compressive strength, and density are familiar to most engineers since they are common to all temperature ranges. However, it has been pointed out that the cost of extracting heat is considerably greater than the cost of supplying it, and the peculiar factors necessary to a good low-temperature insulation take on added significance.

The author recommends periodic inspection of insulated equipment and an adequate maintenance program. To neglect such maintenance is usually costly since it generally leads to the much greater expense of completely reinsulating.

---

[3] Supervisor, Process Development, Union Oil Company of California, Los Angeles, Calif. Mem. ASME.

[4] Pan American Refining Corporation, Texas City, Texas.

The author mentions the need for exercising care to minimize through-metal paths for heat flow. This care is necessary for both low and elevated-temperature services. This fact seems worthy of emphasis because it is not apparent to engineers who are not thoroughly abreast of insulation design that a large amount of heat can be lost or transmitted through a few through-metal conductors in an otherwise well-insulated piece of equipment. The elimination of such heat-conducting paths is a matter of good design and specifications, which the author has emphasized.

From the data presented it appears that plastic-foam materials are excellent for some refrigerated services owing to their very light weight, ease of handling, low conductivity, and low water-vapor permeability. The fact that they are combustible can be overcome by providing fireproof finishes. However, their chief limitation is their maximum temperature limit of 150–175 F. This precludes steaming out of the insulated equipment. Also, in the event of external fire, the cellular structure would collapse owing to melting of the thermoplastic even if a fireproof finish is provided. It is obvious that plastic foam is not suitable for protection, where necessary, of equipment or structures against fire.

A field of insulation closely allied to that covered by the paper is the atmospheric-temperature range where operating temperatures are between 32 F and 212 F. The purpose of insulating equipment in this range is generally for process control or fireproofing. This temperature range poses several problems, especially in humid coastal areas; and many of these problems are those discussed by the author, such as selection of insulation, protection of metal surfaces, adequate weatherproofing, vapor barriers, and so on. Since heat conservation is not the principal purpose of insulating, selection of the insulant is usually governed by such properties as water absorption and vapor permeability, rather than conductivity. Mr. Ray Thomas has written an excellent paper on atmospheric temperature-range insulation.[5]

Table 1 of the paper contains no absolute or comparative costs of the various insulation materials. Does the author possess any relative cost data on these materials? Also, are cellular-glass materials subject to noticeable damage such as breakage or powdering as a result of abrasion in shipment, storage, and handling?

M. S. Northup.[6] The paper is comprehensive in its scope. A fuller explanation of how moisture is driven into insulation by the differential vapor pressure between the inner and outer surfaces might be helpful in stressing the need for a vapor barrier. Also, the life of low-temperature insulation may be extremely short if moisture is allowed to penetrate (particularly when there are cyclic temperature variations) in addition to reducing its insulating efficiency. It should be helpful to point out that there is still a need for a good fireproof and weatherproof coating.

There has been considerable corrosion under cold insulation and it is the writer's opinion that a protective coating on the surface of the equipment is beneficial, since a perfect vapor seal is not possible.

Regarding the economical thickness of insulation, various design bases are used, but one that has received attention is the use of a higher return on investment factor. Using a 50 per cent return, the normally used thicknesses often may be substantially reduced.

[5] "Thermo Insulation for Industrial Requirements—Part 5," by Ray Thomas, *Petroleum Refiner*, vol. 31, July, 1952, pp. 145–149.

[6] Standard Oil Development Company, Esso Engineering Department, Linden, N. J.

Author's Closure

The author wishes to express appreciation for the comments by Messrs. Berg, Cratin, and Northup.

As pointed out by Mr. Berg, there are certainly a number of specific problems associated with application of insulation to equipment that is to be operated at subatmospheric temperatures. The best way to insulate a valve will be determined to a large extent by the type of valve and the type of insulation. If cork insulation is used, preformed covers can be obtained that will conform to the valve shape and eliminate voids between the valve body and insulation. If cellular glass or other rigid-type insulation is used, covers must be fabricated by cutting and fitting the insulation to conform to the valve shape. Voids will undoubtedly result which should be filled with granular insulation. It will sometimes be easiest to simply build a box around the valve with rigid insulation and fill the space between the insulation and valve body with granular insulation. If a flexible-type insulation is used, much less cutting and fitting will be required. Regardless of the type of insulation used, it will be necessary to provide a vapor barrier on the outside of the insulation. If the valve is outdoors a weatherproof covering will also be required. The outside covering should be a material that will not be damaged by product handled in the event of gland leakage. It is desirable to install the valve with the stem looking down, if possible, to prevent condensation on the cold stem or packing gland leaks from dripping on the insulation.

Removable manhole covers can be fabricated in separate units from rigid-type insulation. These covers can be held in place over the manhole during operation of the equipment by a suitable adhesive. When it is desired to remove the cover, the adhesive joint can be easily broken and the cover removed intact. Since the cover must necessarily be large enough to pass over the flange, there will be a void between the nozzle and the insulation cover. This void should be filled with beveled lags or curved segments of rigid insulation, or flexible or granular insulation. Again, it is necessary to provide a suitable vapor barrier and weatherproof coating on the outside of the removable cover.

No relative or comparative cost data of the various insulating material, as requested by Mr. Cratin, was presented in the paper since the cost of the insulating material itself is not representative of the installed cost of the insulation. For one thing, the costs of materials vary in different parts of the country. Comparative costs of materials in Houston may not be applicable in New York. Also, actual installation costs will be affected more by the method of installation, labor costs, and accessory materials used than by the cost of the insulating material itself.

Cellular-glass materials are subject to damage from abrasion. Care must be exercised during storage, shipping, or handling to prevent one block from rubbing against another or against any hard object. Cellular-glass insulation installed on equipment subject to wide temperature fluctuations should have a protective film applied between each layer to prevent abrasion between the blocks during contraction and expansion of the insulation. Several new materials designed to provide a suitable protective film have recently been marketed.

As pointed out by Mr. Northup, the importance of the vapor-pressure differential existing in any low-temperature installation and its effect on the migration of moisture through the insulation cannot be over emphasized. Water vapor will migrate through any insulation in which the temperature at the inner surface is lower than the temperature at the outer surface unless this migration is stopped by use of insulating materials that are impermeable and/or application of an effective vapor barrier. Further information on migration of water vapor through insulation, its causes and effects, is contained in several papers by Mr. Ray

Thomas.[7,8] Care must be exercised in calculating insulation thickness on low-temperature installations to assure that condensation or sweating will not occur on the outer surface. This problem is of particular significance in the coastal areas where high humidity prevails. In the coastal areas, humidity and temperature conditions frequently have more bearing on the selected insulation thickness than the per cent return on investment factor.

[7] "Thermal Insulation for Industrial Requirements—Part 6," by Ray Thomas, *Petroleum Refiner*, vol. 31, August, 1952, pp. 113–116.

[8] "Thermal Insulation for Industrial Requirements—Part 7," by Ray Thomas, *Petroleum Refiner*, vol. 31, October, 1952, pp. 115–121.

Full-Scale Fatigue Testing of Compressor Cylinders

By T. O. KUIVINEN,[1] MOUNT VERNON, OHIO

Present needs for higher-pressure compressor cylinders for natural-gas pipe lines introduce complexities of design and manufacture. Through full-scale fatigue testing, designs incorporating high-strength cast irons are proved suitable at considerable saving to the user. Comparison of the fatigue-test failure of the design to the fatigue strength of the material used indicates the maximum safe working pressures permissible for various suction pressures. In this manner a new design is evaluated, eliminating the risks involved in former practice where field service was the only criterion of performance.

Introduction

THE increasing demand for gas fuel throughout the country produces an ever-expanding program for the many pipeline systems transporting natural gas from producing areas to the market. Pipe-line capacities are being increased by both larger and higher-strength pipe for the newer lines. The larger capacities and higher pressures require many large compressor engines to pump the gas through the lines. These demands present a challenge to engine and compressor manufacturers in the design of suitable reciprocating compressor cylinders to be direct-driven by these large gas engines.

Not too many years ago a pipe-line system with compressors discharging at 500 psi and a compression ratio of about 2.5 was considered to be a high-pressure system. Yet it was possible to design, conservatively, suitable compressor cylinders using gray-iron castings that withstood these pressures for years without failure. The art in this field became well established, and perhaps a large measure of the success was found in the use of generous wall thicknesses based on prior experience. Occasional weaknesses were overcome by "beefing up" the design where necessary.

As pipe-line pressures increased a pressure level was reached where most of us felt that the solution lay in the use of steel castings. Designers could not use heavier walls and still provide ample valve area and gas-passage area to keep work losses to a minimum. Therefore cast steel was adopted for many designs.

Many of the multivalved compressor cylinders for higher capacities and higher pressures introduced difficulties in producing sound steel castings because of the complexity of the structure required for functional purposes. The cost of producing cast-steel cylinders is approximately twice that of cast-iron cylinders, resulting in higher cost to the user. Today procurement is added to the problem because the defense program has taxed to capacity the available steel-foundry production. In spite of these problems commercial acceptance of cast-iron cylinders seems to fall short of the pressure levels required to supply the demand for gas. The precedent of using cast steel seemed firmly entrenched.

This challenged manufacturers to do better engineering and better selling of the high-strength cast irons which have been developed in the last decade as the most efficient material for compressor cylinders.

The designs needed for pumping huge volumes at high pressures and fairly low pressure ratios become complex structures. It is necessary to provide ample valving, means for unloading for varying pressure conditions, and ample inlet and discharge passages. The high-strength-specification cast irons are readily poured into such shapes whereas casting in steel is difficult and expensive.

Test-Proving Designs

Stress calculations for such complex structures require so many assumptions and provoke many opinions as to which fundamental theories best fit the problem that designers must choose between investigating newer mathematical approaches or test-proving the designs. Test-proving produces valuable facts concerning design strength and more convincing sales data.

The convenient resistance-wire-type strain gage is a valuable and well-known tool that tells the engineer the actual stresses occurring in the various parts of a structure. The engineer is able to compare such measured stresses with the known strength of the material used. In many studies he determines the strength of the material by using test bars actually cut out of the castings after the strain-gage measurements have been completed. Through the use of resistance-wire strain gages much of the guesswork has been removed from many problems of design. The use of strain gages is often limited because of the uncertainty of strain measurement on small-radius fillets and sharp corners. Even the smallest gages are too large to indicate the real stress occurring in such areas.

The real proof of performance can be obtained by actually testing full-scale designs under extreme service conditions, accelerating such tests as much as possible. Such testing is expensive, and careful judgment must be made to obtain the desired results with a minimum number of tests.

This paper presents the investigation carried out in fatigue-testing one compressor cylinder design that is in the middle of a design line having close similarity throughout its entire range. A longitudinal section of the cylinder is shown in Fig. 1. It is difficult to show the complexity of the cylinder-head castings in a single view. Some of the casting details are shown to better advantage in illustrations which appear later.

A motor-driven reciprocating single-acting plunger pump of 4 in. bore and 4 in. stroke running at 400 rpm was used to apply a cycling pressure load to the cylinder interior using fuel oil as the liquid. The discharge-valve chambers and the discharge passage of the compressor cylinder were subjected simultaneously to a static pressure equal to the maximum pressure occurring during the cycling within the cylinder. Nearly all of the space within the cylinder was filled with metal so that the compressibility of the remaining volume of fuel oil and air was within the capacity of the 4 × 4 plunger pump, with the pressure cycling higher than the anticipated fatigue strength of the compressor cylinder.

Fig. 2 is the test setup showing in the foreground the motor

[1] Chief Engineer's Assistant, The Cooper-Bessemer Corporation.

Contributed by the Petroleum Division and presented at the Petroleum Mechanical Engineering Conference, Kansas City, Mo., September 22–24, 1952, of The American Society of Mechanical Engineers.

Note: Statements and opinions advanced in papers are to be understood as individual expressions of their authors and not those of the Society. Manuscript received at ASME Headquarters, June 5, 1952. Paper No. 52—PET-22.

driving the horizontal plunger pump in the center, with the compressor cylinder in the background. All compressor valves were removed and dummy plates were installed in the valve openings in order to have better control of the pressures. Fig. 3 is a schematic drawing of the pressure-control system.

The regulating valves are simple intensifiers using o-ring sealed pistons with the manually regulated air pressure setting the desired discharge pressures. A small check valve in one of the dummy discharge valves permits the cycling cylinder pressure to enter the discharge passage where it is controlled by the regulator valve. Excess oil and air bleed back to the open oil-supply tank.

A pair of air-admission valves permit small amounts of air to enter the cylinder from the lower-pressure air tank in case too much air escapes through the regulator valves. Thus the compressibility curve of the fluid and air within the cylinder is used

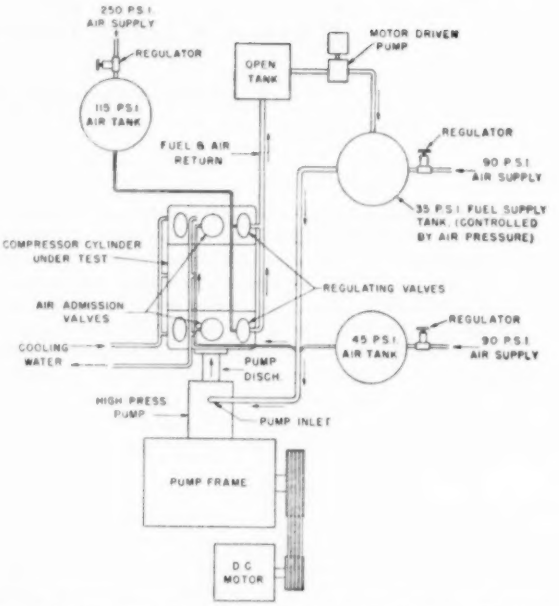

Fig. 3 Pneumatic Control System for Control of Cycling Pressure

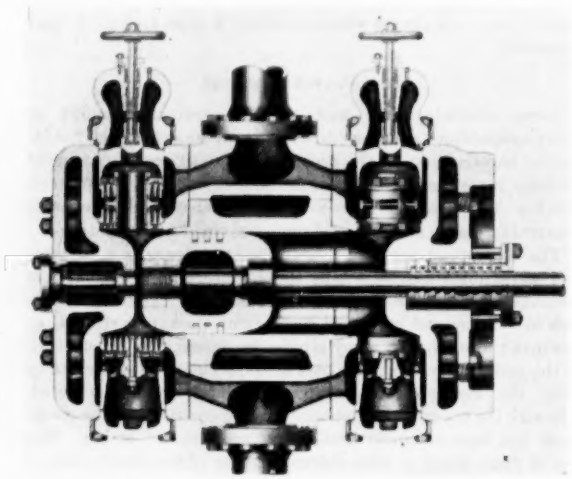

Fig. 1 Compressor-Cylinder Assembly

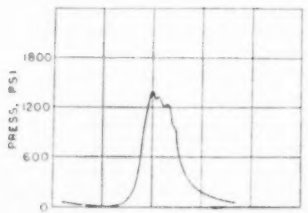

Fig. 4 Typical Cycling-Pressure Diagram

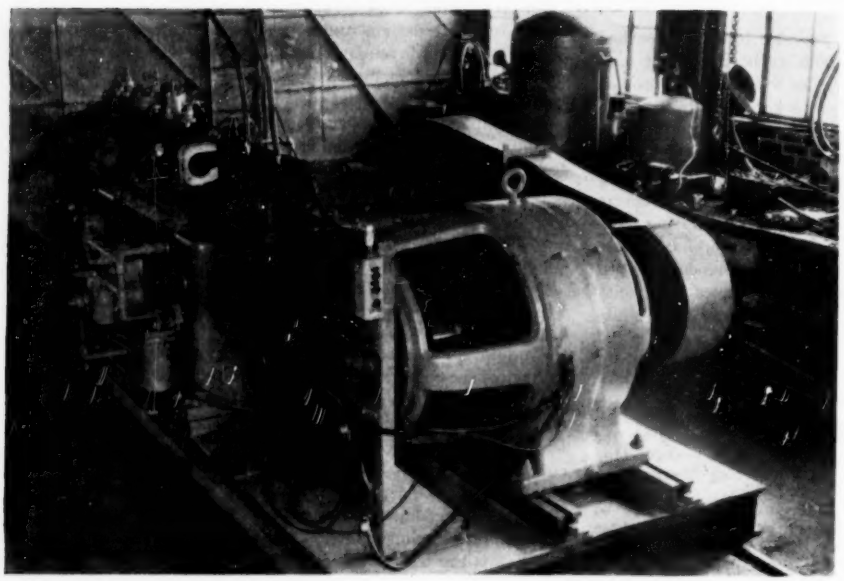

Fig. 2 Compressor-Cylinder Fatigue-Test Setup

to apply the cycling-pressure load. The peak pressure is adjusted by means of regulating the air pressure on top of the intensifier piston. The pressure range is observed by means of a standard high-pressure engine indicator attached to the standard indicator connection of the cylinder. In the first test a strain-gage pickup which fed into a cathode-ray oscilloscope was used to calibrate the equipment. A typical card observed on the oscilloscope is shown in Fig. 4.

Factor of Safety

Before presenting the test results and the conclusions reached it might be wise to review the general understanding of "factor of safety" and the behavior of metal under varying stress. The factor of safety built into any machine is usually understood to be the ratio of the strength of the material to the operating stress. In designing a part by stress calculations alone an engineer arrives at an allowable stress by dividing the ultimate strength of the material used by a factor of safety which is $a \times b \times c$, where

a = allowance for severity of load-application rate in dynamically loaded parts. This is usually set at 2 which is the maximum attained for a condition of pure impact.

b = transfer factor for fatigue strength and is the ratio of tensile strength divided by reverse bending endurance limit. For average steels b runs from 2 to 2.2. For many cast irons b is about 2.8 to 3.

c = real factor of safety put in to allow for material variations, casting dimensional variations, and stress concentrations caused by shape, sharp corners, and so on. The designer usually includes a reserve depending upon the service the part is intended for, his own conservatism, or an "ignorance factor."

Thus we hear engineers discussing factors of safety for various designs ranging from perhaps 6 to 1 to as high as 12 to 14 to 1.

A vast amount of information concerning the behavior of materials under cycling stresses has been obtained from test bars in various types of fatigue machines such as the Moore rotating-beam machine, and others. Some machines are limited to completely reversed alternating stress, while others can provide various ranges of cycling stress.

Test Results

A typical stress versus number of cycles of alternating stress for the 40,000-psi-tensile-strength grade of Meehanite iron used in the test cylinder is shown in Fig. 5. This shows that the reverse bending (complete stress reversal) endurance limit for this grade of iron is approximately 15,000 psi.

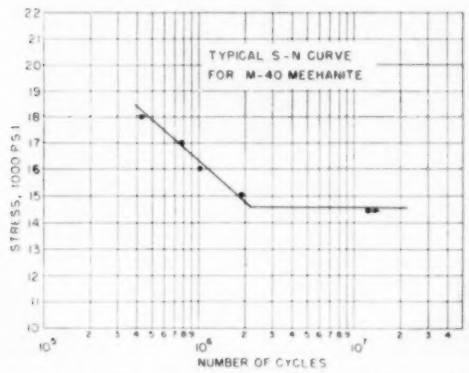

Fig. 5 S-N Curve for Meehanite Cast Iron of 40,000-Psi Tensile Strength

For various ranges of cycling stress the behavior of metals is most easily indicated by the diagram shown in Fig. 6 for an average 70,000-psi tensile-strength steel.

The specification iron used in the test compressor cylinder produces an endurance-strength diagram as shown in Fig. 7.

If an operating condition produces a stress picture as shown by point x in Fig. 7, we can talk about a real factor of safety which will give a true picture of the reserve between the operating

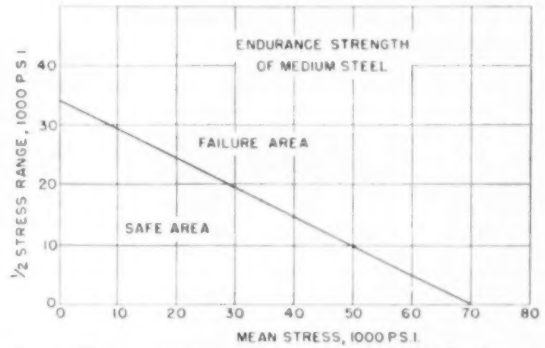

Fig. 6 Endurance-Strength Diagram for 70,000-Psi Steel

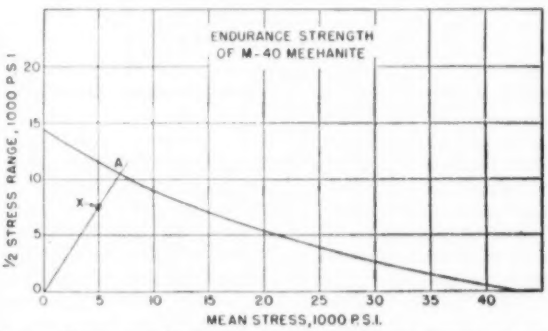

Fig. 7 Endurance-Strength Diagram for Meehanite Cast Iron

stresses and the range needed to produce failure. A line parallel to the endurance-strength line may be drawn through x and its intercept with either axis may be divided into the endurance-strength-line intercept to obtain the safety factor. In a like manner a ray may be drawn through the origin and point x. Then the factor of safety is the distance 0-A, Fig. 7, divided by the distance 0-x. This is the real factor of safety against failure when cycling at the conditions of service represented by the point x.

Table 1 shows the results obtained in stressing the compressor-cylinder assembly at a rate of 400 stress cycles per min for the ranges shown.

TABLE 1 RESULTS OF STRESSING COMPRESSOR-CYLINDER ASSEMBLY

Cycling pressure range, psi	Number of cycles	Results
0–1400	6000000	No failure
0–1600	6000000	No failure
0–1800	5200000	Liner cracked

The cylinder liner cracked through the lubricating-oil check-valve holes. The results indicate that a pressure range of 0–1700 psi is one point on the endurance-strength line for the assembly.

Since the failure occurred at a point that is easily analyzed, it

was felt that nothing had been determined about the actual strength of the complex castings, such as the cylinder heads. Zyglo inspection of all parts revealed no cracks.

Oil check-valve holes are necessary so a new liner was installed with a cast-on strengthening band around the region of the check-valve holes. The revised design is shown in Fig. 8. Table 2 shows the results for the revised design.

TABLE 2 RESULTS OF STRESSING REVISED DESIGN COMPRESSOR-CYLINDER ASSEMBLY

Cycling pressure range, psi	Number of cycles	Results
0–2000	6000000	No failure
0–2200	1900000	Liner cracked

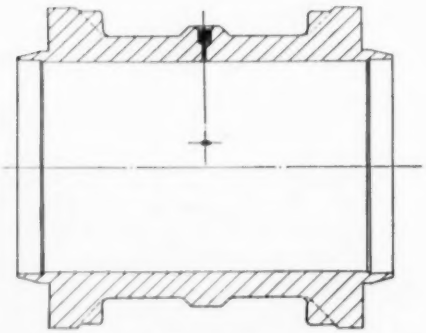

FIG. 8 MODIFIED LINER DESIGN STRENGTHENING OIL CHECK-VALVE HOLE

Again the liner cracked through one of the check-valve holes, indicating that 0–2000-psi pressure range is one point on the endurance-strength line.

A third liner having the same reinforcing band, but with a radius applied to the oilhole at the inner surface of the liner, was installed. After a run of less than 100,000 cycles at 0–2200 psi, it was impossible to hold pressure. The cylinder was dismantled and the heads were found to be cracked from port to port at the discharge valves. Fig. 9 shows one entire head (and the reinforced liner) from the inside with whiting applied to bring out the cracks. Fig. 10 is a close-up of the cracked areas. Fig. 11 is another close-up taken from the opposite side through the discharge-valve pocket to show the extent of crack penetration. This failure indicates that the heads and liner are at the endurance limit at a cycling pressure of 0–2000 psi.

From this limited test a chart may be made to show the allowable pressure ranges that can be used under desirable factors of safety. Refer back to Fig. 7. This is an endurance-strength diagram for the iron used expressed in terms of "psi" stress. A similar diagram, shown in Fig. 12, can be constructed with the strength expressed in psi pressure by drawing a line through the one test point, representing the 0–2000-psi range determined from the fatigue test, that is parallel to the endurance-strength line expressed in terms of stress. Any operating condition can be spotted on the pressure-ordinate chart and the factor of safety determined in the same manner as discussed previously for Fig. 7.

Application engineering of such a compressor cylinder revolves around determination of the liner size for the particular suction and discharge pressures required by the customer. A more suitable chart to determine the allowable pressure ranges for a given factor of safety determined from the fatigue-test results is shown in Fig. 13. This chart is produced by plotting on Fig. 12 two or three points for a given factor of safety by drawing

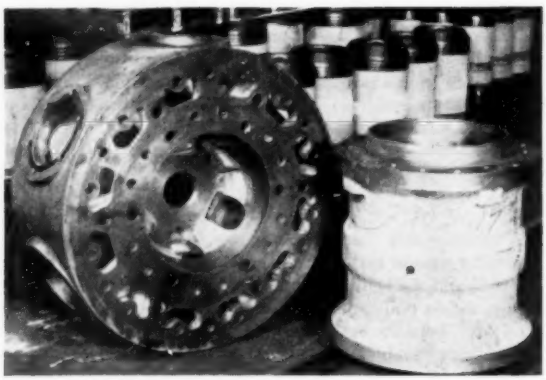

FIG. 9 COMPRESSOR-CYLINDER HEAD SHOWING POINTS OF FAILURE

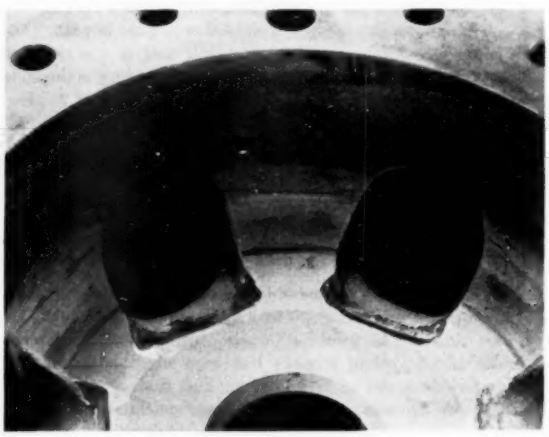

FIG. 10 CLOSE-UP OF CRACKS IN COMPRESSOR-CYLINDER HEAD

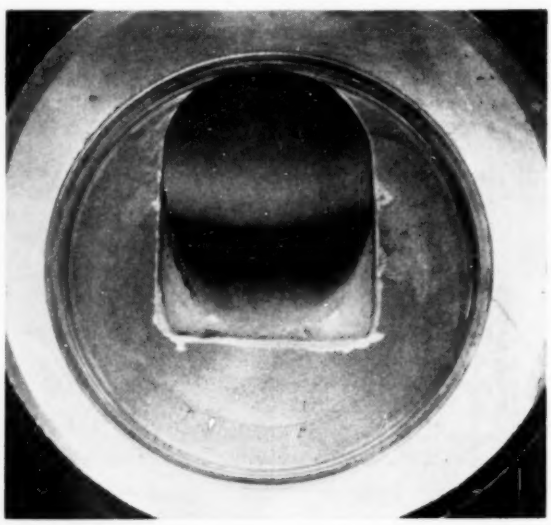

FIG. 11 CLOSE-UP OF DISCHARGE-VALVE POCKET SHOWING OPPOSITE SIDE OF CRACK

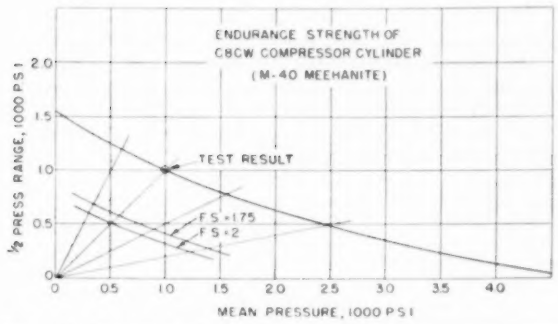

FIG. 12 ENDURANCE-STRENGTH DIAGRAM FOR COMPRESSOR CYLINDER EXPRESSED IN PRESSURE RATHER THAN STRESS

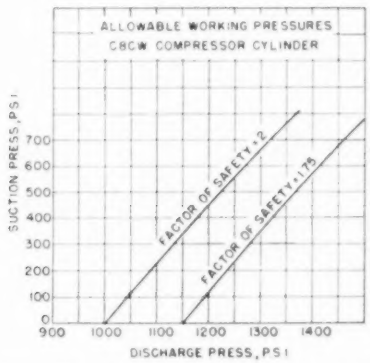

FIG. 13 ALLOWABLE WORKING PRESSURES FOR COMPRESSOR CYLINDER TESTED

rays through chosen points on the endurance-strength line and the origin. The length of each ray is measured and divided by the factor of safety to obtain the reference points. Then a parallel line is drawn through these points to represent various conditions for a given factor of safety. Several points of pressure range are observed and transferred to Fig. 13. This type of chart is easily used and eliminates measurement and calculation from the endurance chart when planning applications of the particular cylinder under consideration.

Conclusion

We recognize that a more precise story over various pressure ranges could be obtained by several tests of the same design so as to have several failure points. In full-size testing this would mean considerably more expense and time. The scheme used herein to make the transition from known material characteristics to evaluating an actual design presents results that are usable for practical applications. Although the tests were limited the results are a long stride ahead of the former practice of designing by experience and limited stress calculations.

It is gratifying to learn that this particular compressor-cylinder design, which we hoped would be suitable for 1000-psi discharge pressure for the usual suction pressures encountered, is actually able to operate at a discharge pressure of 1200 psi with a suction pressure as low as 450 psi with a conservative real safety factor of 2.

Surely this illustrates the suitability of specification cast irons for compressor cylinders in the pressure ranges now being used or contemplated for major pipe lines.

Discussion

H. W. Whiting.[3] The author has pointed out the near futility of calculating with any acceptable accuracy the actual stresses existing in a complex structure such as a large compressor cylinder for the service described.

Designers therefore must depend on full-scale testing of compressor cylinders, either the fatigue type of test described in the paper or the simple hydrostatic test to destruction.

To evaluate both methods of testing we must consider the more accurate safety-factor determination for the over-all cylinder production.

Discounting the fact that thermal stresses are not included in the fatigue-testing method described, the real factor of safety is determined more accurately, permitting in some cases higher operating pressures for the same cylinder where a large "ignorance factor" heretofore had been used. On the other hand, as the author indicates, such a test is expensive and time-consuming, for which reasons tests are run on only one cylinder in the middle of a design line having close similarity throughout its entire range.

Hence, because so few tests are made, we would have no assurance that other cylinders made from the pattern would be as good as the one tested. We know that there are tremendous differences in the strength of cylinders produced from the same pattern due to molding, iron mixture, rate of cooling, annealing, and machining. Recently we have learned that great differences can exist in the two ends of the same cylinder casting.

The foundry of the writer's company cast a cylinder using its standard high-strength cylinder iron designated M3146. This same pattern, generally similar to that described by the author, was shipped to a large, reputable foundry in the east which produced a similar casting of Meehanite A. The same foundry then cast a cylinder of ductile iron. All cylinders were stress-relieved as required, machined completely, and studded for the application of cover plates for hydrostatic testing.

As all of the cylinders tested fractured through the valve ports on the "cope" end only, it was decided to cut the cylinders in two, midway between the ends, and by additional studding and a cover plate, repeat the tests on the "drag" end of the same cylinders. The results of tests are given in Table 3 of this discussion.

TABLE 3 RESULTS OF TESTS ON CYLINDERS, PSI

			M3146	Meehanite A	Ductile iron
Hydrostatic rupture	Cope end...		3300	3500	3600
	Drag end..		4200	4600	5300[a]
Tensile tests 6 bars each	Cope	Low.	38600	40600	34000
		High.	42200	44600	79800
		Avg..	41200	43000	65300
	Drag	Low.	45600	48100	82000
		High.	48400	49200	84800
		Avg..	47000	48600	83400

[a] Cylinder did not rupture, gaskets leaked excessively.

Because we are faced with such inconsistencies in the production of such complex castings the writer believes in the value of an unlimited number of destructive tests on all cylinders and to the extent of repetitive tests on the same cylinder design as just outlined.

Try as we may, we still are faced with the ignorance factor!

Author's Closure

The author would like to thank Mr. Whiting for his interesting contribution. Design engineers must have such knowledge from the foundries so that an intelligent selection of a factor of safety can be made.

It appears that the rupture tests do not correlate too well with

[3] Assistant Executive Engineer, Worthington Corporation, Buffalo, N. Y. Mem. ASME.

the test bars for the specification cast irons. For the M3146 iron, the drag half test bars averaged 14 per cent stronger than the cope half while the rupture test disclosed a 27 per cent increase. Similarly the Mechanite A bars were only 13 per cent stronger whereas the rupture test indicated a 31.5 per cent increase. This indicates that the structure shape effect may have been altered when the castings were sawed in two.

The variation in the ductile-iron casting indicates a need for more research in the use of this new material.

Obviously knowledge obtained from destructive testing is the most reliable, but production economics dictates that an unlimited number of destructive tests on all cylinders cannot be tolerated. Testing of samples followed by close production control appears to be the desired approach.

AN ASME PAPER

Its Preparation, Submission and Publication, and Presentation

To a large degree the papers prepared and presented under the ASME sponsorship are evidence by which its professional standing and leadership are judged. It follows, therefore, that to qualify for ASME sponsorship, a paper must not only present suitable subject matter, but it must be well written and conform to recognized standards of good English and literary style.

The pamphlet on "AN ASME PAPER" is designed to aid authors in meeting these requirements and to acquaint them with rules of the Society relating to the preparation and submission of manuscripts and accompanying illustrations. It also includes suggestions for the presentation of papers before Society meetings.

CONTENTS

PREPARATION OF A PAPER—

General Information—Style, Preferred Spelling, Length Limitation, Approvals and Clearances.

Contents of the Paper—Title, Author's Name, Abstract, Body of Paper, Appendixes, Acknowledgments, Bibliographies, Tables, Captions, Photographs, Other Illustrations.

Writing the Paper—Outline Tabulations, Tables, Graphs, Charts for Computation, Drawings, Mathematics, Accuracy, Headings and Numbering, Lantern Slides, Motion Pictures, Typing, Number of Copies.

SUBMISSION AND PUBLICATION OF A PAPER—

Intention to Submit Paper Required in Advance, Meeting Dates, Due Dates for Manuscript, Discussers, Review and Acceptance, Proofs, Advance Copies and Reprints, Discussion and Closure, Publication by Others.

PRESENTATION OF A PAPER—

Time Limit, Addressing Your Audience, Public Address Systems, Use of Slides.

REFERENCES—

References on Writing and Speaking, Engineering Standards.

Price 40¢. No discount allowed. *A remittance must accompany all orders for $5.00 or less. U. S. Postage Stamps are acceptable.*

THE AMERICAN SOCIETY OF MECHANICAL ENGINEERS

29 West 39th Street, New York 18, N. Y.